

---

# Performance of Concrete Pavements,

---

## Volume III: Improving Concrete

---

### Pavement Performance

---

PB2001-101111



PUBLICATION NO. FHWA-RD-95-111

JUNE 1998



U.S. Department of Transportation  
**Federal Highway Administration**

Research and Development  
Turner-Fairbank Highway Research Center  
6300 Georgetown Pike  
McLean, VA 22101-2296



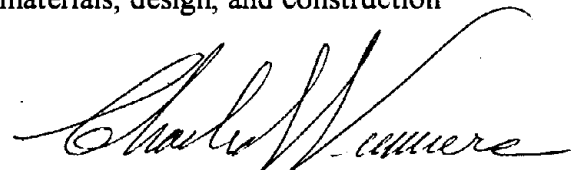
REPRODUCED BY:  
U.S. Department of Commerce **NTIS**  
National Technical Information Service  
Springfield, Virginia 22161

## FOREWORD

This report is part of a four-volume series titled "Performance of Concrete Pavements." The goal of this project was to improve design and construction procedures for conventional Portland Cement Concrete (PCC) pavements. During the field study in 1992 more than 300 test pavement sections located throughout North America were surveyed. The test pavements were previously constructed in individual State research studies. Fifteen States participated in the project: Arizona, California, Florida, Georgia, Illinois, Michigan, Minnesota, Missouri, New Jersey, New York, North Carolina, Ohio, Pennsylvania, West Virginia, Wisconsin and the Province of Ontario. About one-third of the sections were also surveyed in 1987 so some data is also available on trends with time. Data was also gathered on 96 PCC pavements from Europe and 21 PCC sections from Chile. The information was entered into the Rigid Pavement Performance (RIPPER) data base which is based on the SHRP LTPP data base. The RIPPER data base is available from the Federal Highway Administration.

The RIPPER data base was analyzed by researchers from Chile to develop the "Pavement Evaluator" program. These models will comprise part of the World Bank's HDM-4 system. The new models were tested with the Long Term Pavement performance (LTPP) data base. Information assimilated under this project also served as the basis for a set of supplemental AASHTO equations that were approved in 1997. A spreadsheet to perform these checks was built by the LTPP Implementation Program and will aid engineers to optimize PCC designs.

Volume I summarizes the pavement sections and performance data. Volume II presents the results design features. Volume III presents new equations for cracking, faulting, spalling, serviceability, and roughness. Volume IV documents data and key findings from the European and Chilean studies. These findings combined with results from the LTPP program will advance the "state of the practice" for PCC pavement materials, design, and construction procedures.



Charles J. Nemmers, P.E.  
Director, Office of Engineering  
Research and Development

## NOTICE

This document is disseminated under the sponsorship of the Department of Transportation in the interest of information exchange. The United States Government assumes no liability for its contents or use thereof. This report does not constitute a standard, specification or regulation.

The United States Government does not endorse products or manufacturers. Trade and Manufacturers' names appear in this report only because they are considered essential to the object of the document.

1. Report No. FHWA-RD-95-111		3. Recipient's Catalog No.	
4. Title and Subtitle PERFORMANCE OF CONCRETE PAVEMENTS Volume III—Improving Concrete Pavement Performance		5. Report Date June 1998	
		6. Performing Organization Code	
7. Author(s) H.T. Yu, K.D. Smith, M.L. Darter, J. Jiang, and L. Khazanovich		8. Performing Organization Report No.	
9. Performing Organization Name and Address ERES Consultants, Inc 505 W. University Avenue Champaign, IL 61820-3915		10. Work Unit No. (TRAIS) 3C1A	
		11. Contract or Grant No. DTFH61-91-C-00053	
12. Sponsoring Agency Name and Address Office of Engineering and Highway Operations R&D Federal Highway Administration 6300 Georgetown Pike McLean, Virginia 22101-2296		13. Type of Report and Period Covered Final Report October 1991–December 1997	
		14. Sponsoring Agency Code	
15. Supplementary Notes FHWA Contracting Officer's Technical Representative (COTR): Mr. Jim Sherwood, HNR-20 Special thanks are given to the following highway agencies for their assistance in the conduct of this study: Arizona, California, Florida, Georgia, Illinois, Michigan, Minnesota, Missouri, New Jersey, New York, Ohio, Ontario, Pennsylvania, Wisconsin, and West Virginia.			
16. Abstract <p>With the goal of improving future concrete pavement design and construction practices, this project evaluated the performance of 303 inservice concrete pavement sections located throughout North America. An extensive field testing program, consisting of pavement condition surveys, drainage surveys, falling weight deflectometer (FWD) testing, coring/boring operations, and roughness testing, was conducted in order to collect the information needed for analysis. Because many of these pavement sections are part of State-level studies on concrete pavements, a range of design variables (e.g., load transfer, slab thickness, joint spacing, drainage) thought to affect concrete pavement performance are present. Over one-third of the sections was evaluated under a preceding FHWA study, meaning that 5-year performance trends are available for some of the sections. Additional pavement performance data are also available for 96 European concrete pavement sections and for 21 Chilean concrete pavement sections. The average age and average cumulative ESAL loadings for the North American sections are 16 years and 7.1 million, respectively, compared to 21 years and 21.8 million for the European sections and 9 years and 5.9 million for the Chilean sections.</p> <p>This volume presents pavement performance prediction models that were developed from the data collected under this study. Prediction models are presented for transverse joint faulting (doweled and nondoweled), transverse cracking (JPCP and JRCP), transverse joint spalling (JPCP and JRCP), pavement serviceability (JPCP and JRCP), and pavement roughness (JPCP only). Based on the results of the models and on the results of the field evaluation findings, guidelines for the improved design of concrete pavements are presented.</p> <p>This volume is the third of four volumes. The other volumes are:</p> <p>FHWA-RD-94-177 Volume I—Field Investigation  FHWA-RD-95-110 Volume II—Evaluation of Inservice Concrete Pavements  FHWA-RD-95-112 Volume IV—Appendixes</p>			
17. Key Words Concrete pavement, pavement design, pavement performance, performance modeling, design guidelines		18. Distribution Statement No restrictions. This document is available to the public through the National Technical Information Service, Springfield, Virginia 22161.	
19. Security Classif. (of this report) Unclassified	20. Security Classif. (of this page) Unclassified	21. No of Pages	22. Price

# SI\* (MODERN METRIC) CONVERSION FACTORS

## APPROXIMATE CONVERSIONS TO SI UNITS

## APPROXIMATE CONVERSIONS FROM SI UNITS

Symbol	When You Know	Multiply By	To Find	Symbol
<b>LENGTH</b>				
in	inches	25.4	millimeters	mm
ft	feet	0.305	meters	m
yd	yards	0.914	meters	m
mi	miles	1.61	kilometers	km
<b>AREA</b>				
in <sup>2</sup>	square inches	645.2	square millimeters	mm <sup>2</sup>
ft <sup>2</sup>	square feet	0.093	square meters	m <sup>2</sup>
yd <sup>2</sup>	square yards	0.836	square meters	m <sup>2</sup>
ac	acres	0.405	hectares	ha
mi <sup>2</sup>	square miles	2.59	square kilometers	km <sup>2</sup>
<b>VOLUME</b>				
fl oz	fluid ounces	29.57	milliliters	mL
gal	gallons	3.785	liters	L
ft <sup>3</sup>	cubic feet	0.028	cubic meters	m <sup>3</sup>
yd <sup>3</sup>	cubic yards	0.765	cubic meters	m <sup>3</sup>
<b>MASS</b>				
oz	ounces	28.35	grams	g
lb	pounds	0.454	kilograms	kg
T	short tons (2000 lb)	0.907	megagrams (or "metric ton")	Mg (or "t")
<b>TEMPERATURE (exact)</b>				
°F	Fahrenheit temperature	5(F-32)/9 or (F-32)/1.8	Celsius temperature	°C
<b>ILLUMINATION</b>				
fc	foot-candles	10.76	lux	lx
fl	foot-Lamberts	3.426	candela/m <sup>2</sup>	cd/m <sup>2</sup>
<b>FORCE and PRESSURE or STRESS</b>				
lbf	poundforce	4.45	newtons	N
lbf/in <sup>2</sup>	poundforce per square inch	6.89	kilopascals	kPa

Symbol	When You Know	Multiply By	To Find	Symbol
<b>LENGTH</b>				
mm	millimeters	0.039	inches	in
m	meters	3.28	feet	ft
m	meters	1.09	yards	yd
km	kilometers	0.621	miles	mi
<b>AREA</b>				
mm <sup>2</sup>	square millimeters	0.0016	square inches	in <sup>2</sup>
m <sup>2</sup>	square meters	10.764	square feet	ft <sup>2</sup>
m <sup>2</sup>	square meters	1.195	square yards	yd <sup>2</sup>
ha	hectares	2.47	acres	ac
km <sup>2</sup>	square kilometers	0.386	square miles	mi <sup>2</sup>
<b>VOLUME</b>				
mL	milliliters	0.034	fluid ounces	fl oz
L	liters	0.264	gallons	gal
m <sup>3</sup>	cubic meters	35.71	cubic feet	ft <sup>3</sup>
m <sup>3</sup>	cubic meters	1.307	cubic yards	yd <sup>3</sup>
<b>MASS</b>				
g	grams	0.035	ounces	oz
kg	kilograms	2.202	pounds	lb
Mg (or "t")	megagrams (or "metric ton")	1.103	short tons (2000 lb)	T
<b>TEMPERATURE (exact)</b>				
°C	Celsius temperature	1.8C + 32	Fahrenheit temperature	°F
<b>ILLUMINATION</b>				
lx	lux	0.0929	foot-candles	fc
cd/m <sup>2</sup>	candela/m <sup>2</sup>	0.2919	foot-Lamberts	fl
<b>FORCE and PRESSURE or STRESS</b>				
N	newtons	0.225	poundforce	lbf
kPa	kilopascals	0.145	poundforce per square inch	lbf/in <sup>2</sup>


\* SI is the symbol for the International System of Units. Appropriate rounding should be made to comply with Section 4 of ASTM E380.

# TABLE OF CONTENTS

## Volume I Field Investigation

<b>1. INTRODUCTION</b> .....	1
Background .....	1
Project Scope and Objectives .....	2
Sequence of Report .....	3
<b>2. DATA COLLECTION PROCEDURES</b> .....	5
Introduction .....	5
Data Elements .....	6
Office Data Collection .....	6
Field Data Collection .....	6
Data Reduction Procedures .....	25
Data Base .....	34
<b>3. PERFORMANCE OF PAVEMENT SECTIONS</b> .....	35
Introduction .....	35
Performance Summary of Projects in Dry-Freeze Zone .....	37
Performance Summary of Projects in Dry-Nonfreeze Zone .....	58
Performance Summary of Projects in Wet-Freeze Zone .....	78
Performance Summary of Projects in Wet-Nonfreeze Zone .....	183
Overall Summary .....	222
<b>4. CLOSURE</b> .....	223
<b>REFERENCES</b> .....	225

*PROTECTED UNDER INTERNATIONAL COPYRIGHT  
ALL RIGHTS RESERVED  
NATIONAL TECHNICAL INFORMATION SERVICE  
U.S. DEPARTMENT OF COMMERCE*

Reproduced from  
best available copy. 

# TABLE OF CONTENTS

## Volume II Evaluation of Inservice Concrete Pavements

<b>1. INTRODUCTION</b> .....	1
Background .....	1
Research Objectives .....	2
Research Approach .....	2
Advisory Panel .....	3
Overview of Report .....	4
<b>2. OVERVIEW OF PROJECTS EVALUATED IN STUDY</b> .....	5
Introduction .....	5
Description of Projects .....	5
Overall Summary of Projects .....	35
<b>3. EFFECT OF DESIGN FEATURES ON PAVEMENT PERFORMANCE</b> .....	39
Introduction .....	39
Slab Thickness .....	39
Joint Spacing .....	55
Joint Orientation .....	71
Transverse Joint Load Transfer .....	77
Joint Sealant .....	92
Base Type .....	108
Drainage .....	136
Subgrade Type .....	158
Shoulder Type .....	161
Widened Lanes .....	177
Reinforcement .....	179
Maximum Course Aggregate Size .....	186
Pavement Type .....	190
<b>4. EXAMINATION OF BACKCALCULATION RESULTS</b> .....	207
Introduction .....	207
Fundamental Concept .....	208
The "Best Fit" Backcalculation Procedure .....	210
Backcalculation Procedure for Two-Layered Slab .....	214

# TABLE OF CONTENTS

## Volume II (continued)

Determination of In-Place Material Properties .....	221
<b>5. SUMMARY OF EUROPEAN AND CHILEAN CONCRETE PAVEMENT PERFORMANCE .....</b>	<b>231</b>
Introduction .....	231
Evaluation of European Concrete Pavement Performance .....	231
Evaluation of Pavement Performance for Each European Country .....	236
Overall Evaluation of European Pavement Performance .....	259
Evaluation of Chilean Concrete Pavement Performance .....	265
<b>6. SUMMARY AND CONCLUSIONS .....</b>	<b>281</b>
Overview of Report .....	281
Review of Significant Findings .....	282
Closure .....	298
<b>REFERENCES .....</b>	<b>299</b>

# TABLE OF CONTENTS

## Volume III Improving Concrete Pavement Performance

<b>1. INTRODUCTION</b> .....	1
Background .....	1
Research Objectives .....	2
Research Approach .....	2
Advisory Panel .....	3
Overview of Report .....	3
<b>2. DEVELOPMENT OF CONCRETE PAVEMENT PERFORMANCE PREDICTION MODELS</b> .....	5
Introduction .....	5
General Description of Data Used in Model Development .....	7
Joint Faulting Model for Doweled Jointed Concrete Pavements .....	7
Joint Faulting Model for Nondoweled Jointed Concrete Pavements .....	23
Transverse Cracking Model for JPCP .....	34
Crack Deterioration Model for JRCP .....	84
Transverse Joint Spalling Model for JPCP .....	97
Transverse Joint Spalling Model for JRCP .....	114
Present Serviceability Rating Model .....	127
International Roughness Index (IRI) Model for JPCP .....	138
Example Application of Performance Prediction Models .....	140
Summary .....	145
<b>3. CONCRETE PAVEMENT DESIGN RECOMMENDATIONS</b> ....	147
Introduction .....	147
Effect of Site Conditions on Concrete Pavement Performance .....	147
Design Recommendations for Concrete Pavements .....	150
Concrete Pavement Type Selection Considerations .....	254
Summary .....	256
<b>REFERENCES</b> .....	261



# TABLE OF CONTENTS

## Volume IV Appendixes

<b>APPENDIX A—PROJECT SUMMARY TABLES</b> .....	1
Introduction .....	1
General Information for the Projects Included in the Study (Table 5) .....	1
Structural Design Data (Table 6) .....	3
Joint Design Data (Table 7) .....	5
Outer Shoulder and Drainage Design Data (Table 8) .....	8
Traffic Data (Table 9) .....	11
Outer Lane Deflection Data (Table 10) .....	12
Edge Deflection Data (Table 11) .....	14
Primary Outer Lane Performance Data (Table 12) .....	16
Secondary Outer Lane Performance Data (Table 13) .....	18
Continuously Reinforced Concrete Pavement Performance Data (Table 14) .....	21
<b>APPENDIX B—AN EVALUATION OF EUROPEAN CONCRETE PAVEMENTS</b> .....	107
<b>1. INTRODUCTION</b> .....	107
Background .....	107
Analysis of Data .....	108
Description of Summary Report .....	109
<b>2. SUMMARY OF CONCRETE PAVEMENT PERFORMANCE BY     COUNTRY</b> .....	111
Introduction .....	111
European COPES Data Base .....	111
Data Analysis .....	113
France .....	114
Italy .....	137
The United Kingdom .....	147
Belgium .....	164
Switzerland .....	182

# TABLE OF CONTENTS

## Volume IV (continued)

<b>3. SUMMARY OF OVERALL PAVEMENT PERFORMANCE</b> .....	203
Introduction .....	203
Design Features .....	203
Climatic Information .....	208
Traffic Data .....	208
Pavement Performance .....	210
Overall Summary of Important Findings .....	219
<b>4. CLOSURE</b> .....	221
Introduction .....	221
Review of Report Sequence .....	222
Additional Work .....	222
<b>APPENDIX C—AN EVALUATION OF CHILEAN CONCRETE PAVEMENTS</b> .....	225
<b>1. INTRODUCTION</b> .....	225
Background .....	225
Data Analysis .....	226
Description of Summary Report .....	226
<b>2. SUMMARY OF DESIGN AND CONSTRUCTION INFORMATION</b> ..	227
Introduction .....	227
Chilean Program .....	227
Instrumentation .....	227
Design Features .....	229
Climatic Information .....	236
Traffic Data .....	237
Summary .....	241
<b>3. SUMMARY OF OVERALL PAVEMENT PERFORMANCE</b> .....	243
Introduction .....	243
Data Analysis .....	243
Pavement Performance .....	244
Overall Summary of Important Findings .....	260

# TABLE OF CONTENTS

## Volume IV (continued)

APPENDIX D—BIBLIOGRAPHY .....	263
APPENDIX E—REPRINT OF PAPER, <i>A PERFORMANCE EVALUATION OF PCC PAVEMENTS CONSTRUCTED ON PERMEABLE BASES</i> .....	275
REFERENCES .....	295

# LIST OF FIGURES

## Volume I Field Investigation

1.	General location of sections included in the study . . . . .	8
2.	Field survey form—general information collection form . . . . .	10
3.	Field survey form—pavement data collection form . . . . .	11
4.	Drainage survey sheet . . . . .	14
5.	Photographic record form . . . . .	18
6.	Sensor configurations used in the FWD testing . . . . .	22
7.	FWD testing pattern . . . . .	22
8.	Arrangement of pavement temperature measurement holes . . . . .	23
9.	Performance summary for MN 1 & 5 . . . . .	40
10.	Roughness and serviceability for MN 1 & 5 . . . . .	43
11.	Faulting and transverse cracking 5-year performance trends for MN 1 & 5 . . . . .	44
12.	Performance summary for MN 2 . . . . .	47
13.	Roughness and serviceability for MN 2 . . . . .	49
14.	5-year performance trends for MN 2 . . . . .	50
15.	Performance summary for MN 7 . . . . .	56
16.	Performance of dowel coatings on MN 7 . . . . .	57
17.	Roughness and serviceability for MN 7 . . . . .	59
18.	Performance summary for AZ 1 . . . . .	62
19.	Roughness and serviceability for AZ 1 . . . . .	64
20.	5-year performance trends for AZ 1 . . . . .	65
21.	Performance summary for CA 1 . . . . .	70
22.	Roughness and serviceability for CA 1 . . . . .	72
23.	5-year performance trends for CA 1 . . . . .	73
24.	Performance summary for IL 1 . . . . .	83
25.	Roughness for IL 1 . . . . .	84
26.	Performance summary for IL 2 . . . . .	87
27.	Roughness for IL 2 . . . . .	88
28.	Performance summary for MI 1 . . . . .	91
29.	Roughness and serviceability for MI 1 . . . . .	93
30.	5-year performance trends for MI 1 . . . . .	95
31.	Performance summary for MO 1 . . . . .	102
32.	Roughness and serviceability for MO 1 . . . . .	103
33.	Performance summary for NY 1 . . . . .	109
34.	Roughness and serviceability for NY 1 . . . . .	111
35.	5-year performance trends for NY 1 . . . . .	112
36.	Performance summary for NY 2 . . . . .	116
37.	Roughness and serviceability for NY 2 . . . . .	117
38.	5-year performance trends for NY 2 . . . . .	119
39.	Performance summary for OH 1 . . . . .	121

# LIST OF FIGURES

## Volume I (continued)

40.	Roughness measurements for OH 1	123
41.	5-year performance trends for OH 1	125
42.	Performance summary of OH 2 sections, joint faulting and spalling	130
43.	Performance summary of OH 2 sections, transverse and longitudinal cracking	131
44.	Roughness summary of OH 2 sections	132
45.	5-year performance trends of OH 2 sections	137
46.	Performance summary of ONT 1 sections	140
47.	Roughness and serviceability summary of ONT 1 sections	141
48.	5-year performance trends for ONT 1 sections	142
49.	Performance summary for PA 1 sections	148
50.	Roughness and serviceability for PA 1 sections	149
51.	5-year performance trends for PA 1 sections	150
52.	Performance summary for WV 1	153
53.	Roughness and serviceability for WV 1	154
54.	Performance summary for WI 1	157
55.	Roughness and serviceability for WI 1	159
56.	Performance summary for WI 2 and WI 7	162
57.	Roughness and serviceability for WI 2 and WI 7	164
58.	Performance summary for WI 3	167
59.	Roughness and serviceability for WI 3	168
60.	Performance summary for WI 4	172
61.	Roughness and serviceability for WI 4	173
62.	Performance summary for WI 5	177
63.	Roughness and serviceability for WI 5	178
64.	Performance summary for WI 6	181
65.	Roughness and serviceability for WI 6	182
66.	Performance summary for CA 3	186
67.	Roughness and serviceability for CA 3	188
68.	5-year performance trends for CA 3	189
69.	Performance summary for CA 9	193
70.	Roughness and serviceability for CA 9	195
71.	Performance summary for JPCP sections for FL 4	202
72.	Performance summary for CRCP/FRC sections for FL 4	203
73.	Roughness and serviceability for JPCP sections for FL 4	206
74.	Performance summary for GA 1 and GA 2	211
75.	Roughness and serviceability for GA 1 and GA 2	212
76.	Performance summary for NC 1	216
77.	Roughness and serviceability for NC 1	218
78.	5-year performance trends for NC 1	220

# LIST OF FIGURES

## Volume II Evaluation of Inservice Concrete Pavements

1.	General location of projects included in the study . . . . .	7
2.	Hinge joint design details for JRCPC sections in Illinois . . . . .	16
3.	Distribution of projects by age . . . . .	37
4.	Distribution of projects by ESAL applications . . . . .	37
5.	Distribution of slab thickness in sections . . . . .	41
6.	Average transverse joint faulting versus slab thickness for all sections . . . . .	52
7.	Effect of slab thickness on transverse cracking . . . . .	53
8.	Loaded slab corner deflection by slab thickness for all sections . . . . .	55
9.	Distribution of joint spacings for JPCPC . . . . .	56
10.	Distribution of joint spacings for JRCPC . . . . .	57
11.	Effect of joint spacing on JPCPC transverse cracking . . . . .	67
12.	Transverse cracking as a function of $L/\ell$ ratio for aggregate bases . . . . .	68
13.	Transverse cracking as a function of $L/\ell$ ratio for dense-graded stabilized bases . . . . .	68
14.	Faulting of randomly spaced joints . . . . .	70
15.	Effect of joint spacing on JRCPC transverse cracking . . . . .	70
16.	Distribution of sections by joint orientation . . . . .	72
17.	Effect of joint orientation on transverse joint faulting . . . . .	75
18.	Effect of joint orientation on transverse joint spalling . . . . .	75
19.	Effect of joint orientation on IRI . . . . .	76
20.	Effect of joint orientation on corner breaking . . . . .	77
21.	Distribution of doweled and nondoweled sections . . . . .	78
22.	Distribution of dowel coatings . . . . .	78
23.	Comparison of faulting for doweled and nondoweled sections . . . . .	89
24.	Effect of dowel bar diameter on transverse joint faulting . . . . .	90
25.	Effect of load transfer efficiency on transverse joint faulting . . . . .	91
26.	Effect of dowel diameter on transverse joint spalling . . . . .	91
27.	Transverse joint faulting for different dowel bar coatings . . . . .	92
28.	Number of sections sealed with each sealant material (for all sections) . . . . .	94
29.	Transverse joint spalling percentage by sealant type for all sections . . . . .	105
30.	Sealant condition rating by joint sealant type for all sections . . . . .	106
31.	Comparison of IRI for different joint sealant types . . . . .	106
32.	Distribution of different base types . . . . .	109
33.	Average transverse joint faulting for each base type . . . . .	131
34.	Average transverse joint faulting by erodibility class . . . . .	131
35.	Average joint spalling for each base type . . . . .	132
36.	Transverse cracking by base type for JPCPC . . . . .	133
37.	Average deflections for each base type . . . . .	133

# LIST OF FIGURES

## Volume II (continued)

38.	Effect of percentage of cement on transverse joint faulting . . . . .	134
39.	Effect of percentage of cement on corner deflections . . . . .	135
40.	Effect of percentage of asphalt cement on transverse joint faulting . . . . .	135
41.	Effect of percentage of asphalt cement on corner deflections . . . . .	136
42.	Distribution of drainage designs . . . . .	137
43.	Distribution of drainage designs for doweled and nondoweled pavements	137
44.	Transverse joint faulting for each drainage design . . . . .	154
45.	Transverse joint spalling for each drainage design . . . . .	155
46.	Transverse cracking for each drainage design . . . . .	155
47.	Average age for each drainage design . . . . .	156
48.	Transverse joint faulting for various drainage coefficients . . . . .	157
49.	Effect of $P_{200}$ on transverse joint faulting . . . . .	158
50.	Effect of $C_U$ on transverse joint faulting . . . . .	159
51.	Distribution of subgrade types . . . . .	160
52.	Effect of subgrade type on transverse joint faulting of doweled pavements	160
53.	Effect of subgrade type on transverse faulting of nondoweled pavements	161
54.	Effect of edge support on edge deflection . . . . .	174
55.	Effect of edge support on transverse joint faulting . . . . .	174
56.	Effect of edge support on JPCP transverse cracking . . . . .	175
57.	Effect of load offset on calculated stress . . . . .	179
58.	Effect of steel percentage on deteriorated transverse cracking . . . . .	184
59.	Comparison between the "best fit" and AREA-based backcalculation procedures . . . . .	213
60.	Comparison of backcalculated PCC moduli for two sets of modular ratio; Unbonded interface between PCC plate and base . . . . .	219
61.	Comparison of backcalculated PCC moduli for two sets of modular ratio; Bonded interface between PCC plate and base . . . . .	219
62.	Percentage of sections vs. percentage of data kept . . . . .	220
63.	Comparison between backcalculated $E_{pcc}$ before and after screening . . . . .	222
64.	Comparison between backcalculated $k$ before and after screening . . . . .	222
65.	Backcalculated project average PCC moduli values . . . . .	227
66.	Backcalculated subgrade modulus of reactions, $k$ , values . . . . .	227
67.	Comparison of $k$ values determined in 1987 and 1992 . . . . .	228
68.	Effective slab thickness of stabilized base sections . . . . .	229
69.	Days per year (N) of heavy rainfall . . . . .	270

# LIST OF FIGURES

## Volume III Improving Concrete Pavement Performance

1.	Procedures used in the development of mechanistic-empirical statistical models . . . . .	6
2.	General location of sections included in study . . . . .	8
3.	Distribution of projects by age . . . . .	10
4.	Distribution of projects by ESAL applications . . . . .	10
5.	Two-dimensional scatter plot for doweled joint faulting model . . . . .	15
6.	Actual versus predicted faulting for the doweled faulting model . . . . .	20
7.	Predicted versus residual for the doweled faulting model . . . . .	20
8.	Sensitivity plot of the doweled faulting model with ESAL applications and bearing stress . . . . .	21
9.	Sensitivity plot of the doweled faulting model with ESAL applications and joint spacing . . . . .	21
10.	Sensitivity plot of the doweled faulting model with ESAL applications and $C_d$ . . . . .	22
11.	Sensitivity plot of the doweled faulting model with ESAL applications and freezing index . . . . .	22
12.	Sensitivity plot of the doweled faulting model with ESAL applications and mean annual precipitation . . . . .	23
13.	Two-dimensional scatter plot for nondoweled joint faulting model . . . . .	26
14.	Actual versus predicted faulting for the nondoweled faulting model . . . . .	30
15.	Predicted versus residual for the nondoweled faulting model . . . . .	30
16.	Sensitivity plot of the nondoweled faulting model with ESAL applications and slab thickness . . . . .	31
17.	Sensitivity plot of the nondoweled faulting model with ESAL applications and joint spacing . . . . .	31
18.	Sensitivity plot of the nondoweled faulting model with ESAL applications and $C_d$ . . . . .	32
19.	Sensitivity plot of the nondoweled faulting model with ESAL applications and freezing index . . . . .	32
20.	Sensitivity plot of the nondoweled faulting model with ESAL applications and the number of days above 90 °F (32 °C) . . . . .	33
21.	Sensitivity plot of the nondoweled faulting model with ESAL applications and annual precipitation . . . . .	33
22.	Comparison of PCC MR obtained by nondestructive testing and core testing . . . . .	39
23.	Distribution of hourly temperature gradient for CA 1 sections for an average year . . . . .	40
24.	Distribution of hourly temperature gradient for OH 2 sections for an average year . . . . .	41



# LIST OF FIGURES

## Volume III (continued)

25.	Distribution of hourly temperature gradient for GA 1 sections for an average year . . . . .	41
26.	Typical distribution of fatigue damage across a pavement slab . . . . .	55
27.	Preliminary fatigue analysis results given by ERES/COE fatigue model . . .	59
28.	Preliminary fatigue analysis results given by NCHRP 1-26 fatigue model . . . . .	59
29.	Preliminary fatigue analysis results given by Zero-Maintenance fatigue model . . . . .	60
30.	Preliminary fatigue analysis results given by ARE fatigue model . . . . .	60
31.	Edge load stress distribution across a pavement slab at mid-slab . . . . .	61
32.	Fatigue damage distribution across a pavement slab due to the loads placed at various distances away from the pavement edge . . . . .	62
33.	Effects of stress level and mean wheel location on p/c . . . . .	64
34.	Example fatigue damage calculation . . . . .	66
35.	Effects of temperature gradient shifts on critical stresses for fatigue damage . . . . .	67
36.	The effects of slab length on critical stresses in the pavement slab . . . . .	68
37.	Slab cracking data versus total ESAL applied . . . . .	70
38.	Slab cracking versus fatigue damage calculated using load stresses only . .	70
39.	Slab cracking versus fatigue damage calculated considering both load and curling stresses . . . . .	71
40.	Results of fatigue analysis performed using effective slab thickness . . . . .	72
41.	Results of fatigue analysis performed using design slab thickness . . . . .	73
42.	Fatigue analysis results with 4 °F (2.2 °C) shift applied to the temperature gradients . . . . .	75
43.	Fatigue analysis results with 8 °F (4.4 °C) shift applied to the temperature gradients . . . . .	75
44.	Final fatigue analysis results, including slab thickness and temperature gradient adjustments . . . . .	76
45.	The fatigue cracking model . . . . .	77
46.	Sensitivity of JPCP cracking model to slab thickness . . . . .	79
47.	Sensitivity of JPCP cracking model to joint spacing . . . . .	79
48.	Sensitivity of JPCP cracking model to shoulder type . . . . .	80
49.	Sensitivity of JPCP cracking model to bonding condition of base . . . . .	80
50.	Sensitivity of JPCP cracking model to climate . . . . .	81
51.	Sensitivity of JPCP cracking model to modulus of rupture . . . . .	81
52.	Sensitivity of JPCP cracking model to k-value . . . . .	82
53.	Comparison of predicted and actual slab cracking—section by section adjustments for built-in curling . . . . .	83

# LIST OF FIGURES

## Volume III (continued)

54.	Comparison of predicted and actual slab cracking—regional adjustments for built-in curling (DF=11°F [6.1°C]; DN=11.5 °F [6.4 °C]; WF=8°F [4.4 °C]; WN=8.5 °C[4.7 °C]) . . . . .	84
55.	Two-dimensional scatter plot for JRCP crack deterioration model . . . . .	88
56.	Actual versus predicted deteriorated cracking . . . . .	91
57.	Predicted versus residual deteriorated cracking . . . . .	91
58.	Sensitivity plot of the JRCP crack deterioration model showing effect of age and ESAL applications . . . . .	93
59.	Sensitivity plot of the JRCP crack deterioration model showing effect of age and percentage of reinforcement (stabilized base) . . . . .	93
60.	Sensitivity plot of the JRCP crack deterioration model showing effect of age and percentage of reinforcement (nonstabilized base) . . . . .	94
61.	Sensitivity plot of the JRCP crack deterioration model showing effect of age and concrete modulus of elasticity . . . . .	94
62.	Sensitivity plot of the JRCP crack deterioration model showing effect of age and freezing index . . . . .	95
63.	Sensitivity plot of the JRCP crack deterioration model showing effect of age and moisture index . . . . .	95
64.	Comparison of JRCP crack deterioration on selected Ohio sections with the model prediction . . . . .	96
65.	Two-dimensional scatter plot for JPCP spalling model . . . . .	101
66.	Actual versus predicted percentage of JPCP spalled joints . . . . .	105
67.	Actual versus residual percentage of JPCP spalled joints . . . . .	105
68.	Sensitivity plot of the JPCP joint spalling model for age and sealant type (FI = 1650) . . . . .	106
69.	Sensitivity plot of the JPCP joint spalling model for age and sealant type (FI = 1000) . . . . .	106
70.	Sensitivity plot of the JPCP joint spalling model for age and sealant type (FI = 0, Days <sub>90</sub> = 10) . . . . .	107
71.	Sensitivity plot of the JPCP joint spalling model for age and sealant type (FI = 0, Days <sub>90</sub> = 150) . . . . .	107
72.	Sensitivity plot of the JPCP joint spalling model for age and dowel protection . . . . .	108
73.	Sensitivity plot of the JPCP joint spalling model for age and freezing index (liquid sealant) . . . . .	108
74.	Sensitivity plot of the JPCP joint spalling model for age and freezing index (preformed sealant) . . . . .	109
75.	Sensitivity plot of the JPCP joint spalling model for age and freezing index (silicone sealant) . . . . .	109
76.	Sensitivity plot of the JPCP joint spalling model for age and freezing index (no sealant) . . . . .	110

# LIST OF FIGURES

## Volume III (continued)

77.	JPCP joint spalling distribution on Wisconsin sections . . . . .	110
78.	Comparison of JPCP spalling on selected Wisconsin sections with the model prediction . . . . .	111
79.	Comparison of JPCP spalling on selected Minnesota sections with the model prediction . . . . .	111
80.	Comparison of JPCP spalling on selected Arizona sections with the model prediction . . . . .	112
81.	Two-dimensional scatter plot for JRCP spalling model . . . . .	119
82.	Actual versus predicted percentage of JRCP spalled joints . . . . .	122
83.	Actual versus residual percentage of JRCP spalled joints . . . . .	122
84.	Sensitivity plot of the JRCP joint spalling model for age, dowel coating, and sealant type (FI = 1500) . . . . .	123
85.	Sensitivity plot of the JRCP joint spalling model for age, dowel coating, and sealant type (FI = 200) . . . . .	123
86.	Sensitivity plot of the JRCP joint spalling model for age and joint spacing . . . . .	124
87.	Sensitivity plot of the JRCP joint spalling model for age and freezing index (liquid sealant, DOWELCOR = 0) . . . . .	124
88.	Sensitivity plot of the JRCP joint spalling model for age and freezing index (liquid sealant, DOWELCOR = 1) . . . . .	125
89.	Sensitivity plot of the JRCP joint spalling model for age and freezing index (preformed sealant, DOWELCOR = 0) . . . . .	125
90.	Sensitivity plot of the JRCP joint spalling model for age and freezing index (preformed sealant, DOWELCOR = 1) . . . . .	126
91.	Comparison of JRCP spalling on selected Minnesota sections with the model prediction . . . . .	126
92.	Two-dimensional scatter plot for JPCP PSR model . . . . .	129
93.	Actual versus predicted PSR for the JPCP PSR model . . . . .	131
94.	Predicted versus residuals for the JPCP PSR model . . . . .	131
95.	Sensitivity plot of the JPCP PSR model with faulting and transverse cracking . . . . .	132
96.	Sensitivity plot of the JPCP PSR model with transverse cracking and spalling . . . . .	132
97.	Sensitivity plot of the JPCP PSR model with faulting and spalling . . . . .	133
98.	Sensitivity plot of the JPCP PSR model with transverse cracking and longitudinal cracking . . . . .	133
99.	Two-dimensional scatter plot for JRCP PSR model . . . . .	134
100.	Actual versus predicted PSR of the JRCP PSR model . . . . .	135
101.	Predicted versus residual for the JRCP PSR model . . . . .	136

# LIST OF FIGURES

## Volume III (continued)

102.	Sensitivity plot of the JRCP PSR model with faulting and transverse cracking . . . . .	136
103.	Sensitivity plot of the JRCP PSR model with transverse cracking and spalling . . . . .	137
104.	Sensitivity plot of the JRCP PSR model with faulting and spalling . . . . .	137
105.	Two-dimensional scatter plot for JPCP IRI model . . . . .	139
106.	Actual versus predicted PSR for the JPCP IRI model . . . . .	140
107.	Predicted versus residual for the JPCP IRI model . . . . .	141
108.	Sensitivity plot of the JPCP IRI model with faulting and transverse cracking . . . . .	141
109.	Sensitivity plot of the JPCP IRI model with transverse cracking and spalling . . . . .	142
110.	Sensitivity plot of the JPCP IRI model with faulting and spalling . . . . .	142
111.	Soil stabilization selection guidelines . . . . .	151
112.	Flow chart of drainage design recommendations based on $C_d$ (for pavements with design ESAL's greater than 5 million) . . . . .	157
113.	Cross section of a "bathtub" design . . . . .	159
114.	Example permeable base design . . . . .	159
115.	Daylighted pavement cross section . . . . .	160
116.	California drained LCB design . . . . .	161
117.	Effect of drainability on nondoweled joint faulting . . . . .	162
118.	Effect of drainability on doweled joint faulting . . . . .	162
119.	Typical cross section of subsurface drainage systems for crowned section and tied concrete shoulders . . . . .	167
120.	Typical cross section of subsurface drainage system for constant slope cross section and AC shoulders . . . . .	167
121.	Plot of New Jersey gradation . . . . .	168
122.	Recommended edge drain design . . . . .	171
123.	Recommended design for edge drain outlet . . . . .	172
124.	Smooth, long-radius bends and dual outlet system for cleanout and video camera inspection . . . . .	172
125.	A recommended headwall design . . . . .	174
126.	Geotextile wrapped drain . . . . .	175
127.	Partially wrapped drain . . . . .	175
128.	Nonwrapped drain . . . . .	175
129.	Geocomposite edge drain . . . . .	175
130.	Recommended installation detail for fin drains . . . . .	176
131.	Performance of sections on permeable and adjacent nonpermeable bases (nondoweled pavements). . . . .	183

# LIST OF FIGURES

## Volume III (continued)

132.	Performance of sections on permeable and adjacent nonpermeable bases (doweled pavements) . . . . .	183
133.	Effect of stabilized base on nondoweled joint faulting . . . . .	185
134.	Effect of stabilized base on JRCP crack deterioration . . . . .	185
135.	German JPCP design showing widened PCC slab and PCC shoulders. . . . .	193
136.	Types of PCC shoulder construction . . . . .	194
137.	Normalized edge load stress distribution across a slab under varying load locations . . . . .	197
138.	Effect of widened slab on doweled joint faulting . . . . .	198
139.	Sawcut rating as a function of compressive strength . . . . .	200
140.	Cracking performance as a function of $L/\ell$ . . . . .	202
141.	Example nonuniform joint spacing pattern (with skewed joints) . . . . .	205
142.	Illustration of load transfer concept . . . . .	208
143.	Effects of dowel diameter on faulting . . . . .	209
144.	Effect of sealing and sealant type on joint spalling . . . . .	211
145.	Cross section of joint sealant installation . . . . .	215
146.	Longitudinal contraction joint design . . . . .	217
147.	JRCP crack deterioration as a function of reinforcement content . . . . .	219
148.	Illustration of Illinois hinge joint design . . . . .	224
149.	Effects of JPCP slab thickness on mid-panel fatigue cracking for wet-freeze climatic region . . . . .	235
150.	Sensitivity of mid-panel fatigue cracking to joint spacing and slab thickness for wet-freeze climatic region . . . . .	237
151.	Effects of dynamic $k$ -value on stresses in pavement slabs for wet-freeze climatic region . . . . .	239
152.	Effects of subgrade dynamic $k$ on allowable traffic for the wet-freeze climatic region . . . . .	240
153.	Effects of subgrade $k$ and joint spacing on allowable traffic for wet-freeze climatic region . . . . .	241
154.	Effects of concrete strength and slab thickness on cracking performance of JPCP for wet-freeze climatic region . . . . .	242
155.	Effects of concrete strength and $E_{PCC}$ on cracking performance of JPCP for wet-freeze climatic region. . . . .	242
156.	Effects of the base-slab bond condition on cracking performance for wet-freeze climatic region . . . . .	244
157.	Effects of widened slab and tied PCC shoulder on cracking performance for wet-freeze climatic region . . . . .	246
158.	Effects of climate on slab thickness . . . . .	247

# LIST OF FIGURES

## Volume IV Appendixes

1.	Age of pavement sections in France . . . . .	120
2.	Range of slab thicknesses for sections in France . . . . .	120
3.	Distribution of base types for sections in France . . . . .	121
4.	Distribution in transverse joint spacings for sections in France . . . . .	122
5.	Type of drainage features for sections in France . . . . .	123
6.	Number of modernity elements incorporated into sections in France . . . . .	124
7.	Distribution of ESAL applications for sections in France . . . . .	126
8.	Typical load distribution of single axles in France . . . . .	127
9.	Typical load distribution of tandem axles in France . . . . .	127
10.	PSR vs. Age for sections in France . . . . .	130
11.	PSR vs. ESAL's for sections in France . . . . .	131
12.	PSR vs. (Age * ESAL's) for sections in France . . . . .	131
13.	Investigation of effect of base type in PSR vs. (Age * ESAL's) plot . . . . .	132
14.	Investigation of effect of slab thickness in PSR vs. (Age * ESAL's) plot . . . . .	132
15.	Investigation of effect of drainage in PSR vs. (Age * ESAL's) plot . . . . .	133
16.	Investigation of modernity element effect in PSR vs. (Age * ESAL's) plot . . . . .	134
17.	Sensitivity of French model to age and ESAL's . . . . .	135
18.	Sensitivity of French model to drainage conditions . . . . .	136
19.	Sensitivity of French model to slab thickness . . . . .	136
20.	Age of pavement sections in Italy . . . . .	139
21.	Range of slab thicknesses for sections in Italy . . . . .	140
22.	Distribution of base types for sections in Italy . . . . .	140
23.	Number of modernity elements incorporated into sections in Italy . . . . .	141
24.	Distribution of ESAL applications for sections in Italy . . . . .	142
25.	Typical load distribution of single axles in Italy . . . . .	143
26.	Typical load distribution of tandem axles in Italy . . . . .	144
27.	PSR vs. Age for sections in Italy . . . . .	145
28.	PSR vs. ESAL's for sections in Italy . . . . .	146
29.	PSR vs. (Age * ESAL's) for sections in Italy . . . . .	146
30.	Age of pavement sections in the United Kingdom . . . . .	151
31.	Range of slab thicknesses for sections in the United Kingdom . . . . .	151
32.	Distribution of base types for sections in the United Kingdom . . . . .	152
33.	Distribution of shoulder types for sections in the United Kingdom . . . . .	152
34.	Number of modernity elements incorporated into sections in the United Kingdom . . . . .	153
35.	Distribution of ESAL applications for sections in the United Kingdom . . . . .	154
36.	Typical load distribution of single axles in the United Kingdom . . . . .	155
37.	Typical load distribution of tandem axles in the United Kingdom . . . . .	155
38.	PSR vs. Age for sections in the United Kingdom . . . . .	157

# LIST OF FIGURES

## Volume IV (continued)

39.	PSR vs. ESAL's for sections in the United Kingdom . . . . .	158
40.	PSR vs. (Age * ESAL's) for sections in the United Kingdom . . . . .	158
41.	Investigation of effect of base type in PSR vs. ESAL's plot . . . . .	159
42.	Investigation of effect of slab thickness in PSR vs. ESAL's plot . . . . .	160
43.	Investigation of effect of shoulder type in PSR vs. ESAL's plot . . . . .	161
44.	Investigation of effect of joint spacing in PSR vs. ESAL's plot . . . . .	162
45.	Sensitivity of United Kingdom model to age and ESAL's . . . . .	163
46.	Sensitivity of United Kingdom model to slab thickness . . . . .	163
47.	Age of pavement sections in Belgium . . . . .	170
48.	CRCP designs in Belgium . . . . .	170
49.	Range of slab thicknesses for sections in Belgium . . . . .	171
50.	Distribution of base types for sections in Belgium . . . . .	171
51.	Number of modernity elements incorporated into sections in Belgium . . . .	172
52.	Distribution of ESAL applications for sections in Belgium . . . . .	173
53.	Typical load distribution of single axles in Belgium . . . . .	174
54.	PSR vs. Age for sections in Belgium . . . . .	175
55.	PSR vs. ESAL's for sections in Belgium . . . . .	176
56.	PSR vs. (Age * ESAL's) for sections in Belgium . . . . .	176
57.	Investigation modernity element effect in PSR vs. (Age * ESAL's) plot . . . .	177
58.	Investigation of effect of base type in PSR vs. (Age * ESAL's) plot . . . . .	178
59.	Investigation of effect of slab thickness in PSR vs. (Age * ESAL's) plot . . . .	178
60.	Investigation of effect of pavement type in PSR vs. (Age * ESAL's) plot . . .	179
61.	Investigation of effect of freezing index in PSR vs. Age plot . . . . .	180
62.	Sensitivity of Belgian model to age and ESAL's . . . . .	181
63.	Sensitivity of Belgian models to slab thickness . . . . .	182
64.	Age of pavement projects in Switzerland . . . . .	187
65.	Range of slab thicknesses for projects in Switzerland . . . . .	188
66.	Distribution of base types for projects in Switzerland . . . . .	189
67.	Distribution of transverse joints spacings for projects in Switzerland . . . . .	190
68.	Distribution of drainage features for projects in Switzerland . . . . .	190
69.	Number of modernity elements for projects in Switzerland . . . . .	191
70.	Distribution of ESAL applications for projects in Switzerland . . . . .	192
71.	PSR vs. Age for projects in Switzerland . . . . .	194
72.	PSR vs. ESAL's for projects in Switzerland . . . . .	195
73.	PSR vs. (Age * ESAL's) for projects in Switzerland . . . . .	195
74.	Investigation of effect of joint spacing in PSR vs (Age * ESAL's) plot . . . . .	196
75.	Investigation of the effect of slab thickness in PSR vs. (Age * ESAL's) plot .	197
76.	Sensitivity of Swiss faulting model to ages and ESAL's . . . . .	199
77.	Sensitivity of Swiss faulting model to drainage conditions . . . . .	199
78.	Sensitivity of Swiss PSR model to age and ESAL's . . . . .	200

# LIST OF FIGURES

## Volume IV (continued)

79.	Sensitivity of Swiss PSR model to slab thickness . . . . .	200
80.	Age distribution of European COPES sections at the time of survey . . . . .	204
81.	Distribution of pavement types . . . . .	204
82.	Range of slab thicknesses . . . . .	206
83.	Comparison of slab thicknesses . . . . .	206
84.	Range of base types . . . . .	207
85.	Comparison of base types . . . . .	207
86.	Comparison of shoulder types . . . . .	209
87.	Comparison of modernity elements . . . . .	209
88.	Distribution of estimated 80-kN (18-kip) ESAL applications for the European COPES sections . . . . .	211
89.	Comparison of annual traffic . . . . .	211
90.	PSR vs. pavement age for all European COPES sections . . . . .	212
91.	PSR vs. ESAL applications for all European COPES sections . . . . .	212
92.	PSR vs. (Age * ESAL's) for all European COPES sections . . . . .	213
93.	PSR vs. ESAL applications by pavement type, overall sections . . . . .	213
94.	PSR vs. ESAL applications by slab thickness, overall sections . . . . .	215
95.	PSR vs. ESAL applications for doweled and undoweled sections, overall . .	215
96.	PSR vs. ESAL applications by drainage condition, overall sections . . . . .	216
97.	PSR vs. ESAL applications by base type for all European COPES sections .	216
98.	PSR vs. ESAL applications by modernity elements, overall sections . . . . .	217
99.	PSR vs. (Age * ESAL's) by modernity elements, overall sections . . . . .	217
100.	Comparison of PSR vs. Age between European and U.S. sections . . . . .	218
101.	PSR vs. ESAL applications for the U.S. sections . . . . .	218
102.	Instrumentation devices in the test sections . . . . .	228
103.	Schematic layout of instrumentation . . . . .	228
104.	Age of Chilean concrete pavement sections . . . . .	229
105.	Range of slab thicknesses in Chilean sections . . . . .	231
106.	Distribution of base types in Chilean sections . . . . .	232
107.	Distribution of subbase types in Chilean sections . . . . .	232
108.	USCS classification chart, ASTM D-2487 . . . . .	233
109.	Subgrade type in Chilean sections . . . . .	234
110.	Distribution in transverse joint spacings in Chilean sections . . . . .	235
111.	Type of drainage features in Chilean sections . . . . .	235
112.	Number of modernity elements incorporated into Chilean sections . . . . .	237
113.	Days per year (N) of heavy rainfall . . . . .	238
114.	Distribution of ESAL applications in Chilean sections . . . . .	241
115.	Illustration of the curling/warping concept . . . . .	245
116.	Histogram of thermal gradients at a typical test section . . . . .	245
117.	Movement pattern of joint during a complete temperature cycle . . . . .	246



# LIST OF FIGURES

## Volume IV (continued)

118.	Variations in seasonal deflections for corner and interior loading conditions . . . . .	249
119.	Openings of 10 consecutive joints . . . . .	250
120.	Inclination of induced crack . . . . .	252
121.	State of faulting in Chilean concrete pavements . . . . .	253
122.	Faulting vs. ESAL's for Chilean sections . . . . .	255
123.	Faulting vs. (Age * ESAL's) for Chilean sections . . . . .	255
124.	Investigation of the effect of edge drains on faulting . . . . .	256
125.	Investigation of the effect of k-value on faulting . . . . .	256
126.	Comparison of predicted and actual cracking . . . . .	258
127.	Cracking vs. age for Chilean sections . . . . .	258
128.	Cracking vs. ESAL's for Chilean sections . . . . .	259
129.	Cracking vs. (Age * ESAL's) for Chilean sections . . . . .	259
130.	Investigation of the effect of slab length on cracking . . . . .	261
131.	Investigation of the effect of L/l on cracking . . . . .	261
132.	Investigation of the effect of k-value on cracking . . . . .	262

# LIST OF TABLES

## Volume I Field Investigation

1.	List of sections included in the study . . . . .	7
2.	Listing of projects surveyed by automated methods . . . . .	20
3.	Regression coefficients for $d_r^*$ versus $l_k$ relationships . . . . .	31
4.	Summary of sections surveyed in 1987 and 1992 . . . . .	36
5.	Critical values for key performance indicators . . . . .	37
6.	Experimental design matrix for MN 1 and MN 5 . . . . .	38
7.	Summary of 1987 and 1992 outer lane performance data for MN 1 and MN 5 . . . . .	39
8.	Experimental design matrix for MN 2 . . . . .	45
9.	Summary of 1987 and 1992 outer lane performance data for MN 2 . . . . .	46
10.	Design and outer lane performance data for MN 3, MN 4, and MN 6 . . . . .	52
11.	Experimental design matrix for selected sections on MN 7 . . . . .	53
12.	Summary of 1992 outer lane performance data for MN 7 . . . . .	55
13.	Summary of dowel performance on MN 7 . . . . .	55
14.	Experimental design matrix for AZ 1 . . . . .	60
15.	Traffic summary for AZ 1 sections . . . . .	61
16.	Summary of 1987 and 1992 outer lane performance data for AZ 1 . . . . .	61
17.	Summary of 1987 and 1992 outer lane performance data for AZ 2 . . . . .	67
18.	Experimental design matrix for CA 1 . . . . .	67
19.	Summary of 1987 and 1992 outer lane performance data for CA 1 . . . . .	69
20.	Experimental design matrix for CA 2 . . . . .	75
21.	Summary of 1987 and 1992 outer lane performance data for CA 2 . . . . .	75
22.	Design and outer lane performance data for CA 6 . . . . .	76
23.	Design and outer lane performance data for CA 7 and CA 8 . . . . .	78
24.	Design and outer lane performance data for CA 11 . . . . .	79
25.	Summary of sections on IL 1 . . . . .	81
26.	Summary of 1992 performance data for IL 1 . . . . .	82
27.	Summary of sections on IL 2 . . . . .	85
28.	Summary of 1992 performance data for IL 2 . . . . .	86
29.	Experimental design matrix for MI 1 . . . . .	89
30.	Summary of 1987 and 1992 outer lane performance data for MI 1 . . . . .	90
31.	Design and outer lane performance data for MI 3, MI 5, and MI 6 . . . . .	96
32.	Experimental design matrix and performance summary for MI 4 . . . . .	97
33.	Experimental design matrix for MO 1 . . . . .	100
34.	Summary of 1992 outer lane performance data for MO 1 . . . . .	101
35.	Design and outer lane performance data for NJ 2 . . . . .	105
36.	Experimental design matrix for NJ 3 . . . . .	106
37.	Summary of 1987 and 1992 outer lane performance data for NJ 3 . . . . .	106

# LIST OF TABLES

## Volume I (continued)

38.	Experimental design matrix for NY 1 . . . . .	107
39.	Summary of 1987 and 1992 outer lane performance data for NY 1 . . . . .	108
40.	Experimental design matrix for NY 2 . . . . .	114
41.	Summary of 1987 and 1992 outer lane performance data for NY 2 . . . . .	115
42.	Experimental design matrix for OH 1 . . . . .	120
43.	Summary of 1987 and 1992 outer lane performance data for OH 1 . . . . .	122
44.	Experimental design matrix for selected sections on OH 2 . . . . .	127
45.	Summary of 1992 outer lane performance data for OH 2 sections with aggregate base . . . . .	128
46.	Summary of outer lane performance data for OH 2 sections with no base, ATB, and CTB . . . . .	129
47.	Summary of 1992 outer lane performance data for CRCP sections in OH 2 . . . . .	133
48.	Experimental design matrix for ONT 1 . . . . .	138
49.	Summary of 1987 and 1992 outer lane performance data for ONT 1 . . . . .	139
50.	Design and outer lane performance data for ONT 2 . . . . .	145
51.	Experimental design matrix for PA 1 . . . . .	145
52.	Summary of 1987 and 1992 outer lane performance data for PA 1 . . . . .	147
53.	Design and outer lane performance data for WV 1 . . . . .	152
54.	Experimental design matrix for WI 1 . . . . .	156
55.	Summary of 1992 outer lane performance data for WI 1 . . . . .	156
56.	Experimental design matrix for WI 2 and WI 7 . . . . .	160
57.	Summary of 1992 outer lane performance data for WI 2 and WI 7 . . . . .	161
58.	Experimental design matrix for WI 3 . . . . .	165
59.	Summary of 1992 performance data for WI 3 . . . . .	166
60.	Experimental design matrix for WI 4 . . . . .	170
61.	Experimental design matrix for WI 4 . . . . .	171
62.	Experimental design matrix for WI 5 . . . . .	175
63.	Summary of 1992 outer lane performance data for WI 5 . . . . .	176
64.	Experimental design matrix for WI 6 . . . . .	179
65.	Summary of 1992 outer lane performance data for WI 6 . . . . .	180
66.	Experimental design matrix for CA 3 . . . . .	184
67.	Summary of 1987 and 1992 outer lane performance data for CA 3 . . . . .	185
68.	Experimental design matrix for selected sections on CA 9 . . . . .	191
69.	Summary of 1992 outer lane performance data for CA 9 . . . . .	192
70.	Design and outer lane performance data for CA 10 . . . . .	196
71.	Design and outer lane performance data for FL 2 and FL 3 . . . . .	197
72.	Experimental design matrix for selected sections on FL 4 . . . . .	199
73.	Summary of 1992 outer lane performance data for FL 4 . . . . .	201
74.	Experimental design matrix for GA 1 and GA 2 . . . . .	208

# LIST OF TABLES

## Volume I (continued)

75.	Summary of 1992 outer lane performance data for Georgia sections . . . . .	210
76.	Experimental design matrix for NC 1 . . . . .	214
77.	Summary of 1987 and 1992 outer lane performance data for NC 1 . . . . .	215
78.	Design and outer lane performance data for NC 2 . . . . .	222

# LIST OF TABLES

## Volume II Evaluation of Inservice Concrete Pavements

1.	List of projects included in the study	6
2.	Experimental design matrix for AZ 1 (year built in parentheses)	8
3.	Traffic summary for AZ 1 sections	8
4.	Experimental design matrix for CA 1	9
5.	Experimental design matrix for CA 2	10
6.	Experimental design matrix for CA 3	11
7.	Summary of design data for CA 6	11
8.	Experimental design matrix for selected sections on CA 9	13
9.	Experimental design matrix for selected sections on FL 4	14
10.	Experimental design matrix for GA 1 and GA 2	15
11.	Experimental design matrix for IL 1	17
12.	Experimental design matrix for IL 2	17
13.	Experimental design matrix for MI 1	18
14.	Experimental design matrix for MN 1 and MN 5	20
15.	Experimental design matrix for MN 2	21
16.	Experimental design matrix for selected sections on MN 7	22
17.	Experimental design matrix for MO 1	23
18.	Experimental design matrix for NJ 3	24
19.	Experimental design matrix for NY 1	24
20.	Experimental design matrix for NY 2	25
21.	Experimental design matrix for NC 1	26
22.	Experimental design matrix for OH 1	27
23.	Experimental design matrix for selected sections on OH 2	28
24.	Experimental design matrix for ONT 1	29
25.	Experimental design matrix for PA 1	30
26.	Design data for WV 1	31
27.	Experimental design matrix for WI 1	31
28.	Experimental design matrix for WI 2 and WI 7	32
29.	Experimental design matrix for WI 3	33
30.	Experimental design matrix for WI 4	34
31.	Experimental design matrix for WI 5	34
32.	Experimental design matrix for WI 6	35
33.	Range of design features included in study	36
34.	Critical values for key performance indicators	40
35.	Summary of effect of slab thickness for MN 1	42
36.	Summary of effect of slab thickness for MN 2	44
37.	Summary of effect of slab thickness for AZ 1	45
38.	Summary of effect of slab thickness for CA 1	46
39.	Summary of effect of slab thickness for CRCP sections for IL 1	47

# LIST OF TABLES

## Volume II (continued)

40.	Summary of effect of slab thickness for OH 2 . . . . .	48
41.	Summary of effect of slab thickness for ONT 1 . . . . .	49
42.	Summary of selected 1992 deflection data . . . . .	54
43.	Summary of effect of joint spacing for CA 1 . . . . .	58
44.	Summary of effect of actual slab lengths on cracking for CA 1 . . . . .	59
45.	Summary of effect of joint spacing for IL 1 . . . . .	60
46.	Summary of effect of joint spacing for IL 2 . . . . .	61
47.	Summary of effect of joint spacing for MN 1/MN 5 . . . . .	61
48.	Summary of effect of joint spacing for MN 7 . . . . .	63
49.	Summary of effect of joint spacing for NY 2 . . . . .	64
50.	Summary of effect of joint spacing for OH 1 . . . . .	65
51.	Summary of effect of joint spacing for OH 2 . . . . .	66
52.	Summary of effect of joint orientation for FL 4 . . . . .	72
53.	Summary of effect of joint orientation for NC 1 . . . . .	73
54.	Summary of effect of joint orientation for NY 1 . . . . .	74
55.	Summary of effect of load transfer for FL 4 . . . . .	80
56.	Summary of effect of load transfer for GA 1 . . . . .	81
57.	Summary of effect of load transfer for MN 1 . . . . .	82
58.	Summary of effect of load transfer for MN 7 . . . . .	83
59.	Summary of dowel performance on MN 7 . . . . .	84
60.	Summary of effect of load transfer for NC 1 . . . . .	85
61.	Summary of effect of load transfer for NY 1 . . . . .	86
62.	Summary of effect of load transfer for WI 2/WI 7 . . . . .	87
63.	Summary of effect of load transfer for WI 6 . . . . .	88
64.	Pavement performance indicators related to sealing pavements . . . . .	93
65.	Summary of effect of joint sealant type for CA 3 . . . . .	95
66.	Summary of effect of joint sealing for CA 9 . . . . .	96
67.	Summary of effect of joint sealing on OH 2 . . . . .	99
68.	Summary of effect of joint sealant for WI 2/WI 7 . . . . .	100
69.	Summary of effect of joint sealing for WI 5 . . . . .	102
70.	Summary of effect of joint sealing for WI 6 . . . . .	103
71.	Summary of effect of joint sealing for WV 1 . . . . .	104
72.	Summary of effect of base type for AZ 1 . . . . .	110
73.	Summary of effect of base type for CA 1 . . . . .	111
74.	Summary of effect of base type for CA 2 . . . . .	112
75.	Summary of effect of base type for CA 6 . . . . .	113
76.	Summary of effect of base type for FL 4 . . . . .	114
77.	Summary of effect of base type for GA 1 . . . . .	115
78.	Summary of effect of base type for MI 1 . . . . .	116
79.	Summary of effect of base type for MN 1 . . . . .	118

# LIST OF TABLES

## Volume II (continued)

80.	Summary of effect of base type for MO 1	119
81.	Summary of effect of base type for NC 1	120
82.	Summary of effect of base type for NJ 3	121
83.	Summary of effect of base type on JPCP for NY 1	121
84.	Summary of effect of base type on JRCP for NY 1	122
85.	Summary of effect of base type for OH 1	123
86.	Summary of effect of base type for OH 2	123
87.	Summary of effect of base type for ONT 1	124
88.	Summary of effect of base type for PA 1	126
89.	Summary of effect of base type for WV 1	126
90.	Summary of effect of base type for WI 2 & 7	128
91.	Summary of effect of base type for WI 3	128
92.	Summary of effect of drainage for AZ 1	138
93.	Summary of effect of drainage for CA 2	139
94.	Summary of effect of drainage for CA 6	140
95.	Summary of effect of drainage for CA 9	141
96.	Summary of effect of drainage on JPCP for MI 1	142
97.	Summary of effect of drainage on JRCP for MI 1	143
98.	Summary of effect of drainage for NJ 3	144
99.	Summary of effect of drainage for OH 2 (aggregate base)	145
100.	Summary of effect of drainage for OH 2 (stabilized base)	146
101.	Summary of effect of drainage for ONT 1	147
102.	Summary of effect of drainage for PA 1	147
103.	Summary of effect of drainage for WI 2 & 7	149
104.	Summary of effect of drainage for WI 3	150
105.	Summary of effect of drainage for WI 5	151
106.	Summary of effect of shoulder type for AZ 1	163
107.	Effect of shoulder type for CA 3 sections (preformed sealant)	164
108.	Effect of shoulder type for CA 3 sections (no sealant)	165
109.	Effect of shoulder type for FL 4 sections	166
110.	Summary of effect of shoulder type for MI 1	167
111.	Summary of effect of shoulder type for MI 4	168
112.	Summary of effect of shoulder type for MN 2	169
113.	Summary of effect of shoulder type for NY 2	169
114.	Summary of effect of shoulder type for OH 1	170
115.	Effect of shoulder type for OH 2 sections	171
116.	Summary of effect of shoulder type for ONT 1	172
117.	Maximum recommended tie bar spacings	176
118.	Improvement in pavement responses	177
119.	Summary of performance data for sections with widened lanes	178

# LIST OF TABLES

## Volume II (continued)

120.	Summary of effect of reinforcement for CA 1	180
121.	Summary of effect of reinforcement for IL 1	181
122.	Summary of effect of reinforcement for IL 2	182
123.	Overall performance of CRCP sections	185
124.	Summary of effect of maximum coarse aggregate size for MO 1	187
125.	Summary of effect of maximum coarse aggregate size for OH 2 sections constructed on aggregate base	188
126.	Summary of effect of maximum coarse aggregate size for OH 2 sections constructed on no base, ATB, and CTB	189
127.	Performance data summary for NC 1	192
128.	Performance data summary for OH 2	193
129.	Performance data summary for MI 1	195
130.	Performance data summary for WV 1	195
131.	Performance data summary for NY 1	196
132.	Performance data summary for NY 2	197
133.	Performance data summary for OH 1	198
134.	Performance data summary for MN 2	199
135.	Performance data summary for CA 1	200
136.	Performance data summary for IL 1	201
137.	Comparison of performance by pavement type	202
138.	Two sets of the moduli ratios, $E_{pcc}/E_{base}$	218
139.	Results of backcalculation for sections with high percentage of dropped data	221
140.	Distribution of sections by country and pavement type	232
141.	Summary of design features and performance data	237
142.	Design information for Chilean concrete pavement sections	267
143.	Performance data for Chilean sections	276
144.	Summary of effect of design features	293



# LIST OF TABLES

## Volume III Improving Concrete Pavement Performance

1.	Range of design features included in study . . . . .	9
2.	Distribution of the pavement sections used in the development of doweled joint faulting model . . . . .	11
3.	Simplified design matrix for the selection of the overall drainage coefficient, $C_d$ . . . . .	14
4.	Estimates of the coefficients and the associated SEE and P-values for the doweled joint faulting model . . . . .	19
5.	Distribution of the pavement sections used in the development of nondoweled joint faulting model . . . . .	24
6.	Estimates of the coefficients and the associated SEE and P-values for nondoweled joint faulting model . . . . .	29
7.	Distribution of the JPCP sections and designs used in the development of fatigue cracking model . . . . .	36
8.	Distribution of hourly temperature gradients . . . . .	42
9.	Distribution of the pavement sections and designs used in the development of JRCP crack deterioration model . . . . .	85
10.	Distribution of the pavement sections and designs used in the development of JPCP spalling model . . . . .	98
11.	Spalling of JPCP sections located in a cold climate . . . . .	112
12.	Distribution of the pavement sections and designs used in the development of JRCP spalling model . . . . .	115
13.	Distribution of the pavement sections used in the development of PSR model . . . . .	128
14.	Estimates of the coefficients and the associated SEE and P-values for JPCP PSR distress model . . . . .	130
15.	Estimates of the coefficients and the associated SEE and P-values for JRCP PSR model . . . . .	135
16.	Estimates of the coefficients and the associated SEE and P-values for JPCP IRI model . . . . .	140
17.	Example application of prediction models to check adequacy of concrete pavement design . . . . .	144
18.	Critical values for key performance indicators . . . . .	145
19.	Potential for moisture accelerated damage indicated by the MAD index . . .	155
20.	Simplified design matrix for the selection of the overall drainage coefficient, $C_d$ . . . . .	155
21.	Potential for moisture damage indicated by $C_d$ . . . . .	156
22.	Pavement cross section recommendations for enhancing overall drainability	158
23.	Wisconsin standard gradation for permeable aggregate base . . . . .	164
24.	Quality of drainage based on time to drain . . . . .	165
25.	Gradations used in permeable bases . . . . .	168

# LIST OF TABLES

## Volume III (continued)

26.	Typical dense-graded aggregate separator layer gradation . . . . .	170
27.	Summary of PCC pavement base types . . . . .	180
28.	Performance of permeable base sections . . . . .	182
29.	Performance of pavement sections without a base course . . . . .	186
30.	General recommendations on use of shoulder type/edge support . . . . .	192
31.	Summary of performance data for sections with widened lanes . . . . .	196
32.	Recommended maximum joint spacings for JPCP designs . . . . .	204
33.	Summary of effect of joint orientation . . . . .	206
34.	Recommended dowel usage & diameters . . . . .	210
35.	Strain capacity of field-molded joint sealants . . . . .	212
36.	Effect of coarse aggregate size on deteriorated transverse cracking . . . . .	220
37.	Summary of three field developed models for deteriorated transverse cracking of JRCP . . . . .	221
38.	Minimum recommended percent longitudinal reinforcement for JRCP (50 percent level of reliability) . . . . .	222
39.	Effect of reinforcement content on CRCP performance . . . . .	226
40.	Effect of steel reinforcement depth on CRCP performance . . . . .	228
41.	Summary of three prediction models for punchouts and roughness in CRCP	229
42.	Minimum reinforcement contents for CRCP on aggregate base courses and in a wet-freeze climate (50 percent level of reliability) . . . . .	230
43.	Minimum reinforcement contents for CRCP on stabilized base courses and in a wet-freeze climate (50 percent level of reliability). . . . .	231
44.	Comparison of predicted and actual failures (punchouts and deteriorated cracks) from various CRCP sections . . . . .	232
45.	JPCP slab thickness design table for dry-freeze climate (50 percent design reliability) . . . . .	249
46.	JPCP slab thickness design table for dry-nonfreeze climate (50 percent design reliability) . . . . .	250
47.	JPCP slab thickness design table for wet-freeze climate (50 percent design reliability) . . . . .	251
48.	JPCP slab thickness design table for wet-nonfreeze climate (50 percent design reliability) . . . . .	252
49.	Summary of PCC pavement types . . . . .	255
50.	Summary of structural design recommendations for medium- and heavy-trafficked roadways . . . . .	258
51.	Summary of transverse joint design recommendations for medium- and heavy-trafficked roadways . . . . .	259
52.	Summary of longitudinal lane-lane contraction joint design recommendations for medium- and heavy-trafficked roadways . . . . .	260

# LIST OF TABLES

## Volume IV Appendixes

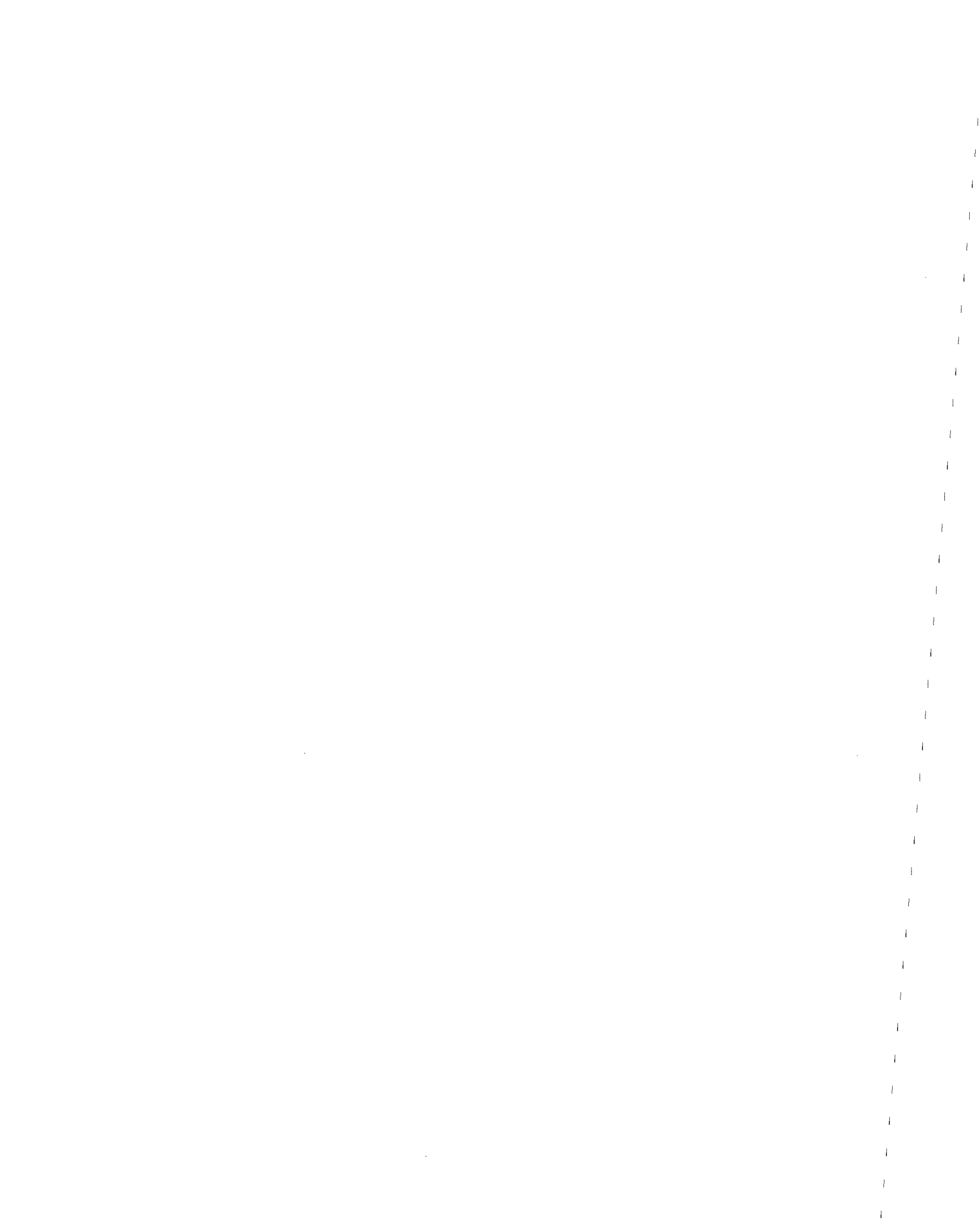
1.	Field testing summary for the sections in the dry-freeze climatic zone . . . .	23
2.	Field testing summary for the sections in the dry-nonfreeze climatic zone .	24
3.	Field testing summary for the sections in the wet-freeze climatic zone . . . .	25
4.	Field testing summary for the sections in the wet-nonfreeze climatic zone .	26
5.	General information for the projects included in the study . . . . .	31
6.	Structural design data . . . . .	32
7.	Joint design data . . . . .	44
8.	Outer shoulder and drainage design data . . . . .	55
9.	Traffic data . . . . .	66
10.	Outer lane deflection data . . . . .	68
11.	Edge deflection data . . . . .	77
12.	Primary outer lane performance data . . . . .	86
13.	Secondary outer lane performance data . . . . .	96
14.	Continuously Reinforced Concrete Pavement performance data . . . . .	106
15.	Distribution of sections by country and pavement type . . . . .	108
16.	Listing of sections included in European COPES analysis . . . . .	111
17.	Design information for COPES concrete pavement sections in France . . . .	115
18.	Performance data for outer traffic lane of COPES concrete pavement sections in France . . . . .	117
19.	Design information for COPES concrete pavement sections in Italy . . . . .	138
20.	Performance data for outer traffic lane of COPES concrete pavement sections in Italy . . . . .	138
21.	Design information for COPES concrete pavement sections in the United Kingdom . . . . .	149
22.	Performance data for outer traffic lane of COPES concrete pavement sections in the United Kingdom . . . . .	150
23.	Design information for COPES concrete pavement sections in Belgium . . .	166
24.	Performance data for outer traffic lane of COPES concrete pavement sections in Belgium . . . . .	168
25.	Design information for COPES concrete pavement sections in Switzerland .	183
26.	Performance data for outer traffic lane of COPES concrete pavement sections in Switzerland . . . . .	185
27.	PSR for COPES concrete pavement sections in Switzerland . . . . .	193
28.	Design information for Chilean concrete pavement sections . . . . .	230
29.	Traffic composition on Chilean sections . . . . .	239
30.	Maximum uplift of corners . . . . .	248
31.	Load transfer for 80-kN (18-kip) load . . . . .	251
32.	Performance data for Chilean sections . . . . .	254

# List of Acronyms and Abbreviations

AASHTO	American Association of State Highway and Transportation Officials
AC	Asphalt Concrete
ADT	Average Daily Traffic
AGG	Dense-Graded Aggregate Base
ATB	Asphalt-Treated Base
$C_d$	Drainage Coefficient
CESAL	Cumulative Equivalent Single Axle Load
COE	Corps of Engineers
COPEs	Concrete Pavement Evaluation System
CRCP	Continuously Reinforced Concrete Pavement
CTB	Cement-Treated Base
CSB	Cement-Stabilized Base
$C_u$	Coefficient of Uniformity
DF	Dry-Freeze
DNF	Dry-Nonfreeze
$D_o$	Load Plate Sensor
E	Concrete Elastic Modulus
ESAL	Equivalent Single-Axle Load
ESAR	Equivalent Single Axle Radius
FI	Freezing Index
FHWA	Federal Highway Administration
FRC	Fiber Reinforced Concrete
FWD	Falling Weight Deflectometer
GRB	Granular Base
IRI	International Roughness Index
JPCP	Jointed Plain Concrete Pavement
JRCP	Jointed Reinforced Concrete Pavement
k	Modulus of Subgrade Reaction
LCB	Lean Concrete Base
LDF	Load Distribution Factor
LEF	Load Equivalency Factor
LTE	Load Transfer Efficiency
LTPP	Long-Term Pavement Performance
MR	Modulus of Rupture
NOAA	National Oceanic and Atmospheric Administration
PAGG	Permeable Aggregate Base (nontreated)
PATB	Permeable Asphalt-Treated Base
P/C	Pass to Coverage Ratio
PCA	Portland Cement Association
PCC	Portland Cement Concrete
PCTB	Permeable Cement-Treated Base

## List of Acronyms and Abbreviations (continued)

PIARC	Permanent International Association of Road Congresses
PSR	Present Servicability Rating
P-value	Probability Value
PVC	Polyvinylchloride
SC	Soil Cement Base
SCS	Soil Conservation Service
SHRP	Strategic Highway Research Program
SEE	Standard Error of the Estimate
SI	International System of Units
TF	Truck Factor
TMI	Thornthwaite Moisture Index
USCS	Unified Soil Classification System
WF	Wet-Freeze
WNF	Wet-Nonfreeze
WWF	Welded-Wire Fabric



# 1. INTRODUCTION

## Background

The need to improve the design and performance of highway pavements is not only indisputable, it is continuous. The introduction and use of innovative designs, new materials, and new construction practices, coupled with increased truck loading of pavement facilities, dictate the need for the monitoring of highway pavement performance so that deficiencies can be identified and addressed by updating current design and construction practices. While such pavement monitoring has been conducted since the earliest days of road building, it has been only in the last two decades that formalized pavement monitoring programs have been implemented. One example of such a monitoring program is the Long-Term Pavement Performance (LTPP) study that was launched by the Strategic Highway Research Program (SHRP) in 1987 and is now being administered by the Federal Highway Administration (FHWA).<sup>(1)</sup> That program is monitoring the performance of both asphalt concrete (AC) and portland cement concrete (PCC) pavements over a 20-year period with the single-minded goal of improving the performance of new pavements.

Before the LTPP program was launched, the FHWA in 1986 sponsored a research study on the evaluation of 95 concrete pavement sections located throughout North America. The goal of the study was to obtain feedback information on the performance of these inservice concrete pavements, many of which are experimental projects containing a variety of design features (e.g., slab thickness, base type, load transfer) that allow for an evaluation of the effect of the design features on pavement performance. That study, completed in 1990, provided much useful information on the performance of concrete pavements, including the development of prediction models for several concrete pavement performance indicators (faulting, spalling, cracking, and serviceability loss). The results are fully documented in a six-volume report.<sup>(2-7)</sup>

One shortcoming of that study was that the findings and results were limited to the pavement designs present in the data base. For example, the data collected under the original study represent a "snapshot" in the performance life of the pavement section. That is, there was no time series performance data that could provide an indication of the section's rate of deterioration, or how the pavement performed over time. Furthermore, many of the sections that incorporated recent design innovations were too new or had not carried enough traffic for drawing meaningful conclusions.

To address these deficiencies while building upon and extending the original study, the FHWA sponsored this follow-up study in 1991. Not only were the original 95 pavement sections reinspected and re-evaluated after receiving 5 more years of traffic loading, but an additional 208 pavement sections were added to the study, thus greatly strengthening the data base used for analysis. Furthermore, many of the new sections that were added to the study contained newer design elements, such as widened lanes or permeable bases. The result is a total of 303 concrete pavement

sections—located throughout North America and representing a broad range of pavement designs—available for analysis.

## Research Objectives

The objectives of this project are as follows:

- To re-evaluate the 95 projects originally surveyed in 1987 to reveal performance trends and to determine deterioration rates.
- To determine the impact of different pavement types, design features, materials, and construction variables on pavement performance, based on additional data collection and testing, data analysis, and performance evaluations.
- To improve design procedures and performance prediction models for jointed concrete pavements, using the expanded data base. Where possible, evaluate the performance of the various rigid pavement types to provide improved guidance on pavement type selection.

In short, the overall objective of this study can be stated as the development of improved guidance on the design and construction of concrete pavements through the field evaluation of the performance of inservice concrete pavements.

## Research Approach

The work conducted under this project can be divided into essentially three distinct phases. The first phase of the project included the collection of performance data for each of the 303 sections included in the study. This field data collection effort consisted of the following major elements:

- A pavement distress survey to quantify the type, amount, and severity of distress occurring on each section.
- A pavement drainage survey to characterize the drainage capabilities of each section.
- Falling Weight Deflectometer (FWD) deflection testing to determine the concrete elastic modulus (E) and the modulus of subgrade reaction (k) of each section, and to characterize the load transfer across transverse joints.
- Coring and boring operations to obtain layer thicknesses and to obtain samples for later laboratory testing.
- Pavement roughness testing using a South Dakota-type road profiler.

A more detailed description of the field data collection activities is reported in volume I.

The second phase of the project consisted of reducing the data collected under the field testing program and, along with pertinent design, construction and traffic data obtained from the participating State Highway Agencies, developing a data base for later analyses. The ORACLE data base management system was selected for this task



because of its use on the FHWA LTPP program.<sup>(8)</sup> The data were extensively cleaned and verified in order to ensure their validity for analysis. A summary of the data for each pavement section is presented in appendix A of volume IV.

The analysis of the data was the third and final phase of the project. Several different analyses were conducted, including an evaluation of the effect of design features on concrete pavement performance, the development of pavement performance prediction models, and the development of guidelines for improving concrete pavement performance.

### **Advisory Panel**

An advisory panel consisting of experienced highway engineers was assembled to provide guidance to the research team in the collection and evaluation of concrete pavement performance data. The advisory panel assisted throughout the project, from arranging for traffic control to providing design and construction information to reviewing project documentation. Members of the advisory panel include:

- Mr. Jamshid Armaghani, Florida Department of Transportation.
- Mr. Chuck Arnold, Michigan Department of Transportation.
- Mr. Roger Green, Ohio Department of Transportation.
- Mr. Terry Rutkowski, Wisconsin Department of Transportation.
- Mr. Larry Scofield, Arizona Department of Transportation.
- Mr. Gordon Wells, California Department of Transportation.
- Mr. Bill Trimm, Missouri Department of Transportation.

In addition, while not serving on the advisory panel, engineers from other highway agencies were also very helpful and cooperative in providing traffic control and inventory data for pavement sections evaluated within their State. These individuals include:

- Mr. Walt Brubaker, West Virginia Parkways Economic Development and Tourism Authority
- Mr. Gaylord Cumberledge, Pennsylvania Department of Transportation.
- Mr. Wouter Gulden, Georgia Department of Transportation.
- Mr. Tom Kazmierowski, Ontario Ministry of Transportation
- Mr. David Lippert, Illinois Department of Transportation.
- Mr. Victor Mottola, New Jersey Department of Transportation.
- Mr. Robert Perry, New York Department of Transportation.
- Mr. David Rettmar, Minnesota Department of Transportation.

### **Overview of Report**

The results of this project are presented in a four-volume final report, with the focus of this volume on improving the performance of concrete pavements. New pavement performance prediction models are presented in this volume, along with guidelines and recommendations for the improved design of concrete pavements.

The performance prediction models were developed using the performance data collected under this study, as well as the performance data from the preceding study. Performance prediction models were developed for the following performance indicators:

- Transverse joint faulting (doweled and nondoweled pavements).
- Transverse slab cracking (JPCP and JRCP).
- Transverse joint spalling (JPCP and JRCP).
- Pavement serviceability (JPCP and JRCP).
- Pavement roughness (JPCP only).

These models can be used to assess the efficacy of an initial pavement design or to evaluate the effect of different design features (e.g., dowel bars) on pavement performance. They may also be useful in forecasting pavement rehabilitation needs and requirements.

This report contains three chapters. Chapter 2 describes the model development efforts and presents the nationwide models for key concrete pavement distress types. Chapter 3 presents the recommended guidelines for the design of concrete pavements, much of which is based on the information provided by the prediction models developed in chapter 2.

## 2. DEVELOPMENT OF CONCRETE PAVEMENT PERFORMANCE PREDICTION MODELS

### Introduction

Pavement performance prediction models are mathematical relationships that predict the development of a key performance indicator (e.g., cracking, faulting) based on design, traffic, and climatic inputs. These models can be mechanistic-based, in which basic pavement responses (stresses, strains, deflections) are calibrated with field observations of pavement performance, or empirically based, in which a statistical regression model is developed solely on the observed performance of the pavement.

Performance prediction models are very useful tools to the design engineer. Among the various applications of performance prediction models are:

- Evaluation of the suitability of a pavement designed by some other method.
- Evaluation of the relative effect of key design features (e.g., dowel bars) on pavement performance.
- Estimation of pavement deterioration for programming rehabilitation.

This chapter presents the pavement performance prediction models that were developed under this study, using the data provided in volume IV of this report series. Prediction models are presented for transverse joint faulting (doweled and nondoweled), transverse cracking (JPCP and JRCP), transverse joint spalling (JPCP and JRCP), present serviceability rating (JRCP and JPCP), and pavement roughness (JPCP only). The models are deterministic in that they predict the mean expected performance indicator based on the input variables. A sensitivity analysis of each model is included to illustrate the effect of key design inputs on the resulting pavement distress.

The development of each model followed the same general step-by-step procedure. This process is illustrated in figure 1 and is described in significant detail for the first prediction model presented to better convey the general model building approach. The S-Plus™ statistical modeling program was used in the model development effort.

It is important to recognize that the models presented herein reflect the designs and performance trends contained in the data base; thus, they are valid only for those conditions. Even though the majority of the North American sections are greater than 15 years old, only 4 of the 303 sections (1 percent) had sustained over 20 million ESAL applications. Therefore, great care must be exercised in extending these models beyond the conditions for which they were developed.

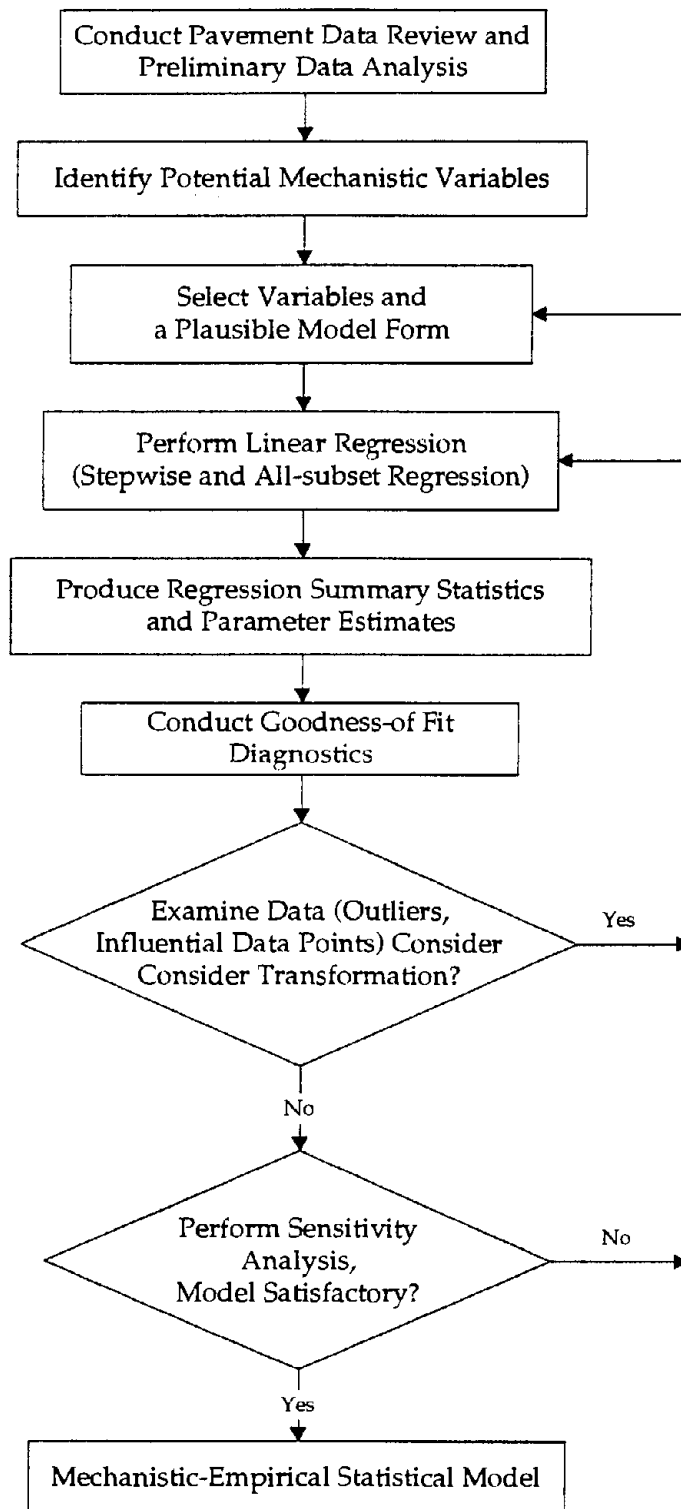


Figure 1. Procedures used in the development of mechanistic-empirical statistical models.

## **General Description of Data Used in Model Development**

The design and performance data used in the development of the various prediction models were collected under this project and under a preceding FHWA project on pavement performance.<sup>(2,3)</sup> A total of 303 concrete pavement sections are available from this study and 95 pavement sections are available from the preceding study. Because the 95 pavement sections were also re-evaluated under the current study, time-series performance data are available for those sections.

The concrete pavement sections evaluated under this study represent a variety of designs. Most of the sections are jointed plain (JPCP) or jointed reinforced concrete pavements (JRCP), although a few continuously reinforced concrete pavements (CRCP) are also included. The sections are located throughout the United States, with the majority located in the upper midwest. In addition, two projects from Canada are also included in the study. Figure 2 depicts the general location of each pavement project included in the study.

A variety of design features (i.e., slab thickness, joint spacing, load transfer, and so on) are present on these pavement sections. The range of design features encountered in these projects is summarized in table 1. This table shows that a significant range of variables exists, although often these ranges occur over different projects located in different climates.

These projects also vary considerably in age and in cumulative traffic loadings (expressed in terms of equivalent single-axle load [ESAL] applications) that they have sustained. Figures 3 and 4 illustrate the range of age and ESAL loadings of the 303 pavement sections. Figure 3 shows that most of the sections are between 15 and 25 years old, with about 20 sections greater than 25 years old. Figure 4 indicates that the majority of the sections have sustained less than 10 million ESAL applications, although 3 sections have carried more than 20 million.

More detailed information on the various concrete pavement projects and on the field data collection activities is presented in volume I.

### **Joint Faulting Model for Doweled Jointed Concrete Pavements**

Transverse joint faulting is a major distress of jointed concrete pavements. Transverse joint faulting is the difference in elevation between abutting slab faces and is primarily the result of a combination of heavy axle loads, free moisture beneath the pavement, and pumping of the supporting base or subbase material from beneath the slab. Pumping occurs when excess moisture is violently ejected from beneath the leave slab corner as it is loaded by a vehicle. The excess moisture that is ejected carries base and subbase fines with it, thereby creating a void or cavity beneath the joint at the leave slab corner while building up loose materials under the approach slab corner. Through the build-up of material beneath the approach corner and through the loss of support under the leave corner, faulting and corner breaks or corner cracking can develop.

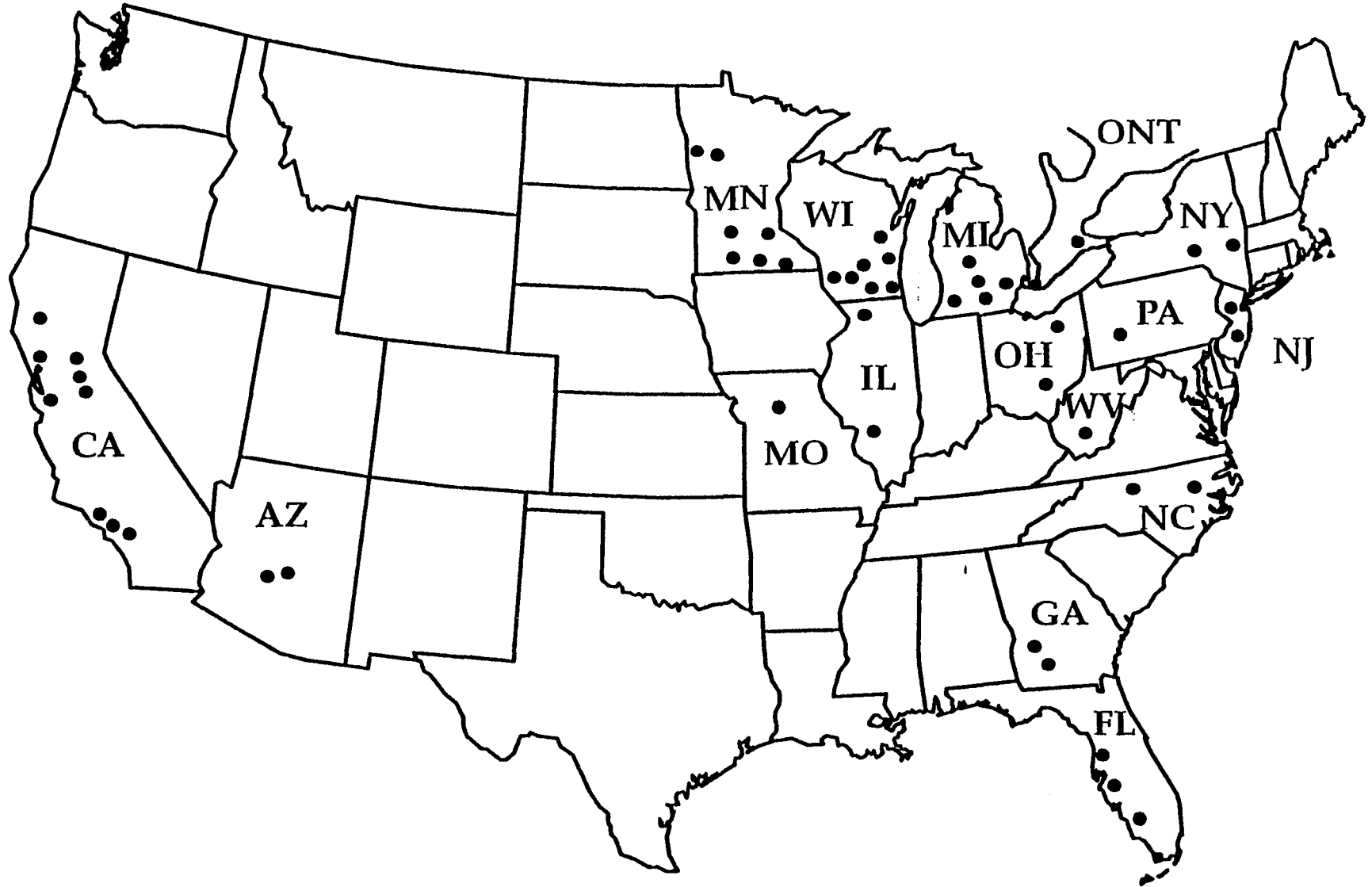


Figure 2. General location of sections included in study.

Table 1. Range of design features included in study.

Design Feature	Range of Design Feature	Distribution of Design Feature	
		Categories	Number in Category
Slab Thickness	7 to 15 in	< 8 in	3
		8 to 9.9 in	234
		10 to 11.9 in	41
		≥ 12 in	25
Joint Spacing—JPCP	5 to 30 ft	< 10 ft	2
		10 to 14.9 ft	7
		15 to 19.9 ft	102
		≥ 20	50
Joint Spacing—JRCP	21 to 78.5 ft	< 25 ft	3
		25 to 39.9 ft	29
		40 to 59.9 ft	61
		≥ 60 ft	24
Joint Orientation		Nonskewed Joints	130
		Skewed Joints	148
Joint Load Transfer		Doweled Joints	154
		Nondoweled Joints	124
Joint Sealant		None	54
		Hot-Poured	120
		Silicone	17
		Preformed	86
Base Type		None	13
		AGG	106
		CTB	65
		ATB	42
		LCB	40
		PAGG	14
		PCTB	7
		PATB	15
Drainage		None	168
		Daylighted	36
		Edge Drains Only	61
		Edge/Trans. Drains	2
		Permeable Base	36
Shoulder Type		AC	246
		PCC	56
		Gravel	1
JRCP Reinforcement	0.04 to 0.25%	< 0.1 percent	45
		0.1 to 0.14 percent	54
		0.15 to 0.19 percent	9
		≥ 0.20 percent	9
Pavement Type		JPCP	161
		JRCP	117
		CRCP	25

Note: 1 in = 25.4 mm; 1 ft = 0.305 m

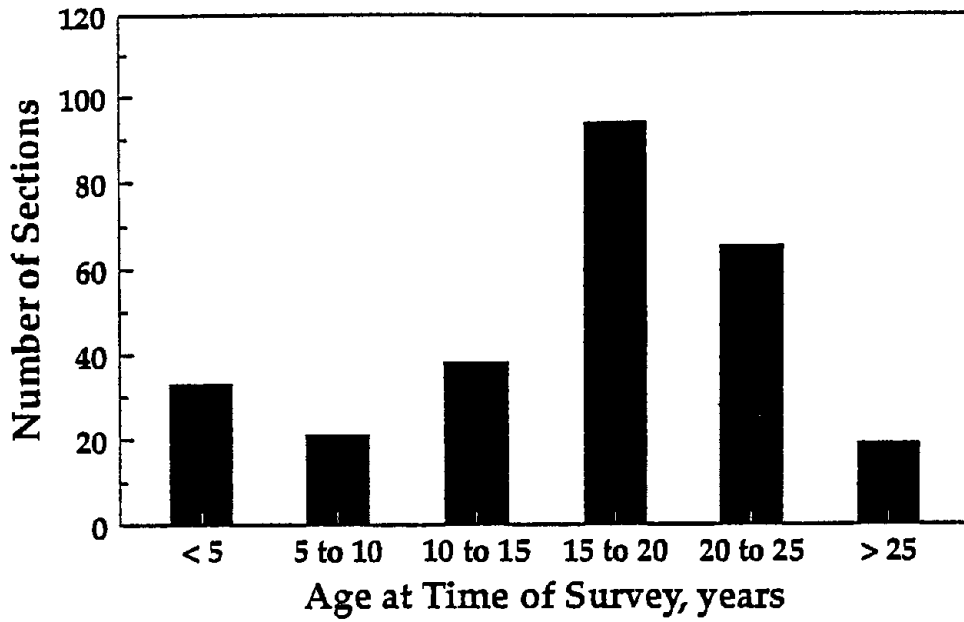


Figure 3. Distribution of projects by age.

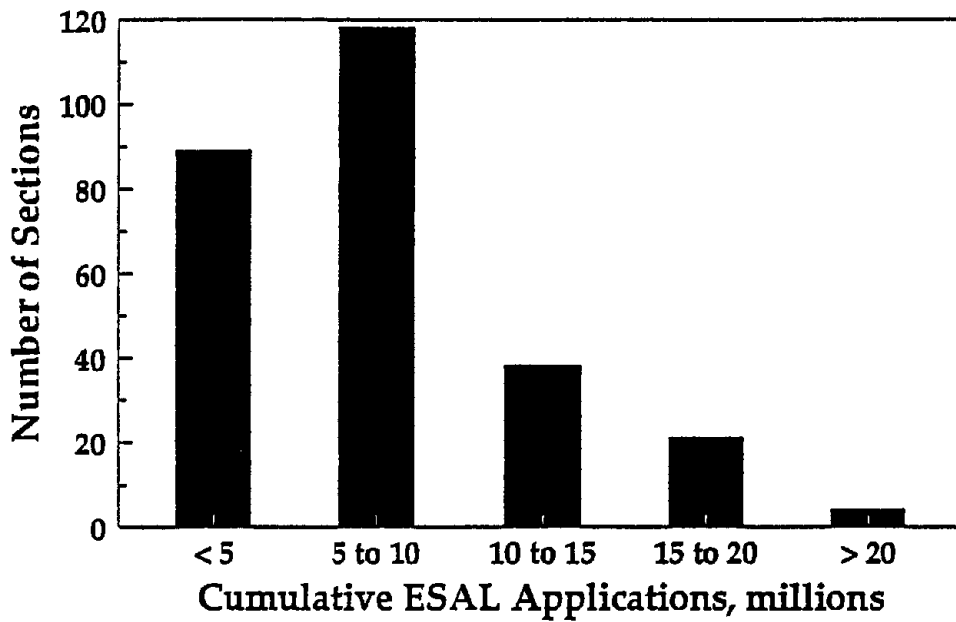


Figure 4. Distribution of projects by ESAL applications.



Poor load transfer across the transverse joint contributes to the development of joint faulting. Load transfer is the mechanism through which wheel loads are conveyed from one slab to the next and is achieved by one of two means in jointed concrete pavements:

- Through the aggregate interlock between the abutting joint faces.
- Through the use of mechanical load transfer devices (e.g., dowel bars) placed across the joint.

Because faulting can occur in both types of load transfer mechanisms, models were developed to predict faulting in both nondoweled (aggregate interlock) and doweled pavements. The development of the doweled model is presented first.

### Preliminary Data Analysis

Several studies have been conducted evaluating the faulting of transverse joints in concrete pavements.<sup>(3,9-13)</sup> Many of those studies produced models for predicting joint faulting, and these models are generally provide reasonable results. However, a major limitation of these models is the limited data base used to develop the models (both in terms of the absolute number of sections and in terms of the inclusion of sections with more recent pavement designs).

The current project data base contains a large number of concrete pavement sections including a range of design features. Furthermore, concrete pavement sections with new design features, such as permeable bases, thicker slabs, widened lanes and dowels in dry climates, are also included. The distribution of pavement sections and designs used in developing the doweled faulting model is given in table 2, broken out by climate, pavement type, and base type. It is observed that most of the sections are JRCP and located in the wet-freeze climatic region. It is also observed that nonstabilized bases are well represented and that few doweled pavements are available in nonfreeze regions.

Table 2. Distribution of the pavement sections used in the development of doweled joint faulting model.

Climatic Region	JPCP		JRCP	
	Nonstabilized Base	Stabilized Base	Nonstabilized Base	Stabilized Base
Wet-Freeze	21	2	48	26
Wet-Nonfreeze	4	7	2	0
Dry-Freeze	6	0	14	14
Dry-Nonfreeze	0	2	0	0

## Explanatory Variables Initially Selected

The dependent variable in the doweled joint faulting model is the mean transverse joint faulting (FaultD, in) measured about 1 ft (0.3 m) from the slab edge on each section. Based on the previous studies of joint faulting modeling, a set of variables were selected from the RIPPER data base. The explanatory variables that were initially considered are:

CESAL:	Cumulative 18-kip (80-kN) equivalent single axle loads, millions.
Age:	Time since construction, years.
Dowdia:	Dowel diameter, in.
Jointspace:	Mean transverse joint spacing, ft.
Slabthick:	PCC slab thickness, in.
Basetype:	Base type (0 = nonstabilized base; 1 = stabilized [asphalt, cement] base).
Baseperm:	Base permeability (0 = not permeable, 1 = permeable).
Widenlane:	Widened lane (0 = not widened, 1 = widened).
Cut:	Percent of the section length located in an area of cut.
Fill:	Percent of the section length located in an area of fill.
Edgesup:	Edge support (1 = tied concrete shoulder; 0 = otherwise).
C <sub>d</sub> :	Modified AASHTO drainage coefficient, calculated from data base information.
DRAIN:	Drainage provisions (0 = no edge drains; 1 = edge drains).
Soiltype:	Subgrade soil type (0 = fine grained; 1 = coarse grained).
Kstatic:	Static backcalculated k-value, lb/in <sup>2</sup> /in.
Bstress:	Maximum dowel/concrete bearing stress, lb/in <sup>2</sup> .
Jtopen:	Calculated joint opening over annual temperature range, in.
Days32:	Number of the days with minimum temperature below 32 °F (0 °C).
Trange:	Annual temperature range, °F.
FTcycle:	Average number of air freeze-thaw cycles.
FI:	Mean annual freezing index, degree-days.
Precip:	Mean annual precipitation, in.

The modified Friberg analysis was used to calculate the maximum bearing stress exerted by the dowels on the surrounding concrete (Bstress, lb/in<sup>2</sup>).<sup>(14,15)</sup> This factor is believed to significantly contribute to the development of transverse joint faulting. The analysis assumes a 9000-lb (40-kN) wheel load placed at the corner, which will produce the maximum stress in the outermost dowel bar. Only dowel bars within a distance of 1.0\* $\ell$  from the center of the load are considered to be active, where  $\ell$  is the radius of relative stiffness, defined as:

$$\ell = [ Eh^3 / 12k(1-\mu^2) ]^{0.25} \quad (1)$$

where:

- E = Concrete modulus of elasticity, lb/in<sup>2</sup>.
- h = Slab thickness, in.

- $k$  = Effective modulus of subgrade reaction, lb/in<sup>2</sup>/in.  
 $\mu$  = Poisson's ratio, fixed at 0.15.

The modified Friberg analysis is based on the assumption that 45 percent of the *load* (not the stress) is transferred across the joint. The formula for the maximum dowel bearing stress is given below:

$$\sigma_{\max} = K * \delta_o \quad (2)$$

where:

- $K$  = Modulus of dowel support, fixed at  $1.5 \cdot 10^6$  lb/in<sup>2</sup>/in ( $4.07 \cdot 10^8$  kN/m<sup>2</sup>/m).  
 $\delta_o$  = Deflection of the dowel at the face of the joint, in  
 $= f_d P_t T (2 + \beta z) / 4 \beta^3 E_s I$

in which

- $f_d$  = Dowel distribution factor.  
 $= 2 * 12 / (\ell + 12)$   
 $\ell$  = Radius of relative stiffness  
 $P_t$  = Shear force acting on dowel, fixed at 9000 lb (40-kN).  
 $T$  = Percent transferred load, set to 0.45.  
 $\beta$  = Relative stiffness of the dowel concrete system, 1/in.  
 $= [(Kd) / (4E_s I)]^{0.25}$ .  
 $E_s$  = Modulus of elasticity of dowel bar, fixed at  $2.9 \cdot 10^7$  lb/in<sup>2</sup> ( $2.0 \cdot 10^5$  MPa).  
 $I$  = Moment of inertia of dowel bar cross-section, in<sup>4</sup>.  
 $= 0.25 * \pi * (d/2)^4$  for dowel diameter  $d$  in inches.  
 $z$  = Width of joint opening, in.

The drainage coefficient,  $C_d$ , is based on the AASHTO drainage coefficient introduced in the AASHTO rigid pavement design procedure in 1986.<sup>(16)</sup> This factor is a reflection of the pavement's ability to drain excessive moisture from within the structure, as well as the pavement's potential for being exposed to near saturated conditions. Although the drainage coefficient represents a major part of the AASHTO design procedure, little guidance is presented for its selection. A rational procedure is presented in reference 6, which was also used in this study to develop drainage coefficients. Using that information, a simplified matrix was developed for the selection of drainage coefficients based on key climatic and pavement design information. This matrix is presented in table 3.

## Model Development

### *Data Review and Correlation Between Variables*

The data extracted from the data base were reviewed to determine if any data expected to be significant were missing. After cells containing missing values of certain variables were eliminated from the data set, a univariate analysis (consisting

Table 3. Simplified design matrix for the selection of the overall drainage coefficient,  $C_d$ .

Edge Drains	Precip. Level	Fine-Grained Subgrade		Coarse-Grained Subgrade	
		Nonpermeable Base	Permeable Base	Nonpermeable Base	Permeable Base
No	Wet	0.70–0.90	0.85–0.95	0.75–0.95	0.90–1.00
	Dry	0.90–1.10	0.95–1.10	0.90–1.15	1.00–1.15
Yes	Wet	0.75–0.95	1.00–1.10	0.90–1.10	1.05–1.15
	Dry	0.95–1.15	1.10–1.20	1.10–1.20	1.15–1.20

- Notes:
1. Coarse subgrade = A-1 through A-3 classes,  
Fine subgrade = A-4 through A-7 classes.
  2. Permeable Base =  $k = 1000 \text{ ft/day (305 m/day)}$  or  $C_u \leq 6$ .
  3. Wet climate = Precipitation  $> 25 \text{ in/year (635 mm/year)}$ ;  
Dry climate = Precipitation  $\leq 25 \text{ in/year (635 mm/year)}$ .
  4. Select mid-point of range and use other drainage features (adequacy of cross slopes, depth of ditches, presence of daylighting, relative drainability of base course, bathtub design, etc.) to adjust upward or downward.

of the determination of the mean, minimum, maximum, and standard deviation of each dependent and independent variable) was conducted.

Two-dimensional scatter plots of the raw data for the key variables were generated to help identify erroneous data points (outliers), and the general trend of the dependent variable with the independent variables. Examples of these two-dimensional scatter plots are given in figure 5. A correlation matrix of each pair of the variables was also obtained to examine the colinearity between the explanatory variables. Based on all of these results, the sections that were identified with missing, questionable, or unreasonable data were either deleted from the data set or marked for evaluation during the model development.

### *Multiple Linear Regression*

Previous studies have shown that faulting increases rapidly with traffic loadings at first, and then levels off at a much decreased rate.<sup>(3,10,11)</sup> The following general model form was adopted:

$$\text{FaultD} = \text{CESAL}^P * [\text{Explanatory Variables}] \quad (3)$$

where:

CESAL = Cumulative 18-kip (80-kN) equivalent single axle loads, millions.

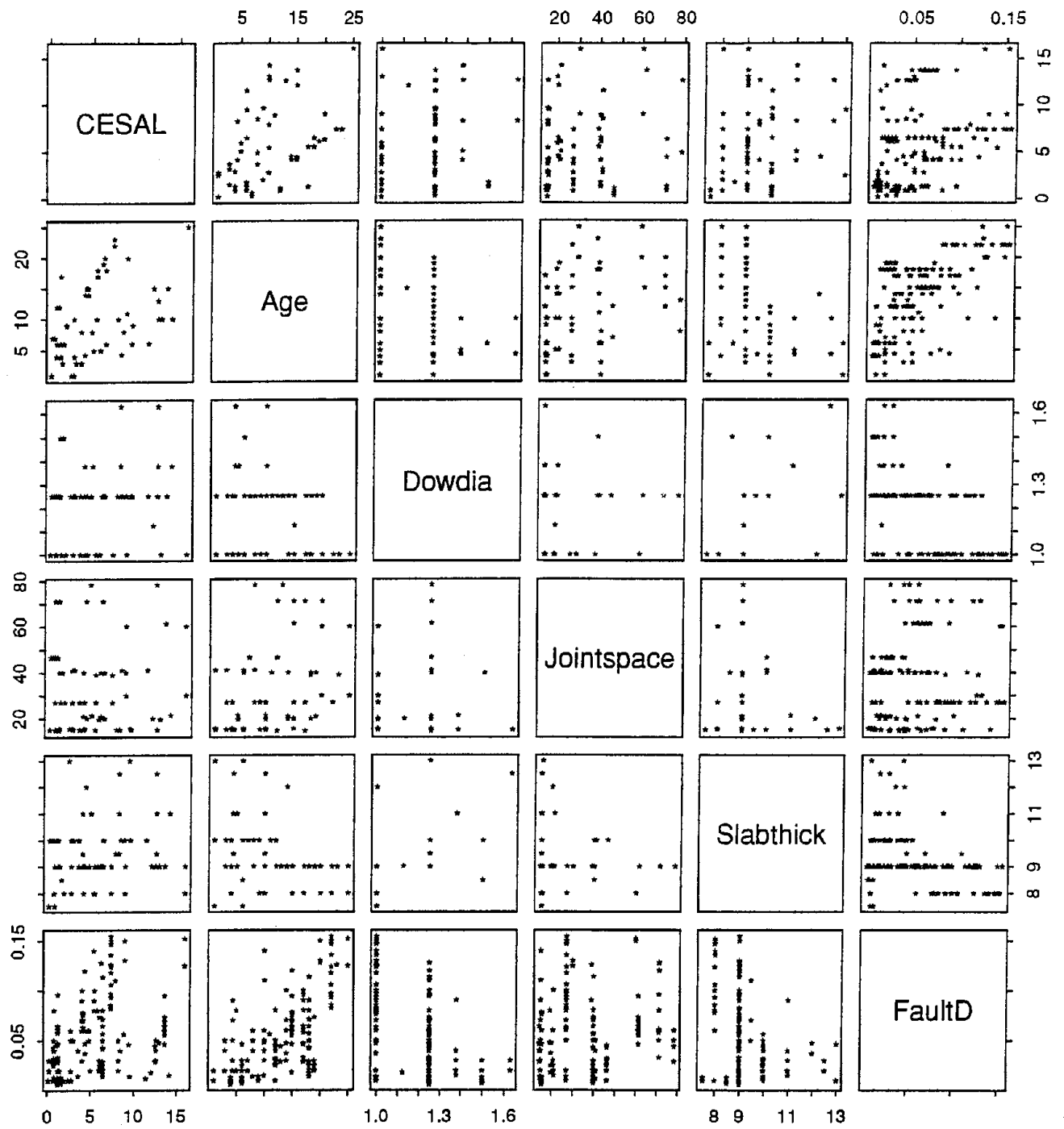


Figure 5. Two-dimensional scatter plot for doweled joint faulting model.

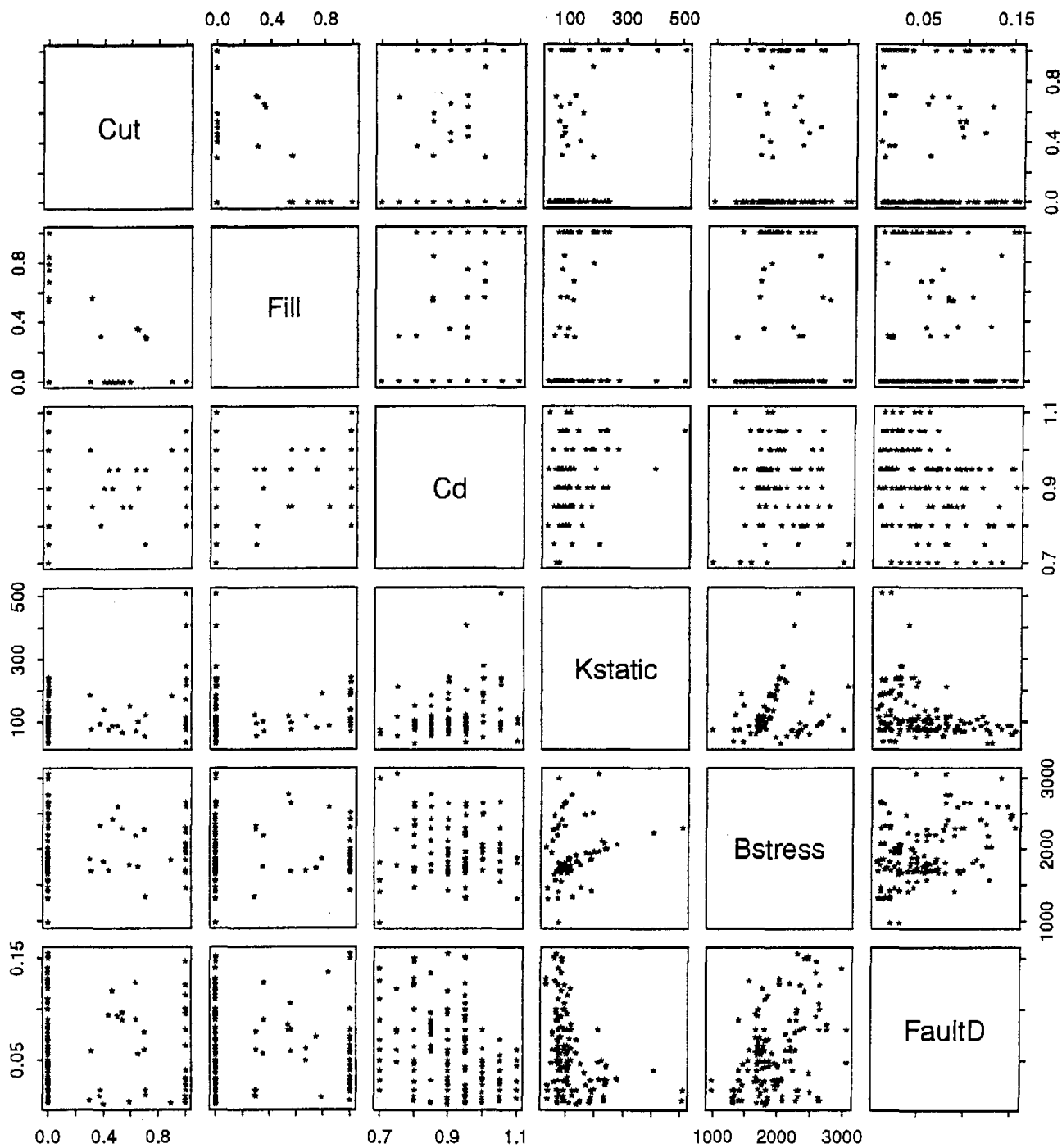


Figure 5. Two-dimensional scatter plot for doweled joint faulting model (continued).

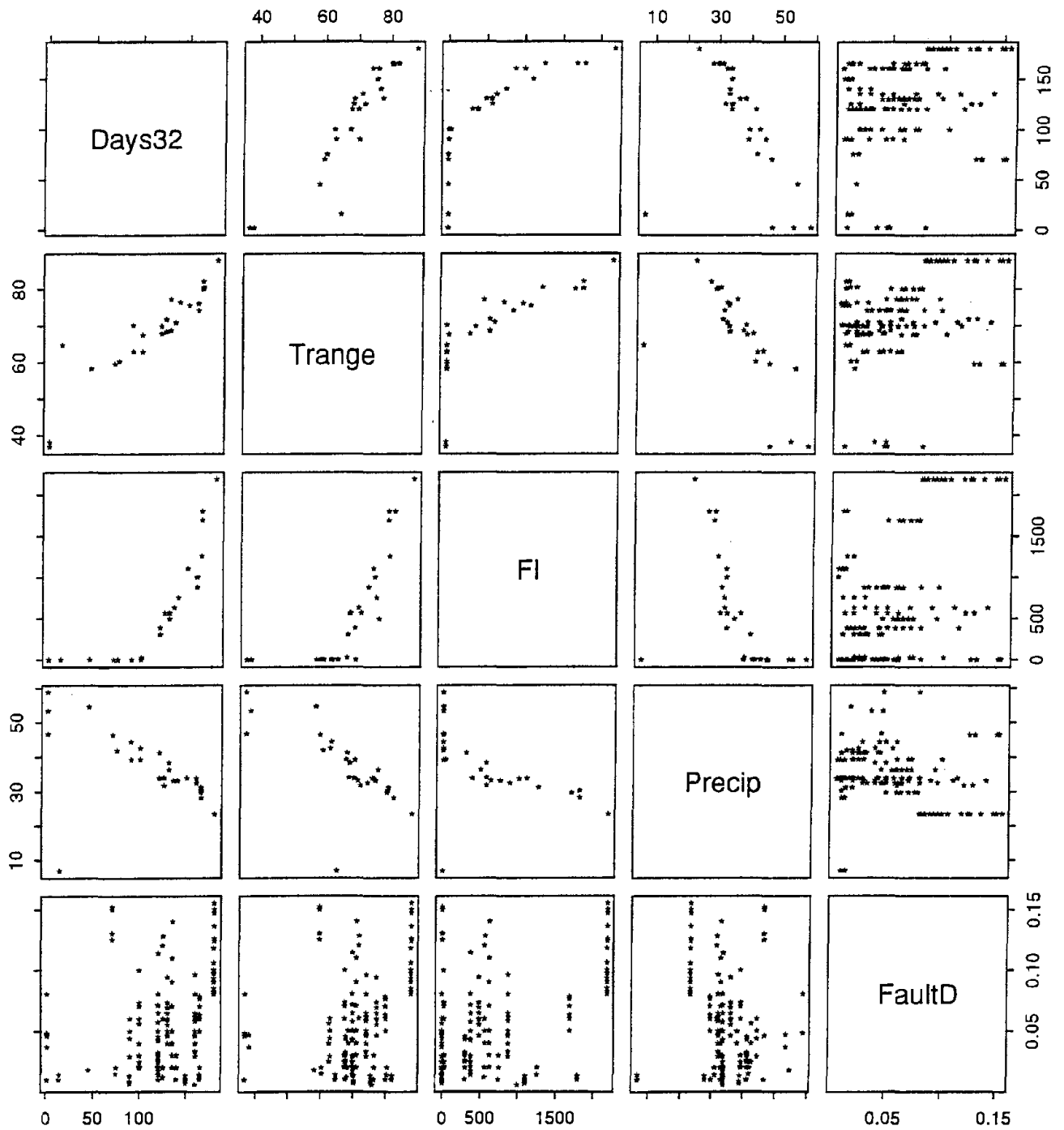


Figure 5. Two-dimensional scatter plot for doweled joint faulting model (continued).

Note that this model form meets the traffic boundary condition of zero faulting at zero CESAL's. Using this model form, explanatory variables were then tested for significance in the overall model using S-Plus™'s step-wise and all-subset linear regression procedures. The previous two-dimensional plots were also examined to determine the best functional form between the dependent variable and the independent variable. The Alternating Condition Expectation (ACE) algorithm introduced by Breiman and Friedman was used to help identify the proper functional forms for each variable.<sup>(17,18)</sup> Through all of this process, engineering judgement and expertise was applied in terms of known mechanics involved.

The final model developed for transverse joint faulting for the jointed concrete pavements (both JPCP and JRCP) with dowel bars is as follows:

$$\begin{aligned} \text{FaultD} = & \text{CESAL}^{0.25} * [0.0628 - 0.0628 * C_d + 0.3673 * 10^{-8} * \text{Bstress}^2 \\ & + 0.4116 * 10^{-5} * \text{Jtspace}^2 + 0.7466 * 10^{-9} * \text{FI}^2 * \text{Precip}^{0.5} \\ & - 0.009503 * \text{Basetype} - 0.01917 * \text{Widenlane} + 0.0009217 * \text{Age}] \end{aligned} \quad (4)$$

N = 146 sections.

R<sup>2</sup> = 0.60.

RSE = 0.022 in (0.56 mm).

where:

CESAL = Cumulative 18-kip (80-kN) equivalent single axle loads, millions.

Bstress = Maximum dowel/concrete bearing stress, lb/in<sup>2</sup>.

Jtspace = Mean transverse joint spacing, ft.

Basetype = Base type (0 = nonstabilized base; 1 = stabilized base).

Widenlane = Widened lane (0 = not widened, 1 = widened).

C<sub>d</sub> = Modified AASHTO drainage coefficient, calculated from data base information.

FI = Mean annual freezing index, degree-days.

Precip = Mean annual precipitation, in.

Age = Pavement age, years.

The regression statistics are defined as follows. N is the total number of pavement sections used in the development of the model. R<sup>2</sup> represents the multiple R-squared value which is defined as the fraction of the total variation in the response accounted for by the variation in the fitted values. The residual standard error (RSE) is the square root of the sum of squared residuals divided by the number of degrees of freedom for residuals (usually the number of observations less the number of coefficients).

The estimate of each coefficient in the equation, the associated standard error of the estimate (SEE) of the coefficients and the probability value (p-value) are provided in table 4. The P-value of each estimated coefficient represents the probability that



Table 4. Estimates of the coefficients and the associated SEE and P-values for the doweled joint faulting model.

Terms	Value	SEE	P-value ( $>  t $ )
Intercept	0.0628	0.0120	<0.0001
$C_d$	-0.0628	0.0129	<0.0001
$B_{stress}^2 \cdot 10^{-8}$	0.3673	0.0948	0.0002
$J_{tspace}^2 \cdot 10^{-5}$	0.4116	0.0950	<0.0001
$FI \cdot Precip^{0.5} \cdot 10^{-9}$	0.7466	0.2048	0.0004
$B_{asetype} \cdot 10^{-2}$	-0.9503	0.2706	0.0006
Widenlane	-0.01917	0.00506	0.0002
$Age \cdot 10^{-3}$	-0.9217	0.2700	0.0008

the coefficient is not significantly different from zero. As shown in the table, all the estimates of the coefficients are significant at  $\alpha = 0.10$  level, where  $\alpha$  is the selected probability value that is used to compare with p-value. In this case, it can be inferred with 90 percent confidence that all of the coefficients are different from zero. The intercept term is the constant term in the bracket of the model equation, while all of the other terms are previously defined.

Figure 6 provides a plot of the predicted versus actual measured faulting from the doweled faulting model using the same data set. The residual versus predicted faulting plot (goodness-of-fitting) is given in figure 7.

#### *Sensitivity Analysis and Discussion*

The sensitivity analysis of the key variables in the doweled model is provided in figures 8 through 12. These three-dimensional plots are drawn by fixing all other variables at a constant value and allowing the selected variables to vary over a range of values. As shown in the graphs, they all take similar shape regarding CESAL, i.e. starting quite steep and then leveling off with increasing CESAL.

Figure 8 provides a sensitivity plot of the doweled joint faulting with CESAL and bearing stress. It is clearly shown that as bearing stress increases, faulting increases. Similarly shown in figure 9 is that faulting increases with increasing joint spacing.

Figure 10 indicates that if drainage coefficient,  $C_d$  increases (meaning improved drainage conditions), faulting will decrease. Figures 11 and 12 show the effect of the climatic factors on faulting. As shown, faulting increases with increasing freezing index (colder climate) and with increasing levels of annual precipitation.

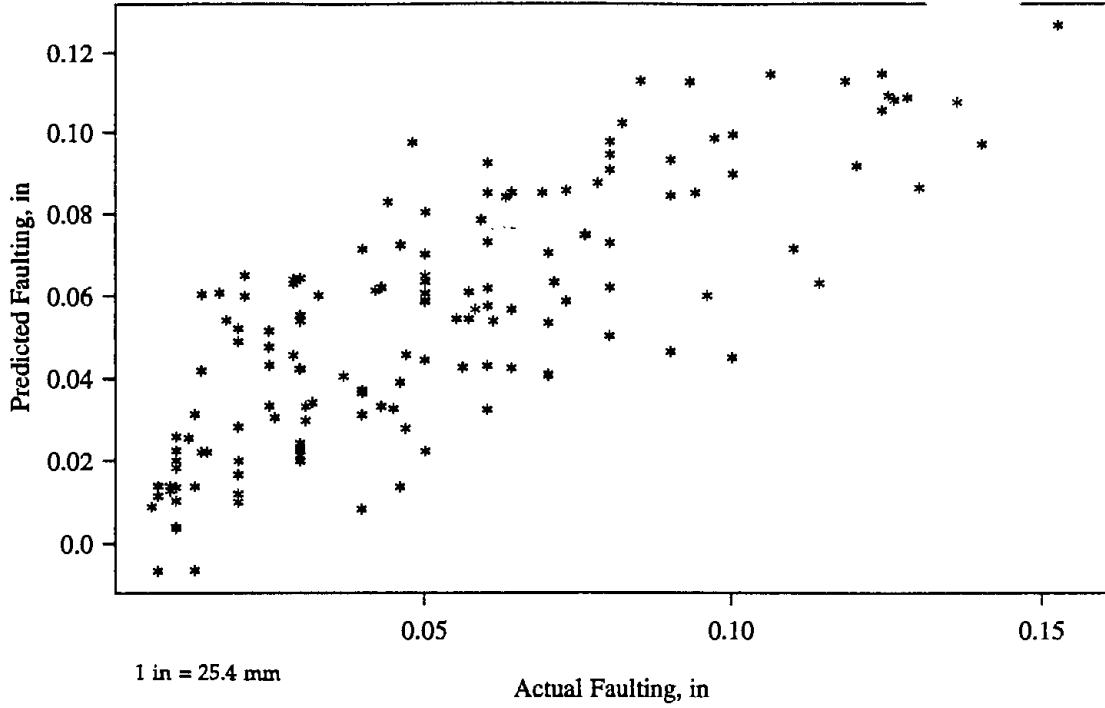


Figure 6. Actual versus predicted faulting for the doweled faulting model.

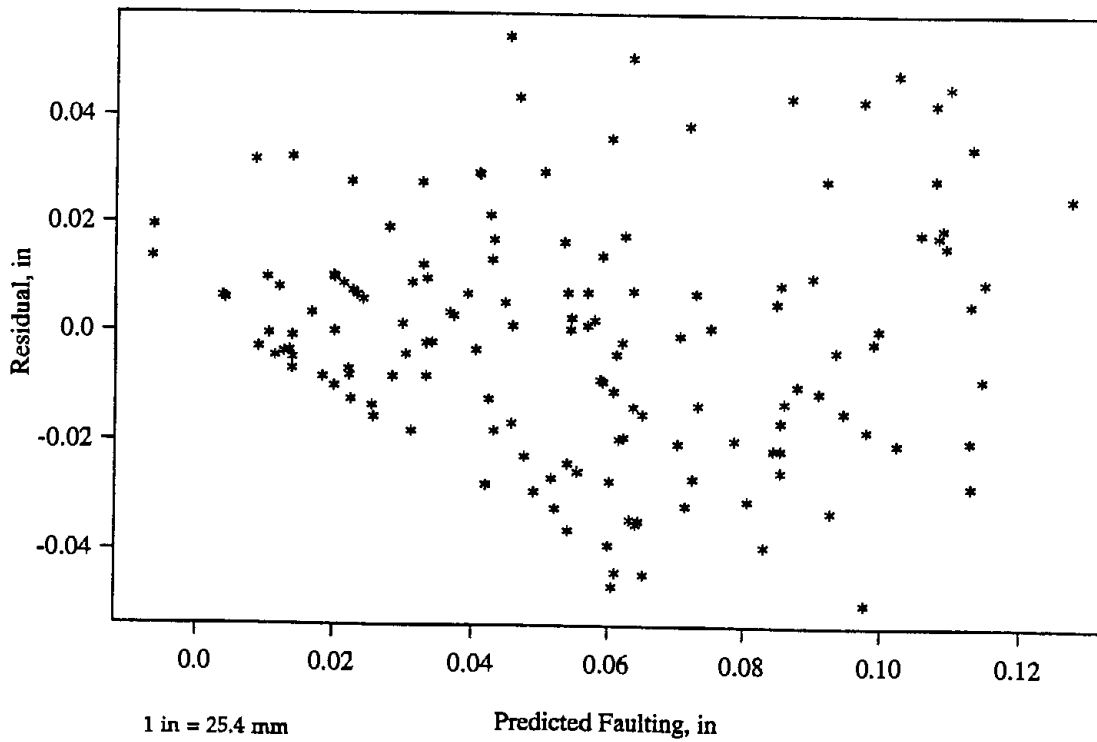
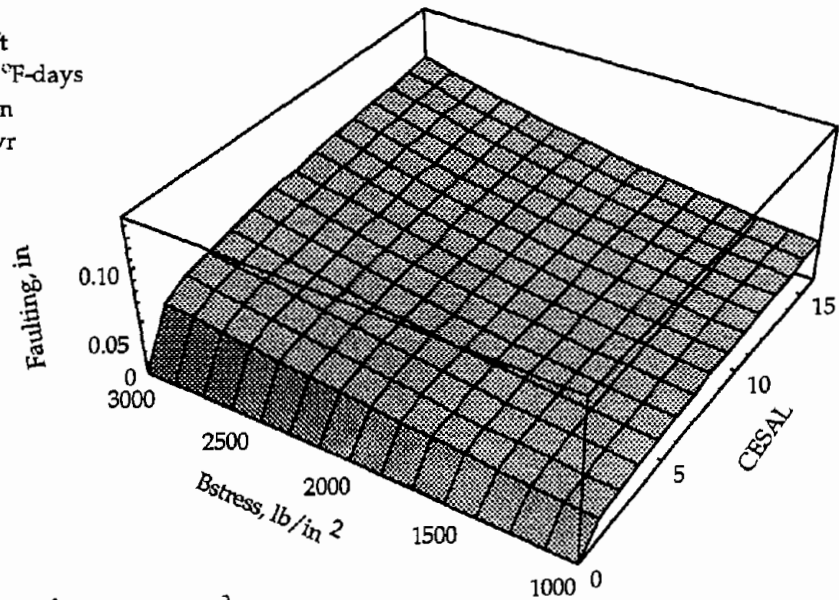


Figure 7. Predicted versus residual for the doweled faulting model.

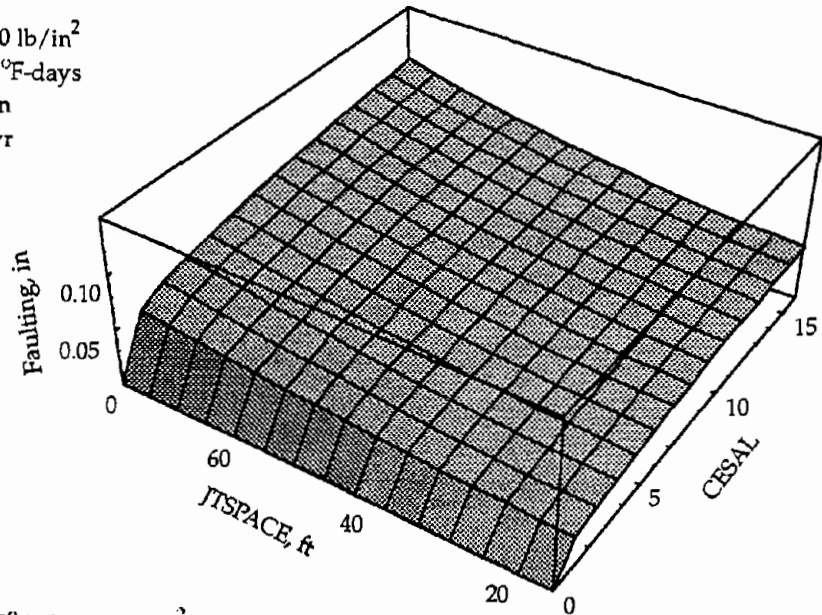
$C_d = 0.9$   
 $Jt\text{space} = 35 \text{ ft}$   
 $FI = 800^\circ\text{F-days}$   
 $\text{Precip} = 35 \text{ in}$   
 $\text{Age} = 13 \text{ yr}$   
 $\text{Basetype} = 1$



1 ft=0.3m;  $1^\circ\text{F-days}=0.555^\circ\text{C-days}$ ;  $1 \text{ lb/in}^2=6.9 \text{ kPa}$ ;  $1 \text{ in}=25.4 \text{ mm}$

Figure 8. Sensitivity plot of the doweled faulting model with ESAL applications and bearing stress.

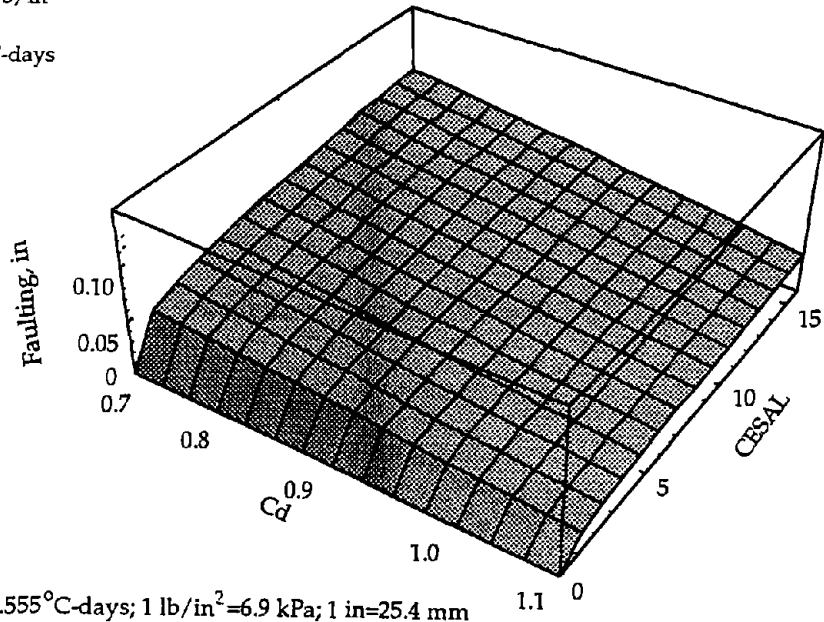
$C_d = 0.9$   
 $B\text{stress} = 2000 \text{ lb/in}^2$   
 $FI = 800^\circ\text{F-days}$   
 $\text{Precip} = 35 \text{ in}$   
 $\text{Age} = 13 \text{ yr}$   
 $\text{Basetype} = 1$



1 ft=0.3m;  $1^\circ\text{F-days}=0.555^\circ\text{C-days}$ ;  $1 \text{ lb/in}^2=6.9 \text{ kPa}$ ;  $1 \text{ in}=25.4 \text{ mm}$

Figure 9. Sensitivity plot of the doweled faulting model with ESAL applications and joint spacing.

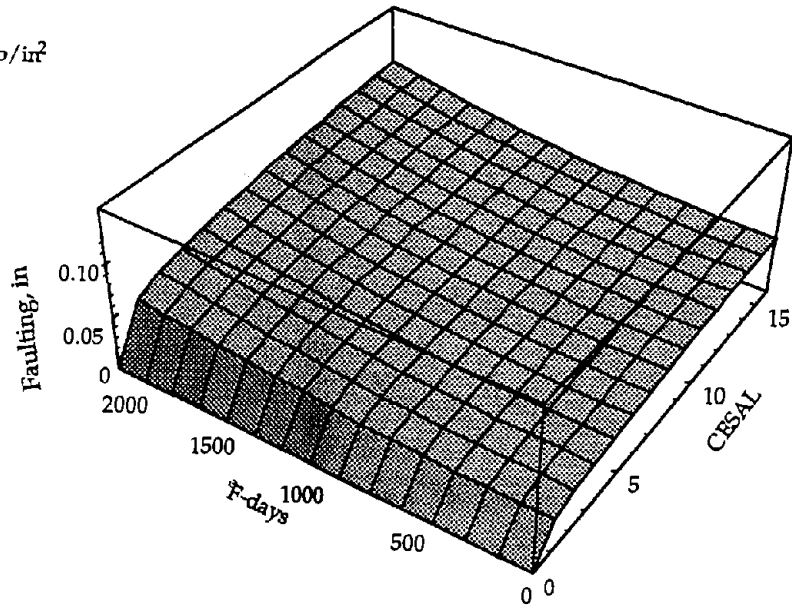
Bstress = 2000 lb/in<sup>2</sup>  
 Jtspace = 35 ft  
 FI = 800° F-days  
 Precip = 35 in  
 Age = 13 yr  
 Basetype = 1



1 ft=0.3m; 1° F-days=0.555° C-days; 1 lb/in<sup>2</sup>=6.9 kPa; 1 in=25.4 mm

Figure 10. Sensitivity plot of the doweled faulting model with ESAL applications and  $C_d$ .

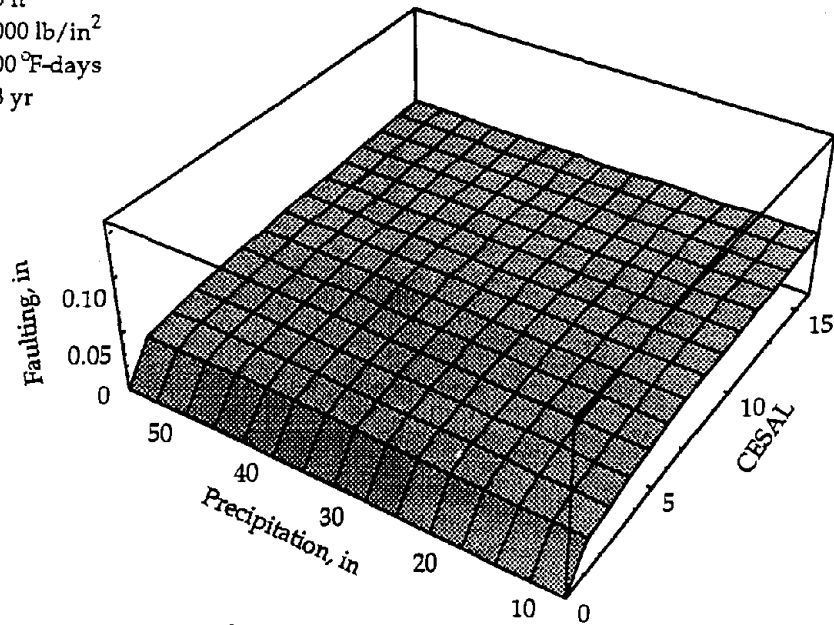
$C_d = 0.9$   
 Jtspace = 35 ft  
 B stress = 2000 lb/in<sup>2</sup>  
 Precip = 35 in  
 Age = 13 yr  
 Basetype = 1



1 ft=0.3m; 1° F-days=0.555° C-days; 1 lb/in<sup>2</sup>=6.9 kPa; 1 in=25.4 mm

Figure 11. Sensitivity plot of the doweled faulting model with ESAL applications and freezing index.

$C_d = 0.9$   
 $J_{tspace} = 35 \text{ ft}$   
 $B_{stress} = 2000 \text{ lb/in}^2$   
 $FI = 800^\circ\text{F-days}$   
 $\text{Age} = 13 \text{ yr}$   
 $\text{Basetype} = 1$



1 ft=0.3m;  $1^\circ\text{F-days}=0.555^\circ\text{C-days}$ ;  $1 \text{ lb/in}^2 = 6.9 \text{ kPa}$ ; 1 in=25.4 mm

Figure 12. Sensitivity plot of the doweled faulting model with ESAL applications and mean annual precipitation.

The faulting model is developed for the range of pavement designs included in the data base as shown in figure 5. Therefore, this model should only be used in the range of each of the variables used in the model.

As shown by the model, several design variables including CESAL's, drainability, joint spacing, dowel diameter, widened lane, base type, and climate conditions significantly affect the faulting of doweled joints. Based on the results of the model, the following design features reduce faulting:

- Large dowel bar size, which results in smaller bearing stress.
- Improved drainability (e.g., edge drains or permeable base).
- Widened lane (most in data base were 2 ft [0.61 m] wide).
- Shorter transverse joint spacing.
- Stabilized base (cement, asphalt).

### Joint Faulting Model for Nondoweled Jointed Concrete Pavements

In nondoweled transverse joints, load transfer is accomplished through aggregate interlock of the abutting joint faces. However, under heavy traffic loadings and under certain environmental conditions, aggregate interlock can become ineffective, leading to pumping and faulting. This section describes the development of the model for faulting of nondoweled pavements.

## Preliminary Data Analysis

The factorial matrix showing the distribution of pavement sections used in the development of the nondoweled joint faulting model is provided in table 5. This table shows a fairly good representation of stabilized base sections in all climatic regions, although there are no sections with joint spacing less than 20 ft (6.1 m) joints in dry-freeze region. Sections with nonstabilized bases are less well represented, with the majority of those sections located in the wet-freeze region.

Table 5. Distribution of the pavement sections used in the development of nondoweled joint faulting model.

Climate Region	Nonstabilized Base		Stabilized Base	
	Joint Spacing $\leq$ 20 ft	Joint spacing $>$ 20 ft	Joint spacing $\leq$ 20 ft	Joint spacing $>$ 20 ft
Wet-Freeze	17	7	19	4
Wet-Nonfreeze	0	4	22	11
Dry-Freeze	2	2	0	0
Dry-Nonfreeze	6	0	37	0

Note: 1 ft = 0.305 m

## Explanatory Variable Initially Selected

As in the development of the transverse joint faulting model for doweled pavements, the independent variable for nondoweled pavements is the average faulting in inches (FaultND). Based on previous studies, the following variables were initially selected to be used in the model development:<sup>(3,10-13,19)</sup>

- CESAL: Cumulative 18-kip (80-kN) equivalent single axle loads, millions.
- Age: Time since construction, years.
- Jointspace: Mean transverse joint spacing, ft.
- Slabthick: PCC slab thickness, in.
- Basetype: Base type (0 = nonstabilized base; 1 = stabilized base).
- Baseperm: Base permeability (0 = not permeable, 1 = permeable).
- Widenlane: Widened lane (0 = not widened, 1 = widened).
- Cut: Percent of the section length located in an area of cut.
- Fill: Percent of the section length located in an area of fill.
- Edgesup: Edge support (1 = tied concrete shoulder; 0 = otherwise).
- C<sub>d</sub>: AASHTO drainage coefficient, calculated from data base information.
- DRAIN: Drainage provisions (0 = no subdrainage; 1 = subdrainage).
- Soiltype: Subgrade soil type (0 = fine-grained; 1 = coarse-grained).
- Kstatic: Static backcalculated k-value, lb/in<sup>2</sup>/in.

Jtopen:	Calculated joint opening, in.
Days32:	Number of the days with minimum temperature below 32 °F (0 °C).
Trange:	Annual temperature range, °F.
FTcycle:	Average number of annual freeze-thaw cycles.
FI:	Mean annual freezing index, degree-days.
Precip:	Mean annual precipitation, in.
MI:	Thornthwaite moisture index.

The magnitude of the corner deflection was also considered in the development of the model. This factor was calculated from the following formula:<sup>(20)</sup>

$$\text{Corner Defl.} = P * (1.2 - 0.88 * 1.4142 * a / \ell) / (K_{\text{static}} * \ell^2) \quad (5)$$

where:

P = Applied wheel load, set to 9000 lb (40-kN).

$\ell$  = Radius of relative stiffness, as defined in equation (2).

a = Radius of the applied load, set to 5.64 in (143 mm), assuming a tire pressure of 90 lb/in<sup>2</sup> (621 kPa).

K<sub>static</sub> = Static backcalculated k-value, lb/in<sup>2</sup>/in.

### Model Development

Figure 13 contains the two-dimensional plots generated between the dependent variable and the selected independent variables. The same modeling development procedure used for doweled pavements was followed in the development of the nondoweled faulting model.

The model selected for transverse nondoweled joint faulting is as follows:

$$\begin{aligned} \text{FaultND} = & \text{CESAL}^{0.25} * [0.2347 - 0.1516 * C_d - 0.000250 * \text{Slabthick}^2 / \text{Jtspace}^{0.25} \quad (6) \\ & - 0.0115 * \text{Basetype} + 0.7784 * 10^{-7} * \text{FI}^{1.5} * \text{Precip}^{0.25} \\ & - 0.002478 * \text{Days90}^{0.5} - 0.0415 * \text{Widenlane}] \end{aligned}$$

N = 131 sections.

R<sup>2</sup> = 0.45.

RSE = 0.034 in (0.86 mm).

where:

CESAL = cumulative 18-kip (80-kN) equivalent single axle loads, millions.

Jtspace = Mean transverse joint spacing, ft.

Slabthick = PCC slab thickness, in.

Basetype = Base type (0 = nonstabilized base; 1 = stabilized base).

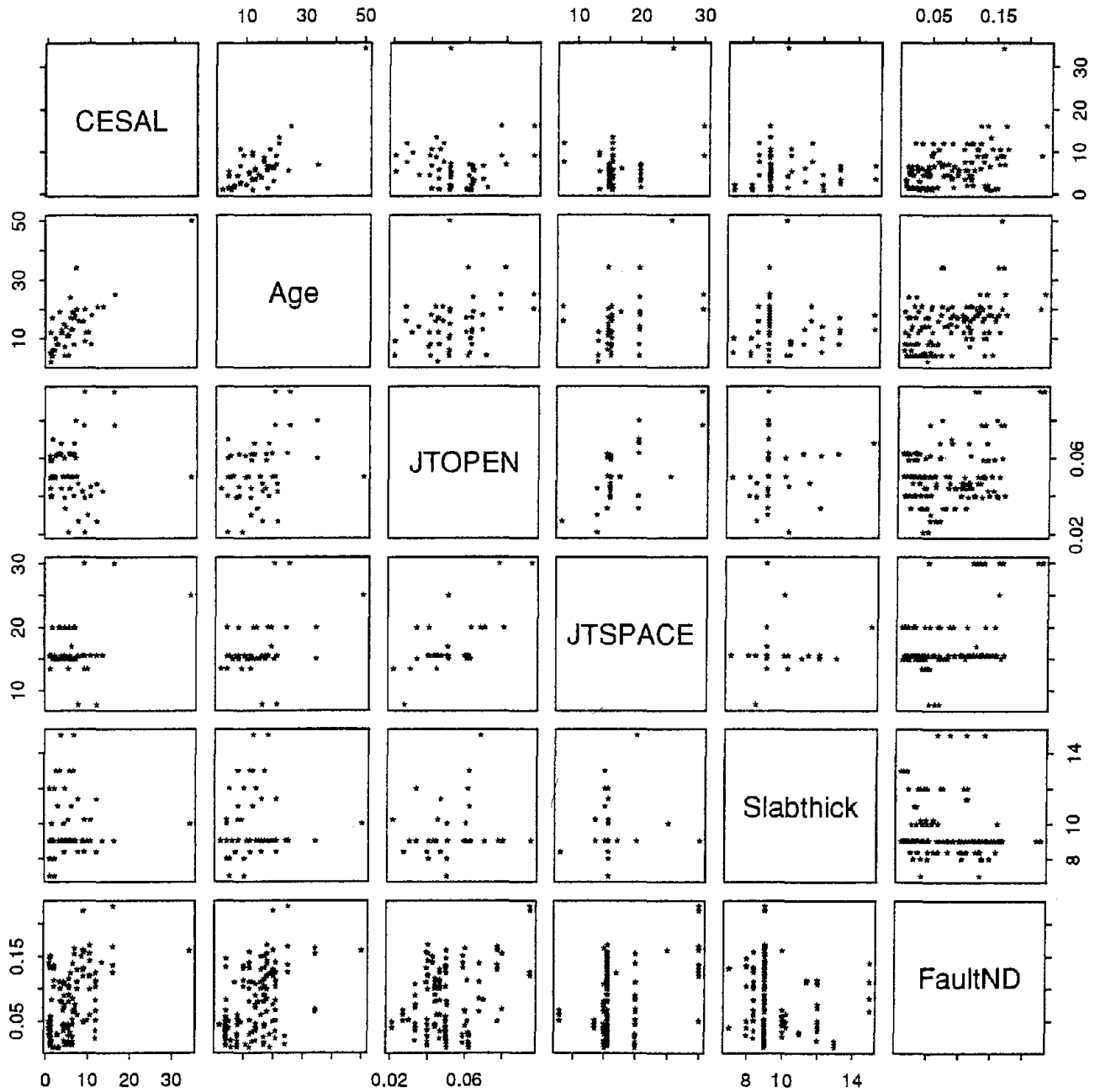


Figure 13. Two-dimensional scatter plot for nondoweled joint faulting model.



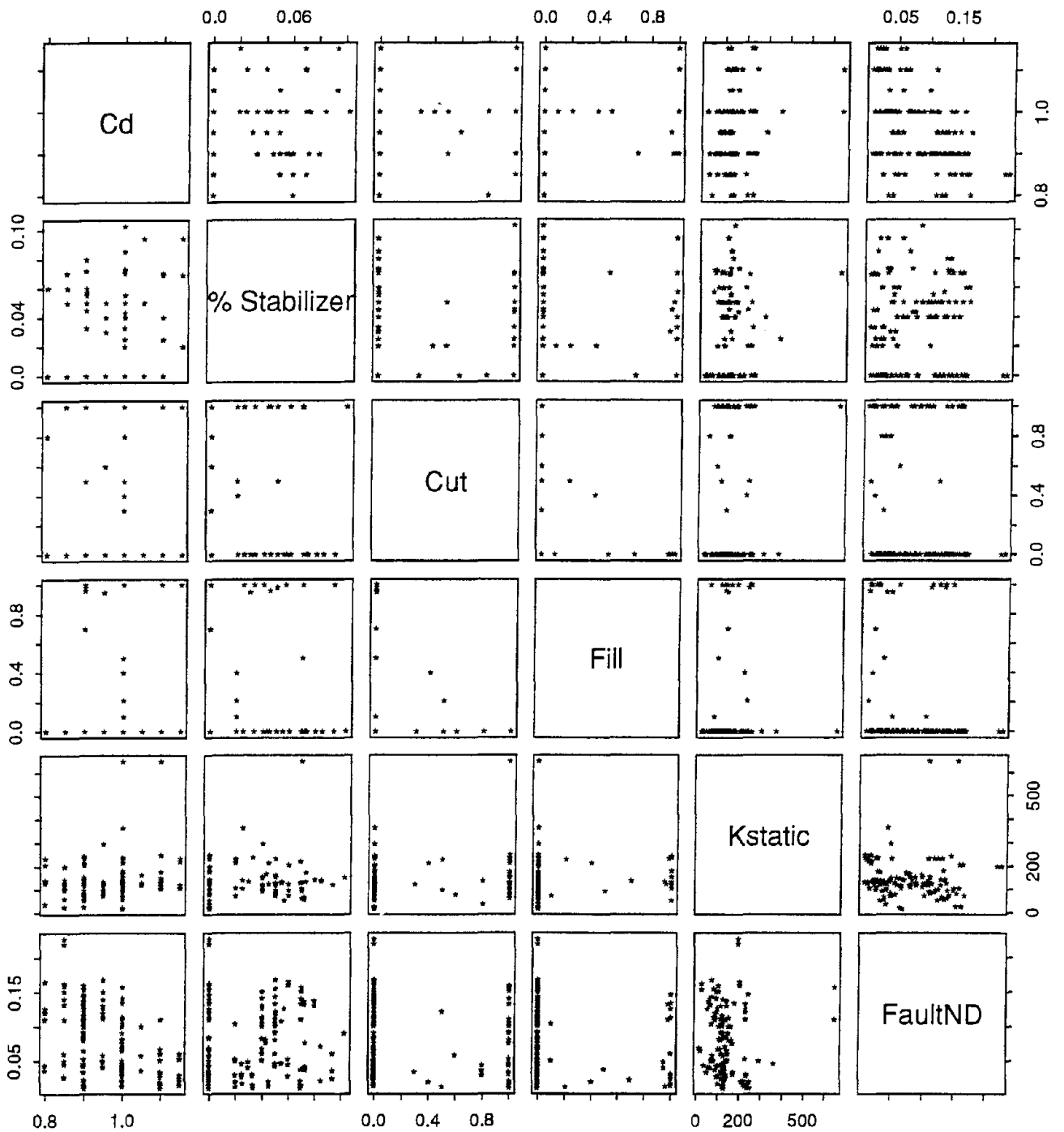


Figure 13. Two-dimensional scatter plot for nondoweled joint faulting model (continued).

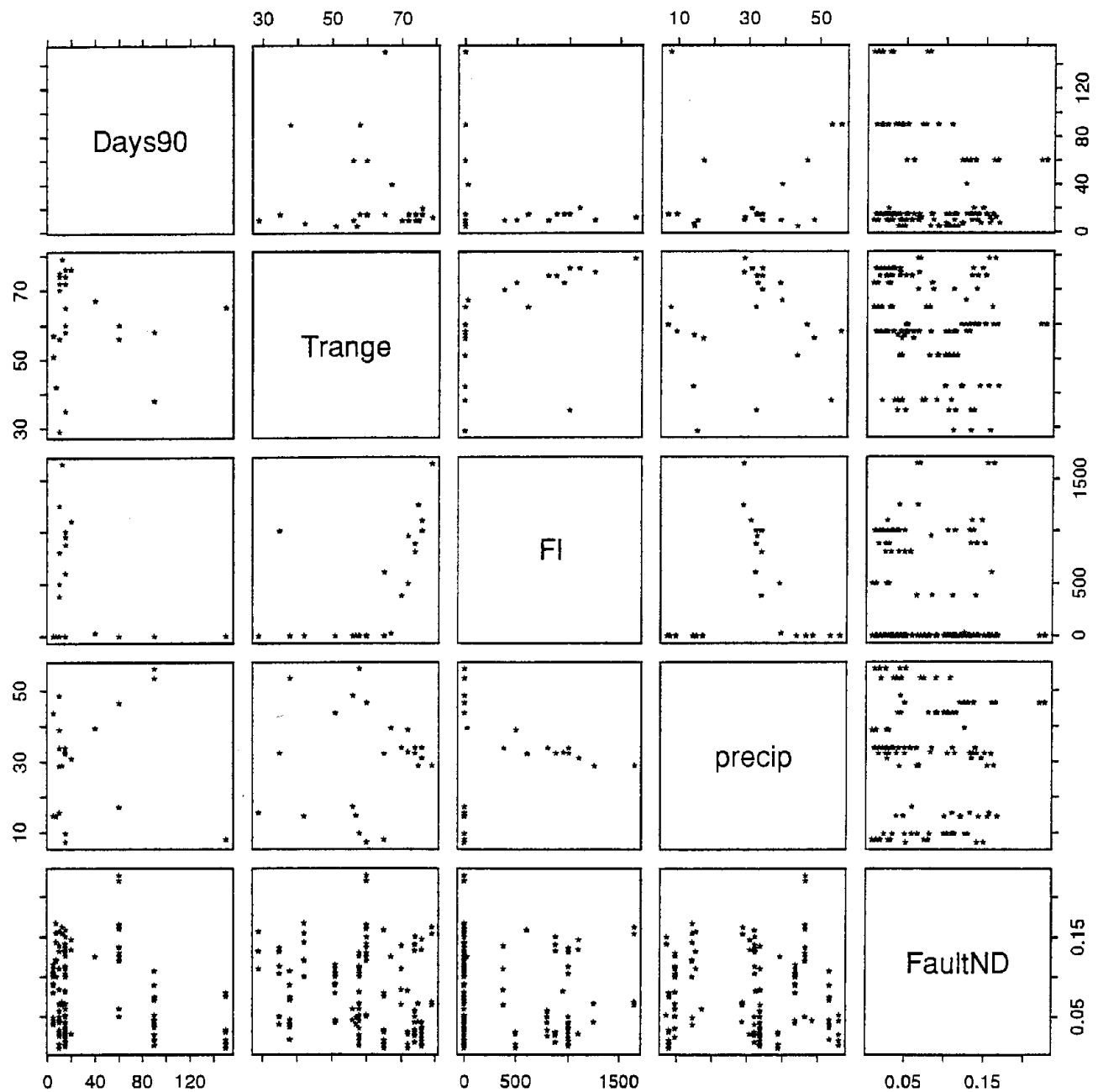


Figure 13. Two-dimensional scatter plot for nondoweled joint faulting model (continued).

Widenlane = Widened lane (0 = not widened, 1 = widened).

$C_d$  = Modified AASHTO drainage coefficient, calculated from data base.

FI=Mean annual freezing index, degree-days.

Precip = Mean annual precipitation, in.

The estimate of each coefficient in the equation, along with the associated SEE and p-value are provided in table 6. As shown in the table, all the estimates of the coefficients are significant at the  $\alpha = 0.10$  level, with reasonably small SEE, except for the FI and Precip term.

Table 6. Estimates of the coefficients and the associated SEE and P-values for nondoweled joint faulting model.

Terms	Value	SEE	P-value (>  t )
Intercept	0.2347	0.0239	<0.0001
Cd	-0.1516	0.0253	<0.0001
Basetype	-0.0115	0.0066	0.0861
Slabthick <sup>2</sup> /Jtspace <sup>0.25</sup>	-0.0250	0.0145	0.0876
FI <sup>1.5</sup> *Precip <sup>0.25</sup> *10 <sup>-7</sup>	0.7784	0.7180	0.2805
Days90 <sup>0.5</sup> *10 <sup>-2</sup>	-0.2478	0.0786	0.0020
Widenlane	-0.0415	0.0069	<0.0001

The plot of actual faulting versus predicted faulting is shown in figure 14, and the plot of the residual versus the predicted faulting plot is given in figure 15. The sensitivity plots of the key variables in the model are provided in the figures 16 through 21.

The sensitivity plots illustrate that, similar to the doweled joint faulting model, nondoweled joint faulting increases rapidly at first and then levels off. Figure 16 gives the sensitivity plot of the nondoweled joint faulting with CESAL and slab thickness, and it shows that as slab thickness increases, faulting decreases. As shown in figure 17, faulting increases with increasing joint spacing. The sensitivity plot of faulting with CESAL and drainage coefficient,  $C_d$ , is provided in figure 18 showing a clear trend of decreasing faulting with increasing  $C_d$  (indicating an improvement in drainage conditions).

Figures 19, 20, and 21 represent the effect of the climatic factors on the faulting. As freezing index increases, or as the number of the days above 90 °F (32 °C) decreases (colder region), faulting increases. Faulting also is observed to increase with increasing level of annual precipitation.

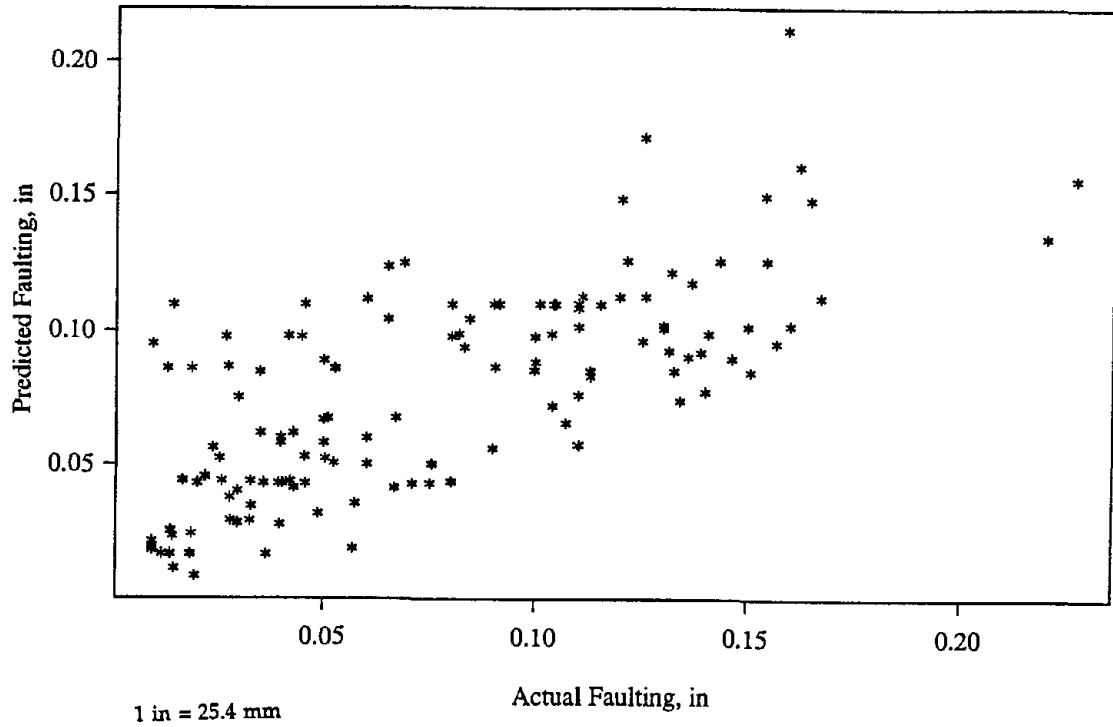


Figure 14. Actual versus predicted faulting for the nondoweled faulting model.

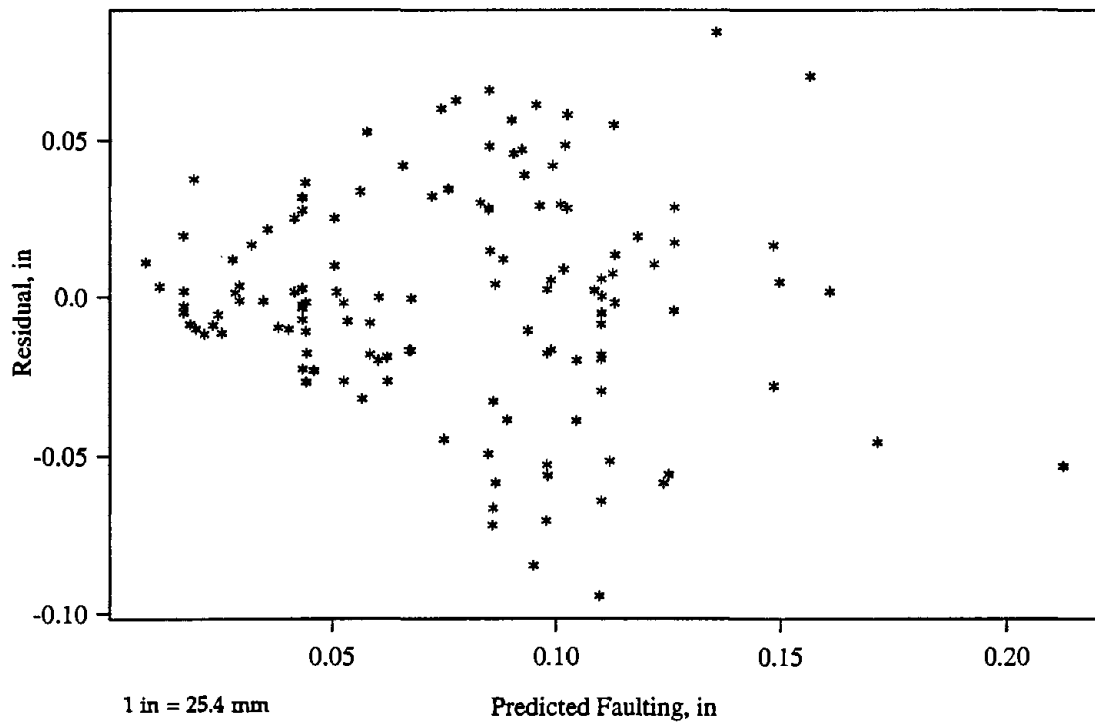


Figure 15. Predicted versus residual for the nondoweled faulting model.

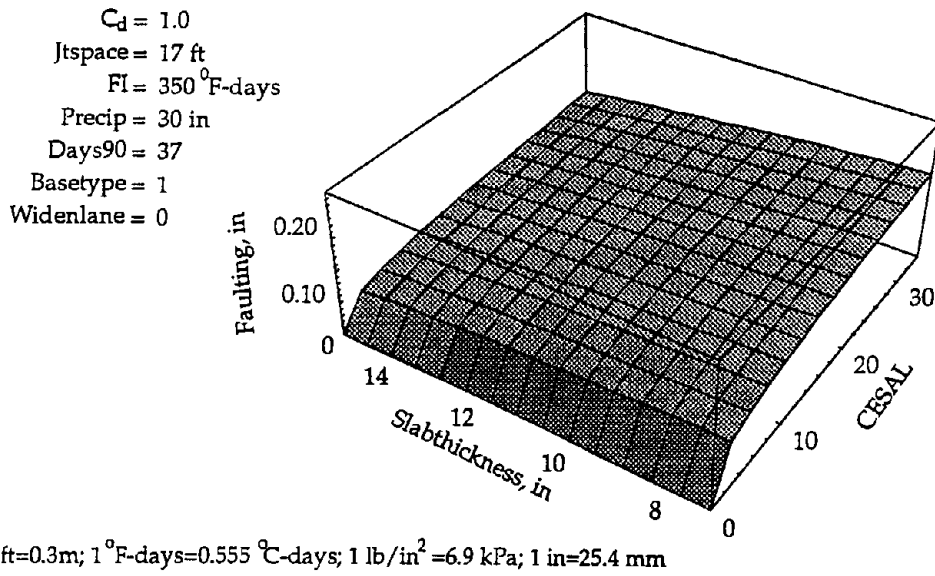


Figure 16. Sensitivity plot of the nondoweled faulting model with ESAL applications and slab thickness.

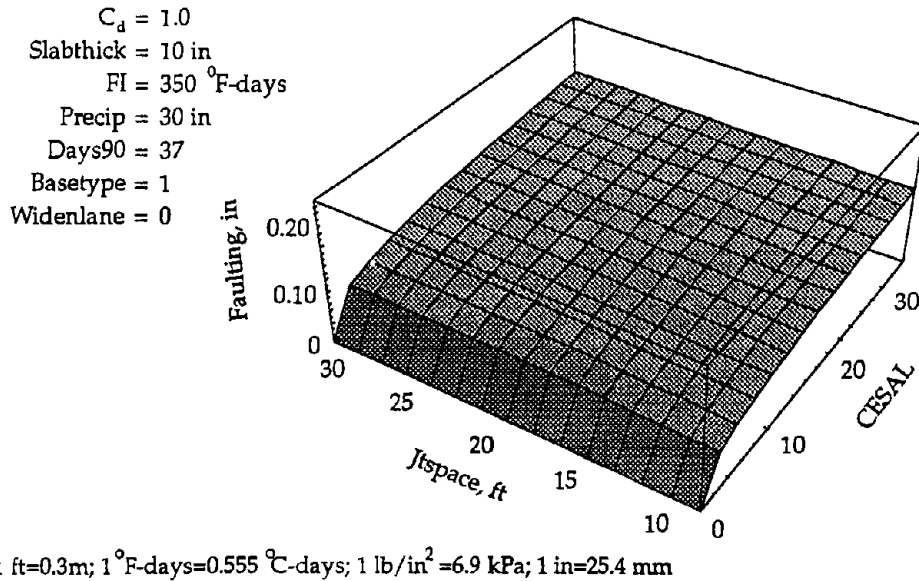


Figure 17. Sensitivity plot of the nondoweled faulting model with ESAL applications and joint spacing.

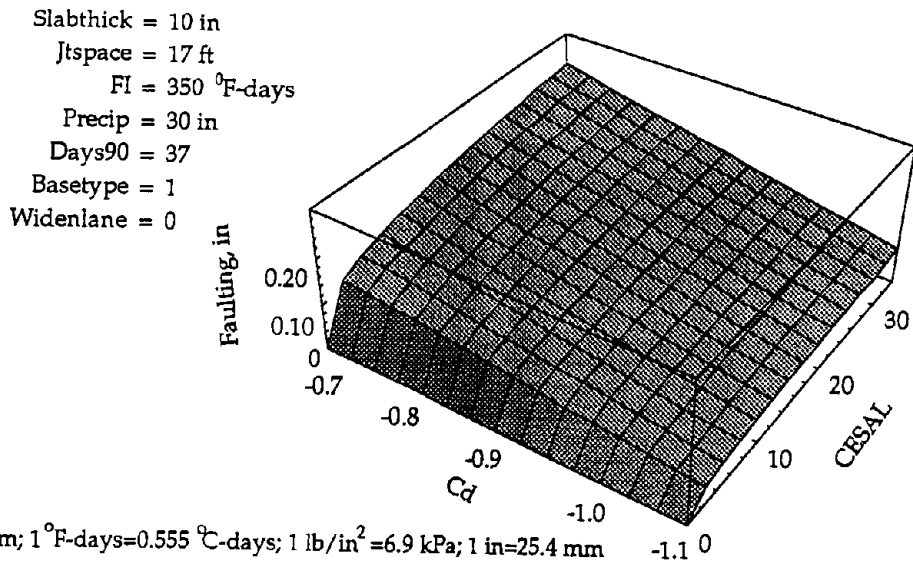


Figure 18. Sensitivity plot of the nondoweled faulting model with ESAL applications and  $C_d$ .

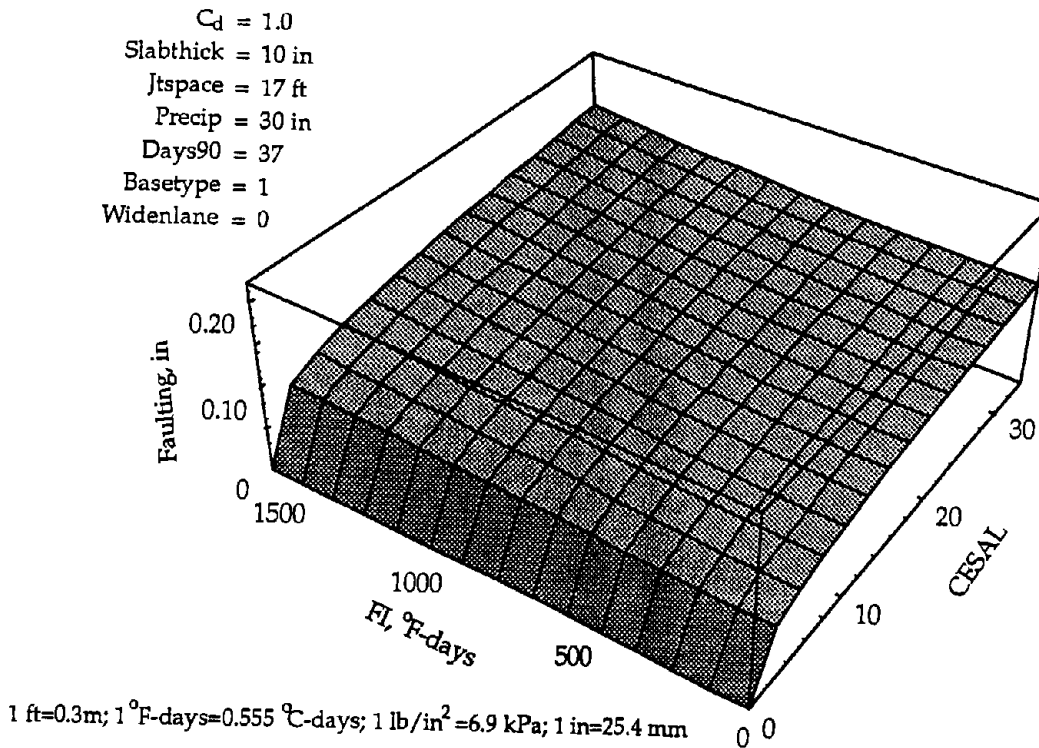
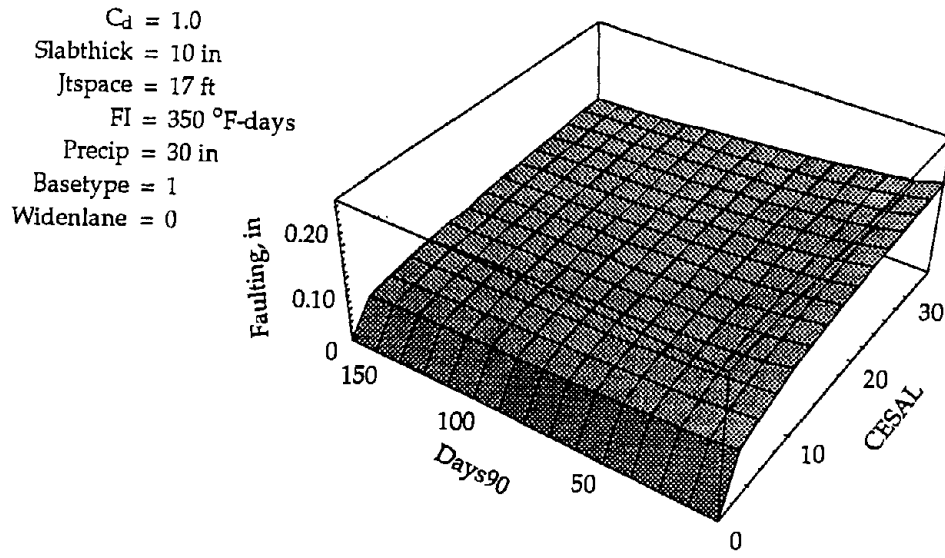
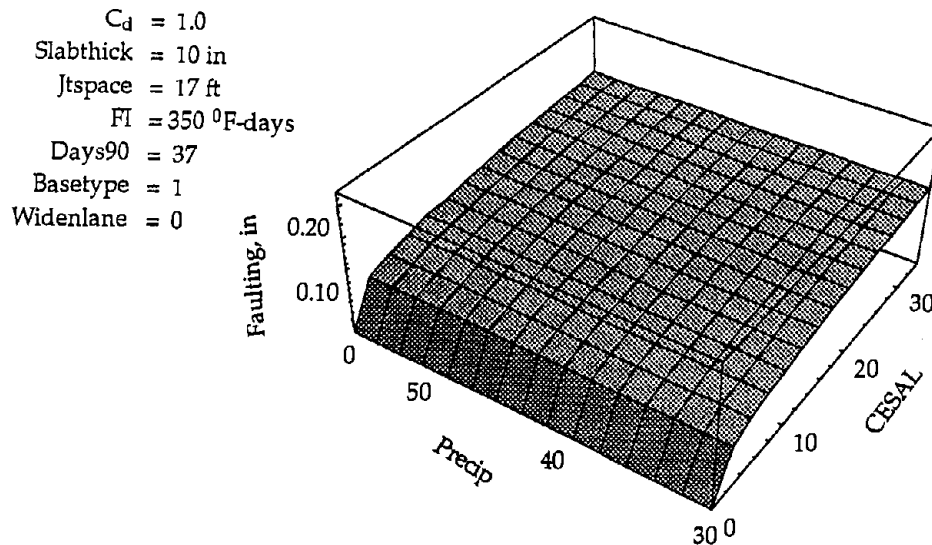


Figure 19. Sensitivity plot of the nondoweled faulting model with ESAL applications and freezing index.



1 ft=0.3m; 1 °F-days=0.555 °C-days; 1 lb/in<sup>2</sup>=6.9 kPa; 1 in=25.4 mm

Figure 20. Sensitivity plot of the nondoweled faulting model with ESAL applications and the number of the days above 90 °F (32 °C).



1 ft=0.3m; 1 °F-days=0.555 °C-days; 1 lb/in<sup>2</sup>=6.9 kPa; 1 in=25.4 mm

Figure 21. Sensitivity plot of the nondoweled faulting model with ESAL applications and annual precipitation.

The main variables significantly affecting nondoweled faulting include ESAL's, drainability, joint spacing, widened lane, base type, and climatic conditions. For nondoweled pavements, it is recommended to use the following design features in order to reduce faulting:

- Improved drainability (e.g., use of edge drain or permeable base).
- Use of stabilized base.
- Use of widened outside lane.
- Shorter joint spacing.
- Thicker concrete slab.

If the predicted faulting for nondoweled pavement is excessive, the use of dowels should be considered.

### **Transverse Cracking Model for JPCP**

Transverse cracking in concrete pavements can occur as a result of either very high stresses in the slabs or fatigue failure. The high stress levels are usually caused by the combined effects of the restraint forces (the restraint against the contraction of PCC in response to either shrinkage or temperature change), thermal curling, moisture warping, and traffic loads. Most of the cracking from these mechanisms occur soon after construction, and concrete pavements are designed to either accommodate such cracking or avoid them all together. For example, a certain amount of transverse cracking is expected in JRCP and CRCP, and reinforcing steel is provided to hold the cracks tightly together. On JPCP, contraction joints are provided at close intervals to prevent the development of any midpanel cracks resulting from the development of excessive restraint forces. Hence, whether or not the cracking from the excessive stress mechanism will be allowed is a design choice, and modeling of this distress mechanism is not warranted.

Fatigue cracking, on the other hand, is a key measure of concrete pavement performance and is a critical item for consideration in the design of concrete pavements. Fatigue cracking is caused by the repeated application of traffic and environmental loading at stress levels less than ultimate. As the loadings are repeated over time, cracking can occur in the slab. The keys to this analysis include the following:

- The accurate determination of stresses in the slab (both traffic and environmentally induced stresses).
- The identification of the critical location in the slab where stresses are greatest.
- The accurate prediction of fatigue damage using a reliable fatigue damage model.

The development of a JPCP fatigue cracking model based on the performance of 144 JPCP sections surveyed under this project is documented in this section. Also documented are the procedures used to determine the accumulated fatigue damage in the slabs. The fatigue cracking model developed under this project gives the



expected amount of slab cracking as function of the accumulated fatigue damage in the slabs. Therefore, in using this model, it is important that the expected fatigue damage is determined accurately using a procedure that is consistent with the one used in the development of the model. The accumulated fatigue damage was determined considering load stress, slab curling, and lateral distribution of traffic in developing the cracking model. The details of how these factors were considered in the damage calculations and how these data were used to develop the fatigue cracking model are presented in the following sections.

### Data Reduction.

The preparation of the input data for the model development is described in this section. The cracking model developed under this project is a function of a single independent parameter, the accumulated fatigue damage, but the determination of the accumulated fatigue damage requires the consideration of a number of additional factors, including traffic, slab design factors, material properties, and climatic factors. The dependent variable in this model is the amount of slab cracking represented in terms of percent slabs cracked. The process of gathering and reducing all of the information needed to perform the necessary analyses are presented below.

#### *Cracking Data*

The distribution of the JPCP sections and designs used in the development of the fatigue cracking model is given in table 7. This table represents 578 data points obtained from 143 JPCP sections. The number of data points is greater than the number of sections because each slab length in the sections with random joint spacing (e.g., 12-13-19-18 ft [3.7-4.0-5.8-5.5 m]) was considered individually, and because 1987 data for 53 original sections are included.

#### *Traffic Data*

To determine the amount of fatigue damage accumulated at the critical damage location, three traffic factors are needed:

- Axle weights.
- Number of traffic passes.
- Lateral traffic wander.

The information regarding the lateral placement of the axle load is important because the edge load stress developed in concrete slabs is highly sensitive to how close the wheel load is placed to the edge of the slab. The edge loading condition is often the critical case in which stresses are the greatest.

The most accurate assessment of the accumulated fatigue damage may be made if the exact lateral placement and axle weights are known for each passing axle. However, such detailed data are not available, and the collection of traffic data to this

Table 7. Distribution of the JPCP sections and designs used in the development of fatigue cracking model.

Climatic Region	Base Type	Thickness < 9.0 in		Thickness = 9.0 in		Thickness > 9.0 in	
		Jt Spc <= 15 ft	Jt Spc > 15 ft	Jt Spc <= 15 ft	Jt Spc > 15 ft	Jt Spc <= 15 ft	Jt Spc > 15 ft
Wet Freeze	Stabilized	14	14	40	48	0	12
	Nonstabilized	4	4	30	44	25	31
Wet Nonfreeze	Stabilized	0	0	30	54	0	8
	Nonstabilized	0	0	0	6	4	4
Dry Freeze	Stabilized	0	0	0	0	0	0
	Nonstabilized	8	8	8	8	0	0
Dry Nonfreeze	Stabilized	40	28	32	22	22	12
	Nonstabilized	0	0	0	0	12	6
Total		66	54	140	182	63	73

1 in = 25.4 mm

1 ft = 0.305 m

level of accuracy may not be warranted given the level of accuracy and variabilities associated with other data involved in the stress calculations.

A reasonable approach to characterizing traffic for fatigue analysis is to use the number of axles at each weight category for each axle type to account for the axle weights and the number of applications (as done in W-4 tables), and to describe the lateral placement of axles using the mean wheel location and standard deviation. This approach has the advantage of directly accounting for the damage caused by mixed traffic rather than using an empirical relationship to first convert the effects of mixed traffic to some equivalent standard measure and then determining the damage caused by the applied traffic.

The next level of approximation is to convert the traffic to the number of 18-kip (80-kN) ESAL applications and assume that a certain fraction of the traffic passes actually pass close enough to the pavement edge to cause the critical edge loading condition. This was done under the preceding FHWA study on concrete pavement performance in which the accumulated number of 18-kip (80-kN) ESAL applications was determined for each JPCP section.<sup>(3)</sup> The edge loading condition was assumed to occur about 5 percent of the time based on the findings of field studies.

The use of the ESAL concept was retained in this study because adequate historical data could not be obtained that would allow the use of load spectra. As

done in the preceding study, the number of 18-kip (80-kN) ESAL applications was determined for each JPCP section and used in the fatigue damage calculations. The use of ESAL's allowed the distress and traffic data from the 1987 study to be used directly in this project.

The effects of the lateral traffic wander was given a more rigorous statistical treatment in this study. Assuming that the lateral wander of traffic is normally distributed, the probable lateral distribution of the traffic wheels was determined. Then, considering the contribution to the fatigue damage at the critical location (longitudinal edge for all normal-width sections) by traffic passing through any point and the probability that the traffic will pass through that point, the pass to coverage (p/c) ratio was determined.

The p/c is simply the ratio that gives the number of traffic passes needed to produce the same amount of fatigue damage at the critical location as one pass that causes the critical loading condition (i.e., edge loading condition). The number of fatigue loading cycles (or coverage) that the applied traffic causes is the number traffic passes divided by p/c. For example, if the p/c is 100, this means that it takes 100 traffic passes to cause the same amount of damage as 1 load placed directly at the edge.

The p/c as described here may be expressed mathematically as follows:

$$p/c = \frac{FD_{D_{ii}}}{\sum_j P(COV_{D_j}) * FD_{D_{ij}}} \quad (7)$$

where:

- $FD_{D_{ii}}$  = Fatigue damage at location  $D_i$  due to the load at  $D_i$ .
- $P(COV_{D_j})$  = Probability that the load will pass through location  $D_j$ .
- $FD_{D_{ij}}$  = Fatigue damage at location  $D_i$  due to the load at  $D_j$ .

The specific details on how the p/c was calculated is discussed later under the subheading *Pass to Coverage Ratio*.

### *Material Properties*

The material properties of interest for the fatigue damage determination include the following:

- Subgrade modulus of reaction, k.
- PCC modulus of elasticity, E.
- PCC modulus of rupture, MR.

The subgrade  $k$  and the PCC modulus of elasticity backcalculated from the FWD testing results were used in this analysis. The procedure for obtaining these values have been previously described, and the results are given in the project summary tables presented in volume IV.

The material testing program under this project included core testing on selected sections. The cores were tested in split tensile to determine the MR. While cores were retrieved from many sections, not all JPCP sections could be tested. An attempt was made to obtain the missing data from the project reports and also by requesting the information from the States, but the MR values could not be obtained for a considerable number of sections.

One way to obtain the missing MR data is to estimate the MR from backcalculated  $E$  using the following empirical correlation:<sup>(21)</sup>

$$MR = 43.5 \left( \frac{E}{10^6} \right) + 488.5 \quad (8)$$

where:

MR = PCC modulus of rupture, lbf/in<sup>2</sup>.

$E$  = Backcalculated PCC modulus of elasticity, lbf/in<sup>2</sup>.

A comparison of the MR values obtained using equation 8 and from core testing is given in figure 22. As shown in this figure, the MR values estimated from the backcalculated  $E$  represent a reasonable average of the values obtained by core testing. The MR values determined from core testing results are also an indirect measure, and the correlation between the split tensile strength and MR can be quite dependent on PCC mix design. Also, the core testing results are based on very limited number of samples (typically 2 per section), leaving the possibility that the testing results may not be representative of the majority of the material in place. Since equation 8 seems to give a reasonable estimate of MR values, the MR values determined from the backcalculated  $E$  were used in all cases for consistency.

### *Climatic Factors*

The climatic factor that has the most significant effect on fatigue cracking in JPCP is when there is a significant difference between the temperature of the top and bottom of the slab. This temperature difference is often referred to as a thermal gradient, which may either be positive (the top of the slab is warmer than the bottom) or negative (the top of the slab is cooler than the bottom). A positive thermal gradient causes the top to curl downward as the slab of the slab expands; this curling is resisted by the weight of the slab, which creates a maximum tensile stress at the bottom of the slab midway between the joints. A negative thermal

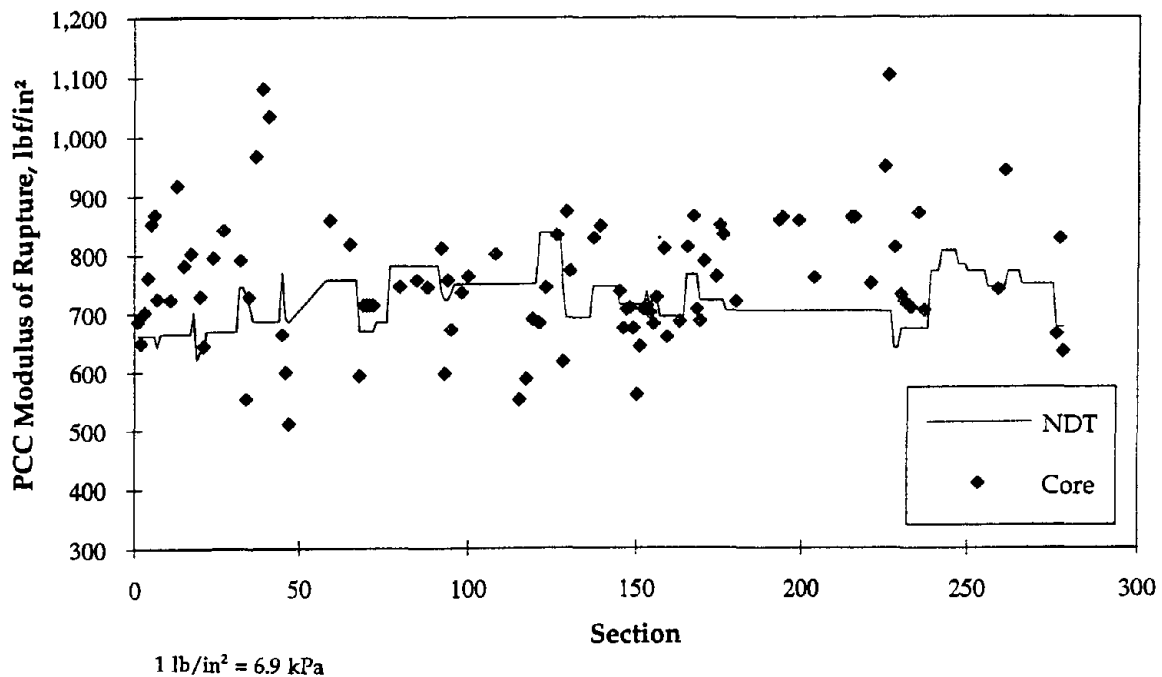


Figure 22. Comparison of PCC MR obtained by nondestructive testing and core testing.

gradient, on the other hand, causes the corners of the slab to curl upward as the top of the slab contracts; again, this curling is resisted by the weight of the slab and thereby creates a maximum tensile stress at the top of the corner region of the slab.

The curling of the pavement slabs caused by the differences in temperatures between the top and bottom of the slabs can dramatically increase the critical stresses in concrete slabs. Depending on the magnitude of the temperature gradient, curling stresses can often equal or exceed load stresses, and when combined with load stress, the resulting stresses can well exceed the concrete MR if transverse joints are not provided at appropriate intervals to alleviate the curling stresses.

The primary factors that affect the magnitude of temperature gradients include air temperature, wind speed, and the amount of time the slabs are exposed to sun. Depending on these factors, the temperature gradient in the pavement slabs change continuously throughout the day. To adequately account for the effects of temperature gradients, hourly temperature gradient data for the entire year from the representative years are needed. Collection of such vast amounts of data is not practical, but a computer program is available that can generate the needed data based on readily-available climatic data. The CMS model considers the climatic factors and material properties to determine through-thickness temperature gradients.<sup>(22)</sup>

Using CMS, the distribution of hourly temperature gradients through concrete slabs for the average year were determined for each pavement section based on 30-year average climatic data. Examples of temperature gradients from the CMS runs are shown in figures 23 through 25. The temperature gradients determined for all of the sections included in this study are given in table 8. In determining the accumulated fatigue damage for each section, the complete temperature distribution data for that section were used to account for the effects of slab curling.

### Stress Calculation

The stress of interest in a fatigue analysis is the maximum tensile stress at the critical damage location. To perform the analysis, the critical damage location must first be determined, and then the combined stress at that location determined considering all factors that significantly affect stresses. In general, the critical damage location is the location in the slab where the maximum stress occurs. The factors that cause stresses in pavement slabs include traffic loads, temperature gradients, moisture gradients, and various factors that cause uniform expansion or contraction of PCC, such as uniform temperature changes and drying shrinkage. In JPCP, because of short joint spacing, the stresses due to the uniform expansion or contraction of PCC are not significant. Therefore, the stress calculation for fatigue analysis involves determining the combined stress due to the traffic loads and slab curling (or warping) at the critical damage location.

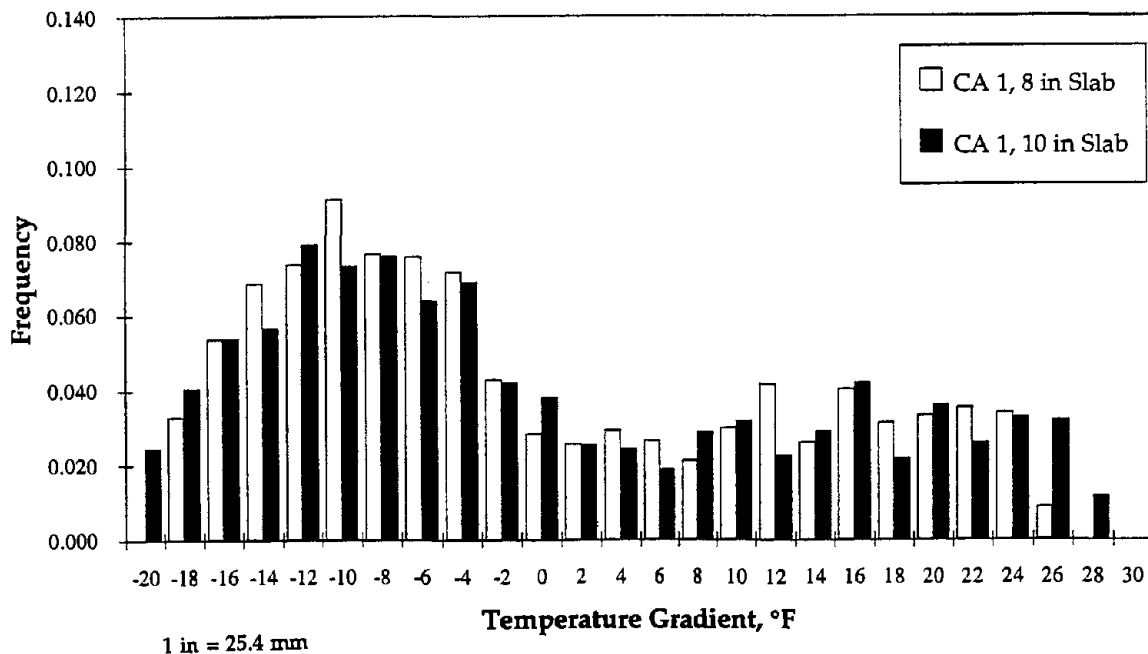


Figure 23. Distribution of hourly temperature gradients for CA 1 sections for an average year.

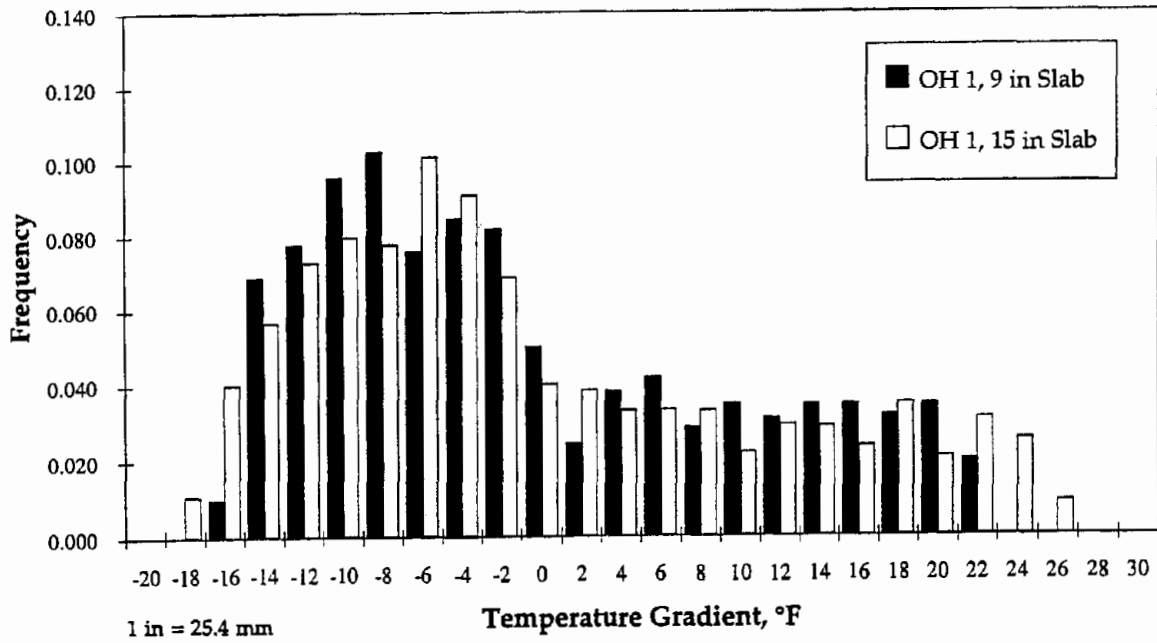


Figure 24. Distribution of hourly temperature gradients for OH 2 sections for an average year.

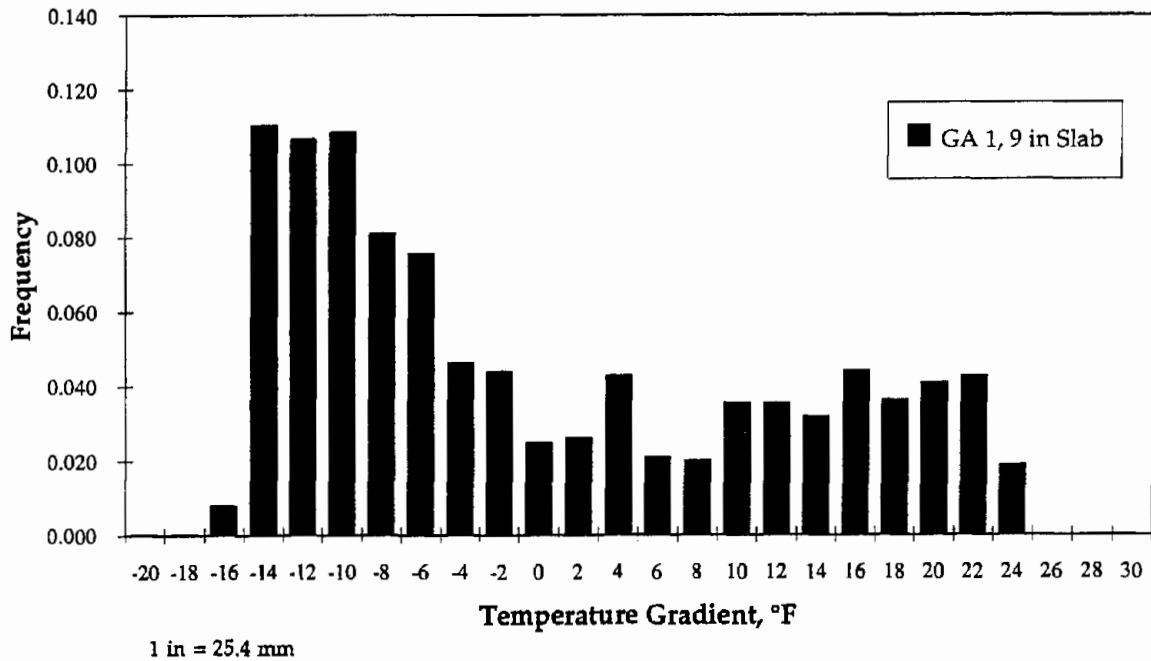


Figure 25. Distribution of hourly temperature gradients for GA 1 sections for an average year.

Table 8. Distribution of hourly temperature gradients.

ΔT °F	Project																							
	az1 9 in	az1 10 in	az1 11 in	az1 13 in	az2 10 in	az2 11 in	az2 12 in	ca1 8 in	ca1 9 in	ca1 10 in	ca1 11 in	ca1 12 in	ca1 13 in	ca1 14 in	ca10 9 in	ca10 10 in	ca11 8 in	ca11 12 in	ca7 10 in	ca11 12 in	ca2 8 in	ca2 10 in	ca2 12 in	
-24	0.000	0.000	0.000	0.000	0.000	0.000	0.000	0.000	0.000	0.000	0.000	0.000	0.000	0.000	0.000	0.000	0.000	0.000	0.000	0.000	0.000	0.000	0.000	0.000
-22	0.000	0.000	0.000	0.000	0.000	0.000	0.000	0.000	0.000	0.000	0.005	0.010	0.013	0.015	0.000	0.000	0.000	0.014	0.000	0.014	0.000	0.000	0.000	0.000
-20	0.000	0.000	0.006	0.016	0.000	0.006	0.011	0.000	0.009	0.024	0.025	0.027	0.028	0.030	0.000	0.007	0.001	0.035	0.035	0.035	0.000	0.000	0.000	0.000
-18	0.020	0.058	0.068	0.071	0.058	0.068	0.077	0.033	0.041	0.040	0.043	0.046	0.042	0.038	0.030	0.036	0.045	0.039	0.039	0.039	0.000	0.000	0.000	0.000
-16	0.097	0.086	0.079	0.073	0.086	0.079	0.073	0.054	0.056	0.054	0.050	0.047	0.046	0.045	0.049	0.051	0.049	0.042	0.045	0.042	0.000	0.028	0.066	0.066
-14	0.097	0.091	0.088	0.077	0.091	0.088	0.085	0.069	0.060	0.057	0.059	0.060	0.061	0.062	0.061	0.053	0.062	0.059	0.058	0.059	0.095	0.120	0.105	0.105
-12	0.098	0.077	0.071	0.063	0.077	0.071	0.065	0.074	0.073	0.079	0.074	0.069	0.066	0.062	0.073	0.084	0.063	0.062	0.070	0.062	0.138	0.120	0.106	0.106
-10	0.065	0.070	0.068	0.065	0.070	0.068	0.066	0.091	0.083	0.073	0.070	0.066	0.067	0.068	0.093	0.076	0.092	0.071	0.068	0.071	0.119	0.097	0.082	0.082
-8	0.067	0.068	0.066	0.065	0.068	0.066	0.064	0.077	0.084	0.076	0.076	0.077	0.074	0.071	0.076	0.078	0.076	0.069	0.083	0.069	0.087	0.073	0.075	0.075
-6	0.059	0.055	0.049	0.049	0.055	0.049	0.042	0.076	0.068	0.064	0.065	0.066	0.069	0.072	0.078	0.078	0.080	0.075	0.070	0.075	0.070	0.062	0.056	0.056
-4	0.043	0.037	0.044	0.045	0.037	0.044	0.052	0.072	0.066	0.069	0.067	0.066	0.059	0.052	0.075	0.066	0.072	0.066	0.068	0.066	0.041	0.042	0.043	0.043
-2	0.033	0.035	0.033	0.038	0.035	0.033	0.031	0.043	0.043	0.042	0.040	0.037	0.043	0.049	0.044	0.050	0.050	0.044	0.042	0.044	0.035	0.038	0.042	0.042
0	0.023	0.023	0.027	0.029	0.023	0.027	0.032	0.028	0.031	0.038	0.037	0.037	0.038	0.039	0.042	0.041	0.031	0.034	0.043	0.034	0.023	0.024	0.030	0.030
2	0.025	0.025	0.024	0.026	0.025	0.024	0.022	0.026	0.025	0.026	0.034	0.042	0.037	0.031	0.025	0.029	0.022	0.039	0.021	0.039	0.036	0.026	0.026	0.026
4	0.021	0.024	0.028	0.031	0.024	0.028	0.032	0.029	0.032	0.024	0.018	0.012	0.019	0.026	0.030	0.021	0.028	0.018	0.028	0.018	0.022	0.033	0.026	0.026
6	0.028	0.021	0.017	0.017	0.021	0.017	0.014	0.027	0.024	0.019	0.019	0.018	0.017	0.016	0.025	0.024	0.031	0.019	0.017	0.019	0.024	0.019	0.019	0.019
8	0.016	0.019	0.016	0.012	0.019	0.016	0.012	0.021	0.019	0.029	0.027	0.025	0.028	0.032	0.026	0.035	0.024	0.024	0.031	0.024	0.024	0.017	0.023	0.023
10	0.016	0.018	0.019	0.020	0.018	0.019	0.021	0.030	0.029	0.032	0.032	0.033	0.027	0.021	0.036	0.029	0.027	0.035	0.028	0.035	0.026	0.028	0.027	0.027
12	0.023	0.024	0.028	0.029	0.024	0.028	0.032	0.042	0.032	0.022	0.023	0.024	0.027	0.029	0.030	0.029	0.044	0.025	0.029	0.025	0.028	0.027	0.017	0.017
14	0.029	0.020	0.016	0.017	0.020	0.016	0.013	0.026	0.031	0.029	0.027	0.025	0.026	0.026	0.037	0.036	0.027	0.024	0.028	0.024	0.037	0.022	0.032	0.032
16	0.022	0.027	0.024	0.021	0.027	0.024	0.021	0.041	0.038	0.042	0.039	0.036	0.033	0.030	0.036	0.034	0.027	0.034	0.036	0.034	0.040	0.040	0.033	0.033
18	0.033	0.031	0.032	0.030	0.031	0.032	0.033	0.031	0.027	0.022	0.026	0.031	0.029	0.027	0.038	0.033	0.039	0.032	0.029	0.032	0.050	0.032	0.023	0.023
20	0.033	0.029	0.030	0.028	0.029	0.030	0.030	0.033	0.037	0.036	0.033	0.029	0.033	0.037	0.032	0.036	0.022	0.021	0.021	0.021	0.048	0.046	0.053	0.053
22	0.036	0.030	0.028	0.027	0.030	0.028	0.027	0.035	0.022	0.026	0.027	0.027	0.024	0.020	0.037	0.029	0.030	0.028	0.037	0.028	0.057	0.055	0.036	0.036
24	0.042	0.041	0.035	0.030	0.041	0.035	0.029	0.034	0.039	0.033	0.032	0.031	0.031	0.032	0.025	0.032	0.032	0.024	0.016	0.024	0.001	0.049	0.058	0.058
26	0.038	0.035	0.038	0.037	0.035	0.038	0.042	0.009	0.028	0.032	0.028	0.025	0.023	0.022	0.003	0.014	0.026	0.024	0.032	0.024	0.000	0.001	0.024	0.024
28	0.020	0.036	0.033	0.031	0.036	0.033	0.030	0.000	0.002	0.012	0.021	0.030	0.030	0.030	0.000	0.000	0.000	0.025	0.027	0.025	0.000	0.000	0.000	0.000
30	0.014	0.018	0.021	0.027	0.018	0.021	0.024	0.000	0.000	0.000	0.003	0.005	0.011	0.016	0.000	0.000	0.000	0.019	0.002	0.019	0.000	0.000	0.000	0.000
32	0.000	0.003	0.011	0.019	0.003	0.011	0.019	0.000	0.000	0.000	0.000	0.000	0.000	0.000	0.000	0.000	0.000	0.001	0.000	0.001	0.000	0.000	0.000	0.000
34	0.000	0.000	0.001	0.009	0.000	0.001	0.003	0.000	0.000	0.000	0.000	0.000	0.000	0.000	0.000	0.000	0.000	0.000	0.000	0.000	0.000	0.000	0.000	0.000

°F = 9/5 \* °C; 1 in = 25.4 mm



Table 8. Distribution of hourly temperature gradients (continued).

ΔT °F	Project																						
	ca3	ca3	ca6	ca6	ca8	ca8	ca9	ca9	ca9	ca9	fl2	fl3	fl3	fl4	fl4	fl4	fl4	ga1	ga1	ga1	ga1	ga2	ga2
	9 in	10 in	9 in	10 in	10 in	12 in	9 in	10 in	11 in	12 in	13 in	9 in	10 in	9 in	10 in	11 in	12 in	9 in	10 in	11 in	12 in	9 in	10 in
-24	0.000	0.000	0.000	0.000	0.000	0.000	0.000	0.000	0.000	0.000	0.000	0.000	0.000	0.000	0.000	0.000	0.000	0.000	0.000	0.000	0.000	0.000	0.000
-22	0.000	0.000	0.000	0.002	0.000	0.014	0.000	0.000	0.000	0.000	0.000	0.000	0.000	0.000	0.000	0.000	0.000	0.000	0.000	0.000	0.000	0.000	0.000
-20	0.000	0.005	0.024	0.036	0.028	0.028	0.000	0.000	0.002	0.003	0.000	0.000	0.005	0.000	0.000	0.000	0.000	0.000	0.000	0.000	0.000	0.000	0.000
-18	0.025	0.034	0.049	0.058	0.052	0.063	0.005	0.024	0.034	0.045	0.000	0.000	0.034	0.000	0.000	0.000	0.000	0.000	0.000	0.000	0.000	0.000	0.000
-16	0.046	0.045	0.069	0.064	0.075	0.070	0.064	0.060	0.057	0.054	0.040	0.001	0.045	0.000	0.005	0.014	0.024	0.008	0.052	0.064	0.077	0.012	0.055
-14	0.062	0.061	0.082	0.085	0.081	0.070	0.074	0.070	0.066	0.062	0.096	0.072	0.061	0.070	0.075	0.070	0.066	0.110	0.086	0.082	0.079	0.116	0.090
-12	0.072	0.074	0.083	0.063	0.070	0.059	0.079	0.076	0.078	0.079	0.112	0.141	0.074	0.155	0.103	0.109	0.114	0.107	0.102	0.101	0.101	0.103	0.101
-10	0.092	0.085	0.064	0.067	0.069	0.067	0.093	0.089	0.084	0.080	0.079	0.128	0.085	0.127	0.124	0.114	0.104	0.108	0.092	0.081	0.069	0.105	0.086
-8	0.085	0.079	0.071	0.061	0.065	0.061	0.087	0.088	0.082	0.077	0.078	0.094	0.079	0.088	0.089	0.084	0.080	0.081	0.077	0.077	0.077	0.079	0.078
-6	0.076	0.079	0.063	0.069	0.060	0.057	0.073	0.067	0.071	0.075	0.068	0.060	0.079	0.060	0.079	0.080	0.080	0.076	0.080	0.076	0.073	0.076	0.078
-4	0.077	0.068	0.045	0.035	0.038	0.040	0.065	0.065	0.062	0.058	0.041	0.043	0.068	0.040	0.049	0.050	0.051	0.046	0.044	0.051	0.058	0.045	0.044
-2	0.043	0.045	0.029	0.035	0.037	0.033	0.044	0.044	0.043	0.042	0.039	0.029	0.045	0.031	0.052	0.046	0.039	0.044	0.047	0.039	0.031	0.044	0.046
0	0.039	0.044	0.028	0.030	0.029	0.039	0.031	0.031	0.033	0.035	0.038	0.029	0.044	0.027	0.029	0.035	0.041	0.025	0.025	0.032	0.038	0.024	0.024
2	0.026	0.029	0.026	0.032	0.029	0.026	0.026	0.025	0.032	0.038	0.034	0.029	0.029	0.029	0.029	0.030	0.030	0.026	0.032	0.035	0.039	0.027	0.031
4	0.032	0.022	0.027	0.018	0.021	0.025	0.036	0.030	0.023	0.017	0.019	0.037	0.022	0.035	0.025	0.027	0.028	0.043	0.032	0.028	0.024	0.043	0.033
6	0.026	0.024	0.018	0.015	0.017	0.016	0.021	0.026	0.022	0.019	0.026	0.017	0.024	0.020	0.031	0.024	0.018	0.021	0.025	0.021	0.017	0.020	0.024
8	0.025	0.034	0.021	0.022	0.020	0.019	0.019	0.019	0.026	0.033	0.026	0.020	0.034	0.017	0.019	0.025	0.031	0.020	0.023	0.028	0.033	0.020	0.023
10	0.036	0.028	0.025	0.030	0.027	0.024	0.037	0.035	0.031	0.026	0.021	0.038	0.028	0.034	0.030	0.030	0.030	0.035	0.031	0.028	0.026	0.034	0.028
12	0.032	0.029	0.018	0.014	0.015	0.020	0.035	0.029	0.027	0.025	0.025	0.019	0.029	0.025	0.034	0.029	0.023	0.035	0.032	0.029	0.026	0.035	0.031
14	0.037	0.042	0.025	0.018	0.019	0.019	0.027	0.030	0.030	0.029	0.030	0.032	0.042	0.025	0.039	0.040	0.041	0.032	0.035	0.035	0.035	0.032	0.034
16	0.035	0.029	0.033	0.042	0.040	0.031	0.050	0.038	0.039	0.040	0.031	0.045	0.029	0.042	0.040	0.039	0.037	0.044	0.035	0.036	0.037	0.042	0.037
18	0.041	0.036	0.026	0.021	0.022	0.024	0.026	0.036	0.031	0.027	0.038	0.041	0.036	0.045	0.041	0.038	0.036	0.036	0.040	0.035	0.031	0.038	0.039
20	0.031	0.034	0.037	0.031	0.038	0.033	0.039	0.033	0.039	0.044	0.038	0.047	0.034	0.042	0.043	0.044	0.046	0.041	0.035	0.037	0.039	0.042	0.039
22	0.040	0.035	0.039	0.040	0.033	0.032	0.040	0.039	0.030	0.022	0.040	0.041	0.035	0.052	0.040	0.037	0.034	0.043	0.038	0.035	0.032	0.043	0.035
24	0.023	0.032	0.036	0.034	0.040	0.035	0.032	0.040	0.040	0.039	0.042	0.035	0.032	0.035	0.024	0.026	0.029	0.019	0.033	0.035	0.036	0.020	0.030
26	0.000	0.008	0.045	0.038	0.043	0.040	0.000	0.005	0.018	0.032	0.028	0.000	0.008	0.001	0.000	0.009	0.017	0.000	0.007	0.015	0.024	0.000	0.013
28	0.000	0.000	0.018	0.030	0.025	0.032	0.000	0.000	0.000	0.000	0.014	0.000	0.000	0.000	0.000	0.000	0.000	0.000	0.000	0.000	0.000	0.000	0.000
30	0.000	0.000	0.001	0.011	0.007	0.019	0.000	0.000	0.000	0.000	0.001	0.000	0.000	0.000	0.000	0.000	0.000	0.000	0.000	0.000	0.000	0.000	0.000
32	0.000	0.000	0.000	0.000	0.000	0.005	0.000	0.000	0.000	0.000	0.000	0.000	0.000	0.000	0.000	0.000	0.000	0.000	0.000	0.000	0.000	0.000	0.000
34	0.000	0.000	0.000	0.000	0.000	0.000	0.000	0.000	0.000	0.000	0.000	0.000	0.000	0.000	0.000	0.000	0.000	0.000	0.000	0.000	0.000	0.000	0.000

°F = 9/5 \* °C; 1 in = 25.4 mm

Table 8. Distribution of hourly temperature gradients (continued).

ΔT °F	Project																							
	ga2 11 in	ga2 12 in	mi1 9 in	mi1 10 in	mi6 10 in	mn2 8 in	mn2 9 in	mn4 8 in	mn7 9 in	nc1 9 in	nc1 10 in	nc1 11 in	nc1 12 in	nc2 11 in	nc2 12 in	ny1 9 in	ny2 9 in	oh1 9 in	oh2 9 in	oh2 15 in	ont1 7 in	ont1 8 in	ont1 9 in	
-24	0.000	0.000	0.000	0.000	0.000	0.000	0.000	0.000	0.000	0.000	0.000	0.000	0.000	0.000	0.000	0.000	0.000	0.000	0.000	0.000	0.000	0.000	0.000	0.000
-22	0.000	0.000	0.000	0.000	0.000	0.000	0.000	0.000	0.000	0.000	0.000	0.000	0.000	0.000	0.000	0.000	0.000	0.000	0.000	0.000	0.000	0.000	0.000	0.000
-20	0.000	0.000	0.000	0.000	0.000	0.000	0.000	0.000	0.000	0.000	0.000	0.000	0.000	0.000	0.000	0.000	0.000	0.000	0.000	0.000	0.000	0.000	0.000	0.000
-18	0.002	0.003	0.000	0.000	0.000	0.000	0.000	0.000	0.000	0.000	0.000	0.000	0.000	0.000	0.000	0.000	0.000	0.000	0.000	0.000	0.011	0.000	0.000	0.001
-16	0.069	0.082	0.018	0.030	0.000	0.000	0.000	0.000	0.000	0.000	0.024	0.044	0.065	0.022	0.043	0.003	0.006	0.019	0.010	0.040	0.000	0.001	0.000	0.000
-14	0.086	0.082	0.059	0.061	0.042	0.031	0.055	0.043	0.046	0.107	0.104	0.093	0.082	0.097	0.088	0.064	0.061	0.083	0.069	0.057	0.002	0.002	0.005	0.000
-12	0.097	0.094	0.075	0.071	0.085	0.103	0.105	0.098	0.094	0.103	0.100	0.097	0.094	0.105	0.097	0.083	0.088	0.082	0.078	0.073	0.021	0.029	0.051	0.000
-10	0.076	0.067	0.096	0.096	0.093	0.119	0.112	0.108	0.109	0.111	0.097	0.089	0.082	0.093	0.088	0.097	0.098	0.096	0.096	0.080	0.125	0.168	0.214	0.000
-8	0.076	0.075	0.101	0.085	0.107	0.102	0.088	0.101	0.099	0.085	0.084	0.082	0.079	0.085	0.082	0.106	0.090	0.084	0.103	0.078	0.206	0.200	0.148	0.000
-6	0.075	0.072	0.094	0.096	0.102	0.089	0.094	0.093	0.103	0.072	0.064	0.065	0.066	0.063	0.061	0.075	0.081	0.091	0.076	0.101	0.119	0.079	0.065	0.000
-4	0.050	0.056	0.072	0.083	0.097	0.086	0.073	0.078	0.072	0.062	0.060	0.067	0.074	0.072	0.083	0.090	0.090	0.072	0.085	0.091	0.080	0.083	0.087	0.000
-2	0.039	0.032	0.076	0.071	0.069	0.054	0.055	0.058	0.060	0.043	0.047	0.038	0.029	0.041	0.032	0.079	0.080	0.065	0.082	0.069	0.065	0.058	0.053	0.000
0	0.031	0.039	0.055	0.048	0.055	0.060	0.062	0.063	0.064	0.028	0.029	0.032	0.034	0.033	0.034	0.049	0.054	0.040	0.050	0.040	0.049	0.047	0.047	0.000
2	0.034	0.038	0.035	0.039	0.027	0.035	0.031	0.033	0.030	0.029	0.032	0.036	0.041	0.036	0.041	0.023	0.033	0.027	0.024	0.038	0.060	0.055	0.060	0.000
4	0.029	0.024	0.040	0.044	0.042	0.034	0.033	0.034	0.036	0.032	0.029	0.025	0.021	0.025	0.020	0.038	0.039	0.029	0.038	0.033	0.062	0.062	0.057	0.000
6	0.020	0.016	0.039	0.029	0.040	0.044	0.045	0.046	0.043	0.026	0.022	0.021	0.021	0.025	0.024	0.041	0.043	0.036	0.042	0.033	0.048	0.047	0.042	0.000
8	0.028	0.033	0.030	0.035	0.030	0.031	0.030	0.030	0.031	0.023	0.026	0.026	0.026	0.025	0.027	0.030	0.029	0.031	0.029	0.033	0.041	0.037	0.033	0.000
10	0.027	0.026	0.031	0.028	0.033	0.042	0.035	0.043	0.033	0.033	0.032	0.032	0.032	0.034	0.034	0.035	0.030	0.038	0.035	0.022	0.037	0.037	0.037	0.000
12	0.027	0.024	0.030	0.024	0.033	0.024	0.027	0.022	0.030	0.037	0.031	0.029	0.027	0.030	0.027	0.033	0.033	0.037	0.031	0.029	0.027	0.031	0.033	0.000
14	0.034	0.035	0.029	0.036	0.031	0.042	0.034	0.041	0.034	0.033	0.037	0.035	0.033	0.039	0.039	0.034	0.031	0.029	0.035	0.029	0.025	0.020	0.021	0.000
16	0.037	0.038	0.030	0.020	0.031	0.028	0.031	0.033	0.035	0.047	0.040	0.041	0.042	0.039	0.039	0.038	0.039	0.033	0.035	0.024	0.022	0.023	0.018	0.000
18	0.036	0.033	0.036	0.038	0.034	0.049	0.036	0.045	0.038	0.036	0.040	0.035	0.031	0.036	0.033	0.032	0.030	0.037	0.032	0.035	0.012	0.021	0.021	0.000
20	0.038	0.037	0.033	0.029	0.034	0.029	0.049	0.033	0.041	0.042	0.036	0.038	0.040	0.037	0.038	0.037	0.035	0.033	0.035	0.021	0.000	0.001	0.009	0.000
22	0.035	0.035	0.021	0.031	0.018	0.000	0.006	0.000	0.001	0.039	0.043	0.037	0.031	0.036	0.033	0.014	0.011	0.034	0.020	0.031	0.000	0.000	0.000	0.000
24	0.031	0.033	0.000	0.006	0.000	0.000	0.000	0.000	0.000	0.012	0.024	0.030	0.035	0.022	0.029	0.000	0.000	0.005	0.000	0.025	0.000	0.000	0.000	0.000
26	0.019	0.024	0.000	0.000	0.000	0.000	0.000	0.000	0.000	0.000	0.000	0.008	0.016	0.005	0.009	0.000	0.000	0.000	0.000	0.009	0.000	0.000	0.000	0.000
28	0.002	0.005	0.000	0.000	0.000	0.000	0.000	0.000	0.000	0.000	0.000	0.000	0.000	0.000	0.000	0.000	0.000	0.000	0.000	0.000	0.000	0.000	0.000	0.000
30	0.000	0.000	0.000	0.000	0.000	0.000	0.000	0.000	0.000	0.000	0.000	0.000	0.000	0.000	0.000	0.000	0.000	0.000	0.000	0.000	0.000	0.000	0.000	0.000
32	0.000	0.000	0.000	0.000	0.000	0.000	0.000	0.000	0.000	0.000	0.000	0.000	0.000	0.000	0.000	0.000	0.000	0.000	0.000	0.000	0.000	0.000	0.000	0.000
34	0.000	0.000	0.000	0.000	0.000	0.000	0.000	0.000	0.000	0.000	0.000	0.000	0.000	0.000	0.000	0.000	0.000	0.000	0.000	0.000	0.000	0.000	0.000	0.000

°F = 9/5 \* °C; 1 in = 25.4 mm

Table 8. Distribution of hourly temperature gradients (continued).

ΔT	Project																				
	ont1	ont1	ont1	ont2	ont2	wi1	wi1	wi1	wi1	wi2	wi2	wi2	wi3	wi4	wi5	wi6	wi7	wi7	wi7	wi7	wv1
°F	10 in	11 in	12 in	9 in	10 in	11 in	12 in	13 in	14 in	9 in	10 in	12 in	8 in	9 in	10 in	10 in	9 in	10 in	11 in	12 in	10 in
-24	0.000	0.000	0.000	0.000	0.000	0.000	0.000	0.000	0.000	0.000	0.000	0.000	0.000	0.000	0.000	0.000	0.000	0.000	0.000	0.000	0.000
-22	0.000	0.000	0.000	0.000	0.000	0.000	0.000	0.000	0.000	0.000	0.000	0.000	0.000	0.000	0.000	0.000	0.000	0.000	0.000	0.000	0.000
-20	0.000	0.000	0.001	0.000	0.001	0.000	0.000	0.000	0.000	0.000	0.000	0.000	0.000	0.000	0.000	0.000	0.000	0.000	0.000	0.000	0.000
-18	0.001	0.001	0.001	0.001	0.000	0.000	0.000	0.000	0.000	0.000	0.000	0.000	0.000	0.000	0.000	0.000	0.000	0.000	0.000	0.000	0.000
-16	0.000	0.001	0.002	0.000	0.001	0.026	0.035	0.040	0.045	0.005	0.019	0.037	0.000	0.000	0.016	0.003	0.002	0.012	0.021	0.030	0.015
-14	0.007	0.015	0.023	0.015	0.022	0.068	0.069	0.069	0.069	0.063	0.068	0.068	0.044	0.050	0.070	0.055	0.058	0.065	0.068	0.071	0.079
-12	0.071	0.097	0.123	0.086	0.107	0.090	0.090	0.087	0.085	0.091	0.083	0.087	0.096	0.091	0.078	0.091	0.099	0.094	0.093	0.091	0.081
-10	0.218	0.196	0.173	0.216	0.200	0.096	0.085	0.083	0.081	0.108	0.106	0.085	0.107	0.103	0.107	0.105	0.109	0.107	0.097	0.087	0.102
-8	0.119	0.108	0.096	0.109	0.092	0.079	0.076	0.072	0.068	0.091	0.083	0.076	0.105	0.106	0.088	0.097	0.091	0.085	0.081	0.076	0.095
-6	0.070	0.074	0.078	0.059	0.063	0.087	0.090	0.093	0.095	0.093	0.085	0.091	0.088	0.095	0.083	0.098	0.096	0.086	0.088	0.090	0.080
-4	0.083	0.081	0.079	0.083	0.080	0.075	0.072	0.074	0.076	0.069	0.079	0.072	0.085	0.078	0.081	0.078	0.066	0.075	0.074	0.074	0.076
-2	0.053	0.051	0.050	0.050	0.051	0.070	0.074	0.074	0.074	0.066	0.067	0.075	0.060	0.067	0.072	0.061	0.064	0.063	0.068	0.073	0.057
0	0.049	0.050	0.052	0.045	0.045	0.047	0.045	0.044	0.042	0.058	0.047	0.046	0.059	0.057	0.045	0.057	0.058	0.051	0.048	0.044	0.040
2	0.057	0.058	0.059	0.054	0.051	0.035	0.035	0.037	0.039	0.033	0.037	0.034	0.032	0.033	0.038	0.034	0.032	0.035	0.037	0.038	0.029
4	0.050	0.048	0.047	0.053	0.050	0.039	0.042	0.038	0.034	0.035	0.037	0.041	0.038	0.033	0.038	0.040	0.036	0.036	0.038	0.040	0.030
6	0.050	0.046	0.043	0.050	0.050	0.028	0.026	0.029	0.033	0.039	0.029	0.026	0.039	0.046	0.028	0.036	0.039	0.033	0.030	0.028	0.025
8	0.032	0.033	0.033	0.034	0.039	0.034	0.031	0.030	0.030	0.032	0.039	0.031	0.033	0.026	0.038	0.034	0.034	0.035	0.032	0.030	0.040
10	0.032	0.030	0.028	0.037	0.030	0.033	0.035	0.031	0.026	0.033	0.030	0.036	0.037	0.036	0.030	0.032	0.033	0.033	0.033	0.033	0.036
12	0.036	0.036	0.037	0.037	0.041	0.023	0.021	0.025	0.029	0.031	0.024	0.021	0.027	0.029	0.025	0.032	0.029	0.026	0.025	0.023	0.032
14	0.020	0.021	0.022	0.022	0.021	0.033	0.029	0.028	0.027	0.031	0.036	0.031	0.040	0.035	0.036	0.028	0.031	0.033	0.031	0.030	0.039
16	0.019	0.018	0.017	0.017	0.021	0.027	0.029	0.027	0.025	0.035	0.024	0.028	0.032	0.037	0.026	0.031	0.034	0.026	0.027	0.028	0.029
18	0.019	0.017	0.016	0.019	0.015	0.036	0.031	0.031	0.031	0.036	0.042	0.031	0.047	0.036	0.041	0.030	0.040	0.037	0.033	0.030	0.042
20	0.015	0.016	0.017	0.015	0.021	0.036	0.035	0.031	0.028	0.041	0.035	0.034	0.031	0.040	0.037	0.042	0.042	0.040	0.038	0.035	0.023
22	0.000	0.003	0.006	0.000	0.000	0.030	0.032	0.032	0.032	0.013	0.028	0.032	0.001	0.005	0.025	0.016	0.007	0.026	0.031	0.035	0.036
24	0.000	0.000	0.000	0.000	0.000	0.009	0.017	0.023	0.029	0.000	0.002	0.018	0.000	0.000	0.000	0.000	0.000	0.001	0.007	0.014	0.015
26	0.000	0.000	0.000	0.000	0.000	0.000	0.000	0.001	0.003	0.000	0.000	0.000	0.000	0.000	0.000	0.000	0.000	0.000	0.000	0.000	0.000
28	0.000	0.000	0.000	0.000	0.000	0.000	0.000	0.000	0.000	0.000	0.000	0.000	0.000	0.000	0.000	0.000	0.000	0.000	0.000	0.000	0.000
30	0.000	0.000	0.000	0.000	0.000	0.000	0.000	0.000	0.000	0.000	0.000	0.000	0.000	0.000	0.000	0.000	0.000	0.000	0.000	0.000	0.000
32	0.000	0.000	0.000	0.000	0.000	0.000	0.000	0.000	0.000	0.000	0.000	0.000	0.000	0.000	0.000	0.000	0.000	0.000	0.000	0.000	0.000
34	0.000	0.000	0.000	0.000	0.000	0.000	0.000	0.000	0.000	0.000	0.000	0.000	0.000	0.000	0.000	0.000	0.000	0.000	0.000	0.000	0.000

°F = 9/5 \* °C; 1 in = 25.4 mm

### *Critical Damage Location*

In this project, the fatigue analysis was conducted assuming that the transverse cracks observed on JPCP are results of fatigue failures initiating at the slab bottom (bottom-up failure). This assumption is accurate if the pavement slabs are flat when the temperature gradient is zero. The critical damage location for this mode of failure is:

- For normal-width (12 ft [3.7 m]) sections, bottom of longitudinal edge, half-way between the two transverse joints that borders the slab.
- For widened lane sections ( $\geq$  12 ft [3.7 m] wide), bottom of the wheel path, also at the midslab location.

On normal-width pavements, the maximum wheel-load stress occurs at the longitudinal edge when the load is placed right at the edge. Edge loading produces stresses that are substantially higher than other loading conditions (about twice that of interior load stresses and about 50 percent higher than corner load stresses). And, as also described previously, the stresses resulting from slab curling can also add significantly to the load stresses when the slabs are exposed to high positive temperature gradients (slab surface hotter than bottom, causing the slabs to curl down). Combined, the magnitude of stresses at the longitudinal edge is so much greater than the stresses at any other location that fatigue cracking in JPCP is controlled by the few axle loads that pass through or near the slab edge while the slab is under a large positive temperature gradient.

When pavement slabs are subjected to large positive temperature gradients, the curling stress component of the combined stress at the longitudinal edge can equal or exceed the load stress component. Negative temperature gradients cause compressive stress at the bottom of longitudinal edge, and therefore, reduces the combined stress at that location. Since the amount of fatigue damage caused during a loading cycle is very sensitive to the applied stress level, only the traffic passes at large positive temperature gradients are significant to fatigue damage accumulation at the longitudinal edge.

The negative temperature gradients are important to the combined stress under the corner loading condition, especially on nondoweled pavements. The negative temperature gradients cause tensile stresses at the slab surface that are additive to the load stresses under corner loading condition. The magnitude of corner load stresses are generally about 70 percent that of edge load stresses. If dowels are provided, this stress is significantly reduced, but the corner load stress can still become critical even on a doweled pavement if the pavement is subjected to sufficiently large effective negative temperature gradients. Such conditions can develop because a number of factors other than temperature gradients also cause upward curling of pavement slabs, including the following:

- Moisture gradient—the top of slab is usually drier than the bottom throughout most of the year. Therefore, moisture gradients generally tend to cause lifting

of the slab corners. The moisture gradients could be treated as equivalent temperature gradients, but insufficient information is available to adequately quantify this effect.

- Differential drying shrinkage—field moisture measurements have shown that surface shrinkage of PCC occurs only to a depth of about 2 in (51 mm).<sup>(23)</sup> The net effect of this phenomenon is an equivalent temperature gradient (temperature difference between top and bottom) of about -2.5 °F (-1.4 °C) for a 10-in (250-mm) slab.
- Built-in temperature gradient (residual temperature gradient)—if the PCC was hardened with any positive temperature gradient, this gradient will remain with the slab permanently, but as a negative gradient. Since the slab was flat when it hardened with a positive temperature gradient, the slab will be curled up, when that temperature gradient is removed (i.e., at zero temperature gradient). A slab hardened under such condition will only become flat when it is subjected to a positive temperature gradient of the same magnitude that was present at hardening. Effectively, then, this slab has a built in negative temperature gradient (negative, since the slab will be curled up when the temperature gradient is zero) of the same magnitude as the gradient that was present at hardening. Daytime construction will generally cause positive temperature gradients in PCC at hardening, causing built-in negative temperature gradients in the slabs. Since pavement slabs are exposed to daily cycling of temperature gradients, from large positive gradient at midday to negative gradients at night, any relaxing of the residual gradients through creep effects are not likely. Studies have shown that the magnitude of this residual temperature gradient in many highway pavements is -2.5 °F/in (.055 °C/mm) or more, which translates to -25 °F (-14 °C) gradient in a 10-in (250-mm) slab.<sup>(24)</sup>

All three factors above cause upward curling of the pavement slabs, and the effects of the last two are permanent. According to the above, the magnitude of negative residual temperature gradient could be very significant in many pavement sections.

The effects of all factors that cause curling or warping of pavement slabs can be expressed in terms of an effective temperature gradient and combined to determine their net effect. The magnitude of curling stress depends on the net result of all factors at work. Hence, the initial upward curling has the effect of shifting the actual temperature gradients in the negative direction by the amount corresponding to the degree of initial curling. The initial upward curling, therefore, reduces the combined stress at the longitudinal edge, but increases the critical tensile stresses at the surface under corner loading condition.

If the magnitude of the initial upward curling is sufficiently high (high negative residual temperature gradient), then the stresses under corner loading can become more critical and fatigue cracking can initiate at the slab surface (top-down cracking). This mode of failure could be a very significant cause of transverse cracking in JPCP,

and it is very possible that both top-down and bottom-up cracking would have to be considered in designing concrete pavements.

The top-down cracking mode was investigated further to determine the magnitude of stresses involved. The preliminary results suggest that this mode of cracking could be more critical than bottom-up, particularly on short slabs (12-ft [3.7-m] or 13-ft [4.0-m] slabs). However, complete fatigue analysis for this mode of failure could not be conducted because of a lack of data. The most important information needed to conduct this analysis is the magnitude of the actual residual temperature gradients. This information can be determined from curling measurements taken from the inservice pavement sections, but the process is very time-consuming. For the corner loading condition to become critical for fatigue cracking, the residual temperature gradient in the pavement slab would have to be about -15 °F (-8.3 °C) or more. According to reference 24, this condition is not uncommon. Further details on top-down cracking, including the results of a preliminary stress analysis, are given later under *Critical Failure Mode*.

The cracking model developed under this project is based on the fatigue damage determined for the edge loading condition. The stresses for this analysis were determined using the regression equations developed under NCHRP Project 1-26.<sup>(25)</sup> These equations are based on the results given by the finite element program ILLI-SLAB, and they provide an accurate and efficient means of determining the combined stress due to axle loads and slab curling under the edge loading condition. The stress calculation procedures are described in the section.

#### *Load Stress*

The NCHRP 1-26 equations utilize Westergaard's edge stress equation for a circular load and various adjustment factors to reproduce the results given by the ILLI-SLAB finite element program. The NCHRP 1-26 equation for the load stress has the following form:

$$\sigma_{load} = f1 * f2 * f3 * f4 * \sigma_e \quad (9)$$

where:

- $\sigma_{load}$  = Load stress, lbf/in<sup>2</sup>.
- f1, f2, f3, f4 = Adjustment factors for slab size, stabilized base, widened lane, and tied concrete shoulder.
- $\sigma_e$  = Stress obtained using Westergaard's edge load equation for circular loads, lbf/in<sup>2</sup>.

The equivalent single-axle radius (ESAR) concept is used to handle multiple wheel loads, and adjustments are made to account for the slab size effect, widened traffic lane, tied concrete shoulder, and the presence of a stabilized base. The ESAR is the equivalent single wheel radius of a multiple wheel load that will produce the same

stress intensity at the critical location. The application of the ESAR concept allows the use of a closed form solution to determine the maximum stress under a multiple wheel load.

The edge load stress is calculated using the equation given in Westergaard's 1948 paper for circular load given below, substituting the radius of the applied load with the equivalent single axle radius.<sup>(26)</sup>

$$\sigma_e = \frac{3(1 + \mu)P}{\pi(3 + \mu)h^2} \left[ \ln \frac{Eh^3}{100ka^4} + 1.84 - \frac{4\mu}{3} + \frac{1 - \mu}{2} + 1.18(1 + 2\mu) \frac{a}{\ell} \right] \quad (10)$$

where:

- P = Total applied load, lbf.
- $\mu$  = Poisson's ratio.
- E = Modulus of elasticity of PCC, lbf/in<sup>2</sup>.
- h = Slab thickness, in.
- k = Modulus of subgrade reaction, lbf/in<sup>2</sup>/in.
- a = Radius of the applied load, in.
- $\ell$  = Radius of relative stiffness, in, defined as follows:

$$\ell = \left[ \frac{Eh^3}{12(1 - \mu^2)k} \right]^{0.25} \quad (11)$$

where:

- E = Modulus of elasticity of PCC, lbf/in<sup>2</sup>.
- h = Slab thickness, in.
- $\mu$  = Poisson's ratio.
- k = Modulus of subgrade reaction, lbf/in<sup>2</sup>/in.

The equivalent single-axle radius for the dual wheel load is obtained using the following equation:

$$\begin{aligned} \frac{a_{eq}}{a} = & 0.909 + 0.339485 \frac{S}{a} + 0.103946 \frac{a}{\ell} - 0.017881 \left( \frac{S}{a} \right)^2 - 0.045229 \left( \frac{S}{a} \right)^2 \frac{a}{\ell} \\ & + 0.000436 \left( \frac{S}{a} \right)^3 - 0.301805 \frac{S}{a} \left( \frac{a}{\ell} \right)^3 + 0.034664 \left( \frac{S}{\ell} \right)^2 + 0.001 \left( \frac{S}{a} \right)^3 \frac{a}{\ell} \end{aligned} \quad (12)$$

Limits:  $0 \leq S/a \leq 20$   
 $0 \leq a/\ell \leq 0.5$

$R^2 = 1.0$

where:

- $a_{eq}$  = Equivalent single axle radius of dual wheels, in.
- $a$  = Radius of the applied load, in.
- $S$  = Dual wheel spacing, in.
- $l$  = Radius of relative stiffness, in.

The use of the equivalent load radius in equation 10 gave results that match those of ILLI-SLAB analysis almost exactly.

In the NCHRP 1-26 procedure, the load stress is determined by applying various adjustment factors to the edge stress calculated using Westergaard's equation (equation 10). The adjustments are made for the slab size effect, widened lane, tied concrete shoulder, and stabilized base. Regression equations are provided for determining each of these factors, but only the factor for widened lane was used in this project for the following reasons:

- The adjustment factor for the slab size effect was not used, because the ILLI-SLAB analysis performed to validate all procedures used in this project showed that the use of this factor could result in overcompensation for the slab size effect. This factor was originally introduced because the load stress in short slabs can be significantly less than that in an infinite slab assumed in the Westergaard solution. The stresses are lower in short slabs because some of the load on short slab is carried by the rigid body motion of the slab (i.e., slabs sinking into the subgrade). If this rigid body motion is prevented, by the adjacent slabs for example, the stresses in short slabs can be even higher than that in infinite slabs. The analysis has shown that the response of multiple slab system with even a moderate load transfer efficiency at the transverse joints closely approximate that of an infinitely long slab. For highway pavements, this factor is significant only for very short slabs (12 ft [3.7 m] or less), even if the slabs have very poor load transfer efficiency.
- The effects of tied concrete shoulder were treated by directly considering the stress load transfer efficiency (LTE). The stress LTE was determined from deflection LTE using the following regression equation:<sup>(27)</sup>

$$\begin{aligned} \text{Log}_{10}(LTE_{\sigma}) = & 0.064787 + 0.0047221 LTE_{\Delta} + 0.00089586 LTE_{\Delta}^2 \\ & - 0.16478 \times 10^{-4} LTE_{\Delta}^3 + 0.89222 \times 10^{-7} LTE_{\Delta}^4 \end{aligned} \quad (13)$$

where:

- $LTE_{\sigma}$  = Stress LTE, percent.
- $LTE_{\Delta}$  = Deflection LTE, percent.

For sections provided with tied concrete shoulder or other forms of edge support (such as adjacent lane or tied curb and gutter), the load stress was multiplied by the following factor to account for the edge support:



$$f_{LTE} = \frac{100}{100 + LTE_{\sigma}} \quad (14)$$

where:

$f_{ES}$  = Adjustment factor for edge support.  
 = 1.0 if no edge support.

$LTE_{\sigma}$  = Stress LTE, percent.

- The effects of stabilized bases were considered directly using the effective slab thickness. The effective slab thickness was determined from FWD testing results, and it represents the equivalent thickness of a single concrete layer that would give the same structural response as the actual pavement structure (slab and base). The procedure used to determine the effective slab thickness is described in chapter 4 of volume II. The effective slab thickness as determined in this project accounts for the structural contribution of all pavement layers and any interaction between layers. On those section where the effective slab thickness was used, the following equation was used to determine the maximum tensile stress at the bottom of the pavement slab:

$$f_{SB} = \frac{2 (h - x)}{h_e} \quad (15)$$

where:

$f_{SB}$  = Adjustment factor for stabilized base.

= 1.0 if  $h_e = h$ .

$h$  = Actual slab thickness, in.

$h_e$  = Effective slab thickness, in.

$x$  = neutral axis location:

$$x = \frac{\frac{h_1^2}{2} + \frac{E_2}{E_1} h_2 \left( h_1 + \frac{h_2}{2} \right)}{h_1 + \frac{E_2}{E_1} h_2} \quad (16)$$

where:

$h_1$  = Slab thickness, in.

$h_2$  = Base thickness, in.

$E_1$  = Concrete modulus of elasticity, lbf/in<sup>2</sup>.

$E_2$  = Base modulus of elasticity, lbf/in<sup>2</sup>.

Unlike other adjustment factors,  $f_{sb}$  is applied to the combined stress, because this factor is an adjustment for the slab thickness.

On widened lane sections, the critical location for fatigue damage is the bottom of slab, directly under the wheel path. Studies have shown that the slabs are almost never loaded at the outer edge on widened lane sections.<sup>(28)</sup> Therefore, the following adjustment factor was used to obtain the maximum stress directly under the wheel load:

$$f_{WL} = 0.454147 + \frac{0.013211}{D/\ell} + 0.386201 \frac{a}{D} - 0.24565 \left(\frac{a}{D}\right)^2 + 0.053891 \left(\frac{a}{D}\right)^3 \quad (17)$$

where:

- $f_{WL}$  = Adjustment factor for widen lane.
- = 1.0 if standard-width lane.
- $a$  = Radius of loaded area, in.
- $D$  = Mean wheel location, inches from outer edge.
- $\ell$  = Radius of relative stiffness, in.

The load stress can now be determined using the following equation:

$$\sigma_{Load} = f_{ES} f_{WL} \sigma_e \quad (18)$$

where:

- $\sigma_{Load}$  = Load stress, lbf/in<sup>2</sup>.
- $f_{ES}$  = Adjustment factor for edge support (equation 14).
- $f_{WL}$  = Adjustment factor for widened lane (equation 17).
- $\sigma_e$  = Westergaard's edge stress (equation 10), lbf/in<sup>2</sup>.

### *Curling Stress*

The curling stress is determined using the following equation and then combined with the load stress using a regression coefficient in the NCHRP 1-26 procedure:

$$\sigma_c = \frac{C E \alpha_T \Delta T}{2} \quad (19)$$

where:

- $\sigma_c$  = Curling stress, lbf/in<sup>2</sup>.
- C = Curling stress coefficient.
- E = Concrete modulus of elasticity, lbf/in<sup>2</sup>.
- $\alpha_T$  = Concrete coefficient of thermal expansion ( $5.5 \times 10^{-6}$ ).
- $\Delta T$  = Temperature difference between the top and bottom of the slab, °F.

This equation was developed by Westergaard, and Bradbury developed the coefficients for solving this equation.<sup>(29,30)</sup> For maximum stress at the longitudinal edge, the curling stress coefficient is given by the following equation:<sup>(25)</sup>

$$C = 1 - \frac{2 \cos\lambda \cosh\lambda}{\sin 2\lambda + \sinh 2\lambda} (\tan\lambda + \tanh\lambda) \quad (20)$$

where:

$$\lambda = \frac{L}{\ell \sqrt{8}} \quad (21)$$

- L = Slab length, in.
- $\ell$  = Radius of relative stiffness, in.

### *Combined Stress*

The combined stress due to load and curling is obtained using the following equation:

$$\sigma_{combined} = f_{SB} (\sigma_{load} + R * \sigma_{curl}) \quad (22)$$

where:

- $\sigma_{combined}$  = Combined edge stress, lbf/in<sup>2</sup>.
- $f_{SB}$  = Adjustment factor for stabilized base (equation 15).
- $\sigma_{load}$  = Load stress, psi.
- R = Regression coefficient.
- $\sigma_{curl}$  = Curling stress, lbf/in<sup>2</sup>.

The regression coefficient R is determined using the following equation:

$$\begin{aligned}
R = & 1.062 - 0.015757 dT - 0.0000876k - 1.068 \frac{L}{\ell} + 0.387317 dT \frac{L}{\ell} \\
& + 1.17 \times 10^{-11} E dT k - 1.81 \times 10^{-12} E dT^2 k - 1.051 \times 10^{-9} E \left( \frac{L}{\ell} \right)^2 k dT \\
& + 1.84 \times 10^{-11} E dT^2 \frac{L}{\ell} k - 1.7487 \left( \frac{L}{\ell} \right)^2 dT + 0.000034351 dT^3 \\
& + 86.97 \left( \frac{L}{\ell} \right)^3 - 0.00816396 dT^2 \frac{L}{\ell}
\end{aligned} \tag{23}$$

where:

$$\begin{aligned}
dT &= \alpha \Delta T \times 10^5. \\
\alpha &= \text{PCC coefficient of thermal expansion, } \epsilon / ^\circ\text{F}. \\
\Delta T &= \text{Temperature difference through the slab, } ^\circ\text{F}. \\
k &= \text{Subgrade modulus of reaction, lbf/in}^2/\text{in}. \\
L &= \text{Slab length, in.} \\
\ell &= \text{Radius of relative stiffness, in (equation 11).} \\
E &= \text{Modulus of elasticity of PCC, lbf/in}^2.
\end{aligned}$$

The coefficient R is needed because the load and curling stresses are not directly additive. Curling causes various parts of the slab to lift off of the base, invalidating the full contact assumption made in the load stress calculation. The regression coefficient R provides the necessary adjustment to the curling stress to give the correct combined stress.

### Fatigue Damage Determination

The fatigue damage was determined using the linear damage accumulation approach proposed by Miner:<sup>(31)</sup>

$$FD = \sum \frac{n}{N} \tag{24}$$

where:

$$\begin{aligned}
FD &= \text{Fatigue Damage} \\
n &= \text{number of applied 18-kip (80-kN) single axle loads} \\
N &= \text{number of allowable 18-kip (80-kN) single axle loads}
\end{aligned}$$

According to Miner's theory, failure, or cracking, is expected when the FD reaches 1.0, and the allowable number of load repetitions, N, depends on the applied stress level. The allowable number of load repetitions is the very basis of fatigue concept,

but this N is not so easily determined for pavement slabs and warrants some discussion.

The allowable number of load repetitions is easy to determine, at least conceptually, for simple structures, such as simply supported beams used in laboratory testing. A simply supported beam has no redundancy in the structure to redistribute load once it cracks. More importantly, on a beam, the critical damage location spans across the entire width of the beam; therefore, when the fatigue damage reaches a critical point, the cracking may be expected to spread very quickly over the entire width of the beam, causing failure. The fatigue failure in a beam test, therefore, is easily detected, since it coincides with structural failure. This is not true on a pavement slab.

On pavement slabs, the maximum fatigue damage at the longitudinal edge is confined to a very small area, at the bottom of the outermost edge of the slab, and the amount of accumulated fatigue damage is drastically less at locations even a short distance away from the edge. Figure 26 illustrates the typical fatigue damage distribution across the slab at the midslab location. Because of the fatigue damage distribution has such a steep gradient across the slab, pavement slabs are able to withstand a considerable number of load applications beyond the initial failure. Also, because of the slab geometry, the cracking would have to progress a considerable length toward the center of the slab before a visible cracks first appear at the slab surface.

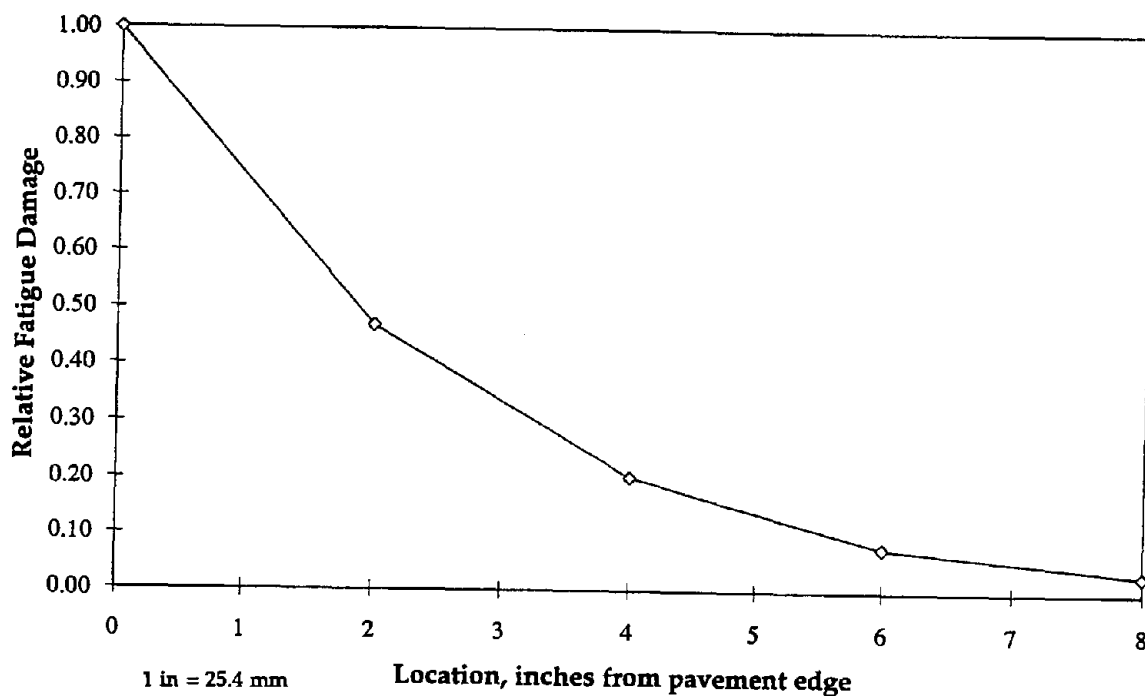


Figure 26. Typical distribution of fatigue damage across a pavement slab.

Therefore, on pavement slabs the fatigue failure at the critical damage location does not necessarily lead to immediate cracking, and the N is much more difficult to define. Although the N to fatigue failure at the critical damage location is expected to be the same for both pavement slabs and beams, the failure on pavement slabs does not have the same practical significance as the failure on beams because the failure is highly localized. For design purposes, the N to slab cracking is a much more practical measure of fatigue life than fatigue failure at the critical damage location.

A number of fatigue models for pavement slabs have been developed based on the performance of inservice pavements. These models have been developed to give the allowable number of load applications until slab cracking. The difficulty in developing a fatigue model based on performance of inservice pavements, rather than laboratory testing results, is that the accumulated damage is very difficult to determine. The material properties and the pavement structure itself are much more variable on inservice pavements than on laboratory samples. Many factors affect stresses in pavement slabs, including traffic loads, temperature curling, moisture warping, and as previously discussed, the residual temperature gradients. Since traffic wanders about the wheel path, the effective number of applied load repetitions is also a major unknown, even if accurate traffic data were available. Therefore, there is a considerable variation in the N predicted by different models, depending on how the effects of various factors affecting fatigue were treated in the model.

Several orders of magnitude difference in the N predicted by different fatigue models is not uncommon. However, this may not have a serious practical significance. The large differences in the N predicted by different fatigue models means that the amount of fatigue damage at which the slabs are expected to crack can vary considerably depending on the model used. For design purposes, as long as a given fatigue model gives consistent results for a range of parameters, the absolute amount of fatigue damage at which the slabs are expected to crack is not important.

The objective of conducting a fatigue analysis in this project is to develop a performance model that can be used to determine the expected amount of slab cracking for design and planning purposes. A model in the following form is desired:

$$\text{PercentSlabsCracked} = f (FD) \quad (25)$$

To develop such a model, the accumulated fatigue damage in the pavement sections must be determined and correlated to the amount of cracking observed on those sections. A fatigue model is needed for this calculation.

The approach taken in this project was to try various existing fatigue models and used the one that gives the best correlation, rather than developing a new fatigue model. The "best correlation" would be judged by the consistency in the results (i.e., high correlation coefficient and low standard error), not by the absolute damage

amount at which various amount of cracking is expected. It would be possible to iteratively adjust both the fatigue model and the cracking model to normalize the models, so that the model predicts 50 percent slab cracking at fatigue damage of 1.0, but this would not improve the results. As previously discussed, it is important to note that a pavement slab is not necessarily expected to crack when the accumulated fatigue damage at the critical location reaches 1.0.

### *Fatigue Model*

Four different fatigue models were tried in this project, including three that were developed based on field performance of full-scale slabs, and one based on laboratory beam testing results:

- ERES/COE model—this model was developed from Corps of Engineers (COE) data from 51 full-scale field sections. The edge load stress was calculated using H-51 program (computerized Pickett and Ray charts) and multiplied by 0.75 to account for the edge support in the sections.<sup>(32)</sup>

$$\log N = 2.13 SR^{-1.2} \quad (26)$$

where:

- N = Number of allowable load applications.
- SR = Stress to strength ratio ( $\sigma$ /MR).
- $\sigma$  = Critical tensile stress, lbf/in<sup>2</sup>.
- MR = PCC modulus of rupture, lbf/in<sup>2</sup>.

This model was originally developed for airfield pavements, but has shown good results in various other applications.

- NCHRP 1-26 model—this model was developed using the COE and AASHO road test data. This model is also based on edge load stress.<sup>(25)</sup>

$$\log N = \left[ \frac{-SR^{-5.367} \log(1 - P)}{0.0032} \right]^{0.2276} \quad (27)$$

where:

- N = Number of allowable load applications.
- SR = Stress-to-strength ratio ( $\sigma$ /MR).
- P = Probability of failure.

For 50 percent probability of failure ( $P = 0.5$ ) this model reduces to the following:

$$\log N = 2.81 SR^{-1.22} \quad (28)$$

where:

SR = Stress-to-strength ratio ( $\sigma/MR$ ).

- Zero-Maintenance model—this model is based on laboratory testing results of 140 beams.<sup>(13)</sup>

$$\log N = 17.61 - 17.61 SR \quad (29)$$

where:

SR = Stress-to-strength ratio ( $\sigma/MR$ ).

- ARE model—this model was developed based the on AASHO Road Test data. The actual loadings were converted to 18-kip (80-kN) ESAL's using the AASHTO load equivalency factors, and the maximum midslab stresses calculated using elastic layer theory was used.<sup>(33)</sup>

$$N = 23,440 SR^{-3.21} \quad (30)$$

where:

SR = Stress-to-strength ratio ( $\sigma/MR$ ).

The preliminary fatigue analysis results given by the four different fatigue damage models are shown in figures 27 through 30. The ERES/COE and NCHRP 1-26 models have similar forms and gave very similar results. The Zero-Maintenance model gave the most scatter. The ARE model gave the narrowest range of the damage values, but the results do not show a logical trend. Further refinements were made to the calculated damage considering a more refined pass-to-coverage ratio, and consideration of moisture gradient and residual temperature gradients. The details of these refinements are discussed later in the *Model Development* section.

#### *Pass to Coverage*

The pass to coverage ratio (p/c) was discussed earlier. The p/c is commonly taken as a percentage of traffic that passes close to the pavement edge. In this approach, the traffic passing within a certain distance of the outer edge is assumed to cause one edge loading application. In this project, the concept "fatigue damage per pass" (FD/Pass) was introduced to more precisely determined the amount of fatigue damage cause by passing traffic.



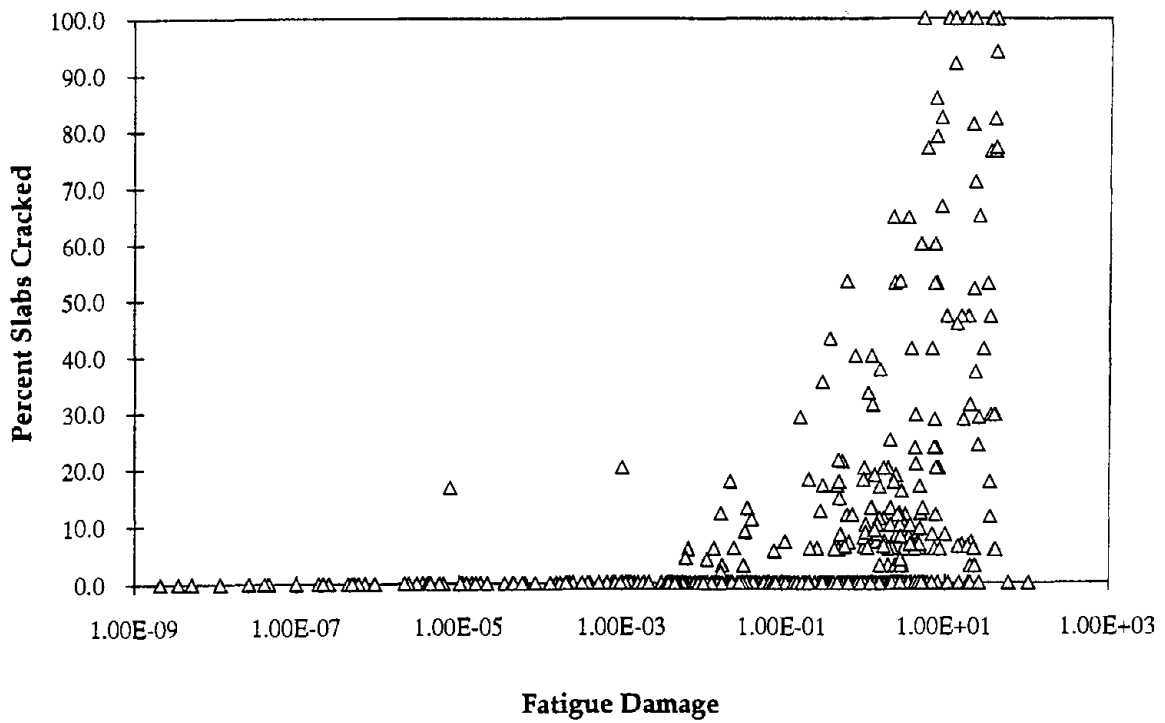


Figure 27. Preliminary fatigue analysis results given by ERES/COE fatigue model.

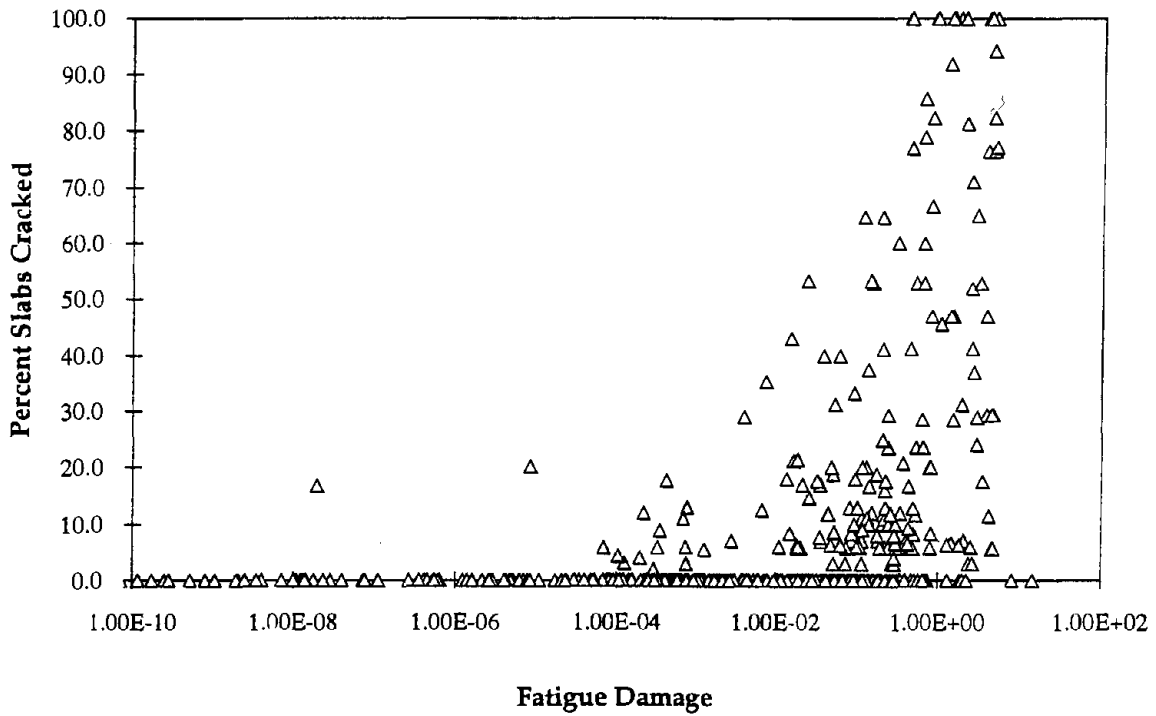


Figure 28. Preliminary fatigue analysis results given by NCHRP 1-26 fatigue model.

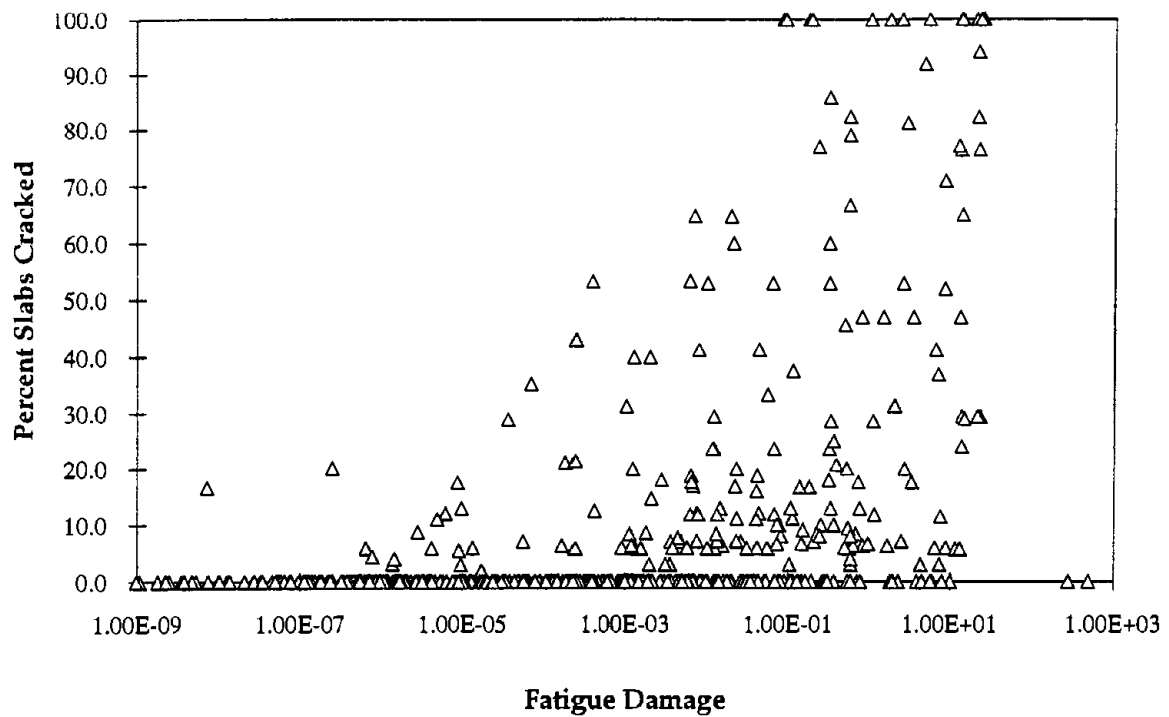


Figure 29. Preliminary fatigue analysis results given by Zero-Maintenance fatigue model.

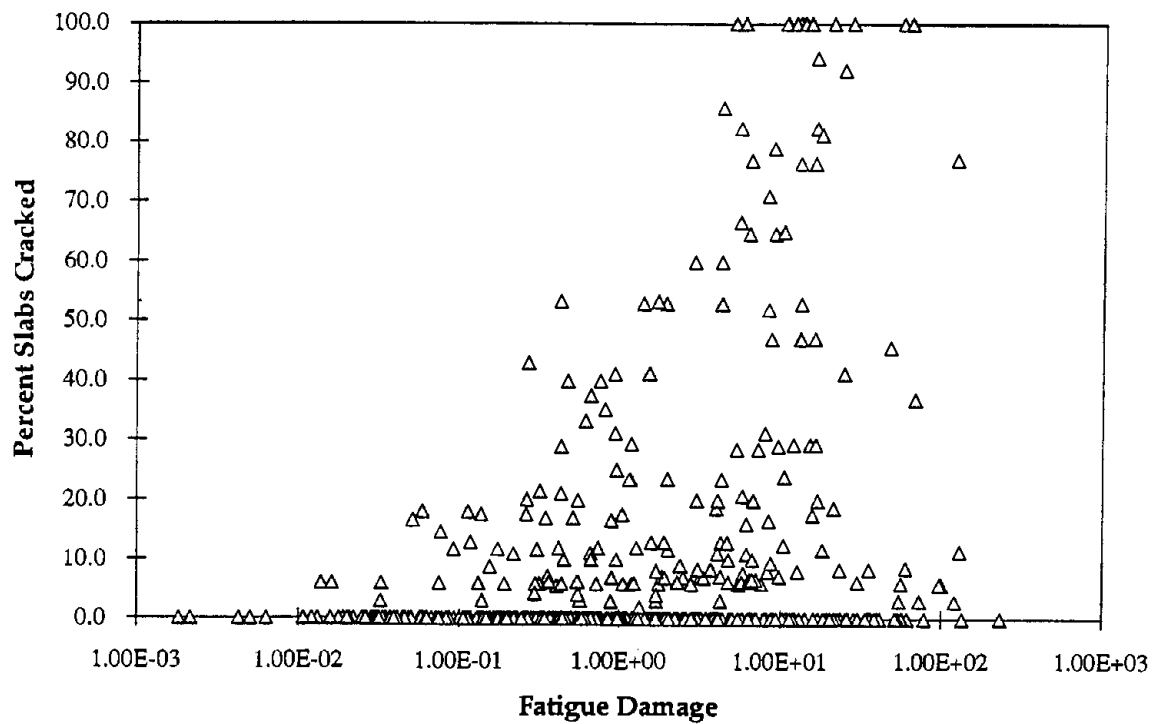


Figure 30. Preliminary fatigue analysis results given by ARE fatigue model.

A more precise determination of  $p/c$  is warranted because the edge load stress on concrete slabs is extremely sensitive to the load location. The edge load distribution due to a dual wheel load is illustrated in figure 31. Each line in this figure is the normalized stress at various location across the slab due to the load placed at a certain distance from the edge. The load placement shown in figure 31 starts at 0 in from the outer edge to 30 in (762 mm) from the edge. As shown in this figure, the edge stress drops rapidly, as the load is placed away from the edge. Even the load placed 2 in (51 mm) away from the edge produces stresses that are considerably less (about 12 percent drop) than the load placed directly at the edge. In terms of fatigue damage, the stress trends shown in figure 31 are much more significant (figure 32). To accurately determine the accumulated fatigue damage at critical location, the fatigue contribution by the traffic passing near the pavement edge needs to be determined more accurately.

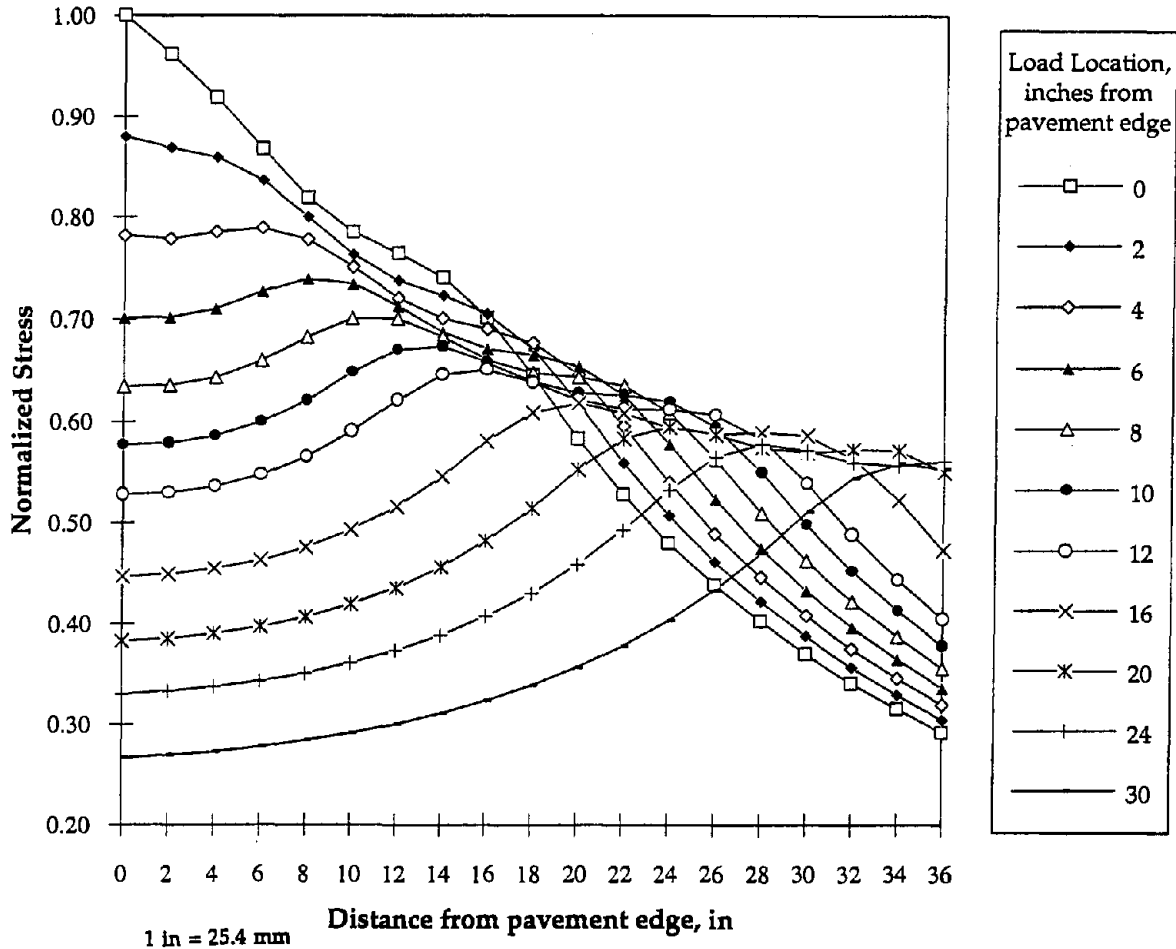


Figure 31. Edge load stress distribution across a pavement slab at mid-slab.

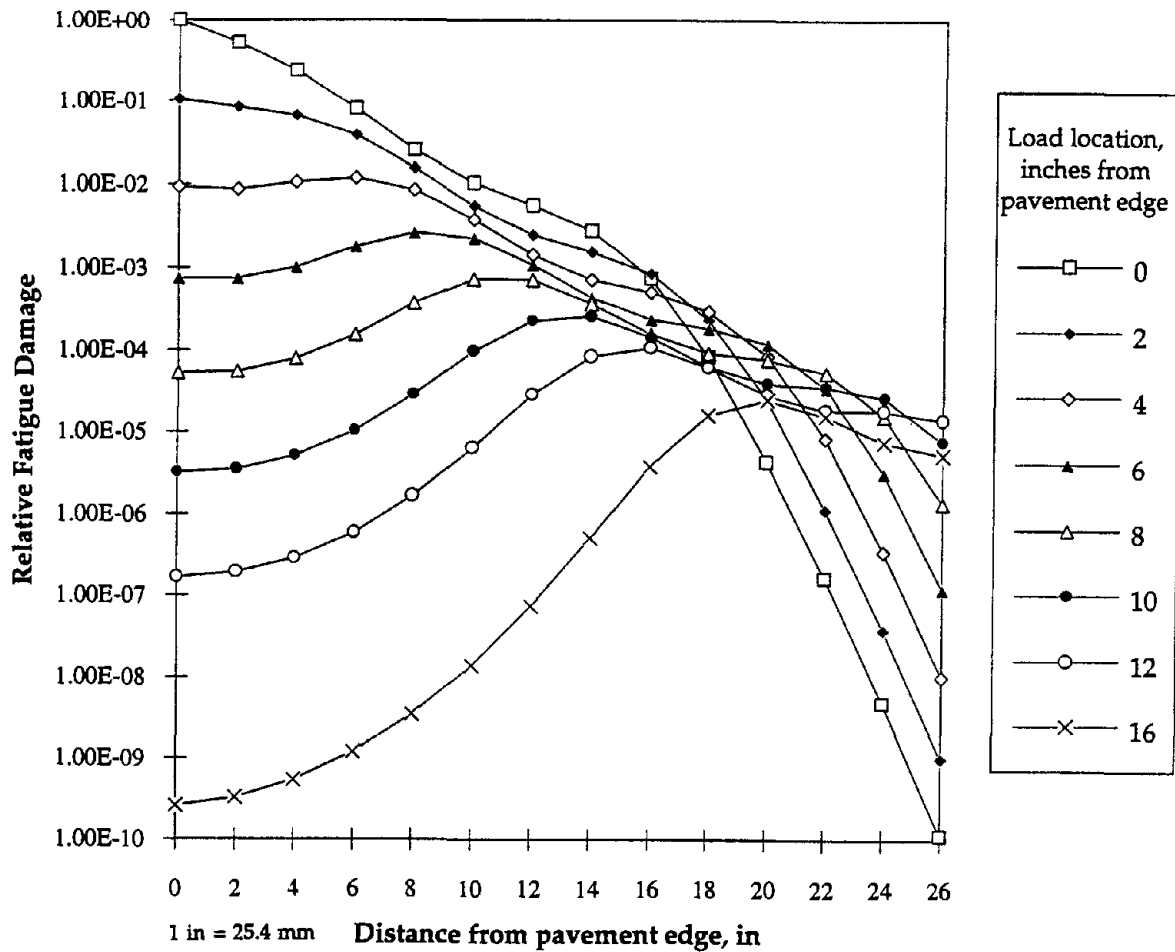


Figure 32. Fatigue damage distribution across a pavement slab due to the loads placed at various distances away from the pavement edge.

The fatigue damage caused by the traffic at any point on a pavement slab may be determined using  $FD/Pass$ . The  $FD/Pass$  may be defined as follows:

$$FD_{D_i}/Pass = \sum_j P(COV_{D_j}) * FD_{D_{ij}} \quad (31)$$

where:

- $FD_{D_i}/Pass$  = Fatigue damage per pass at the damage location  $D_i$ .
- $P(COV_{D_j})$  = Probability that the load will pass through location  $D_j$ .
- $FD_{D_{ij}}$  = Fatigue damage at location  $D_i$  due to the load at  $D_j$ .

The  $FD/Pass$  as defined above, represents the probabilistic amount of damage caused at the damage location  $D_i$  due to the applied traffic. It is important to note that  $FD/Pass$  is determined for a specific point on the pavement. To determine  $FD/Pass$ ,

the stress at the location of interest due to the loads placed at all relevant locations must be determined. Figure 31 is an example of the type of data needed to determine FD/Pass.

For fatigue analysis of JPCP, the most relevant location of interest is the longitudinal edge. Once the FD/Pass is determined, this number can be converted to p/c to show the number of equivalent load cycles (edge load applications) produced by the applied traffic. Taking fatigue damage as  $1/N$ , equation 32 can be used to determine p/c based on FD/Pass. Rewriting equation 7,

$$p/c_{D_i} = \frac{1/N_{D_{ii}}}{\sum_j P(\text{COV}_{D_j}) 1/N_{D_{ij}}} \quad (32)$$

where:

- $p/c_{D_i}$  = p/c at location  $D_i$ .
- $N_{D_{ii}}$  = Allowable number of load applications based on stress at location  $D_i$  due to the load placed at  $D_i$ .
- $P(\text{COV}_{D_j})$  = Probability that the load will pass through location  $D_j$ .
- $N_{D_{ij}}$  = Allowable number of load application based on stress at location  $D_i$  due to the load at  $D_j$ .

The traffic is assumed to be normally distributed. The subscript on p/c above denotes that the p/c determined above converts the traffic placed on the pavement to the equivalent number of load applications by the loads placed directly at  $D_i$  for fatigue damage at  $D_i$ . Equation 32 reduces to the following:

$$p/c_{D_i} = \frac{1}{\sum_j P(\text{COV}_{D_j}) \frac{N_{D_{ii}}}{N_{D_{ij}}}} \quad (33)$$

The p/c as defined in equation 33 involves a considerable amount of analysis; however, since it is a measure of relative damage caused by the loads placed at various locations, it is not very sensitive to the pavement structure. Therefore, p/c determined for the average case may be used. The p/c is, however, affected by several factors, including the following:

- Mean wheel location.
- Standard deviation of traffic wander.
- Stress level.

The mean wheel location and standard deviation of traffic is somewhat variable, and both of these factors have a significant effect on  $p/c$ . In this project the figures reported in reference 28 were used:

- Average wheel location = 22 in from pavement edge.
- Standard deviation = 8.4 in.

These results are based on 1,300 observations. The average wheel location on widened lane sections were about 2 in closer to the paint stripe; however, since the critical damage location on widened lane sections is directly under the wheel path, the  $p/c$  is close to 1.0 (i.e., almost every wheel passes through the critical location).

The effects of mean wheel location and stress level on  $p/c$  is illustrated in figure 33. The  $p/c$  is smaller (meaning more damaging) at higher stress levels, because the stresses due to loads placed greater distances away from the edge become significant. The following regression equation was developed for  $p/c$  and used in the analysis:

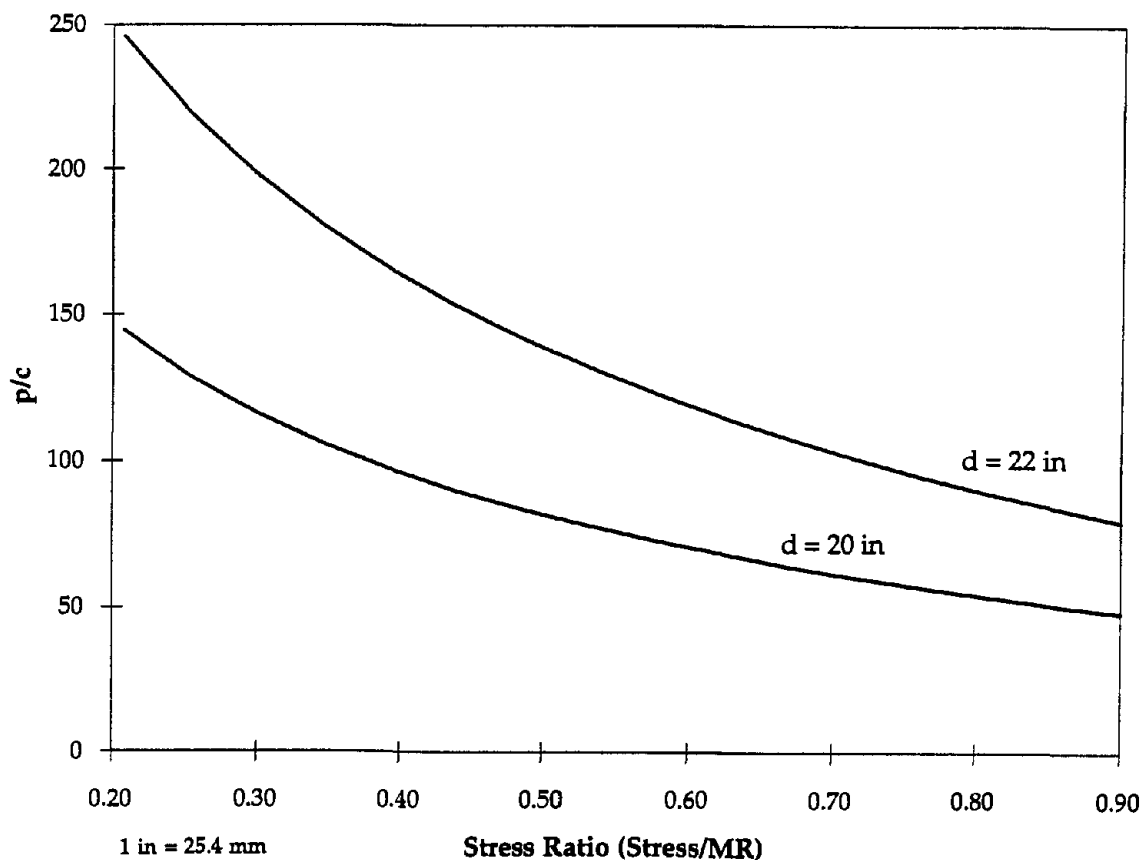


Figure 33. Effects of stress level and mean wheel location on  $p/c$ .

$$p/c = 418.9 - 1148.6SR + 1259.9SR^2 - 491.55SR^3 \quad (34)$$

$$R^2 = 1.0$$

where:

$$SR = \text{Stress-to-strength ratio } (\sigma/MR).$$

### *Consideration of Curling*

The hourly temperature gradients determined for each project (by slab thickness) were used directly to account for the effects of slab curling. Assuming that traffic is evenly distributed at all temperature gradients, the total traffic was multiplied by the frequency of the temperature gradients given in table 8 to estimate traffic passes at each temperature condition. The combined stress at each temperature gradient was then calculated. Using the traffic and the stress determined for each temperature gradient, the fatigue damage incurred at each temperature was obtained and summed to determine the total damage accumulated in each section. The calculations were performed on a spreadsheet using the equations described in this section. An example calculation is given in figure 34.

### *Critical Failure Mode*

The critical failure mode assumed in this project is the cracks initiating at the bottom of the slab at the longitudinal edge. The edge stress, which promotes this type of failure, is normally the most critical stress in pavement slabs. However, under certain conditions, JPCP slabs can also crack from top-down under corner loading. The residual negative temperature gradients and other factors that cause upward curling of pavement slabs, such as moisture gradient and differential drying of concrete, play a major role in this mode of failure.

The stresses that would lead to top-down cracking become significant only if the pavement slabs have a fair amount (about 15 °F [8.3 °C]) of residual, or built-in, negative effective temperature gradient. However, as discussed earlier, the conditions that cause negative residual temperature gradients in pavement slabs are not uncommon. In fact, based on references 23 and 24, most pavement slabs may be expected to be curled up to some degree. Although the corner-load stresses are much lower on doweled sections, top-down cracking can occur even on doweled pavements.

The residual negative temperature gradients have the effect of shifting the entire temperature gradient distribution in the negative direction. This, in turn, has the effect of simultaneously reducing the edge load stress and increasing the corner load stress. The effects of this temperature shift on the critical slab stresses are illustrated in figure 35. Because negative temperature gradients occur much more frequently than positive temperature gradients at all locations, the corner load stress does not have to be greater than the edge stress for the top-down cracking to become critical.

MR, psi = 700      Total Traffic = 20 MESAL  
 Stress LTE = 0.0      Wheel Load = 9,000 lbs      F Damage = 0.453  
 T Shift = 8.0      Tire Pressure = 95 psi      Cracking = 16.0%

h	Slab L, ft	Ec MPsi	k	Temp Diff	Freq	Traffic ESAL	Load Stress	Temp Stress	Stress L+T	FD ERES
10.0	15	5.00	200	-36.0	0.000	0	221.4	-316.4	203.0	0.000
10.0	15	5.00	200	-34.0	0.000	0	221.4	-298.9	172.0	0.000
10.0	15	5.00	200	-32.0	0.000	0	221.4	-281.3	147.0	0.000
10.0	15	5.00	200	-30.0	0.000	0	221.4	-263.7	127.5	0.000
10.0	15	5.00	200	-28.0	0.001	69	221.4	-246.1	113.0	0.000
10.0	15	5.00	200	-26.0	0.041	2,828	221.4	-228.5	103.1	0.000
10.0	15	5.00	200	-24.0	0.071	4,842	221.4	-211.0	97.4	0.000
10.0	15	5.00	200	-22.0	0.072	4,870	221.4	-193.4	95.4	0.000
10.0	15	5.00	200	-20.0	0.082	5,515	221.4	-175.8	96.7	0.000
10.0	15	5.00	200	-18.0	0.073	5,012	221.4	-158.2	101.0	0.000
10.0	15	5.00	200	-16.0	0.062	4,364	221.4	-140.6	107.9	0.000
10.0	15	5.00	200	-14.0	0.067	4,927	221.4	-123.1	117.1	0.000
10.0	15	5.00	200	-12.0	0.070	5,357	221.4	-105.5	128.2	0.000
10.0	15	5.00	200	-10.0	0.049	3,952	221.4	-87.9	141.1	0.000
10.0	15	5.00	200	-8.0	0.034	2,965	221.4	-70.3	155.3	0.000
10.0	15	5.00	200	-6.0	0.028	2,527	221.4	-52.7	170.7	0.000
10.0	15	5.00	200	-4.0	0.024	2,406	221.4	-35.2	186.9	0.000
10.0	15	5.00	200	-2.0	0.019	2,023	221.4	-17.6	203.9	0.000
10.0	15	5.00	200	0.0	0.027	3,151	221.4	0.0	221.4	0.000
10.0	15	5.00	200	2.0	0.029	3,589	221.4	17.6	239.1	0.000
10.0	15	5.00	200	4.0	0.027	3,626	221.4	35.2	257.0	0.000
10.0	15	5.00	200	6.0	0.037	5,423	221.4	52.7	275.0	0.002
10.0	15	5.00	200	8.0	0.033	5,330	221.4	70.3	292.8	0.005
10.0	15	5.00	200	10.0	0.033	5,724	221.4	87.9	310.4	0.013
10.0	15	5.00	200	12.0	0.035	6,650	221.4	105.5	327.7	0.034
10.0	15	5.00	200	14.0	0.031	6,315	221.4	123.1	344.6	0.065
10.0	15	5.00	200	16.0	0.033	7,225	221.4	140.6	361.2	0.140
10.0	15	5.00	200	18.0	0.019	4,568	221.4	158.2	377.3	0.154
10.0	15	5.00	200	20.0	0.003	735	221.4	175.8	392.9	0.040
10.0	15	5.00	200	22.0	0.000	0	221.4	193.4	408.2	0.000
10.0	15	5.00	200	24.0	0.000	0	221.4	211.0	423.1	0.000
10.0	15	5.00	200	26.0	0.000	0	221.4	228.5	437.6	0.000
<b>SUM</b>					1.000	1.04E+05	<b>Total Fatigue Damage</b>		0.453	

P	p	a eq	SR	l	C	R	L/l	.01 L/l	DT	Lam	p/c
9,000	95	6.88	0.29	38.2	0.64	0.058	4.7	0.047	-19.800	1.666	189.1
9,000	95	6.88	0.25	38.2	0.64	0.165	4.7	0.047	-18.700	1.666	216.4
9,000	95	6.88	0.21	38.2	0.64	0.264	4.7	0.047	-17.600	1.666	240.7
9,000	95	6.88	0.18	38.2	0.64	0.356	4.7	0.047	-16.500	1.666	261.0
9,000	95	6.88	0.16	38.2	0.64	0.440	4.7	0.047	-15.400	1.666	276.9
9,000	95	6.88	0.15	38.2	0.64	0.517	4.7	0.047	-14.300	1.666	288.2
9,000	95	6.88	0.14	38.2	0.64	0.588	4.7	0.047	-13.200	1.666	294.9
9,000	95	6.88	0.14	38.2	0.64	0.651	4.7	0.047	-12.100	1.666	297.3
9,000	95	6.88	0.14	38.2	0.64	0.709	4.7	0.047	-11.000	1.666	295.8
9,000	95	6.88	0.14	38.2	0.64	0.761	4.7	0.047	-9.900	1.666	290.7
9,000	95	6.88	0.15	38.2	0.64	0.807	4.7	0.047	-8.800	1.666	282.8
9,000	95	6.88	0.17	38.2	0.64	0.847	4.7	0.047	-7.700	1.666	272.4
9,000	95	6.88	0.18	38.2	0.64	0.883	4.7	0.047	-6.600	1.666	260.2
9,000	95	6.88	0.20	38.2	0.64	0.914	4.7	0.047	-5.500	1.666	246.7
9,000	95	6.88	0.22	38.2	0.64	0.940	4.7	0.047	-4.400	1.666	232.4
9,000	95	6.88	0.24	38.2	0.64	0.961	4.7	0.047	-3.300	1.666	217.7
9,000	95	6.88	0.27	38.2	0.64	0.979	4.7	0.047	-2.200	1.666	202.9
9,000	95	6.88	0.29	38.2	0.64	0.993	4.7	0.047	-1.100	1.666	188.3
9,000	95	6.88	0.32	38.2	0.64	1.003	4.7	0.047	0.000	1.666	174.2
9,000	95	6.88	0.34	38.2	0.64	1.010	4.7	0.047	1.100	1.666	160.8
9,000	95	6.88	0.37	38.2	0.64	1.015	4.7	0.047	2.200	1.666	148.1
9,000	95	6.88	0.39	38.2	0.64	1.016	4.7	0.047	3.300	1.666	136.3
9,000	95	6.88	0.42	38.2	0.64	1.016	4.7	0.047	4.400	1.666	125.3
9,000	95	6.88	0.44	38.2	0.64	1.013	4.7	0.047	5.500	1.666	115.3
9,000	95	6.88	0.47	38.2	0.64	1.008	4.7	0.047	6.600	1.666	106.2
9,000	95	6.88	0.49	38.2	0.64	1.002	4.7	0.047	7.700	1.666	97.9
9,000	95	6.88	0.52	38.2	0.64	0.994	4.7	0.047	8.800	1.666	90.4
9,000	95	6.88	0.54	38.2	0.64	0.985	4.7	0.047	9.900	1.666	83.6
9,000	95	6.88	0.56	38.2	0.64	0.976	4.7	0.047	11.000	1.666	77.6
9,000	95	6.88	0.58	38.2	0.64	0.966	4.7	0.047	12.100	1.666	72.1
9,000	95	6.88	0.60	38.2	0.64	0.956	4.7	0.047	13.200	1.666	67.2
9,000	95	6.88	0.63	38.2	0.64	0.946	4.7	0.047	14.300	1.666	62.8

1 psi = 6.9 KPa  
 1 lb = .45 kg

Figure 34. Example fatigue damage calculation.



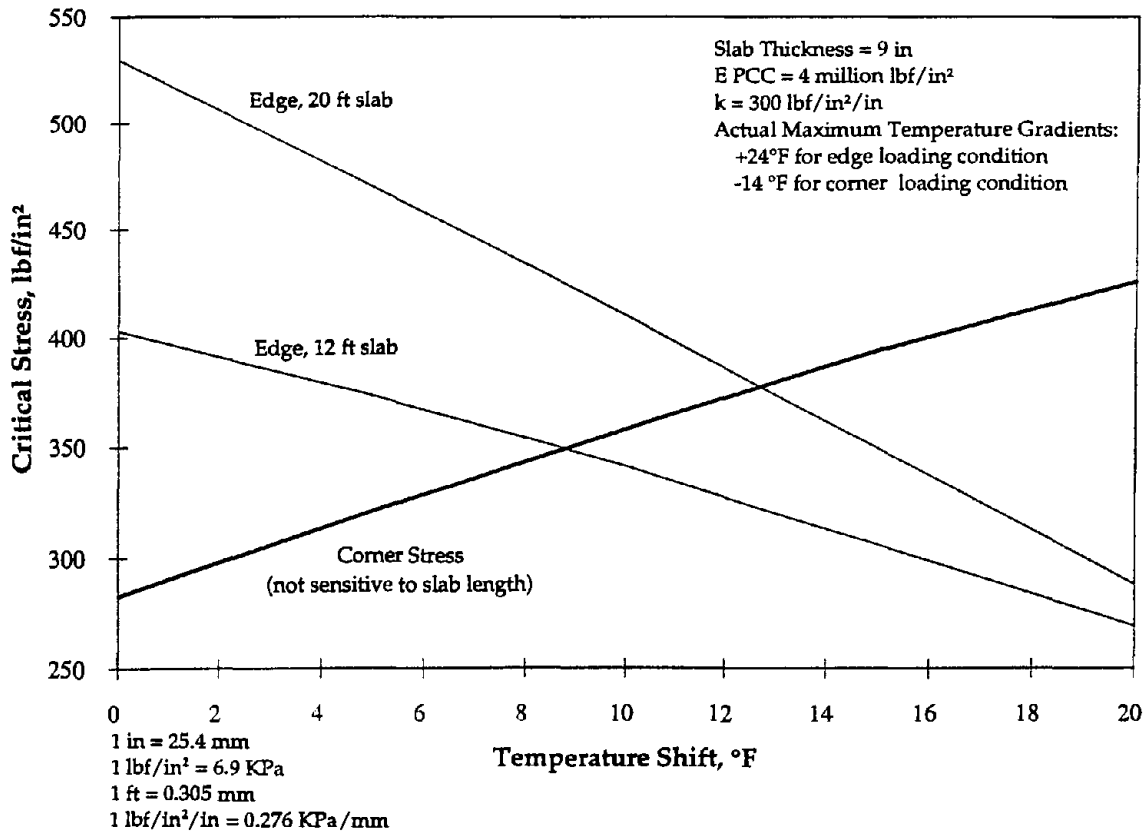


Figure 35. Effects of temperature gradient shifts on critical stresses for fatigue damage.

The top-down cracking is more critical on shorter slabs than longer slabs, because the corner load stresses are not very sensitive to slab length. While the slab length is critical to the curling stress at the longitudinal edge, it does not have as great an effect on the curling of the slab corners because the curling of the slab corners depends on both the slab length and width. Therefore, bottom-up cracking is more likely to be critical on long slabs, while top-down cracking is likely to be critical on short slabs. For top-down cracking, the foundation stiffness ( $k$ ) is a more critical factor than slab length. The effects of slab length and  $k$  on the critical slab stresses are illustrated in figure 36.

As discussed earlier, the top-down cracking needs further investigation. The factors that significantly affect top-down cracking include the following:

- Magnitude of residual temperature gradient.
- Dowels.
- Base type.
- Subgrade  $k$ .

Of the factors listed above, the most difficult information to obtain is the magnitude of residual temperature gradient.

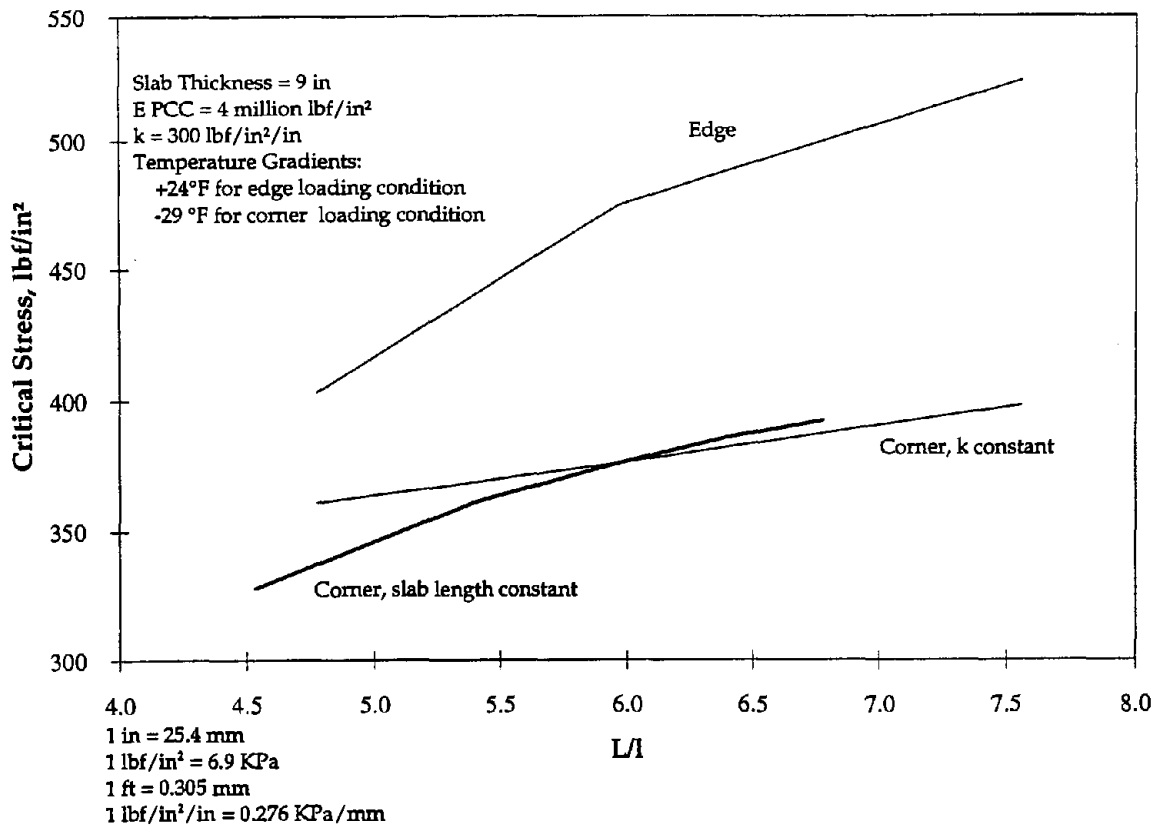


Figure 36. The effects of slab length on critical stresses in the pavement slab.

Based on preliminary analysis, it appears that while the top-down cracking could be the critical mode of failure in some cases, the magnitudes of fatigue damage involved in both types of cracking are similar; that is, even if the temperature gradients are significantly shifted, so that the top-down cracking becomes critical, the fatigue damage calculated assuming the edge loading as the critical mode of failure would not lead to gross errors. The only exception is for short slabs. Further study is needed to model top-down cracking.

### Model Development

The progression of the model development, from raw data to the finished model, are described in the following. The cracking model relates the amount of fatigue cracking to the accumulated fatigue damage in the pavement section. In developing this model, a detailed analysis was performed to determine the accumulated fatigue damage in the pavement sections included in the evaluation. The factors considered in this analysis include the following:

- Thermal curling.
- Edge support and widened lanes.
- Structural contribution of stabilized bases.
- p/c.

The above list represents all of the factors normally considered to have a significant effect on the stresses in pavement slabs, except moisture warping. These

factors were given a very thorough treatment in this evaluation to ensure that their effects are accurately incorporated in the fatigue analysis. Nevertheless, the initial analysis results showed a considerable scatter (figures 27 through 30).

Further refinements were made to the data, considering the effects of the others factors that cause upward curling of pavement slabs, to improve the correlation between the calculated fatigue damage and observed slab cracking. When all of the adjustments were made, a best-fit curve was fitted through the data to obtain the fatigue cracking model. In the following, the details of the model development is presented, along with a discussion of the rationale and justification for some of the adjustments made to the data.

### *Preliminary Analysis*

The cracking data collected under this project and those from the preceding study are shown in figure 37. As expected, a simple plot of traffic versus percent slab cracking does not show any trend, demonstrating that the slab design factors are important to pavement performance.

The next level of refinement is illustrated in figure 38. In this figure, the fatigue damage estimate was performed considering load stresses only. Figure 38 shows that the slabs are more likely to crack when the fatigue damage is high and less likely to crack when the fatigue damage is low. However, there is still a considerable amount of scatter in the data, and the figure still does not show a clear relationship.

When curling stresses are included in the analysis, the results show a very clear trend of an increasing amount of cracking for an increasing amount of fatigue damage. The results based on for ERES/COE fatigue damage model are shown in figure 39; those for all of the damage models considered in this study are given in figures 27 through 30. As previously discussed, these results still show a considerable scatter, indicating that not all factors significantly influencing fatigue cracking have been taken into consideration.

On the preliminary analysis, the ERES/COE model gave the best results; therefore, this model was selected for use in this evaluation and in all subsequent refinements. The NCHRP 1-26 model also gave similar results, but the results were shifted to the left by one order of magnitude. This in itself is not important, but since the two models gave very similar results the one that seems to give the damage numbers in more conventional range (about 50 percent cracking at fatigue damage of 1.0) was selected.

Refinements were made in the fatigue analysis to account for the effects of the following factors:

- Effective slab thickness.
- Residual temperature gradients.

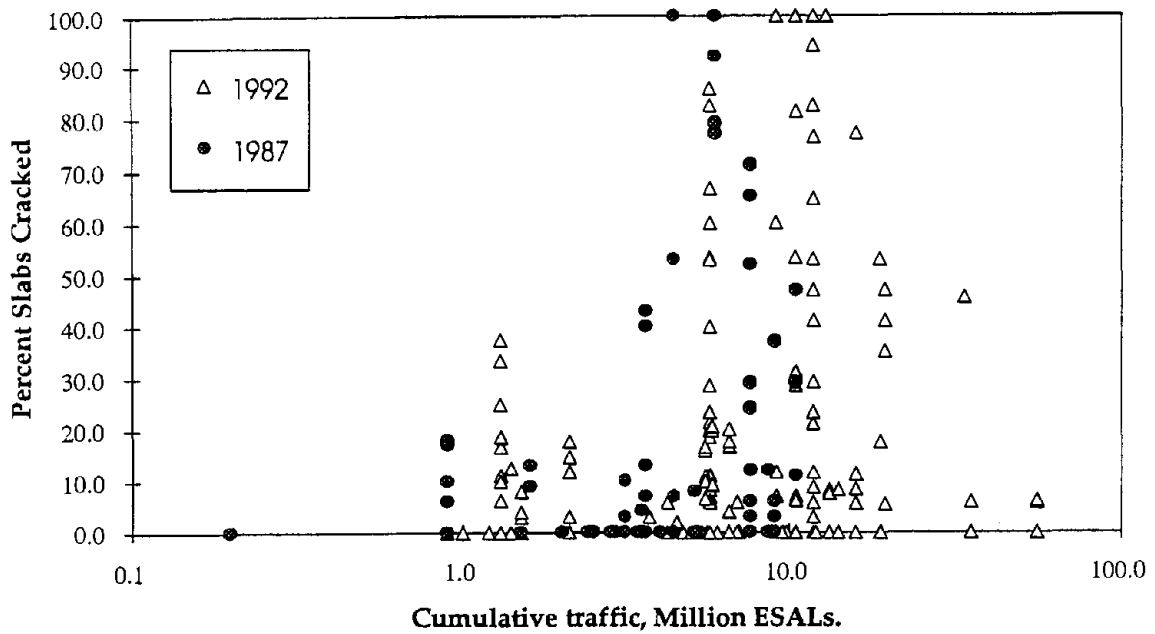


Figure 37. Slab cracking data versus total ESAL applied.

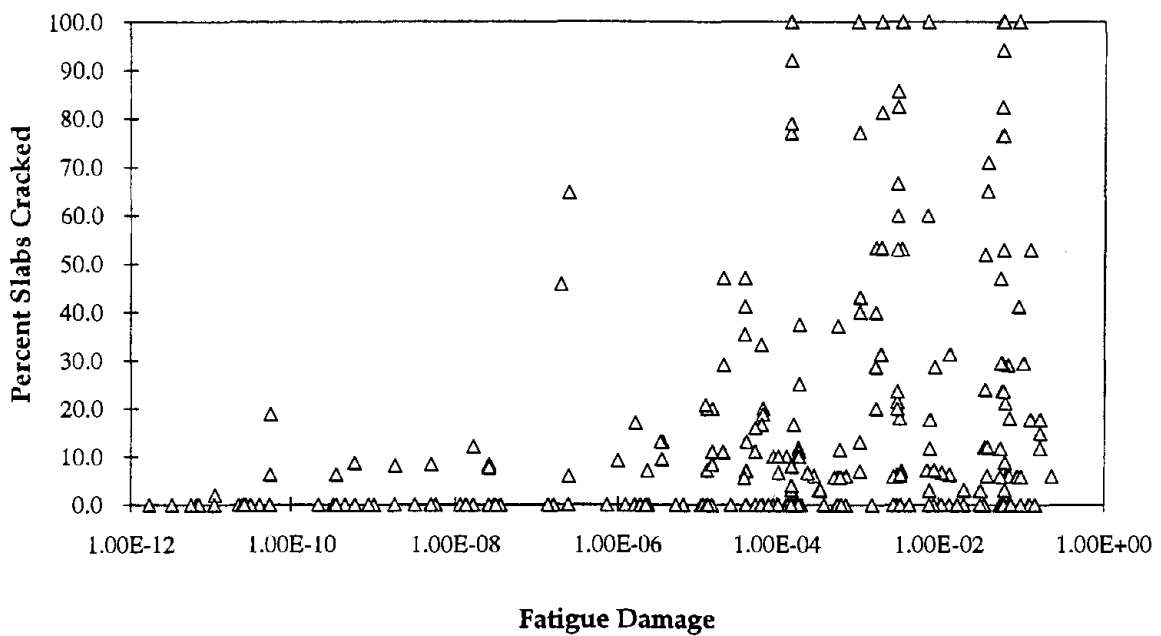


Figure 38. Slab cracking versus fatigue damage calculated using load stresses only.

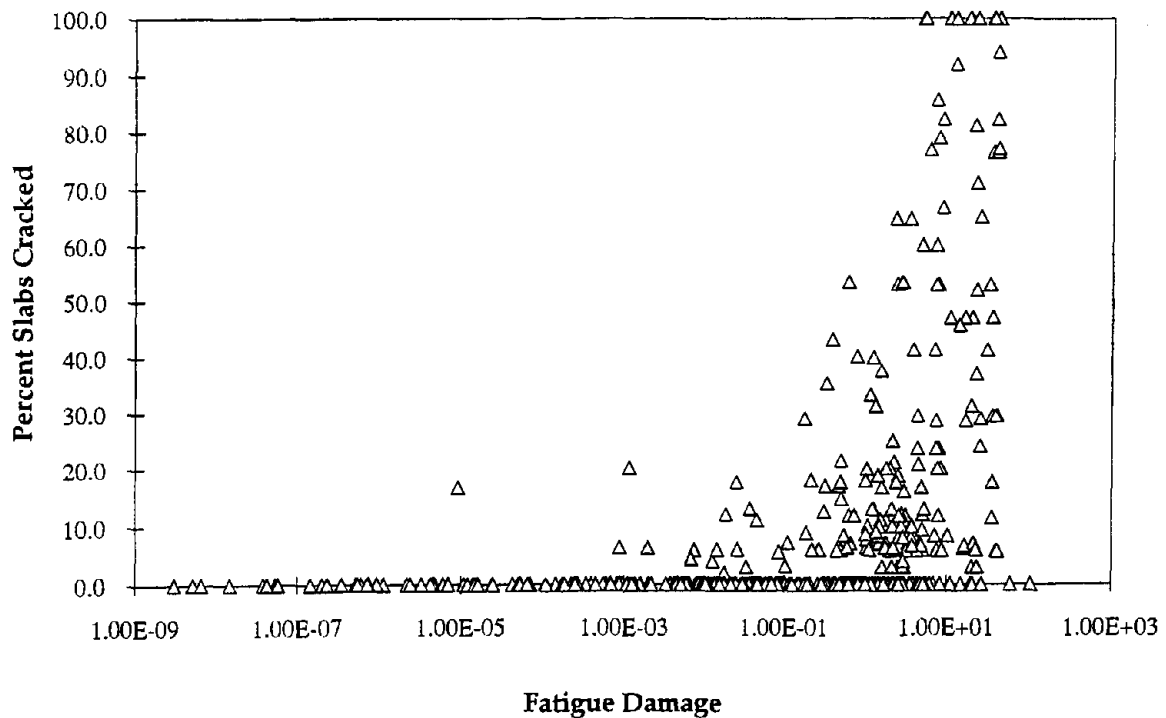


Figure 39. Slab cracking vs fatigue damage calculated considering both load and curling stresses.

#### *Consideration of Effective Slab Thickness*

As discussed in chapter 4 of volume II, the effective slab thickness was used in this project to account for the structural contribution of stabilized bases. The effective slab thickness was determined either directly from the backcalculated  $l$  or theoretically, using the parallel axes theorem (equation 29, volume II). In theory, the structural contribution of a stabilized base can be considerable if it can be assumed bonded to the pavement slab. A recent study has shown that the actual physical bonding of the two pavement layers is not necessary to obtain the bonded structural response.<sup>(34)</sup> The bonded response may be obtained if sufficient friction exists between the two pavement layers. The FWD testing results also showed that the bonded response was obtained from virtually all stabilized base sections. However, the fatigue analysis results did not support these findings.

The results of fatigue analysis based on the effective slab thickness is shown in figure 40. This figure shows a wide scatter in the analysis results. When the analysis was repeated, using the slab thickness only, the results showed a very clear trend (figure 41). There may be at least two possible reasons for these unexpected results:

- Some of the cracking observed in the stabilized base sections may be from top-down cracking. The slab corners are particularly susceptible to the debonding, even in bonded concrete overlay sections, due to large deflections at those locations. If the pavement slab is not bonded to the base, the corner stresses

under high negative temperature gradients could become excessive, leading to slab cracking.

- The FWD testing for backcalculation is normally conducted at the interior locations, near the slab center. The deflections at the interior locations are significantly less than those at either the slab corners or edges. Also, if the pavement slabs are curled up most of the time, as discussed earlier, then the slab centers would be further pressed against the base by the lifting of the slab corners and edges. Therefore, while the pavement slab may be effectively bonded to the stabilized base at the center locations, it may not be able to develop enough frictional forces at the slab edges to give the bonded response.

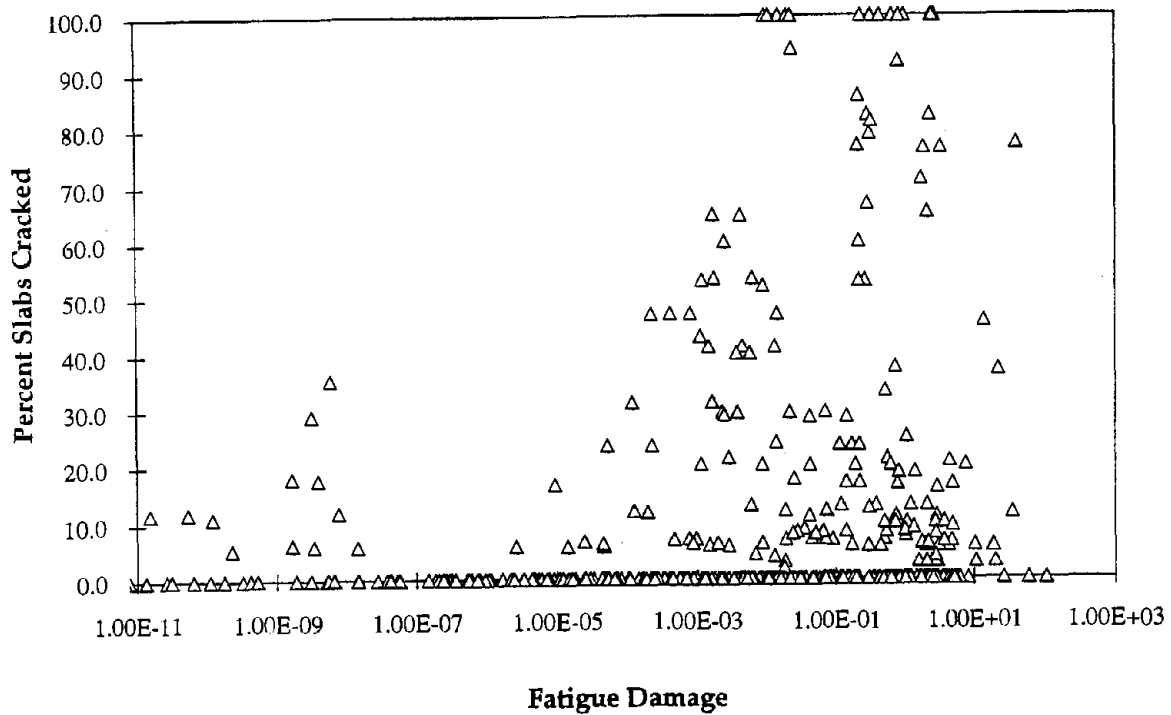


Figure 40. Results of fatigue analysis performed using effective slab thickness.

Although not all stabilized base sections exhibited bonded behavior, the performance given by some of the sections seem to indicate that an effective bond exists between the pavement slab and the stabilized base. This is evidenced by low levels of slab cracking, or no slab cracking, at high calculated fatigue damage. On those sections, the use of the effective slab thickness gave a more reasonable correlation between percent slab cracking and fatigue damage. Those sections exhibiting bonded response were individually identified and on those sections, the effective slab thickness was used.

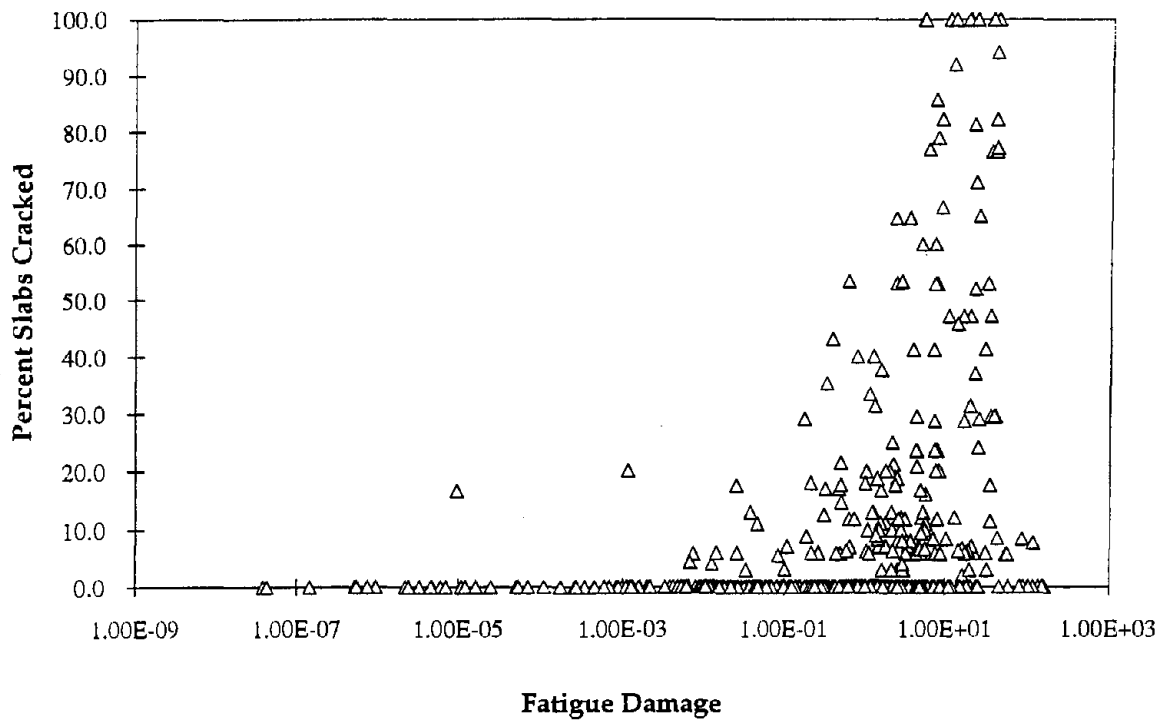


Figure 41. Results of fatigue analysis performed using design slab thickness.

All thickness changes were made uniformly in any given section to ensure that the thickness assignment is reasonable and consistent. Most sections analyzed were represented by two or more data points, resulting from the use of 1987 and 1992 data for the sections included in the preceding study, and many of the JPCP sections included in this model contain random joint spacings. Since each slab length in random joint sections were broken out as a separate section, four subsections were included for each actual random joint section in the analysis. Any thickness changes were made uniformly within an actual pavement section. This requirement provided the verification that the thickness assignment was reasonable. Random joint sections typically include a wide range of slab sizes (e.g., 12 ft [3.7 m] to 19 ft [5.8 m]). Since the edge stress is very sensitive to both slab thickness and slab length, any changes in the slab thickness has a significant effect on fatigue damage and therefore the changes in the calculated fatigue damage is very different for different length slabs. Since the slab thicknesses was required to be assigned consistently within a pavement section, the fatigue damage calculated had to be reasonable for all slab sizes for the assignment to be made.

Figure 39 already include the results of thickness adjustments. Although the change from figure 41 (slab thickness only) to figure 39 is not readily visible, this

adjustment resulted in a very significant improvement. Note the changes for the section having high fatigue damage but no cracking between the two figures. The thickness adjustment shifted a large number of sections with no cracking to the left in figure 39, showing more reasonable fatigue values for many of these sections.

### *Consideration of Moisture and Residual Temperature Gradients*

Regardless of the cause, any curling or warping of pavement slabs has a significant effect on critical stresses in a pavement slab. As discussed earlier, numerous factors can cause upward curling of pavement slabs. The effects of slab curling by other factors are directly additive to the effects of thermal curling; therefore, significant error can result if considerations are given only to thermal curling.

In this project, the cumulative effects of curling (or warping) caused by all factors other than temperature gradients were addressed by shifting the temperature gradients determined for each pavement section. The actual magnitude of the effective residual curling is unknown. However, using the same logic used to make the thickness adjustments, the consistency within the data set could be used as the guide to make relative adjustments. Again, consistent adjustments were made for all data points within an actual pavement section, and the reasonableness of the results was used as the guide in making these adjustments.

The analysis results with 4 °F (2.2 °C) shift for the residual curling in selected sections is shown in figure 42. After this initial shift, the sections requiring further temperature shifts were identified and an 8 °F (4.4 °C) shift was made (figure 43). Following the same procedure, further fine adjustments were made, applying up to 16 °F (8.9 °C) shifts on selected sections to obtain the final result shown in figure 44. The data points shown by the shaded circles in figure 44 are those suspected to be caused by top-down cracking and other outliers. These data points, totaling 13 (out of 578), were removed before performing regression to obtain the cracking model.

The type of variation in the applied temperature shifts is reasonable, since the temperature gradients during construction (more specifically, the temperature gradient at the time of concrete hardening) is a major contributor of residual curling. Paving operations normally begin early in the morning and continue until late in the afternoon. During this time, the concrete is exposed to continuously variable temperature conditions. This would lead to the same variation in residual curling.

### *Regression*

A nonlinear regression was performed on the final fatigue analysis results shown in figure 44 to obtain the slab cracking model. The following form of equation was selected for the equation:



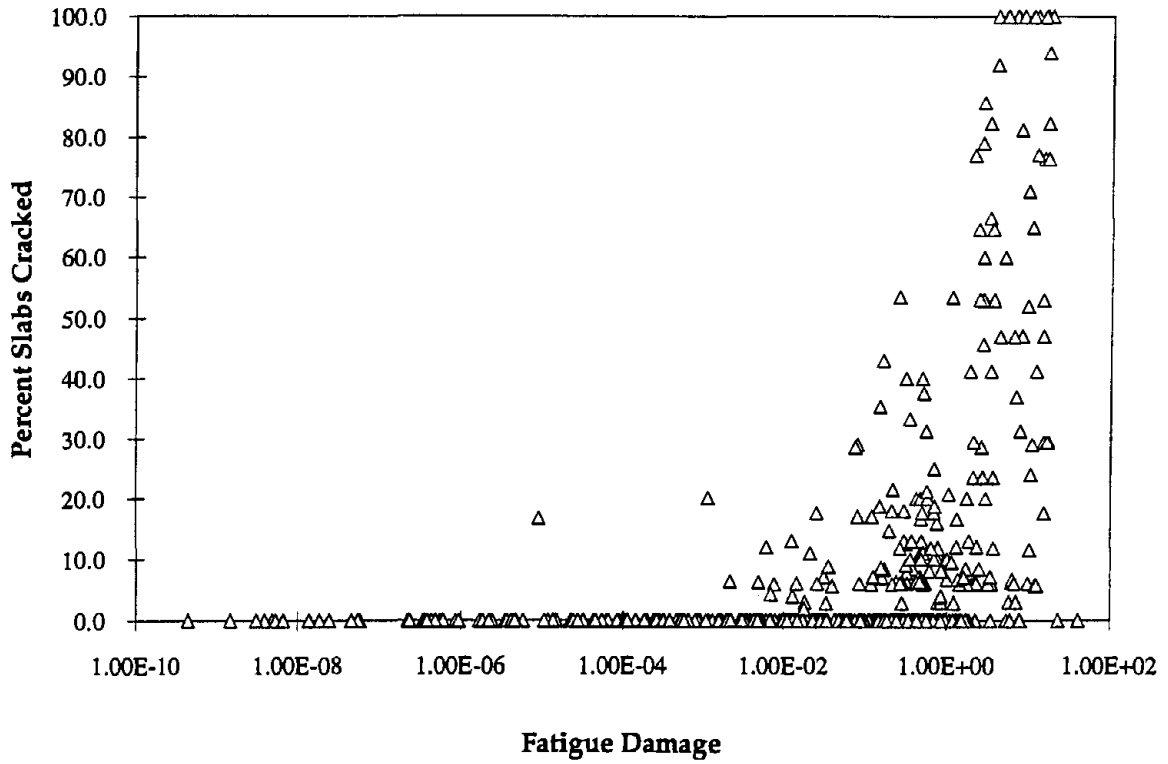


Figure 42. Fatigue analysis results with 4 °F (2.2 °C) shift applied to the temperature gradients.

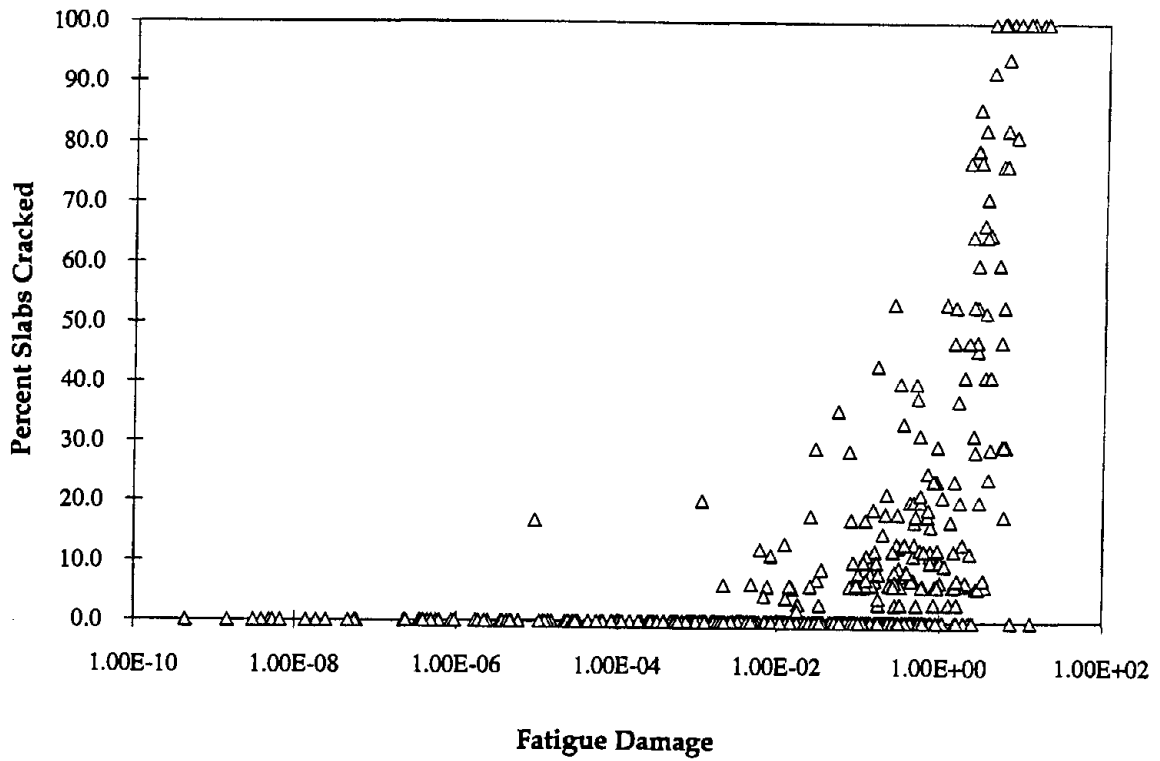


Figure 43. Fatigue analysis results with 8 °F (4.4 °C) shift applied to the temperature gradients.

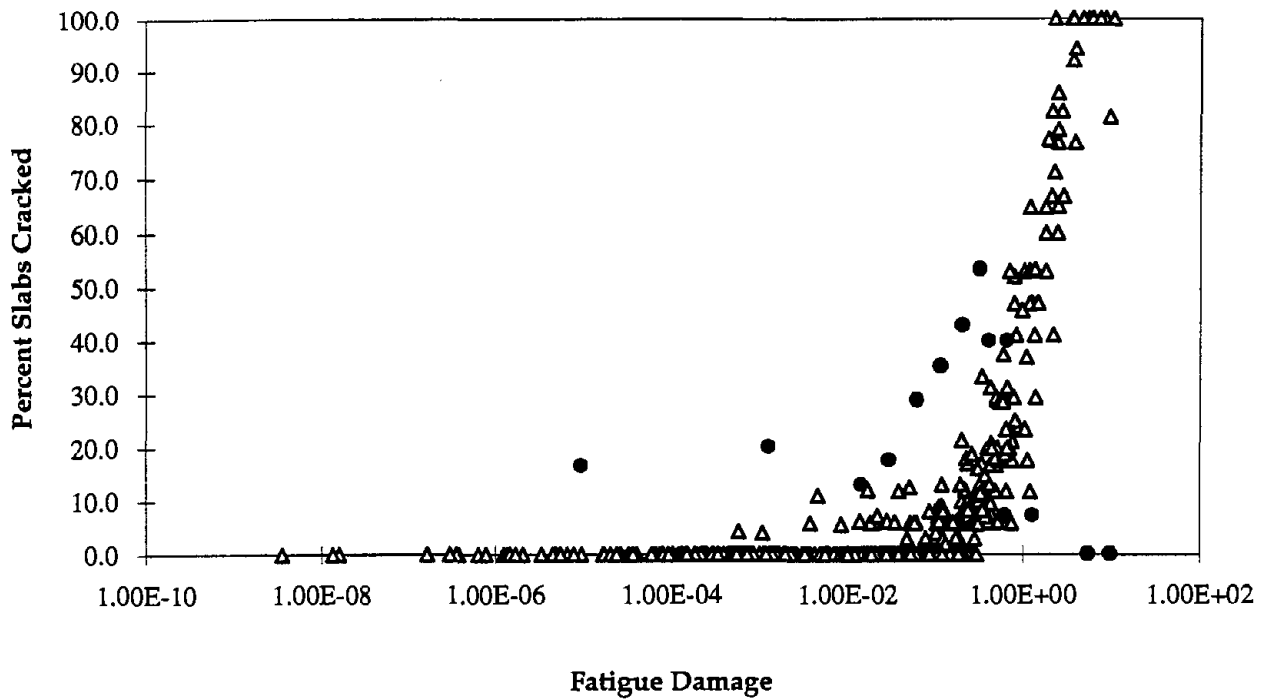


Figure 44. Final fatigue analysis results, including slab thickness and temperature gradient adjustments.

$$\text{Percent Cracking} = \frac{FD^n}{a^n + FD^n} \quad (35)$$

where:

- FD = Accumulated fatigue damage ( $\sum n/N$ ).
- a, n = Regression constants.

This form of equation was selected, because it is representative of the characteristic curve for the cracking model and satisfies the boundary conditions:

- 0 percent cracking at FD = 0.
- 100 percent cracking at FD =  $\infty$

The regression coefficients a and n were determined by minimizing the error in the predicted slab cracking. Once these coefficients were determined, the following equation was obtained by simplifying equation 35:

$$\text{Percent Cracking} = \frac{100}{1 + 1.41 \text{FD}^{-1.66}}$$

$$\begin{aligned} R^2 &= 0.91 \\ \text{SEE} &= 6.8 \\ n &= 465 \end{aligned}$$

where:

FD = Accumulated fatigue damage ( $\Sigma n/N$ ).

The regression result is shown in figure 45.

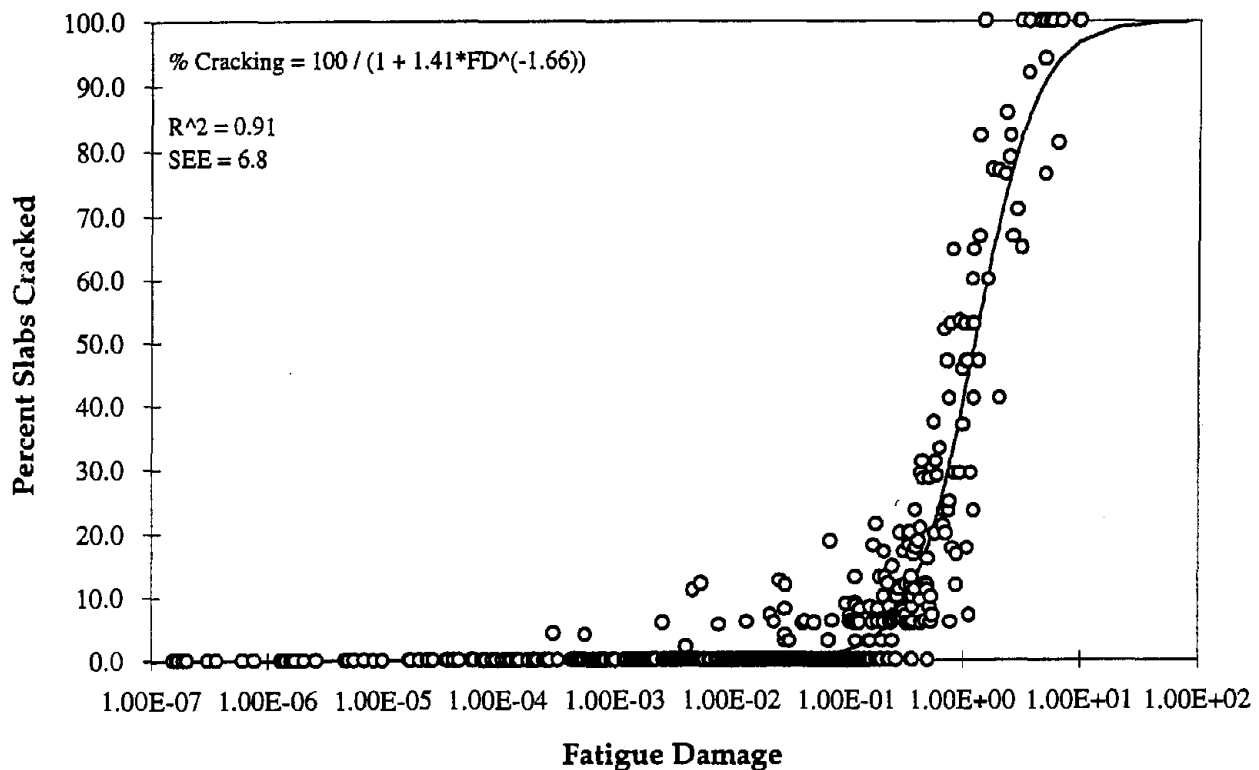


Figure 45. The fatigue cracking model.

### Sensitivity Analysis

The sensitivity of various concrete pavement design factors were evaluated using the cracking model developed under this project. The results of this analysis are shown in figures 46 through 52. The design factors evaluated include the following:

- Slab thickness (figure 46).
- Joint spacing (figure 47).
- Shoulder type (figure 48).
- Stabilized base (figure 49).

- Climate (figure 50).
- k-value (figure 51).
- PCC modulus of rupture (figure 52).

The results show that fatigue cracking is very sensitive to slab thickness, joint spacing, and shoulder type. The curling stresses in the pavement slabs increase rapidly with the increasing joint spacing, leading to increased slab cracking (figure 47). Figure 48 shows that a tied PCC shoulder and widened slabs can significantly reduce the amount of slab cracking. The tied PCC shoulders improve cracking performance by reducing stresses at the pavement edge. The effectiveness of the tied PCC shoulder depends on the load transfer efficiency across the lane-shoulder joint. Widened slabs effectively move the traffic away from the pavement edges, thus allowing the interior stresses (rather than much higher edge stresses) to control fatigue cracking.

Other factors that affect cracking of JPCP include stabilized base, climate, subgrade support (k-value) and PCC modulus of rupture. The stabilized base can have a significant effect on slab cracking if the base may be considered bonded to the pavement slabs (figure 49); however, the effect is negligible if the bonded response cannot be obtained. Figure 50 shows that the climate can have a significant effect on slab cracking. The conditions in the hotter climates generally lead to more slab cracking because of the higher temperature gradients. For top-down cracking, moisture conditions may also be important; drier conditions cause greater amounts of cracking because of the greater differential shrinkage. Figure 51 shows that the PCC modulus of rupture also has a significant effect on slab cracking. The subgrade modulus of reaction has a relatively minor effect (figure 52), but the difference between the extreme conditions can be significant.

In general, the performance trends predicted by the cracking model appear reasonable and consistent with the field observations. More details on the effects of various factors on fatigue performance of JPCP are given in chapter 3, *Concrete Pavement Design Recommendations*.

### Application of the Cracking Model

The JPCP cracking model developed under this study (equation 36) is based on the fatigue damage that was determined considering the effects of various factors that cause built-in, upward curling of PCC slabs (e.g., differential shrinkage, temperature gradients built into the slabs during construction). The excellent correlation shown in figure 45 was achieved by applying various equivalent temperature gradients to account for the effects of built-in curling. The equivalent temperature gradients were introduced in the damage calculation by shifting the actual distribution of temperature gradients (obtained using CMS) by the magnitude of the effective temperature gradient. The applied equivalent temperature gradients ranged from 4 to 16 °F (2.2 to 8.9 °C). When this model is used without considering the built-in upward curling of slabs, the model is likely to predict an excessively high amount of cracking.

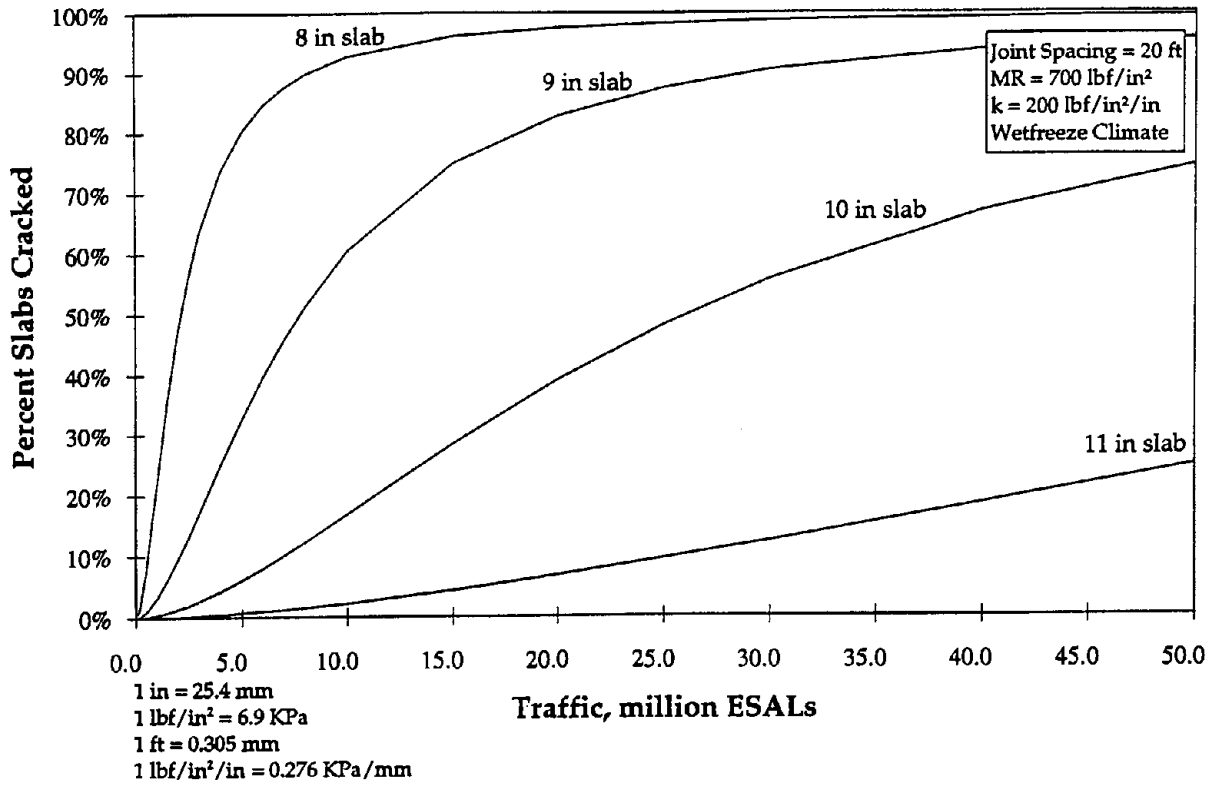


Figure 46. Sensitivity of JPCP cracking model to slab thickness.

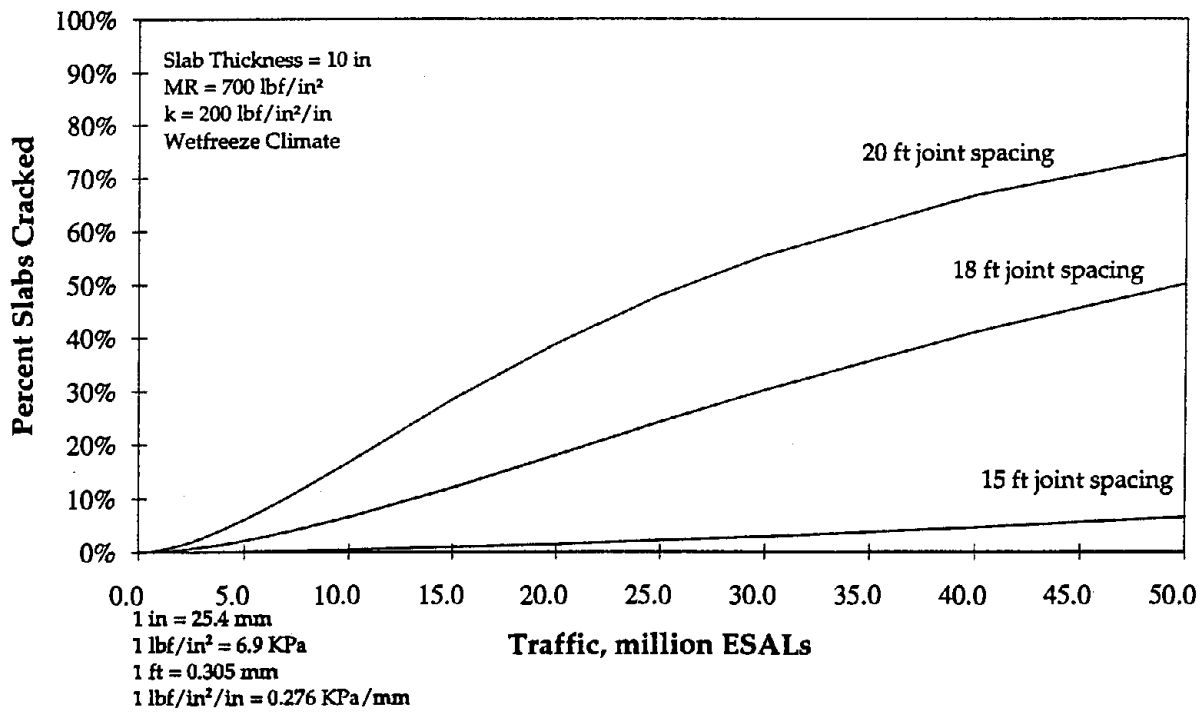


Figure 47. Sensitivity of JPCP cracking model to joint spacing.

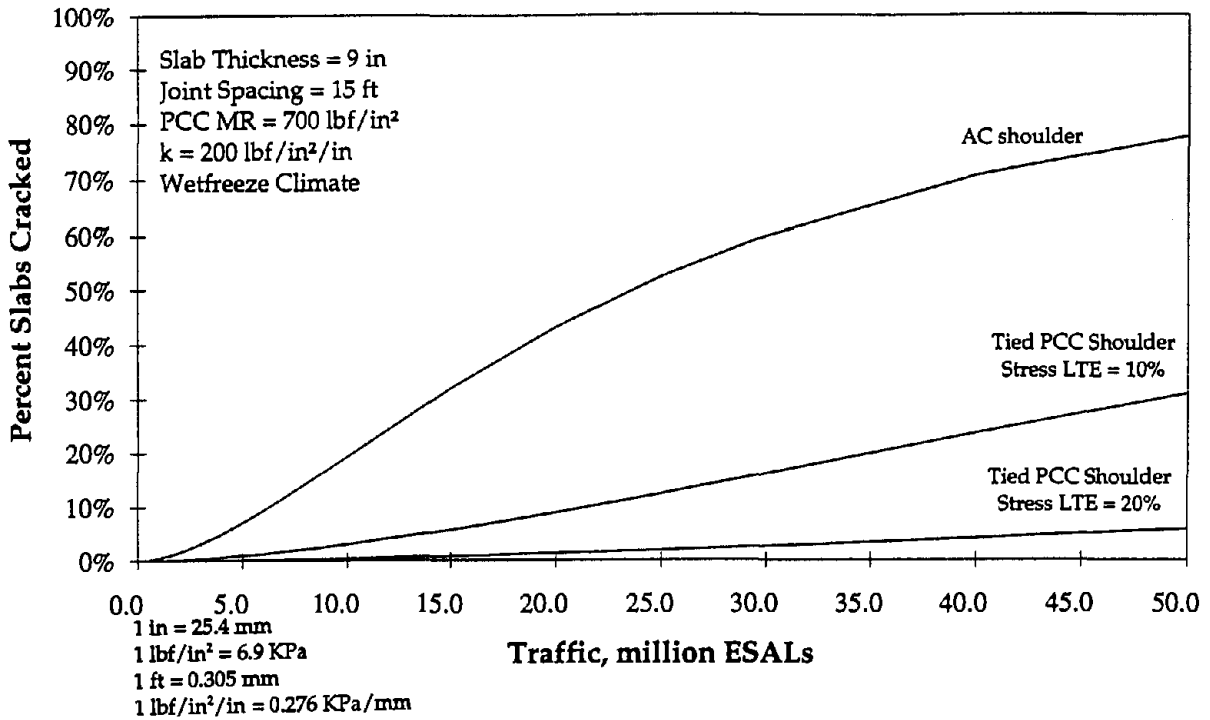


Figure 48. Sensitivity of JPCP cracking model to shoulder type.

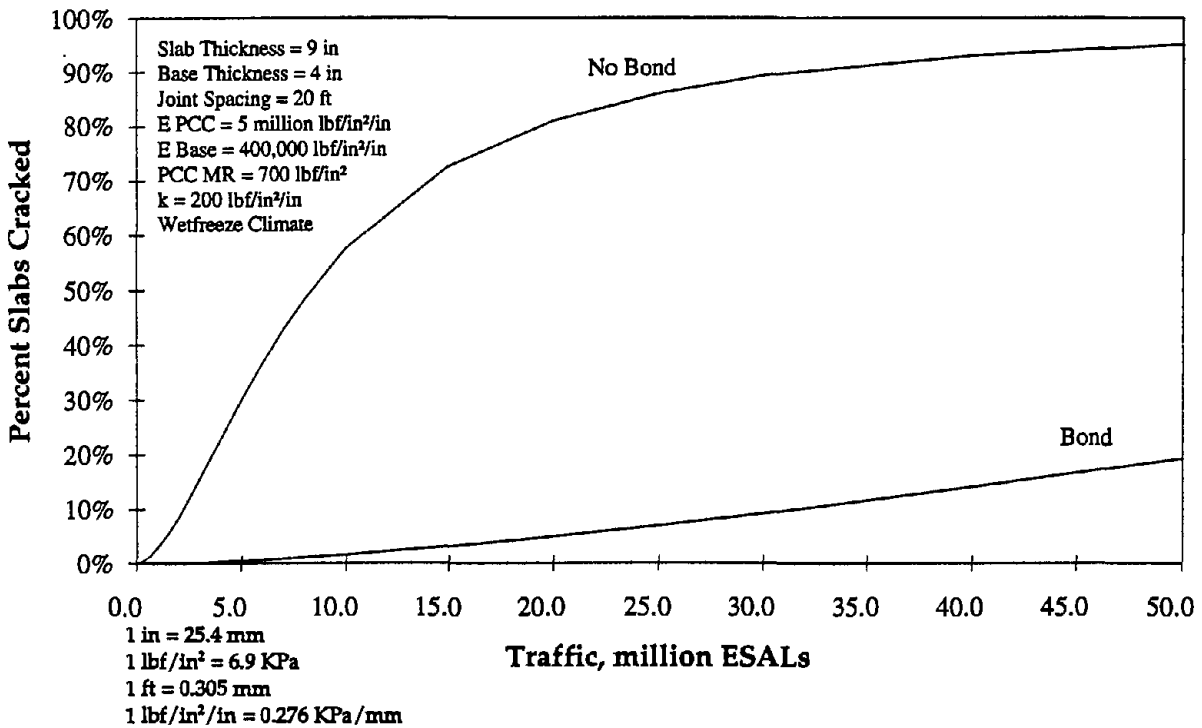


Figure 49. Sensitivity of JPCP cracking model to bonding condition of base.

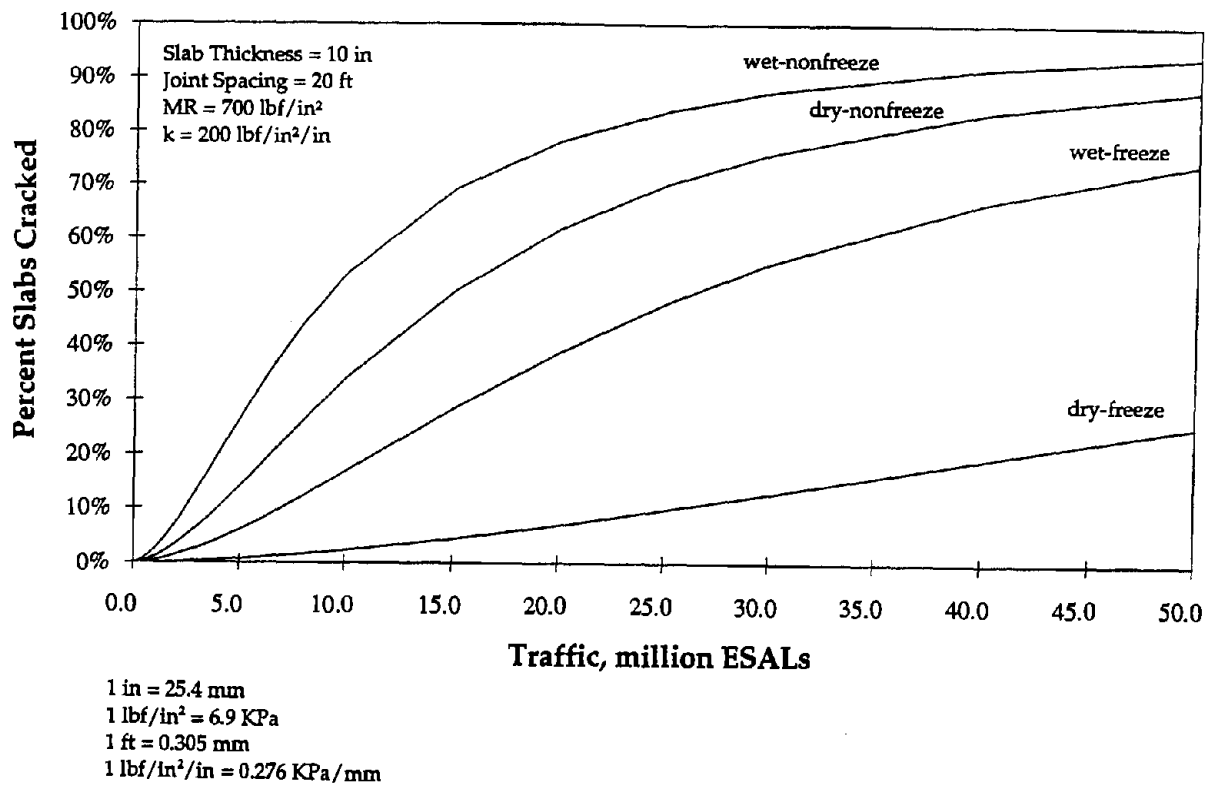


Figure 50. Sensitivity of JPCP cracking model to climate.

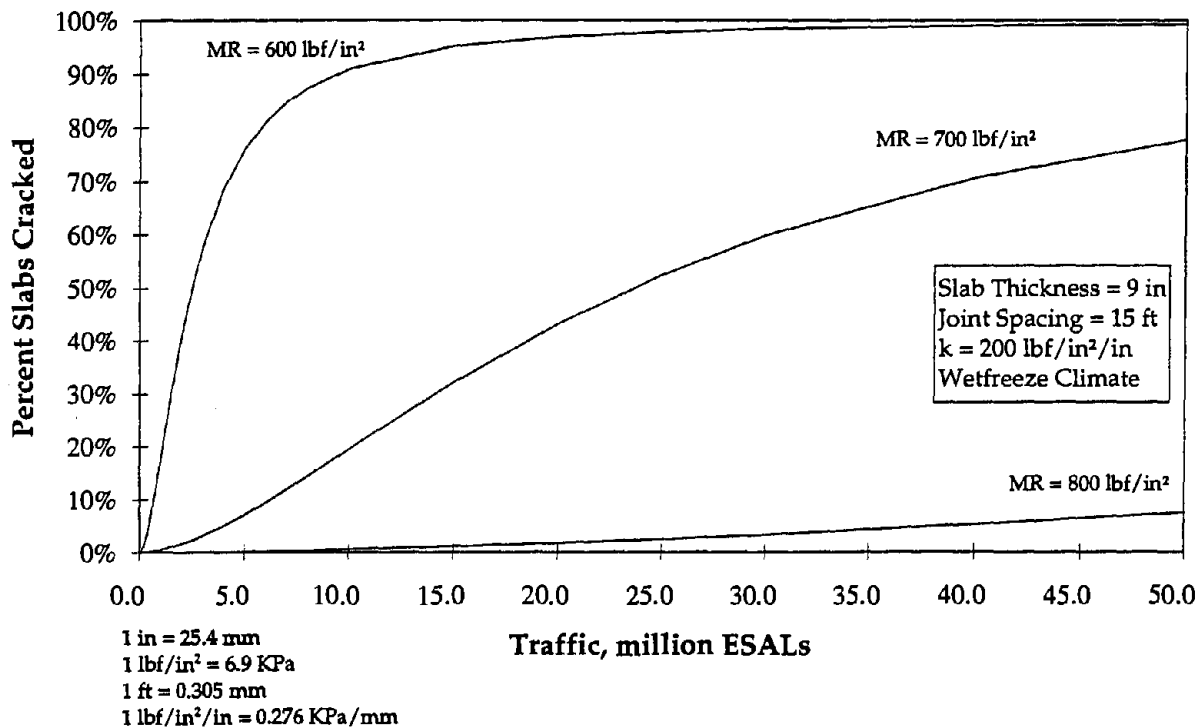


Figure 51. Sensitivity of JPCP cracking model to modulus of rupture.

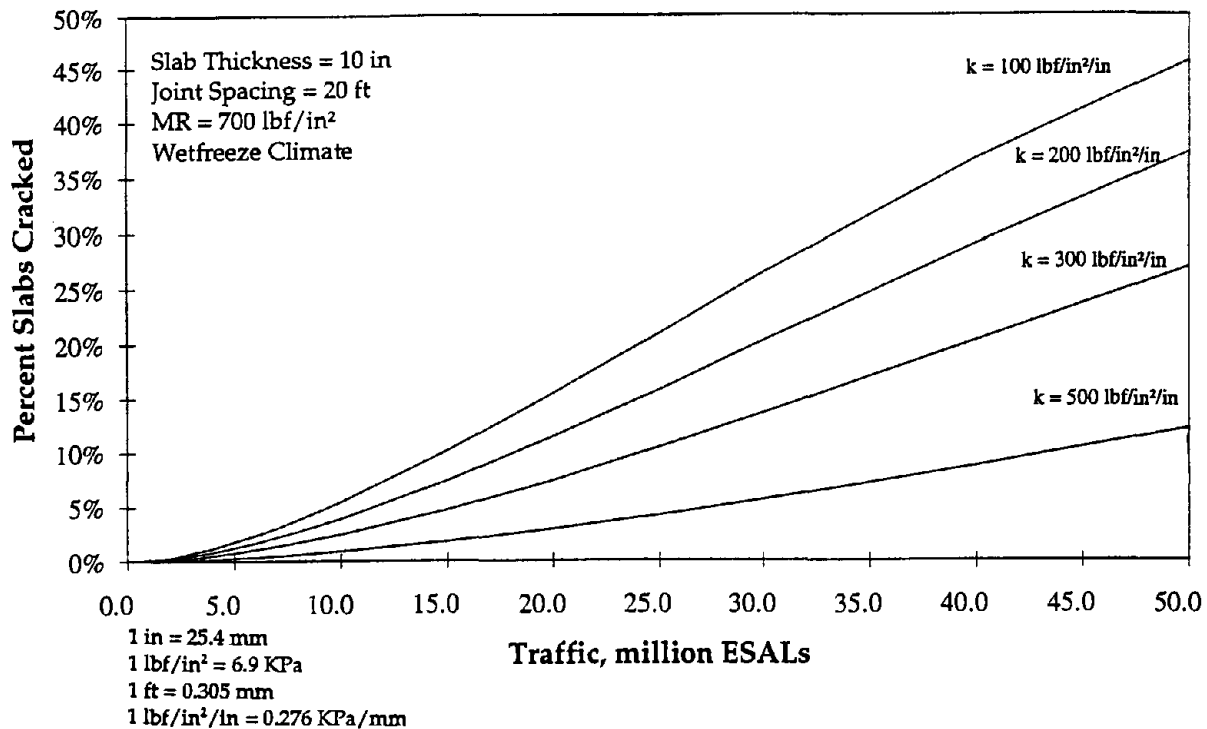


Figure 52. Sensitivity of JPCP cracking model to k-value.

To determine the appropriate temperature shift factor for use with the cracking model, the average effective temperature gradients used in the development of the cracking model was reviewed. Based on this review, it was determined that, at least in the United States, four climatic regions are adequate for shift factors: Dry-Freeze (DF), Dry-Nonfreeze (DN), Wet-Freeze (WF), and Wet-Nonfreeze (WN). The temperature regions address the amount of construction curling, and the moisture regions address the amount of drying shrinkage. The average values determined for the U.S. are as follows:

- DF — 11 °F (6.1 °C)
- DN — 11.5 °F (6.4 °C)
- WF — 8 °F (4.4 °C)
- WN — 8.5 °F (4.7 °C)

The above values are the temperatures that should be subtracted from the actual temperature gradients when using the cracking model, and they represent (approximately) the temperature gradients needed to bring the pavement slabs to the flat condition. These values are consistent with those that have been measured in the field.<sup>(24,35)</sup> For the slab thicknesses in the range of 8 to 13 in (203 to 330 mm) a fixed value of the temperature shift factor may be used because the factors that cause built-in curling have offsetting effects: the amount of residual temperature curling increases with the slab thickness, whereas the effects of differential shrinkage decreases with the slab thickness. For the slab thicknesses beyond this range the above values are conservative.



The accuracy of the cracking model is shown in figures 53 and 54. Figure 53 shows the data on which the cracking model is based. This data set was obtained by making adjustments for built-in curling on a section-by-section basis. Figure 54 is the result of applying the fixed temperature shift factors suggested for each climatic region. Figure 54 shows a considerably greater amount of scatter, but considering the possible range of built-in curling and the sensitivity of slab cracking to curling stresses, more accurate predictions may not be possible. The actual reliability of the cracking model will likely be much better than that shown in figure 54 because more accurate material, structural, and traffic data would be available in most cases where the model will be used.

It is also important to note the following in calculating the accumulated fatigue damage:

- The k-valued used in the model is the backcalculated dynamic k. The dynamic k may be taken as twice the static k obtained by laboratory testing.
- The PCC modulus of rupture and  $E_{PCC}$  are long-term values. The long-term concrete strength is typically about 10 percent greater than the 28-day strength.

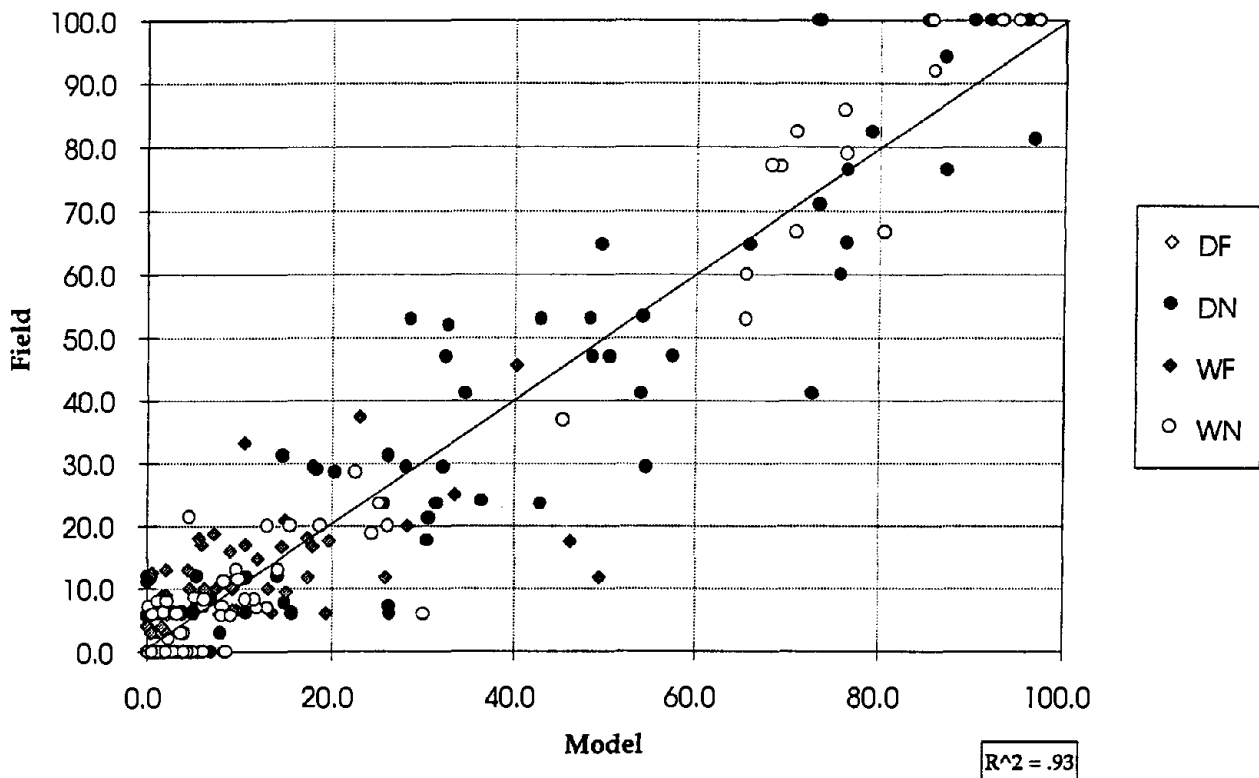


Figure 53. Comparison of predicted and actual slab cracking—section by section adjustments for built-in curling.

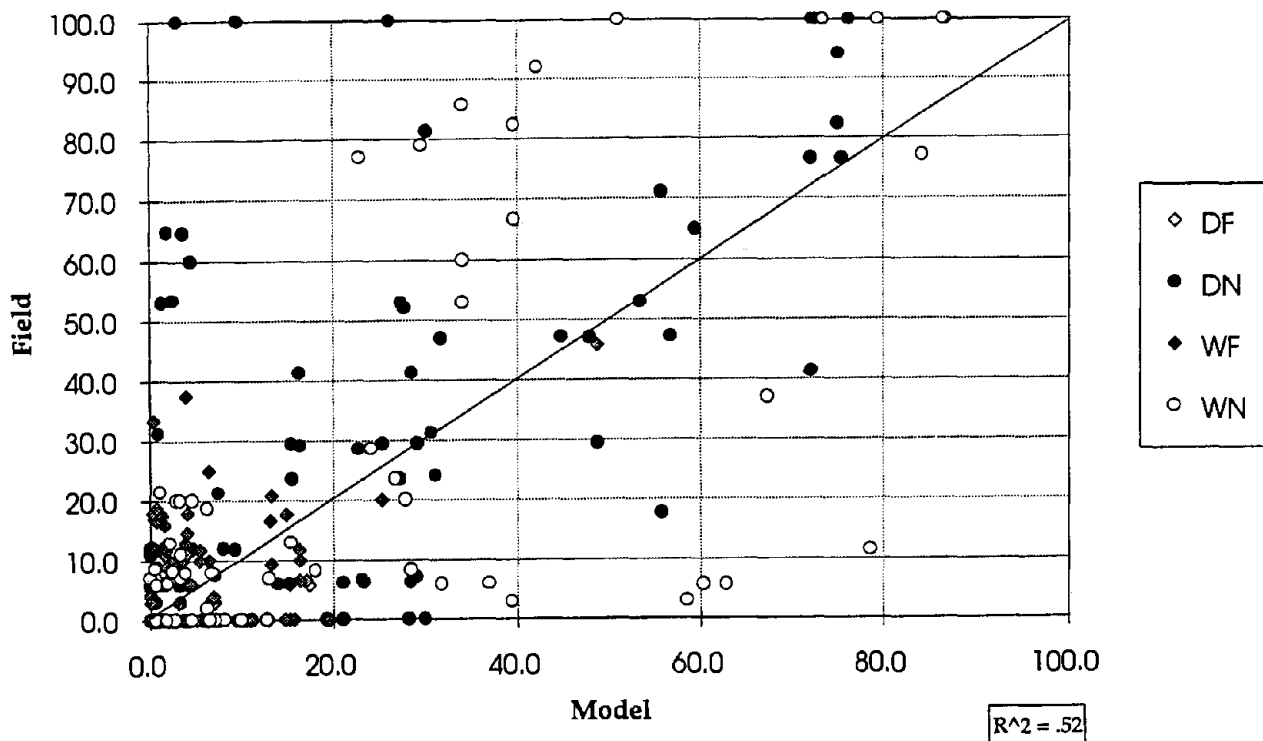


Figure 54. Comparison of predicted and actual slab cracking—regional adjustments for built-in curling (DF = 11 °F [6.1 °C]; DN = 11.5 °F [6.4 °C]; WF = 8 °F [4.4 °C]; WN = 8.5 °F [4.7 °C];).

### Crack Deterioration Model for JRCP

Low-severity transverse cracks are a normal occurrence in JRCP. These cracks are expected to develop as the slab responds to drying shrinkage, thermal curling, and thermal contractions. Reinforcement is placed in JRCP to hold the cracks tight and prevent deterioration. However, repeated heavy load applications, environmental effects, and inadequate steel design can result in the cracks breaking down and deteriorating. Medium- and high- severity transverse cracks in JRCP cause localized failures, increased roughness, user discomfort, and trigger the need for rehabilitation.

#### Preliminary Data Analysis

The project data base contains information on 159 JRCP sections, including time-series performance data for both 1987 and 1992. However, these sections were examined and cleaned to remove pavement sections that exhibit severe D-cracking (medium- and high- severity) and a few that were considered as outliers.

The factorial matrix of the distribution of the remaining 111 pavement sections is shown in table 9, separated by climatic region, percentage of longitudinal

Table 9. Distribution of the pavement sections and designs used in the development of JRCR crack deterioration model.

Climatic Region	PERSTEEL percent	Age, years 0 - 10		Age, years 11 - 25	
		Nonstabilized Base	Stabilized Base	Nonstabilized Base	Stabilized Base
FI <200	0.04-0.10	0	0	9	4
	0.11-0.29	1	4	3	1
FI >200	0.04-0.10	7	4	29	30
	0.11-0.29	2	4	8	5
Total		10	12	49	40

reinforcement (PERSTEEL), and age. The climate is categorized as cold (FI greater than 200) and warm (FI less than 200). Two age brackets are included (0 to 10 and 11 to 25), two types of bases are considered (stabilized and nonstabilized), and two reinforcement brackets (0.6 to 0.10 percent and 0.11 to 0.29 percent) are evaluated.

Overall, this table shows a fairly good distribution for pavements greater than 10 years old. The majority of the sections are located in cold climates and have a reinforcement steel content between 0.04 and 0.10 percent. There is also a fairly even distribution of pavement sections constructed on both stabilized and nonstabilized bases.

#### Review of Available Models

Several models for predicting crack deterioration of JRCR are currently available. One model, developed under the NCHRP 277 contract, has the following form:<sup>(10)</sup>

$$\begin{aligned}
 \text{CRACKS} = & \text{CESAL}^{0.897} [7130.0 \text{ JTSPACE}/(\text{ASTEEL} * \text{THICK } 5.0)] \\
 & + \text{CESAL}^{0.10} (2,281 \text{ PUMP}^{5.0}) \\
 & + \text{CESAL}^{2.16} [1.81/(\text{BASETYP} + 1)] \\
 & + \text{AGE}^{1.3} [0.0036 (\text{FI} + 1)^{0.36}]
 \end{aligned}
 \tag{37}$$

where:

- CRACKS = total length of medium and high severity cracks, ft/mi.
- CESAL = cumulative 18-kip (80-kN) ESAL's in traffic lane, millions.
- JTSPACE = Mean transverse joint spacing, ft
- ASTEEL = area of reinforcing steel, in<sup>2</sup>/ft width.

THICK = slab thickness, in.  
 PUMP = pumping severity (=0, if no pumping exists; =1, low severity; =2, medium severity; =3, high severity).  
 BASETYP = base type (= 0, nonstabilized aggregate; =1 stabilized aggregate [cement, asphalt]).  
 AGE = time since construction, years.  
 FI = freezing index.

A more recent model has the following form:<sup>(11)</sup>

$$\begin{aligned}
 \text{CRACKJR} = & -72.9 + 1.9 \text{ CESAL} + \frac{0.182}{\text{PERSTEEL}^2} + \frac{2473}{\text{KSTATIC}} \\
 & + 0.687 \text{ PRECIP}
 \end{aligned}
 \tag{38}$$

where:

CRACKJR = number of transverse cracks (medium- and high-severity)/mi.  
 CESAL = cumulative 18-kip (80-kN) ESAL applications in traffic lane, millions.  
 PERSTEEL = percentage of steel (longitudinal reinforcement).  
 KSTATIC = backcalculated static modulus of subgrade reaction, lb/in<sup>2</sup>/in.  
 PRECIP = average annular precipitation, in.

Collectively, these models suggest several important variables influencing the development of deteriorated cracks in JRPC: ESAL applications, steel percentage, base type/support, joint spacing, and climatic factors (freezing index and precipitation).

### Explanatory Variables Initially Selected

The initial explanatory variables that were considered are as follows:

AGE:	time since construction, years.
CESAL:	cumulative 18-kip (80-kN) ESAL's in traffic lane, millions.
JTSPACE:	mean transverse joint spacing, in.
THICK:	PCC slab thickness, in.
Cd:	adapted AASHTO drainage coefficient.
JTOPEN:	joint opening, in.
JTWIDTH:	mean joint width, in.
JTSEALNT:	joint seal type (several types are listed in the data base).
Epc:	mean backcalculated modulus of elasticity of concrete, million lb/in <sup>2</sup> .
Kdyn:	mean backcalculated modulus of subgrade reaction, lb/in <sup>3</sup> .
MI:	Thornthwaite moisture index.
Days90:	number of days temperature greater than 90 °F.
TRANGE:	mean monthly temperature range.
FI:	freeze index, degree-days below freezing.
PRECIP:	average annular precipitation, in.
FTCY:	mean annular air freeze-thaw cycles.

DOWELCOR: dowel potential corrosion (=0, if no dowels exist or dowels are coated [epoxy, plastic, stainless steel]; =1, if dowels do not have special protective coating).  
 BASE: base type (= 0, nonstabilized aggregate; =1, stabilized aggregate [cement, asphalt]).  
 PERSTEEL: percentage of steel (longitudinal reinforcement).

Although aggregate type and maximum aggregate size are important parameters that affect load transfer across the crack and, therefore, may have effect on crack deterioration, lack of this information in the data base did not permit inclusion of these parameters into a JRCP crack deterioration model. Two-dimensional scatter plots of the raw data for some of the key variables are shown on figure 55.

### Model Development

The final model developed for crack deteriorating in JRCP is as follows:

$$\begin{aligned}
 CRACKJR = & AGE^{2.5} * [6.88 * 10^{-5} * FI/THICK \\
 & + (0.116 - 0.073 \text{ BASE}) * CESAL * (1 - e^{-0.032 * a}) \\
 & * e^{(7.55188 - E_{pcc} - 66.5 \text{ PERSTEEL} + 5 \text{ PERSTEEL} * E_{pcc})}
 \end{aligned} \tag{39}$$

where:

CRACKJR = number of transverse cracks (medium- and high- severity)/mi.  
 CESAL = cumulative 18-kip (80-kN) ESAL's in traffic lane, millions.  
 PERSTEEL = percentage of steel (longitudinal reinforcement).  
 E<sub>pcc</sub> = mean backcalculated modulus of elasticity of concrete million lb/in<sup>2</sup>.  
 THICK = PCC slab thickness, in.  
 a = MI, Thornthwaite moisture index, if MI is greater than 1.  
 = 1, if MI is less than 1.  
 BASE = 0, if nonstabilized base exists.  
 = 1, if stabilized base exists.  
 FI = Freezing Index, degree days below freezing.

Statistics:

N = 111.  
 R<sup>2</sup> = 0.67.  
 RSE = 32.0 cracks/mi.

The actual versus predicted crack deterioration and residual versus predicted crack deterioration are given in figures 56 and 57, respectively. These figures show that prediction errors are symmetrically distributed around zero.

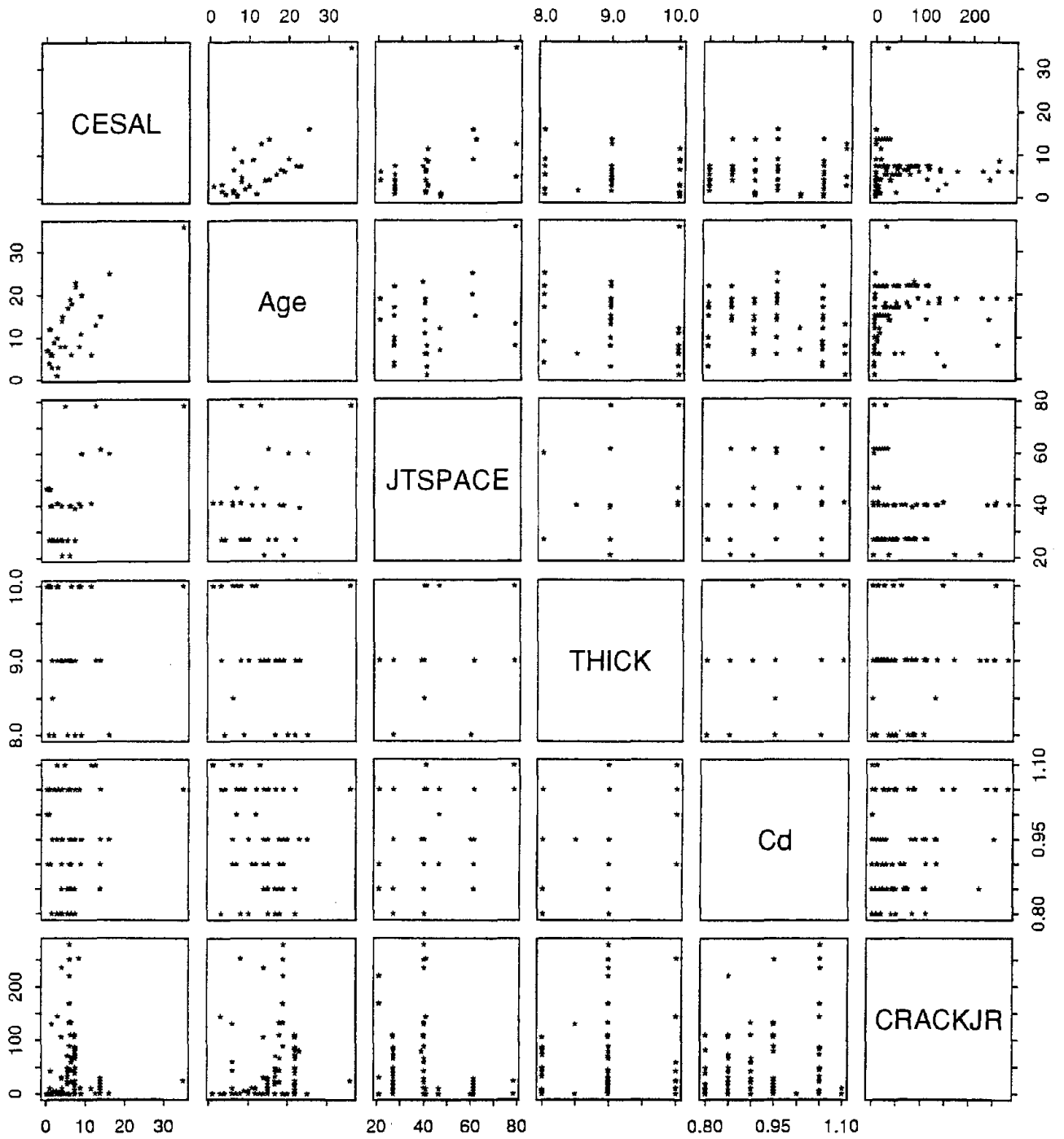


Figure 55. Two-dimensional scatter plot for JRCP crack deterioration model.

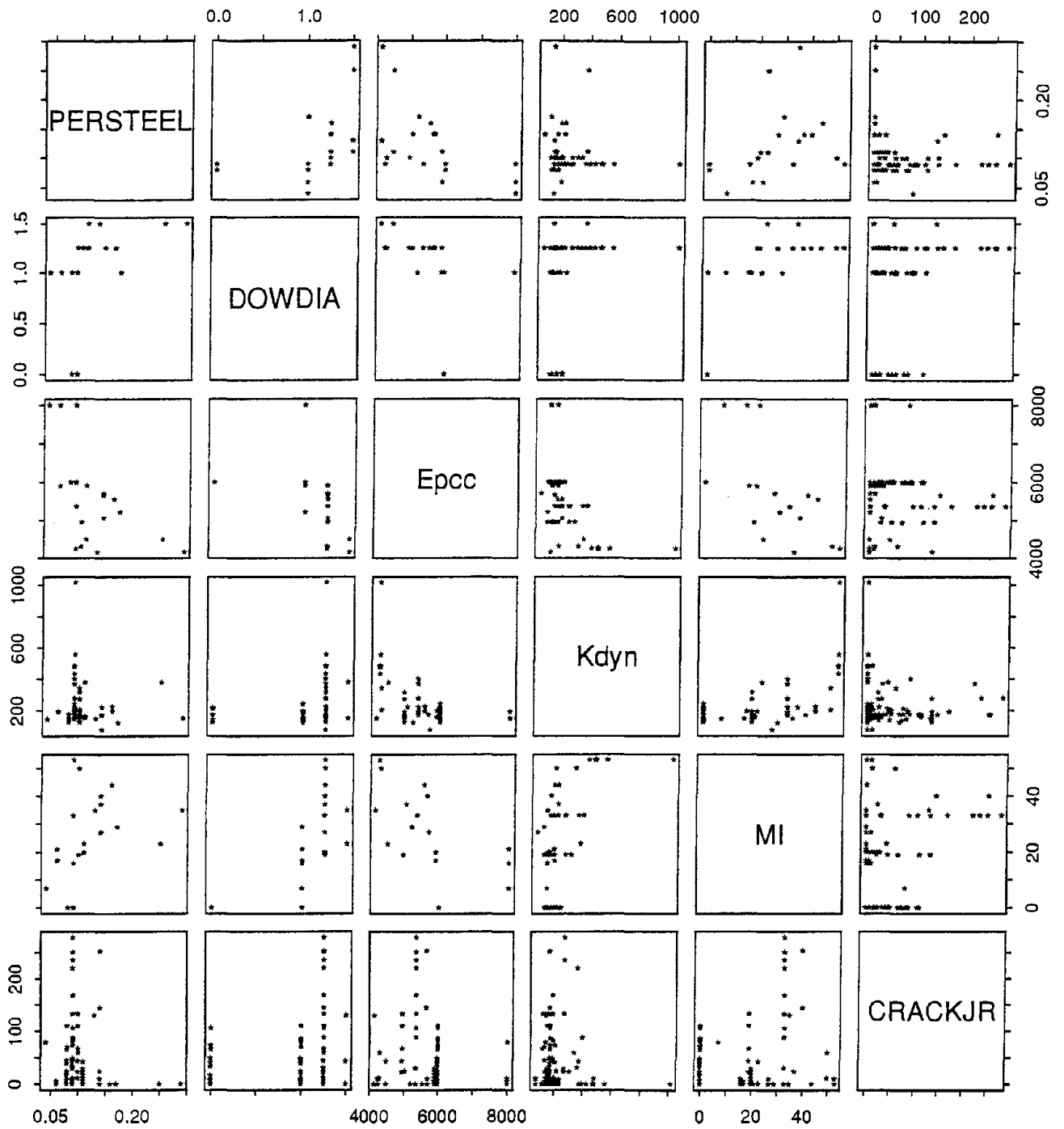


Figure 55. Two-dimensional scatter plot for JRCP crack deterioration model (continued).

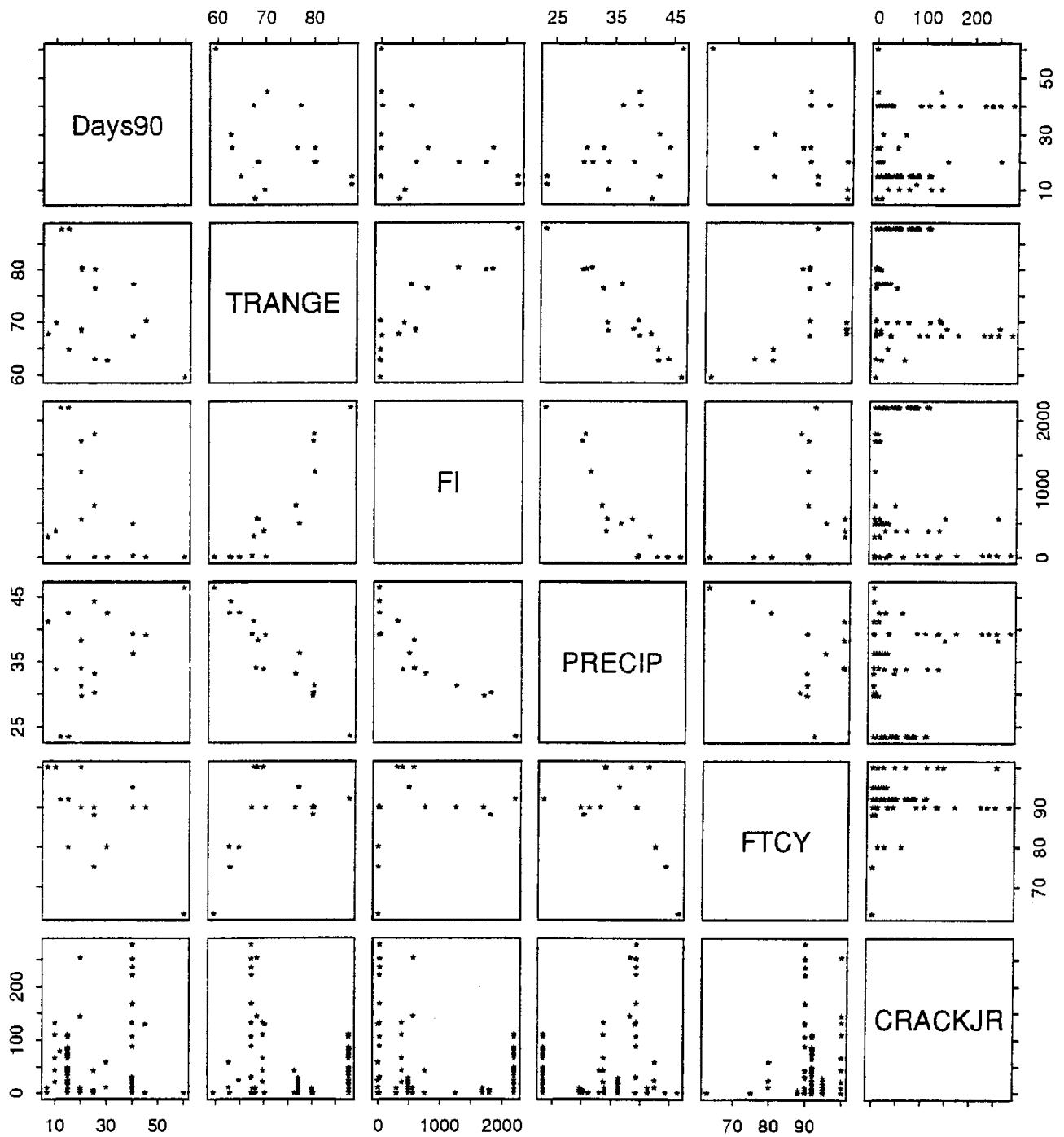


Figure 55. Two-dimensional scatter plot for JRCP crack deterioration model (continued).



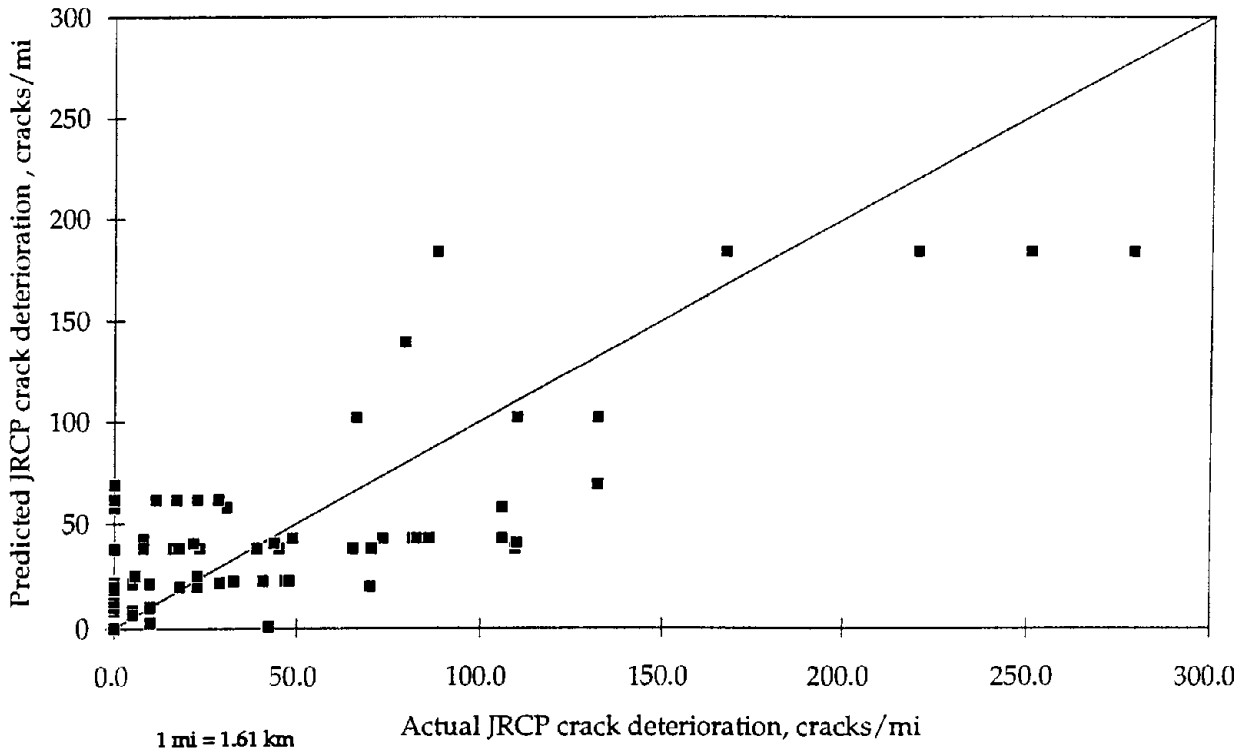


Figure 56. Actual versus predicted deteriorated cracking.

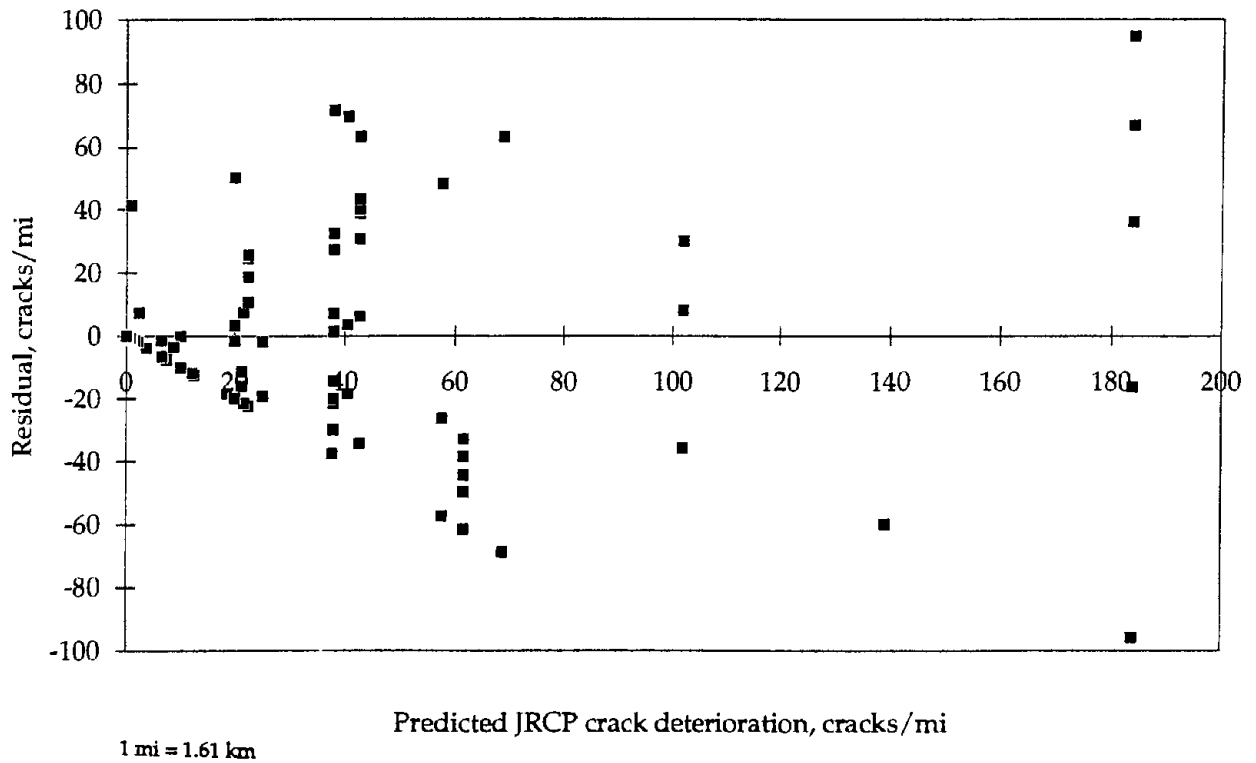


Figure 57. Predicted versus residual deteriorated cracking.

## Sensitivity Analysis and Discussion

The sensitivity plots of the key variables in the model are provided in the figures 58 through 64. These three-dimensional plots are developed by varying the selected variables over a range of values and fixing all other variables at constant values. Because cumulative traffic is changing with age, it is assumed in these examples that traffic increases 3 percent annually; the actual traffic growth rates may be much higher in some cases. In the plots the traffic is characterized through cumulative traffic after 20 years.

Figure 58 shows the combined effect of traffic and aging on JRCP crack deterioration. The JRCP is 9 in (229 mm) thick, modulus of elasticity of concrete is 5,000,000 lb/in<sup>2</sup>, and longitudinal reinforcement is 0.1 percent. An increase in the amount of traffic and pavement age leads to an increase in crack deterioration. Aging represents many mechanisms of cracks deterioration, such as cyclic opening and closing of cracks, corrosion of reinforcement, and freeze-thaw cycles. Heavy traffic loading causes the reinforcement to rupture, allowing the cracks to begin accommodating slab movements, thereby leading to additional deterioration.

Figures 59 and 60 illustrate that a higher percentage of longitudinal reinforcement better prevents cracks from deterioration. This agrees with the results of a laboratory study conducted at the Michigan State University that showed the effect of greater reinforcement on delaying the deteriorating of transverse cracks. <sup>(36, 37)</sup> Effective longitudinal reinforcement holds cracks tight and increases shear resistance. A comparison of figures 59 and 60 also shows that the presence of a stabilized base reduces crack deterioration.

JRCP with more durable PCC should better resist crack deterioration. Because the modulus of elasticity of concrete is one of the indicators of concrete strength, it may be expected that an increase in modulus of elasticity improves pavement performance. Figure 61 shows that the model predicts a decrease in crack deterioration when the concrete modulus increases.

The effects of climatic conditions are shown in figures 62 and 63. One can observe that crack deterioration is higher in cold and wet climates. One possible explanation of this effect is that greater use of deicing salts and increased moisture level accelerate corrosion of the reinforcement.

Figure 64 presents a comparison of JRCP crack deterioration on selected sections located in Ohio with the model prediction. Reasonable agreement is observed between the model predictions and field test data.

It is interesting to note that, like the LTPP crack deterioration model, the model developed in this study does not predict dependence of crack deterioration on joint spacing. This might be explained by the presence in the data base of several long-jointed sections, such as MO 1 sections, that performed exceptionally well.

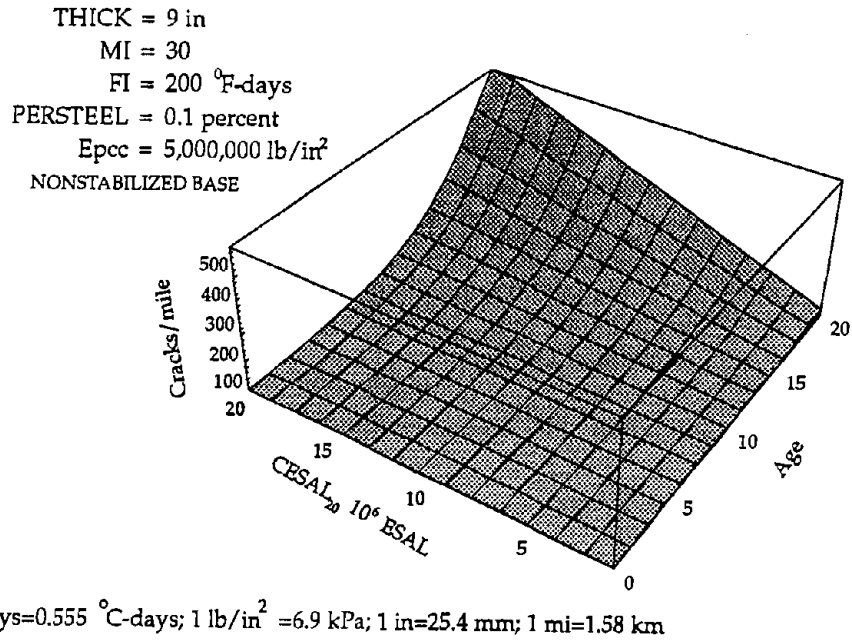


Figure 58. Sensitivity plot of the JRCR crack deterioration model showing effect of age and ESAL applications.

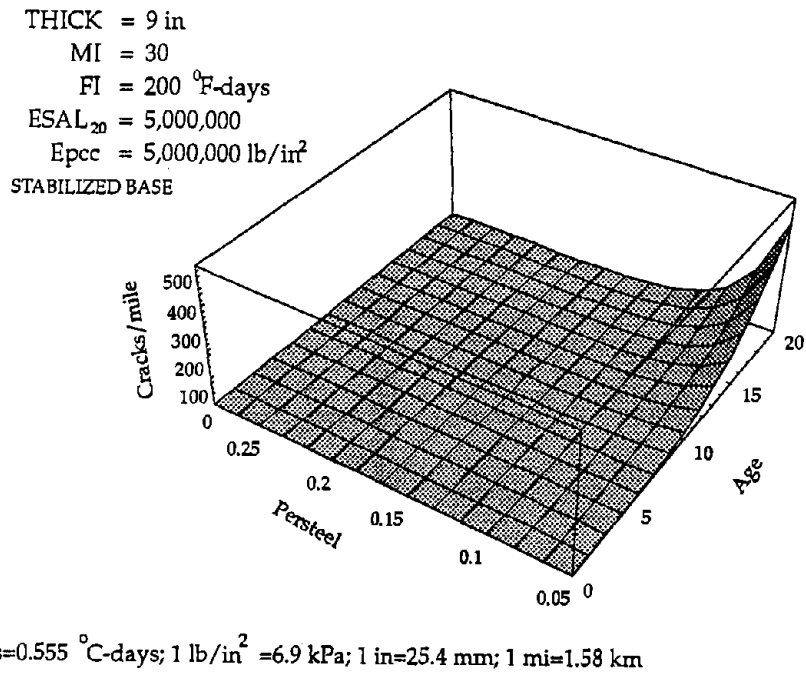
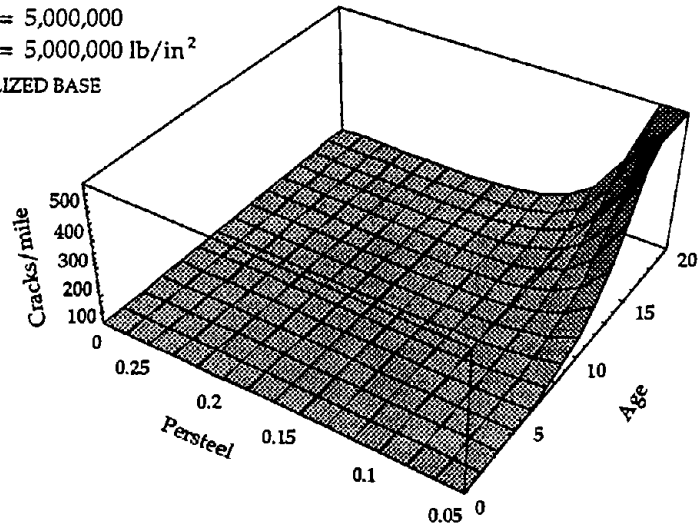


Figure 59. Sensitivity plot of the JRCR crack deterioration model showing effect of age and percentage of reinforcement (stabilized base).

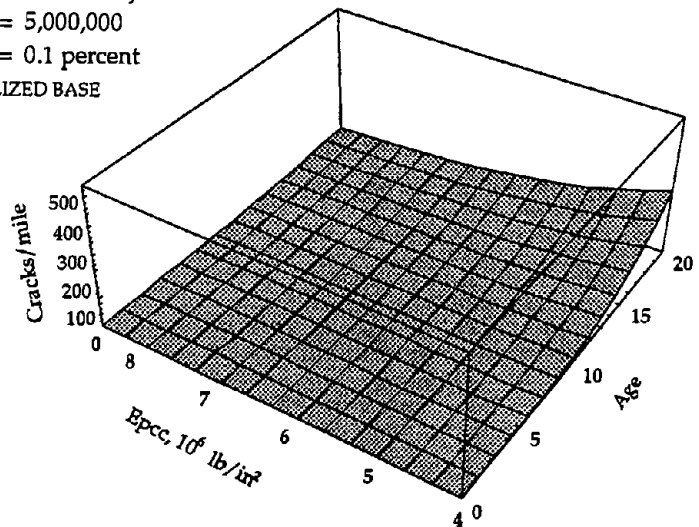
THICK = 9 in  
 MI = 30  
 FI = 200 °F-days  
 ESAL<sub>20</sub> = 5,000,000  
 E<sub>pcc</sub> = 5,000,000 lb/in<sup>2</sup>  
 NONSTABILIZED BASE



1 °F-days=0.555 °C-days; 1 lb/in<sup>2</sup> =6.9 kPa; 1 in=25.4 mm; 1 mi=1.58 km

Figure 60. Sensitivity plot of the JRCP crack deterioration model showing effect of age and percentage of reinforcement (nonstabilized base).

THICK = 9 in  
 MI = 30  
 FI = 200 °F-days  
 ESAL<sub>20</sub> = 5,000,000  
 PERSTEEL = 0.1 percent  
 NONSTABILIZED BASE



1 °F-days=0.555 °C-days; 1 lb/in<sup>2</sup> =6.9 kPa; 1 in=25.4 mm; 1 mi=1.58 km

Figure 61. Sensitivity plot of the JRCP crack deterioration model showing effect of age and concrete modulus of elasticity.

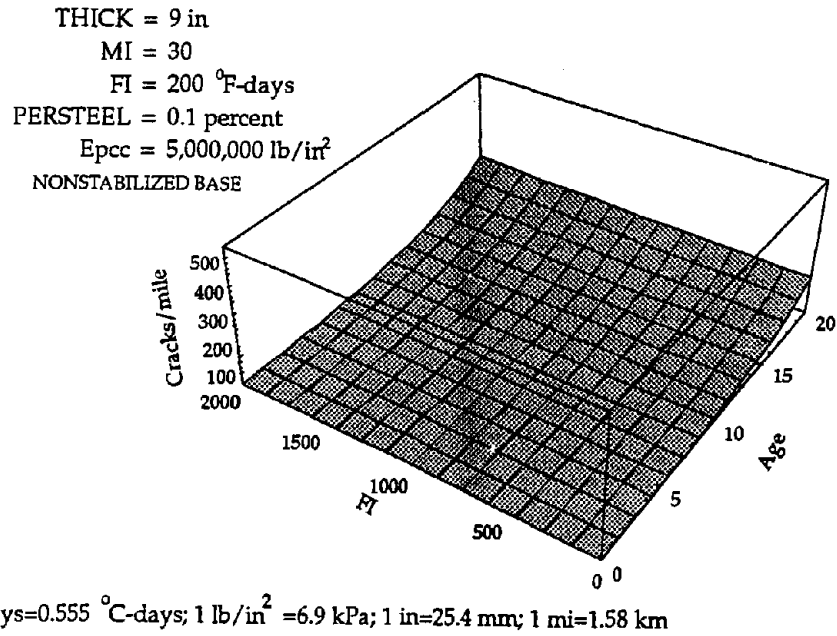


Figure 62. Sensitivity plot of the JRCP crack deterioration model showing effect of age and freezing index.

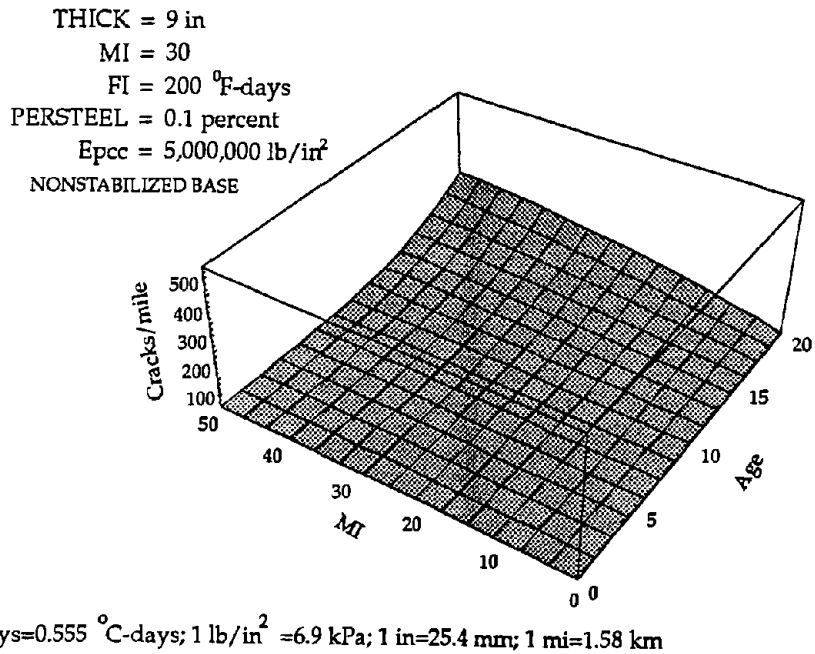


Figure 63. Sensitivity plot of the JRCP crack deterioration model showing effect of age and moisture index.

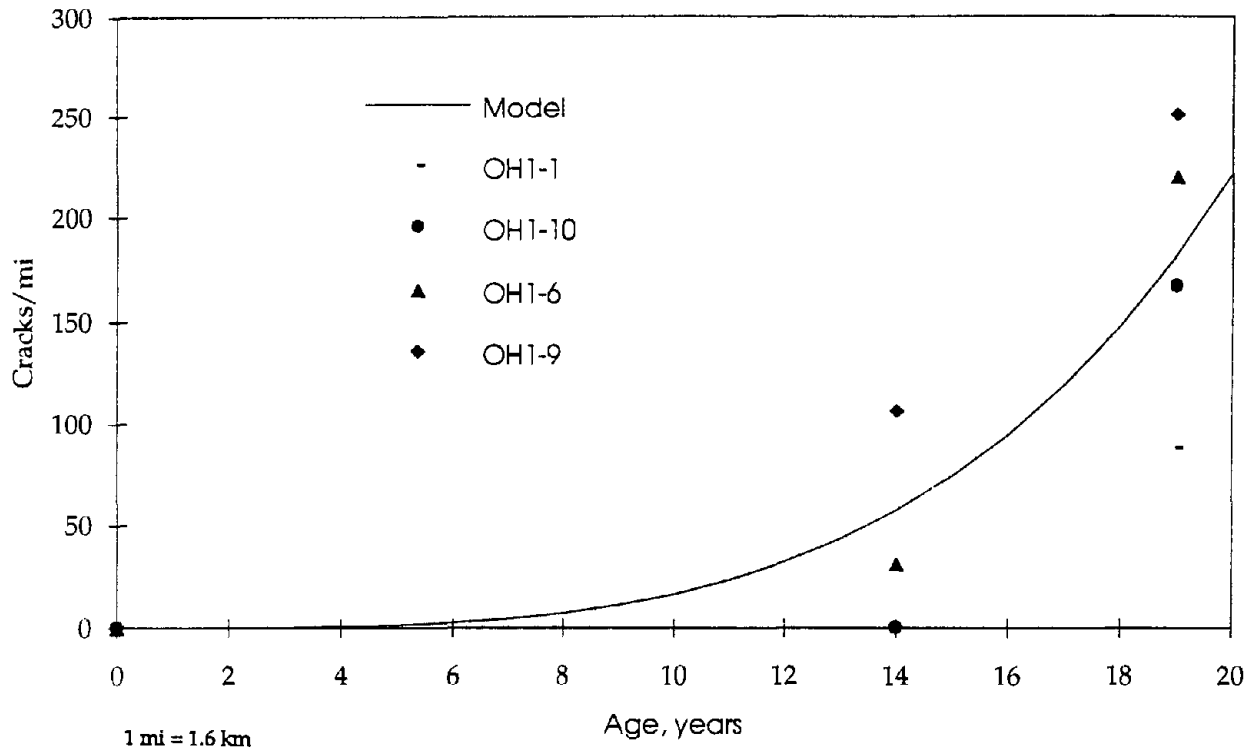


Figure 64. Comparison of JRCP crack deterioration on selected Ohio sections with the model prediction.

The following is a summary of conclusions observed from the JRCP crack deterioration model:

- Crack deterioration increases with pavement age and traffic.
- Crack deterioration becomes significant 10 years after construction.
- An increase in the amount of longitudinal reinforcement significantly reduces the number of deteriorated cracks.
- Crack deterioration is greater in cold and wet climates.
- The presence of a stabilized base decreases the amount of deteriorated cracks.
- An increase in modulus of elasticity of the concrete decreases the number of deteriorated cracks.

Based on the results of the model, the following design features can be recommended to reduce JRCP crack deterioration:

- Higher percentage of reinforcement (greater than 0.11 percent).
- Use of more durable PCC in cold climate.
- Thicker PCC slab.
- Stabilized base.

## Transverse Joint Spalling Model for JPCP

Transverse joint spalling is the chipping or fracturing of the slab edges within a few feet of the joint. Transverse joint spalling usually does not extend vertically through the entire slab thickness, but rather is limited to the upper portion of the slab. Transverse joint spalling can be caused by a variety of factors, including:

- The presence of incompressible materials in the joints that cause excessive stresses at the joint as the slab expands in warm weather.
- Poor durability of the concrete, either due to an inadequate air void system or to aggregate durability problems such as D-cracking or reactive aggregate.
- Inadequate consolidation of the concrete at the joint.
- Misaligned and corroded load transfer devices.

Transverse joint spalling models were developed for both JPCP and JRCP pavements to account for different behavioral characteristics of each pavement type. The model for JPCP is presented first.

### Preliminary Data Analysis

The project data base contains information on 208 JPCP pavement sections, including time-series performance data from both 1987 and 1992. Wisconsin sections were resurveyed in 1997. These sections were examined and cleaned to remove pavement sections that exhibited severe D-cracking (medium- or high- severity), that contained unusual load transfer mechanisms (e.g., ACME devices), and a few that were identified as outliers.

The inference space (factorial matrix) of the distribution of the remaining 164 pavement sections is shown in table 10, divided by climatic region, sealant type, and age. The climate is categorized as cold (FI greater than 200), mild (FI less than 200 and number of days with temperatures above 90 °F [32 °C], Days90, less than 100), and hot (number of days with temperatures above 90 °F [32 °C] greater than 100). Three age brackets are included (0 to 10, 11 to 20, and 21 to 35), and four joint sealant types are evaluated:

- Preformed (compression) sealant.
- Liquid sealant (including hot-applied, asphaltic-based sealants, polyurethanes, PVC coal tars).
- Silicone sealant.
- None (indicating sections whose joints have not been sealed even at construction).

An analysis of the factorial matrix indicates the following limitations:

- The nonsealed sections in the cold region (FI greater than 200) are all relatively new.

Table 10. Distribution of the pavement sections and designs used in the development of JPCP spalling model.

Climatic Region	Sealant	Age, years 0 - 10	Age, years 11 - 20	Age, years 21 - 35
COLD FI >200 (OH, NY, WI, MN, ONT)	Preformed	12	3	4
	Liquid	8	2	8
	Silicone	8	2	0
	None	16	0	0
MILD FI <200 Days90<100 (GA, NC, OH, FL, CA)	Preformed	0	18	0
	Liquid	1	11	17
	Silicone	4	0	0
	None	6	21	10
HOT FI <200 Days90 >100 (AZ)	Preformed	0	0	0
	Liquid	5	8	0
	Silicone	0	0	0
	None	0	0	0
Total		60	65	39

- Very few sections exist in hot regions (number of days with temperatures above 90 °F [32 °C] greater than 100), and the only sealant type in this region is liquid.
- Most of the sections with silicone sealant are less than 10 years old.

Overall, a good distribution of age exists up to 35 years.

#### Review of Available Models

Several models for predicting spalling of JPCP pavements have been developed. One model developed in 1990 under the preceding FHWA contract on pavement performance has the following form:<sup>(3)</sup>

$$\begin{aligned}
 JTSPALL = AGE^{2.178} * [ 0.0221 + 0.5494 DCRACK & \hspace{10em} (40) \\
 - 0.0135 LIQSEAL - 0.0419 PREFSEAL + 0.0000362 FI ] &
 \end{aligned}$$



where

- JTSPALL = Number of medium- and high-severity spalled joints/mi.  
AGE = Age since original construction, years.  
DCRACK = 0, if no D-cracking exists.  
= 1, if D-cracking exists.  
LIQSEAL = 0, if no liquid sealant exists in joint.  
= 1, if liquid sealant exists in joint.  
PREFSEAL = 0, if no preformed sealant exists in joint.  
= 1, if preformed sealant exists in joint.  
FI = Freezing Index, degree-days below freezing.

Another model was developed from an early analysis of the SHRP LTPP data.<sup>(11)</sup>  
This model has the following form:

$$SPALLJP = 9.79 + 10.09 * [-1.227 + 0.022 * (0.9853 AGE + 0.1709 FTCY)^2] \quad (41)$$

where

- SPALLJP = Mean percentage of medium- and high-severity spalled joints.  
AGE = Age since original construction, years.  
FTCY = Mean annual air freeze-thaw cycles.

An examination of these models shows that joint spalling depends on pavement age, climatic conditions, and joint sealant. Furthermore, the rate of increase in spalling is low over the first few years and then increases more rapidly. Both models predict that pavement age is not linearly related to joint spalling, and that greater spalling will occur for pavements in colder climates. The SHRP model, however, does not account for sealant type, whereas the FHWA model predicts much lower spalling when preformed sealant are used.

#### Explanatory Variables Initially Selected

The initial explanatory variables that were considered follow:

- |           |   |
|-----------|---|
| AGE:      | Time since construction, years.   |
| CESAL:    | Cumulative 18-kip (80-kN) ESALs in traffic lane, millions.                          |
| JTSPACE:  | Mean transverse joint spacing, ft.  |
| THICK:    | PCC slab thickness, in.   |
| Cd:       | Adapted AASHTO drainage coefficient.  |
| JTOPEN:   | Joint opening, in.  |
| JTWIDTH:  | Mean joint width, in.   |
| JTSEALNT: | Joint seal type (several types are listed in the data base).                        |
| Epsc:     | Mean backcalculated modulus of elasticity of concrete, million lb/in <sup>2</sup> . |
| Kdyn:     | Mean backcalculated modulus of subgrade reaction, lb/in <sup>2</sup> /in.           |
| MI:       | Thornthwaite moisture index.  |

Days90:	Number of days temperature greater than 90 °F.
TRANGE:	Mean monthly temperature range.
FI:	Freeze index, degree-days below freezing.
PRECIP:	Average annual precipitation, in.
FTCY:	Mean annual air freeze-thaw cycles.
DOWELCOR:	Dowel potential corrosion (=0 if no dowels exist or dowels are coated [epoxy, plastic, stainless steel], =1 if dowels do not have protective coating).

Engineering experience suggests that corrosion of dowels significantly increases joint spalling. It is not easy, however, to predict precisely the extent of corrosion that exists in a pavement. Therefore, an index of potential corrosion was developed such that dowels with special coating of epoxy, plastic, or stainless steel were categorized differently than dowels without corrosion protection.

### Model Development

Two-dimensional scatter plots of the raw data for the some of the key variables are shown in figure 65. The functional form used in the 1990 FHWA model was selected as the basis for further model development:

$$SPALLJP = AGE^p * [ \textit{Explanatory Variables} ] \quad (42)$$

Since D-cracked sections were excluded from consideration, the DCRACK variable is not needed in the model. Although the previous FHWA model predicts much greater spalling for pavements in cold climates, an analysis of the data base shows that pavements in very hot climates may also develop significant joint spalling. To provide a better fit of the field test data, an additional climatic variable, Days90, was included in the model.

The final model developed for joint spalling for jointed plain concrete pavements is as follows:

$$\begin{aligned}
 SPALLJP = & AGE^2 * 10^{-6} * JTSPACE * [551.6 - 847.3 * ( LIQSEAL + PREFSEAL) \\
 & + 0.936 * Days90^3 * 10^{-3} + 364 * DOWELCOR \\
 & + (2.783 - 1.400 * LIQSEAL - 2.368 * PREFSEAL \\
 & - 0.676 * SILSEAL) * FI] \quad (43)
 \end{aligned}$$

where

SPALLJP = Percent of medium- and high-severity spalled joints.  
 AGE = Age since original construction, years.

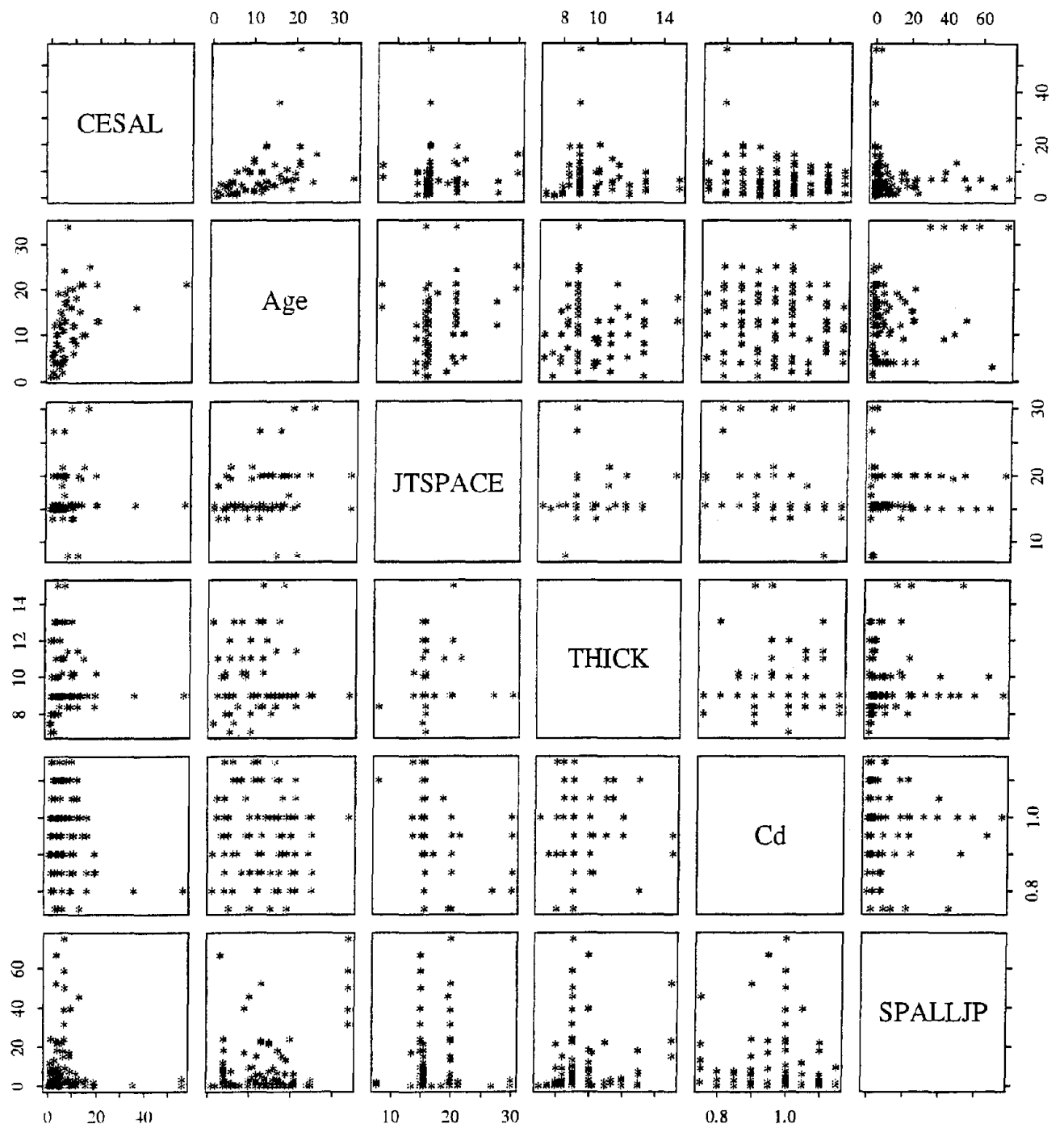


Figure 65. Two-dimensional scatter plot for JPCP spalling model.

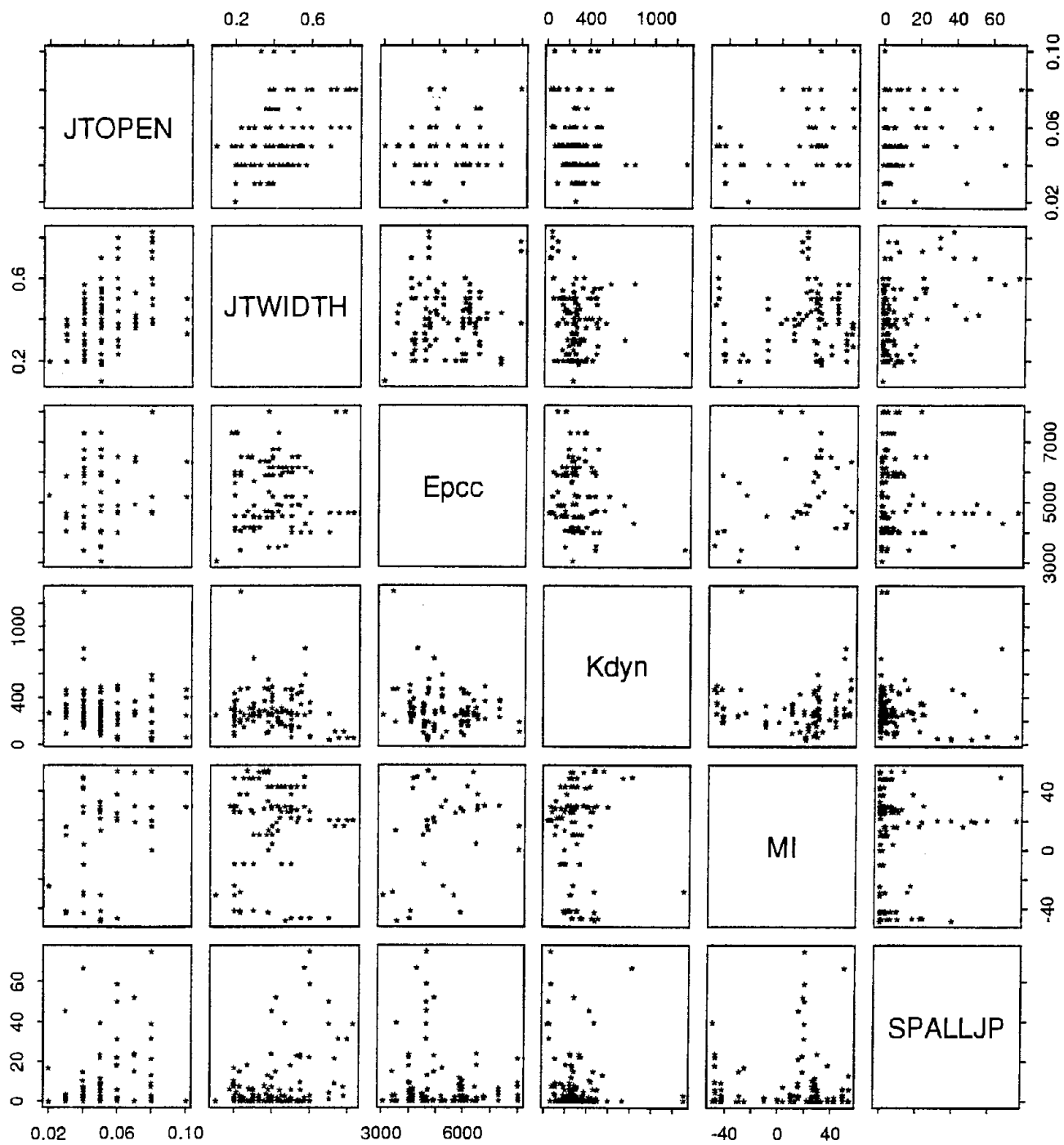


Figure 65. Two-dimensional scatter plot for JPCP spalling model (continued).

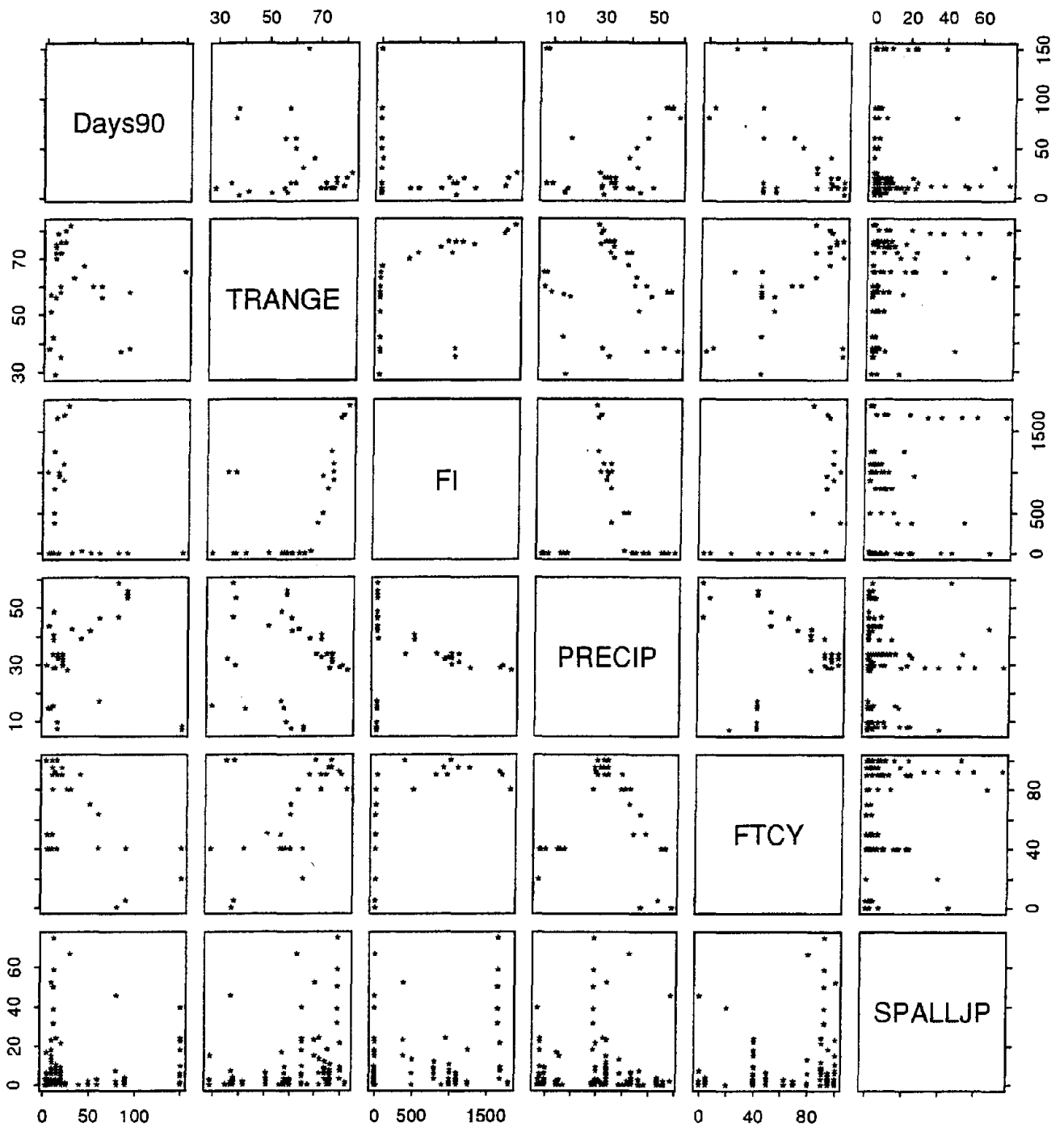


Figure 65. Two-dimensional scatter plot for JPCP spalling model (continued).

DOWELCOR = Dowel corrosion.  
= 0, if no dowels exist, or dowels are protected from corrosion.  
= 1, if dowels are not protected from corrosion.  
JTSPACE = Mean transverse joint spacing, ft.  
LIQSEAL = 0, if no liquid sealant exists in joint.  
= 1, if liquid sealant exists in joint.  
PREFSEAL = 0, if no preformed sealant exists in joint.  
= 1, if preformed sealant exists in joint.  
SILSEAL = 0, if no silicone sealant exists in joint.  
= 1, if silicone sealant exists in joint.  
FI = Freezing Index, degree-days below freezing.  
Day90 = Number of days with temperature greater than 90 °F.

Excellent statistics were obtained for this model, as shown:

N = 163  
R<sup>2</sup> = 0.76  
RSE = 5.1 percent of joints

A plot of the actual spall versus the predicted joint spalling is given in figure 66, and a plot of the residual versus the predicted joint spall is shown on figure 67. These figures show that prediction errors are symmetrically distributed around zero.

### Sensitivity Analysis and Discussion

The sensitivity analysis of the key variables in the JPCP spalling model are provided in figures 68 through 80. Figures 68 through 71 present sensitivity analysis of age, sealant type, and joint spalling to show the average effects that joint sealants have on JPCP joint spalling in different climatic conditions. These plots were prepared by fixing the climatic variables, Days90 and FI, at constant typical values for cold, warm, and hot regions. It is assumed that no dowel corrosion exists, but similar trends can be observed for sections with dowel corrosion. The plots show that the amount of joint spalling always increases with age, and that the rate of the increase in spalling increases with age.

Figures 68 and 69 show that, in a cold climate, preformed sealant reduces spalling much better than liquid and silicone sealants, and liquid sealant performs better than silicone. To illustrate this conclusion with actual data, several sections exposed to similar climatic conditions were considered. Table 11 summarizes information on those sections.

The sections with silicone sealant show a much larger percentage of spalled joints than the older sections with liquid and preformed sealants. A possible explanation for this is that the silicone sealant pulls open microcracking that has developed along the joint during the sawing operation. This phenomenon has been reported on several projects with silicone sealant.

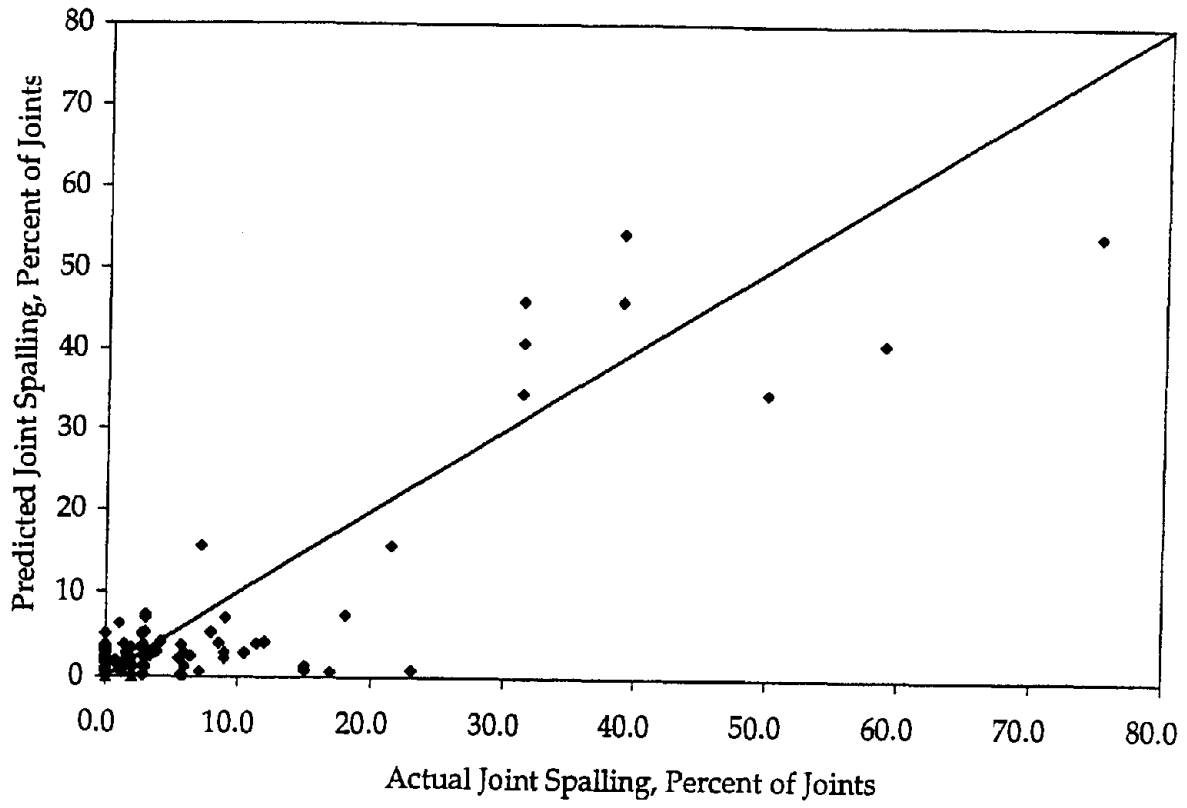


Figure 66. Actual versus predicted percentage of JPCP spalled joints.

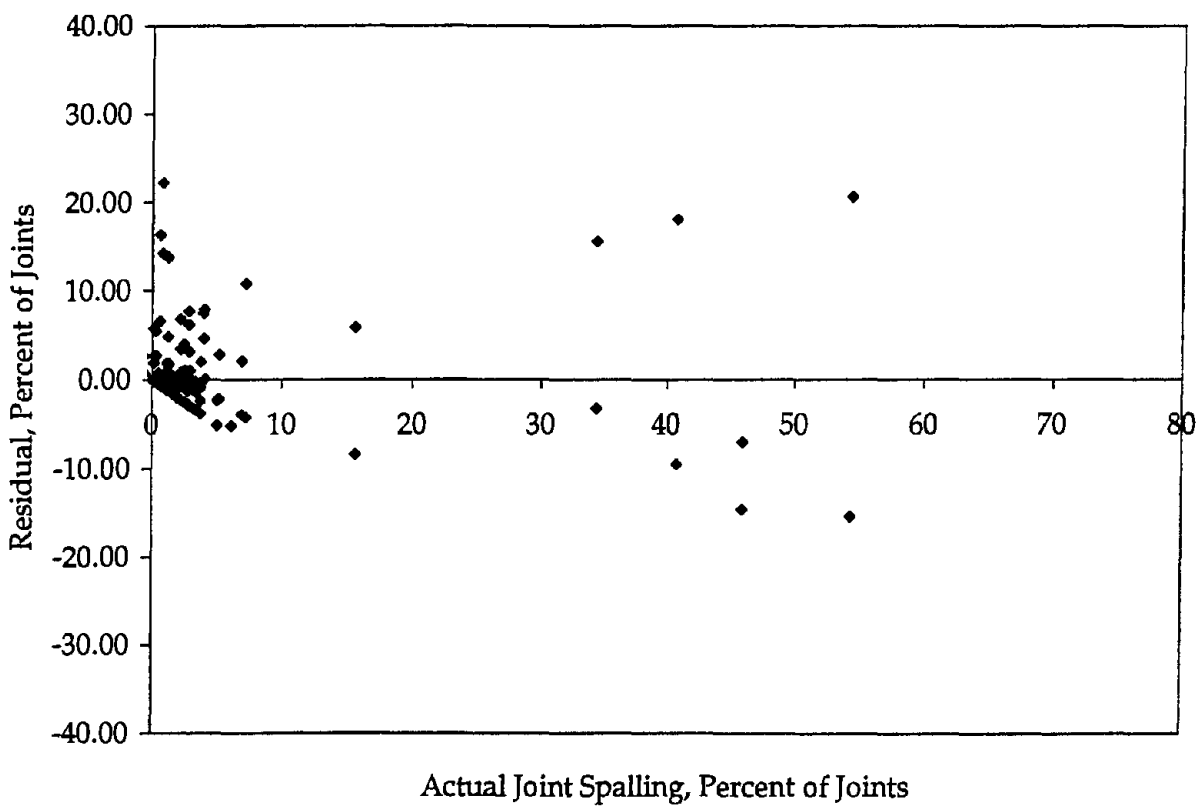


Figure 67. Actual versus residual percentage of JPCP spalled joints.

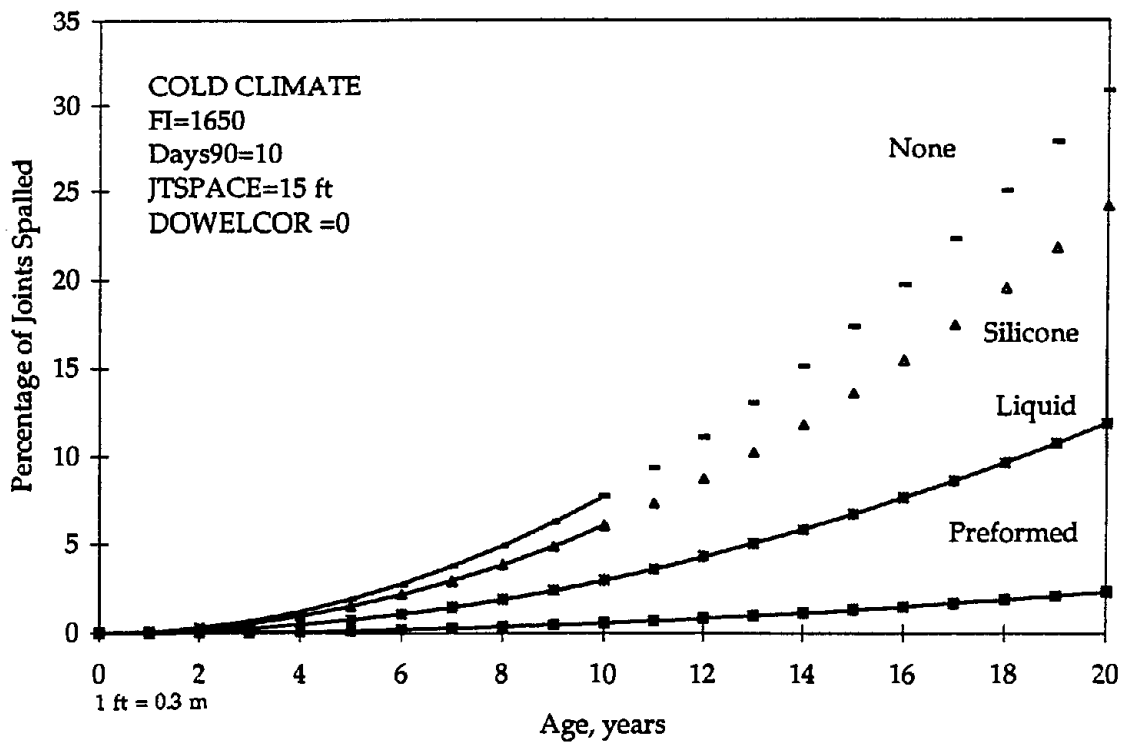


Figure 68. Sensitivity plot of the JPCP joint spalling model for age and sealant type (FI = 1650).

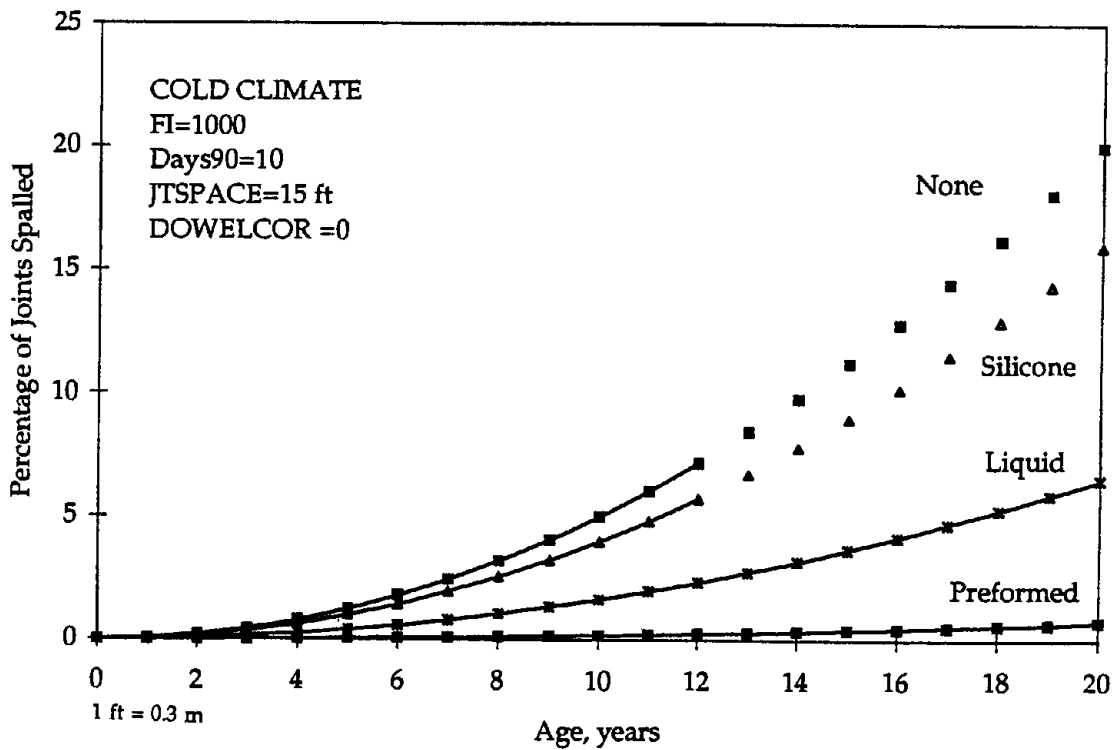


Figure 69. Sensitivity plot of the JPCP joint spalling model for age and sealant type (FI = 1000).



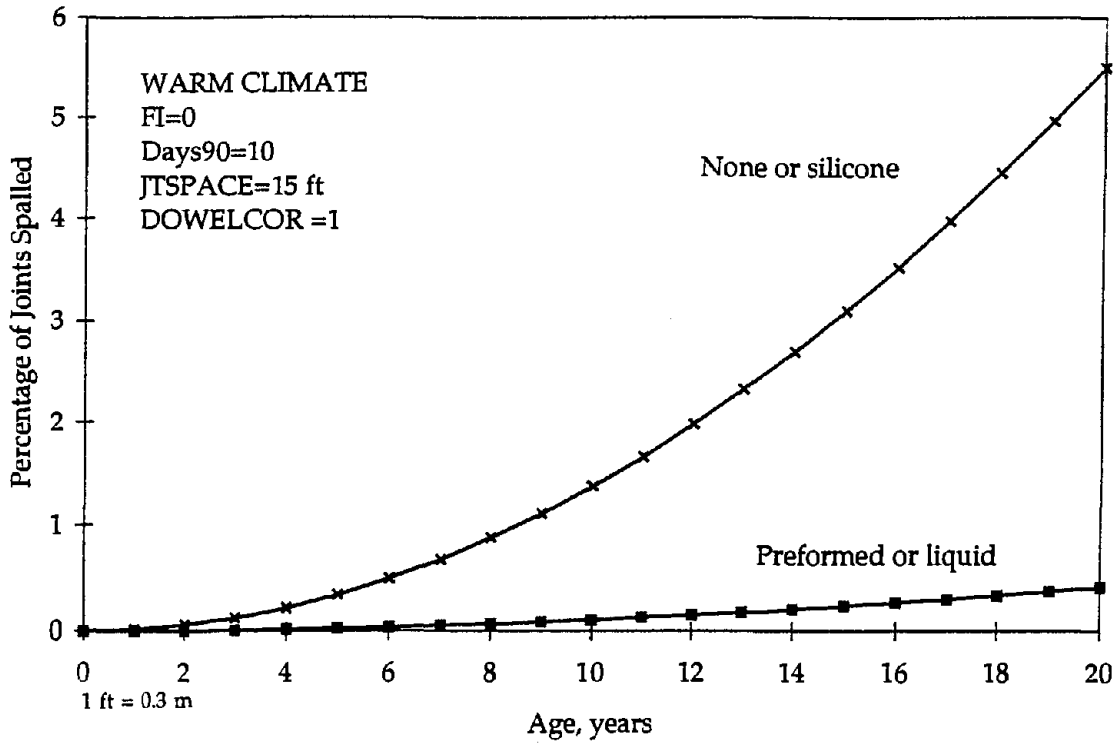


Figure 70. Sensitivity plot of the JPCP joint spalling model for age and sealant type (FI = 0, Days90 = 10).

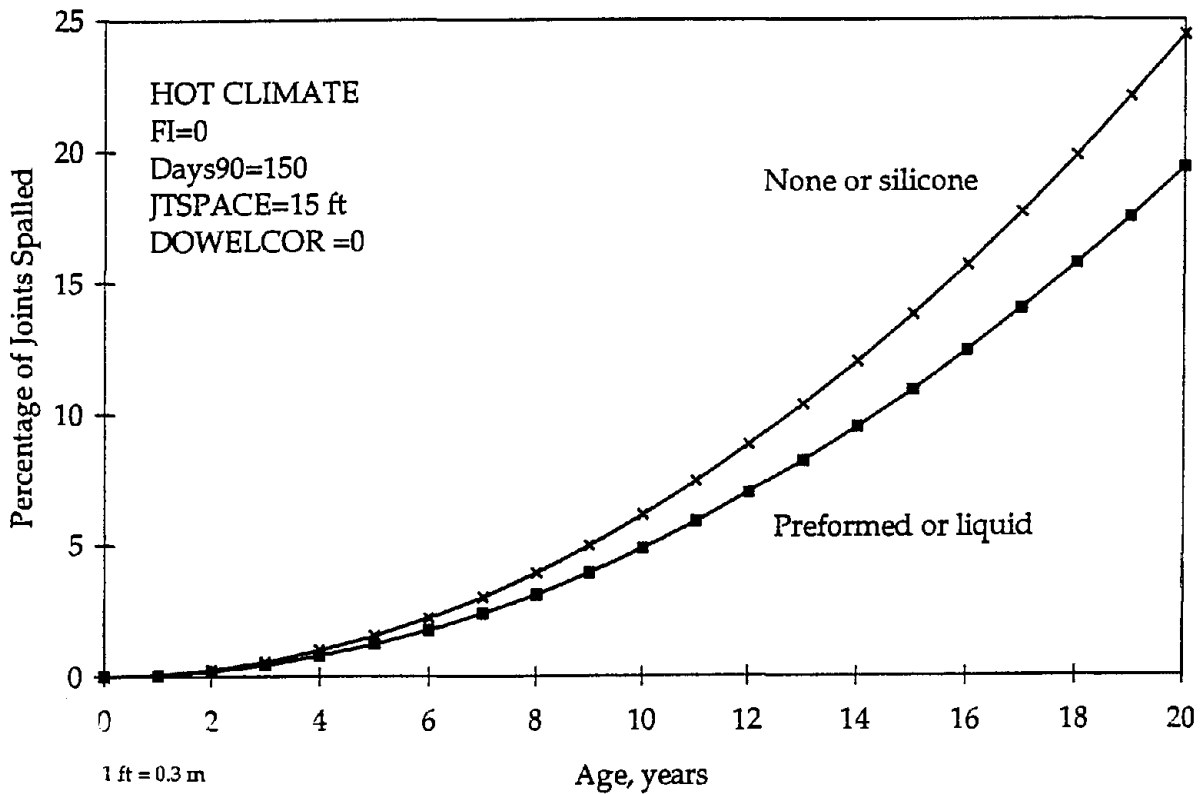


Figure 71. Sensitivity plot of the JPCP joint spalling model for age and sealant type (FI = 0, Days90 = 150).

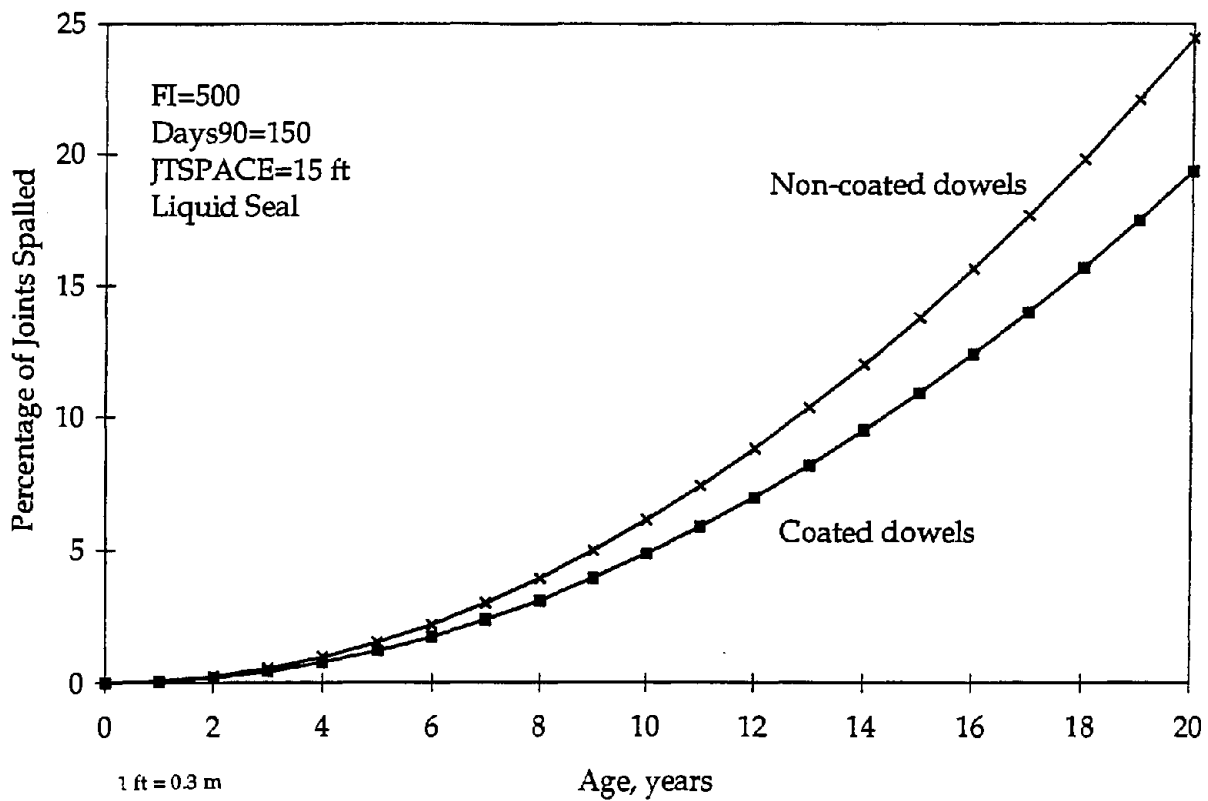


Figure 72. Sensitivity plot of the JPCP joint spalling model for age and dowel protection.

LIQUID SEALANT  
 Days90 = 10  
 JTSPACE = 15 ft  
 DOWELCOR = 0

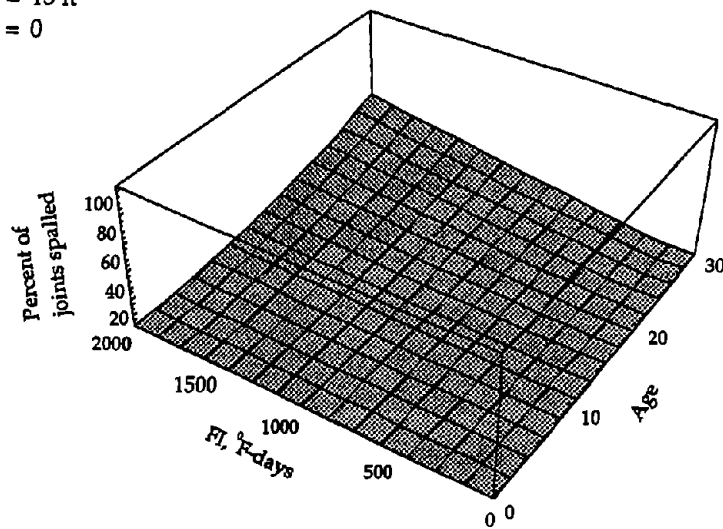
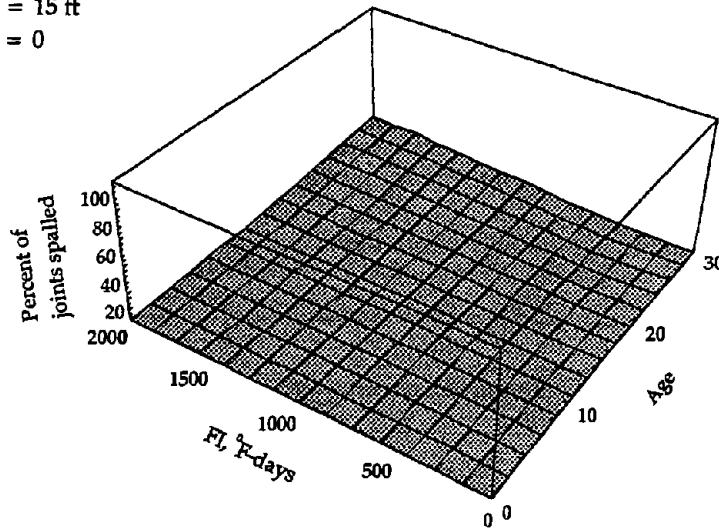


Figure 73. Sensitivity plot of the JPCP joint spalling model for age and freezing index (liquid sealant).

PREFORMED SEALANT

Days90 = 10  
JTSPACE = 15 ft  
DOWELCOR = 0

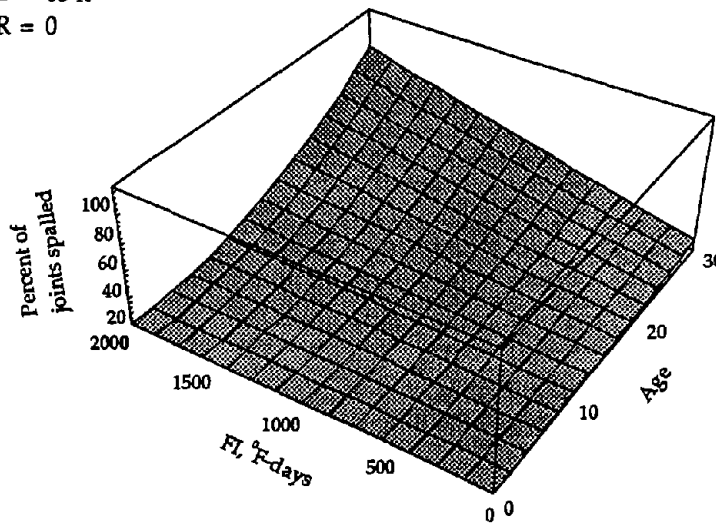


1 ft=0.3m; 1 °F-days=0.555 °C-days

Figure 74. Sensitivity plot of the JPCP joint spalling model for age and freezing index (preformed sealant).

SILICON SEALANT

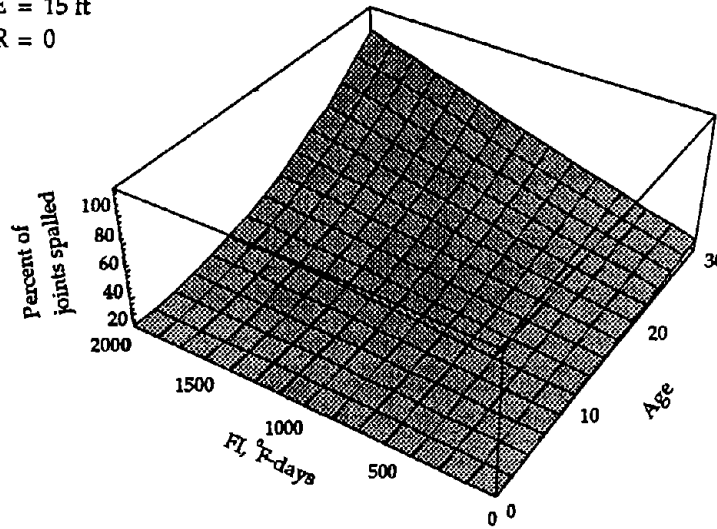
Days90 = 10  
JTSPACE = 15 ft  
DOWELCOR = 0



1 ft=0.3m; 1 °F-days=0.555 °C-days

Figure 75. Sensitivity plot of the JPCP joint spalling model for age and freezing index (silicone sealant).

NO SEALANT  
 Days90 = 10  
 JTSPACE = 15 ft  
 DOWELCOR = 0



1 ft=0.3m; 1 °F-days=0.555 °C-days

Figure 76. Sensitivity plot of the JPCP joint spalling model for age and freezing index (no sealant).

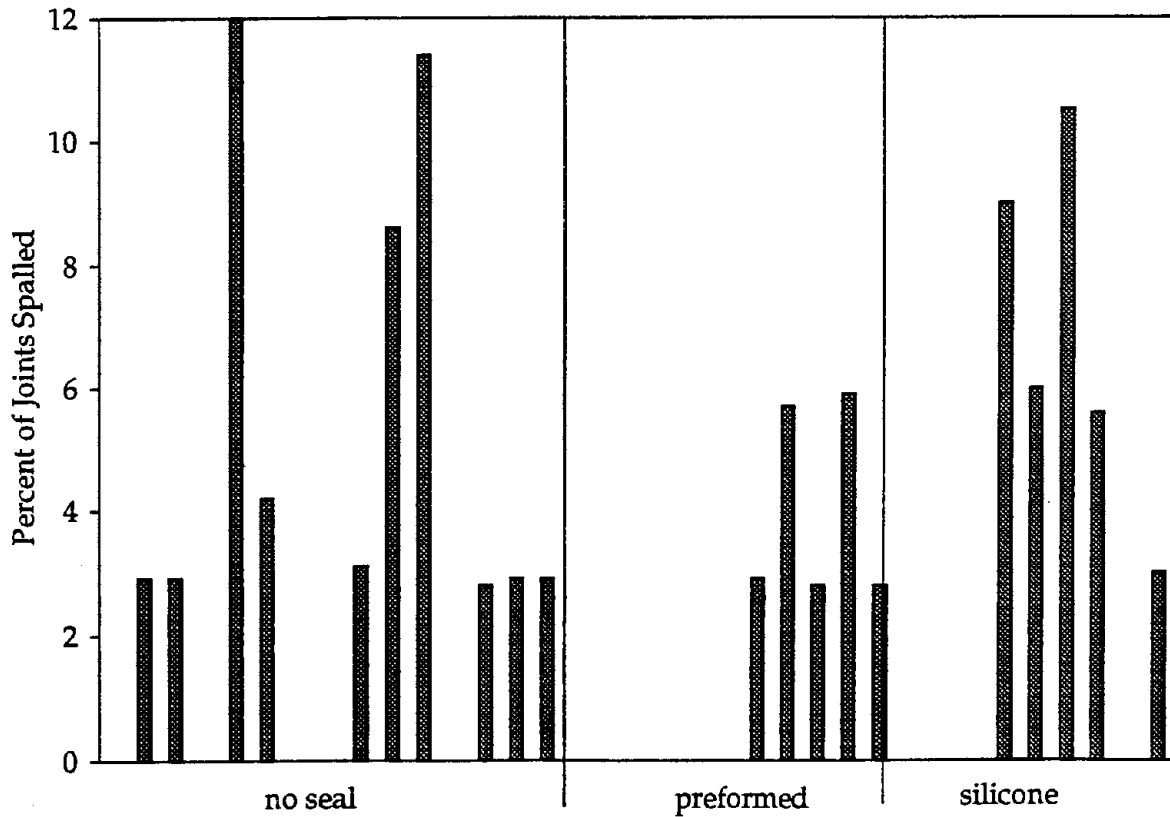


Figure 77. JPCP joint spalling distribution on Wisconsin sections.

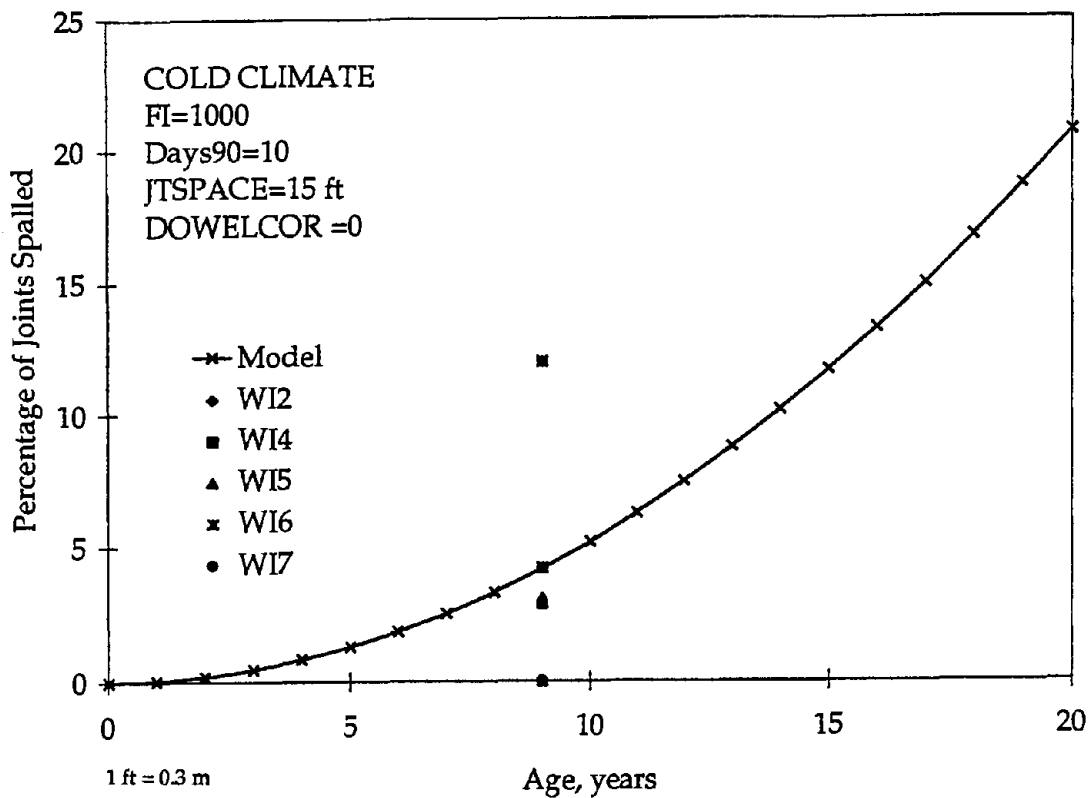


Figure 78. Comparison of JPCP spalling on selected Wisconsin sections with the model prediction.

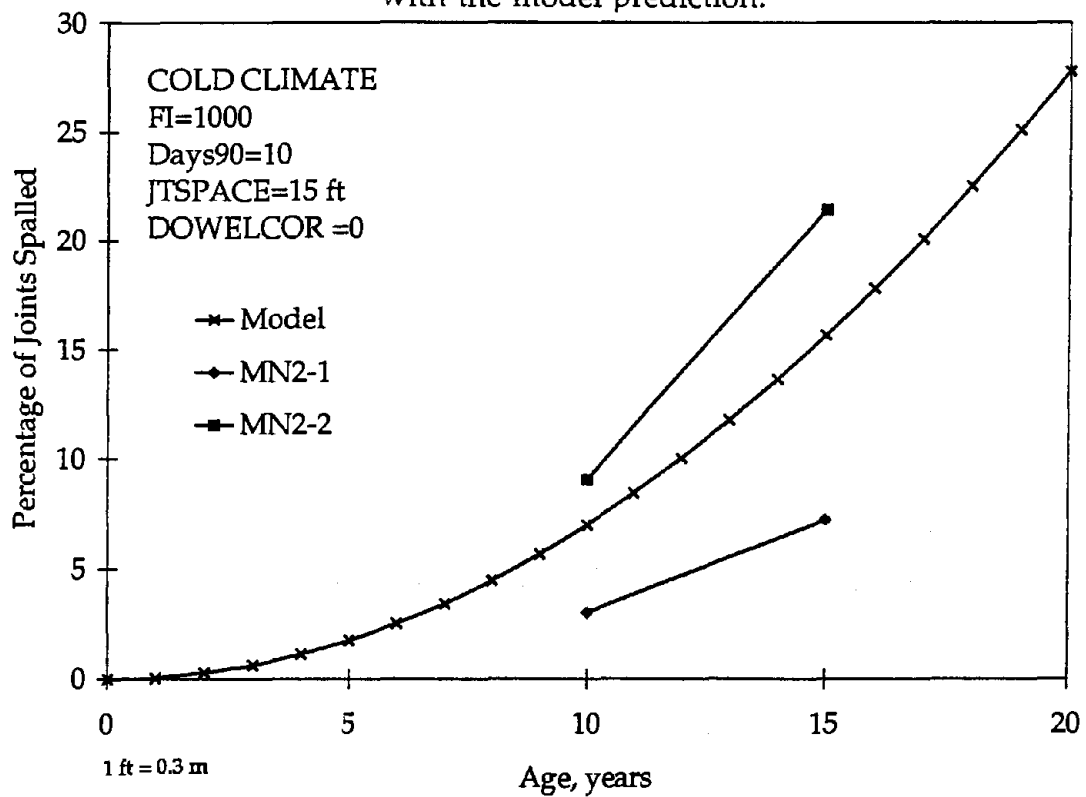


Figure 79. Comparison of JPCP spalling on selected Minnesota sections with the model prediction.

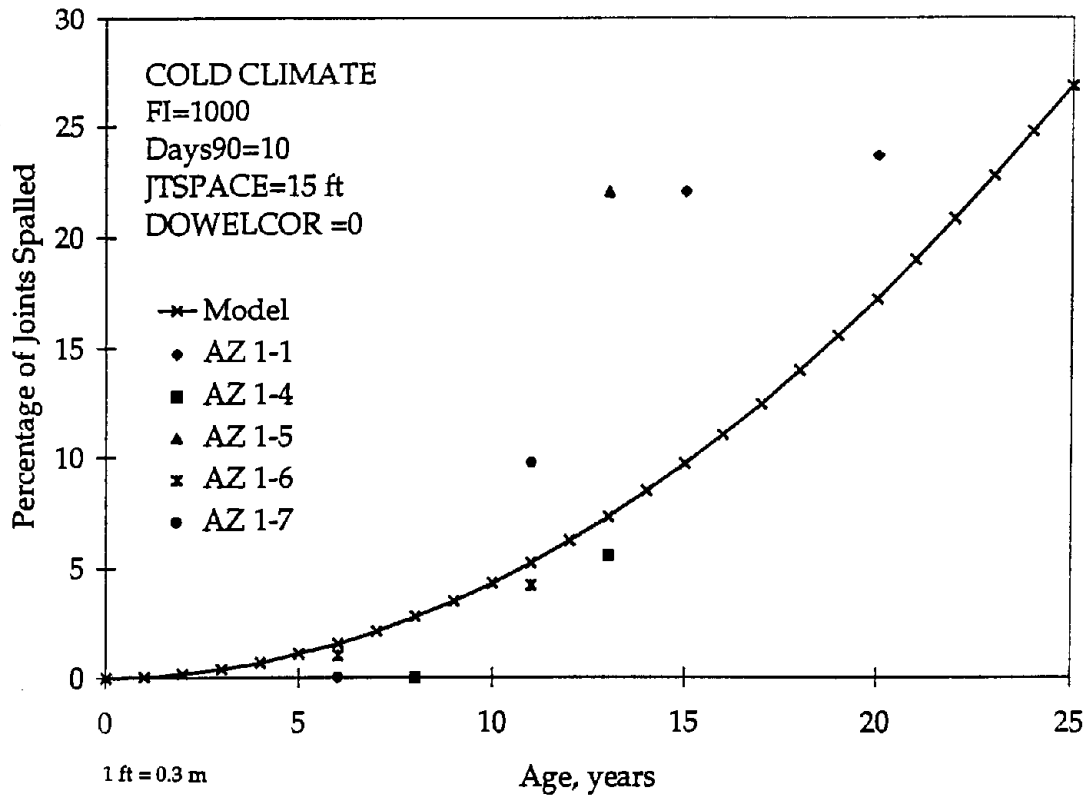


Figure 80. Comparison of JPCP spalling on selected Arizona sections with the model prediction.

Table 11. Spalling of JPCP sections located in a cold climate.

Section	Sealant	Age	SPALLJP
ONT 1-2	Liquid	10	0.7
ONT 1-1	Liquid	10	0
WI 5-1	Silicone	9	6
WI 5-5	Silicone	9	3
ONT 2-1a	Preformed	21	3
ONT 2-1	Preformed	21	0

The proposed model predicts a very large percentage of spalled joints in a cold climate if no sealant is present (see figures 68, 69 and 76). This prediction may not be reliable because of a lack of data for older, nonsealed sections located in a cold climate. At the same time, several 9-year old sections, such as WI 6-4, WI 6-1, and

WI 4-4, exhibit a high percentage of spalled joints (12, 11, and 9 percent, respectively), while older Wisconsin sections with sealant exhibit less spalling (see figure 77). This observation supports the conclusion that the absence of sealant may increase spalling in a cold climate, although it might be not so pronounced as is predicted by the model. A considerable number of older nonsealed sections exist in a warm climate, and some of them also show higher spalling than sealed sections. This does not mean, however, that nonsealed joints exhibited significantly worse overall performance. The majority of spalls observed in Wisconsin sections with nonsealed joints, including the spalls rated as medium- and high-severity according to SHRP classification, were less than 0.6 m (2 ft) wide and seemed not to affect pavement ride quality. Although the nonsealed joints were filled by fine incompressibles, it appeared that those incompressibles did not cause any significant damage to the pavement and helped the pavement to keep large incompressibles out of the joints, acting like a natural sealant.

The spalling model also predicts that sealants are not so effective in climates with a large number of hot days, as can be observed from figure 71. However, the database contains information for only a few sections located in a hot climate, and all of these sections have liquid sealant.

Figure 72 shows results of the sensitivity analysis of age, potential dowel corrosion, and joint spalling. This plot illustrates the effect of dowel corrosion in a cold climate (FI = 500, Days90 = 10). The plot shows that climate dowel corrosion may double the percentage of spalled joints. Therefore, corrosion protection of dowels is very important.

The three-dimensional plots given in figures 73 through 76 show the effect of the interaction between climate conditions and pavement age on the performance of each type of sealant. The number of days with temperatures above 90 °F (32 °C), Days90, is fixed at 10, and the variation of FI from 0 to 2000 represent variation in climate from mild to cold. One can observe that percentage of joints spalled increases with age and freezing index. It is predicted that significant spalling of sealed joints does not begin until about 10 or 15 years after construction, but rapidly increases after that, especially in cold climates. This effect can be explained by the increase in the number of freeze-thaw cycles to which the pavements is exposed.

Figures 78 through 80 present comparisons of JPCP spalling on selected sections located in Wisconsin, Minnesota, and Arizona, respectively, with the model prediction. Reasonable agreement is observed between the model predictions and field test data.

Based on the results provided by the JPCP joint spalling model, the following conclusions may be drawn:

- Transverse joint spalling increases with the pavement age to the second power.
- Significant transverse joint spalling does not begin until about 10 or 15 years after construction.

- Preformed joint sealant reduces transverse joint spalling more effectively than other sealant types considered.
- Transverse joints without sealant exhibit the largest amount of spalling.
- Silicone sealants perform worse than liquid sealants, presumably because of the silicone pulling on the sidewalls of the young concrete before it has gained sufficient strength.
- An increase in joint spacing increases the percent of joints spalled.
- The amount of spalling is greater in very cold climates and in very hot climates, but lower in moderate climates.
- An appropriate protection of dowels from corrosion (e.g., epoxy-coating) reduces joint spalling.

Based on the results of the modeling, the following design features are recommended to reduce JPCP spalling:

- Preformed sealant, especially in cold climates.
- More durable PCC in freeze-thaw.
- Corrosion protection of dowels.

The model also shows that the pavement aging has a tremendous effect on JPCP spalling. Effective maintenance strategies, which include cleaning and resealing of joints at regular intervals, may reduce the effect of aging and, therefore, significantly reduce spalling.

### **Transverse Joint Spalling Model for JRCP**

Transverse joint spalling of jointed reinforced concrete pavements is caused by mechanisms similar to those that cause joint spalling in jointed plain concrete pavements. However, there are some complicating issues, such as the presence of transverse cracks at midpanel that may rupture the reinforcement and become working cracks, which could reduce movements at the joints. Also, longer joint spacings result in larger joint openings and present a more difficult sealing problem. These and other factors must be accounted for in the development of a spalling model for JRCP.

### **Preliminary Data Analysis**

The project database contains information on 159 JRCP sections, including time-series performance data for both 1987 and 1992. As in the JPCP spalling model development, these data were examined and cleaned to remove pavement sections that exhibit severe D-cracking (medium- and high-severity), that contain unusual load transfer mechanisms (e.g. ACME devices), and outliers.

The factorial matrix of the distribution of the remaining 109 pavement sections is shown in table 12, separated by climatic region, sealant type, and age. The climate is categorized as cold (FI greater than 200) and warm mild (FI less than 200). Two age



Table 12. Distribution of the pavement sections and designs used in the development of JRCP spalling model.

Climatic Region	Sealant	Age, years 0 - 10		Age, years 11 - 25	
		Nonstabilized Base	Stabilized Base	Nonstabilized Base	Stabilized Base
FI <200	Preformed	0	4	10	4
	Liquid	1	1	3	1
	Silicone	0	0	0	0
	None	0	0	0	0
FI >200	Preformed	6	5	0	0
	Liquid	3	3	30	32
	Silicone	2	0	2	0
	None	0	0	2	0
Total		12	13	47	37

brackets are included (0 to 10, and 11 to 25), two types of bases are considered (stabilized and nonstabilized), and four joint sealant types are evaluated:

- Preformed sealant.
- Liquid sealant (including hot-applied, asphaltic-based sealants, polyurethanes, PVC coal tars)
- Silicone sealant.
- None (indicating section whose joints have not been sealed even at construction).

An analysis of the factorial matrix indicates the following limitations:

- There are only two nonsealed sections and only two sections with silicone sealant in the data base. Thus, the effect of these variables cannot be considered in the development of a JRCP joint spalling model.
- There are no sections greater than 10 years old with preformed sealant and located in the cold region.
- Very few sections with liquid sealants exist in warm regions.

#### Review of Available Models

Several models for predicting transverse joint spalling of JRCP pavements are available. One model developed under a FHWA contract has the following form:<sup>(3)</sup>

$$JTSPALL = AGE^{4.1232} * [0.00024 + 0.0000269 DCRACK + 0.000307 REACTAGG(44) - 0.000033 LIQSEAL - 0.0003 PREFSEAL + 0.00000014 FI]$$

where:

- JTSPALL = Number of medium- and high- severity spalled joints/mi.
- AGE = Age since original construction, years.
- DCRACK = 0, if no D-cracking exists.  
= 1, if D-cracking exists.
- REACTAGG = 0, if no reactive aggregate exists.  
= 1, if reactive aggregate exists.
- LIQSEAL = 0, if no liquid sealant exists in joint.  
= 1, if liquid sealant exists in joint.
- PREFSEAL = 0, if no preformed sealant exists in joint.  
= 1, if preformed sealant exists in joint.
- FI = Freezing Index, degree days below freezing.

Another model was developed from an early analysis of the SHRP LTPP data.<sup>(11)</sup> This model has the following form:

$$SPALLJR = -79 + 0.604 * AGE^{1.5} + 0.129 * TRANGE^{1.5} \quad (45)$$

where:

- SPALLJP = Mean percentage of medium- and high- severity spalled joints:
- AGE = Age since original construction, years.
- TRANGE = mean monthly temperature range, °F.

An examination of these models shows that joint spalling depends on pavement age, climatic conditions, joint sealant, and concrete durability. The models show that a parabolic relationship between the age of the JRCP and the number of spalled joints exist. Aging probably represents many mechanisms, such as the number of freeze-thaw cycles, the cyclic opening and closing of joints, sealant aging, and infiltration of incompressibles. One should note, however, that the SHRP LTPP model is based on a smaller number of young sections, which results in a small exponent on the age term. On the other hand, the exponent of 4.12 on the age term in the 1990 FHWA model appears to be high.

#### Explanatory Variables Initially Selected

The initial explanatory variables that were considered are as follows:

- AGE: time since construction, years.
- CESAL: cumulative 18-kip (80-kN) ESAL's in traffic lane, millions.
- JTSPACE: mean transverse joint spacing, in.
- THICK: PCC slab thickness, in.

Cd:	adapted AASHTO drainage coefficient.
JTOPEN:	joint opening, in.
JTWIDTH:	mean joint width, in.
JTSEALNT:	joint seal type (several types are listed in the data base).
Epcc:	mean backcalculated modulus of elasticity of concrete, million lb/in <sup>2</sup> .
Kdyn:	mean backcalculated modulus of subgrade reaction, lb/in <sup>2</sup> /in.
MI:	Thornthwaite moisture index.
Days90:	number of days temperature greater than 90 °F.
TRANGE:	mean monthly temperature range.
FI:	freeze index, degree-days below freezing.
PRECIP:	average annular precipitation, in.
FTCY:	mean annular air freeze-thaw cycles.
DOWELCOR:	dowel potential corrosion (=0 if no dowels exist or dowels are coated [epoxy, plastic, stainless steel], =1 if dowels do not have a protective coating).
BASE:	base type (= 0 nonstabilized base, =1 stabilized base).

As was done for the jointed plain pavements, sections with dowel coatings were categorized differently than sections without.

### Model Development

It was observed from the data base that pavement sections with stabilized bases have more spalling than sections with nonstabilized bases for sections located in similar climatic conditions. This might be explained by poor drainage conditions often associated with stabilized bases. It was also found that the presence of preformed sealant compensates for this negative effect caused by the stabilized base.

Two-dimensional scatter plots of the raw data for the some of the key variables are shown on figure 81. The final model developed for joint spalling for the joint plain concrete pavements is as follows:

$$\begin{aligned}
 SPALLJR = & AGE^3 * JTSPACE * (1.94 DOWELCOR \\
 & + 8.819 BASE * (1 - PREFSEAL) + 0.00701 FI) * 10^{-5}
 \end{aligned}
 \tag{46}$$

where:

- SPALLJR = Mean percentage of medium- and high-severity spalled joints.
- AGE = Age since original construction, years.
- JTSPACE = mean transverse joint spacing, ft.
- DOWELCOR = dowel corrosion potential.
- = 0 if no dowels exist, or if dowels are protected from corrosion.
- = 1 if dowels are not protected from corrosion.
- PREFSEAL = 0, if no preformed sealant exists in joint.
- = 1, if preformed sealant exists in joint.
- BASE = 0, if nonstabilized base.

= 1, if stabilized base (cement treated, asphalt treated, lean concrete).  
FI = Freezing Index, degree days below freezing.

Some excellent statistics were obtained for this model:

N = 109.  
R<sup>2</sup> = 0.76.  
RSE = 14.4 percent of joints.

The model has an acceptable level of R<sup>2</sup>, but a relatively high RSE. It should be noted, however, that the RSE has the same order of magnitude as the accuracy of the field measurements. For example, the OH 1-9 section is 400 ft (122 m) with a joint spacing is 40 ft (12.2 m). This means that 11 joints were evaluated. Therefore, each spalled joint increases the percentage of spalling by 9 percent, meaning that there can be a significant amount of variability associated with any section.

The actual versus predicted joint spalling and residual versus predicted joint spalling are given in figures 82 and 83, respectively. These figures show that prediction errors are symmetrically distributed around zero.

#### Sensitivity Analysis and Discussion.

The sensitivity plots of the key variables in the model is provided in the figures 84 through 91. Figures 84 and 85 show sensitivity studies for age, sealant type, potential corrosion of dowels, and JRPC joint spalling in a cold and in a warm climate, respectively. One can observe that dowel protection may reduce joint spalling by 10 to 50 percent. The effect of preformed sealants can be even more pronounced. However, the effect of these design features do not become evident until after about 10 or 15 years.

Figure 86 shows the effect of joint spacing on the joint spalling for sections located in a cold climate, constructed on a stabilized base, and containing preformed joint sealants. As would be expected, an increase in joint spacing significantly increases the percentage of spalled joints. This difference is even more pronounced with liquid sealant. It should be noted, however, that the longer joint spacing results in only an increase in the percentage of spalled joints; the actual number of spalled joints per mile remains the same. For example, figure 86 shows that after 20 years the increase in joint spacing from 40 ft (12.2 m) to 60 ft (18.3 m) increases the percentage of spalled joints from 4.49 to 6.73 percent. However, the total number of joints per mile decreases from 132 joints/mi (5280/40) to 88 joints/mi (5280/60) and, therefore, the actual number of spalled joints per mile remains the same for each design (5.92 joints/mi, obtained by multiplying 0.0339\*132 or by 0.0673\*88).

Figures 87 through 90 presents three-dimensional sensitivity plots for age, freezing index, type of sealant, and dowel corrosion protection. The model predicts higher spalling for pavement sections for older pavements located in a colder climate. Similar to what was observed for JPCP pavements, the percent of joints spalled

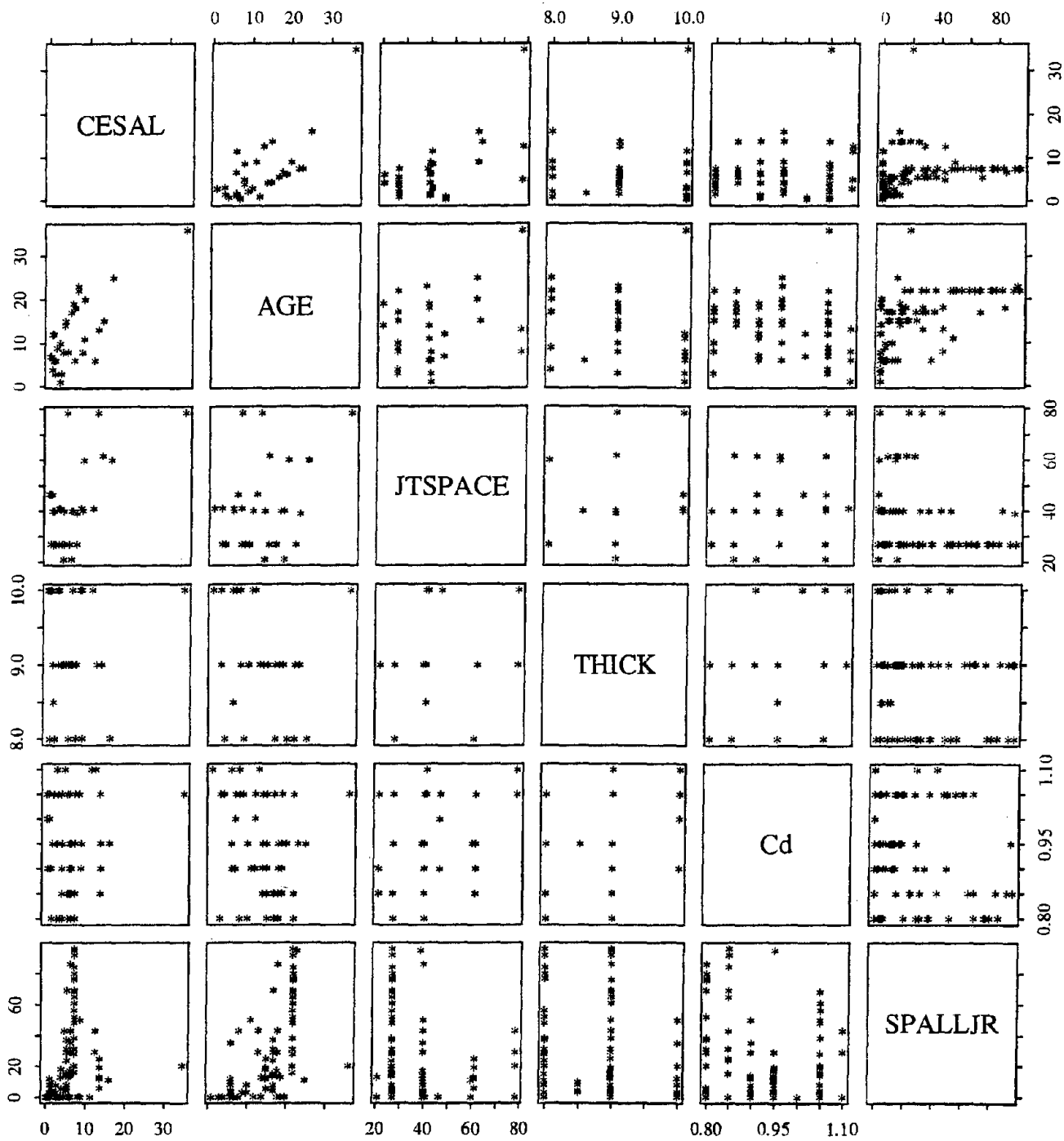


Figure 81. Two-dimensional scatter plot for JRCP spalling model.

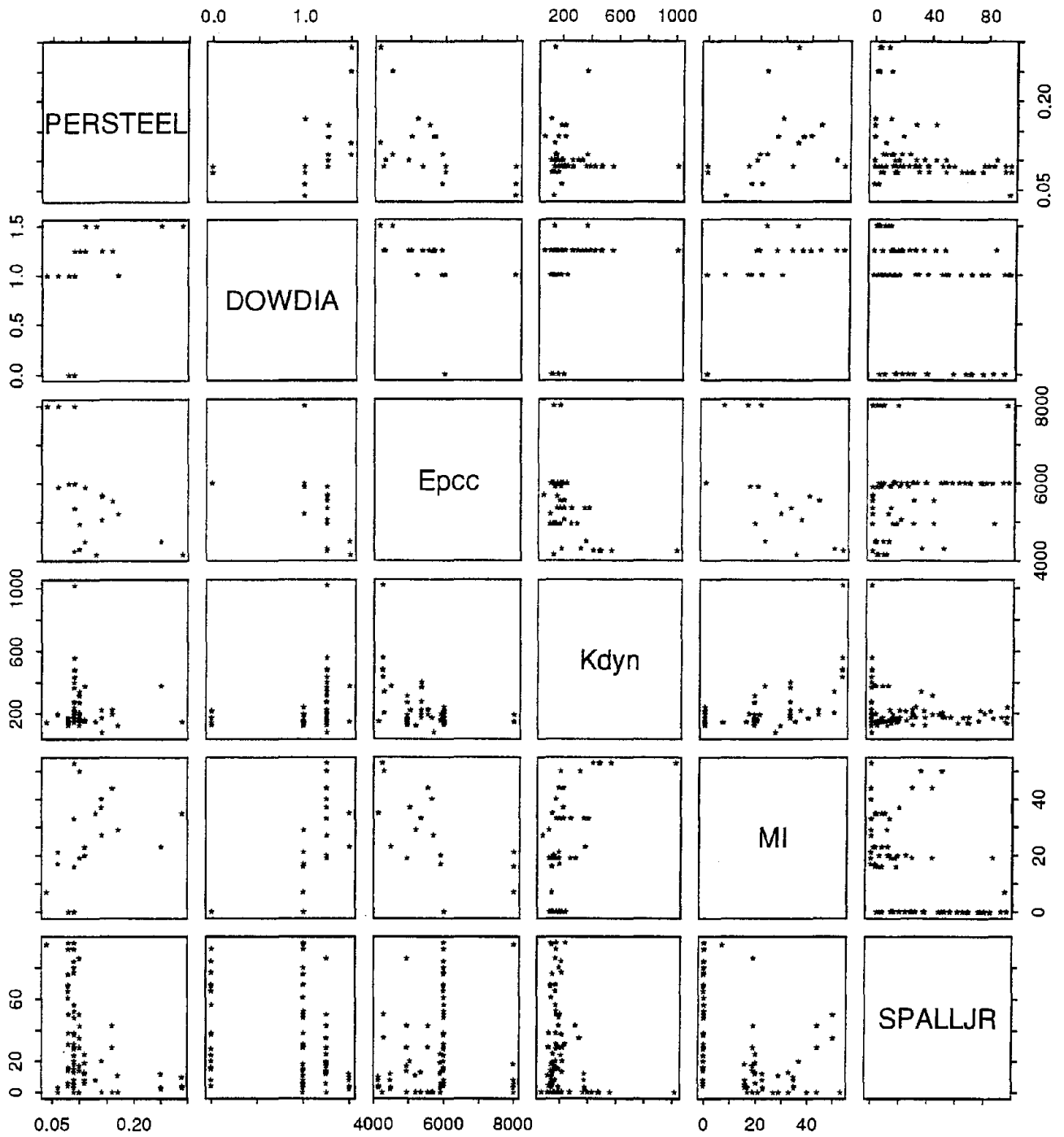


Figure 81. Two-dimensional scatter plot for JRCP spalling model (continued).

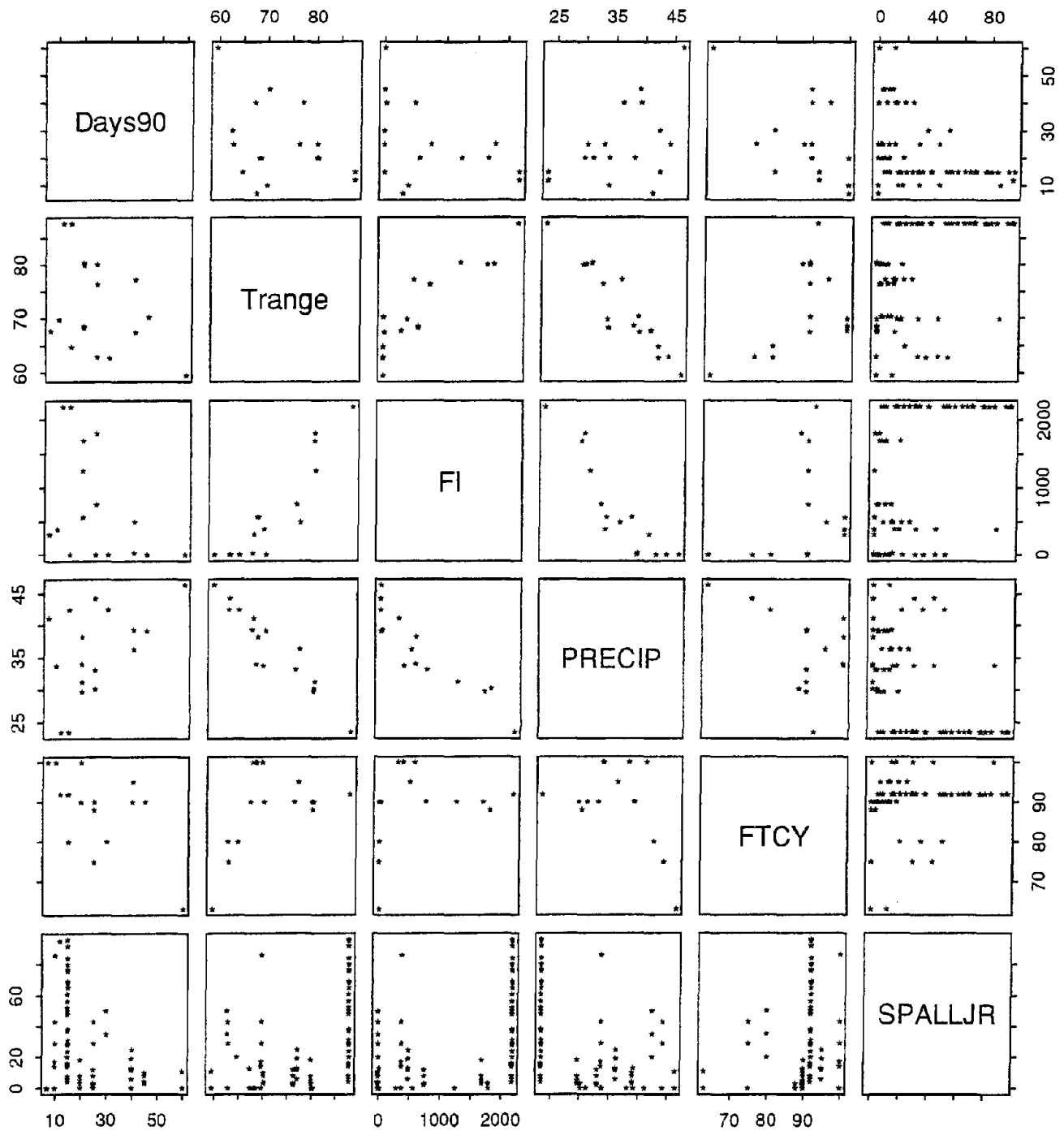


Figure 81. Two-dimensional scatter plot for JRCP spalling model (continued).

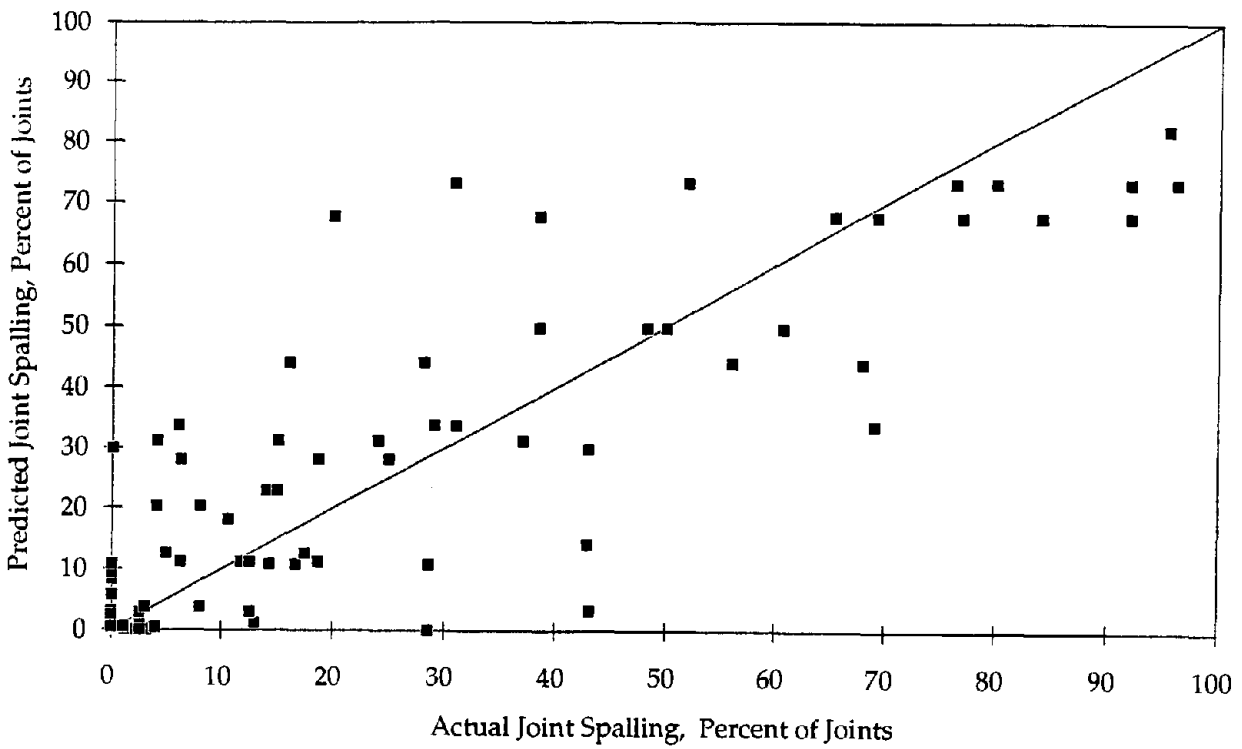


Figure 82. Actual versus predicted percentage of JRCP spalled joints.

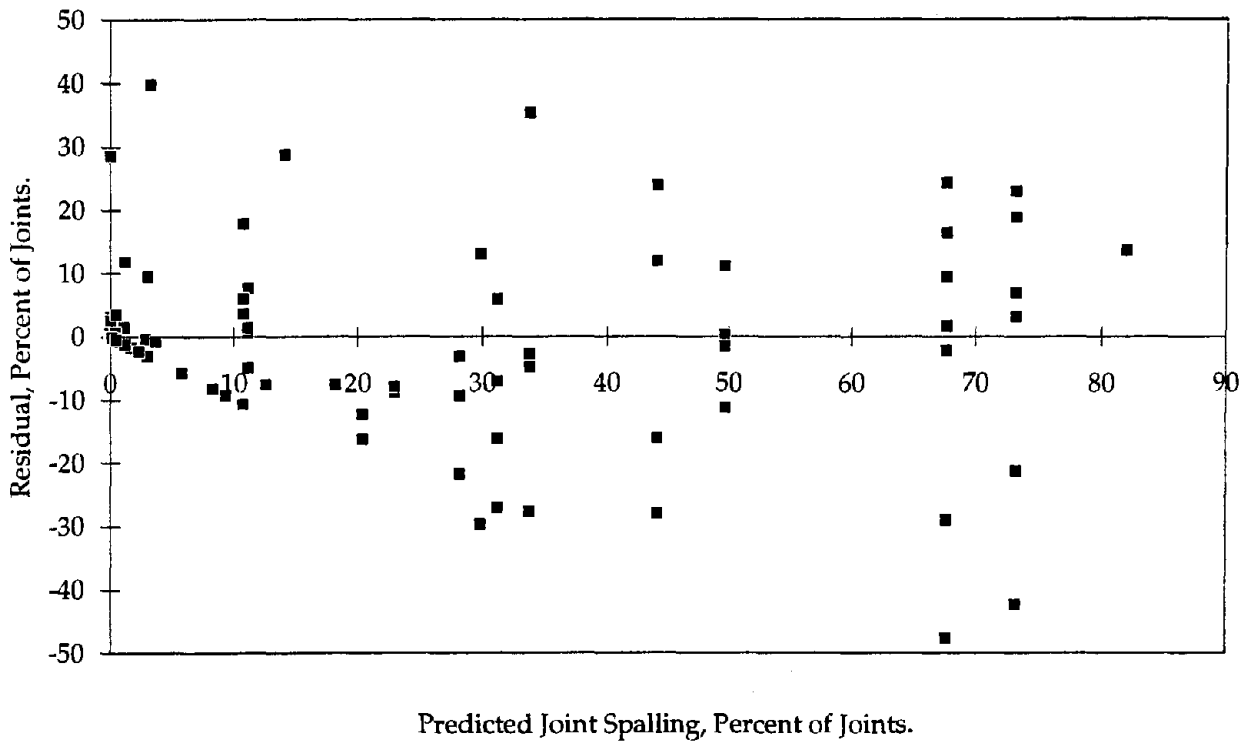


Figure 83. Actual versus residual percentage of JRCP spalled joints.



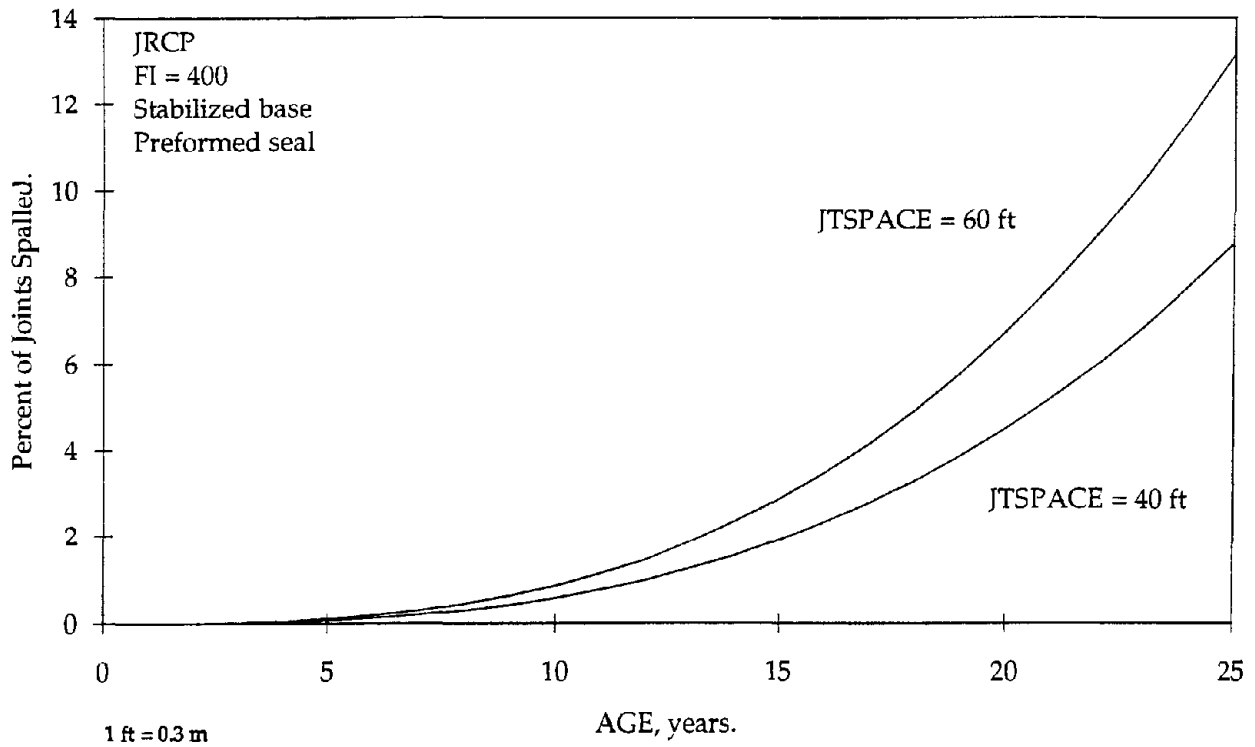


Figure 84. Sensitivity plot of the JRCP joint spalling model for age, dowel coating, and sealant type (FI = 1500).

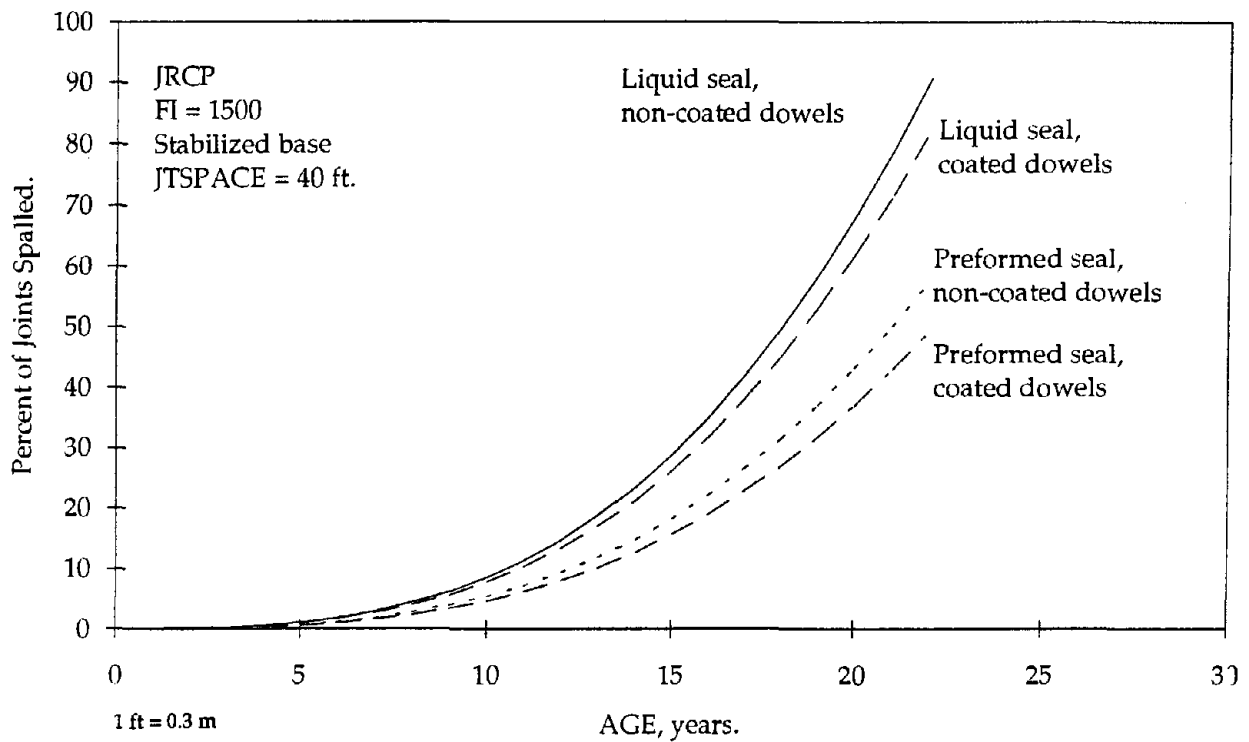


Figure 85. Sensitivity plot of the JRCP joint spalling model for age, dowel coating, and sealant type (FI = 200).

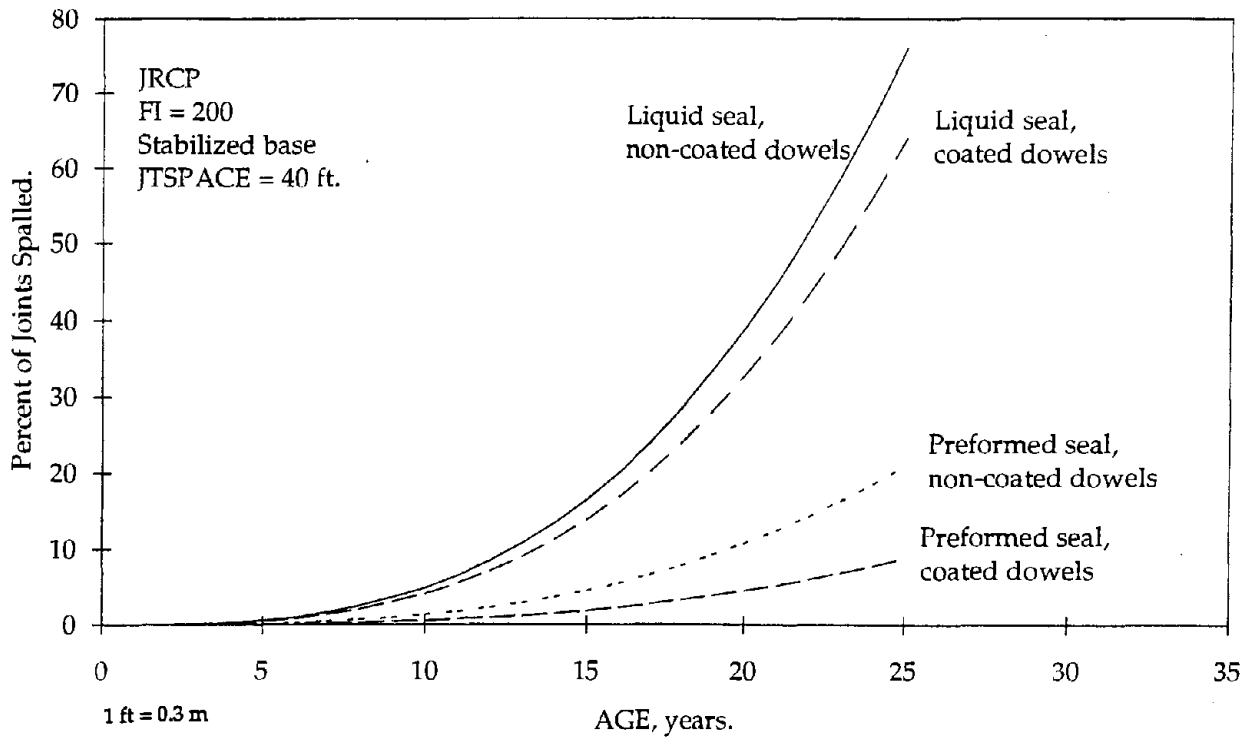


Figure 86. Sensitivity plot of the JRCP joint spalling model for age and joint spacing.

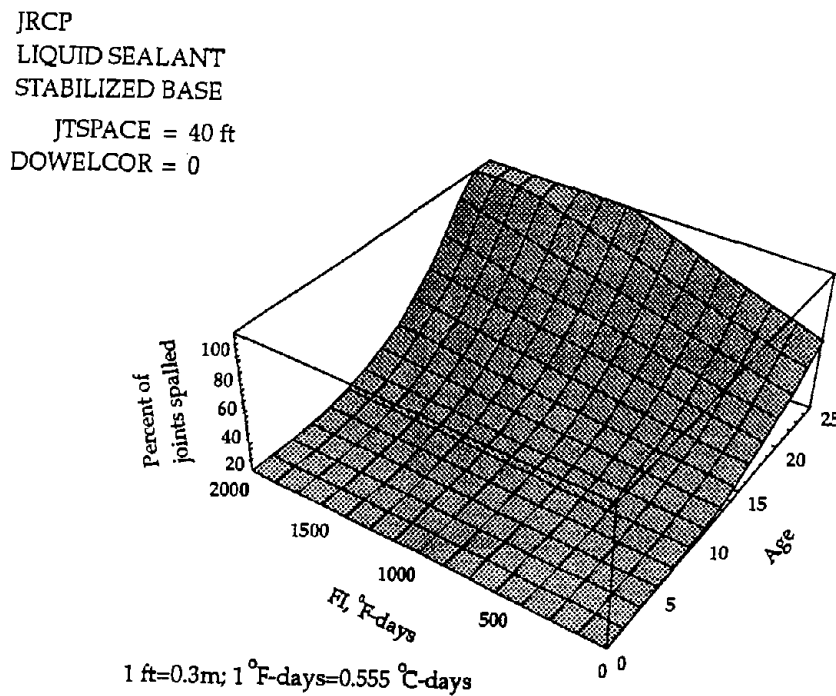
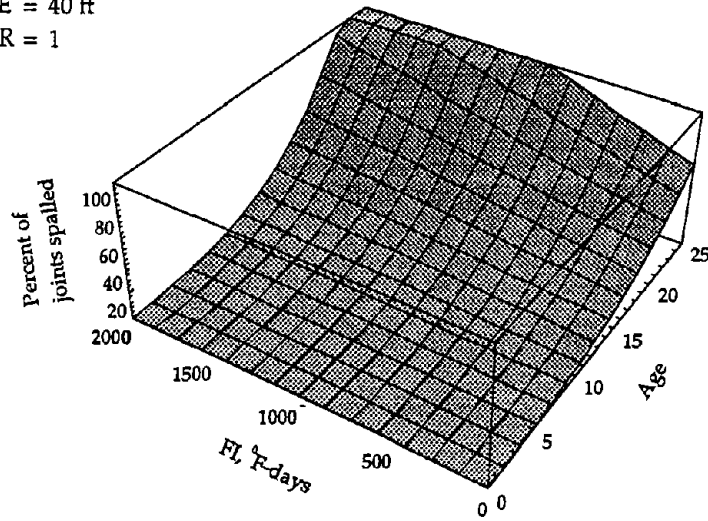


Figure 87. Sensitivity plot of the JRCP joint spalling model for age and freezing index (liquid sealant, DOWELCOR = 0).

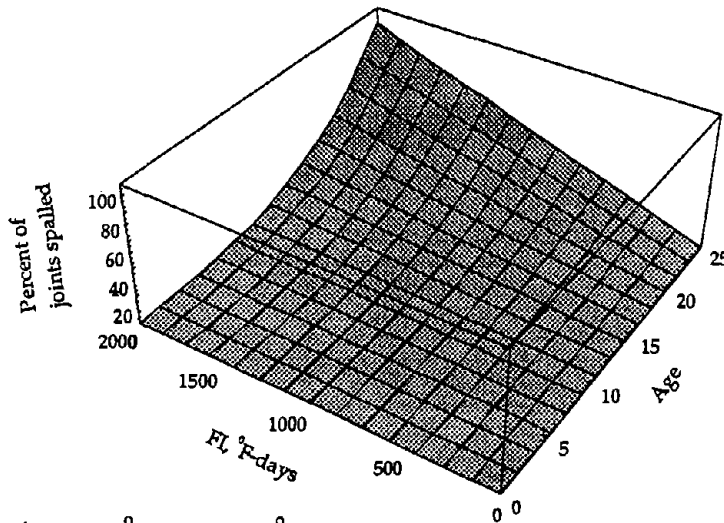
JRCP  
LIQUID SEALANT  
STABILIZED BASE  
JTSPACE = 40 ft  
DOWELCOR = 1



1 ft=0.3m; 1 °F-days=0.555 °C-days

Figure 88. Sensitivity plot of the JRCP joint spalling model for age and freezing index (liquid sealant, DOWELCOR = 1).

JRCP  
PREFORMED SEALANT  
STABILIZED BASE  
JTSPACE = 40 ft  
DOWELCOR = 0



1 ft=0.3m; 1 °F-days=0.555 °C-days

Figure 89. Sensitivity plot of the JRCP joint spalling model for age and freezing index (preformed sealant, DOWELCOR = 0).

JRCP  
 PREFORMED SEALANT  
 STABILIZED BASE  
 JTSPACE = 40 ft  
 DOWELCOR = 0

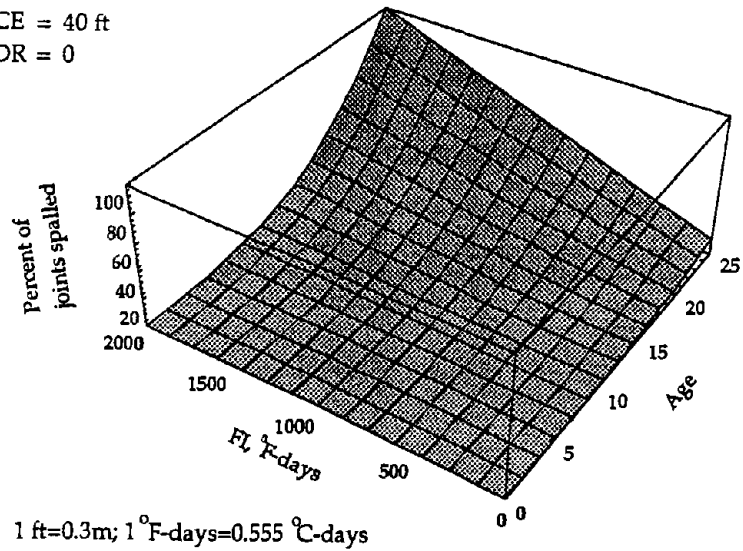


Figure 90. Sensitivity plot of the JRCP joint spalling model for age and freezing index (preformed sealant, DOWELCOR = 1).

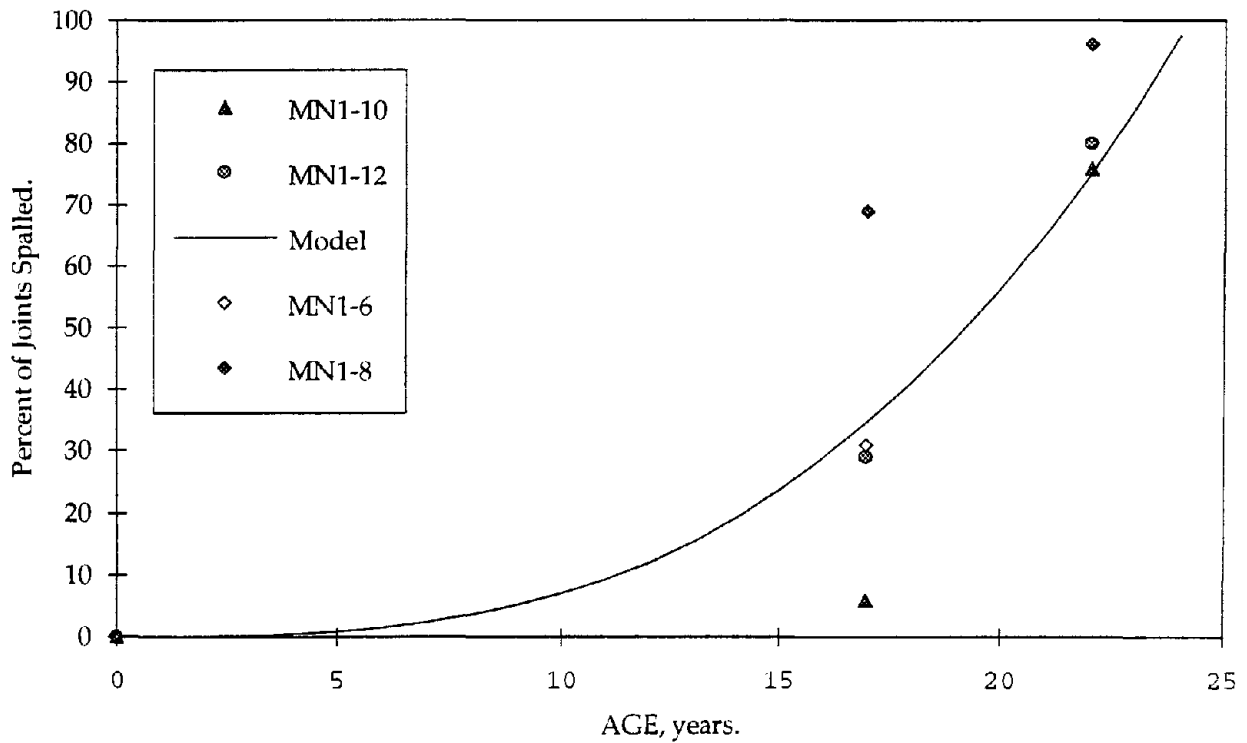


Figure 91. Comparison of JRCP spalling on selected Minnesota sections with the model prediction.

increases with age and freezing index. It is predicted that if joint are sealed then significant spalling does not begin until 10 years after construction, but rapidly increases after that, especially in cold climates. Again, this effect can be explained by an increase in the number of freeze-thaw cycles to which the pavements is exposed. Figure 91 presents a comparison of JRCP spalling on selected sections located in Minnesota. Reasonable agreement is observed between the model predictions and field test data.

Analysis of the results of the JRCP spalling model leads to the following conclusions:

- Transverse joint spalling increases rapidly with pavement age (to the third power).
- Significant transverse joint spalling does not occur until 10 years after construction.
- Transverse joint spalling is greater in cold climates than in warmer climates.
- An increase in transverse joint spacing results in an increase in the percentage of joints spalled, however, the actual number of spalled joint per mile remains the same.
- Joints having dowels with corrosion protection show reduced spalling.
- The presence of a dense stabilized base increases spalling if preformed sealant is not used.
- A preformed sealant reduces spalling for pavements with stabilized bases.

Based on the results of the sensitivity analysis, the following design features are recommended to reduce JRCP spalling:

- Preformed sealant, especially in cold climates and with stabilized base.
- Use of nonstabilized base.
- Use of more durable PCC in cold climates.
- Corrosion protection of dowels.

The model also shows that the pavement aging has a tremendous effect on JRCP spalling. Effective maintenance strategies, which include cleaning and resealing of joints at regular intervals, may reduce the effect of aging, and, therefore, significantly reduce spalling.

### **Present Serviceability Rating Model**

The present serviceability rating (PSR) is a subjective user rating of the existing ride quality of the pavement condition. PSR has been correlated with various roughness indicators, such as slope variance and IRI. As such, it is a reflection of the user response to pavement condition. A PSR model, based on key distress types, is useful in the mechanistic-empirical design of pavements to approximately relate physical pavement deterioration (such as faulting and cracking that are estimated using other models) to serviceability, or user response. PSR prediction models are

developed for both JPCP and JRCP using key pavement distresses. The available number of sections for each pavement type and climatic region is shown in table 13.

Table 13. Distribution of the pavement sections used in the development of PSR model.

Climatic Region	JPCP	JRCP
Wet-Freeze	84	52
Wet-Nonfreeze	44	8
Dry-Freeze	28	22
Dry-Nonfreeze	30	8

The explanatory variables initially considered are:

FaultTT: Total joint faulting per mile, in/mi.

T-crack: Amount of transverse cracking, number of cracks/mi.

Spall: Percentage of the joints spalled, percent.

L-crack: Amount of longitudinal cracking, ft/mi.

Although suspected to have a significant effect on serviceability, the number of full-depth repairs was not selected as an independent variable due to the absence of such repairs on most of the study sections.

### Model Development

Following the same model building procedure used in the development of the transverse joint faulting and joint spalling models, PSR models were developed for both JPCP and JRCP.

#### *Jointed Plain Concrete Pavements*

Figure 92 provides the two-dimensional plot for the variables evaluated for PSR in JPCP. The final model for the PSR using the sections of jointed plain concrete pavement is as follows:

$$\text{PSR} = 3.95 - 0.010276 * \text{FaultTT} - 0.001014 * \text{T-crack} - 0.009421 * \text{Spall} - 0.003911 * \text{L-crack}^{0.5} \quad (47)$$

$$R^2 = 0.51.$$

$$N = 186.$$

$$\text{RSE} = 0.30.$$

where:

FaultTT = Total joint faulting per mile, in/mi.

T-crack = Amount of transverse cracking, number of cracks/mi.

Spall = Percentage of the joints spalled, percent.

L-crack = Amount of longitudinal cracking, ft/mi.

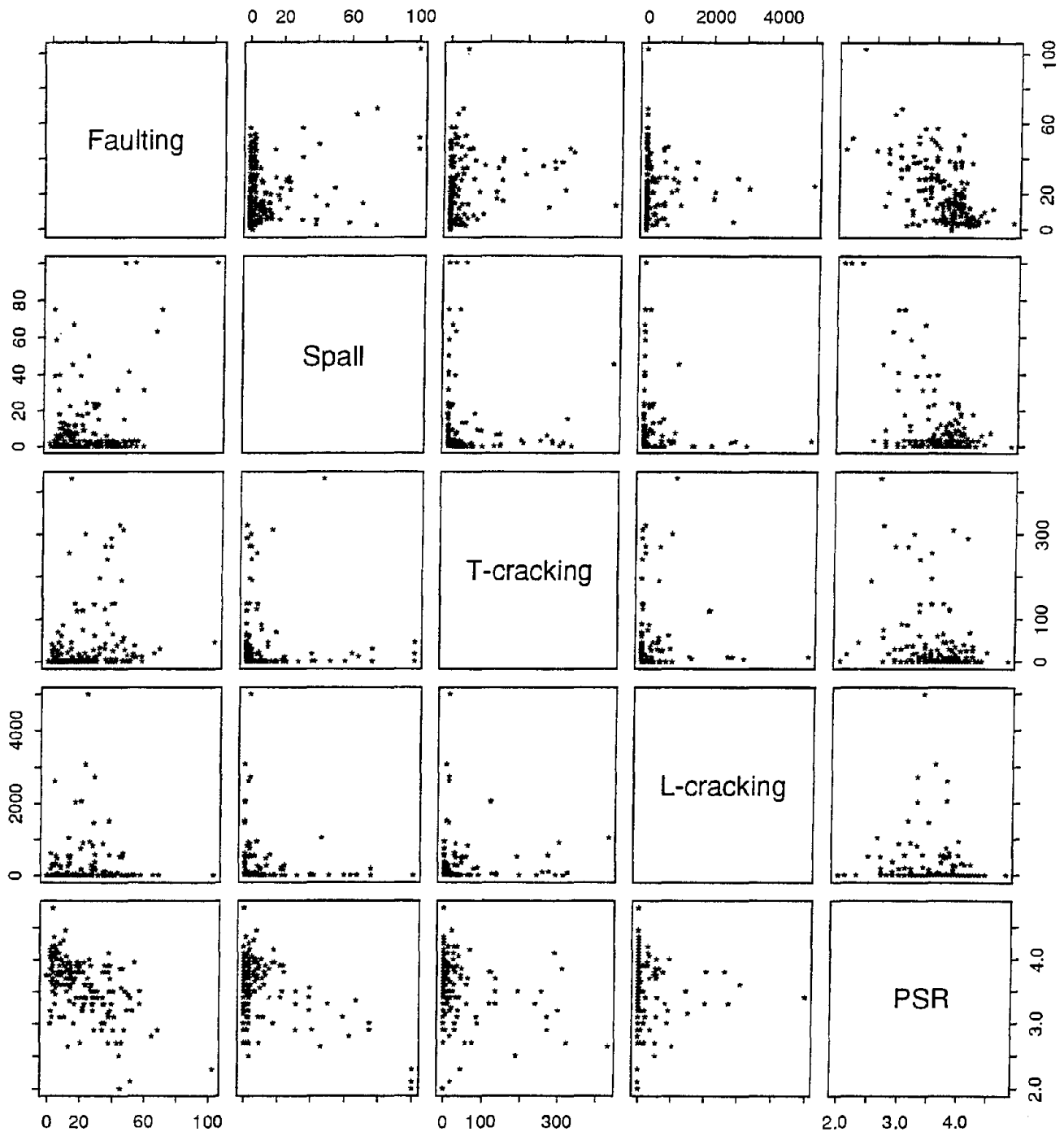


Figure 92. Two-dimensional scatter plot for JPCP PSR model.

The estimate of each coefficient in the equation, the associated standard error of estimate and p-value are provided in table 14. Again, all of the estimates of the coefficients are significant at  $\alpha = 0.10$  level, with a reasonably small Standard Error Estimates (SEE).

Table 14. Estimates of the coefficients and the associated SEE and P-values for JPCP PSR distress model.

Terms	Value	SEE	P-value (> t )
Intercept	3.95	0.0370	<0.0001
FaultTT	-0.010276	0.00145	<0.0001
T-crack	-0.001014	0.000336	<0.0001
L-crack <sup>0.5</sup>	-0.003911	0.001845	0.0319
Spall	-0.009421	0.00132	0.0024

The goodness-of-fit plots for the JPCP PSR model are provided in figures 93 and 94. Sensitivity analysis was conducted as shown in figures 95 through 98. Figure 96 shows that PSR decreases as the total joint faulting and total number of the transverse cracking increase while holding the percentage of the joints spalled and the longitudinal cracking measurements fixed at their mean values. Similar trends are shown in figures 96, 97 and 98, as the PSR decreases as any of the four distresses increases while holding the other measurements constant.

#### *Jointed Reinforced Concrete Pavements*

Figure 99 gives the two-dimensional plot between the variables and the final model selected is presented below. The estimates of the coefficients, the associated SEE, and P-values for JRCPSR model are given in table 15.

$$\text{PSR} = 4.165 - 0.06694 * \text{FaultTT}^{0.5} - 0.00003228 * \text{T-crack}^2 - 0.1447 * \text{Spall}^{0.25} \quad (48)$$

$$\begin{aligned} R^2 &= 0.66. \\ N &= 90. \\ \text{RSE} &= 0.28. \end{aligned}$$

where:

- FaultTT = Total joint faulting per mile, in/mi.
- T-crack = Amount of transverse cracking, number of cracks/mi.
- Spall = Percentage of the joints spalled, percent.



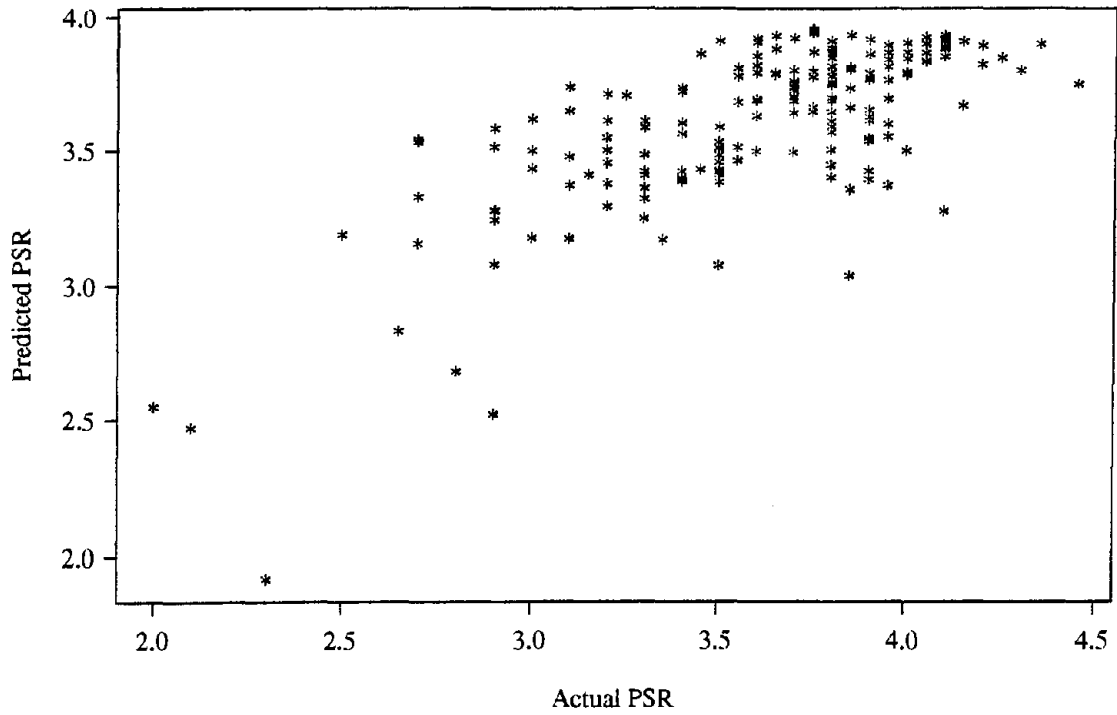


Figure 93. Actual versus predicted PSR for the JPCP PSR model.

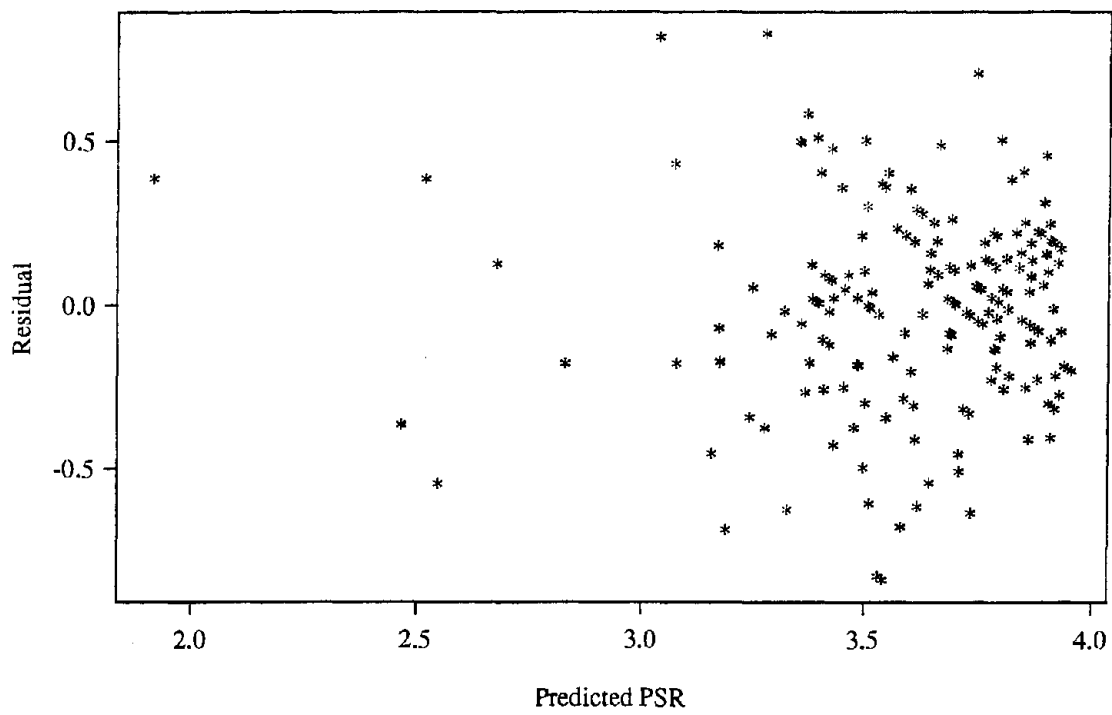
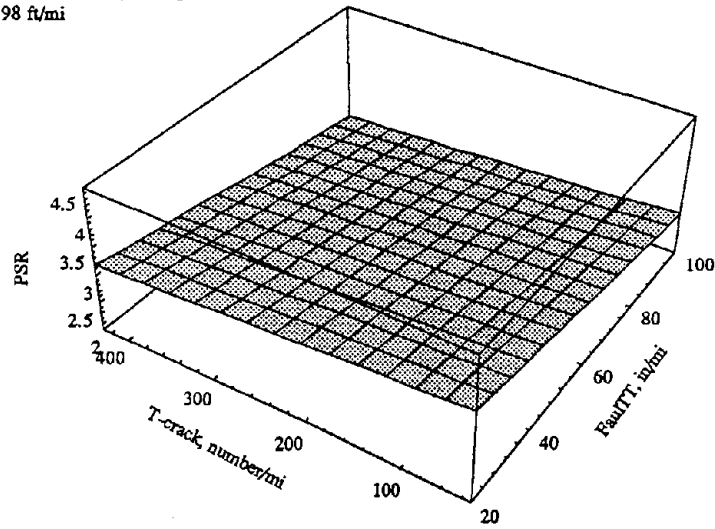


Figure 94. Predicted versus residuals for the JPCP PSR model.

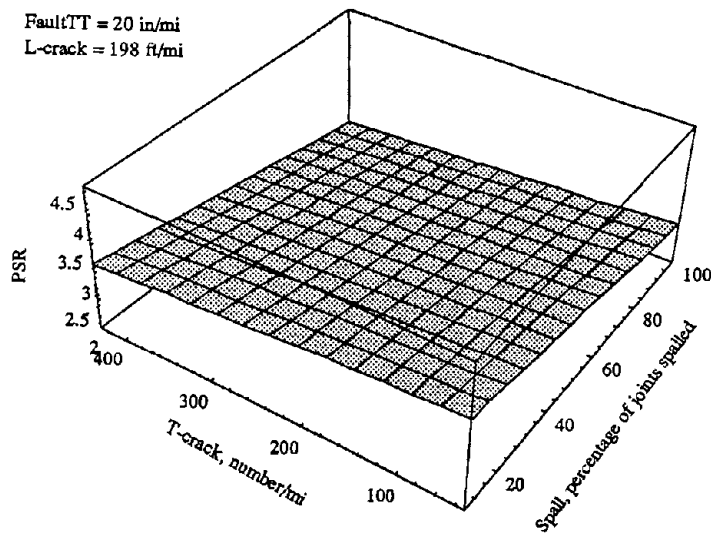
Spall = 9 percentage of joints spalled  
L-crack = 198 ft/mi



1 mi=1.6km; 1 in=25.4mm

Figure 95. Sensitivity plot of the JPCP PSR model with faulting and transverse cracking.

Fault/TT = 20 in/mi  
L-crack = 198 ft/mi



1 mi=1.6km; 1 in=25.4mm

Figure 96. Sensitivity plot of the JPCP PSR model with transverse cracking and spalling.

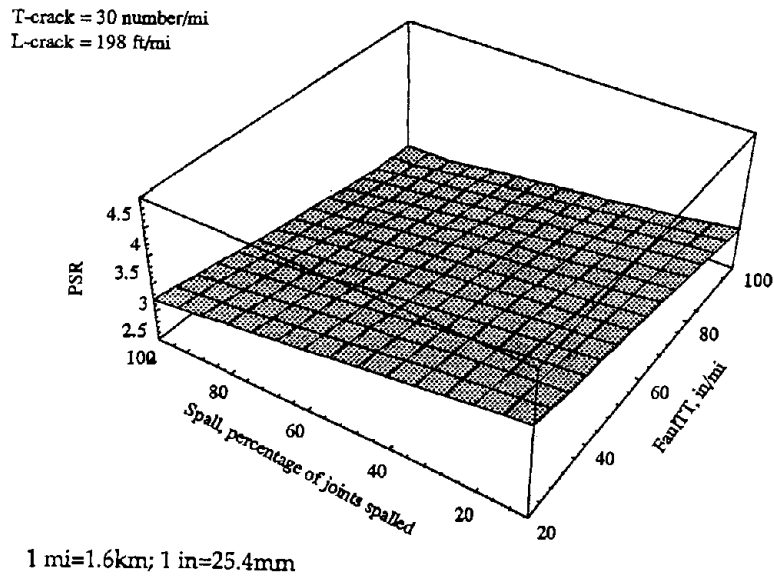


Figure 97. Sensitivity plot of the JPCP PSR model with faulting and spalling.

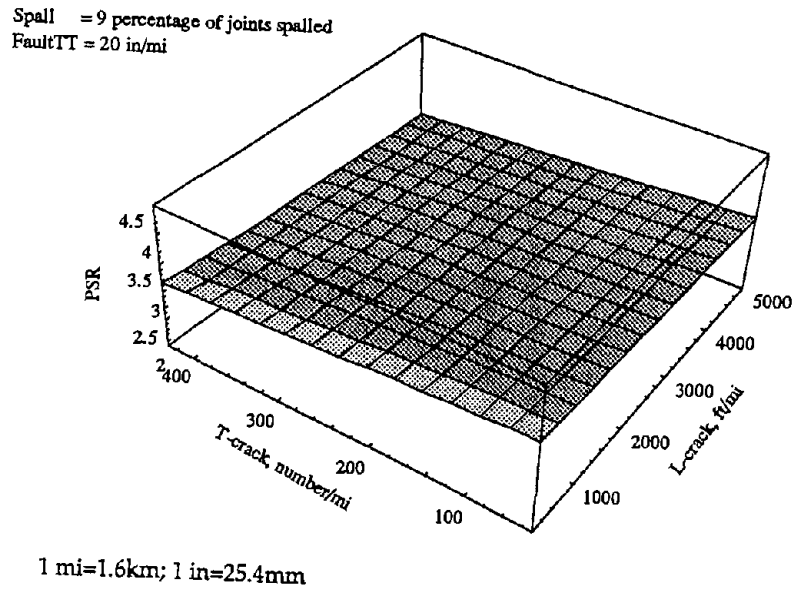


Figure 98. Sensitivity plot of the JPCP PSR model with transverse cracking and longitudinal cracking.

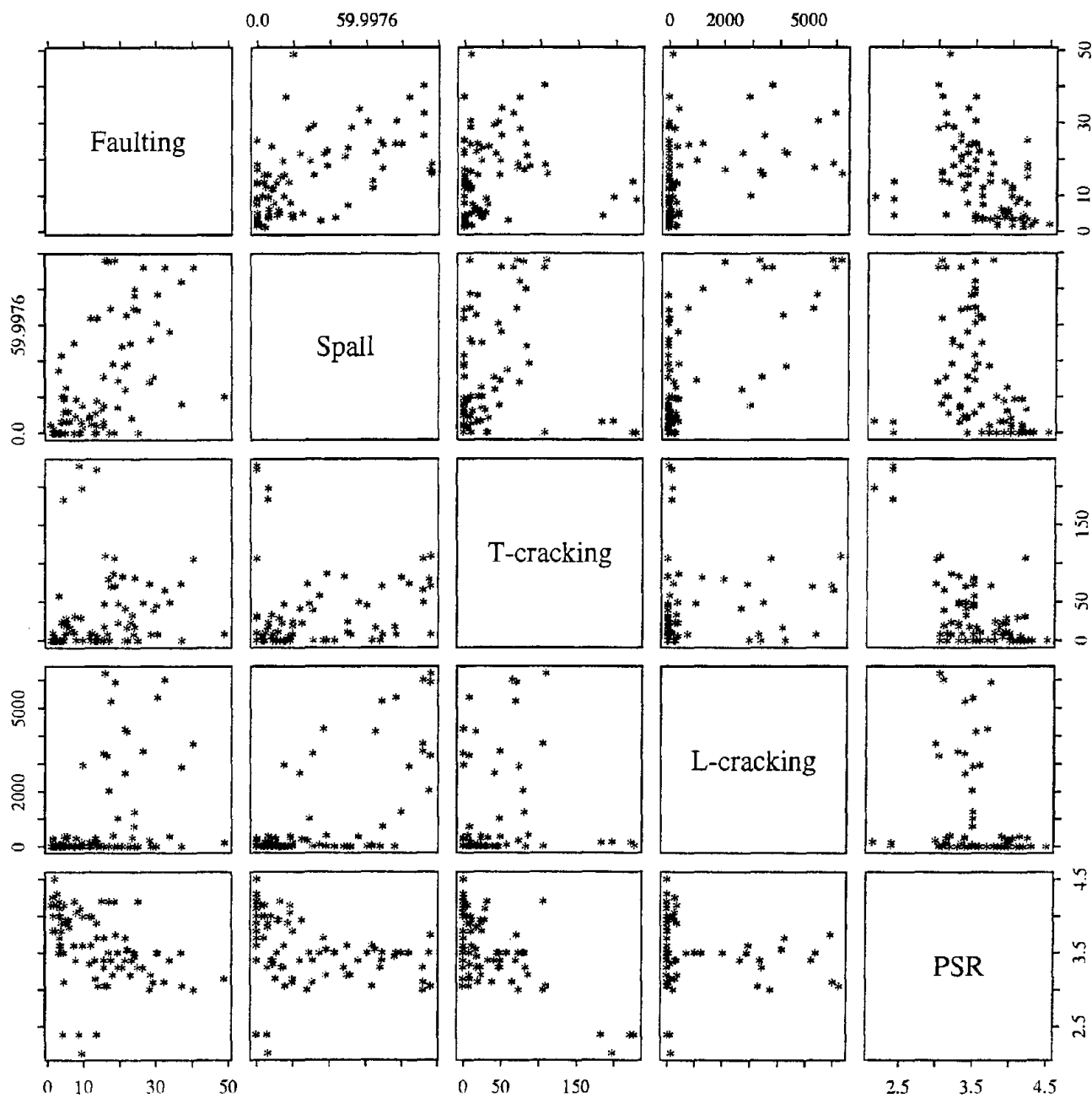


Figure 99. Two-dimensional scatter plot for JRCP PSR model.

Table 15. Estimates of the coefficients and the associated SEE and P-values for JRCP PSR model.

Terms	Value	SEE	P-value ( $> t $ )
Intercept	4.165	0.076	<0.001
FaultTT <sup>0.5</sup>	-0.06694	0.026	0.0120
T-crack <sup>2</sup>	-0.00003228	0.000	<0.001
Spall <sup>0.25</sup>	-0.1447	0.033	<0.001

Figures 100 and 101 provide the actual versus predicted PSR and the residual versus the predicted value plot, respectively. Figures 102 through 104 provide the sensitivity analysis plots for the JRCP PSR model. As shown in figure 102, PSR decreases as either the total joint faulting per mile or the total number of the transverse cracking per mile increases. Similarly, figure 103 indicates that PSR decreases with increasing spalling or transverse cracking. Finally, figure 104 shows that if faulting or spalling increases, faulting decreases.

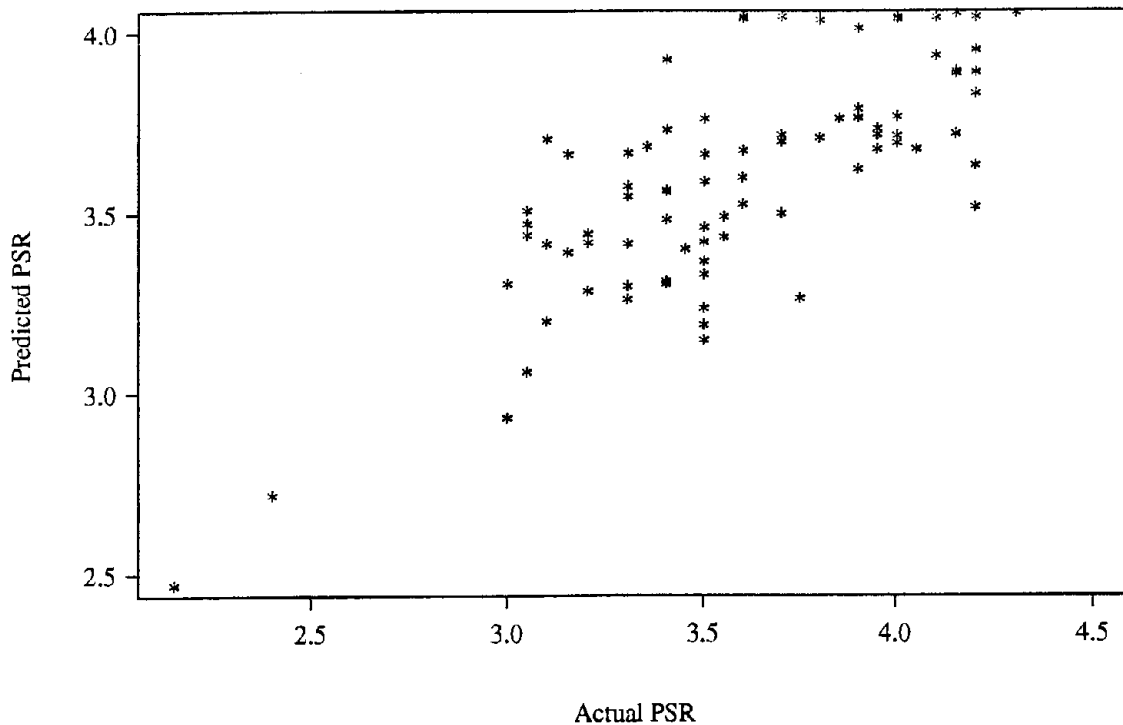


Figure 100. Actual versus predicted PSR of the JRCP PSR model.

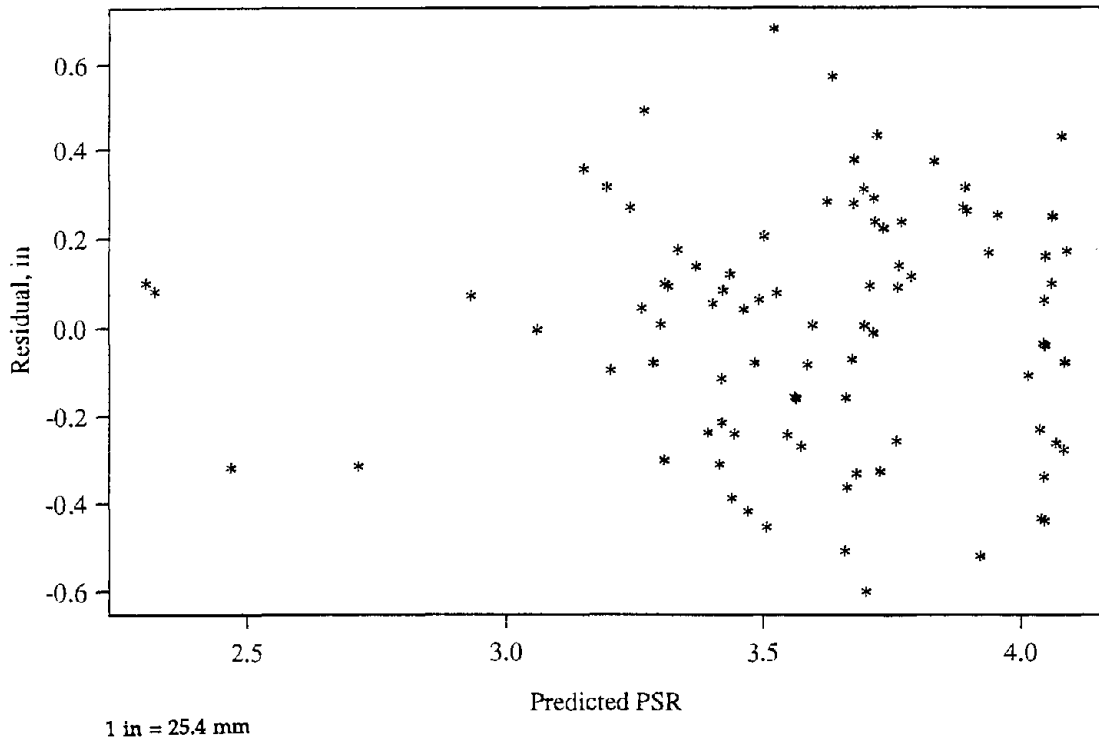


Figure 101. Predicted versus residual for the JRCP PSR model.

Spall = 26 percentage of joints spalled

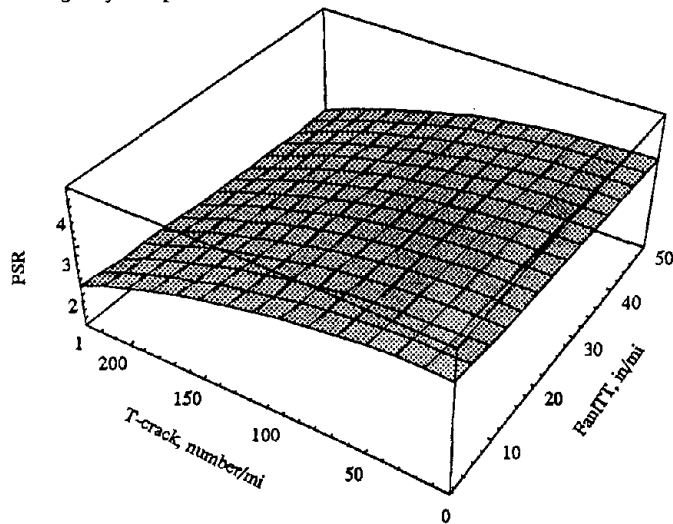


Figure 102. Sensitivity plot of the JRCP PSR model with faulting and transverse cracking.

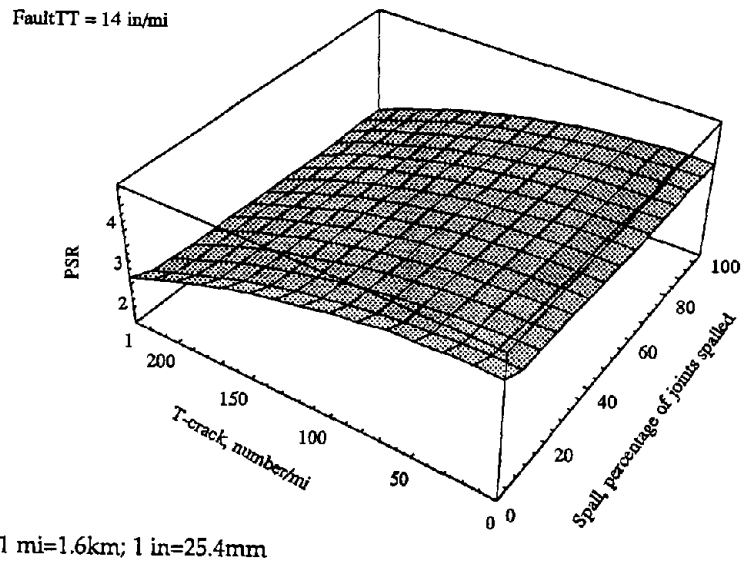


Figure 103. Sensitivity plot of the JRCP PSR model with transverse cracking and spalling.

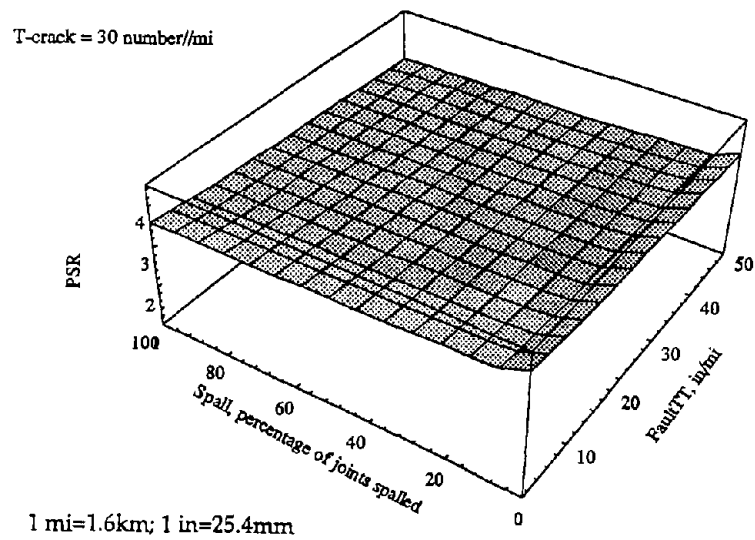


Figure 104. Sensitivity plot of the JRCP PSR model with faulting and spalling.

## International Roughness Index (IRI) Model for JPCP

The international roughness index (IRI) is a roughness indication calculated from the longitudinal profile and is reported in units of in/mi. IRI has been shown to correlate very well with the subjective rating of users (PSR) and is a function of the pavement distresses. In this section, the development of a distress model for IRI of the jointed plain concrete pavement as a function of the joint faulting, spalling and transverse cracking is described.

The explanatory variables initially considered are:

FaultTT: Total joint faulting per mile, in/mi.

T-crack: Amount of transverse cracking, number of cracks/mi.

Spall: Percentage of the joints spalled, percent.

L-crack: Amount of longitudinal cracking, ft/mi.

Figure 105 provides the two-dimensional scatter plot between the variables. The final model developed for JPCP is shown below:

$$IRI^2 = 99.59 + 2.6098 * \text{FaultTT} + 1.8407 * \text{Spall} + 2.2802 * 10^{-6} * \text{T-crack}^3 \quad (49)$$

$$R^2 = 0.61.$$

$$N = 144.$$

$$RSE = 64.11.$$

where:

FaultTT = Total joint faulting per mile, in/mi.

T-crack = Amount of transverse cracking, number of cracks/mi.

Spall = Percentage of the joints spalled.

One major problem encountered in the development of the IRI model is that the initial IRI value is not known. If this value were known, it would likely explain a significant amount of the variation.

The estimate of each coefficient in the equation, the associated standard error of estimate and p-value are provided in table 16. All of the estimates of the coefficients are significant at  $\alpha = 0.10$  level.

Figures 106 and 107 provide the goodness-of-fit plots for the JPCP IRI model, and sensitivity analysis plots are shown in figures 108 through 110. Figure 108 gives the sensitivity plot showing that IRI increases with increasing faulting or transverse cracking. Figure 109 indicates that IRI increases as either transverse cracking or spalling increase. Similarly, figure 110 shows that IRI increases as either faulting or spalling increases.



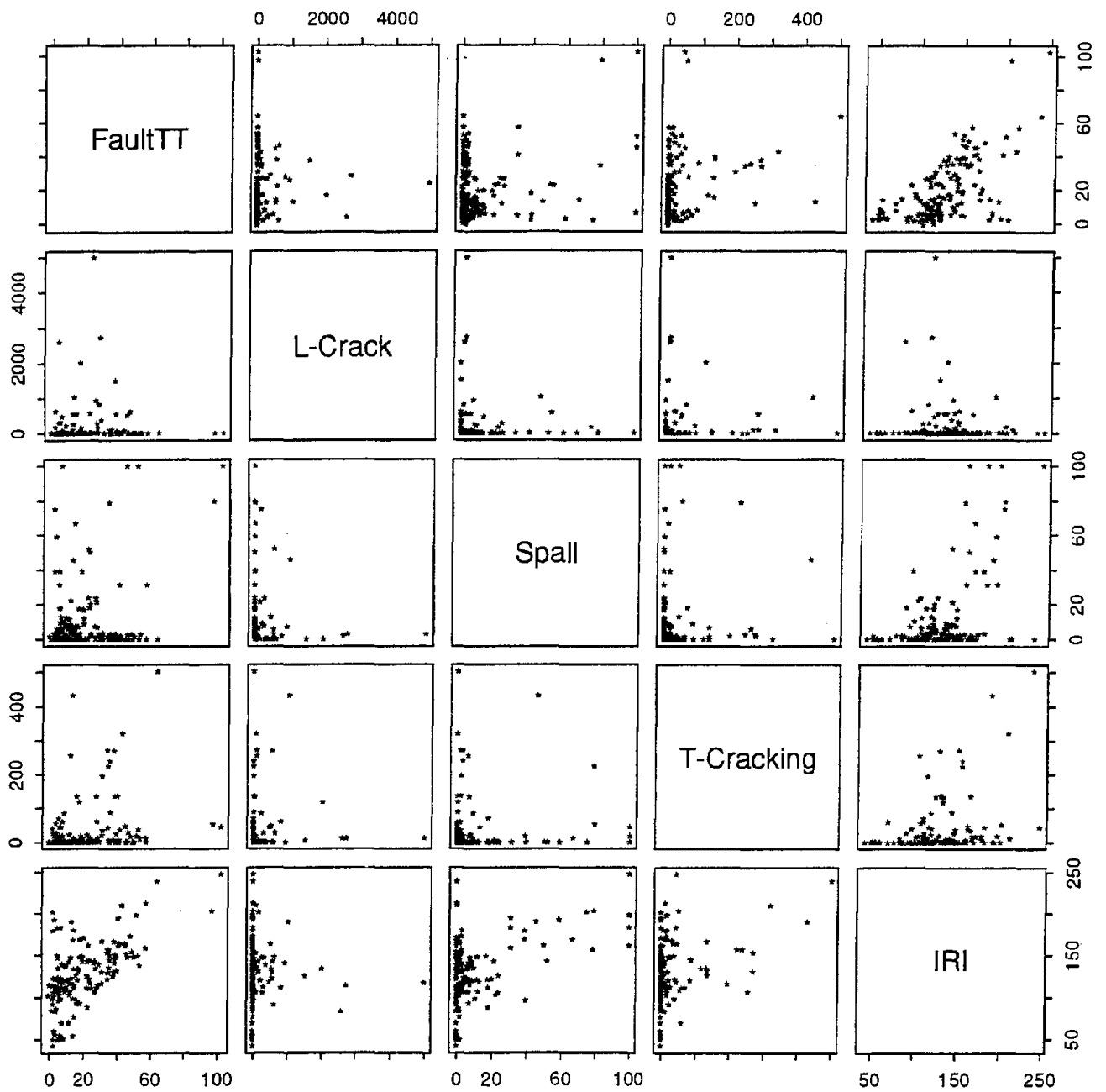


Figure 105. Two-dimensional scatter plot for JPCP IRI model.

Table 16. Estimates of the coefficients and the associated SEE and P-values for JPCP IRI model.

Terms	Value	SEE	P-value (>  t )
Intercept	99.59	8.17	<0.0001
FaultTT	2.6098	0.315	<0.0001
T-crack <sup>3</sup>	2.2808*10 <sup>-6</sup>	0.422*10 <sup>-6</sup>	<0.0001
Spall	1.8407	0.2527	<0.0001

The IRI measurements of jointed reinforced concrete pavement in the data base showed little dependence on the distress indicators. Therefore, no model was developed for IRI of JPCP in this study.

### Example Application of Performance Prediction Models

As described earlier, the performance prediction models developed under this study may be used for a variety of applications, including the evaluation of a pavement design obtained through a given pavement design procedure. The inputs used in the development of that original pavement design can be used in the performance prediction models to predict the pavement distress at the end of the

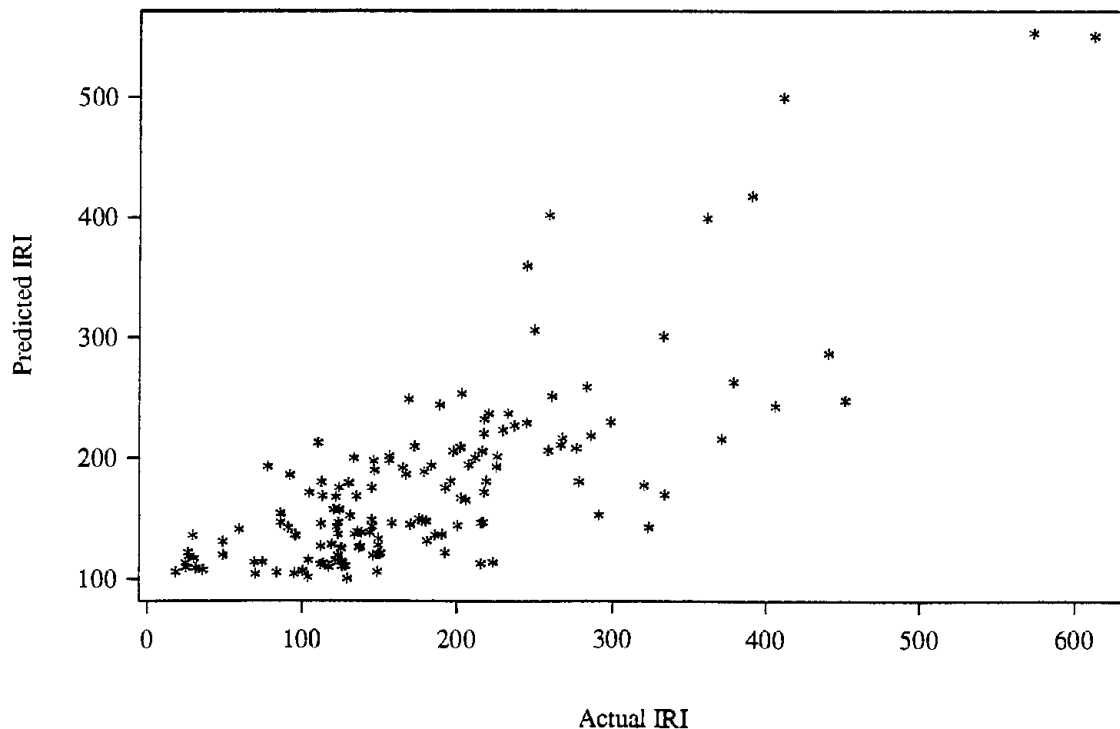


Figure 106. Actual versus predicted PSR for the JPCP IRI model.

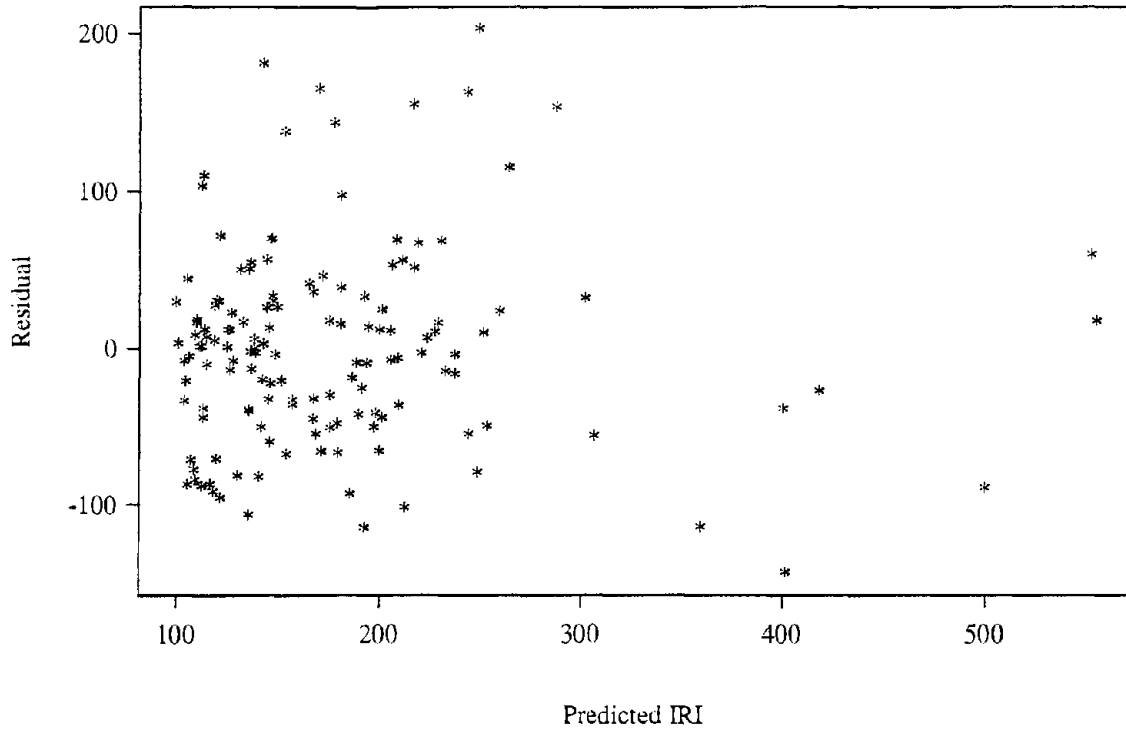


Figure 107. Predicted versus residuals for the JPCP IRI model.

Spall = 11 percentage of joints spalled

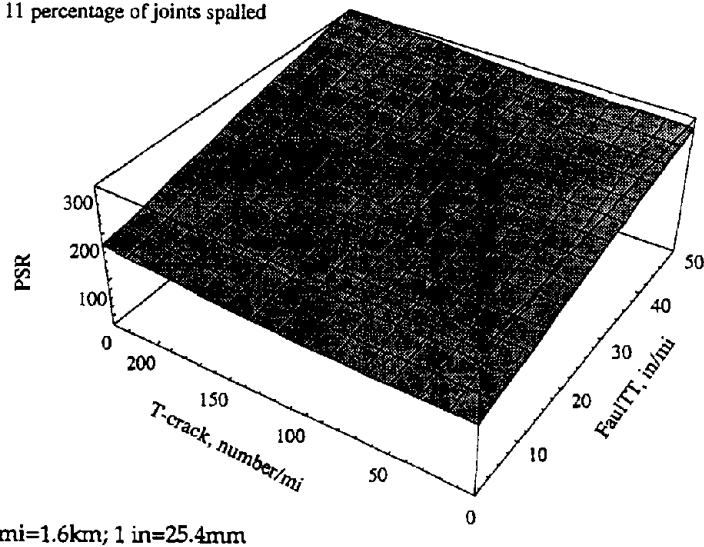
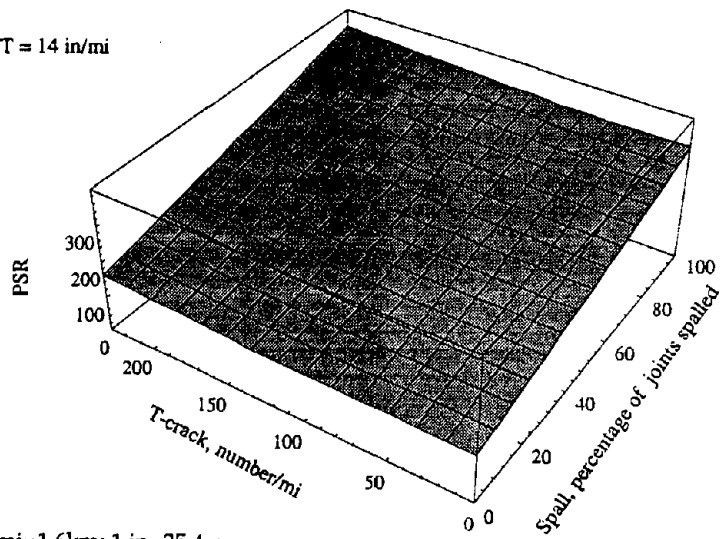


Figure 108. Sensitivity plot of the JPCP IRI model with faulting and transverse cracking.

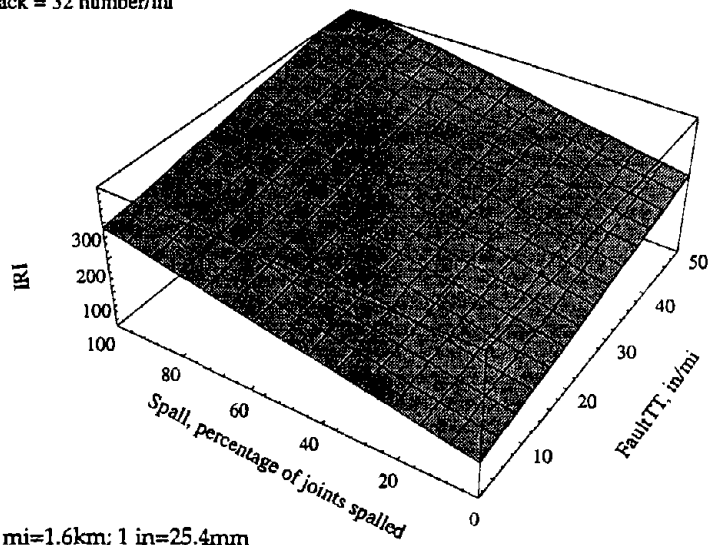
Fault/TT = 14 in/mi



1 mi=1.6km; 1 in=25.4mm

Figure 109. Sensitivity plot of the JPCP IRI model with transverse cracking and spalling.

T-crack = 32 number/mi



1 mi=1.6km; 1 in=25.4mm

Figure 110. Sensitivity plot of the JPCP IRI model with faulting and spalling.

initial performance period. If the predicted distress at the end of the initial performance period exceeds some defined critical level, then that pavement design may be considered inadequate and modifications to certain design inputs may be appropriate.

However, the inputs to be adjusted in making modifications to a pavement design must be carefully selected. For example, if a nondoweled pavement with an aggregate base is being considered, one means of reducing the faulting on the pavement is to use a stabilized base course. However, depending upon the joint spacing and the climatic conditions, this could significantly increase the amount of transverse cracking that could occur in the pavement. Therefore, the design engineer must be cognizant of these type of tradeoffs when modifications to the pavement design are considered.

Table 17 illustrates applicability of the models for concrete pavement design check. It is assumed that the thickness of the slab has been determined using an agency-approved method and that the various design features (load transfer, base type, AC shoulder, etc.) have been selected in accordance with agency policy or procedures. The various pavement design variables, climatic variables, and pavement performance variables are listed at the top of table 17.

The initial pavement design was tested using the models. In the first iteration, the level of faulting (0.13 in [3.3 mm]) and the amount of transverse slab cracking (67 percent of the slabs) are both considered unacceptable. However, the amount of transverse joint spalling (5 percent of the joints) and the estimate of the overall serviceability level (3.3) is acceptable for this pavement type and traffic loading. The acceptability of the distress levels is based on table 18, which presents recommendations for critical levels of pavement distress at which some form of rehabilitation is appropriate.

In order to reduce the levels of faulting and cracking to acceptable levels, the joint spacing of the pavement is reduced from 20 ft (6.1 m) to 15 ft (4.6 m). This revised design was again tested using the models in the second iteration. The result of this change is that joint faulting is marginally acceptable and transverse slab cracking is marginally unacceptable. Joint spalling is still acceptable and the PSR is quite adequate.

However, to ensure the integrity of the design, one more iteration is warranted to control the development of the joint faulting and the transverse slab cracking. In the third iteration, a tied PCC shoulder is added, the base is changed to a permeable gradation, and the dowel diameter is increased to 1.25 in (32 mm). The evaluation of this design indicates that the design is quite adequate.

Table 17. Example application of prediction models to check adequacy of concrete pavement design.

---

**Initial Pavement Design Variables**

Evaluate the adequacy of the following pavement design using the performance prediction models.

<u>Pavement Design</u>	<u>Climatic Variables</u>	<u>Performance Variables</u>
10 in JPCP	Wet Climate (30 in/yr)	Performance Period = 20 years
Asphalt-treated base (k = 250)	Cold Climate (FI = 400)	ESAL applications = 20 million
20-ft joint spacing	Days > 90 °F = 10	
1 in epoxy-coated dowels	Temperature Range = 70 °F	
Hot-poured joint sealant		
Elastic modulus = 4,000,000 lbf/in <sup>2</sup>		
Modulus of rupture = 700 lb/in <sup>2</sup>		
Standard lane width (12 ft)		
AC shoulders		
No Drainage (C <sub>d</sub> = 0.80)		
Fine-grained subgrade		

**Evaluation of Design**

**Iteration No. 1—Initial Pavement Design.**

Predicted Faulting	= 0.13 in (34.45 in/mi)	(from Eq. 4)
Predicted Cracking	= 67 percent of the slabs (176.9 crack/mi)	(from Eq. 36)
Predicted Spalling	= 5 percent of the joints	(from Eq. 43)
Predicted PSR	= 3.4	(from Eq. 47)

Design not adequate; slab cracking and faulting unacceptable.

**Iteration No. 2—Keeping all other design variables the same, reduce joint spacing to 15 ft.**

Predicted Faulting	= 0.12 in (42.36 in/mi)
Predicted Cracking	= 11 percent of the slabs (38.7 cracks/mi)
Predicted Spalling	= 2 percent of the joints
Predicted PSR	= 3.5

Design marginally adequate for faulting and slab cracking.

**Iteration No. 3—Keeping the design from iteration 2, specify a PCC shoulder; add a permeable base (C<sub>d</sub> = 1.05); increase dowel diameter to 1.25 in.**

Predicted Faulting	= 0.05 in (17.65 in/mi)
Predicted Cracking	= 1.0 percent of the slabs (assuming 25 percent stress load transfer across the shoulder) (3.5 cracks/mi)
Predicted Spalling	= 2 percent of the joints
Predicted PSR	= 3.7

Based upon the results of this iteration, the design, as revised, is acceptable.

---


$$1 \text{ in} = 25.4 \text{ mm}; 1 \text{ ft} = 0.305 \text{ m}; 1 \text{ lbf/in}^2 = 6.9 \text{ kPa}; \text{ } ^\circ\text{C} = (\text{ } ^\circ\text{F} - 32) * (5/9)$$

Table 18. Critical values for key performance indicators.

Performance Indicator	JPCP	JRCP
Joint Faulting	0.13 in	0.26 in
Transverse Cracking	10% slabs cracked, or 70 cracks/mi	70 deteriorated (medium- and high-severity) cracks/mi
Longitudinal Cracking	500 ft/mi (all levels)	500 ft/mi (all levels)
Joint Spalling	15-20% joints spalled, or 50 spalls/mi	20-30% joints spalled, or 25 spalls/mi
PSR	3.0-3.5	3.0-3.5
IRI	125-175 in/mi	125-175 in/mi

1 in = 25.4 mm; 1 ft = 0.305 m; 1 mi = 1.61 km

### Summary

This chapter has presented several performance prediction models for concrete pavements. Models are presented for doweled transverse faulting, nondoweled transverse faulting, JPCP transverse cracking, JRCP transverse cracking, JPCP transverse joint spalling, JRCP transverse joint spalling, and for JPCP and JRCP serviceability. A combination of theory, mechanistic variables, and field performance data was utilized in the development of the models.

The models have a variety of application within the pavement field. For example, the models can be used to assess the suitability of a given pavement design, to evaluate the effect of key design features (e.g., dowel bars) on pavement performance, and to estimate pavement deterioration to assist in programming rehabilitation and maintenance activities. However, the models must be used with care and not be extended beyond the conditions from which they were developed.





### 3. CONCRETE PAVEMENT DESIGN RECOMMENDATIONS

#### Introduction

This study has produced many interesting and significant findings concerning the performance of concrete pavements. In an effort to harness that information in a more useful form, guidelines and recommendations for the design and construction of concrete pavements have been developed. These guidelines are based primarily on the results of this study, but applicable information from other studies are cited where appropriate.

In considering these recommendations, it must be realized that a pavement structure is a complex system with many interacting components. Because of this, the consideration of one design feature by itself may lead to significant problems in other elements of design. Therefore, any recommended change in a design feature must fully consider the impacts on other design features for a range of site conditions. In other words, the total pavement system (i.e., support, drainage, thickness, jointing, materials, reinforcement, and so on) must be considered together in developing a reliable concrete pavement design. In addition, site conditions (traffic, subgrade, climate) must be fully considered as some design recommendations may be more applicable to some site conditions than others.

In this chapter, the importance of specific site conditions on concrete pavement performance is first described, followed by recommendations on the design and use of various concrete pavement design features. Major site conditions covered include climate, subgrade, and traffic. Key design considerations are provided for subgrade preparation, subsurface drainage, base type, shoulder type, widened PCC slabs, transverse joint design (including joint spacing, joint orientation, joint load transfer, and joint sealant), longitudinal joint design, JRCP steel reinforcement, CRCP steel reinforcement, and slab thickness. Also included in this chapter are guidelines on the selection of concrete pavement type.

#### Effect of Site Conditions on Concrete Pavement Performance

Site conditions are those factors—each unique to a particular paving project—that have a large effect on the design requirements of a pavement. Three site conditions (traffic, climate, and subgrade) are identified and their effect on concrete pavement performance is described below.

#### Traffic

Repeated traffic loads cause tensile stresses (in combination with thermal and moisture induced stresses) at the top and bottom of concrete slabs that eventually lead to crack initiation and propagation throughout the slab. These cracks eventually break down and deteriorate, resulting in crack faulting, crack spalling, and increased

roughness. Repeated traffic loads also cause large deflections at joints and at unsupported slab edges and corners that can lead to pumping and erosion beneath the slab, factors that strongly contribute to joint faulting and corner breaks.

In this study, traffic loading was expressed in terms of the number of 18-kip (80-kN) ESAL applications. The range of ESAL applications for this study was from just less than 1 million to greater than 56 million, with a mean of just over 7 million. Of course, the accumulated traffic loadings are confounded with age; since the mean age of these sections at the time of evaluation is 16 years, the mean number of ESAL applications per year is 0.44 million.

It should be noted that, even though the majority of the North American sections are greater than 15 years old, only 4 of the 303 sections (1 percent) had sustained over 20 million ESAL applications. This is one reason data from several European countries were included, where 45 of 96 sections (47 percent) had sustained over 20 million ESAL applications.

Traffic loadings, as expressed in ESAL applications, were found to be the significant driving variable for in the development of the following distresses: faulting of doweled and of nondoweled joints, transverse cracking of JPCP, transverse crack deterioration of JRCP, and increased roughness (through joint faulting and slab cracking). The only distress that traffic did not appear to have a significant effect was joint spalling (in which case pavement age was found to be more significant).

### Climate

Climatic site conditions include moisture and temperature variables that cause significant stresses, deflections, or deformations in a pavement structure. For example, temperature and moisture gradients cause significant curling and warping stresses in slabs that, by themselves or in conjunction with load stresses, can lead to significant amounts of slab cracking. Freeze-thaw cycles can lead to loss of strength of concrete and spalling if an inadequate air void system exists. Deicing salts used to reduce pavement icing can lead to corrosion of dowels, reinforcement, and tie bars. Deep frost penetration into frost susceptible soils can lead to differential frost heaving. Excess moisture beneath slabs and bases can lead to pumping and erosion that causes faulting and increased stresses.

Climate was considered in this study through the following variables: thermal gradient through the slab, mean annual temperature, number of annual freeze-thaw air temperature cycles, frost depth (freezing index), number of days above 90 °F (32 °C), number of days below 32 °F (0 °C), mean annual precipitation, and the Thornthwaite Moisture Index. All four major climatic zones (wet-freeze, wet-nonfreeze, dry-freeze, and dry-nonfreeze) were represented in the data, although not all climates and geographical areas were well represented by the data.

Climatic effects were found to be significant in the following distresses: faulting of doweled joints (annual precipitation, freezing-index), faulting of nondoweled joints

(annual precipitation, freezing-index, number of days with maximum temperature above 90 °F (32 °C), transverse cracking (thermal gradient through slab which is related to geographic area of the US and various climatic variables such as annual temperature and precipitation, wind speed), crack deterioration for JRCP (age which represents numbers of climatic cycles such as freeze-thaw, freezing-index which is an indication of use of deicing salts and low temperatures, Thornthwaite moisture index), joint spalling (age, freezing-index, number of days having a maximum temperature greater than 90 °F [32 °C], age), PSR (through faulting, cracking, and spalling), and IRI (through faulting, cracking, and spalling).

### Subgrade

The degree of subgrade support affects the magnitude of slab stresses that are caused by both traffic loading and environmental forces. It has been shown that as subgrade support increases, load stresses decrease but thermal curling and moisture warping stresses increase. In addition, as the subgrade support increases, curling stresses increase at a faster rate than the corresponding rate of decrease in the load stresses (this is true except for very soft subgrades where the static  $k$  is less than 100 lb/in<sup>2</sup>/in [27 kPa/mm]). For very stiff subgrades, there is a point where the curling stresses level off with increasing values of  $k$ . However, the subgrade stiffness under typical design conditions is usually much lower than that at which the curling stresses reach a maximum value. Therefore, a stiff subgrade is not desirable for JPCP, but may be desirable for JRCP and continuously reinforced concrete pavements (CRCP) because of the beneficial effects of a stiff subgrade in reducing deflections at transverse cracks in these designs.

The degree of subgrade support was expressed in terms of a  $k$ -value backcalculated from FWD data. This backcalculated  $k$ -value represents the dynamic support of the embankment or subgrade and not that of the base course.<sup>(34)</sup> A static  $k$ -value may be determined by dividing the dynamic  $k$ -value by a factor of 2. If deflection data were unavailable, subgrade support was indicated indirectly through the subgrade soil classification (fine- or coarse-grained). For the pavements evaluated in this study, the backcalculated static  $k$ -values ranged from 18 to 649 lbf/in<sup>2</sup>/in (4.9 to 175 kPa/mm), and averaged 121 lbf/in<sup>2</sup>/in (32.7 kPa/mm).

The type of subgrade is also an important factor in design. Coarse-grained subgrades tend to allow more bottom drainage of a pavement structure than fine-grained materials, and are also less sensitive to moisture and thermal effects. A related subgrade effect is whether a pavement section is in an area of cut or fill; a cut area may not have as good drainage as a fill area, yet may provide better support.

Subgrade support effects were found to be significant in the development of the following distresses: faulting of doweled joints (fine/coarse grained soil,  $k$ -value), faulting of nondoweled joints (fine/coarse grained soil), JPCP transverse cracking ( $k$ -value), PSR (via faulting and cracking), and IRI (via faulting and cracking). The base course also had a significant effect on these distresses and that is discussed later.

## Design Recommendations for Concrete Pavements

This section presents general design and construction recommendations for concrete pavements. Information is presented on various key components of concrete pavement design, and this is based both on the results of this study and on other current research work on these topics.

### Subgrade Preparation

Preparation of the subgrade prior to the placement of the overlying paving layers is important to the performance of the pavement. A stable and uniformly compacted subgrade is desirable for pavement construction, and often the native or imported embankment is unable to provide those qualities. In such cases, the unsuitable material may be removed and replaced with select granular material, or some kind of treatment of the subgrade may be required.

Even if an existing subgrade material is determined suitable, subcutting, mixing, and recompacting of the material is often desirable to improve the uniformity of support and to reduce the potential for significant volumetric changes of the material. This is perhaps most critical in transition areas between cut and fill.

In general, granular or more coarse-grained subgrades are more desirable for a pavement than fine-grained materials, but fine-grained soils are far more prevalent throughout the country. Coarse-grained materials generally provide a stronger, more stable working platform than fine-grained materials, and generally have some degree of permeability that can contribute to the overall drainability of the pavement system.

In order to ensure a suitable subgrade for a concrete pavement, some agencies specify a minimum level of subgrade support. For example, one agency requires a minimum California Bearing Ratio (CBR) of 6, below which subgrade stabilization is required.<sup>(38)</sup> Furthermore, several European countries also require a minimum level of subgrade support to ensure stability and a strong working platform. For instance, Spain requires a minimum CBR of 10, below which the subgrade must be removed; if the CBR is between 10 and 20, a granular subbase layer is required.<sup>(39)</sup> Similarly, Germany specifies a minimum subgrade bearing value of 6525 lb/in<sup>2</sup> (45 MPa), determined using a modified plate load test.<sup>(40)</sup> Austria also specified a minimum bearing value for its subgrades (5075 lb/in<sup>2</sup> [35 MPa]), below which soil replacement or stabilization is required.<sup>(39)</sup>

Based on the above information, it is recommended that subgrades for PCC pavement construction have a minimum CBR of 6 in the top 12 in (305 mm) in order to provide stability and uniformity for paving operations. As previously indicated, this can be achieved through either replacement or stabilization of the existing subgrade material. The preferred method will depend on the specific conditions of each individual project (length, depth of unsuitable material, type of subgrade, availability of alternate materials, paving requirements, and so on). A dynamic cone

penetrometer (DCP), a long, narrow device that can be driven into the subgrade to estimate the in-place CBR of the soil, can be used for construction control.

Stabilization of the existing subgrade is one method of addressing problem soils. The type of stabilizing agent to be used is strongly dependent on the type of subgrade. Figure 111 provides recommendations for determining suitable stabilizing agents based on subgrade soil properties.<sup>(41)</sup> The following types of stabilizers are commonly used:<sup>(41)</sup>

- Lime
  - a. Appropriate for medium-, moderately fine-, and fine-grained soils with moderate to high plasticity.
  - b. Most suited to soils with plasticity index (PI) greater than 10 and more than 25 percent passing No. 200 sieve.
  - c. Suitable soils: AASHTO classification A-4, A-5, A-6, A-7, and some A-2-6 and A-2-7 materials.

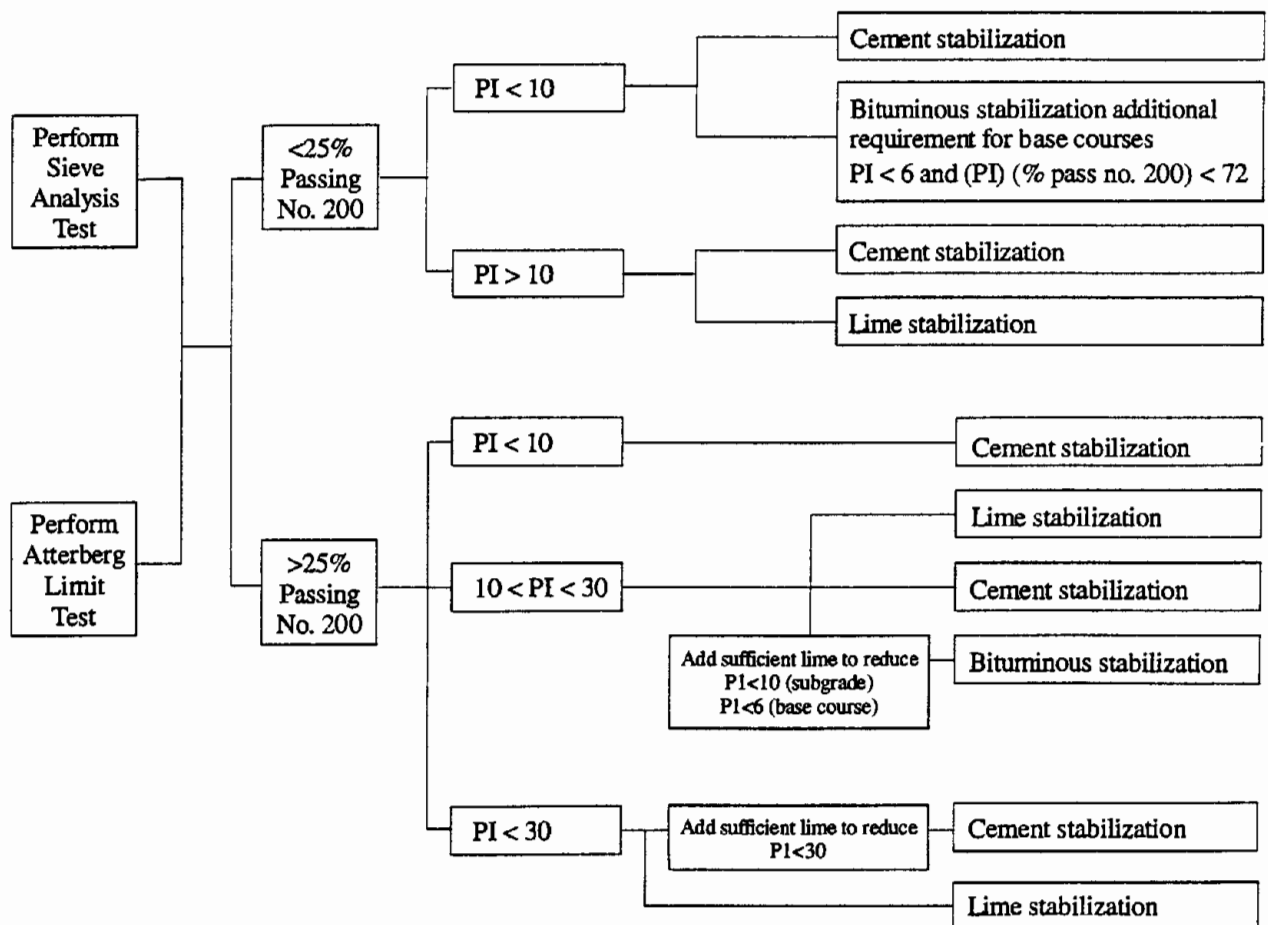


Figure 111. Soil stabilization selection guidelines.<sup>(42)</sup>

- Cement
  - a. Generally appropriate for coarse-, medium-, and fine-grained soils having low to moderately high plasticity.
  - b. Most suited to
    - sandy soils with  $PI < 30$ .
    - fine-grained soils with  $PI < 20$  and  $LL < 40$
    - coarse-grained soils with  $PI > (20 + [50 - \text{fines content}])$
  - c. Suitable soils: AASHTO classification A-1, A-2-4, A-2-5, A-3, A-4 and A-5 materials.
- Asphalt
  - a. Generally suited to medium- and coarse-grained soils with low plasticity.
  - b. Most suited to:
    - sands with less than 25 percent passing the number 200 sieve and  $PI < 6$ .
    - coarse grained material with less than 15 percent passing the number 200 sieve and  $PI < 6$ .
  - c. Suitable soils: AASHTO classification A-2-4, A-2-6, A-3, A-4 and low plasticity A-6 soils.

Additional information on the selection and mix design of stabilizing agents are found in references 42 through 46.

Another critical consideration in the preparation of the subgrade is the potential for frost heave. Frost heave is the upward expansion that occurs when certain frost susceptible soils freeze; this upward expansion is caused not so much by the freezing of water, but rather by the additional water that moves upward toward the freezing front, resulting in the formation and continuing expansion of ice lenses.<sup>(47)</sup> The upward expansion causes cracking and distorted roadway surfaces, resulting in increased roughness. In addition, weakened support and instability can result during the spring thawing as moisture from the thawing upper layers is trapped between the surface and the still-frozen soil below.<sup>(47)</sup> Three factors are necessary for frost heave to occur:<sup>(47)</sup>

1. Extended period of time with below freezing temperatures.
2. Availability of sufficient water to support the growth of ice lenses.
3. Presence of a frost susceptible soil. A soil (or base or subbase course) is considered frost susceptible if it contains more than 3 percent by weight of particles smaller than 0.020 mm.<sup>(47)</sup>

Where frost heave is a problem, susceptible soils should be replaced with a nonfrost-susceptible material. Alternatively, the addition of a select nonfrost-susceptible material over the problem soil may be effective, with the result of raising the gradeline above natural ground.<sup>(47)</sup> Many European countries place thick granular layers (8 to 20 in [203 to 508 mm]) between the subgrade and the base course to help control frost heave.<sup>(39)</sup> The layer thickness required for frost protection is generally taken as one-half to three-fourths of the depth of the local frost penetration. Finally, subcutting, remixing, and recompacting suitable quality soils will increase the level of support and decrease problems due to nonuniformity of the in-place material.

In addition to frost heave, swelling (or expansive) soils represent another potential subgrade problem. These soils exhibit significant volume changes in reaction to changing moisture contents. Possible solutions for these types of soils include removal, placement of a more suitable material, compaction at water contents 1 to 2 percent above optimum, compaction to 102 percent of optimum using ASTM T-99, and lime or cement stabilization. More exotic treatments (such as membrane encapsulation) may be required for severe swelling soils.

In characterizing the subgrade support for concrete pavement design, the modulus of subgrade reaction (or k-value) is used. Previously, the k-value for use in design was taken to be the "top of the base" k-value, that is, the level of support provided to the slab by the base/subbase/subgrade system. As previously noted, recent research indicates that the most appropriate k-value for design is actually the elastic k-value of the subgrade.<sup>(34)</sup>

### Subsurface Drainage

The importance of subsurface drainage to pavement performance has long been recognized, but it has only been in the last few decades that it has received more emphasis in design. An effective subsurface drainage system removes excess water from the pavement structure, thereby preventing or reducing the development of key moisture-related distresses, such as faulting, pumping, and loss of support. However, in order for a subsurface drainage system to be cost effective, it must increase pavement life in proportion to its additional cost of installation. According to a recent survey, the average increase in construction costs for replacing a conventional dense-graded aggregate base with a permeable base drainage system (including longitudinal pipe edge drains) ranged from 14 percent for a permeable aggregate base to 23 and 24 percent for asphalt-stabilized and cement-stabilized permeable bases, respectively.<sup>(48)</sup> Thus, roughly speaking, a concomitant increase in life of 14 to 24 percent is needed in order to offset these additional construction costs.

### *Identifying the Need for Drainage*

The need for drainage depends on both the natural drainage characteristics of the subgrade soil and the amount of precipitation. For example, the need for drainage is not as critical in dry regions with coarse-grained subgrades as in wet regions with fine-grained subgrades. The anticipated traffic levels are also important in determining the need for drainage, as the need for drainage on medium and high-trafficked highways is far greater than on lower volume roadways. A drainage analysis should be conducted as a part of normal pavement design practices to determine the need for drainage.

The most comprehensive guidelines for determining the need for drainage are given in reference 49. This report defines a moisture-accelerated distress (MAD) index that considers both internal (drainage capacity) and external (exposure) factors and their interactions to provide guidelines on the susceptibility of a pavement structure to moisture-related damage. The MAD index was developed for evaluating

the potential for MAD in existing pavements, but it is also useful for determining the need for subsurface drainage in new pavements.

The MAD index is determined considering the following factors:

- Climatic region — three regions are defined based on moisture.
- Seasonal moisture concentration.
- Temperature — high temperature, freeze-thaw activity, and frost areas.
- Drainage quality of base material.
- Natural drainage characteristic of subgrade soil.

Each of these factors affects the numerical value of the MAD index. For example, an initial MAD index is assigned to each of the three climatic regions.<sup>(50)</sup>

- Climatic region I—moderate potential for MAD, numerical value = 47.
- Climatic region II—normal potential for MAD, numerical value = 67.
- Climatic region III—low potential for MAD, numerical value = 85.

The resultant index value is then either increased, decreased, or unchanged depending on the other factors. For example, the value is unchanged if the moisture condition is fairly constant throughout the year; 7 points are deducted for moderate seasonal concentration of moisture; and 14 points are deducted for a large seasonal concentration of moisture. Similarly, 14 points are deducted for frost areas, 7 points are deducted for freeze-thaw areas, and the numerical value is left unchanged for high temperature areas. If the base material is of acceptable quality, 7 points are added; 7 points are deducted for unacceptable base. The potential for moisture-accelerated distress indicated by the MAD index is given in table 19.

A simple procedure for characterizing the drainage condition of pavement structures that also takes into consideration the external and internal factors affecting drainage was developed under the current study for use in the development of the performance models. This approach employs a simple matrix for selecting the overall drainage coefficient,  $C_d$ . This factor, which is based on the AASHTO drainage coefficient (see reference 50), indicates the pavement's ability to drain excess water from within the structure as well as the exposure condition, similar to the MAD index. As shown in table 20,  $C_d$  depends on the base type, the presence of edge drains, and moisture exposure condition. Table 21 provides guidelines for interpreting the meaning of  $C_d$ .

Combined, tables 20 and 21 provide a simple procedure for determining the need for drainage. In general, pavements should be designed to minimize the potential for moisture-related damage in order to obtain good long-term performance. If a high potential for moisture damage exists (as indicated by a low  $C_d$ ), the use of a permeable base and associated edge drain should be considered. A flow chart of drainage design recommendations based on  $C_d$  is given in figure 112.



Table 19. Potential for moisture accelerated damage indicated by the MAD index.<sup>(49)</sup>

MAD Index	MAD Potential	Description
85-100	Negligible	This pavement would not show any moisture-related problems during its lifetime—drainage not needed.
70-85	Low	This pavement contains a combination of properties that make it moisture insensitive, but climatic influences and maintenance must be carefully watched to maintain the good performance.
55-70	Normal	This pavement is composed of average materials exposed to average situations. Moisture damage is likely unless adequate drainage and maintenance are kept at a high level.
35-55	Moderate	Lower quality materials and a slightly inferior climate will produce large amounts of moisture damage unless extensive care is given to drainage considerations and routine maintenance.
15-35	High	Even with adequate drainage moisture damage will appear due to variability in materials. Without drainage there would be excessive moisture damage.
0-15	Excessive	The combination of climate and materials precludes any effectiveness of drainage in reducing moisture damage. Severe problems will develop, excessive maintenance should be planned for.

Table 20. Simplified design matrix for the selection of the overall drainage coefficient,  $C_d$ .

Edge Drain	Precipitation	Fine Grained Subgrade (A-4 through A-7)		Coarse Grained Subgrade (A-1 through A-3)	
		Nonpermeable Base	Permeable Base	Nonpermeable Base	Permeable Base
No	Wet	0.70-0.90	0.85-0.95	0.75-0.95	0.90-1.00
	Dry	0.90-1.10	0.95-1.10	0.90-1.15	1.00-1.15
Yes	Wet	0.75-0.95	1.00-1.10	0.90-1.10	1.05-1.15
	Dry	0.95-1.15	1.10-1.20	1.10-1.20	1.15-1.20

- Notes:
1. Permeable Base  $k = 1000$  ft/day or  $C_u \leq 6$ . 1 ft = 0.3 m
  2. Wet climate = Precipitation > 15 in/year; 1 in = 25.4 mm  
 Dry climate = Precipitation  $\leq$  15 in/year.
  3. The available data provided no information on the effectiveness of permeable bases without edge drains, and the data ranges provided in the table are estimates. This design is generally not recommended, although on a coarse-grained subgrade some vertical drainage may occur.
  4. Generally select mid-point of range and use other drainage features (adequacy of cross slopes, depth of ditches, etc.) to adjust upward or downward.

Table 21. Potential for moisture damage indicated by  $C_d$ .

$C_d$	Potential for Moisture Damage
1.10–1.20	Negligible
1.00–1.10	Low
0.90–1.00	Moderate
0.80–0.90	High
0.70–0.80	Excessive

Expected traffic levels are also an important factor in determining the need for drainage. For example, the need for drainage is much more critical on Interstate-type highways carrying high traffic volumes and heavy commercial vehicles where the potential for damaging interactive effects of load and moisture are very high. The flow chart presented in figure 112 and the guidelines presented in this section are for medium- and high-trafficked roadways (design ESAL's greater than 5 million).

#### *Pavement Cross Section Characteristics*

Certain pavement cross section characteristics are also important in determining the need for pavement drainage. Items such as cross slopes, depth of ditches, and longitudinal grade of ditches are critical in evaluating drainage needs and should not be ignored. For example, if any of these factors are inadequate (i.e., flat cross slope, shallow drainage ditches, or no longitudinal grade), drainage of the pavement will not occur, no matter how well designed or elaborate the other components of the drainage system. In other words, key pavement cross section characteristics such as cross slopes, depth of ditches, and longitudinal ditch grades must be considered as part of the overall drainage system or the pavement will effectively be a nondrained structure.

A minimum cross slope of 2 percent is recommended for the mainline pavement structure, and this should be increased to 3 or 4 percent for the shoulder surface. In areas of cut or at grade, a 3 to 4 ft (0.9 to 1.2 m) wide ditch is recommended, the depth of which will be dependent upon the anticipated amount of water that will be flowing in the ditch. A minimum depth of 4 ft (1.2 m) beneath the edge of the mainline pavement surface is recommended, although this may need to be increased depending on the expected inflow. The longitudinal grade of the ditch should be a minimum of 1 percent. These recommendations are summarized in table 22.

Special consideration should be given to sag vertical curves, crest vertical curves, superelevation transitions, and cut-to-fill transitions in order to maintain the ability of the pavement structure to drain water.

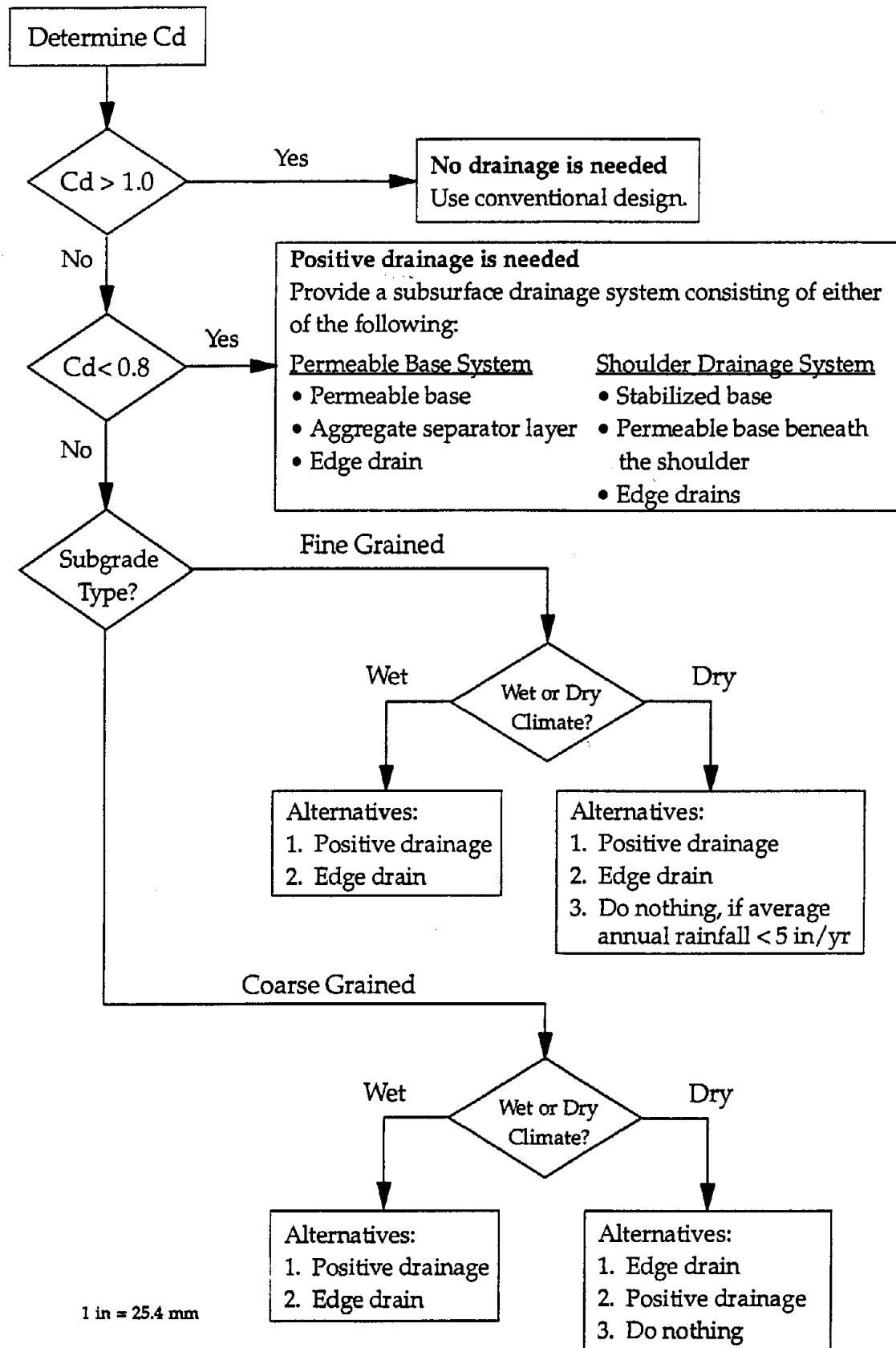


Figure 112. Flow chart of drainage design recommendations based on  $C_d$  (for pavements with design ESAL's greater than 5 million).

Table 22. Pavement cross section recommendations for enhancing overall drainability.

Cross Section Feature	Recommendation
Pavement Cross Slope	Minimum 2 percent
Shoulder Cross Slope	Minimum 3 percent
Width of Ditches	3 to 4 ft
Depth of Ditches	Minimum 4 ft ( <i>deeper if greater flows anticipated</i> )
Longitudinal Grade of Ditchline	Minimum 1 percent

1 ft = 0.305 m

The cross-sectional design of the base course is also an important factor influencing the drainability of pavements. In the past (and in several of the pavements on this study), a stabilized or dense-graded base was placed beneath the pavement, and also was placed beneath the thin (2 to 3 in [51 to 76 mm]) AC shoulder surfacing. Such a layout created a “bathtub” section in which free water is unable to drain either vertically or laterally through the dense-graded material (see figure 113). Such cross sections must be avoided so that excess moisture may effectively be removed.

#### *Effectiveness of Different Drainage Designs*

The performance data from this study showed that sections constructed on permeable bases are performing superior to sections containing other drainage designs. Also, direct comparisons between sections with permeable and nonpermeable bases indicate that the permeable base sections are performing better. This enhanced performance is generally manifested in lower faulting and fewer transverse cracks. In some cases, joint spalling is also less for the permeable base sections, probably due to the joints being less saturated. In addition, on at least one project, the incidence of D-cracking was noticeably less on a permeable base section built than on an adjacent stabilized base section (both sections had the same D-cracking susceptible aggregate). However, the sections included in this study were all relatively young and had not been exposed to substantial traffic loadings. Figure 114 shows an example permeable base design, including all key design elements.

Pavement sections containing only longitudinal edge drains (and no permeable base) show only a small advantage in pavement performance when compared to nondrained systems. This could be due to free moisture being unable to migrate to the longitudinal drain because of the relative impermeability of the base course. Thus, the water remains within the pavement, essentially creating a nondrained structure.

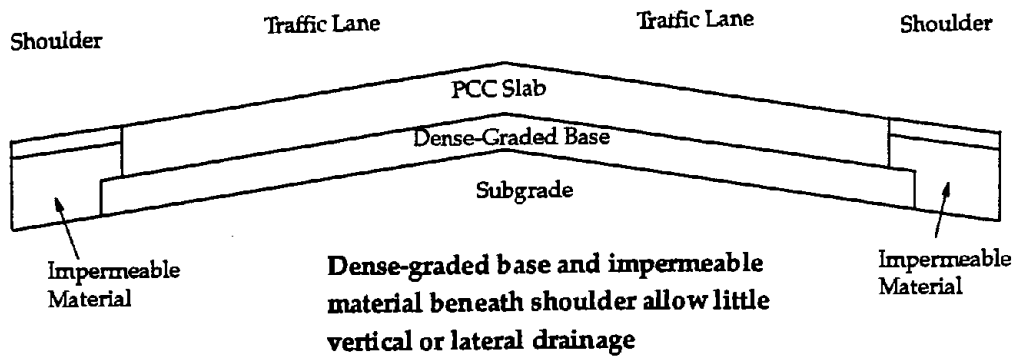


Figure 113. Cross section of a "bathtub" design.

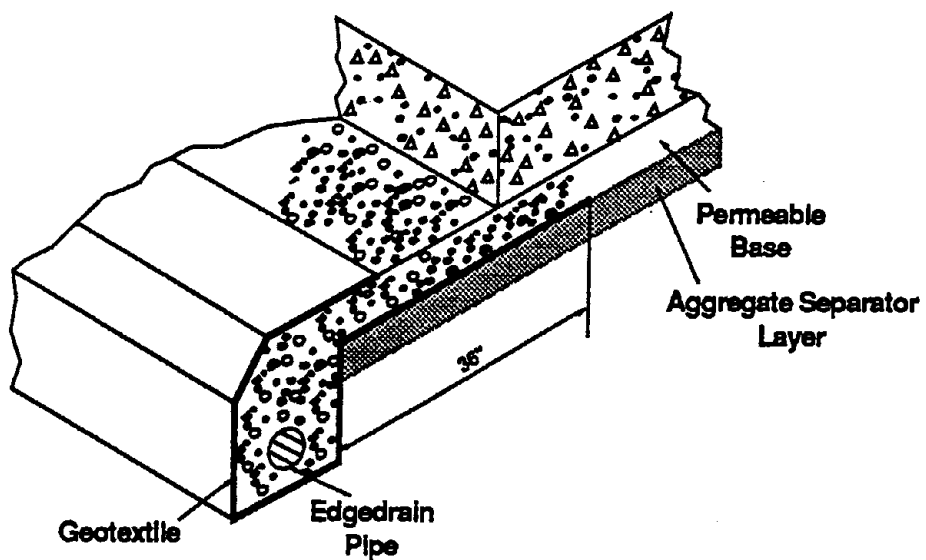


Figure 114. Example permeable base design.<sup>(51)</sup>

Daylighted cross sections, in which an aggregate base course extends out beyond the shoulders to the ditches, is another means of providing drainage to a pavement structure. In this design, shown in figure 115, excess water can flow through the aggregate base and directly to the ditches, if the aggregate base has some degree of permeability. However, these designs are generally not recommended (even with a permeable base) because they are not maintainable. The "outlet" portion of the daylighted base frequently clogs with dirt, grass, and other debris, serving to keep free moisture within the pavement system and accelerating the development of distress.

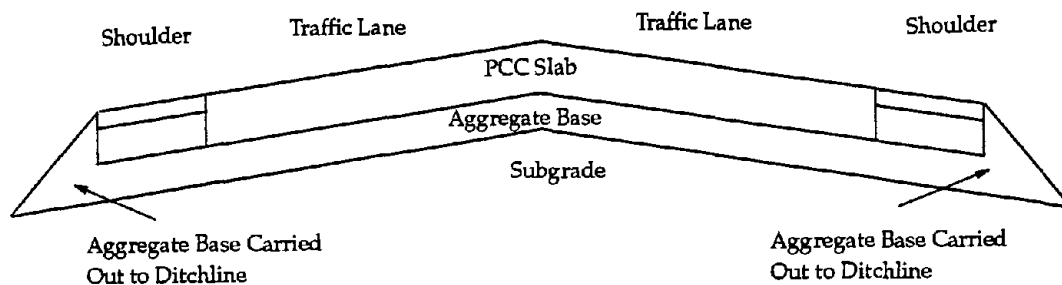


Figure 115. Daylighted pavement cross section.

Although no such sections were included in this study, an interesting PCC pavement drainage design adopted by the California Department of Transportation is shown in figure 116. In this design, an LCB is placed directly beneath the PCC slab and on top of a granular subbase material. Drainage is provided by the placement of a permeable base course beneath the shoulders. Longitudinal edge drains are placed in the permeable base course to carry the excess moisture from the pavement structure. This design is now required for all high-type PCC pavements in California (pavements designed for more than 2.5 million ESAL's).

The overall drainability of the pavement sections included in this study was assessed using the  $C_d$  coefficient previously described. Sections with relatively good drainability typically will have a  $C_d$  greater than 1, whereas sections with relatively poor drainability will have a  $C_d$  less than 1. An evaluation of the performance data generally shows that pavements with higher a  $C_d$  exhibit better performance than pavements with a lower  $C_d$ , particularly in terms of faulting. In fact, the  $C_d$  coefficient was found to be a very significant factor in the development of the joint

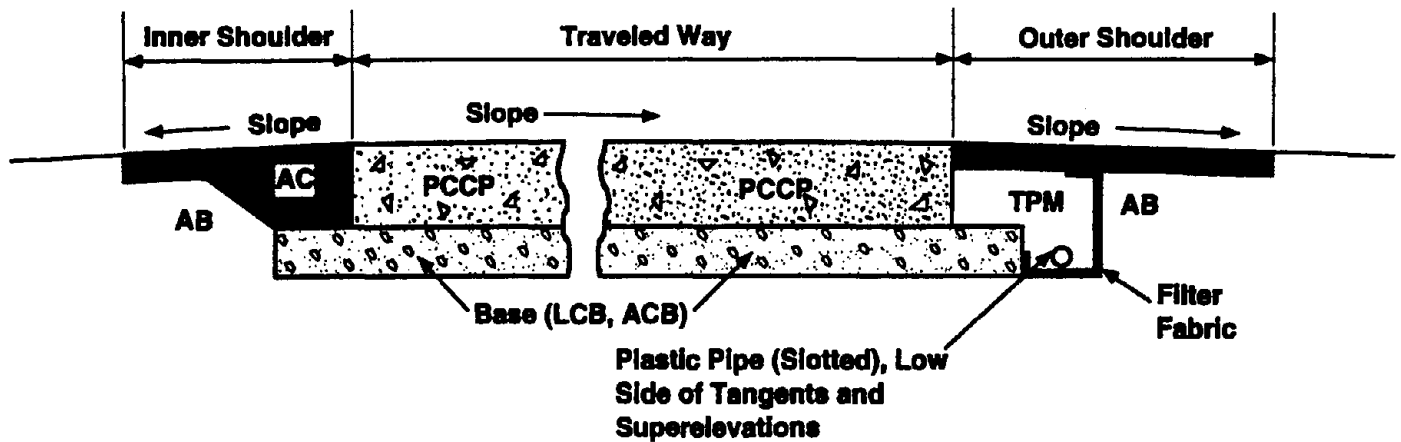


Figure 116. California drained LCB design.<sup>(52)</sup>

faulting models presented in chapter 2. Those models were used to develop figures 117 (nondoweled joints) and 118 (doweled joints). These figures illustrate how improved drainability (as expressed in terms of  $C_d$ ) significantly reduces the development of joint faulting.

#### *Example State Drainage Guidelines*

Many States have established policies on the use of subsurface drainage and its design. The type of drainage policies vary considerably, ranging from a simple blanket statement (e.g., permeable bases shall be used under all new pavements) to one that specifies when and what type of base is to be used. The following are some examples:

- Pennsylvania requires the placement of an open-graded base as an interlayer between PCC pavements and dense-graded aggregate subbase.<sup>(53)</sup>
- The Ministry of Transportation of Ontario (MTO) requires a 4-in (100-mm) layer of open-graded drainage layer to be placed directly beneath the PCC slab on all expressway facilities.<sup>(54)</sup>
- California formerly required treated permeable bases under all pavements except when the mean annual rainfall is less than 5 in (127 mm) per year or when the permeability of subgrade soil is more than 100 ft/day (30 m/day).<sup>(51)</sup> However, this guideline is currently undergoing revision, with modifications allowing the use of permeable bases for low and medium trafficked pavements

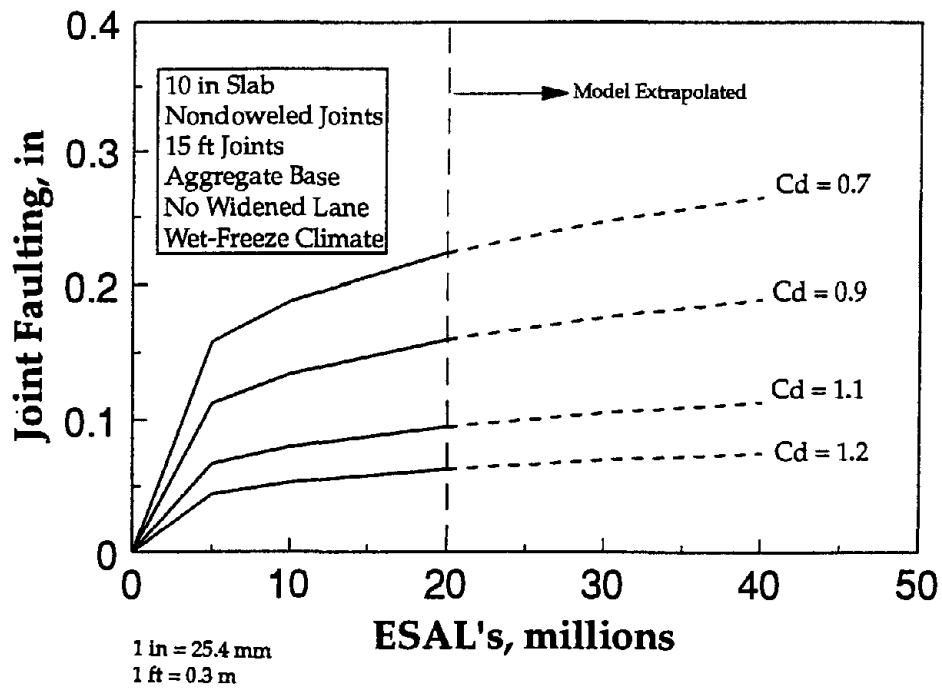


Figure 117. Effect of drainability on nondoweled joint faulting.

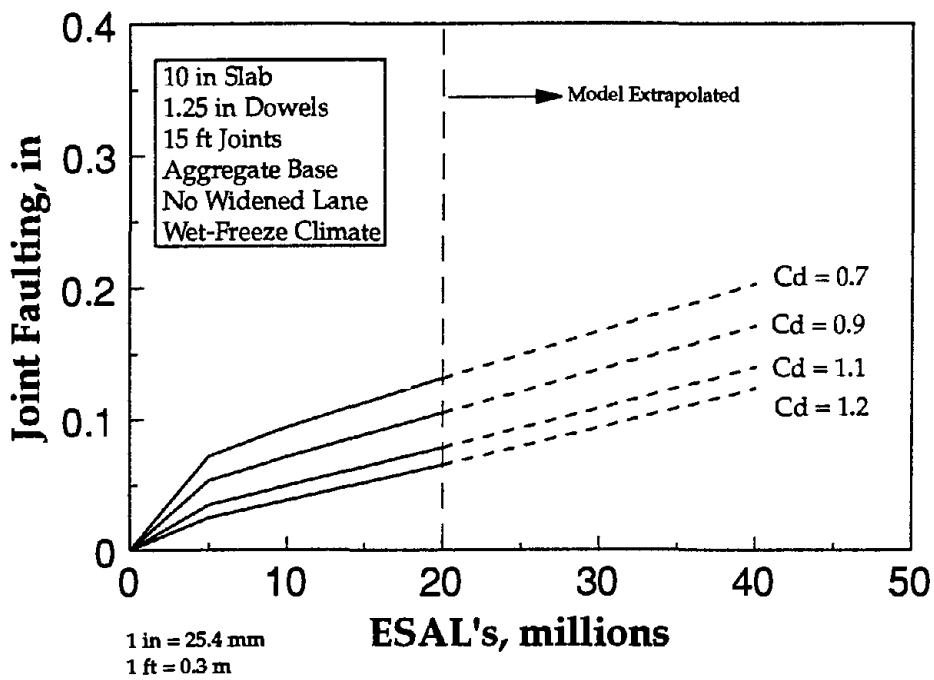


Figure 118. Effect of drainability on doweled joint faulting.



only.<sup>(55)</sup> As previously described, for more than 2.5 million ESAL's, California stipulates the use of an LCB on top of a granular subbase, with drainage provided by a permeable base beneath the shoulder and accompanying longitudinal edge drains.<sup>(55)</sup>

- The Washington State Department of Transportation (WSDOT) requires the use of either a permeable cement-treated or permeable asphalt-treated base course for all PCC pavements with design ESAL's greater than 25 million.<sup>(56)</sup> For under 25 million ESAL's, nondoweled pavements over a high-type AC base are allowed.
- The Minnesota Department of Transportation (Mn/DOT) recommends the use of permeable bases based on subgrade type and projected traffic levels. For nongranular subgrades, the use of permeable bases is recommended on all Interstate roadways, as well as all non-Interstate roadways with 20-year design ESAL's greater than 4.5 million.<sup>(57)</sup> For granular subgrades, the use of permeable bases is recommended for both Interstate and non-Interstate roadways with 20-year design ESAL's greater than 15 million.<sup>(57)</sup> The placement of a deep granular subbase is also recommended.
- The New York State Department of Transportation (NYDOT) requires the use of either a permeable cement-treated or permeable asphalt-treated base course for all new and reconstructed rigid pavement structures.<sup>(58)</sup> A 12-in (305-mm) granular subbase and up to 24 in (710 mm) of select granular subgrade is also required.
- The Missouri Highway and Transportation Department (MHTD) stipulates the use of a permeable base course beneath all heavy duty pavements (pavements carrying more than 1000 trailer combinations per day).<sup>(59)</sup>
- The Wisconsin Department of Transportation has a general guidelines for determining when and which type of permeable base should be used.<sup>(51)</sup>
  - When the subgrade permeability is less than 10 ft/day (3 m/day), the following is required:
    - Subbase: 6-in (152-mm) dense-graded aggregate.
    - Base: minimum 4-in (102-mm) Wisconsin standard No. 1 (AASHTO No. 67) permeable aggregate (PAGG).
  - When the subgrade permeability is 10 ft/day (3 m/day) or greater, a minimum 6-in (152-mm) layer of Wisconsin standard No. 2 PAGG base is placed directly on the subgrade. This design is based on vertical flow of water into the subgrade, and filter layer criteria is checked to ensure material compatibility between subgrade and the PAGG.

The gradation of Wisconsin PAGG's are given in table 23. For both gradations, 90 percent of particles retained on No. 4 sieve are required to have at least one fractured face. Wisconsin also uses treated permeable bases.

Table 23. Wisconsin standard gradation for permeable aggregate base.<sup>(51)</sup>

Sieve Size		Wisconsin No. 1 PAGG (AASHTO No. 67)	Wisconsin No. 2 PAGG
in	mm		
1.5	38.10		100
1	25.40	100	75-100
3/4	19.05	90-100	
3/8	9.525	20-55	55-75
No. 4	4.750	0-10	30-55
No. 10	2.000	0-5	10-25
No. 40	0.425		0-10
No. 200	0.075		0-5
Target Permeability		10,000 ft/day (3,000 m/day)	500 ft/day (152 m/day)

Several of the guidelines listed above include the subgrade type or permeability as a criterion for determining the need for a permeable base. This is considered critical because the "vertical drainage" provided by subgrades with sufficient permeability can go a long way in aiding the drainability of the pavement structure. Where the subgrade has sufficient permeability, this "vertical drainage" should be exploited by not placing a nonpermeable layer directly above the subgrade.

#### *Estimating Drainage Capacity for Design*

Most of the existing guidelines for drainage are based on determining the capacity needed to drain the pavement structure to an acceptable moisture condition within a set time period following a saturating rain. The common guidelines for acceptable drainage times are given in table 24.<sup>(50,60)</sup>

The time to drain to 50 percent saturation criterion given in table 24 was established in 1952, and has been adopted by many agencies, including the Corps of Engineers.<sup>(61)</sup> While this is the most commonly used criteria for drainage design, the basis for this criteria is somewhat arbitrary. More recently, a rational criterion has been proposed based on the observation that permanent deformation of coarse-grained materials increases dramatically when the level of saturation is over 85 percent.<sup>(49,62)</sup>

Table 24. Quality of drainage based on time to drain.<sup>(50,60)</sup>

Quality of Drainage	50% Saturation Achieved Within	85% Saturation Achieved Within
Excellent	2 hours	2 hours
Good	1 day	2 to 5 hours
Fair	1 week	5 to 10 hours
Poor	1 month	Greater than 10 hours
Very Poor	Water will not drain	Much greater than 10 hours

One shortcoming of the time-to-drain approach is that it considers only the capacity of a drainage system to remove water from the pavement structure (starting from a fully saturated condition) without any regard to either the rate or frequency of rainfall. Nevertheless, this approach is generally recommended for determining the required drainage capacity for pavement design.

If the time-to-drain requirement is not satisfied, the base permeability may have to be increased. Other options include increasing the cross slope or reducing the length of flow path (the distance the water has to travel to drain).

Another approach to determining the drainage requirements is the inflow-outflow analysis.<sup>(51,63)</sup> In this approach, the drainage system is designed to provide adequate capacity to remove all infiltrated water under peak-flow conditions in addition to meeting the time-to-drain requirements. While this approach gives consideration to the rate of rainfall, inadequate data are currently available to assess whether or not it is important to prevent saturation of pavement structures at all times.

#### *Permeable Base Drainage Design Recommendations*

As discussed in the previous section, there are varying degrees of need for pavement drainage. In some cases, the combination of exposure conditions and natural drainage capacity of the subgrade soil may allow pavements to be constructed without a subsurface drainage system. Or on low-volume roadways, the use of a subsurface drainage system may not be justified in light of the significant increase in construction costs. Since a permeable base drainage system can add about 20 percent to the cost of a concrete pavement, there must be a strong need for improved drainage of the pavement.

As previously discussed, the pavement cross section (cross slopes, depth of ditches, longitudinal ditch grade) must be carefully evaluated so that no water is trapped in the system. If water is trapped in a permeable base and unable to drain from the structure, inherently a weaker structure exists that is less capable of providing support in a saturated condition, and rapid failure of the pavement may ensue.

For new pavements that have been identified as having a strong need for drainage, the most effective system for pavement subsurface drainage consist of the following three elements:

- Permeable base—to provide rapid drainage of free water infiltrating the pavement structure.
- Separator layer—to prevent migration of fines into the permeable base. This is an essential element of the drainage system to prevent clogging of the permeable base.
- Longitudinal edge drain collector system—to collect and remove water draining from the permeable base layer.

Where positive drainage is needed (as indicated by the MAD index or a low  $C_d$  given in table 20, for example), a drainage system consisting of the above three design elements should be provided. Proper design, construction, and maintenance of each component are extremely important in order to obtain full benefits from the drainage system. In addition, other key aspects of concrete pavement design—particularly joint design—must still be carefully considered and effectively designed. The provision of positive drainage will not overcome the effects of poor practices in other design areas.

Recommended subsurface drainage designs are shown in figure 119 (for PCC pavements with PCC shoulders) and figure 120 (for PCC pavements with AC shoulders). In these figures, both pre-pave (placement of the edge drain prior to mainline paving operations) and post-pave (placement of the edge drain after mainline paving operations) edge drain installations are shown. The following sections describe the various components of the permeable base drainage system.

### Permeable Base

The permeable base should be placed directly below the PCC slabs to intercept water infiltrating the pavement structure. A minimum thickness of 4 in (102 mm) is recommended for permeable bases, and the base should extend 1 to 3 ft (0.3 to 0.9 m) beyond the edge of the pavement.<sup>(51)</sup>

The minimum recommended permeability is 1,000 ft/day (300 m/day). The permeabilities of commonly used gradations are typically much greater than 3,000 ft/day (911 m/day). Several States use the AASHTO No. 57 gradation for their stabilized permeable bases. The AASHTO No. 67 gradation is also commonly used. Many agencies have their own gradation for permeable bases. Example gradations are given in table 25; a graphical illustration of the New Jersey gradation is provided in figure 121.

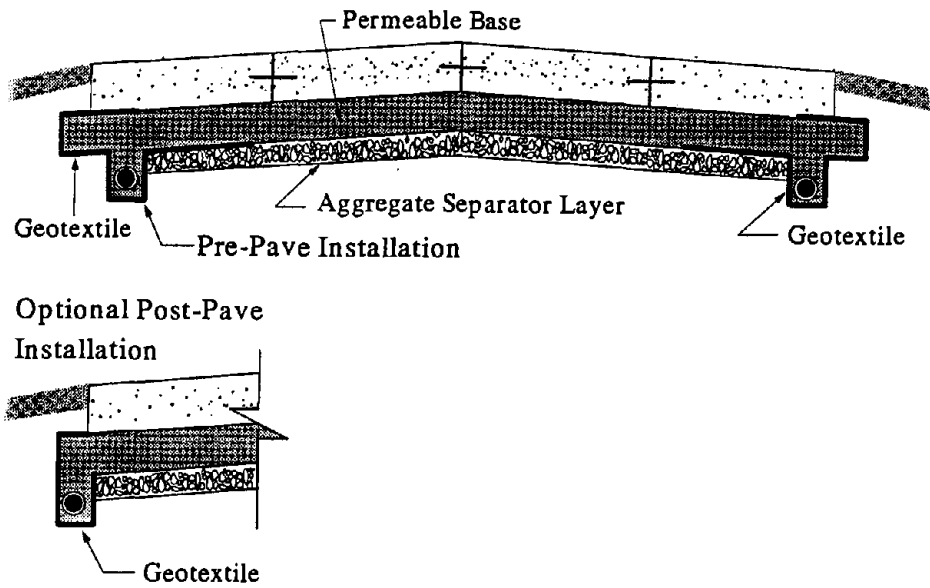


Figure 119. Typical cross section of subsurface drainage systems for crowned section and tied concrete shoulders.<sup>(51)</sup>

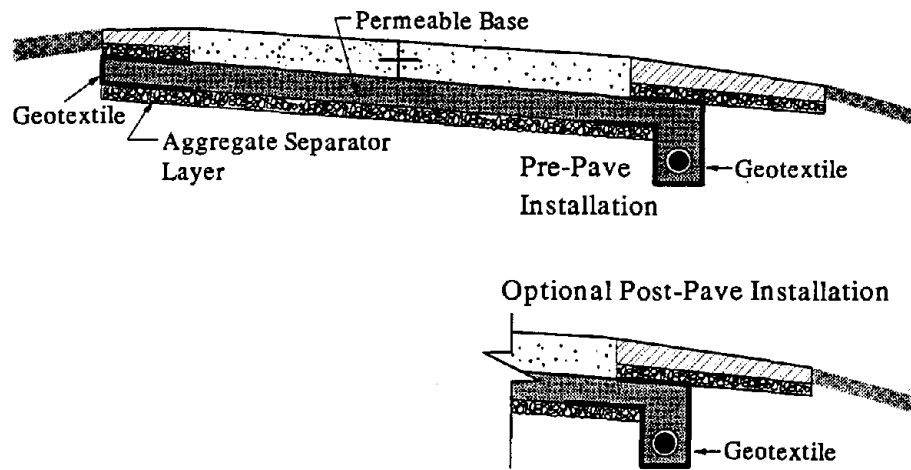


Figure 120. Typical cross section of subsurface drainage system for constant slope cross section and AC shoulders.<sup>(51)</sup>

Table 25. Gradations used in permeable bases.

Sieve Size		Percent Passing					
in	mm	AASHTO 57	AASHTO 67	Pennsylvania		New Jersey	
1	25.4	95-100	100			95	100
3/4	19.0		90-100	52	100		
1/2	12.7	25-60				60	80
3/8	9.53		20-55	35	65		
#4	4.75	0-10	0-10	8	40	40	55
#8	2.36	0-5	0-5			5	25
#16	1.18			0	12	0	8
#30	.60			0	8		
#50	.300					0	5
#200	.075				5		
Target Permeability		6,800 ft/day (2,070 m/day)	5,200 ft/day (1,580 m/day)	1,000 ft/day (305 m/day)		2,000 ft/day (610 m/day)	

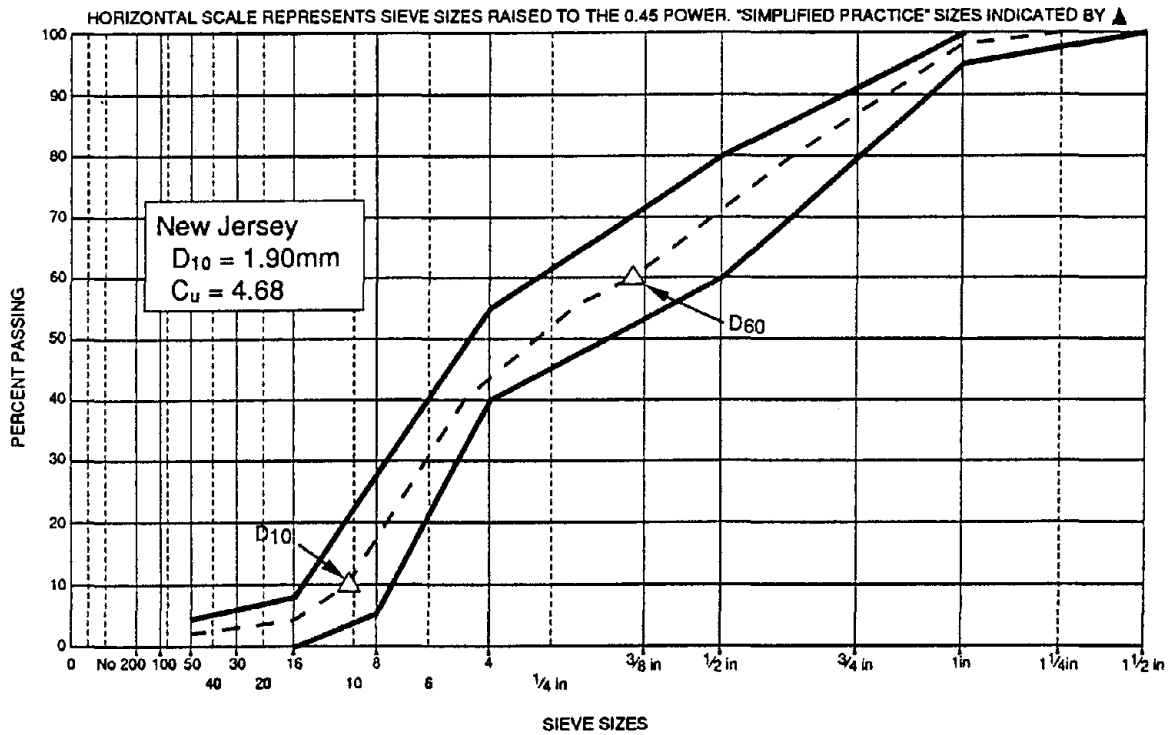


Figure 121. Plot of New Jersey gradation.<sup>(51)</sup>

Some States limit base permeability out of concern for possible erosion under the base that may result from excessive flow velocities. However, limiting the base permeability may not necessarily prevent the erosion problem; it is possible for the erosion to take place as a result of built-up of excessive pore pressure when the flow capacity of the permeable base is exceeded, in much the same way that erosion occurs in a nondrained pavements. For example, California determined that stripping of asphalt-treated permeable material occurred when insufficient quantities of asphalt binder was used.<sup>(64)</sup>

The FHWA recommends the use of 100 percent crushed stone in permeable bases to ensure stability.<sup>(51)</sup> One agency recommends a minimum  $C_u$  of 4 to provide adequate stability. The coefficient of uniformity is an indicator of how densely graded the material is and is determined as follows:

$$C_u = \frac{D_{60}}{D_{10}} \quad (50)$$

where:

$D_{60}$  = Particle size (mm) of a gradation at which 60 percent of the material (by weight) are smaller.

$D_{10}$  = Particle size (mm) of a gradation at which 10 percent of the material (by weight) are smaller.

Some studies recommend  $C_u$  less than 3.5.<sup>(65)</sup> Field evaluations by numerous highway agencies (including New Jersey, Ontario, Pennsylvania, and Wisconsin) have shown that untreated permeable bases do not pose significant construction problems.<sup>(51)</sup>

Permeable bases may be treated with either asphalt cement (AC) or portland cement to improve stability. The use of a treated permeable base is recommended if construction traffic will be allowed on the base. The type of asphalt cement most commonly used is AC-20, but AC-40 can also be used to provide additional stability. Permeable asphalt-stabilized bases should be treated with between 2 to 2.5 percent AC by weight, although one study has suggested using 3 percent.<sup>(64)</sup> Permeable cement-stabilized base should be treated with between 2 to 3 bags of portland cement per yd<sup>3</sup> (112 to 167 kg/m<sup>3</sup>).

### Separator Layer

Permeable bases must be placed over a separator layer to prevent contamination by the fines migrating up from the underlying layers. A dense-graded aggregate layer of adequate thickness (4 in [102 mm] is inadequate over soft soils, up to 12 in [300 mm] may be required) is recommended.

The following filtration criteria should be satisfied for a dense aggregate separation layer.<sup>(51)</sup>

$$D_{15}(\text{Separator Layer}) \leq 5D_{85}(\text{Subgrade}) \quad (51)$$

$$D_{50}(\text{Separator Layer}) \leq 25D_{50}(\text{Subgrade}) \quad (52)$$

$$D_{15}(\text{Permeable Base}) \leq 5D_{85}(\text{Separator Layer}) \quad (53)$$

$$D_{50}(\text{Permeable Base}) \leq 25D_{50}(\text{Separator Layer}) \quad (54)$$

In addition, the separator layer should contain no more than 12 percent fines (material passing the No. 200 sieve) and have a coefficient of uniformity ( $C_u$ ) greater than 20.<sup>(51)</sup> An example gradation for the separator layer meeting these requirements is given in table 26. As with the permeable base, the material for the separator layer should consist of durable, crushed aggregates.

Table 26. Typical dense-graded aggregate separator layer gradation.<sup>(51)</sup>

Sieve Size		Percent Passing
in	mm	
1-1.5	38.10	100
3/4	19.05	95-100
No. 4	4.750	50-80
No. 40	0.425	20-35
No. 200	0.075	5-12

Some agencies use geotextile materials as separator layers between the subgrade and the permeable base. The most important component in the selection of a geotextile material as a separator layer is the determination of the required apparent opening size (AOS) of the material. Detailed information on the selection of an appropriate geotextile material to serve as a separator layer is found in reference 51.

#### Edge Drain Collector System

A conventional pipe edge drain is recommended to drain permeable bases. The edge drain must have the necessary hydraulic capacity to handle water being discharged from the permeable base. A geocomposite fin drain or an aggregate trench drain without a pipe is not recommended to drain permeable bases because neither provide adequate hydraulic capacity nor can they be maintained.<sup>(51)</sup>



The recommended edge drain design is shown in figure 122. The trench for the drain should be made deep enough to place the top of the drainage pipe at least 2 in (52 mm) below the bottom of the permeable base. In deep freeze areas, a deeper placement may be necessary to avoid freezing problems. The recommended horizontal locations of the edge drain are shown in figures 119 and 120. The placement of the edge drain depends on the sequence of construction. The drains should not be placed in the trackline of paver nor in the wheelpath of the pavement.

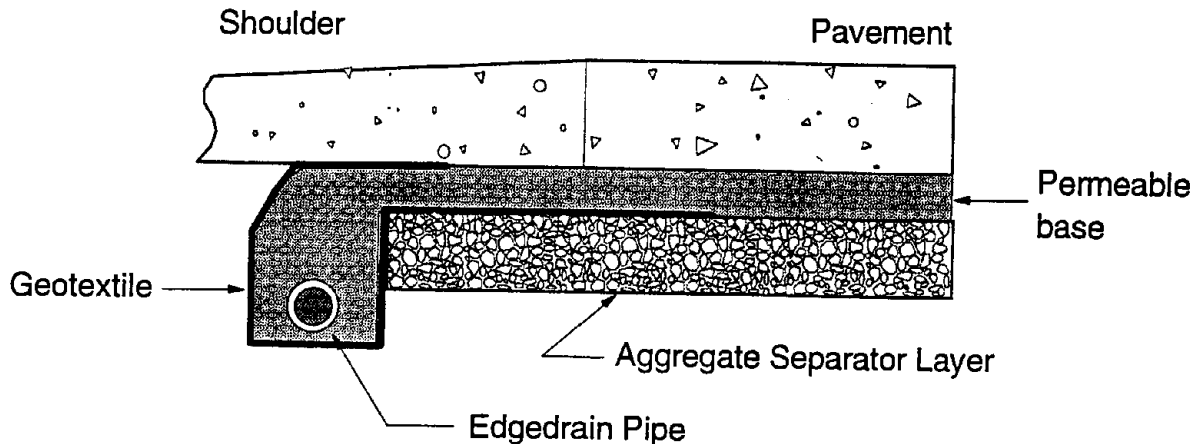


Figure 122. Recommended edge drain design.<sup>(51)</sup>

The pipe size required for the edge drain is controlled by the spacing of the outlets and longitudinal grade. For maintenance considerations, minimum 4-in (102-mm) diameter pipes and maximum outlet spacings of 250 ft (76 m) are recommended.<sup>(51)</sup> However, in areas where the grade is very flat, outlet spacings may need to be decreased in order to facilitate removal of the water from the edge drain.

Most highway agencies use either flexible, corrugated polyethylene (CPE) pipe or smooth, rigid polyvinyl chloride (PVC) pipe for longitudinal edge drains. CPE pipe is governed by AASHTO M 252, whereas PVC pipe is governed by AASHTO M 278.

The backfill material for the trench should be at least as permeable as the permeable base material. Nonstabilized pea-gravels are not recommended as the backfill material because they cannot be compacted satisfactorily.<sup>(66)</sup> Proper compaction of the backfill material is important to avoid settlement over the edge drain.

Outlets for the edge drains are required at regular intervals (no more than 250 ft [76 m]) so that water collected by the edge drains may be released to the ditches. The recommended design for outlet pipes is shown in figures 123 and 124. Solid-walled rigid pipes are recommended for the lateral outlet pipes. For maintenance considerations, smooth, long-radius bends and dual outlet system are recommended. The dual outlet system allows flushing equipment to enter the edge drain from either end, and also permits easy inspection of the system using video inspection equipment. The outlets should be placed close enough together so that only one headwall is required.

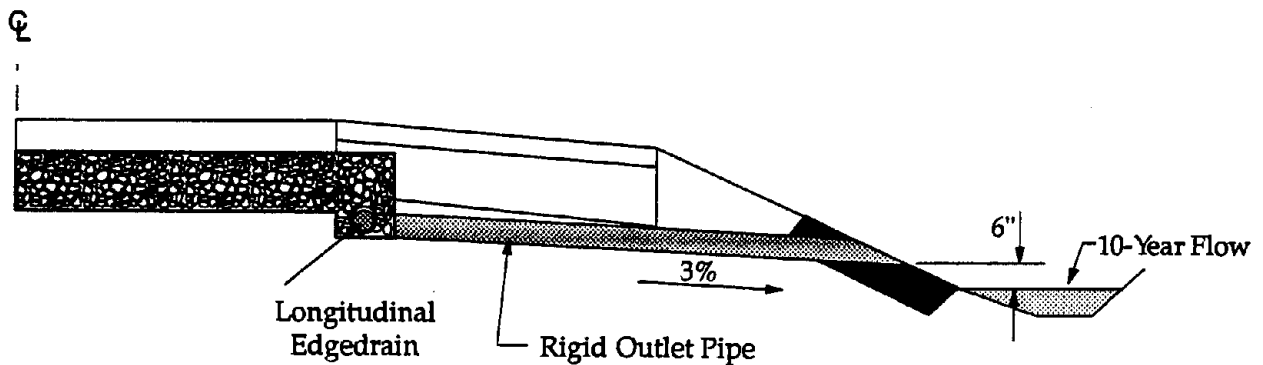


Figure 123. Recommended design for edge drain outlet.<sup>(51)</sup>

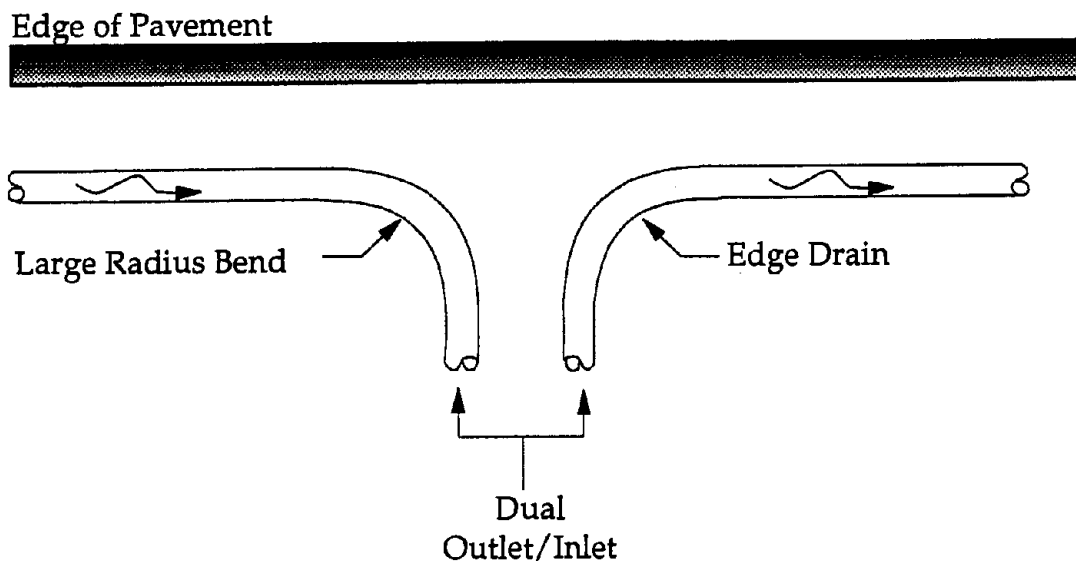


Figure 124. Smooth, long-radius bends and dual outlet system for cleanout and video camera inspection.<sup>(51)</sup>

The outlet pipes should have at least 3-percent slope toward the drainage ditch, and the discharge end of the pipe should be placed at least 6 in (152 mm) above the 10-year design flow in the ditch; the same requirements apply even when the outlet pipes are discharging into the storm drain system. In most cases, these requirements place the ditchline a minimum of 4 ft (1.2 m) below the pavement surface. The flow capacity of the drainage ditch is important to performance of drainage system. The ditch must be cut deep enough to provide the required freeboard at the discharge end of the outlet pipes under the maximum design flow condition, taking into consideration the discharge from surface drainage as well as subsurface drainage. Inadequate clearance at the discharge end will not allow free flow of water out of the pavement structure, and if the water level in the ditch rises above the outlet level, backflow could occur, thereby flooding, rather than draining, the structure. If ditch depths are not adequate to allow discharge of water from the pavement structure, permeable bases should not be constructed.

Headwalls are recommended at the ends of drainage outlets to protect outlet pipes from damage, to prevent slope erosion, and to aid in location of the drainage outlets. Headwalls should be placed flush with the slope so that they do not impair mowing operations or become a roadside hazard.<sup>(51)</sup> A recommended headwall design is shown in figure 125. Removable rodent screens are recommended to discourage rodents from building nests in the pipe drains. The screens should be easily removable to allow maintenance access and cleaning.

### *Transverse Drains*

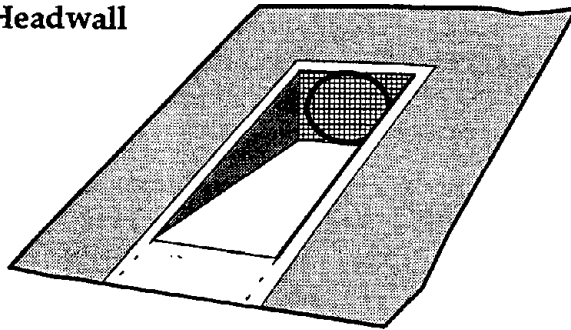
Any time the longitudinal or transverse slopes of a roadway approach zero, a strong potential for drainage problems exists. Examples of this include transition areas before and after superelevated curves (in which the cross slope of the pavement is zero) and sag vertical curves (in which the longitudinal slope is zero). In these cases, consideration should be given to the use of transverse drains, which are drains installed transversely beneath the pavement structure. Transverse drains can effectively remove excess water at these problem locations, but must be placed with sufficient grade to do so. In addition, the depth of the ditches must be deep enough for the anticipated water flows, particularly in the case of sag vertical curves.

A combination of transverse drains and longitudinal collector drains can provide a very effective means for rapid removal of water from the pavement system. The design details of transverse drains are the same as those of longitudinal edge drains.

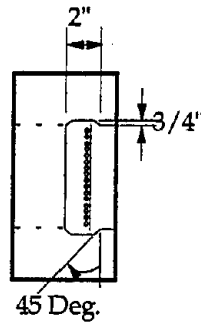
### *Edge Drains*

Longitudinal edge drains (placed without a permeable base) have been used as a means of providing subsurface drainage in both new and in existing pavements. However, opinions differ on the effectiveness of edge drains by themselves in improving pavement performance. Based on the results of the current study, it is believed that edge drains placed without a permeable base are generally not effective

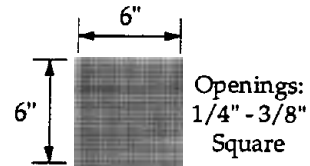
**Precast Concrete Headwall  
In Slope**



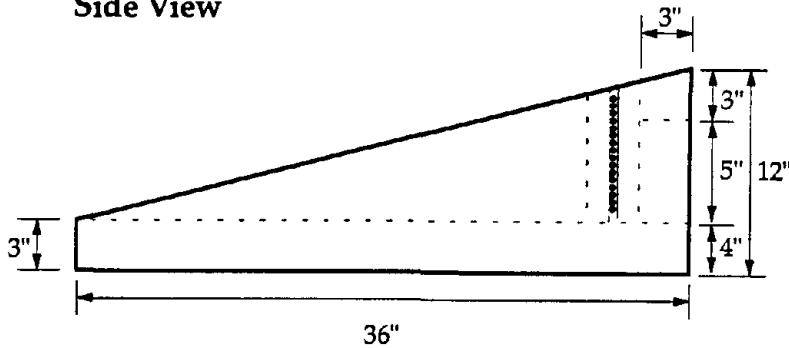
**Top View Detail of  
Slotted Headwall**



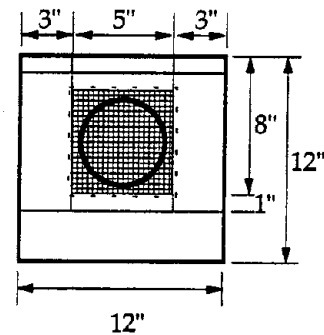
**Rodent Screen Detail**



**Side View**



**Front View**



1 in = 25.4 mm

Figure 125. A recommended headwall design.<sup>(51)</sup>

because infiltrated water cannot readily flow through a dense-graded base to reach the drain. Nevertheless, although the current trend is move toward the use of permeable bases, edge drains are used routinely in a number of States.

There are two basic types of edge drains—trench type, and geocomposite fin drains—but depending on the installation detail four different types may be identified as shown in figures 126 through 129. Of the four types, the partially wrapped and nonwrapped drains are the least problem prone. Other types are more sensitive to quality of construction. When properly installed, fin drains can perform equally or better than other types, but obtaining the intimate contact with the edge of pavement is not always easy.<sup>(67)</sup> The recommended installation details for fin drains to obtain more consistent results are shown in figure 130.<sup>(67,68)</sup> The recommended

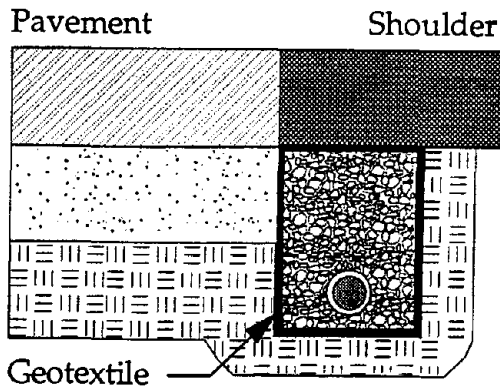


Figure 126. Geotextile wrapped drain.<sup>(67)</sup>

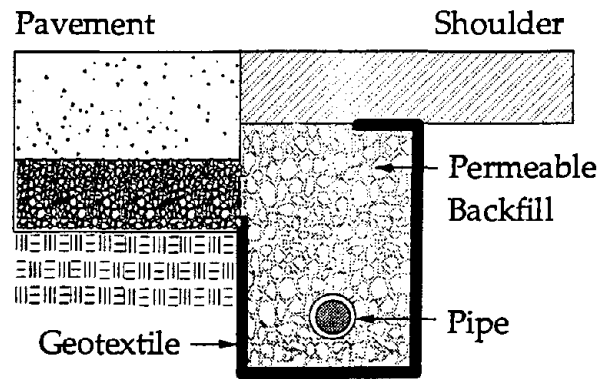


Figure 127. Partially wrapped drain.<sup>(67)</sup>

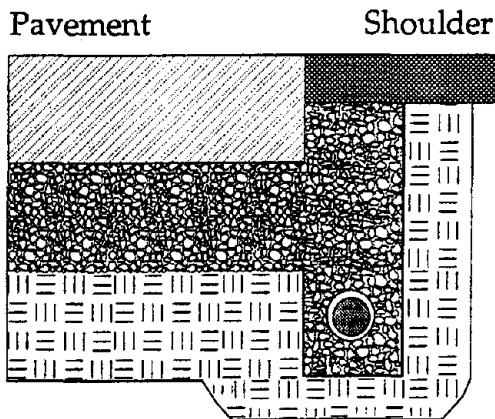


Figure 128. Nonwrapped drain.<sup>(67)</sup>

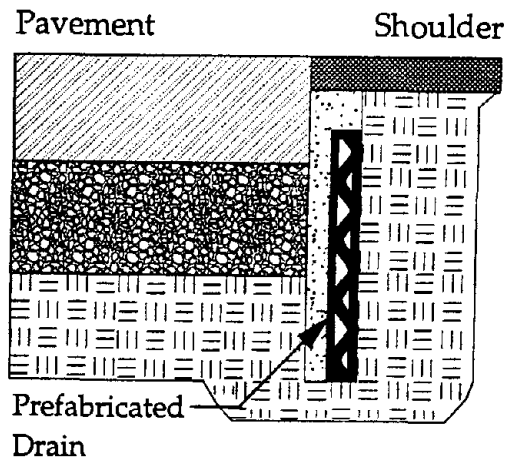


Figure 129. Geocomposite edge drain.<sup>(67)</sup>

outlet designs for the edge drains are the same as those for the edge drains provided with permeable bases.

As previously indicated, either flexible CPE pipe or smooth PVC pipe are commonly used for longitudinal edge drains. However, rigid outlet pipes are always required to prevent crushing during construction and maintenance activities.

### Daylighting

The effect of daylighting on pavement performance was discussed previously. Generally, these designs have not resulted in improved performance because of their tendency to clog with dirt and other debris. If the daylighted base becomes clogged, free moisture is kept within the pavement system and accelerates the development of pavement distress.

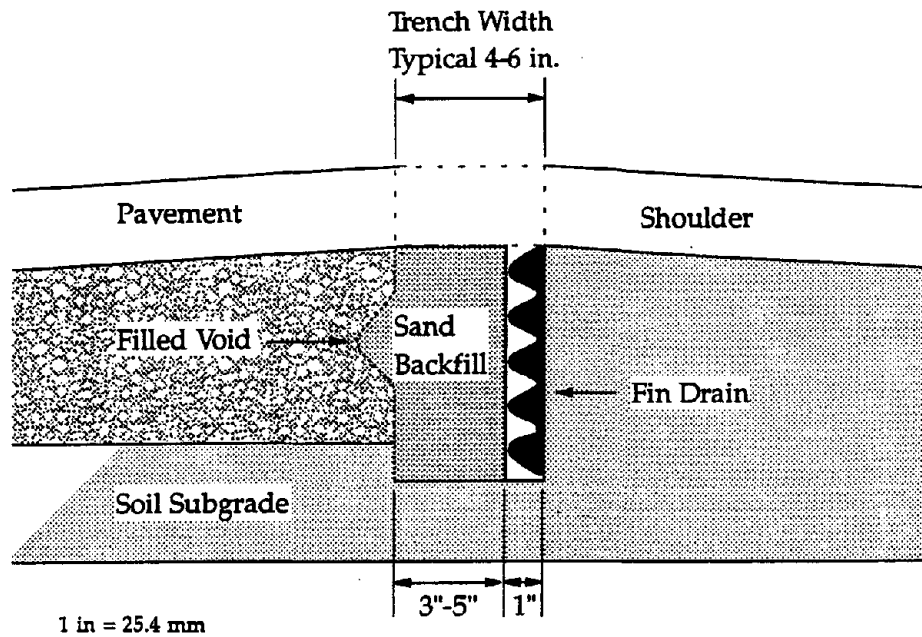


Figure 130. Recommended installation detail for fin drains.<sup>(67)</sup>

### Construction Issues

A key concern regarding the construction of drained pavements is whether or not permeable base materials provide adequate stability to support construction traffic. The experiences by State Highway Agencies clearly show that even nontreated permeable bases can provide adequate stability. Whether or not construction traffic should be allowed on a permeable base, however, is another issue.

Most States do not allow construction traffic on a permeable base to prevent contamination. Typically, the only traffic allowed on permeable bases are the paving train and haul trucks that are backing up to feed the paver. Ontario places a further restriction on how long a permeable base may remain exposed before paving: the contractors are required to place the surface layer within 30 days of placement of the open-graded drainage layer to prevent contamination of the drainage layer from prolonged exposure.<sup>(54)</sup> No data are available to show whether contamination of permeable bases during construction is a serious problem.

Obtaining a uniform base thickness can also be a problem for permeable bases. Kazmierowski et al. noticed a large variation in core thickness (2.6 to 3.9 in [65 to 100 mm]) of a nontreated permeable aggregate base during the construction of a test section in Ontario.<sup>(54)</sup> Solberg recommends trimming the separator layer prior to placing the permeable base when a treated permeable base will be used in order to obtain the desired layer thickness.<sup>(69)</sup> This construction variability is the main reason for recommending a minimum design permeable base thickness of 4 in (102 mm).

The compaction of permeable bases also requires special considerations. The conventional approach of requiring a fixed percentage of a standard or target density is not applicable because of difficulties in measuring density. The purpose of compacting a permeable base is to merely seat the aggregate; over-rolling can cause degradation of the material and a subsequent loss of permeability. Specifying a level of consolidation which results in no appreciable displacement of the base following compaction is recommended for permeable bases. For both stabilized and nonstabilized permeable bases, most State Highway Agencies specify one to three passes of a 5- to 10-ton (4.5- to 9-Mg) steel-wheeled roller.<sup>(51)</sup>

The placement of cement-treated permeable base (PCTB) may require some special considerations. Because PCTB is typically a harsh mix, a subgrade planer or similar equipment with the ability to spread harsh material the width of the highway may be needed to place PCTB.<sup>(70)</sup> Anchoring dowel baskets on PCTB can also be difficult. This problem could be avoided by using a paver equipped with a dowel bar inserter. FHWA recommends that the method of dowel placement be a contractor option provided that specified placement tolerances are met.

If the PCTB is used, curing of the base material may also be of concern, although the need for curing the treated base has not been well established. Illinois finds curing PCTB to be unnecessary.<sup>(70)</sup> Methods that can be used to cure cement-stabilized permeable base include the following:

- Covering with polyethylene sheeting for 3 to 5 days.
- Applying fine water mist several times on the day after the base is placed.
- Applying curing compound by itself or in conjunction with one of the methods above.

As discussed previously, the inclusion of permeable bases in a pavement design requires that ditches be of adequate depth and that longitudinal and transverse slopes are sufficient to provide drainage. Special consideration must be given to permeable base subsurface drainage design details in areas of superelevated curve transitions, in sag and crest vertical curves, or in any other areas where longitudinal grades or transverse cross slopes are at or near zero.

### *Maintenance of Drainage Systems*

Proper maintenance is important to ensure proper functioning of the drainage systems. Maintenance activities consist primarily of keeping the drainage pipes and outlets free of vegetation, debris, and sediments. Regular inspection of the drainage system is also recommended in order to monitor its performance. Video equipment can be used to inspect the internal condition of pavement drainage systems.<sup>(71,72)</sup>

Clogging of edge drains can be a major problem in drainage systems. One study found the most severe clogging problems in edge drains placed on very flat slopes.<sup>(72)</sup> The same study also found that smooth-walled plastic outlet pipes performed better than corrugated steel pipes because corrosion and sedimentation are more

pronounced in the steel pipes.<sup>(72)</sup> Such clogged drains can be effectively cleaned by flushed with high pressure water jets, provided that the outlets are designed with curved connections to allow cleaning of the longitudinal edge drain.

Clearly marked drainage outlets are extremely important for maintenance. Marking facilitates the location of the drainage outlets for routine inspection and maintenance work and helps to prevent damage by construction equipment and mowers. Metal posts can be used to mark the location of the outlet along with a paint stripe on the shoulder to help mark the general location of the outlet. In one Kentucky project, 11 of 14 drainage outlets were damaged by guardrail posts driven through the drainage pipes.<sup>(73)</sup> The potential for these types of problems can be greatly reduced by clearly marking the drainage outlets, in conjunction with a headwall.

### Base Type

Base courses are placed beneath concrete pavements to provide increased structural capacity, to prevent pumping of materials, and to provide a working platform for subsequent paving operations. The performance of concrete pavements is greatly affected by base type, most notably in the development of joint faulting and slab cracking. The use of a base course under concrete highway pavements is strongly recommended, as slab-on-grade designs (i.e., pavements without a base course) on Interstate-type pavements have not performed well even under moderate traffic loadings. Furthermore, the presence of a strong, durable base course make it possible to construct smoother pavements.

A variety of base types is available for use under PCC pavements, including aggregate (granular) bases, cement-treated bases, asphalt-treated bases, lean concrete bases, and permeable (both stabilized and nonstabilized) bases. Although good performance has been obtained with all of these base types, the results of this study show considerable variability in their performance. Some of this variability is due to differences in the pavement structural design elements, but significant differences in base material properties, cross sectional designs, and climatic conditions are also responsible. For example, inadequate stabilizer contents, placement of the base in a "bathtub" configuration, and areas of heavy moisture and severe freeze-thaw conditions all can result in significant differences in performance.

### *Use of Granular Subbase Beneath Base Course*

The use of a granular subbase beneath the base course is recommended for most medium- and high-trafficked roadways. This granular layer serves several purposes, including:

- Provision of strong construction platform.
- Provision of additional frost protection.
- Prevention of pumping of the subgrade.



- Provision of additional support to the pavement structure and for future rehabilitation activities.

Many European countries employ a granular subbase beneath stabilized base layers and have experienced good performance.<sup>(39)</sup> These subbase layers may range in thickness from 8 to 20 in (203 to 508 mm), depending upon the degree of frost protection required. In the U.S., a study in Wisconsin indicated that JRC sections constructed with a granular subbase have provided an average of 7 additional years of life before requiring rehabilitation (as compared to sections with either a stabilized or nonstabilized base and no subbase).<sup>(74)</sup>

### *Selection of Base Type*

In selecting a suitable base type for a concrete pavement, several factors should be evaluated:

- Type of subgrade (stabilized bases more effective on fine-grained subgrades).
- Local experience and success with the various base types.
- Need for positive drainage beneath the pavement structure.
- Erodibility of the base course material (or the subgrade beneath a stabilized base).
- Anticipated traffic loadings and level of support requirements.
- Availability of materials.
- Contractor construction experience with the various base types.
- Overall construction considerations (working platform, sensitivity of base to moisture during construction).
- Pavement type.
- Need for frost protection of lower layers.
- Need for a strong working platform for the current construction and future reconstruction.
- Cost of the base course.

It is believed that any of the available base types, if designed and constructed properly, can provide adequate performance. However, the base type should not be considered as a separate entity but selected and designed in accordance with the overall pavement structure. Relative advantages and disadvantages of the different base types, along with key design considerations, are summarized in table 27.

The erodibility of the base course can have a significant effect on the ability of the base course to support the overlying slab. Extensive studies have been conducted by the Permanent International Association of Road Congresses (PIARC) on the erodibility of different base course materials, and offer the following classifications:<sup>(75,76)</sup>

- Class A (Extremely Erosion Resistant)—LCB with 8 percent cement or ATB with 6 percent asphalt.
- Class B (Erosion Resistant)—plant-mixed CTB with 5 percent cement.

Table 27. Summary of PCC pavement base types.

Base Type	Advantages	Disadvantages	Key Design Considerations	Recommended Traffic Levels
Permeable Base (stabilized and nonstabilized)	Removes water from pavement Low susceptibility to erosion Decrease in moisture-related distresses (faulting, D-cracking, etc.)	Difficult to construct ( <i>particularly nonstabilized</i> ) Granular separator layer required May have to limit construction traffic High cost (from 14 to 24 percent greater than conventional aggregate base)	Design of separator layer Collector/outlet pipe design Adequate stabilizer contents ( <i>generally 200–250 lb/yd<sup>3</sup> of cement or 2–3% of asphalt</i> ) Compaction/curing	Medium to High
Lean Concrete	Easy to construct Strong stable platform Strong resistance to erosion Improves pavement rideability Reduces slab stresses ( <i>if bonded</i> )	High cost (about 22 percent greater than conventional aggregate base) Increased friction with slab Increased slab curling Granular subbase required to prevent pumping	Shorter JPCP joint spacing Curing of base Bonding of base Notching of joints in base if bonded to slab	Medium to High ( <i>with granular subbase</i> )
Asphalt Stabilized	Easy to construct Strong stable platform Some resistance to erosion Improves pavement rideability Reduces slab stresses ( <i>if bonded</i> )	High cost (about 8–15 percent greater than conventional aggregate base) May be susceptible to stripping Increased friction with slab Increased slab curling Granular subbase required to prevent pumping	Shorter JPCP joint spacing Asphalt content ( <i>5–6% recommended</i> ) Proper compaction Whitewashing of base prior to paving Bonding of base	Medium to High ( <i>with granular subbase</i> )
Cement Stabilized	Easy to construct Strong stable platform Some resistance to erosion Improves pavement rideability Reduces slab stresses ( <i>if bonded</i> )	High cost (about 8–15 percent greater than conventional aggregate base) May be susceptible to erosion Increased friction with slab Increased slab curling Granular subbase required to prevent pumping	Shorter JPCP joint spacing Cement content ( <i>6–8% recommended</i> ) Compaction Bonding of base	Medium to High ( <i>with granular subbase</i> )
Dense-Graded Aggregate	Easy to construct Low cost Low friction with slab	Susceptible to erosion May retain moisture for long periods	Compaction ( <i>to 95% of AASHTO T180</i> ) Controls on liquid limit, plastic limit, and percentage of fines	Low to Medium

- Class C (Erosion Resistant Under Certain Conditions)—plant-mixed CTB with 3.5 percent cement or ATB with 3 percent asphalt.
- Class D (Fairly Erodible)—CTB with 2.5 percent cement or untreated aggregate materials.
- Class E (Very Erodible)—untreated fine soils.

A U.S. study on the erodibility of various base course materials also showed the importance of cement and asphalt content on minimizing erosion.<sup>(77)</sup>

The sections constructed on permeable bases in this study showed good performance under low to medium traffic levels, provided that an effective separator layers and edge drains were present; the performance of these sections is summarized in table 28. Figures 131 and 132 illustrate the faulting performance of the permeable base sections included in this study for nondoweled and doweled pavements, respectively. These figures include several direct comparisons between adjacent permeable and nonpermeable pavements, and the permeable bases sections consistently show lower levels of faulting. However, a few of the nondoweled permeable base sections did not perform well due to design deficiencies (one did not contain a separator layer and one had an AC layer over the PCTB) and these are noted in figure 131. These results show that a dense AC layer should not be placed between the PCC slab and the permeable base course.

While the projects included in this study have performed well, some agencies have experienced significant problems with pavements constructed on permeable bases. Early cracking of slabs has been one problem, which is likely due to the increased bond and friction that exists between the slab and the base. This increased bond and friction is probably caused by the concrete penetrating into the open surface of the permeable base. Other problems that have aggravated the performance of some permeable base sections include inadequate joint sawing depth, absence of a separator layer, and the stability of untreated permeable base courses. Furthermore, doweled joints are considered essential to their performance.

It should be noted that the permeable base sections included in this study were generally less than 5 years old and had not been exposed to substantial traffic loadings. Because of this, continued monitoring of the long-term performance of pavements constructed on permeable bases is warranted.

Pavements constructed on lean concrete bases have performed well under high traffic loadings, given that certain design and materials criteria are met. The results of this study showed that these designs performed well when shorter joint spacings were employed to counteract the increase in curling stresses created by the stiffer foundation support. A granular subbase layer beneath the LCB is recommended to prevent pumping of the subgrade; this is particularly important if the base is to be bonded to the slab. Dowel bars were also found to be critical for this design in providing effective joint load transfer.

Table 28. Performance of permeable base sections.

Project ID	Base Type	ESAL's, millions	Age, years	Dowel Diameter, in	Joint Faulting, in	JPCP, % Cracked Slabs	JRCP M-H Tr. Cracks/mi	PSR	IRI, in/mi
CA 2-2	AC/PCTB	7.3	12	0.00	0.16	3	N/A	4.0	137
CA 6-2	PATB	12.0	12	0.00	0.05	0.00	N/A	3.8	170
CA 10	PATB	0.8	2	0.00	0.05	0.00	N/A	3.9	93
MI 1-4a	PATB	1.3	17	0.00	0.03	0.00	N/A	3.8	106
MI 3	PAGG	10.4	6	1.25	0.01	N/A	10	3.8	122
MI 5	PAGG	7.6	8	1.25	0.04	N/A	253	3.4	188
MN 6	PATB	1.9	9	1.0	0.01	N/A	5	4.2	143
MO 1-6	PATB	4.0	15	1.25	0.06	N/A	6	4.2	164
NJ 3-1	PAGG	7.6	13	1.25	0.04	N/A	0.00		191
NJ 3-2	PATB	7.6	13	1.25	0.03	N/A	0.00		199
ONT 1-2	PATB	2.3	10	0.00	0.10	0.00	N/A	3.9	135
PA 1-2	PATB	0.6	12	1.25	0.01	N/A	0.00	4.2	150
PA 1-3	PAGG	0.6	12	1.25	0.03	N/A	0.00	4.1	178
PA 1-4	PAGG	0.6	12	1.25	0.03	N/A	0.00	4.0	159
WI 1-1	PCTB	1.8	2	1.25	0.01	0.00	N/A	3.7	100
WI 1-2	PCTB	1.8	2	1.25	0.01	0.00	N/A	3.8	84
WI 1-3	PCTB	1.8	2	1.25	0.00	0.00	N/A	3.8	114
WI 2-1	PCTB	1.4	4	1.25	0.01	0.00	N/A	4.1	122
WI 2-2	PATB	1.4	4	1.25	0.01	0.00	N/A	4.0	106
WI 2-3	PAGG	1.4	4	1.25	0.01	0.00	N/A	4.0	112
WI 3-1	PATB	0.8	4	0.00	0.03	0.00	N/A	4.0	109
WI 6-1	PAGG	1.1	4	0.00	0.07	0.00	N/A	4.0	88
WI 6-2	PAGG	1.1	4	0.00	0.04	0.00	N/A	3.9	77
WI 6-3	PAGG	1.1	4	1.25	0.00	0.00	N/A	3.8	81
WI 6-4	PAGG	1.1	4	1.25	0.00	0.00	N/A	3.8	102
WI 7-1	PAGG	1.4	4	0.00	0.03	0.00	N/A	4.3	136
WI 7-2	PAGG	1.4	4	0.00	0.03	6	N/A	4.2	113
WI 7-3	PCTB	1.4	4	0.00	0.01	0.00	N/A	4.5	120
WI 7-4	PCTB	1.4	4	0.00	0.04	6	N/A	4.1	147
WI 7-5	PATB	1.4	4	0.00	0.01	0.00	N/A	4.0	147
WI 7-6	PATB	1.4	4	0.00	0.02	0.00	N/A	4.1	86

1 in = 25.4 mm

1 mi = 1.61 km

### Joint Faulting, in

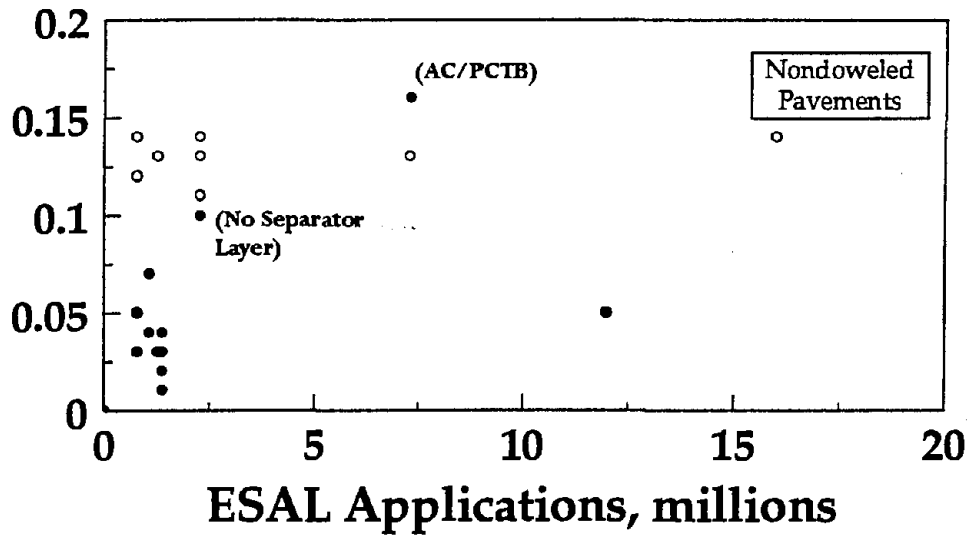


Figure 131. Performance of sections on permeable and adjacent nonpermeable bases (nondoweled pavements).

### Joint Faulting, in

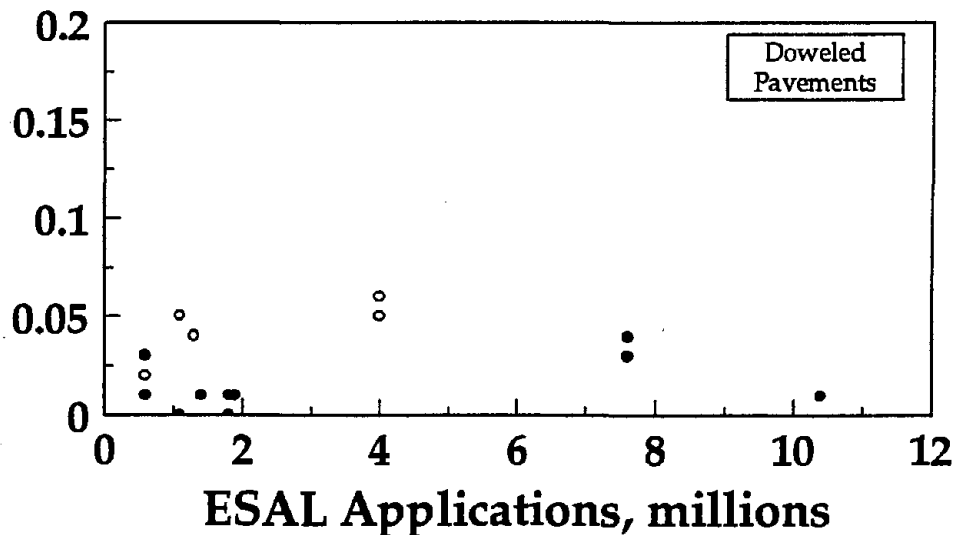


Figure 132. Performance of sections on permeable and adjacent nonpermeable bases (doweled pavements).

Good performance can be obtained from asphalt- and cement-treated bases if quality aggregates and sufficient quantities of stabilizer are used in the base and if shorter transverse joint spacings and dowel bars are employed. Their use may be more suitable to medium- to high-trafficked roadways. In this study, the performance of sections constructed on ATB and CTB varied considerably, but most of these sections had stabilizing levels less than 6 percent. Similar to LCB, shorter joint spacings may be needed for JPCP to help control thermal curling stresses.

The effectiveness of stabilized bases (including LCB) in preventing joint faulting and JRCP crack deterioration is shown in figures 133 and 134. Figure 133 illustrates the predicted faulting for pavements constructed on an aggregate and stabilized base using the nondoweled faulting model presented in chapter 2; the faulting for the stabilized base course section is less than that of the aggregate base section. Figure 134 illustrates the beneficial effect of a stabilized base in preventing the development of deteriorated transverse cracking in JRCP using the JRCP crack deterioration model from chapter 2. In JPCP, however, stabilized bases can cause increased thermal curling stresses, so it is imperative that shorter transverse joint spacings be employed. Doweled joints are also essential to prevent pumping and loss of support under medium and heavy traffic loadings.

Aggregate base courses are believed to be most appropriate for low- to medium-trafficked roadways. The results of this study indicated that sections constructed on aggregate bases exhibited fair to good performance. While these sections were somewhat susceptible to faulting (probably because of the erodibility of the base material), they did exhibit less cracking than sections constructed over other base types.

As previously described, the use of a thick granular subbase beneath all base courses should be considered, particularly for high-type concrete pavements. Many European countries employ a substantial granular subbase beneath the base course on their concrete pavements, not only for frost protection but also to provide additional support and to decrease pumping potential beneath the base course.<sup>(39)</sup>

It is worth reiterating that a base course is strongly recommended for most highway pavement construction in which medium to high traffic volumes are expected (i.e., design ESAL's greater than 3 million). In this study, pavements that were constructed directly on grade without benefit of a base course show poor to fair performance, as illustrated in table 29. Even though these were often thicker slabs, these designs were susceptible to pumping and exhibited excessive levels of faulting even under relatively low traffic.

Overall, each of the base types are believed capable of providing good performance, but only if designed and constructed properly. Careful consideration must still be given to other key design elements (e.g., joint design) in order to obtain the full benefits of a particular base type. For example, regardless of base type, dowels are believed to be a necessity for all PCC pavements except those exposed to very light traffic levels.

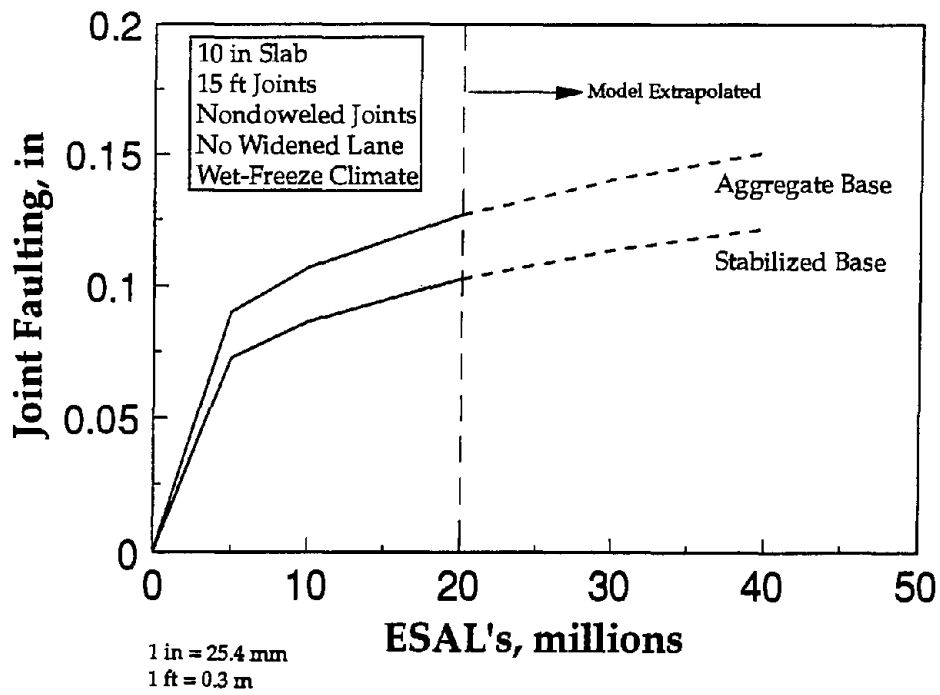


Figure 133. Effect of stabilized base on nondoweled joint faulting.

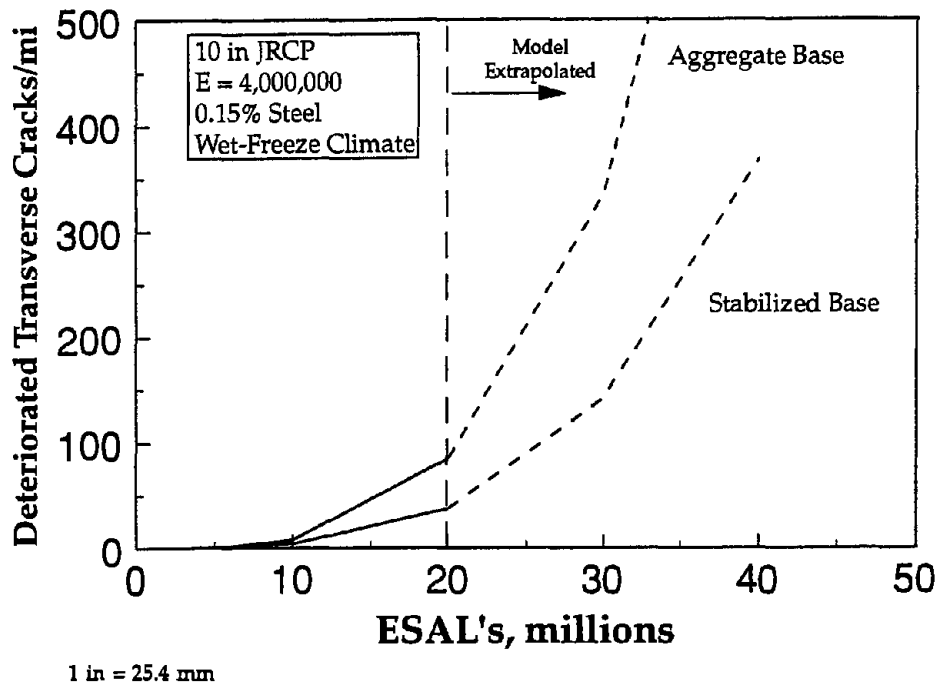


Figure 134. Effect of stabilized base on JRCP crack deterioration.

Table 29. Performance of pavement sections without a base course.

Section ID	Thickness, in	ESAL's, millions	% Slabs Cracked	Joint Faulting, in
AZ 1-5	11	6.0	0	0.03
OH 2-2	15	6.5	0	0.08
OH 2-3	15	6.5	4	0.14
ONT 1-1	12	2.1	0	0.11

1 in = 25.4 mm

General recommendations on the design and construction of each base type are provided in the following sections.

#### *Permeable Bases*

As discussed in the preceding section on subsurface drainage, permeable bases are an effective means of removing surface-infiltration water from beneath the concrete pavement. Both stabilized and nonstabilized permeable bases have been used with success, and at this time no significant differences in performance between the two types have been noted. A minimum thickness of 4 in (102 mm) is recommended for all permeable base types, and this should be adequate for most cases.

A variety of gradations have been used for permeable base design. An open gradation with few fines is required, and examples of gradations that have been successful are shown in table 25. Again, only high-quality, crushed aggregates should be used in the construction of permeable base.<sup>(51)</sup> Nonstabilized permeable aggregate bases draw their stability from the interlock of the aggregate particles. One agency recommends a minimum  $C_u$  of 4 to provide adequate stability, which is particularly important if construction traffic is allowed on the base.

Stabilized permeable bases offer the advantage of increased stability and the provision of a strong working platform; their permeability is generally much higher than nonstabilized permeable bases (typically 10,000 ft/day [3050 m/day] vs. 1000 ft/day [305 m/day]) since nonstabilized permeable bases require some smaller size particles to provide stability whereas stabilized permeable bases obtain their stability from the cementing agents (asphalt or portland cement). However, this stability may degrade over time depending on the amount of stabilizer and on environmental forces, which is why only high-quality crushed stone materials are recommended for use in permeable bases.

Permeable asphalt-treated bases are typically stabilized with between 2 and 2.5 percent asphalt cement. However, California has discovered stripping on many of



its asphalt-treated permeable bases, and subsequently has recommended a minimum of 3 percent asphalt.<sup>(64)</sup> A harder grade of asphalt (AC 40) may be used to improve the stability of the base during construction.<sup>(51)</sup>

Permeable cement-treated bases typically contain 2 to 3 bags of portland cement per cubic yard as a stabilizer. A minimum of 200 lb/yd<sup>3</sup> (119 kg/m<sup>3</sup>) is recommended for general use, with 250 lb/yd<sup>3</sup> (148 kg/m<sup>3</sup>) suggested for areas with questionable support or where heavy construction traffic on the base course is expected.<sup>(78)</sup>

Other key components of the permeable base system are the separator layer and the pipe collector system. The separator layer is placed between the subgrade and the permeable base to prevent the migration of fines into the permeable base that could otherwise compromise its water-carrying capability and reduce support. The pipe collector system gathers the water from the permeable base and then carries it to the ditches at regular intervals. Detailed information on both of these components was provided in the preceding section.

The use of a permeable base subsurface drainage system does come with a cost. According to a recent survey, the inclusion of a permeable base on a concrete pavement (in lieu of a conventional dense-graded aggregate base) increases the cost of that pavement by an average of 14 to 24 percent.<sup>(48)</sup> In order for this to be cost effective, a corresponding increase of 14 to 24 percent in performance or life must also be realized.

### *Lean Concrete Bases*

A lean concrete base is similar to conventional concrete in makeup and composition, but generally contains less cement and is therefore has strengths lower than conventional concrete. In some cases, a lower quality aggregate may be used, a mixture often referred to as econcrete, although the two terms are often used synonymously regardless of the composition.

A lean concrete base provides uniform support to the pavement and provides a strong construction platform for paving operations. For construction purposes, it represents an "all weather" base and is considered "extremely erosion resistant" according to PIARC guidelines if a minimum of 8 percent cement is used.<sup>(75,76)</sup>

Typically, lean concrete contains between 200 and 350 lb/yd<sup>3</sup> (119 and 207 kg/m<sup>3</sup>) of cement, resulting in 28-day compressive strengths between 750 and 1500 lb/in<sup>2</sup> (5.2 and 10.4 MPa). However, due to erodibility concerns, cement contents and strengths in the upper portion of those ranges are preferred. Production and placement of lean concrete bases are essentially the same as for conventional concrete pavements, with thicknesses ranging from 4 to 6 in (102 to 152 mm).

For heavily-trafficked roadways, the use of higher quality materials and greater cement contents (8 percent minimum) is recommended. Germany specifies a strength

of 2000 lb/in<sup>2</sup> (13.9 Mpa), with construction traffic allowed when the base achieves a strength of 1400 lb/in<sup>2</sup> (9.7 Mpa).<sup>(40)</sup>

The current practice in the U.S. is to treat the surface of the lean concrete base with two layers of a wax-based curing compound in order to break the bond between the base and the overlying slab. The purpose of this is to minimize the potential for random cracking in the base to reflect through the concrete slab. However, it is standard practice in several European countries to take active steps to *promote* the bond between the slab and the base.<sup>(39)</sup> For example, Germany builds a 6-in (152-mm) lean concrete or cement-treated base that is bonded to the overlying PCC slab; notches are cut in the lean concrete base course at locations to coincide with the transverse joints in the PCC slab.<sup>(40)</sup> The bonding of these layers provides a thick monolithic slab, which decreases edge stresses, deflections, thermal curling, moisture warping, and interlayer erosion.<sup>(39)</sup> Moreover, a thicker, monolithic structure would allow for increases in transverse joint spacing, although there is some concern about the longevity of the bonding. German officials estimate that the bond will remain effective for only about 4 years before debonding begins to occur at the joints and slab edges.<sup>(40)</sup> Nevertheless, increasing the bond and friction between the base and the slab can have a beneficial effect in reducing pumping and erosion of the pavement.

Because of the strong potential for improvement in concrete pavement performance, consideration should be given to this design philosophy of bonding the base and the slab. Consideration should also be given to providing an aggregate subbase beneath the LCB to prevent pumping and loss of support beneath the LCB. German designs use a thick granular blanket layer beneath the stabilized base, ranging in thickness from 8 to 20 in (203 to 508 mm).<sup>(39)</sup> The use of the thick granular layer beneath the LCB is likely an important design feature that contributes to excellent performance of the bonded-base design used in Germany.

Lean concrete bases are commonly used in Europe and have provided excellent performance in that continent, even under greater ESAL loadings and higher legal load limits than are encountered in the U.S. (see reference 79 and volume II of this report series). Similar performance with LCB has been observed in California, where concrete pavement sections constructed on LCB show significantly less faulting than comparable sections placed on CTB or ATB.<sup>(80)</sup> Because of their outstanding performance, California now requires the use of a drained LCB on all high-trafficked JPCP pavements, along with doweled joints and a thick granular subbase.<sup>(64)</sup> Similarly, as seen in this study, Georgia has constructed doweled JPCP over an LCB and an 8-in (203-mm) granular base that have performed very well. However, because of the increased foundation stiffness, shorter joint spacings (15 ft [4.6 m] maximum) are generally required to reduce the possibility of transverse cracking due to thermal curling effects.

As with the use of permeable bases, consideration must be given to the additional construction cost of lean concrete bases. According to a recent survey, the use of a

lean concrete base in lieu of a conventional dense-graded aggregate base increases the construction cost by an average of 22 percent.<sup>(48)</sup>

### *Stabilized (Cement and Asphalt) Bases*

Stabilized base courses may be placed under concrete pavements to increase support, reduce susceptibility to moisture and erosion, and to provide a strong working platform for paving operations. Both asphalt- and cement-treated bases have been used successfully under concrete pavements.

Cement-treated and asphalt-treated bases may consist of either plant-mixed or road mixed materials, although plant-mixed materials are recommended. Agency-approved aggregates and gradations should be used in the mixture, with granular materials preferred. In order to increase the erodibility resistance of these materials (and hence the overall quality of the mixtures), a minimum of 8 percent cement and 6 percent asphalt is recommended.<sup>(75,76)</sup> Thicknesses of 4 to 6 in (102 to 152 mm) generally have worked well for both base types.

The asphalt grade used in asphalt-treated bases will depend on the climate, and should be consistent with the grade the highway agency uses for its conventional hot-mix AC pavements. Hot-mixed asphalt-treated bases are preferred, with a minimum 6 percent asphalt and a minimum Marshall stability of 500. If hot weather is expected during the paving operation, a lime slurry "whitewash" of the base course may be required to prevent excessive heat buildup in the base layer which can cause shrinkage cracking in the concrete slabs. For the best results, the whitewash should be applied one day before the concrete placement.

Cement-treated base courses often are required to meet a minimum unconfined compressive strength requirement, primarily to ensure resistance to freeze-thaw damage. Commonly, 7-day compressive strengths between 400 and 750 lb/in<sup>2</sup> (2.8 and 5.2 MPa) are specified. Again, to increase the erosion resistance of the base, a minimum 8 percent cement is recommended.

Because of increased stiffness of stabilized bases, shorter transverse joint spacings (15 ft [4.6 m] or less) may be required to minimize slab curling effects. However, the increased stiffness of the base also can reduce slab stresses under loading. For example, in a recent instrumentation study, it was found that the presence of a 7-in (178 mm) existing AC pavement beneath an 11.25-in (286 mm) JPCP significantly reduced slab load stresses even though no specific actions were taken to promote bond.<sup>(81)</sup> Consideration should also be given to the use of a thick granular subbase beneath the stabilized base to increase support and minimize pumping.

The performance of stabilized bases has been mixed. On many projects containing stabilized bases, pumping, erosion, and faulting erosion have been observed. In these cases, the stabilized bases were unable to prevent moisture damage. On other projects, excessive transverse slab cracking has been observed, presumably due to larger thermal curling stresses when layers are separated.

Increased stabilizer contents, improved joint load transfer design (including the use of dowels on all pavements except those on very low traffic roadways), and shorter joint spacings in combination are believed necessary for the improved effectiveness of stabilized bases. In addition, the use of a granular subbase material beneath the stabilized base course is considered critical to the performance of the pavement under medium and high traffic volumes.

### *Dense-Graded Aggregate Bases*

Dense-graded aggregate bases have been the traditional base course material placed beneath concrete pavements. In the early days of concrete road building, research studies indicated the susceptibility to pumping of concrete pavements placed directly on the subgrade, and it was found that the placement of a granular base course beneath the slab helped to alleviate (but did not always totally eliminate) that problem. Dense-graded base course thickness of 6 in (152 mm) are commonly used to provide a stable construction platform.

Dense-graded bases are generally granular materials consisting of high-quality crushed stone or gravel. A certain amount of fines are present in the base course to add some stability and aid in the placement of the material. Recommended gradations for dense-graded bases are provided in reference 82. Other recommendations included in reference 82 include limiting the fraction passing the No. 200 sieve to two-thirds of the fraction passing the No. 40 sieve, limiting the liquid limit to 25, limiting the plasticity index to 6, and providing compaction to 95 percent relative density (following AASHTO T180, method D).

Performance evaluations of pavements that have been constructed on dense-graded aggregate base course show some susceptibility to pumping and erosion. Results from the AASHTO Road Test showed that the dense-graded aggregate base pumped extensively, ultimately causing the failure of most of the JCP sections.<sup>(83)</sup> Erodibility tests conducted by PIARC indicate most unbound, dense-graded aggregate base courses to be very erodible.<sup>(75,76)</sup> Nevertheless, because of reduced stiffness and frictional qualities, pavements constructed over dense-graded based performed fairly well in this study under moderate traffic loadings. Furthermore, it is worth noting that one section in this study that was constructed on a dense-graded aggregate base (NJ 2) was 41 years old at the time of survey and had sustained over 35 million ESAL applications, and was still exhibiting good performance. This is probably due to a combination of some drainability of the base, durable materials, presence of a subbase material, and effective expansion joint design (1.25-in [32-mm] diameter dowels with stainless steel sleeves).

For aggregate base courses on medium to high traffic routes, the use of a thick subbase is recommended to provide additional support to the pavement structure and to increase vertical drainage of the base. A subbase will also provide sufficient support in the future to allow recycling or reconstruction of the pavement structure without additional base/subgrade corrections that might be required if only a dense-graded base course had been placed over the subgrade.

## Shoulder Type/Edge Support

Traffic loading at the outside edge and corner of a PCC pavement produce critical stresses and deflections in the slab. Depending upon their magnitude, these critical stresses and deflections can have a significant effect on the performance of the pavement, most notably in the development of transverse fatigue cracking and transverse joint faulting.

Several design alternatives have been employed to reduce the magnitude of these critical edge stresses and corner deflections. One means is through the addition of a concrete shoulder that is tied to the mainline pavement; this serves to provide lateral support to the mainline pavement, thereby reducing the magnitude of the edge stresses and corner deflections. Concrete shoulder also provide an easily maintained lane-shoulder joint that eliminates the continual maintenance problems associated with PCC mainline-AC shoulder joints.

Another design alternative for reducing critical edge and corner stresses is to construct widened PCC slabs, in which the outer lane is constructed 13 to 14 ft (4.0 to 4.3 m) wide but the painted traffic lane width is maintained at 12 ft (3.7 m). This moves the traffic away from the slab edge, thereby producing a more interior loading condition and providing a significant reduction in pavement stresses and deflections.

If properly designed and constructed, both of these methods can positively contribute to the performance of the pavement. In this study, the use of widened PCC slabs appears to be more effective than tied PCC shoulders in enhancing pavement performance, although many of the widened PCC slab sections have not experienced significant traffic loadings. Nevertheless, there are certain instances where the use of a tied PCC shoulder may be more appropriate. General guidelines on the use of these edge support features and shoulders are presented in table 30.

Table 30 shows that the use of widened PCC slabs is recommended for most rural Interstate-type PCC pavement construction. The cost of constructing widened PCC slabs is about 2 percent greater than a conventional 12-ft (3.6-m) slab width design with AC shoulders.<sup>(48)</sup> This is an insignificant cost when compared to the benefits that are derived.

Table 30 shows that a tied PCC shoulder is recommended for most Interstate-type pavements in urban areas to provide lateral support to the mainline pavement and for the possibility of serving as a emergency travel lane (in case of accidents or during maintenance/rehabilitation activities). The cost of adding a PCC shoulder in place of an AC shoulder ranges from about 13 to 21 percent, depending upon the thickness of the PCC shoulder.<sup>(48)</sup> Additional information on the various types of PCC shoulder construction are provided in the next section.

Although widened PCC slabs are most ideally suited for rural conditions (and in conjunction with an AC shoulder), they could also be used in urban areas with or

without a tied PCC shoulder. For example, Germany uses this combination design on their high-volume roadways (see figure 135) and report good performance.<sup>(39)</sup>

As table 30 shows, widened PCC slabs and tied PCC shoulders are also recommended for arterial roadway classifications because of the potential performance improvements. However, on lower volume roadways, the potential benefits of these design features may not be fully realized so their use may not be as appropriate in those situations.

Because both widened PCC slabs and tied PCC shoulders reduce critical slab stresses and deflections, their incorporation on a design project suggests that a thinner PCC slab may be appropriate. Although this is true strictly from a fatigue damage standpoint, this practice is not currently recommended. The effect of widened PCC slabs and tied PCC shoulders on slab cracking is discussed in a later section.

General recommendations on the design and construction of the two edge support methodologies are provided in the following sections.

#### PCC Shoulder Design Recommendations

The use of tied PCC shoulders has grown considerably in the last few years, but evaluations of their effectiveness have shown mixed results. In this study, for example, low load transfer across the lane-shoulder joint was observed on several sections, suggesting an ineffective tie bar system. Similarly, in a study of CRCP

Table 30. General recommendations on use of shoulder type/edge support.

Functional Class	Recommended Shoulder Type/Edge Support	
	Rural	Urban
Interstates/Freeways	<ol style="list-style-type: none"> <li>1. Widened Lane with AC Shoulder</li> <li>2. PCC Shoulder (paved monolithically)</li> </ol>	<ol style="list-style-type: none"> <li>1. PCC Shoulder (paved monolithically)</li> <li>2. Widened Lane with PCC Shoulder</li> </ol>
Arterials	<ol style="list-style-type: none"> <li>1. Widened Lane with AC Shoulder</li> <li>2. PCC Shoulder</li> <li>3. None (AC Shoulder)</li> </ol>	<ol style="list-style-type: none"> <li>1. PCC Shoulder (paved monolithically)</li> <li>2. Widened Lane with PCC Shoulder</li> </ol>
Collectors	<ol style="list-style-type: none"> <li>1. None (AC, Gravel, or Turf Shoulder)</li> </ol>	<ol style="list-style-type: none"> <li>1. PCC Shoulder</li> <li>2. Curb and Gutter</li> </ol>
Locals	<ol style="list-style-type: none"> <li>1. None (Gravel or Turf Shoulder)</li> </ol>	<ol style="list-style-type: none"> <li>1. PCC Shoulder and Curb and Gutter</li> <li>2. Curb and Gutter</li> <li>3. None (AC, Gravel, or Turf Shoulder)</li> </ol>

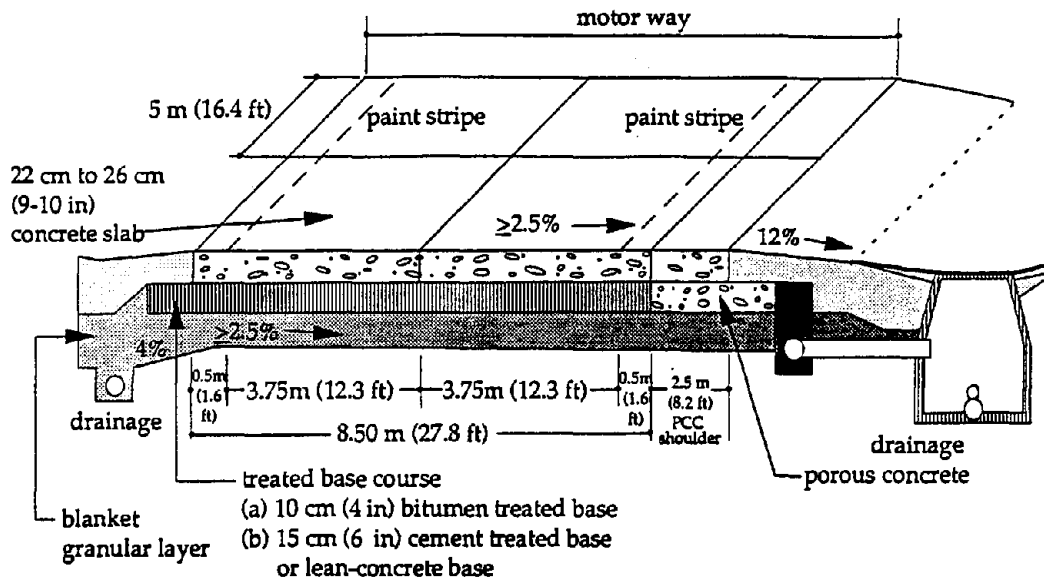
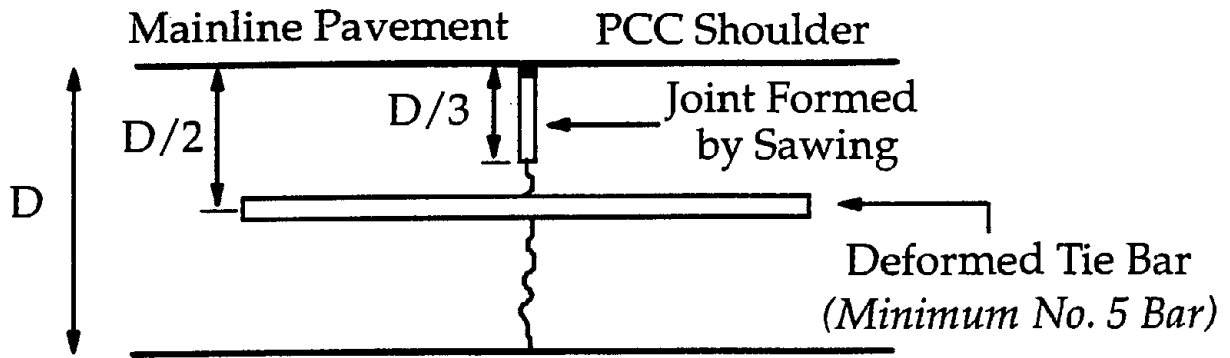


Figure 135. German JPCP design showing widened PCC slab and PCC shoulders.<sup>(39)</sup>

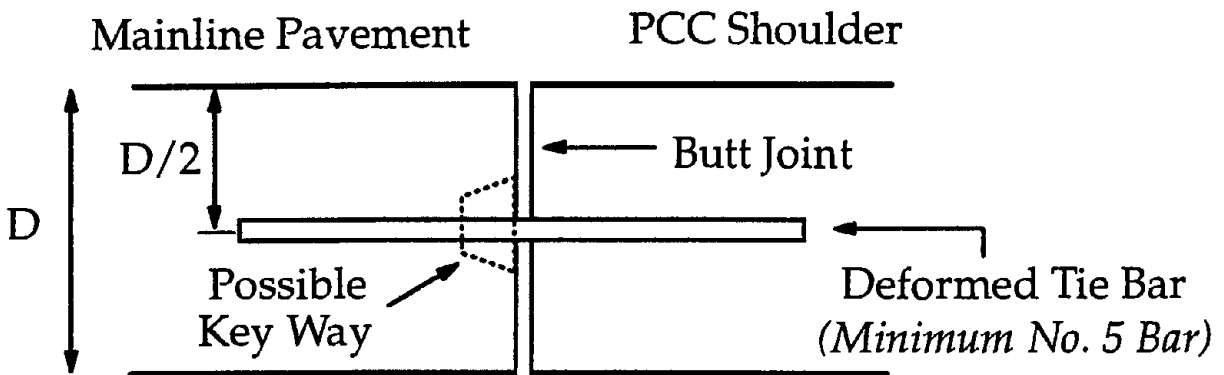
performance, it was found that the tied PCC shoulders did not appear to have a significant impact on reducing edge deflections, again perhaps due to a poor tie bar design.<sup>(84,85,86)</sup>

The effectiveness of PCC shoulders in improving concrete pavement performance is a function of both the method in which they are constructed and the competency of the tie bar design used to secure the shoulders to the mainline pavement. In broad terms, PCC shoulders can be constructed in one of three ways (see figure 136):

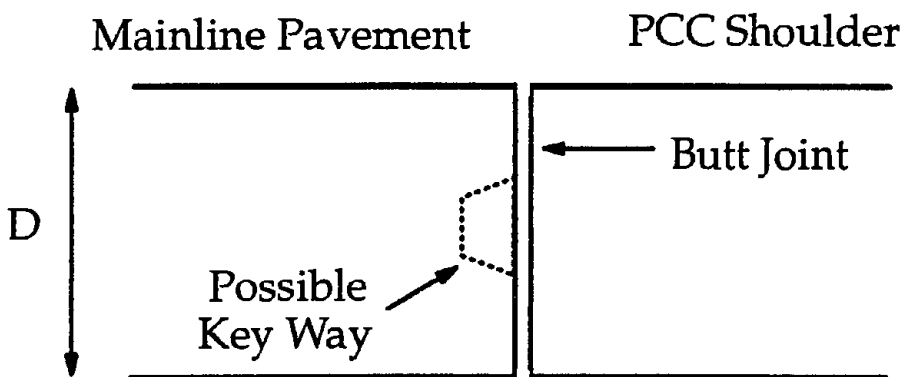
1. Tied PCC shoulder constructed monolithically with the mainline pavement. In this case, the full width of the pavement (including the shoulders) is paved in a single pass, with tie bars set on the grade ahead of the paving or inserted into the plastic concrete at the prescribed intervals. The longitudinal lane-shoulder joint is then later sawed to a depth of one-third of the slab thickness directly above the tie bars, creating a longitudinal weakened plane or warping joint. Because of the monolithic paving, aggregate interlock load transfer is present along the joint in addition to the support provided by the tie bars. This method is considered the most effective means of providing lateral support to the mainline pavement and is highly recommended.
2. Tied PCC shoulder placed after the paving of the mainline pavement. This method is more commonly used in PCC pavement construction and involves "tying in" a PCC shoulder to the mainline pavement at some time after the



**PCC Shoulder Paved Monolithically**



**PCC Shoulder Paved Separately (tied)**



**PCC Shoulder Paved Separately (not tied)**

Figure 136. Types of PCC shoulder construction.



mainline pavement has been placed. One way of accomplishing this is to have bent tie bars mechanically inserted at the outside edge of the pavement; the bars are bent so they do not impede on construction activities and straightened immediately before placement of the PCC shoulder (if bending of the bars is to be allowed, Grade 40 steel is recommended). Other alternatives include two-piece threaded tie bar systems or drilling holes in the hardened mainline pavement and grouting in tie bars prior to the placement of the PCC shoulder. The performance of tied PCC shoulders constructed after the placement of the mainline pavement have shown mixed results, with the effectiveness of this procedure much more dependent upon a competent tie bar design (tie bar diameter and spacing). Pull-out tests (as described in reference 87) of the tie bars are recommended to help ensure both sufficient embedment lengths and adequate bonding.

In this type of construction, keyways are sometimes used in PCC lane-shoulder joints. Keyways are small grooves or protrusions formed by a groover inside the side plates of the paver; they are often added to help provide load transfer across the lane-shoulder joint. However, because they often shear off under traffic loading (resulting in cracking/spalling over the length of the joint), their use is not recommended.

3. PCC shoulder (generally paved separately from the mainline pavement) not tied to the mainline pavement. In this case, no positive means of tying the PCC shoulder to the mainline pavement are employed; rather, the shoulder is merely placed adjacent to the mainline pavement. Rarely used, this design provides little (if any) lateral support to the mainline pavement and has not been effective.<sup>(88)</sup> Consequently, this design is not recommended.

The tie bar system used to secure the PCC shoulder to the mainline pavement is a critical component of their design; of particular importance is the tie bar diameter and the spacing between adjacent tie bars. Based on the results of this study, No. 5 bars (0.62 in or 16 mm diameter) are recommended as the minimum size bars to tie the PCC shoulders to the mainline pavements; No. 4 bars (0.5 in or 13 mm diameter) were shown to be inadequate in many cases. Larger diameter bars may be required on heavy truck routes, particularly on ramps, truck lanes, or other merging areas where trucks frequently cross the longitudinal joints. Maximum spacing limits of 30 to 36 in (762 to 914 mm) are recommended in order to provide adequate support to the mainline pavement.

Tie bars should be deformed in order to effectively tie the shoulder to the mainline pavements. Tie bar lengths of 30 in (762 mm) are recommended, as is epoxy-coating of the bars to help prevent corrosion. As described previously, pull-out tests of tie bars are suggested to ensure sufficient embedment lengths and to ensure adequate bonding.

It is recommended that the thickness of the PCC shoulder be the same as that of the mainline pavement. This helps reduce the possibility of differential frost heave in

cold regions (as described in reference 89), and also provides a sufficient structure that can be used as a travel or emergency lane during maintenance or rehabilitation activities. California has recently adopted the use of PCC shoulders (of the same structural thickness as the mainline pavement) for all new PCC pavement construction.<sup>(52)</sup>

The transverse joints in the PCC shoulder should match those of the mainline pavement in order to prevent "sympathetic" cracking in the mainline pavement from joints in the shoulder. If the PCC shoulders are envisioned to carry significant truck traffic at some point in time (during rehabilitation of the mainline pavement, for example), consideration should be given to doweling the joints, a practice followed in Germany.<sup>(40)</sup>

### Widened PCC Slab Recommendations

Pavements evaluated in this study containing widened PCC slabs show outstanding performance, exhibiting low faulting and very few transverse cracks. Table 31 summarizes the various projects from this study that incorporate widened PCC slabs. This table shows that the sections are performing very well, although many are not that old and have not been exposed to substantial traffic loadings.

Table 31. Summary of performance data for sections with widened lanes.

Project	Lane Width	Age, Years	ESAL's, millions	Faulting, in	Deter Cracks/mi	Longitudinal Cracks, ft/mi	% Joints Spalled	IRI, in/mi (PSR)
CA 8	14	9	9.1	0.05	0	0	17	148 (4.0)
FL 2	14	6	9.5	0.05	0	0	7	93 (3.7)
MN 3	14	8	3.7	0.01	0	0	0	100 (4.2)
MN 4	14	6	0.9	0.01	0	0	1	149 (4.4)
MN 6	14	9	2.0	0.01	5	0	3	143 (4.2)
WI 1	14	2	5.0	0.01	0	0	0	99 (3.8)
WI 2	14	4	1.3	0.01	0	0	3	117 (4.0)
WI 5	14	4	1.4	0.05	2	91	8	139 (3.8)
WI 6	14	4	4.2	0.03	0	0	6	87 (3.9)
WI 7	14	4	1.3	0.03	2	58	5	119 (4.1)
WV 1	15	1	3.7	0.04	10	0	67	168 (3.4)

1 in = 25.4 mm; 1 ft = 0.305 m; 1 mi = 1.61 km

Widened PCC slabs have also been used extensively in Europe. For example, Germany and France both widen their PCC slabs by 1.6 ft (0.5 m), and indicate

improvements in pavement performance.<sup>(39)</sup> Also, an experimental pavement project in Belgium showed that widened lanes and doweled joints significantly improved pavement performance.<sup>(90)</sup>

Because of the possibility of longitudinal cracking, it is recommended that widened PCC slabs be limited to widths of 14 ft (4.3 m) or less. Furthermore, analytical data indicate that for slab widths greater than 14 ft (4.3 m), the accompanying reduction in stresses and deflections is quite small, meaning that there is little structural benefit to widening slabs more than that width. This is illustrated in figure 137, which illustrates the normalized slab stresses (normalized to the maximum edge stress and calculated at the mid-point between the joints and under a 9000-lb [40-kN] dual wheel load at different locations from the slab edge) as a function of the load distance from the pavement edge.<sup>(81)</sup> This figure shows the maximum stress occurs when the load is at the edge (0 distance from the slab edge to the outside of the dual tires), and also illustrates reductions of 12, 22, and 30 percent in the edge stress when the load is moved in by only 2, 4, and 6 in (51, 102, 152 mm), respectively.

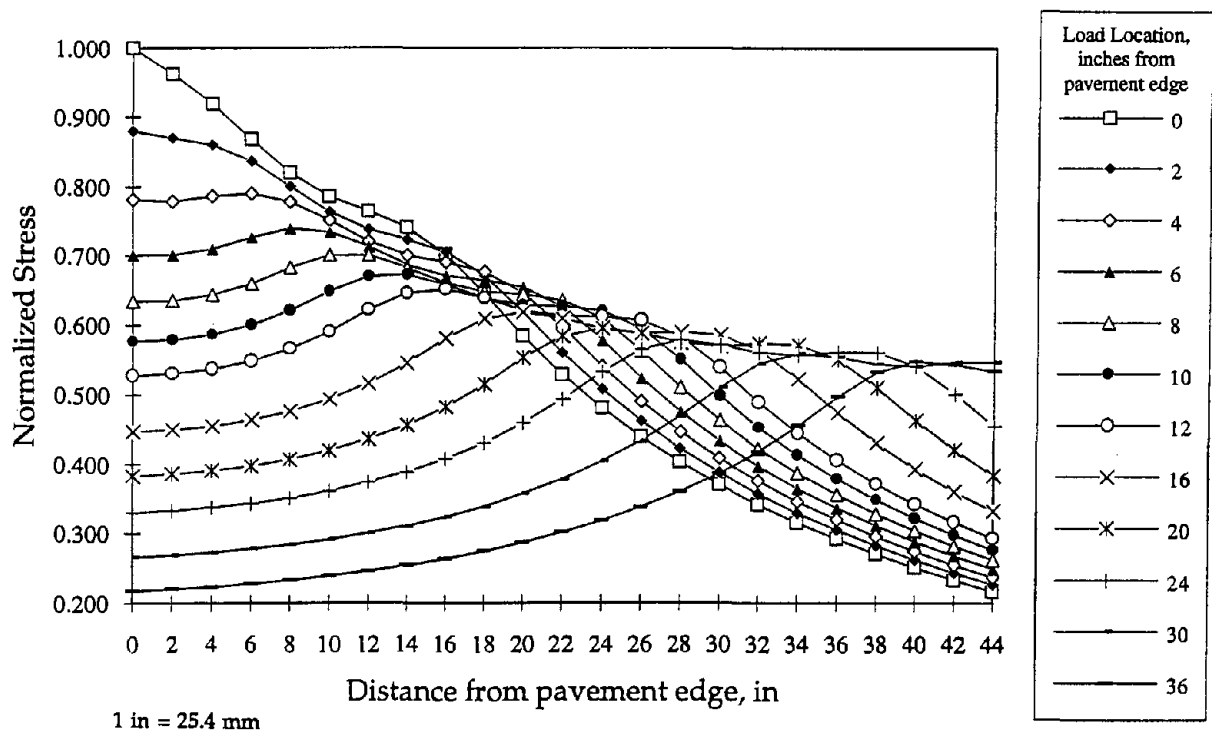


Figure 137. Normalized edge load stress distribution across a slab under varying load locations.<sup>(81)</sup>

Figure 137 also indicates how the critical stress location shifts as the load is moved away from the slab edge. For example, if the load is shifted 6 in (152 mm) away from the slab edge, the critical stress is no longer at the slab edge but rather at a point about 10 to 12 in (254 to 305 mm) away from the slab edge. As the load

continues to be moved away from the slab edge, the magnitude of the maximum stress is reduced, with the greatest reductions occurring to about 24 in (610 mm). At load locations greater than 24 in (610 mm) from the slab edge, the maximum stress continues to decrease, although not as drastically.

The effects of widened PCC slabs were found to be strongly significant in the development of the joint faulting and JPCP slab cracking models described in chapter 2. For example, figure 138 illustrates the effect of widened PCC slab on the development of faulting in a 10-in (254-mm) doweled pavement. The faulting of the widened PCC slab section is about two-thirds of the nonwidened PCC slab. Widened PCC slabs offer similar benefits to transverse slab cracking in JPCP, as discussed in the *Slab Thickness* section.

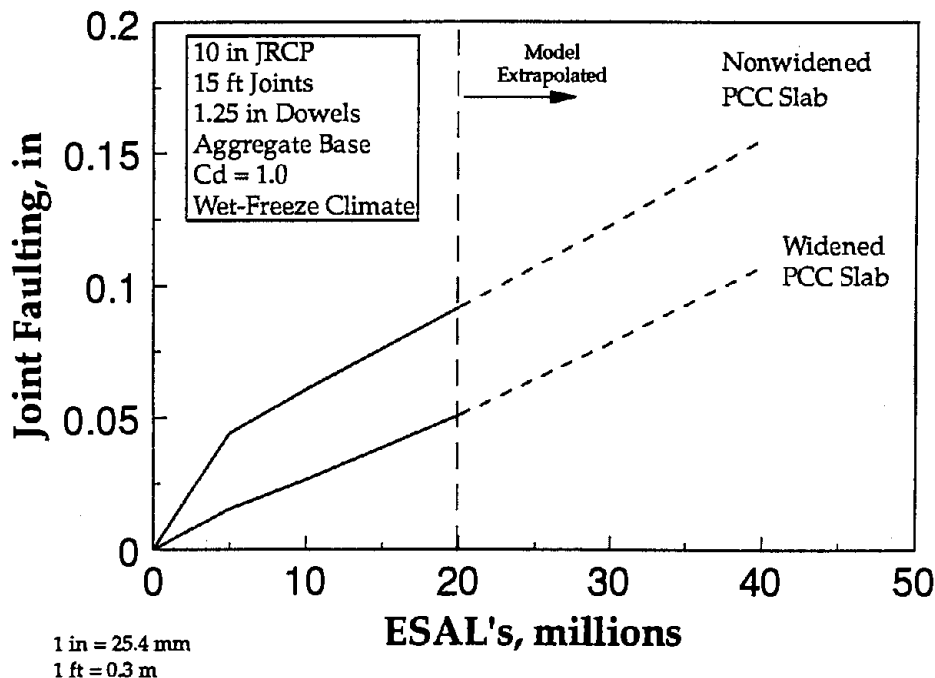


Figure 138. Effect of widened slab on doweled joint faulting.

### Transverse Joint Design

Transverse joints are placed in jointed concrete pavements to relieve internal slab stresses caused by shrinkage, temperature and moisture gradients, and frictional restraint from the underlying base course, stresses that can all lead to the development of random, uncontrolled cracking in the slab. While transverse joints are a necessary and integral part of concrete pavement design and construction, there are many problems associated with their design, construction, and performance. Indeed, the performance of many jointed concrete pavements has historically not been driven by its structural capacity, but rather by its joint design. Excessive joint spacing, insufficient joint load transfer design, and inadequate joint reservoir design

are examples of critical joint design factors that have impaired the performance of many jointed concrete pavements.

Transverse joint design consists of many different design elements, including sawcut depth, joint spacing, uniformity of joint spacing, joint orientation, load transfer, and joint sealant. An effective joint design, specifically addressing each of these three subjects, is needed in order to ensure the long-term performance capabilities of a jointed concrete pavement. Each of these factors is discussed below.

### *Sawcut Depth*

In the construction of the transverse joint, it is important that the depth of the sawcut in a slab be deep enough to ensure the formation of the crack beneath it. However, in order to achieve maximum joint sawing production rates, it is desirable to saw to the minimum depth necessary to ensure the formation of the crack. Also, on nondoweled joints, it is desirable to limit the depth of sawing in order to provide a greater aggregate interlock load transfer.

Conventional practice has been to saw transverse joints to a depth of 25 percent of the slab thickness. While this depth has worked well in most cases, the type of underlying base course may also have an affect on the required depth of sawing. Stabilized bases produce more friction between the slab and the base, and therefore can induce larger tensile stresses in the slab. In addition, slabs placed on permeable bases often end up slightly thicker than the design thickness due to the open texture of the base course material. Thus, to ensure the formation of the crack, the sawcut depth of transverse joints may need to be greater for slabs placed on stabilized and permeable bases (say, 33 percent of the slab thickness).

Another way to address the problem associated with friction caused by stabilized bases is to notch the surface of the treated base course at the prescribed transverse joint spacings to ensure the formation of the cracks at that location in the treated base. This practice is routinely conducted in Germany on their cement-treated bases.<sup>(40)</sup> After placement of the pavement on top of the base, Germany specifies that the joints in the PCC slab be sawed to 30 percent of the slab thickness.<sup>(40)</sup>

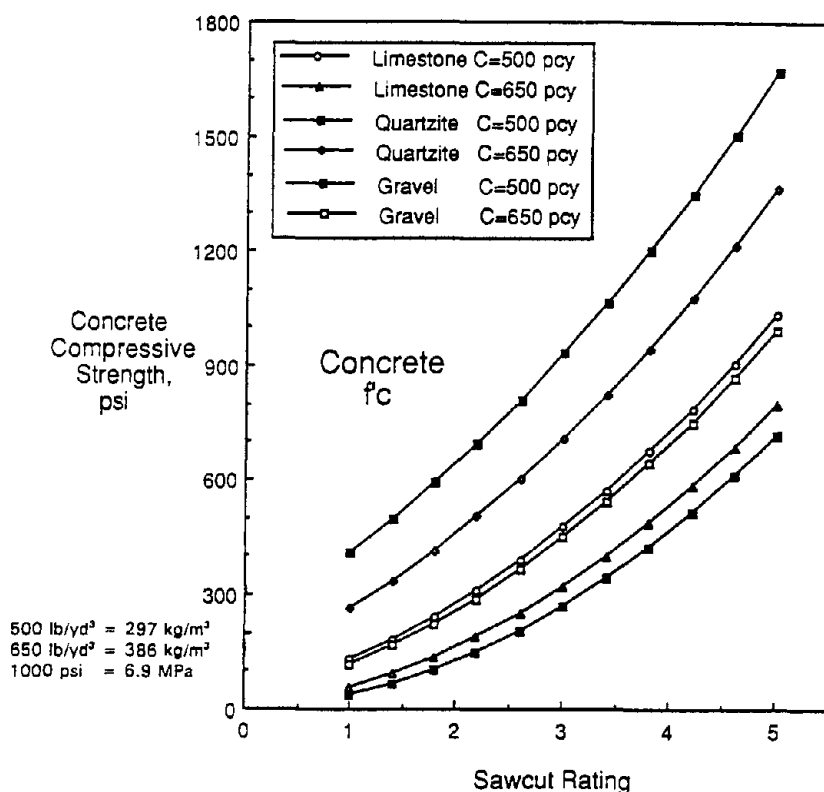
For initial sawcutting operations, most joints are sawed to a width of 0.125 in (3 mm) prior to widening for joint reservoir. Some saw blade manufacturers now produce a blade that can produce the initial sawcut and the reservoir sawcut in a single pass.

### *Sawcut Timing*

A critical aspect of the joint sawing operations is the timing of the actual sawing of the slab. If this sawing is performed too early (i.e., before the slab has hardened sufficiently), spalling or raveling of the joint can occur. On the other hand, if the joint sawing is performed too late (after the development of internal slab stresses), uncontrolled cracking will develop. Since the occurrence of the latter is of more

critical concern than the former, it is desirable to begin sawing as soon as possible, generally within 4 to 12 h.

A recent FHWA research study was conducted on identifying the earliest time (near limit) and the latest time (far limit) that joint sawing operations could be performed.<sup>(91,92)</sup> For the near limit, or the earliest time that sawing could be conducted, that study correlated the compressive strength of different concrete mixes to the desired rating (appearance) of the joint sawcut.<sup>(91)</sup> These results are illustrated in figure 139, where the joint ratings are defined. Generally, a minimum rating of 3 would be desired if sealant reservoir widening is to be done. For example, for a mix with a cement content of 650 lb/yd<sup>3</sup> (386 kg/m<sup>3</sup>) and a quartzite aggregate, a compressive strength of 700 lb/in<sup>2</sup> (4.8 MPa) is required before sawing. Harder aggregates (e.g., quartzite) require greater compressive strengths than softer aggregates (e.g., limestone). The reason that lower cement contents require greater strengths is because of the lower volume of cement paste.



**Sawcut ratings:**

- 1 = badly spalled
- 2 = unacceptable
- 3 = acceptable if widening is to be done
- 4 = good
- 5 = excellent

Figure 139. Sawcut rating as a function of compressive strength.<sup>(91)</sup>

In order to use the relationship in figure 139, an estimate of the concrete compressive strength is needed. This can be determined by testing cylinders cast from the mix at early ages or by nondestructive means such as maturity monitoring or pulse-velocity testing.

The far limit, or the latest time that sawing can be done to prevent the occurrence of random cracking, is dependent upon the development of restraint stresses in the slab. These restraint stresses primarily are made up of frictional restraint stresses and thermal curling stresses. During the first 24 h of paving, the concrete slabs are very sensitive to the development of restraint stresses.<sup>(91)</sup> Field observations and testing has shown that a primary indicator of the latest time that sawing can be performed is when the temperature of the concrete surface cools more than 15 °F (8 °C).<sup>(91)</sup> However, because of the difficulty in determining that time, and because the surface may cool off very rapidly (due to late afternoon cooling, rainshowers, and so on), it is recommended that joint sawing be performed as soon as the concrete can be sawed without significant raveling of the joints. This is particularly true for slabs placed on stabilized bases, since these pavements can develop greater frictional restraint stresses. Additional time for sawcutting may be made available for sawcutting if paving is performed at night or very early in the morning (completing by 10 or 11 a.m.) to minimize the development of temperature gradients through the slab.<sup>(91)</sup>

In the past, some agencies have used skip joint sawing procedures, in which only every second or third joint is initially sawed. This is usually done in an effort to keep up with the paving operation, and the skipped joints are sawed later. However, this practice can result in the development of transverse cracks at or near the joints that were skipped, particularly on slabs over stabilized bases. Also, the joints sawed first are typically wider, creating nonuniform joint movements and variable performance of joint sealants.

#### *Transverse Joint Spacing—JPCP Pavements*

Transverse joints are needed in JPCP to control random cracking that would occur from excessive shrinkage and curling stresses if joints were not provided. Shrinkage and curling stresses in concrete slabs increase rapidly with increasing joint spacing. To obtain the desired performance, transverse joints must be provided at appropriate intervals to limit the critical stresses to an acceptable level. Along with slab thickness, concrete strength, and edge support (tied PCC shoulders and widened slab) transverse joint spacing is a key design factor affecting cracking performance of JPCP.

One way of determining the appropriate joint spacing is to conduct a fatigue analysis. In general, stresses in pavement slabs decrease with decreasing joint spacing because curling stress decreases; however, no fatigue advantages can be gained by using a joint spacing less than 12 ft (3.7 m). The use of slabs shorter than 12 ft (3.7 m) is also not recommended because short slabs tend to rock under heavy traffic (particularly if they are not doweled). The FHWA recommends maximum joint spacings of 15 ft (4.5 m) for JPCP.<sup>(93)</sup> However, longer joint spacings may be

considered for thicker slabs, and if acceptable performance can be demonstrated through current performance or a fatigue analysis, joint spacings of up to 20 ft (6.1 m) may be desirable (particularly for pavements placed on nontreated bases).

The base type and the subgrade  $k$  have a significant effect on stresses in pavement slabs: the stiffer the foundation, the greater the curling stress. Therefore, concrete pavements constructed on stiff subgrades or on a stabilized base require shorter joint spacing. A shorter joint spacing may also be required when a stabilized base is used. A stabilized base has a similar effect on curling stresses as a stiff foundation if the base is not bonded to the pavement slab. If the design procedure being used does not account for curling stresses in determining the required slab thickness, then a conservative joint spacing should be used to ensure acceptable performance. This may be accomplished by selecting the joint spacing recommended for higher  $k$ -values.

The guidelines for JPCP joint spacings are often given in terms of the ratio of the slab length to the radius of relative stiffness ratio,  $L/\ell$ . However, as shown in figure 140, the correlation between  $L/\ell$  and the amount of slab cracking is very approximate. The theoretical relationship between  $L/\ell$  and slab cracking depends on the  $k$ -value, concrete modulus of elasticity, and slab thickness. Furthermore, the limits on maximum  $L/\ell$  values will also vary with climate. However, within a narrow range of values for these parameters, it may be possible to establish workable guidelines based on  $L/\ell$ .

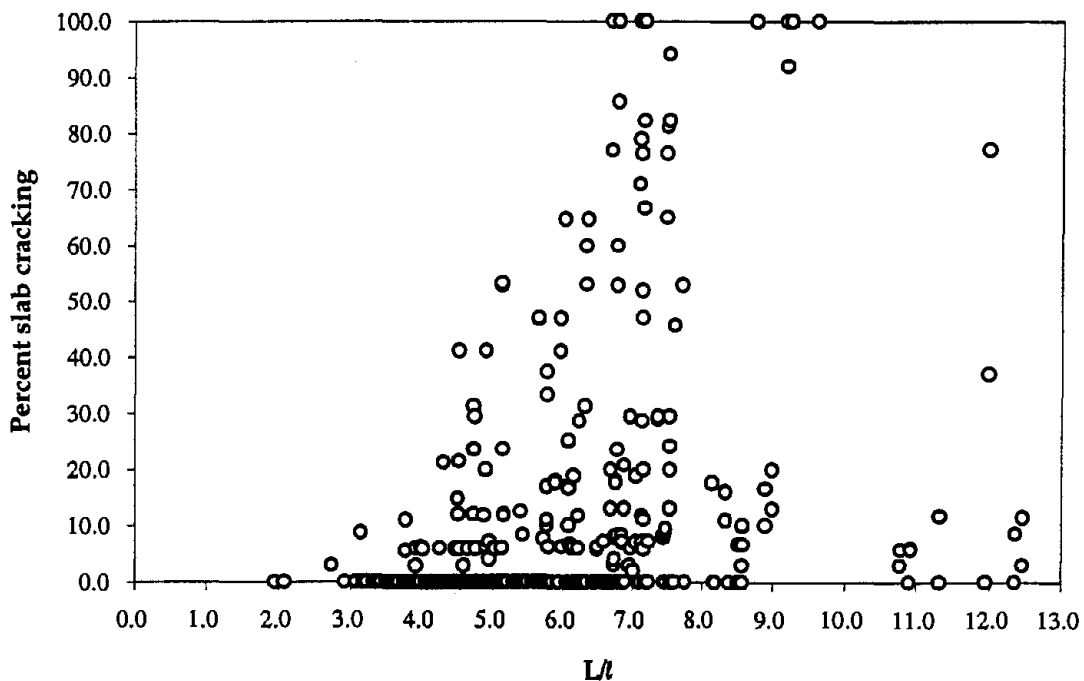


Figure 140. Cracking performance as a function of  $L/\ell$ .



Figure 140 shows that, for highway pavements, satisfactory performance may be achieved by keeping  $L/\ell$  less than about 4.5. In general, adequate cracking performance can be obtained if  $L/\ell$  is kept less than about 4.5; however, the  $L/\ell$  limit of 4.5 is overly conservative for thick slabs (10 in [254 mm] or thicker) and for a very stiff foundation (dynamic  $k$ -value greater than about 400 lbf/in<sup>2</sup>/in [108 kPa/mm]). And, as previously indicated, the  $L/\ell$  limits will also vary by climatic region.

Because of these limitations, it is believed that the best way of determining the maximum joint spacing for JPCP is based on computing expected fatigue damage. Such an analysis has been conducted, and recommended maximum joint spacings are provided in table 32 for a range of key design features. These results are based on the cracking model presented in chapter 2 and consider the effects of thermal curling and built-in construction curling.

### *Transverse Joint Spacing—JRPC Pavements*

The primary concern for joint spacing in JRPC is the joint performance. Although joint spacings of up to 100 ft (30 m) have been used in the past, the current trend is to use much shorter joint spacing. The shorter joint spacing reduces horizontal slab movements, which the effects of dowel misalignment and joint lock up less critical.<sup>(93)</sup> Less slab movements also put less stress on joint sealant systems, allowing them to function more effectively over time.

The JRPC projects evaluated under this study showed mixed results when evaluating the effect of joint spacing. While most of the shorter-jointed JRPC designs (less than 30 ft [9.1 m]) displayed good performance, a few did not. On the other hand, many of the longer-jointed JRPC designs (greater than 60 ft [18.2 m]) also performed fairly well, although there were only a few sections in that category.

In light of these mixed findings, it is difficult to make a recommendation regarding joint spacings for JRPC. Recent trends have been toward the use of shorter joint spacings in order to reduce the amount of slab movement and to provide a more easily sealed and maintained transverse joint design. The FHWA currently recommends a maximum joint spacing of 30 ft (9.1 m) for JRPC.<sup>(87)</sup> However, this recommendation should be tempered with local experience.

### *Uniformity of Joint Spacing*

Traditionally, joints in concrete pavements have been placed at uniform intervals. However, in the late 1950's, research was conducted on the effect of the faulting of uniformly spaced joints on the rideability of the pavement.<sup>(94)</sup> The study determined that faulting of uniformly spaced joints produced a rhythmic response in certain full-sized automobiles, significantly affecting the rideability of the pavement. It was found that this response was reduced the most by employing a nonuniform joint spacing of 12-13-19-18 ft (3.7-4.0-5.8-5.5 m). It was further indicated that slab spacing patterns in multiples of 7.5 ft (2.3 m) should be avoided.

Table 32. Recommended maximum joint spacings for JPCP designs.

Design	ESAL's =	E <sub>pcc</sub> =	Slab	Dry-Freeze			Dry-Nonfreeze			Wet-Freeze			Wet-Nonfreeze		
				Subgrade k, 1bf/in <sup>2</sup> /in			Subgrade k, 1bf/in <sup>2</sup> /in			Subgrade k, 1bf/in <sup>2</sup> /in			Subgrade k, 1bf/in <sup>2</sup> /in		
				100	200	400	100	200	400	100	200	400	100	200	400
2 million	3 million	1bf/in <sup>2</sup> /in	6-in Slab	12	12	12	12	12	12	12	12	12	12	12	12
			7-in Slab	12	14	14	12	14	14	12	14	14	12	12	14
			8-in Slab	16	16	16	16	16	16	16	16	16	16	16	16
	5 million	1bf/in <sup>2</sup> /in	6-in Slab	12	12	12	12	12	12	12	12	12	12	12	12
			7-in Slab	12	12	14	12	12	12	12	12	12	12	12	12
			8-in Slab	16	16	16	14	15	16	15	15	16	13	13	13
5 million	3 million	1bf/in <sup>2</sup> /in	7-in Slab	12	14	14	12	12	14	12	12	14	12	12	12
			8-in Slab	16	16	16	15	16	16	16	16	16	14	16	16
			9-in Slab	18	18	18	18	18	18	18	18	18	18	18	18
	5 million	1bf/in <sup>2</sup> /in	7-in Slab	12	12	12	12	12	12	12	12	12	12	12	12
			8-in Slab	14	15	16	12	12	12	12	13	13	12	12	12
			9-in Slab	18	18	18	16	16	15	18	17	18	16	15	14
10 million	3 million	1bf/in <sup>2</sup> /in	8-in Slab	16	16	16	13	16	16	14	16	16	12	13	16
			9-in Slab	18	18	18	18	18	18	18	18	18	18	18	18
			10-in Slab	20	20	20	20	20	20	20	20	20	20	20	20
	5 million	1bf/in <sup>2</sup> /in	8-in Slab	12	13	14	12	12	12	12	12	12	12	12	12
			9-in Slab	18	18	18	15	14	13	16	15	15	14	14	13
			10-in Slab	20	20	20	19	18	17	20	19	19	18	17	15
20 million	3 million	1bf/in <sup>2</sup> /in	9-in Slab	18	18	18	18	18	18	18	18	18	16	18	18
			10-in Slab	20	20	20	20	20	20	20	20	20	20	20	20
			11-in Slab	20	20	20	20	20	20	20	20	20	20	20	20
	5 million	1bf/in <sup>2</sup> /in	9-in Slab	16	15	16	14	13	12	14	14	13	13	12	12
			10-in Slab	20	20	20	18	16	15	19	17	16	17	16	14
			11-in Slab	20	20	20	20	19	17	20	20	19	20	18	17
50 million	3 million	1bf/in <sup>2</sup> /in	10-in Slab	20	20	20	20	20	20	20	20	20	20	20	20
			11-in Slab	20	20	20	20	20	20	20	20	20	20	20	20
			12-in Slab	20	20	20	20	20	20	20	20	20	20	20	20
	5 million	1bf/in <sup>2</sup> /in	10-in Slab	18	17	16	16	15	13	17	15	14	16	14	13
			11-in Slab	20	20	19	19	17	15	20	18	17	19	17	15
			12-in Slab	20	20	20	20	19	17	20	20	19	20	19	17
100 million	3 million	1bf/in <sup>2</sup> /in	11-in Slab	20	20	20	20	20	20	20	20	20	20	20	20
			12-in Slab	20	20	20	20	20	20	20	20	20	20	20	20
			13-in Slab	20	20	20	20	20	20	20	20	20	20	20	20
	5 million	1bf/in <sup>2</sup> /in	11-in Slab	20	18	17	18	16	14	19	17	15	18	16	14
			12-in Slab	20	20	19	20	18	16	20	20	17	20	18	16
			13-in Slab	20	20	20	20	20	18	20	20	20	20	20	18

Note: k-values are dynamic values obtained directly from backcalculation (dynamic = 2\* static).

1in = 25.4 mm  
 1 lbf/in<sup>2</sup>/in = 0.276 Kpa/mm

Based on those findings, many agencies adopted nonuniform joint spacings (sometimes referred to as random joint spacings) in their JPCP designs in the 1960's and 1970's. Initially, the 12-13-19-18-ft (3.7-4.0-5.8-5.5-m) pattern was commonly used, but transverse cracking often occurred on the longer 19- and 18-ft (5.8- and 5.5-m) slabs. Consequently, shorter nonuniform joint spacings (such as 12-15-13-14-ft [3.7-4.6-4.0-4.3-m]) are more commonly used today, as illustrated in figure 141.

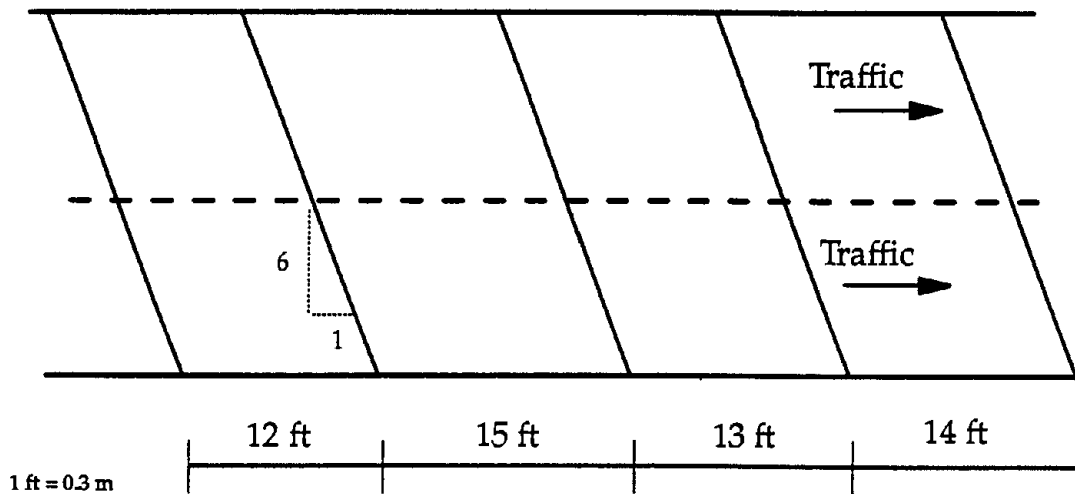


Figure 141. Example nonuniform joint spacing pattern (with skewed joints).

The results of this investigation did not reveal any strong advantages or disadvantages to the use of nonuniform joint spacings. If used, it is recommended that nonuniform joint spacings be kept relatively short without large differences in the length of the slabs that make up the joint spacing pattern.

Although many States currently employ nonuniform joint spacing in their JPCP designs, it is not known if their use is warranted for the wheelbases and suspension systems found on today's vehicles. It is also not known if nonuniform joint spacings are needed when dowel bars are specified in the design, since the dowel bars are expected to provide load transfer and reduce joint faulting. Because of the prevalence of dowels in JRCP and in most high-type JPCP, the use of nonuniform joint spacings on these design types may not be warranted.

#### *Joint Orientation*

Joint orientation refers to the angle of the transverse joint with respect to the centerline of the pavement. Perpendicular joints are constructed perpendicular to the centerline, whereas skewed joints are placed at an angle to the centerline, usually

offset about 2 ft (0.6 m) per 12-ft (3.7-m) lane in the counterclockwise direction (see figure 141). The purpose of skewing the transverse joint is so that the wheels of an axle do not cross the joint at the same time, thereby reducing the potential deflection at the joint.

Based on the results of this study, the use of skewed joints is recommended for nondoweled slabs (this corresponds to pavements designed for 5 million ESAL applications or less). In such designs, skewed joints have been observed to show less faulting than perpendicular joints. The direct performance comparisons of sections from this study with and without skewed joints are summarized in table 33. This table shows that sections with skewed joints show about one-half of the faulting levels as the sections with nonskewed joints (all joints are not doweled).

Table 33. Summary of effect of joint orientation.

Section	Skewed Joints	ESAL's, millions	Faulting, in	% Slabs Cracked	IRI, in/mi (PSR)
FL 4-2	yes	4.5	0.02	0	139 (3.8)
FL 4-7	no	4.5	0.07	0	110 (3.7)
FL 4-3	yes	4.5	0.04	0	122 (3.7)
FL 4-8	no	4.5	0.08	0	106 (3.6)
FL 4-6	yes	4.5	0.05	0	95 (3.7)
FL 4-9	no	4.5	0.11	1	125 (3.2)
NC 1-1	yes	16.0	0.13	11	111 (3.3)
NC 1-8	no	16.0	0.23	77	131 (3.3)
NY 1-8a	no	5.5	0.01	10	112 (4.2)
NY 1-8b	yes	5.5	0.03	7	111 (3.9)

1 in = 25.4 mm  
 1 ft = 0.305 m  
 1 mi = 1.61 km

Note: All sections contain nondoweled joints.

Because sections with skewed joints are also more susceptible to corner breaks, this suggests the need to limit the amount of skewing. Maximum skews of no more than 2 ft (0.6 m) per 12-ft (3.7-m) lane are recommended, with some suggesting a maximum skew of 1 ft (0.3 m) per 10-ft (3-m) of pavement width.<sup>(95,96)</sup>

If transverse joints are to be doweled, skewed joints are not recommended due to their reduced effectiveness.<sup>(97)</sup> In addition, dowel alignment problems may be more apt to occur in skewed joint construction.<sup>(96)</sup>

### *Load Transfer*

Transverse joint load transfer is the mechanism through which wheel loads are conveyed from one slab to the next. It is an important consideration in the design of concrete pavements because the effective transfer of the wheel load from one slab to the next will reduce significantly the magnitude of the stresses and deflections in the slab at the joints. This, in turn, will help to reduce such joint distresses as pumping, faulting, loss of support, and corner breaks.

The effectiveness of the joint in transferring load from one side of the joint to another is called the load transfer efficiency (LTE). While there are several ways of expressing LTE, one common means is expressing it in terms of measured deflections:

$$LTE_{\delta} = (\delta_{\text{unloaded}} / \delta_{\text{loaded}}) \times 100 \quad (55)$$

where:

$$\begin{aligned} LTE_{\delta} &= \text{Deflection load transfer efficiency, percent} \\ \delta_{\text{unloaded}} &= \text{Deflection of the adjacent unloaded slab, in} \\ \delta_{\text{loaded}} &= \text{Deflection of the loaded slab, in} \end{aligned}$$

If the load transfer is perfect, or 100 percent, the unloaded slab deflects the same amount as the loaded slab. If the load transfer is 0 percent, the unloaded slab does not deflect at all. This concept is illustrated in figure 142.

Another way of expressing the load transfer is in terms of stress. Stress load transfer is defined as the ratio of the stress of the loaded slab to the stress of the unloaded slab:

$$LTE_{\sigma} = (\sigma_{\text{unloaded}} / \sigma_{\text{loaded}}) \times 100 \quad (56)$$

where:

$$\begin{aligned} LTE_{\sigma} &= \text{Stress load transfer efficiency, percent} \\ \sigma_{\text{unloaded}} &= \text{Stress in loaded slab, lbf/in}^2 \\ \sigma_{\text{loaded}} &= \text{Stress in adjacent unloaded slab, lbf/in}^2 \end{aligned}$$

It is important to note that deflection load transfer efficiency does not equal stress load transfer efficiency. In fact, there is no unique relationship between the two, as they are a function of slab properties (thickness, elastic modulus, Poisson's ratio), support conditions, and the radius of the applied load.<sup>(98)</sup> Deflection LTE normally is

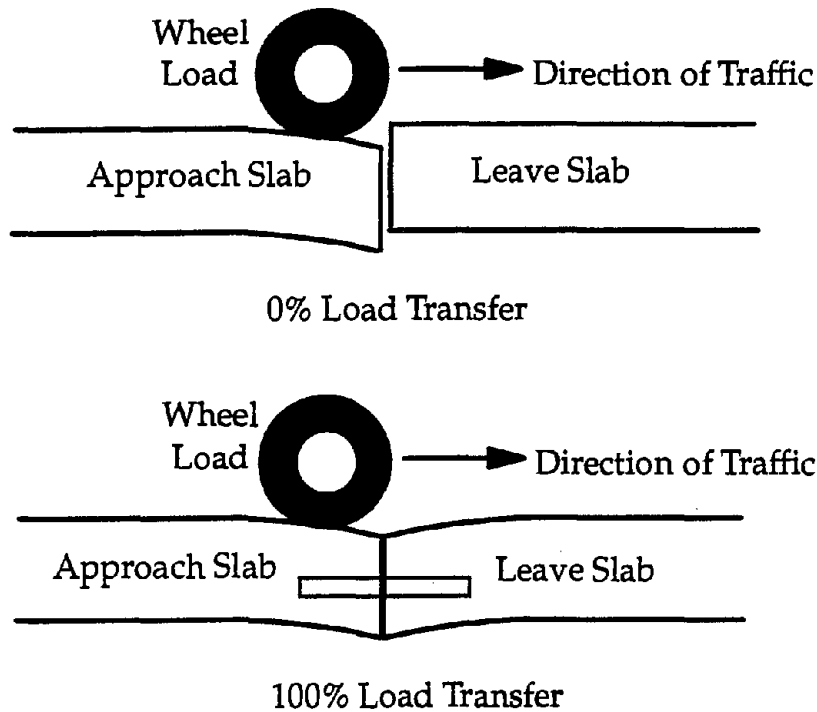


Figure 142. Illustration of load transfer concept.

used in evaluating the effectiveness of the joint load transfer system since it can be readily obtained from nondestructive deflection testing. Generally, it is desirable to maintain deflection load transfer efficiencies above 70 percent to ensure good long-term performance (i.e., to prevent pumping and faulting).<sup>(50)</sup>

Load transfer across a transverse joint is achieved either through the aggregate interlock between the abutting joint faces or through the use of mechanical load transfer devices (e.g., dowel bars) placed across the joints at the mid-depth of the slab. The use of dowel bars is recommended for nearly all jointed concrete pavement designs, with the possible exception of those pavements designed for extremely light truck traffic volumes. Even in those cases, the use of dowel bars should be carefully considered in light of the ability to accurately forecast truck loadings. If properly designed and installed, dowel bars are an effective means of load transfer and go a long way to ensuring a reliable, long-lasting pavement.

The selection of an adequate dowel bar diameter is critical in the design of the load transfer system. For example, figure 143 illustrates the effect of dowel diameter on predicted faulting for a standard pavement using the doweled faulting prediction model presented in chapter 2. This figure shows the large effect that dowel diameter has on controlling faulting.

Guidelines on the use of dowel bars and the selection of dowel diameters are summarized in table 34. These results are based on the faulting prediction models

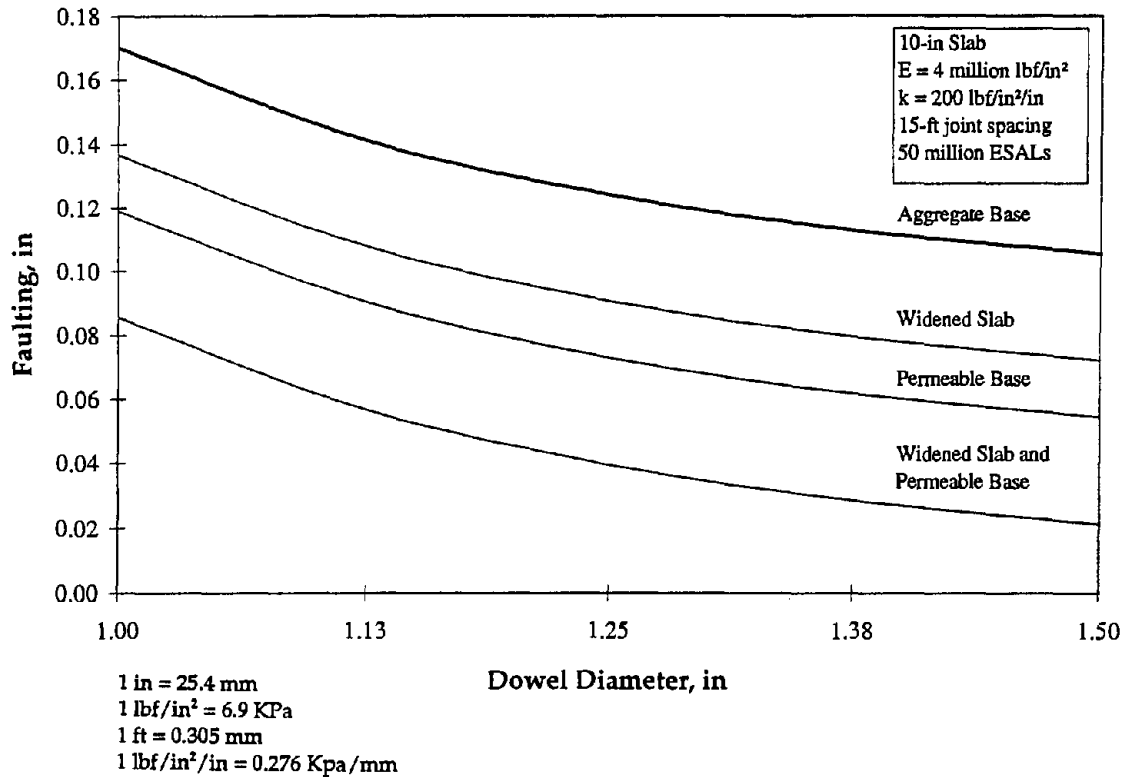


Figure 143. Effects of dowel diameter on faulting.

presented in chapter 2 and a maximum faulting limit of 0.10 in (2.5 mm). The table illustrates that the use of dowels is recommended for pavements designed for ESAL's of 5 million or more. However, because limited data were available for sections with more than 20 million ESAL's, the recommendations for dowel diameters in the higher ESAL categories should be used with caution.

Dowel bars are generally 18 in (457 mm) long, and typically spaced at uniform 12 in (305 mm) intervals across the joint.<sup>(87,93)</sup> However, nonuniform dowel spacings may also be used to concentrate the dowels directly under the wheelpaths, where they are needed the most. For example, the German design calls for 4 to 5 dowels at 10-in (254-mm) spacings in the wheelpaths, whereas between the wheelpaths, dowels are placed at 20-in (508-mm) spacings.<sup>(40)</sup> Similar designs have been used in the U.S. in retrofitted dowel installations.<sup>(99)</sup>

Dowel alignment and coating are also very important to their effective performance. The FHWA recommends the alignment tolerance (both vertical and horizontal) of 0.25 in/ft (21 mm/m).<sup>(87,93)</sup> The use of corrosion-resistant material or coating is recommended to prevent corrosion of the dowel, which could result in lock-up of the joint. Materials that have been successfully used as a rust inhibitor include epoxy coatings, plastic coatings, and stainless steel sleeves.

Table 34. Recommended dowel usage and diameters.

	Lanes	PCC Thickness, in	Dry-Freeze Climate			Dry-Nonfreeze Climate			Wet-Freeze Climate			Wet-Nonfreeze Climate		
			Base Type			Base Type			Base Type			Base Type		
			AGG	Treated	Perm	AGG	Treated	Perm	AGG	Treated	Perm	AGG	Treated	Perm
Design ESALS = 1 million	All	6-8	NR	NR	NR	NR	NR	NR	NR	NR	NR	NR	NR	NR
Design ESALS = 5 million	Widened No	7-9 7-9	NR 1.25	NR 1.00	NR 1.00	NR 1.25	NR 1.00	NR 1.00	NR 1.25	NR 1.25	NR 1.25	NR 1.25	NR 1.25	NR 1.25
Design ESALS = 10 million	All	8-10	1.25	1.25	1.00	1.25	1.00	1.00	1.50	1.25	1.25	1.38	1.25	1.25
Design ESALS = 20 million	All	9-11	1.25	1.25	1.25	1.25	1.25	1.25	1.50	1.50	1.25	1.50	1.25	1.25
Design ESALS = 50 million	All	11-13	1.50	1.25	1.25	1.38	1.25	1.25	1.50	1.50	1.50	1.50	1.50	1.25
Design ESALS = 100 million	All	11-13	1.50	1.38	1.25	1.50	1.25	1.25	1.50	1.50	1.50	1.50	1.50	1.50



## Joint Sealant and Reservoir Design

Joint sealing is an issue of current debate among many highway engineers. Some believe that a well-designed and maintained joint reservoir is critical in preventing the entry of incompressibles and moisture into the pavement structure, whereas others believe that the benefits derived from joint sealing are not enough to offset the costs associated with its placement.

The results of this study showed that, in direct project comparisons, sections with sealed joints had less spalling than sections with nonsealed joints, although the differences were not that significant. Moreover, overall performance of nonsealed joints was not worse than sealed joints.

Model development efforts presented in chapter 2 produced a joint spalling model that relates the various joint sealant types to the development of joint spalling. This model is based on all data that were available from the study, not just those involved in head-to-head comparisons. Figure 144 illustrates the joint spalling predictions from the model for JPCP. It is observed that those sections with a sealant material display less spalling than nonsealed sections, and sections with preformed compression seal show the least amount of spalling.

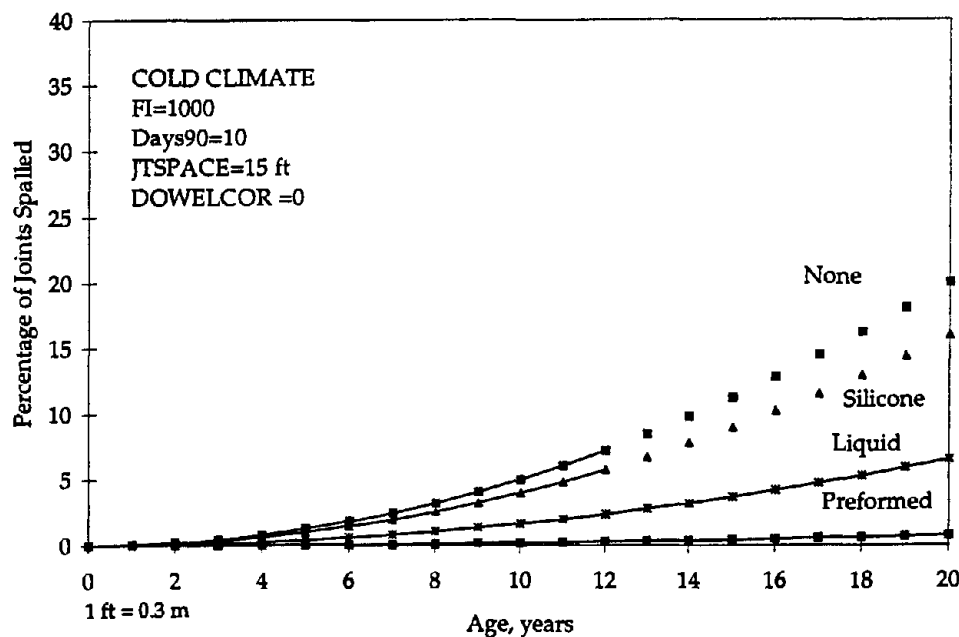


Figure 144. Effect of sealing and sealant type on joint spalling.

This, however, does not mean that the overall performance of nonsealed joints necessarily should be worse than the performance of sealed joints. The decision to seal or not seal joints in concrete pavements should be based on many factors, including (but not limited to) climate, joint design, base type, and local experience. Of these, local experience is probably the most important, as agencies should have an indication of what works and does not work for their local conditions. Wisconsin's

experience with nonsealed joints, which exhibited good overall performance 9 years after traffic opening, suggests that Wisconsin's joint design (1/8-in [3-mm] wide, unfilled, and unsealed) is an attractive and cost-effective alternative that needs to be investigated and tested for other climatic regions.

If determined necessary, the joint reservoir is designed in conjunction with both the type of sealant to be used in the pavement and the anticipated movements expected at the joint. The following three items must be considered:

- The type of sealant to be used (and the allowable sealant strain).
- The anticipated joint movement.
- The recommended shape factor for the type of sealant.

Each of these items is discussed in more detail below.

### Joint Sealant Type

Joint sealants may be grouped into two types: field poured and preformed. Field-poured sealants that are used in highway work fall into two general classes:

- Hot-poured thermoplastics—materials that become soft on heating and hard on cooling.
- Thermosetting—one- or two-component materials that cure by chemical reaction from an original liquid state to a nonreversible solid state.

The strain capacity of field-molded joint sealants is shown in table 35.

Table 35. Strain capacity of field-molded joint sealants.<sup>(100)</sup>

Sealant Class	Example Material	Compression Limit, %	Extension Limit, %
Thermoplastic (hot-poured)	Asphalt rubber (ASTM D 5078)	--	5
	Rubberized Asphalt (ASTM D 3405)	--	10 - 25*
	PVC coal tar (ASTM D 3406)	--	25
Thermosetting	Silicone	-50	100
	Polyurethane	--	25
	Polysulfide	--	25
	Epoxy based	--	<25

\* Depends on the manufacturer.

Hot-poured thermoplastic sealants used on highway pavements include asphalt rubber, rubberized asphalt, and polyvinyl chloride (PVC) coal tar. Asphalt rubber is a blend of asphalt and suspended, unmelted rubber particles that result in improved elasticity, greater cohesiveness, and an increased softening point. Rubberized asphalt is an asphalt cement-based sealant that incorporates various types of polymers and melted rubber to improve extensibility and resistance to high-temperature softening and tracking. In the past 15 years, rubberized asphalt has become the most commonly used sealant. PVC coal tar sealants are fuel and jet blast resistant, have a high softening point, and bond well to concrete. Installation of PVC coal tar requires accurate temperature control, care in adding fresh sealant, and adherence to continuous heating limits. PVC sealants are not widely used because of variable performance and potential health hazards.<sup>(101)</sup>

Thermosetting sealants used on highway pavements include silicones, polyurethanes, polysulfides, and epoxies. Silicone sealants are one-part, cold-applied materials that have been used in the paving industry since the 1970s. These sealants offer good extensibility, resistance to weathering, and temperature susceptibility resistance.<sup>(101)</sup> Polyurethanes, polysulfides, and epoxies are two-component materials that cure through chemical reaction. The two-component sealants are not widely used because of the two component nature, which adds an additional step and possible source of error, and their performance has been variable.

Preformed compression sealants are premolded strips of styrene, urethane, neoprene, or other synthetic materials that are designed to be placed in PCC pavement joints in a state of compression. Generally these seals are designed to be compressed 20 to 50 percent of their uncompressed widths.<sup>(101)</sup>

The factors to consider in the design and selection of poured sealants include the following:<sup>(96)</sup>

- Adhesion to the joint faces.
- Cohesion throughout the range of temperatures the sealant will experience.
- Ductility at low temperatures.
- Resistance to infiltration at high temperatures.
- Strain capacity.
- Durability under weather and traffic.
- Potential health hazard to workers.
- Pot life during installation.
- Operational latitudes—sensitivity of the material to variations in construction conditions, limitations on heating, and mixing.

Based on material properties, silicone sealants may be expected to provide good performance, but the performance observed in the field is mixed. Although silicone sealants have excellent extensibility, high stresses can develop at the joint face unless a low modulus sealant is used. At least two agencies found problems with an incompatibility between silicone seals and concrete made with dolomitic

aggregates.<sup>(96)</sup> In general, silicone sealants offer desirable properties, and many agencies have adopted silicone seals for their "high type" sealing purposes.

Among the pavement sections evaluated under this study, those containing preformed sealants exhibited the least amount of joint spalling. Where D-cracking is not a problem, preformed compression seals were highly effective in maintaining the joints clean and free of spalling, even in older sections (up to 21 years, in one case). Proper installation is important to obtain good performance using preformed compression sealants. Both excessive joint opening and excessive compression of the sealant can cause failures; the compression seals must be installed to maintain 20 to 50 percent compression of the sealant at all times.<sup>(101)</sup> Preformed compression sealants are used to seal both longitudinal and transverse joints in Germany.<sup>(39)</sup>

### Estimating Joint Movements

The amount of opening experienced by a joint is a function of the joint spacing, the friction between the slab and the base, the concrete coefficients of thermal expansion and of drying shrinkage, and the temperature drop. Equation 57 may be used to obtain an estimate of the average joint opening for a concrete pavement design:<sup>(13)</sup>

$$\Delta L = C L (\alpha \Delta T + \epsilon) \quad (57)$$

where:

- $\Delta L$  = Joint opening caused by temperature changes and drying shrinkage of the PCC, in
- $\alpha_c$  = Thermal coefficient of expansion of the PCC slab, °F  
(typical range  $3.8 \times 10^{-6}$  to  $6.6 \times 10^{-6}$ )
- $T$  = Temperature difference from time of PCC placement to minimum temperature, °F
- $\epsilon$  = Drying shrinkage coefficient of the PCC slab,  
in/in (typical range  $2 \times 10^{-4}$  to  $8 \times 10^{-4}$ )
- $L$  = Joint spacing, in
- $C$  = An adjustment factor for friction between slab  
and base; 0.80 for granular untreated subbase and  
0.65 for stabilized base

### Shape Factor

The shape factor is the ratio of the sealant width to the sealant depth, and is based on research conducted in the late 1950's.<sup>(102)</sup> This research showed that, for the same width, sealants placed deeper were subjected to greater strains when subjected to thermal movement than those placed shallower.<sup>(102)</sup> Recognition of this fact led to the

consideration of sealant strains in the design of the joint reservoir and in the selection of the sealant.

Figure 145 shows a cross section of a concrete pavement joint, showing the width and depth of the joint seal. The desired joint shape factor is achieved by installing a backer rod, as shown in figure 145. In addition to obtaining the desired joint shape factor, the backer rod prevents three-sided adhesion. It is important that the backer rod be compatible with the selected sealant material.

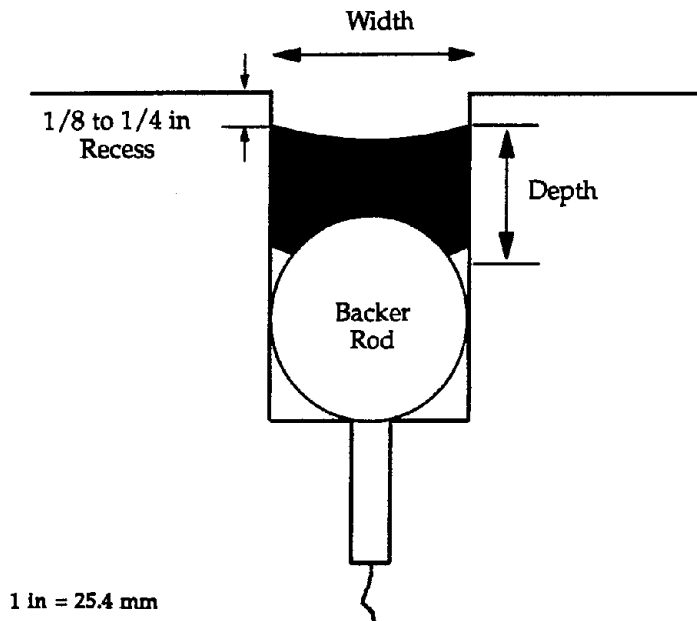


Figure 145. Cross section of joint sealant installation.

#### Determining Design Joint Width

After the sealant has been selected and the joint openings estimated, the determination of the design joint width is a fairly simple computation. The required joint design width is computed from the following equation:

$$W = \Delta L / S \quad (58)$$

where:

- W = Design width of transverse contraction joint, in
- $\Delta L$  = The joint opening caused by temperature changes and drying shrinkage of the PCC, in
- S = Allowable strain in the joint sealant material, in/in

The allowable strain in the sealant will depend on the sealant material. Most thermoplastic materials sealants typically have a maximum tensile strain of 0.25 in/in (25 percent), whereas silicone sealants normally have a maximum tensile strain of 0.50 in/in (50 percent).

The depth of the sealant reservoir is determined by the desired joint reservoir shape factor (width to depth ratio). Different sealants require different shape factors, and manufacturers' recommendations should be followed for their specific type of sealant. The shape factor is generally in the range of 0.67 to 1.5, with a shape factor of 1 common for asphaltic-based sealants and a shape factor of 2 common for silicone sealants. A minimum sealant depth of 0.5 in (13 mm) is recommended for transverse joints.

Different requirements exist for preformed compression seals. These seals are placed in the joint under compression and are required to be compressed 20 to 50 percent of their normal width throughout its life. The determination of the required joint reservoir width and the selection of a proper preformed compression seal is an iterative procedure that should include input from the manufacturer. Consideration should be given to the possibility of needing different compression seal sizes for a project due to the differences in widths of cracked and noncracked joints.

### Longitudinal Contraction Joint Design

Longitudinal contraction joints (also referred to as longitudinal weakened plane joints or longitudinal warping joints) are placed between adjacent lanes to prevent the development of longitudinal cracking. On conventional 24-ft (7.3-m) wide concrete pavement, longitudinal contraction joints are placed at the mid-point of the width of the paving, typically 12 ft (3.7 m) from the edge of the slab. On multilane facilities, the maximum longitudinal contraction joint spacing is 14 ft (4.3 m), which corresponds with the maximum recommended width for PCC slab widening.

It is recommended that longitudinal contraction joints be established through sawcutting of the pavement to a depth of one-third of the slab thickness. This is generally deep enough to produce a weakened plane at that location, forcing the pavement to crack directly beneath the sawcut. As with the sawing of transverse joints, the timing of the longitudinal sawing operations is critical to preventing the development of random cracking; this is perhaps most crucial when paving in cold weather and over stabilized base courses.<sup>(96)</sup> The recommendations presented previously on the timing of transverse joint sawing operations should be consulted for guidance on longitudinal joint sawing operations as well.

Another way of forming longitudinal contraction joints is through the use of a plastic insert that is mechanically installed off the rear of the paver. While once very popular, this method is not recommended and has been dropped by most agencies.<sup>(96)</sup> This is because there are questions regarding the effectiveness of the plastic insert in forming the longitudinal contraction joint; it was observed in this study that significant longitudinal cracking occurred on many concrete pavements in which the

longitudinal contraction joint was formed using a plastic insert, particularly for those pavements constructed on stabilized bases.

Most longitudinal joints are sawed to a width of 0.12 to 0.25 in (3 to 6 mm) and filled with a rubberized-asphalt sealant material. Because typical longitudinal joint movements are so small, many agencies consider a designed joint sealant reservoir unnecessary.<sup>(96)</sup> Figure 146 shows a typical longitudinal contraction joint design.

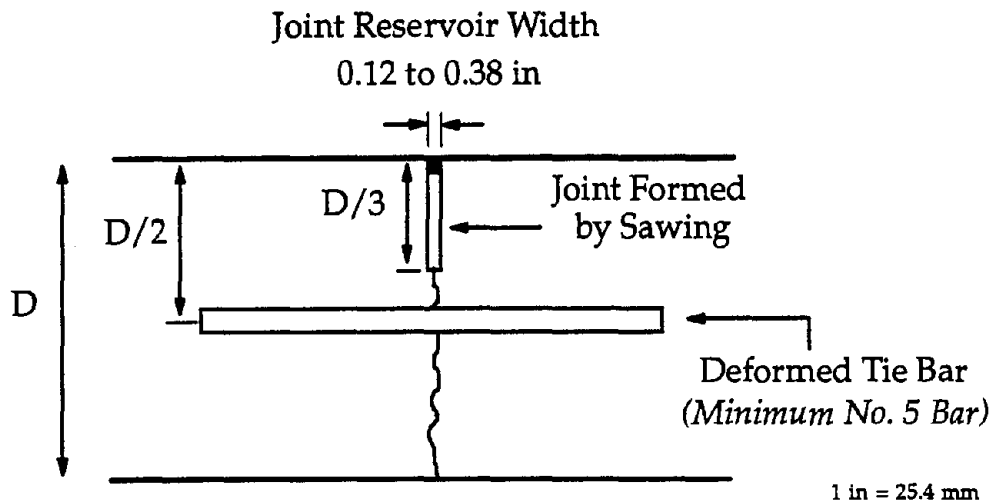


Figure 146. Longitudinal contraction joint design.

Tie bars are typically placed at the mid-depth of the PCC slab at the longitudinal contraction joint location through mechanical implantation. The primary purpose of the tie bars is not to provide load transfer but rather to hold the lanes together so that lane separation and differential vertical movements are prevented.

An adequately designed tie bar system is critical to ensuring the effectiveness of the longitudinal construction joints. In cases where tie bars were omitted altogether from the longitudinal contraction joint design, significant horizontal separation and vertical elevation differences have occurred between lanes.<sup>(94)</sup> Such observations were also noted in this study where tie bars were not present between lanes or on several pavements with small tie bars (No. 4 [13 mm] or less) or large tie bar spacings.

Most agencies are currently using No. 4 (13 mm) or No. 5 (16 mm) bars, 30-in (762-mm) long, and spaced at 30-in (762-mm) intervals.<sup>(96)</sup> For most medium- and high-trafficked roadways, it is recommended that No. 5 (16 mm) bars be employed at 30-in (762-mm) intervals. However, larger diameter bars at closer spacings are suggested in areas frequently crossed by truck traffic (e.g., acceleration/deceleration lanes, truck climbing lanes, and high-volume merge areas).<sup>(96)</sup> For example, Germany uses between three and five bars (0.8-in [20-mm] diameter and 31.5-in [80-mm] long) for every 16.4 ft (5 m) slab on its high-type pavements.<sup>(40)</sup>

## JRCP Longitudinal Reinforcement Design

Transverse cracks occur in JRCP as a result of a combination of many factors, including shrinkage stresses caused by both low temperatures and loss of moisture from the concrete, thermal curling stresses due to temperature differences between the top and bottom of the slab, and stresses due to repeated traffic loadings. Longitudinal reinforcement is provided in JRCP to hold these transverse cracks tightly together, thereby maintaining load transfer across the crack and reducing the development of crack spalling and faulting. The steel is not intended to provide structural load carrying capacity.

The amount of longitudinal reinforcement required to hold these cracks tightly together is usually computed using the "subgrade drag theory." This procedure determines the amount of steel required to "drag" the slab across the base or subgrade without yielding the reinforcement. However, this method does not include many variables that are believed to affect the deterioration of a crack, such as crack width (which affects vertical load transfer), repeated traffic loading applications (which creates vertical shear forces across the crack), base/subgrade support conditions, friction between the slab and base, lock-up of joints from corroded dowels that opens adjacent transverse cracks, and corrosion of reinforcement at the crack face.

Field data from this study and several other studies (see, for example, references 10, 11, 36, 103, and 104) have illustrated that transverse cracks in JRCP deteriorate with time and traffic. These deteriorated cracks cause roughness and increased maintenance requirements (i.e., full-depth repairs), and also generate the need for early rehabilitation (such as overlays). These cracks also create reflection crack problems in AC overlays if they are not repaired. Thus, there is a great need for improved longitudinal reinforcement design for JRCP to prevent this mode of damage if JRCP is to remain a viable pavement design alternative. This section includes guidelines for improved design of JRCP reinforcement to prevent the deterioration of transverse cracks.

### *Key Factors*

Various field and laboratory studies over the past 15 years have shown that the following variables affect the deterioration of transverse cracks in JRCP:

- **Reinforcement content.** Increased reinforcement content reduces the amount of deteriorated cracks.<sup>(10,11,37)</sup> JRCP containing less than 0.10 percent steel typically have a significant amount of deteriorated cracks, whereas JRCP with more than 0.20 percent steel typically exhibit very low amounts. A recent study evaluated the effectiveness of the AASHTO Design Guide (subgrade drag theory) to provide reinforcement for JRCP and found that the typical percentages determined for aggregate bases would result in large amounts of deteriorated cracking.<sup>(14)</sup> Researchers in Texas found that the steel percentages obtained from the AASHTO Guide are inadequate and should be more in the range of 0.20 to 0.30 percent.<sup>(105)</sup>



Still other researchers found that in laboratory tests (fatigue loading across reinforced cracks) on large-scale test specimens, 0.17 percent steel content commonly used in Michigan is inadequate for loading conditions encountered in the field.<sup>(37)</sup>

An example of the effect of reinforcement content on the development of deteriorated transverse cracks is shown in figure 147. This is based on the JRCP crack deterioration model presented in chapter 2. It is observed that reinforcement content has a very significant effect on deteriorated transverse cracks.

- **Base/subgrade support.** Stabilized bases and stiffer subgrades reduce the amount of deteriorated cracks in JRCP.<sup>(10,37)</sup> A stabilized base has a very large effect on reducing the amount of deteriorated transverse cracks in JRCP as shown in figure 147.
- **Climate.** JRCP's constructed in colder and wetter climates exhibited more transverse crack deterioration than those constructed in warmer climates, probably due to larger crack openings.<sup>(10,11)</sup> Reinforcement design must consider local temperature and moisture conditions.

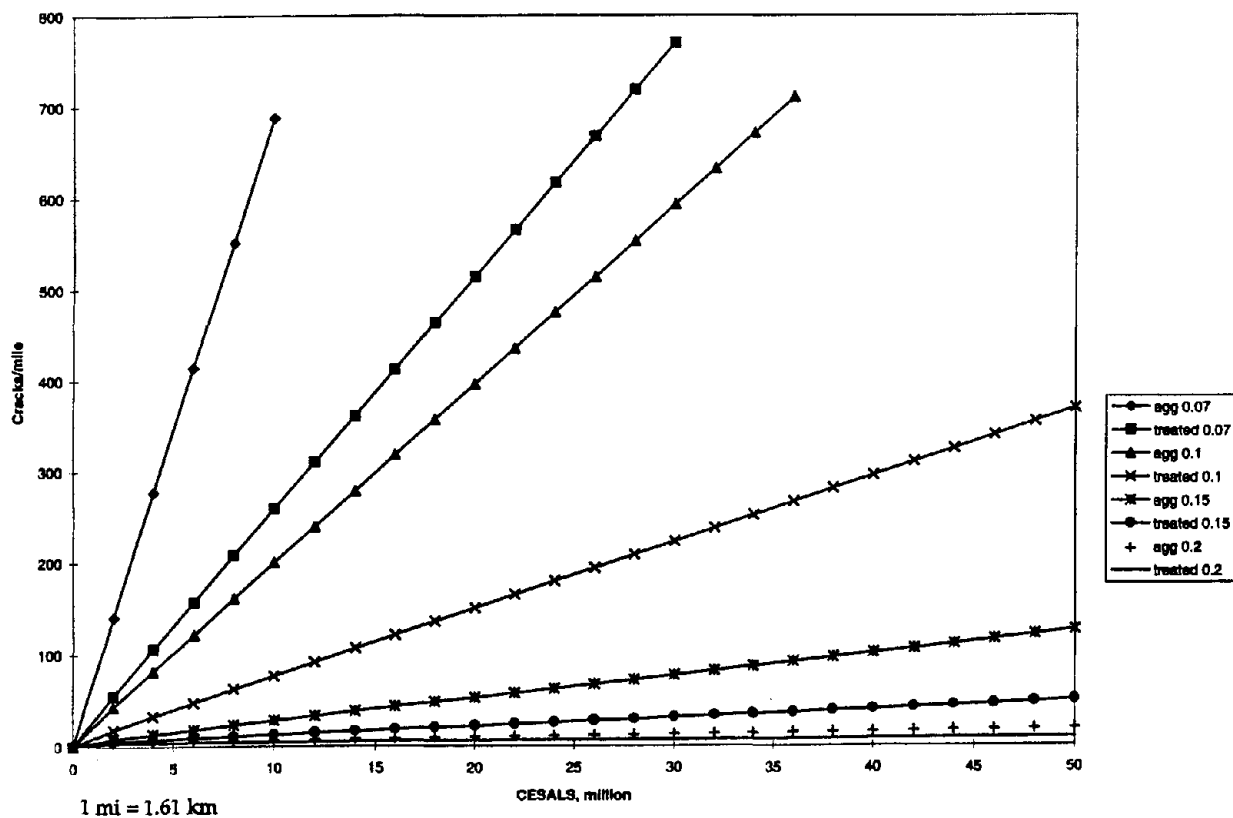


Figure 147. JRCP crack deterioration as a function of reinforcement content.

- Traffic. Increased traffic loadings (ESAL's) result in increased crack deterioration.<sup>(10,11,37)</sup> The relative effect of ESAL's on crack deterioration is also shown in figure 147.
- Type of reinforcement. In laboratory studies, the use of deformed wire mesh reinforcement resulted in fewer deteriorated transverse cracks, as compared to smooth wire mesh.<sup>(36)</sup> Deformed reinforcing bars also produced excellent performance.
- Maximum coarse aggregate size. The use of "large" top size durable coarse aggregate is effective at maintaining load transfer across transverse cracks. Smaller top size aggregates (i.e., 0.5 in [13 mm] or less) result in straight cracks through the depth and across the slab with little aggregate interlock to help provide load transfer.<sup>(36, 106)</sup> Field results from this study also showed that JRCP with larger maximum coarse aggregate exhibit less deteriorated cracks than those with a smaller maximum coarse aggregate size. Data averaged over similar sections with different maximum aggregate sizes (but the same type of coarse aggregate) from the OH 2 project in Vermilion, Ohio gave the results shown in table 36.

Table 36. Effect of coarse aggregate size on deteriorated transverse cracking.

Maximum Coarse Aggregate Size, in	Deteriorated Cracks/mi	Cracking Ratio (to 1.5-in Max. Size)
1.5	92	1.0
1.0	110	1.2
0.5	230	2.5

1 in = 25.4 mm; 1 mi = 1.61 km

Over the years, many of these factors influencing JRCP crack deterioration have been incorporated into performance prediction models. At least three performance prediction models for transverse crack deterioration have been developed using relatively large data bases: the NCHRP 1-19 model (see reference 10), the SHRP LTPP GPS-4 model (see reference 11), and the new prediction model presented in chapter 2. These models are empirical in nature and are based on completely different national data bases, yet they show consistent effects for most of the above mentioned variables. A summary of the features of these different models is given in table 37.

#### *JRCP Longitudinal Reinforcement Recommendations*

The crack deterioration model presented in chapter 2 is believed to be the most comprehensive model available at this time. This model can be used to compute the required percent of reinforcement for any desired limiting criteria. A limiting value

Table 37. Summary of three field developed models for deteriorated transverse cracking of JRCP.

Prediction Model	NCHRP 1-19 Model <sup>(10)</sup>	LTPP GPS-4 Model <sup>(11)</sup>	New FHWA Model (see chapter 2)
Data Base	4 States, 268 sections	15 States, 28 sections	10 States, 111 sections
Reinforcement Content	Increased reinf., decreased crack deterioration	Increased reinf., decreased crack deterioration	Increased reinf., decreased crack deterioration
Slab Thickness	Increased thickness, decreased crack deterioration	Not included	Increased thickness, decreased crack deterioration
Joint Spacing	Increased joint spacing, increased crack deterioration	Not included	Not included
Base Type	Stabilized base, less crack deterioration	Not included	Stabilized base, less crack deterioration
Subgrade Stiffness	Not included	Increased k-value, decreased crack deterioration	Not included
Traffic (ESAL's)	Increased ESAL's, increased failures	Increased ESAL's, increased failures	Increased ESAL's, increased failures
Climate	Increased freezing index, increased crack deterioration	Increased precipitation, increased crack deterioration	Increased freezing and moisture index, increased crack deterioration

of 25 deteriorated transverse cracks/mi (16 cracks/km) is reasonable for design purposes. Based on that value, recommended longitudinal reinforcement contents are shown in table 38.

As shown in table 38, a minimum of 0.10 percent longitudinal reinforcing steel is recommended for JRCP. This value increases with increasing traffic loadings and in more severe climates. It should be noted that the design criteria of 25 deteriorated cracks/mi (16 cracks/km) is a mean predicted value, and that no safety factor has been included. Thus, the recommendations shown in table 38 represent a 50 percent level of reliability (that is, the selected reinforcement content should provide adequate performance in 50 of 100 pavements). To achieve a higher level of design reliability, the design engineer should select a greater amount of reinforcing steel.

It should be noted that the recommendations for reinforcement contents at the higher ESAL categories are based on extrapolations of the prediction model; only a few sections existed that had sustained greater than 20 million ESAL's. Thus, the design recommendations for those higher ESAL categories should be used with caution.

Table 38. Minimum recommended percent longitudinal reinforcement for JRCP (50 percent level of reliability).

Base Type	ESAL's millions	Wet-Freeze Climate	Wet-Nonfreeze Climate	Dry-Freeze Climate	Dry-Nonfreeze Climate
Aggregate	1	0.12	0.10	0.11	0.10
	5	0.15	0.10	0.15	0.10
	10	0.17	0.10	0.16	0.10
	25	0.19	0.12	0.18	0.12
	50	0.20	0.14	0.20	0.13
	100	0.22	0.15	0.21	0.15
Stabilized	1	0.10	0.10	0.10	0.10
	5	0.13	0.10	0.10	0.10
	10	0.15	0.10	0.10	0.10
	25	0.17	0.10	0.10	0.10
	50	0.18	0.12	0.11	0.11
	100	0.20	0.13	0.13	0.13

Notes: A minimum of 0.10 percent reinforcement is recommended.

Deformed bars or deformed welded wire fabric strongly recommended.

Base type: aggregate (nonstabilized) or stabilized (asphalt or cement).

ESAL's: 18-kip (80-kN) single-axle load applications in traffic lane, millions.

Climatic zone: Wet-freeze (Freezing Index = 500; Thornthwaite Moisture Index = 30).

Wet-nonfreeze (Freezing Index = 0; Thornthwaite Moisture Index = 30).

Dry-freeze (Freezing Index = 500; Thornthwaite Moisture Index = 0).

Dry-nonfreeze (Freezing Index = 0; Thornthwaite Moisture Index = 0).

In the design and construction of JRCP, the use of deformed bars or deformed welded wire fabric (WWF) is strongly recommended. Although smooth bars or wires have been commonly used in the past, deformed bars or wires are more effective in keeping transverse cracks held tightly together. Smooth WWF fabric is governed by ASTM A 185, whereas deformed WWF is governed by ASTM A 497.

A variety of WWF sizes are available for use in JRCP, and the sizes should be carefully selected in order to obtain the required reinforcing content. Generally, a minimum 0.225 in (6 mm) diameter wire is recommended for both transverse and longitudinal reinforcement.<sup>(106)</sup> Minimum spacings of 4 in (102 mm) are recommended for both longitudinal and transverse wires to facilitate placement and vibration of concrete, whereas maximum spacings of 12 in (305 mm) and 6 in (152 mm) are recommended for longitudinal and transverse wires, respectively.<sup>(106)</sup> A minimum 2.5 in (64 mm) cover is suggested for most WWF installations.

## *Alternate JRCP Designs*

Over the years, several design variations of conventional JRCP have been constructed that are worth noting. For example, Japan has conducted experimental studies using combined load and curling stresses and discovered that the critical edge load position (where many transverse cracks begin to spall in JRCP) was minimized by providing additional 0.5-in (13-mm) diameter deformed bars along the outside longitudinal edge of the PCC slab.<sup>(107)</sup> This proved to be extremely effective at reducing crack widths and, subsequently, crack deterioration.<sup>(107)</sup> Performance studies in Japan indicate that JRCP with wire mesh, the most common pavement type in Japan, have exhibited excellent performance, with the use of a 1-in AC interlayer found to significantly increase pavement durability.<sup>(108)</sup>

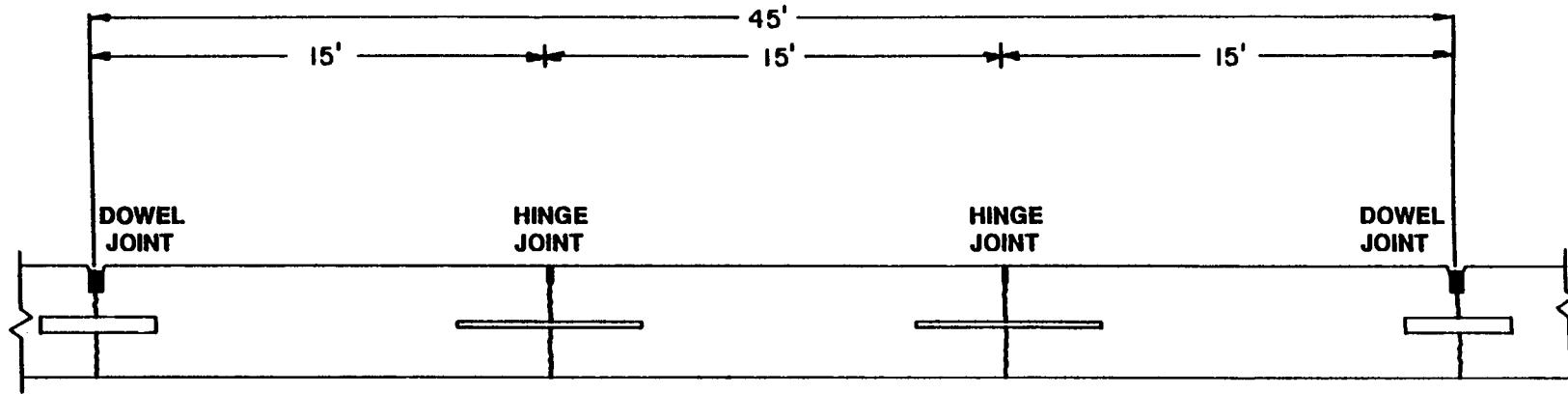
Interestingly, the use of the a steel reinforcing bar at the outside edge of the slab can be traced back to at least the Bates Road Test of the early 1920's.<sup>(109)</sup> In that study, it was found that the inclusion of a 0.75-in (19 mm) diameter longitudinal deformed "marginal bar" at the outside edge of the pavement was quite effective at reducing the severity of transverse and corner cracks.<sup>(109)</sup>

More recently, the Illinois DOT has also developed an alternative JRCP design, as illustrated in figure 148.<sup>(110)</sup> In this design, termed the "hinge joint" design, doweled transverse contraction joints are sawed at 45 ft (13.7 m) intervals, and two sawed "hinge" joints are cut at the third points of the 45-ft (13.7-m) slab. Deformed tie bars (No. 6 [19 mm] diameter bars, 36 in [914 mm] long) are placed across these intermediate hinge joints at 18-in (457-mm) intervals, thus clustering the steel at key stress points in the pavement and providing an effective steel percentage of 0.26 to 0.29 percent. The results of this study show that this hinge joints design has performed well, although there are some reports of cracking problems when the designed has been used in urban intersections.

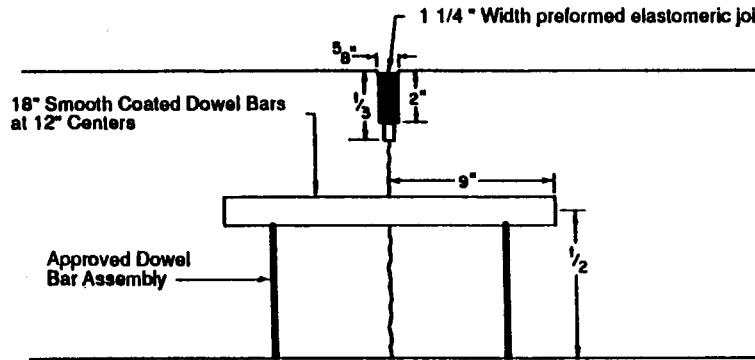
## CRCP Longitudinal Reinforcement Design

Continuously reinforced concrete pavements (CRCP) are constructed with continuous longitudinal reinforcement and contain no transverse joints other than construction joints. The amount of longitudinal reinforcement required in CRCP is much greater than that used in JRCP, but the purpose of the steel reinforcement is the same: to hold transverse cracks tightly together to prevent their deterioration (faulting, spalling) under traffic and environmental loadings. If an inadequate amount of reinforcement is provided, the spacing between transverse cracks becomes excessive, resulting in wide cracks that deteriorate over time. These in turn can lead to punchouts and localized failures in the CRCP, distresses that can result in premature failure of the pavement.

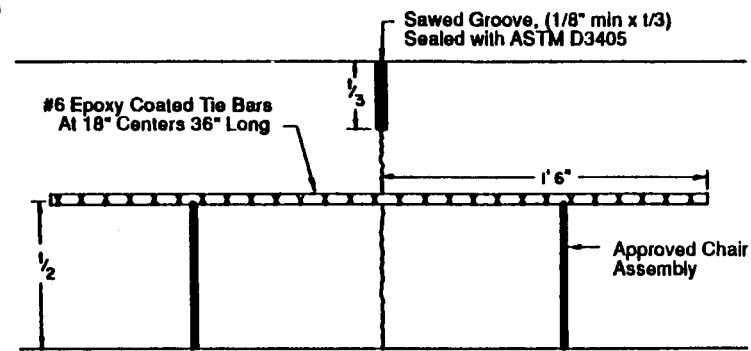
Determining the appropriate amount of reinforcement prior to construction is a complex issue because the formation of the transverse cracks depends not only on material properties and design features, but also on the climatic conditions during and shortly after construction. Material properties include concrete tensile strength,



LONGITUDINAL CROSS - SECTION



DOWEL JOINT DETAIL



HINGE JOINT DETAIL

1 in = 25.4 mm  
1 ft = 0.3 m

Figure 148. Illustration of Illinois hinge joint design.<sup>(110)</sup>

shrinkage, and coefficient of expansion; design features include items such as slab/base friction, and amount and depth of reinforcement.

Transverse cracks in CRCP usually develop during the first few months after construction and then remain relatively constant for many years. The crack width is very critical to crack deterioration and depends in part on crack spacing and reinforcement content. If the cracks remain tight and are not allowed to open significantly, they will not likely cause performance problems. Strong support beneath the CRCP is also very critical for minimizing the deterioration of transverse cracks and the development of punchouts.

Due to the many complexities involved, the determination of the amount of longitudinal reinforcement for CRCP is often determined from local experience. There are several approximate analytical methods available (see, for example, references 50, 111, and 112), but none of these consider all of the variables that affect the crack spacing (e.g., climate) or the deterioration of a crack (crack width, crack spalling and faulting) after it forms. Key factors affecting the deterioration of a crack include traffic loadings (vertical shear forces across the crack), base/subgrade support conditions, friction between the slab and base, steel-concrete bond, and corrosion of reinforcement.

Field data from this study and other studies (see references 14, 84, 85, 86, 111, 112, 113, and 114) have shown that while CRCP has generally performed well, there have been several major failures over the years that have prompted many SHA's to stop building CRCP. Many of these failed projects exhibited severe crack deterioration (spalled and faulted) and steel ruptures. This severe crack deterioration led to punchouts and increased roughness, which accelerated the need for maintenance and rehabilitation activities. These deteriorated cracks and punchouts also can cause reflection cracking problems in AC overlays if they are not repaired.

Although the focus of this study was not on the performance of CRCP, several CRCP sections were included in the field evaluations. Nevertheless, based on the limited results from this study and information gained from other studies, some guidance on CRCP longitudinal reinforcement design is offered. More detailed information on the design and construction of CRCP is found in references 84, 85, and 86.

### *Key Factors*

Various performance studies that have been conducted over the past 50 years have shown that the following major variables affect the deterioration of transverse cracks in CRCP:

- Reinforcement content. Increased reinforcement content causes increased restraint within the CRCP and results in closer crack spacings and smaller crack widths.<sup>(40,111,113,115)</sup> Consider, for example, the performance results shown in table

39, which are taken from the Vandalia, IL CRCP experimental study after 20 years.<sup>(115)</sup>

This table shows the strong effect of reinforcement content on pavement performance. This pavement was also recently observed (after nearly 50 years of service and over 10 million ESAL applications) and those sections containing 0.7 and 1.0 had no failures, even though the crack spacing was very small (less than 2 ft [0.6 m]). CRCP in Illinois has been constructed with about 0.72 percent reinforcement for many years. This practice has led to very short crack spacings, but very tight cracks and excellent performance. Crack spacings on CRCP in the Chicago area, for example, is about 2 to 3 ft [0.6 to 0.9 m]; however, they remain tight, and few punchouts have developed after many years and millions of ESAL applications.<sup>(113)</sup>

Similar results have been observed for CRCP in Belgium. The original Belgium design was built during the 1970's and included 0.85 percent longitudinal reinforcement in an 8-in (203-mm) slab. A high strength concrete was also used, and the pavement was placed on an LCB with a thin AC interlayer between the slab and base. Over 62 mi (100 km) of this design were constructed, and after 20 years and 30 to 40 million ESAL applications, none of the pavements displayed any punchouts.<sup>(39)</sup> However, by the late 1970's, many of these CRCP exhibited very tight and closely spaced cracks (16 to 24 in [406 to 610 mm]), which was thought to be too close and might ultimately lead to fragmentation. Thus, the design was altered in the late 1970's to include only 0.67 percent reinforcing steel and no AC interlayer.<sup>(39)</sup> These design changes did increase the crack spacing to an average of 4.9 ft (1.5 m), but they also resulted in the development of a greater number of punchouts.<sup>(39)</sup>

Table 39. Effect of reinforcement content on CRCP performance  
(adapted from reference 115)

Percent Reinforcement	Mean Crack Spacing, ft	Mean Crack Width, in	PSR	Approximate Extent of Failures
0.3	9.5	0.042	3.3	Many
0.5	7.8	0.027	3.6	Some
0.7	6.2	0.021	3.5	None
1.0	5.9	0.011	4.0	None

1 ft = 0.305 m  
1 in = 25.4 mm

Note: Results are for 8 in (203 mm) CRCP.  
Age of Pavement: 20 Years  
Approximate ESAL applications: 4.3 million



Other European countries have also constructed some CRCP with higher reinforcement contents. For example, one pavement constructed in France with 0.73 percent steel was touted as the best performing CRCP in France.<sup>(39)</sup> France also constructs CRCP with trapezoidal cross sections and with 2.5-ft (0.75 m) widened slabs that have performed well.<sup>(39)</sup> Spain has also built some CRCP with 0.73 and 0.85 percent longitudinal reinforcement that have performed very well.<sup>(39)</sup>

These data strongly support the belief that CRCP constructed with greater reinforcement contents (and containing the resultant short crack spacings and narrow crack widths) show outstanding performance. Although it is often mentioned in the literature that the reinforcement content should be limited in order to produce a minimum crack spacing of 3 ft (0.9 m), the above cases illustrate that many inservice CRCP perform well with even 2 ft (0.6 m) average crack spacing because the cracks remain very tight.

- Base/subgrade support. CRCP require strong base/subbase/subgrade support in order to perform well. By providing stronger support and being less susceptible to erosion, stabilized bases reduce the amount of deteriorated cracking and punchouts, and help sustain long-term rideability.<sup>(11,14,111,113)</sup> Similar results have been obtained in Belgium, in which the use of strong, nonerodible base materials, along with the use of high steel contents and high quality concrete, provided better performance than thicker slabs placed with less steel and on weaker subgrades.<sup>(39)</sup>
- Strength of lean concrete base. Data from a CRCP project in South Carolina showed that the compressive strength of the lean concrete base strongly related to pumping/erosion and the development of punchout failures in the pavement.<sup>(116)</sup> Sections constructed on a stronger LCB experienced less punchout failures than sections constructed over weaker LCB.
- Climate. The Illinois models were developed for CRCP located in a wet-freeze climate.<sup>(14,111)</sup> The LTPP model for IRI of CRCP based on sections all over the U.S. surprisingly did not show any climatic variable as significant.<sup>(11)</sup> However, it is very likely that climate does play a significant role in performance of CRCP. For example, States in the north have often used greater amounts of longitudinal reinforcement than States in the south, most likely to maintain tight cracks.
- Traffic. Increased traffic loadings (ESAL's) result in increased crack deterioration and increased roughness.<sup>(11,14,111,115)</sup>
- Depth of reinforcement. As previously stated, the purpose of the reinforcing steel in a CRCP is not to carry load, but rather to hold the cracks tightly together. As such, the closer the reinforcement is to the surface, the tighter the cracks remain and the fewer failures that develop. For example, the data shown in table 40 are from long-term performance studies in Illinois and clearly show the effect of steel depth on CRCP performance.<sup>(117)</sup> A study of the performance of a CRCP project in South Carolina showed similar results.<sup>(116)</sup>

Table 40. Effect of steel reinforcement depth on CRCP performance.<sup>(117)</sup>

Reinforcement Depth, in	Crack Spacing, ft	Crack Width, in	Patching, ft <sup>2</sup> /1000 ft <sup>2</sup>
2	2.4	0.0187	7 (6 failures/mi)
3	3.8	0.0312	12.7 (11 failures/mi)
4 (mid-depth)	5.4	0.0327	30.9 (27 failures/mi)

1 in = 25.4 mm; 1 mi = 1.61 km

However, practical considerations in construction and minimizing chlorides impacts requires a concrete cover of about 3 in (76 mm) minimum. Illinois has specified a cover of 3 in (76 mm) regardless of thickness and this has provided excellent performance.

- Maximum coarse aggregate size. The observations of the effect of maximum coarse aggregate size on JRCP performance may well apply to CRCP performance. In this study, the use of larger top size durable coarse aggregate improved load transfer across transverse cracks in JRCP, while smaller top size aggregates (i.e., 0.5 in [13 mm]) resulted in straight cracks both through the depth and across the width of the slab, thereby producing little aggregate interlock load transfer.

Many of these key factors have been incorporated into performance prediction models for CRCP. For example, in 1989, a prediction model was produced under an FHWA study for the development of punchouts.<sup>(14)</sup> More recently, a punchout model was developed for the Illinois Department of Transportation (IDOT) in 1994.<sup>(111)</sup> Under the early data analysis work conducted under the SHRP LTPP program, a prediction model for IRI was developed for CRCP projects.<sup>(11)</sup> These three field models show consistent effects for most of the above mentioned variables. A summary of the features of these models is given in table 41.

#### *CRCP Longitudinal Reinforcement Recommendations*

The IDOT CRCP failure model is believed to be the most comprehensive model available at this time.<sup>(111)</sup> This model was used to provide recommendations for CRCP longitudinal reinforcement content, assuming a limiting criteria of 5 failures/mi (3 failures/km). Failures include punchouts, deteriorated transverse cracks where the steel has ruptured, and other localized failures. The design recommendations over a range of traffic levels and slab thicknesses are shown in table 42 for aggregate bases and in table 43 for stabilized bases.

The ability of the model to predict the performance of actual, inservice CRCP projects is summarized in table 44. This table compares the predicted failures to the

Table 41. Summary of three prediction models for punchouts and roughness in CRCP.

Prediction Model	FHWA 1989 Model (Punchouts) <sup>(14)</sup>	IDOT 1993 Model (Punchouts) <sup>(110)</sup>	LTPP 1994 Model (IRI) <sup>(11)</sup>
Data Base	Illinois, 137 sections	Illinois, 408 sections	25 States, 42 sections
Reinforcement Content	Increased reinf., decreased failures	Increased reinf., decreased failures	Increased reinf., lower IRI
Slab Thickness	Increased thickness, decreased failures	Increased thickness, decreased failures	Increased thickness, lower IRI
Reinforcement Type	Deformed bars slightly fewer failures than deformed fabric	Not included	Not included
Reinforcement Placement	Not included	Chairs slightly fewer failures than tubes	Not included
Stabilized Base	Stabilized base fewer failures than nonstabilized	Stabilized base fewer failures than nonstabilized	Not included
Subgrade type	Not included	Not included	Coarse grain soil lower IRI than fine grain soil
Traffic (ESAL's)	Increased ESAL's, increased failures	Increased ESAL's, increased failures	Increased ESAL's, increased failures
Widened slab (14 ft vs. 12 ft)	Not included	Not included	Widened slab fewer failures

1 ft = 0.305 m

actual failures for the 17 CRCP sections included in this study, for 19 sections from references 84, 85 and 86, and for 3 sections from Belgium. The model's predictions are reasonably close for the wet-freeze zone where the model was derived, but appear to produce conservative results in other climatic zones.

A reinforcement content of 0.60 percent is included as the minimum allowable steel content in tables 42 and 43. Note that the recommendations provided in tables 42 and 43 are based on the *mean* predicted limiting value of 5 failures/mi (3 failures/km), and that no safety factor has been included. In other words, the recommendations represent a 50 percent level of reliability, meaning that they will not always be adequate. Because of the many uncertainties involved in CRCP design, and due to the severe problems that develop when a CRCP begins to fail, it is recommended that higher steel contents be generally selected in order to increase overall design reliability and performance. Design engineers are encouraged to modify the recommendations provided in tables 42 and 43 with engineering judgment and local experience so that suitable reinforcement contents can be selected for their specific conditions.

As with the recommendations for JRCP steel design, the recommendations for CRCP reinforcement contents at the higher ESAL categories are based on extrapolations of the prediction model. Thus, the design recommendations for those

Table 42. Minimum reinforcement contents for CRCP on aggregate base courses and in a wet-freeze climate (50 percent level of reliability).

ESAL's, millions	Slab Thickness, in	% Longitudinal Steel	Projected Failures/mi
1	8	0.60	0.74
1	9	0.60	0.42
1	10	0.60	0.22
1	11	0.60	0.11
1	12	0.60	0.05
5	8	0.65	4.21
5	9	0.60	3.32
5	10	0.60	1.76
5	11	0.60	0.87
5	12	0.60	0.40
10	9	0.70	4.19
10	10	0.65	3.09
10	11	0.60	2.13
10	12	0.60	0.99
10	13	0.60	0.43
20	10	0.75	3.90
20	11	0.65	3.74
20	12	0.60	2.41
20	13	0.60	1.05
20	14	0.60	0.42
40	11	0.75	4.72
40	12	0.70	3.05
40	13	0.65	1.84
40	14	0.60	1.04
40	15	0.60	0.39
60	12	0.75	3.69
60	13	0.65	3.10
60	14	0.60	1.75
60	15	0.60	0.66
60	16	0.60	0.24
100	12	0.85	3.69
100	13	0.75	3.09
100	14	0.65	2.42
100	15	0.60	1.28
100	16	0.60	0.45

1 in = 25.4 mm  
1 mi = 1.61 km

Notes: A minimum of 0.60 percent steel is recommended.  
The use of deformed steel is strongly recommended.

Table 43. Minimum reinforcement contents for CRCP on stabilized base courses and in a wet-freeze climate (50 percent level of reliability).

ESAL's, millions	Slab Thickness, in	% Longitudinal Steel	Projected Failures/mi
1	8	0.60	0.57
1	9	0.60	0.33
1	10	0.60	0.17
1	11	0.60	0.09
1	12	0.60	0.04
5	8	0.60	4.56
5	9	0.60	2.58
5	10	0.60	1.37
5	11	0.60	0.68
5	12	0.60	0.32
10	9	0.65	4.54
10	10	0.60	3.34
10	11	0.60	1.66
10	12	0.60	0.77
10	13	0.60	0.33
20	10	0.70	4.22
20	11	0.65	2.91
20	12	0.60	1.88
20	13	0.60	0.81
20	14	0.60	0.33
40	11	0.75	3.68
40	12	0.65	3.30
40	13	0.60	1.99
40	14	0.60	0.81
40	15	0.60	0.31
60	12	0.70	4.00
60	13	0.65	2.31
60	14	0.60	1.36
60	15	0.60	0.52
60	16	0.60	0.18
100	12	0.80	3.99
100	13	0.70	3.35
100	14	0.60	2.62
100	15	0.60	1.00
100	16	0.60	0.35

1 in = 25.4 mm  
1 mi = 1.61 km

Notes: A minimum of 0.60 percent steel is recommended.  
The use of deformed steel is strongly recommended.

Table 44. Comparison of predicted and actual failures (punchouts and deteriorated cracks) from various CRCP sections.

Section ID Climate	Thick, in	% Reinf.	Base Type	ESAL's, million	Age, years	Mean Crack Space, ft	Predicted Failures/mi	Actual Failures/ mi
<b>Wet-Freeze</b>								
IL 1-1	9	0.72	LCB	1.7	6	3.4	0.4	0.00
IL 1-2	8	0.73	LCB	1.7	6	3.0	0.6	0.00
IL 1-3	7	0.70	LCB	1.7	6	3.5	1.2	0.00
IL-2*	8.8	0.59	CTB	10	15	4.2	9.3	12.4
IL-3 *	8.3	0.60	ATB	10	20	3.6	9.4	2.8
IL-4 *	9.3	0.60	ATB	20	20	2.1	12.8	1.8
IL-5 *	8.5	0.70	CTB	5	5	3.0	2.2	1.0
IA-1 *	8.2	0.65	CTB	10	20	5.9	8.8	0.00
IA-2 *	8.0	0.65	ATB	11	22	3.0	9.0	3.6
IA-3 *	8.0	0.65	ATB	8	15	3.0	6.0	3.2
OH 2-47/48	9	0.61	ATB	6.5	18	3.1,4.1	3.4	0.00
OH 2-98/99	9	0.61	CTB	6.5	18	4.1,6.1	4.2	0.00
OH2-CRC, -Sa, -Sb	9	0.61	AGG	6.5	18	3.3, 3.0, 3.4	4.4	0 and 13
PA-1*	9.2	0.45	AGG	10	15	4.8	10.0	0.00
PA-2*	9.4	0.55	AGG	11	22	4.3	10.3	10.6
WI-1*	8.4	0.65	AGG	10	18	2.9	8.3	6.2
WI-2*	10.2	0.67	AGG	6	6	2.9	1.2	0.00
WI-3*	10.2	0.67	AGG	7	7	3.5	1.5	0.8
WI-4*	10.6	0.67	AGG	7	7	4.6	1.1	1.4
WI-5*	7.9	0.61	AGG	16	16	3.4	25.8	21.4
MEAN WF							6.2	3.6
<b>Wet-NonFreeze</b>								
NC 1-9	8	0.60	AGG	16	25	4.3	26	0.00
OK-1*	9.2	0.5	ATB	2	4	8.4	1.4	0.3
OK-3*	10.3	0.5	ATB	2	3	4.8	0.7	0.00
OK-5*	10.1	0.61	CTB	1	2	6.1	0.2	0.5
OR-1*	12.4	0.60	AGG	7	7	4.0	0.5	0.00
OR-2*	10.1	0.60	CTB	4	4	5.6	1.3	0.00
MEAN WNF							5.0	0.1
<b>Dry-NonFreeze</b>								
CA 1-11 to 1-16	8.4	0.56	CTB	11.9	21	2.5 to 4.0	18.0	0 to 48
MEAN DNF							18.0	8.0
<b>BELGIUM</b>								
BEL-01	8	0.85	ATB/LCB	29.5		< 2	8.6	0.00
BEL-02	8	0.85	ATB/LCB	29.5		< 2	8.6	0.00
BEL-03	8	0.85	ATB/LCB	37.6		< 2	11.8	0.00

1 in = 25.4 mm  
 1 ft = 0.305 m  
 1 mi = 1.61 km

\* Data obtained from study documented in references 86 and 87.

higher ESAL categories should be used with caution. Furthermore, for CRCP greater than 10 to 12 in (254 to 305 mm) thick, the percentage of steel reinforcement and the quality of the subgrade support are believed to be more important to CRCP performance than slab thickness.

As discussed previously, the crack spacing and crack width are two crucial elements of CRCP reinforcement design. Conventional wisdom has decreed that crack spacings between about 3 and 8 ft (0.9 to 2.4 m) are required, but based on the Illinois (see references 115, 113, and 117) and European (see reference 39) experiences, crack spacings as short as 1.5 ft (0.5 m) can provide good performance. With regards to crack width, a maximum width of 0.025 in (0.6 mm) is considered necessary to provide good performance.

In CRCP reinforcement, generally No. 4 (13 mm), No. 5 (16 mm), or No. 6 (19 mm) diameter deformed bars are used, although deformed wire fabric has also been used with success. Deformed bars or wire are considered essential to ensuring that the cracks are held tightly together and not allowed to open. Grade 60 steel conforming to AASHTO M31, M42, or M53 is recommended for longitudinal CRCP reinforcement. The spacing between adjacent longitudinal bars should be between 4 and 9 in (102 and 229 mm).<sup>(115)</sup>

The depth of the steel from the slab surface can greatly affect the performance of the pavement; the closer the steel is to the surface, the tighter the cracks are held together. However, a minimum cover of 2.5 to 3 in (64 to 76 mm) is generally recommended.

In recent years, many agencies have adopted the use of epoxy-coated steel in their CRCP projects in order to minimize corrosion of the reinforcement. This has raised some concerns, however, about the bonding condition between the reinforcing steel and the concrete, a factor that can influence the crack pattern. Although the long-term effect of epoxy coating on pavement performance are not yet known, a recent field evaluation of CRCP projects suggests that the use of epoxy coating did not result in an undesirable crack pattern.<sup>(86)</sup> Additional research is needed to quantify the effects of epoxy coating on the development of the crack pattern and on the long-term performance of CRCP projects.

Some agencies include transverse steel in their CRCP designs, but many believe that it is not always needed.<sup>(118)</sup> However, its use may be required in areas where subgrade soil movements are anticipated.

### Concrete Strength

Concrete strength directly affects slab cracking and also influences other aspects of concrete pavement performance, including wear resistance, durability, and spalling. Higher concrete strengths can have a large positive effect on fatigue cracking and may also provide better wear resistance and lower permeability. The benefits of

reduced permeability include improved freeze-thaw durability of the concrete paste and better protection against steel corrosion that can cause spalling.

In terms of cracking performance, the consideration for the use of high-strength concrete is primarily a cost issue because slab thickness can be selected for any strength material to obtain the same cracking performance. Other benefits of using higher strength concrete are more difficult to assess. A Utah study showed that cement content may have a greater effect on wear resistance than concrete strength, but wear resistance was a problem only in the section with very low cement content (428 lbf/yd<sup>3</sup> [254 kg/m<sup>3</sup>]).<sup>(19)</sup> In Europe, special attention is given to the quality of concrete, especially the material placed near the pavement surface, to ensure adequate wear resistance and durability.<sup>(39)</sup>

Many countries in Europe use much higher-strength concrete than in the U.S. The minimum 28-day flexural strength is 800 lbf/in<sup>2</sup> (5.5 MPa) in Germany and 940 lbf/in<sup>2</sup> (6.5 MPa) in Austria.<sup>(40)</sup> The mean values are considerably higher: 1,100 lbf/in<sup>2</sup> (7.6 MPa) in Austria and 1,200 lbf/in<sup>2</sup> (8.3 MPa) in Italy. Often, two different mixes are used so that a durable, high-quality, high-strength material can be placed in the top portion of the slab (top 1.5 to 3 in [38 to 76 mm]) at a reasonable cost. A special paver is used to place the two different mixes in a single pass. No durability problems were found in any of the European sections inspected during the 1992 U.S. tour of European highways even though some of the sections had been exposed to severe freeze-thaw conditions and heavy use of deicing materials.<sup>(39)</sup>

Other than the effects on slab cracking, the pavement sections evaluated under this study did not show any strength-dependent performance trends. The average 28-day flexural strength estimated for the pavement sections evaluated under this study was about 650 lbf/in<sup>2</sup> (4.5 MPa). This value was estimated from the long-term flexural strengths determined for the pavement sections, assuming that the long-term strength is about 10 percent higher than 28-day strength. The 28-day flexural strength of 650 lbf/in<sup>2</sup> (4.5 MPa) is representative of the typical design strength for concrete pavements in the U.S. Based on the observations from this study, the following may be said about concrete strength:

- For the design conditions in the U.S., a minimum 28-day flexural strength of 650 lbf/in<sup>2</sup> (4.5 MPa) appears to be adequate to avoid any strength-related problems.
- Concrete strength is an important design factor affecting fatigue life of concrete slabs, but the structural capacity of concrete slabs also depend on slab thickness and joint spacing. The use of higher strength concrete might be considered for economic reasons, because the use of higher strength concrete reduces the required slab thickness.
- Based on excellent performance of European designs, the use of higher strength concrete merits further evaluation in the U.S.



## JPCP Slab Thickness

Slab thickness is a key design feature that has a major effect on the performance of concrete pavements. Slab thickness most directly affects fatigue cracking, but since slab thickness also affects deflections, all concrete pavement distresses that are influenced by slab deflections (pumping, faulting, and crack deterioration) are also affected by slab thickness to some extent. However, deflections are usually not a major factor for consideration in slab thickness design because deflection-related distresses are addressed more efficiently through the use of other design factors such as dowels, drainage, and widened PCC slabs. In general, slab thickness beyond that needed to limit mid-panel or corner fatigue cracking is not warranted when conventional concrete mixes are used.

The effects of slab thickness on mid-panel fatigue cracking are shown in figure 149. This figure shows the extreme sensitivity of slab cracking to slab thickness. For design traffic of 20 million ESAL's, a 0.5-in (13-mm) increase in slab thickness from 8.5 in (216 mm) to 9.0 in (229 mm) reduces the slab cracking from 62 percent to about 27 percent. The effects are just as dramatic in terms of allowable traffic. For example, if 20 percent slab cracking is selected as the failure criterion, the same 0.5-in (13-mm) increase in slab thickness (from 8.5 in to 9 in [216 mm to 229 mm]) increases the allowable traffic from 6.1 million ESAL's to 15 million ESAL's. That is, in terms of mid-panel slab cracking, a 0.5-in (13-mm) increase in slab thickness doubles the design life of a concrete pavement for slab thicknesses in the range of 8 and 9 in (203 and 229 mm).

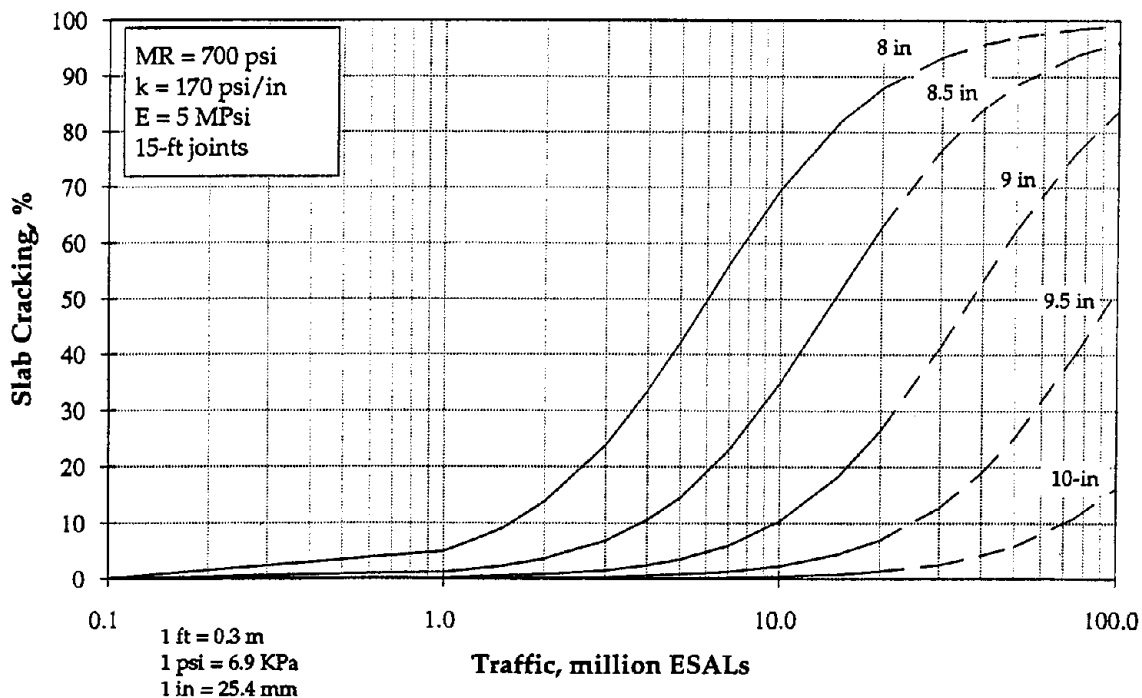


Figure 149. Effects of JPCP slab thickness on mid-panel fatigue cracking for wet-freeze climatic region.

Numerous factors in addition to slab thickness affect mid-panel fatigue cracking in concrete pavements. In general, all factors that affect stresses in concrete slabs (more accurately, the stress to strength ratio) affect fatigue cracking, but major factors are slab thickness, joint spacing, subgrade stiffness ( $k$ -value), concrete modulus of rupture (MR), concrete elastic modulus ( $E_{PCC}$ ), base type, slab/base friction, widened slab, shoulder type, and climate. To obtain the desired performance, slab thickness should be selected considering the effects of the key design factors and their interactions on mid-panel fatigue performance of concrete slabs. This may be accomplished using the mid-panel fatigue analysis procedure presented in chapter 2 of this report.

The JPCP calibrated mechanistic cracking model presented in chapter 2 is based on the development of fatigue cracking at the mid-point of the slab, and the slab thickness recommendations presented later are based on that assumed failure mode. However, it is possible that fatigue cracking can also develop near slab corners when the slab is subjected to traffic loading under a negative (slab surface cooler than slab bottom) temperature gradient. In this case, cracking will actually initiate at the top of the slab due to the slab corners being curled up; thus, in addition to the factors listed above, the inclusion of dowel bars is a critical factor influencing top-down fatigue cracking (near the slab corner).

Although top-down fatigue cracking can be the critical failure mode in some cases, the magnitudes of fatigue damage accumulated in both top-down and mid-panel fatigue cracking are similar. Because of this, the required slab thicknesses computed using either a top-down fatigue cracking analysis or a mid-panel fatigue cracking analysis will likely be very close, except on shorter slabs (less than 15 ft [4.6 m]). In those cases with very short joint spacing, the required slab thicknesses computed using a top-down fatigue analysis would be slightly greater.

The mid-panel JPCP fatigue cracking model gives reasonable predictions, and the predictions compare well with the field data, including the cracking data from the AASHO road test.<sup>(83)</sup> Compared to the AASHTO rigid pavement design charts (which are based on serviceability loss), however, the allowable traffic given by the cracking model is much lower than AASHTO for thin slabs (less than 7.5 in [191 mm]) but substantially greater than AASHTO for thick slabs (greater than 10 in [250 mm]). The reason for the difference is attributable to the difference in the design criteria (i.e., the AASHTO design procedure is based on serviceability) and to the consideration of corner loading conditions in the development of the AASHTO design equation.

Although slab cracking is a major factor affecting serviceability, slab cracking does not affect serviceability until the cracks develop faulting and spalling. On lower-volume roads, it may be possible to accommodate greater amount of traffic on cracked slabs because of the lighter axle loads. The fact that AASHTO requires greater slab thicknesses at high traffic levels (20 million ESAL's or more) is believed to be caused by an extrapolation beyond the data. None of the AASHO Road Test JPCP test sections having a thickness of 11 in (279 mm) or more cracked, even after

14 years of service on I-80. However, the main cause of roughness in concrete pavements is faulting, and dowels are much more effective at reducing faulting than additional slab thickness; as observed in this study, additional slab thickness is ineffective at reducing faulting. In general, the cracking model gives slab thicknesses that are slightly less than AASHTO (by about 0.5 in [13 mm]) for typical highway design conditions. For low traffic conditions, however, the cracking model gives substantially greater thicknesses.

The key findings of the cracking analysis conducted under this project are presented in the following discussion, along with a discussion of how to incorporate this information in the thickness design of concrete pavements.

*Effect of Joint Spacing on JPCP Slab Thickness Design*

Joint spacing greatly affects curling stresses that develop in concrete slabs. Within the range of recommended joint spacing for jointed plain concrete highway pavements (12 to 20 ft [6.1 to 7.6 m]), curling stresses increase rapidly with increasing joint spacing. Depending on joint spacing and temperature gradients, curling stress can make up a significant portion of the combined stress (load and curling) in a pavement slab. In longer slabs, curling stresses may exceed load stresses when the slabs are exposed to high temperature gradients. Because of the higher curling stresses a greater slab thickness is required to obtain the same level of performance as the slab length is increased.

The effects of joint spacing on slab thickness design is illustrated in figure 150. In this figure and in other sensitivity plots, a level of 20 percent slab cracking was used

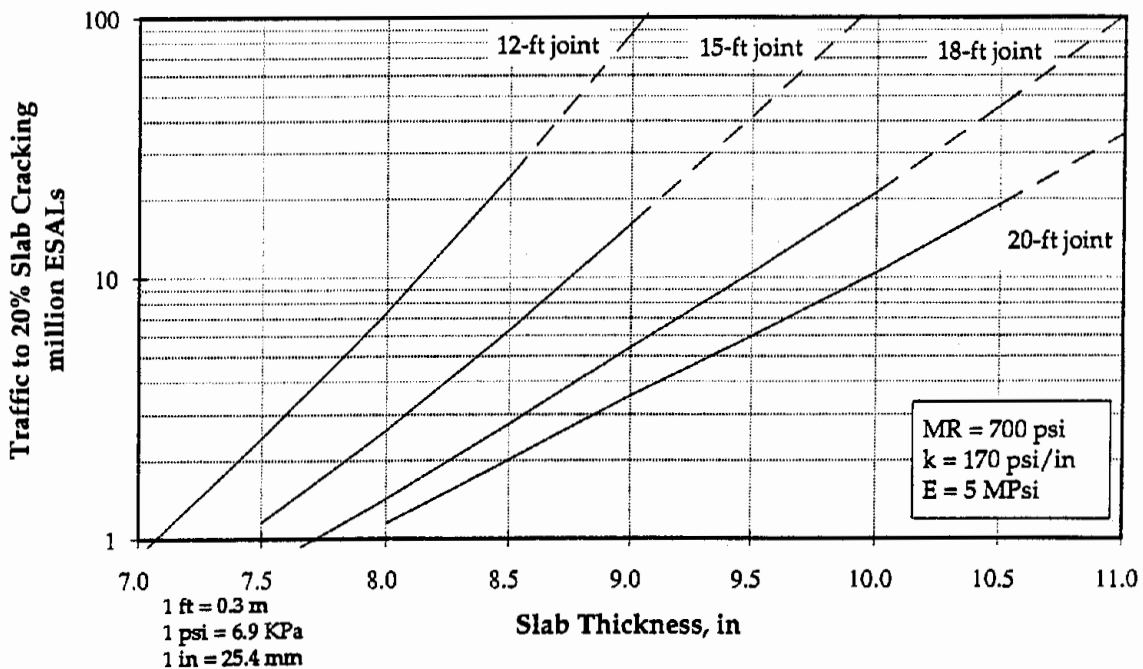


Figure 150. Sensitivity of mid-panel fatigue cracking to joint spacing and slab thickness for wet-freeze climatic region.

as the failure criteria. This choice is arbitrary, and it was selected to provide a consistent basis for comparisons only; however, 20 percent slab cracking is a reasonable choice of failure criteria for design purposes because it is representative of the onset of rapid cracking of slabs (see figure 149). Some agencies use similar criteria to determine the timing of structural rehabilitation.

Figure 150 shows that the desired level of performance can be obtained for any joint spacing by selecting the appropriate slab thickness. For example, a design traffic of 20 million ESAL's may be accommodated using 12-ft (3.7-m), 15-ft (4.6-m), 18-ft (5.5-m), or 20-ft (6.1-m) joint spacing by selecting the appropriate slab thickness. Both 8.5-in (216-mm) slabs at 12-ft (3.7-m) joint spacing and 10.5-in (267-mm) slabs at 18-ft (6.1-m) joint spacing satisfy the design requirements, and in terms of cracking performance the two designs are equivalent. The selection of joint spacing, however, involves consideration of other factors, including spalling, pumping, and stability of pavement slabs.

The recommended minimum and maximum joint spacings for highway pavements are 12 ft (3.7 m) and 20 ft (6.1 m), respectively. The selection of joint spacing within this range is largely a matter of economics and designer preference. If a short joint spacing is used, then the required slab thickness is less but the cost of sawing and maintaining joints is higher; if greater joint spacings are used, the cost of joints is less but thicker slabs are required. Slab thickness and joint spacing design involves balancing between the cost of providing and maintaining joints against the cost of additional slab thickness required by increasing joint spacing.

If either joint spacing or slab thickness has been selected, the other parameter can be determined using the cracking model or a chart similar to that shown in figure 150. Design charts such as that shown in figure 150 are useful for numerous purposes, including the following:

- Determining the maximum allowable joint spacing given slab thickness.
- Determining the required slab thickness given joint spacing.
- Determining the sensitivity of slab cracking to slab thickness and joint spacing.

Because the results shown in figure 150 depend on concrete strength, subgrade dynamic  $k$ , elastic modulus of concrete, and climate the chart must be developed for the specific design condition at hand.

#### *Effect of Subgrade $k$ on JPCP Slab Thickness Design*

Although subgrade support is not a particularly sensitive factor affecting stresses in concrete slabs, it is an important factor for consideration in slab thickness design because even a small change in stress has a large effect on the mid-panel fatigue life of concrete slabs. Relatively large changes in  $k$ -value are required to significantly alter stresses in the pavement slabs. However, large variations in  $k$ -values do occur in the field (variations in the order of 100 lbf/in<sup>2</sup>/in [27 kPa/mm] or more), and the

resulting variations in critical stresses are significant for mid-panel fatigue performance.

The effects of subgrade dynamic  $k$  on slab stresses are shown in figure 151. An increase in dynamic  $k$ -value reduces the load stress but increases the curling stress. The net effect depends on the relative rates of change in load and curling stresses as the dynamic  $k$ -value is increased. Figure 151 shows a net positive effect, but the result can be either positive (increase in combined stress) or negative (decrease in combined stress). Without slab curling, the net result is a decrease in stresses with increasing dynamic  $k$ -value; however, all pavements are exposed to daily temperature cycles which cause slab curling. In typical highway design conditions, the combined stress increases with increasing dynamic  $k$ -value.

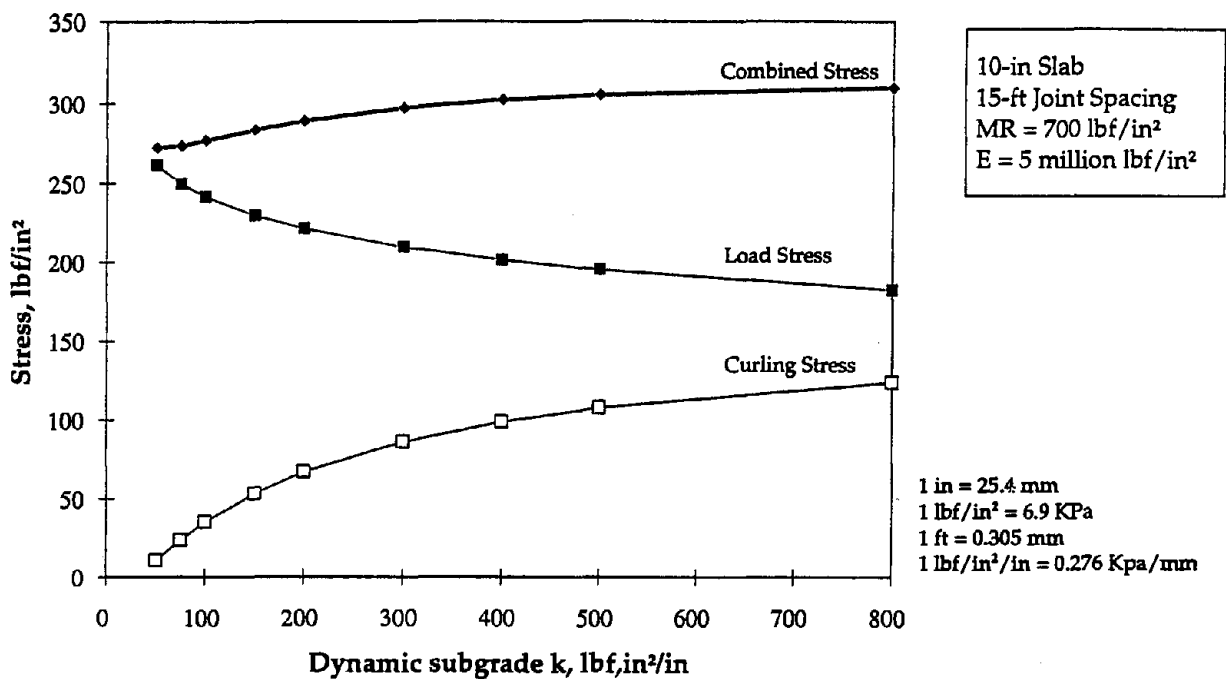


Figure 151. Effects of dynamic  $k$ -value on stresses in pavement slabs for wet-freeze climatic region.

The effects of subgrade dynamic  $k$  on cracking performance are shown in figure 152. Subgrade  $k$  does not have as dramatic an effect on cracking performance as either slab thickness or joint spacing, but the effects are not insignificant. For example, the difference in allowable traffic for a 9-in (229-mm) slab constructed on a subgrade with a dynamic  $k$  of 100 lbf/in<sup>2</sup>/in (27 kPa/mm) and a dynamic  $k$  of 200 lbf/in<sup>2</sup>/in (54 kPa/mm) is 20 percent. For a 9.5-in (241-mm) slab, the difference is nearly 40 percent. Compared to the effect of a 0.5-in (13-mm) increase in slab thickness on cracking performance, which results in an increase factor of 3 in allowable traffic, the doubling of dynamic  $k$ -value has a relatively minor effect. However, a 20-percent reduction in service life is significant from a design perspective.

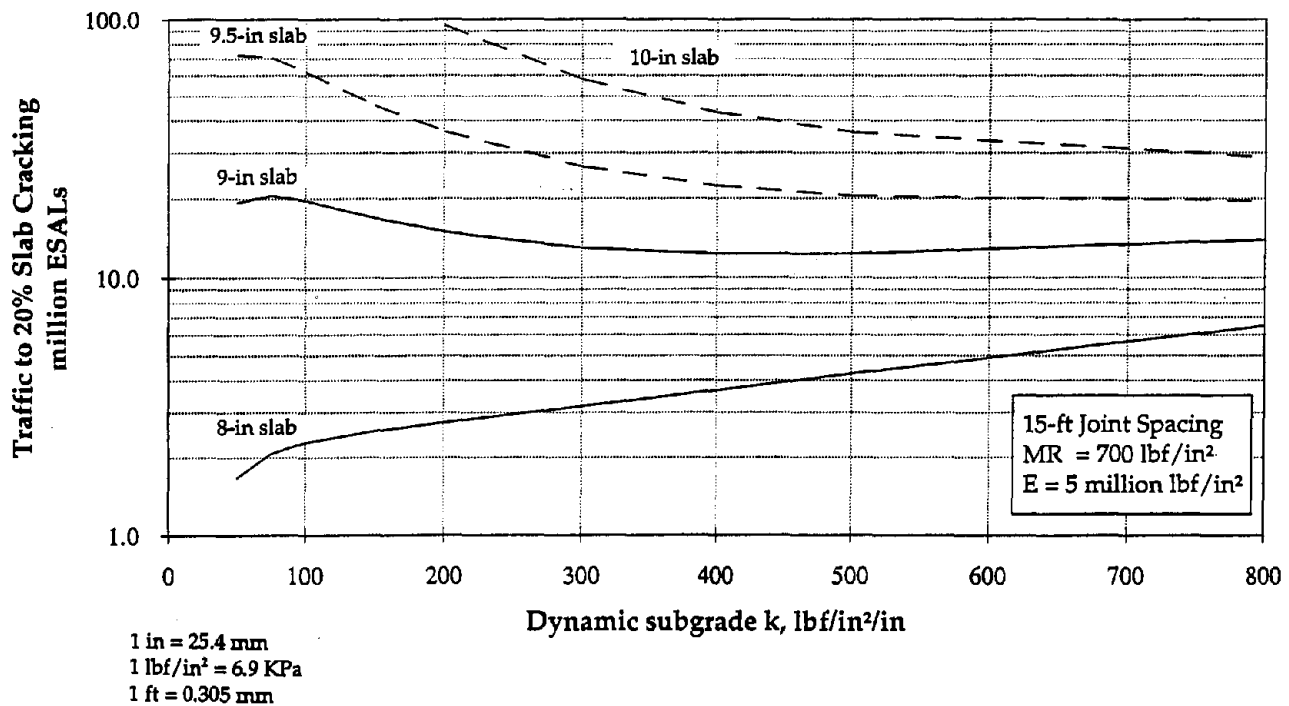


Figure 152. Effects of subgrade dynamic  $k$  on allowable traffic for the wet-freeze climatic region.

For cracking performance, there is also a strong interaction between the subgrade  $k$  and the joint spacing. The effects of subgrade  $k$  and joint spacing on mid-panel fatigue cracking is shown in figure 153. Again, the net effect of increasing dynamic  $k$ -value depends on the relative changes in curling and load stresses in the slab as the dynamic  $k$ -value is increased.

Depending on the site conditions, the subgrade  $k$  can be highly variable, and as shown in figures 152 and 153, taking a lower value of design  $k$  is not always conservative. To ensure satisfactory performance the design  $k$ -value must be selected with care. The trends shown in figures 152 and 153 are consistent with the findings from a recent research project that investigated the effects of foundation support on pavement performance.<sup>(34)</sup>

Most design procedures give thinner slabs for higher  $k$ -values when in fact thicker slabs are required to compensate for the increased curling stress. The reason for this is that most design procedures do not consider the effects of slab curling in thickness design. The lack of adequate consideration for the effects of foundation stiffness on curling stresses in design can lead to premature failures. The use of sensitivity plots (similar to figure 152) is highly recommended to ensure that the trend given by the design procedure is reasonable. Design checks using the procedures described in chapter 2 of this report are also recommended.

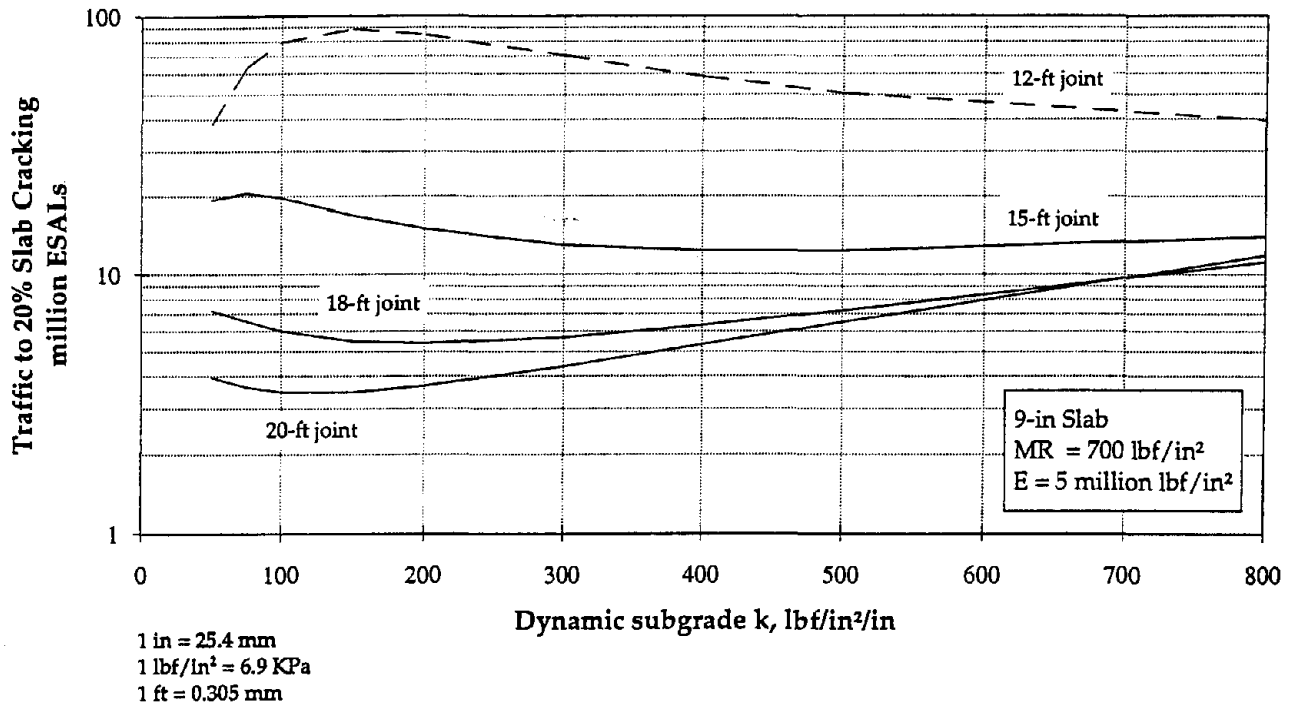


Figure 153. Effects of subgrade  $k$  and joint spacing on allowable traffic for wet-freeze climatic region.

The  $k$ -values used in this report are dynamic  $k$ -values obtained by backcalculation using FWD data. The dynamic  $k$ -values are approximately twice the static  $k$ -value commonly used in design. Only the estimated dynamic  $k$ -value at the top of subgrade should be used with the procedure presented in chapter 2.

#### *Effect of Concrete Strength and Elastic Modulus on JPCP Slab Thickness Design*

The concrete modulus of rupture (MR) directly affects the stress-to-strength ratio, which determines the fatigue life of the concrete slab. Because fatigue cracking is very sensitive function to the stress ratio, significant improvement in cracking performance can be achieved by increasing the concrete strength. The effects of concrete MR on cracking performance is shown in figure 154. Figure 154 shows that a 0.5 in (13 mm) reduction in slab thickness is possible if MR is increased by about 7 percent (about 50 lb/in<sup>2</sup> [345 kPa] in this case). However, an increase in concrete strength is usually accompanied by a corresponding increase in the  $E_{PCC}$ . Because a higher  $E_{PCC}$  causes higher stresses in concrete slabs, the actual improvement in cracking performance with an increase in MR is somewhat less than consideration of MR alone. This effect is shown in figure 155.

Figure 155 shows that if the increase in MR is accompanied by a 10 percent increase in  $E_{PCC}$ , about a 10 percent increase in strength (rather than 7 percent indicated by the consideration of MR alone) is needed to reduce slab thickness by 0.5

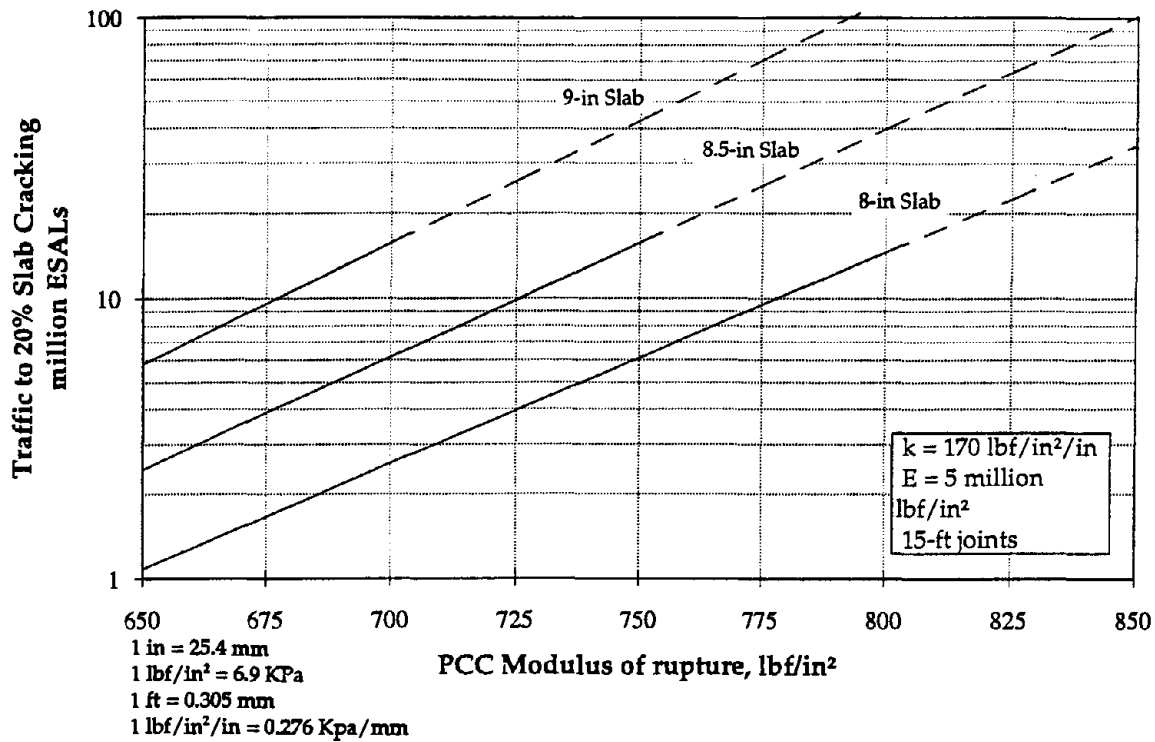


Figure 154. Effects of concrete strength and slab thickness on cracking performance of JPCP for wet-freeze climatic region.

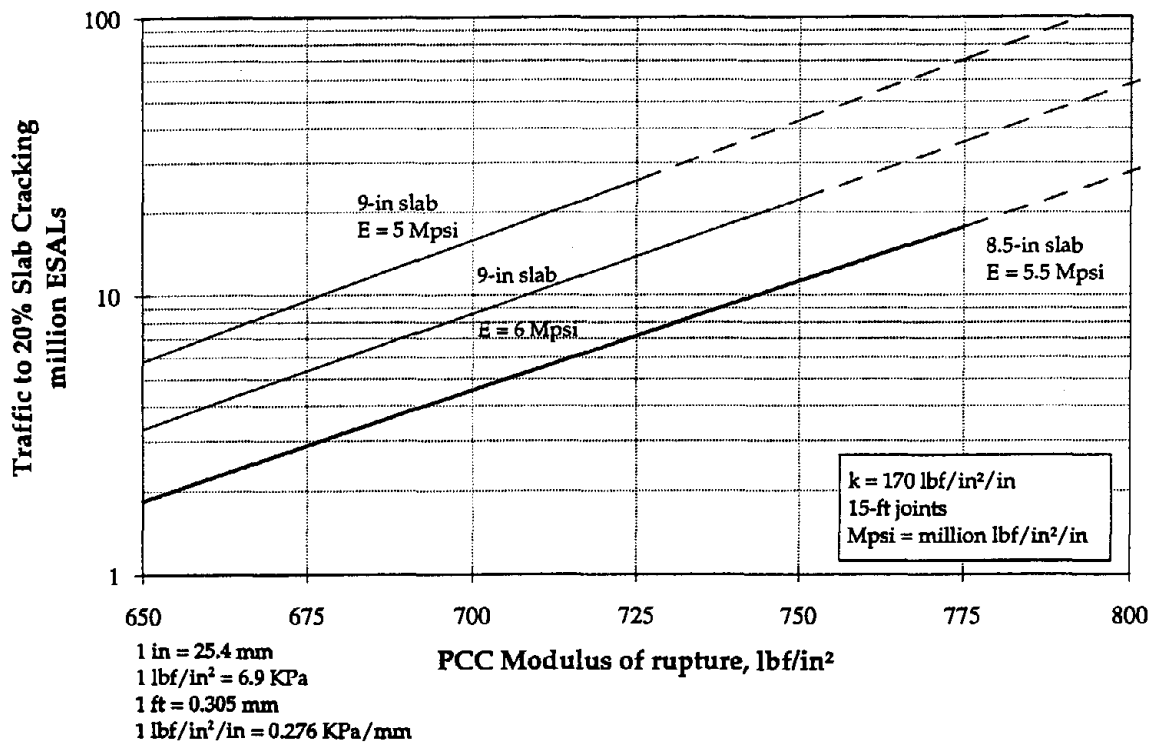


Figure 155. Effects of concrete strength and  $E_{PCC}$  on cracking performance of JPCP for wet-freeze climatic region.



in. If  $E_{PCC}$  is 20 percent higher, then a 5 percent higher strength has no net effect (i.e., no improvement in performance).

For the consideration of mid-panel fatigue cracking only, the design slab thicknesses can be reduced by using higher strength concrete; however, excessive reductions in slab thickness is not advisable because of concerns for excessive deflection. Slab deflections affect faulting performance and crack deterioration in JRCF and CRCP, but inadequate information is currently available to provide guidelines on what limits should be placed on maximum deflections. Thus, prudent practice may be to not go below the lower limit of the typical slab thicknesses for the class of pavement being designed; that is, use high-strength concrete only to obtain structural capacity beyond that which can be obtained using minimum thickness and normal-strength concrete. For example, if the lower limit of slab thicknesses for a highway pavement in the wet-freeze climatic zone were 8 in (203 mm) and the design traffic were 20 million ESAL's, then 820 lbf/in<sup>2</sup> (5.7 MPa) concrete may be used with the 8-in (203-mm) slab to satisfy the design requirements; however, higher strength concrete should not be used to reduce slab thicknesses below the 8-in (203-mm) minimum. The lower limit of slab thicknesses may vary depending on the highway, base type, climate, and local conditions.

#### *Effect of Slab-Base Bonding on JPCF Slab Thickness Design*

A stabilized base can have a significant effect on slab thickness design if it is bonded to the pavement slab, as illustrated in figure 156. The presence of the stabilized base has negligible effect on the slab thickness if it is not bonded to the slab. The bonding of the base enhances the mid-panel fatigue performance in two ways:

- The bonding allows the two pavement layers to function monolithically as a single effective layer. The effective thickness depends on the layer thickness and modulus of individual layers. In the example shown in figure 156, the 4-in (102-mm) stabilized base adds about 1 in (25 mm) to the effective thickness of the combined base-slab system for the 7-in (178-mm) slab.
- The location of critical stress remains at the bottom of the concrete layer in the combined structure because  $E_{PCC}$  is so much greater than  $E_{Base}$  (by a factor of 12.5 in the figure 156 example). Because the critical stress location is now much closer to the neutral axis, the critical stress is significantly less than the effective thickness alone would suggest. In this example, the performance given by the 7-in (178-mm) slab on 4-in (102-mm) stabilized base is equivalent to that given by about 9.2-in (234-mm) slab on grade. In other words, the 4-in (102-mm) base is providing performance equivalent of 2.2 in (56 mm) of additional slab thickness.

The bonded assumption must be used with care because debonding and layer slippage may eventually occur. In Germany, pavement slabs are routinely bonded to cement stabilized base as a matter of standard practice.<sup>(39)</sup> Germans report that the

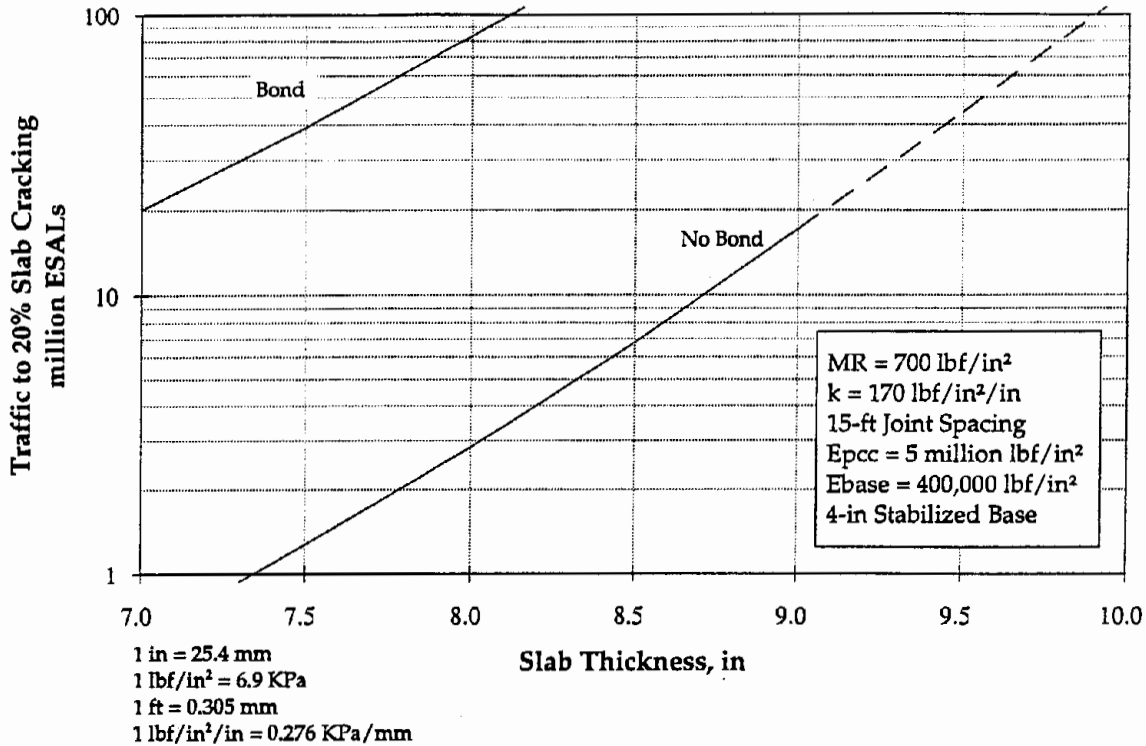


Figure 156. Effects of the base-slab bond condition on cracking performance for wet-freeze climatic region.

bond remains effective for 4 to 5 years, but debonding will eventually occur at the corners and edges.<sup>(40)</sup> Recent studies have shown that the actual bond is not necessary to obtain some of the benefits of the bonding; some of the bonded response can be obtained through the interface friction.<sup>(34,80)</sup>

The mid-panel fatigue analysis results of this study showed that, in terms of cracking performance, most of the sections evaluated under this study exhibited unbonded behavior; however, backcalculation of FWD testing results showed bonded response in almost all stabilized base sections. The backcalculation results suggest that bonded response can be achieved through friction alone; however, the fatigue analysis results show that the bond between a stabilized base and slab is not reliable, and that friction alone is usually not adequate to provide bonded response at the pavement edges. A small amount of slippage between the layers results in a significant increase in slab bending stresses.

Further investigation is needed to determine the effectiveness of the bond between a stabilized base and concrete slab. Further investigation is also needed to determine the effects of a stabilized base on stresses in concrete slabs when the two layers are not bonded. If the two layers are not bonded, it is possible for the stabilized base to act as a very stiff foundation and cause high curling stresses in the pavement slab; however, this effect was not evidenced in the data collected under this study, indicating that the base layer does provide some structural benefit to the pavement

slabs. Nevertheless, for design purposes, unless special efforts are made to intentionally bond the base and slab, the unbonded assumption should be used.

### *Effect of Widened PCC Slabs and Tied PCC Shoulders on JPCP Slab Thickness Design*

Widened PCC slabs and tied PCC shoulder improve cracking performance of concrete pavements by reducing the critical bending stresses at the edge of the slab. In widened slab sections, the reduction in the critical stress is achieved by moving the critical edge further away from the wheel path, thereby reducing the frequency of traffic encroachment to the pavement edge. The critical location for mid-panel fatigue damage in widened PCC slabs is directly under the outer wheelpath, and the critical stress is about 60 percent of that occurring in a standard-width (12-ft [3.7-m]) slab.

In tied PCC shoulder sections, the reduction in the critical stress is achieved by transferring part of the load to the shoulder slabs through aggregate interlock. The effectiveness of tied PCC shoulders depend on the stress load transfer efficiency (LTE) across the lane-shoulder joint. For design purposes, a conservative value of LTE should be used because the LTE tend to degrades with pavement age. The recommended values of stress LTE are 20 percent for the shoulders that are constructed monolithically with the mainline (sawed lane-shoulder joint) and 10 percent for separately constructed shoulders (smooth or keyed joint faces at the lane-shoulder joint).

The effects of widened slab and tied shoulders on thickness design are shown in figure 157. According to figure 157, the following adjustments to slab thickness are possible:

- 0.5-in (13-mm) reduction for tied PCC shoulders with 10 percent stress LTE.
- 1.0-in (25-mm) reduction for tied PCC shoulders with 20 percent stress LTE.
- 1.5-in (38-mm) reduction for widened slab.

The above findings for tied PCC shoulders are consistent with the findings of a Minnesota study, which showed that 1-in (25-mm) reduction in slab thickness is possible when tied PCC shoulders are provided.<sup>(120)</sup> Similarly, results from a Colorado study showed that the structural benefit provided by effectively tied PCC shoulders was roughly equivalent to 1 in (25 mm) of PCC slab thickness.<sup>(81)</sup>

However, the possible slab thickness reductions described above are based on considerations of mid-panel fatigue cracking only. As discussed previously, the potential for excessive deflections is a major concern when slab thickness is reduced. As before, a similar cautionary note is applicable: design features such as tied PCC shoulder and widened slab should not be used to reduce slab thickness below the minimum of the typical pavement thicknesses for the class of pavement being designed.

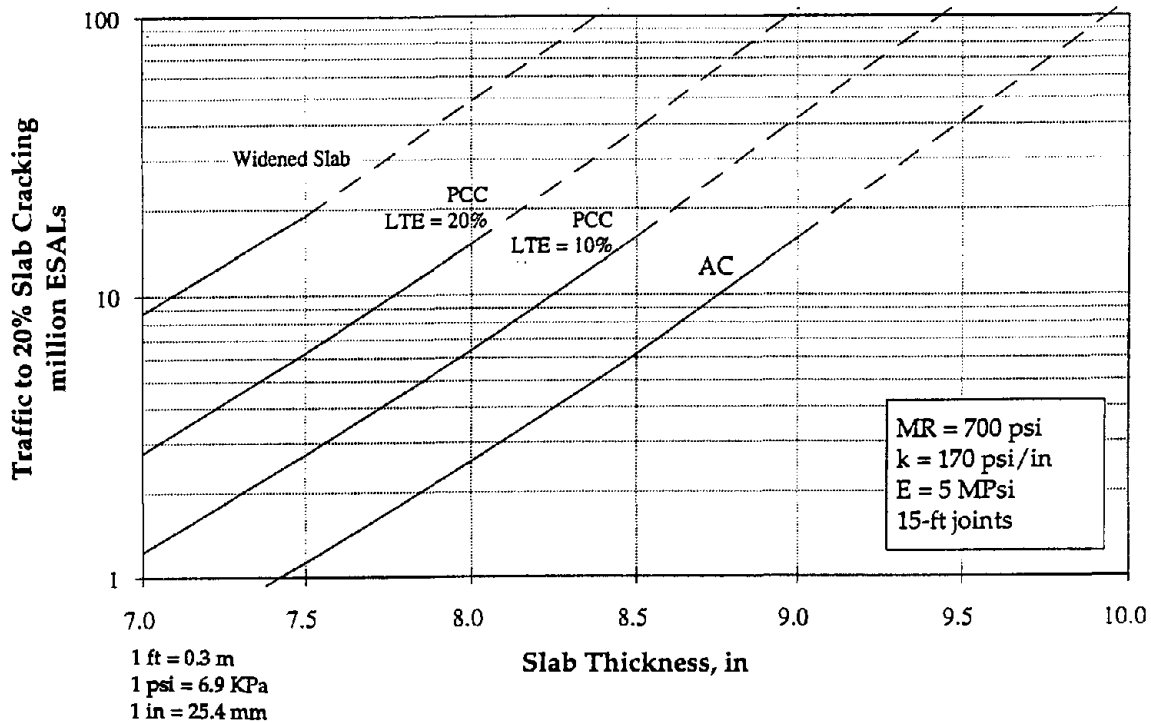


Figure 157. Effects of widened slab and tied PCC shoulder on cracking performance for wet-freeze climatic region.

In general, widened PCC slabs are more effective at improving cracking performance than tied PCC shoulders, and widened slabs cost considerably less. However, if the assumed LTE for design is very high, it is possible for the design thickness obtained for tied PCC shoulder to be less than that required for widened slab sections. This is because the critical damage is assumed to occur at the lane-shoulder joint for tied PCC shoulder sections and under the outer wheelpath for widened slab sections. If a very high LTE is assumed, the damage at the interior location can become more critical than the damage at the lane-shoulder joint. If the assumed stress LTE is 20 percent or greater, the thickness for widened slab design should also be checked to ensure that the slab thickness is adequate according to fatigue damage at both locations.

#### *Effect of Climate on JPCP Slab Thickness Design*

Pavements in different climates are subjected to different temperature and moisture conditions. The different temperature conditions affect curling stresses, and the different moisture conditions affect differential shrinkage and moisture warping. The effects of the environmental exposure conditions on slab thickness is shown in figure 158. The four climatic regions specified by LTPP are used in this analysis. The four regions were shown to adequately describe the exposure conditions affecting the cracking performance of concrete pavements. The different temperature and moisture conditions in different climatic regions can significantly affect cracking performance.

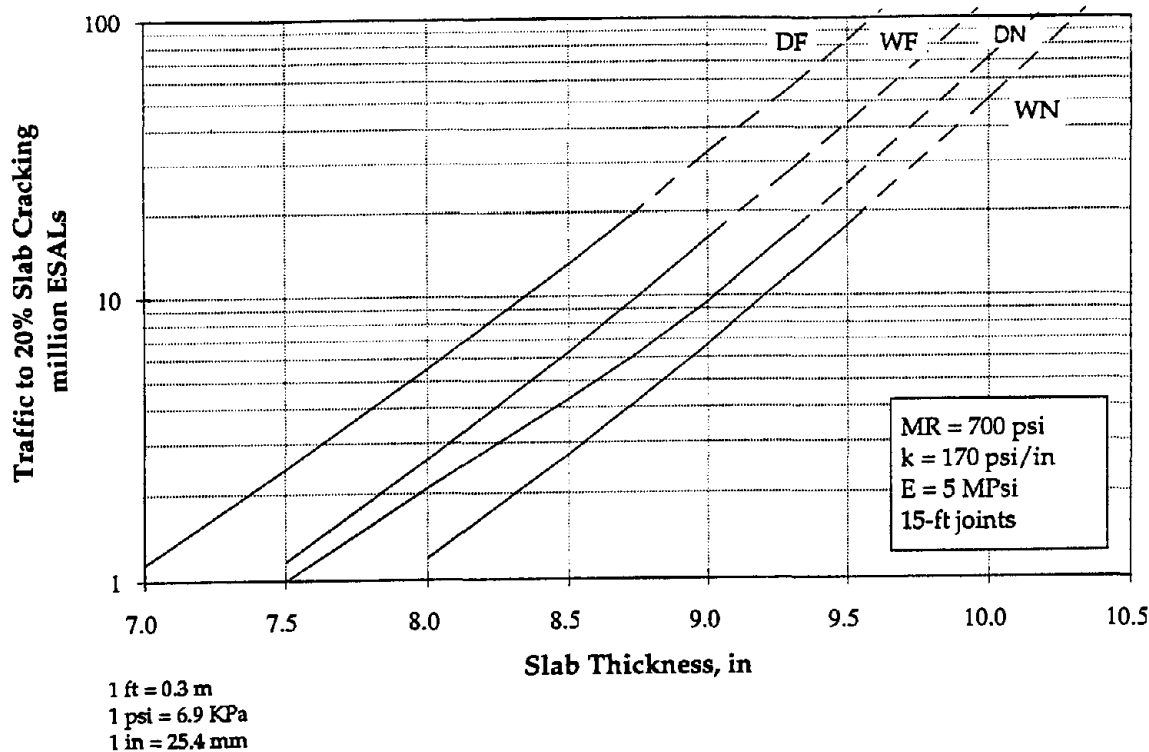


Figure 158. Effects of climate on slab thickness.

Figure 158 shows that the difference in the required slab thickness due to environmental conditions can be as much as 1 in (25 mm). Thicker slabs are required in nonfreeze regions because of exposure to higher temperature gradients. The required slab thicknesses are slightly less in dry regions because concrete slabs are exposed to greater amount of differential shrinkage which counters the curling stresses. The procedure for determining the accumulated mid-panel fatigue damage considering the environmental effects are described in chapter 2. This procedure may be used to determine the required slab thickness for the different design conditions.

#### *Design Slab Thickness Tables for JPCP*

The design slab thicknesses determined using the mid-panel fatigue cracking model are summarized in tables 45, 46, 47, and 48 for the dry-freeze, dry-nonfreeze, wet-freeze, and wet-nonfreeze regions, respectively. These tables provide the required slab thickness in 0.25-in (6-mm) increments for the given conditions. The variables considered in these tables are:

- Joint spacing—12, 15, 18, and 20 ft (3.7, 4.6, 5.5, and 6.1 m).
- Subgrade dynamic  $k$ —100, 200, and 400 lbf/in<sup>2</sup>/in (27, 54, and 109 kPa/mm).
- Base type—aggregate and stabilized bases.
- Tied PCC shoulder—10 percent and 20 percent LTE.
- Widened slab.
- Traffic—1, 5, 10, 20, 50, and 100 million ESAL's.

The following parameters were held constant:

- Long-term concrete modulus of rupture—700 lbf/in<sup>2</sup> (4.8 MPa).
- Concrete modulus of elasticity—5 million lbf/in<sup>2</sup> (34.5 GPa).
- Base thickness—5 in (127 mm).

Because the results are based on a mid-panel fatigue analysis, the inclusion of dowels in the transverse joints is irrelevant. The concrete strength above is representative of long-term values. The 28-day MR may be estimated by reducing the long-term concrete strength by 10 percent.

Tables 45 through 48 may be used to verify thickness designs. However, the values shown in these tables are values representative of a 50 percent level of reliability. Thus, slight increase in thickness over those shown in these tables may be desirable to improve reliability; however, given the sensitive of cracking performance to slab thickness, thickness increases in excess of 0.5 in (13 mm) are not warranted.

It should also be noted that the recommendations for the higher ESAL categories in tables 45 through 48 are based on gross extrapolations of the prediction model; only a few sections included in the data base had been exposed to more than 20 million ESAL applications. Thus, the recommendations provided for those higher ESAL categories should be used with caution.

For comparison with AASHTO design thicknesses, table 47 (wet-freeze climatic region) should be used. The slab thicknesses for 15 or 18 ft (4.6 or 5.5 m) joint spacing in table 47 compare reasonably with the AASHTO thicknesses at 50 percent reliability level. When a higher reliability level is used, the AASHTO design thicknesses are substantially higher. The change in design thickness corresponding to the changes in design reliability from 50 percent to 90 percent is nearly 2 in (51 mm) for a typical highway pavement. Considering the sensitivity of cracking performance to slab thickness, an increase of this magnitude seems excessive. The AASHTO design thicknesses are significantly less than those given in table 47 at low traffic levels (5 million ESAL's or less) but substantially greater at very high traffic levels (50 million ESAL's or more). For average highway design traffic levels, AASHTO thicknesses and the table 47 values show reasonable agreement.

### JRCP and CRCP Slab Thickness

Common design practice in the U.S. is to build JRCP and CRCP to the same thickness as JPCP. This practice is suited for designs using the AASHTO design procedure, which does not include joint spacing as one of the factors in determining the required slab thickness. In the AASHTO design procedure, the joint spacing for JPCP is selected to minimize fatigue cracking over the design period. For JRCP and CRCP, the basic design philosophy in the AASHTO procedure is that slab cracking can be tolerated because the reinforcing steel will hold the cracks tight. The problem has been that the amount of reinforcement provided has often not been sufficient to

Table 45. JPCP slab thickness design table for dry-freeze climate (50 percent design reliability).

Traffic million ESAL's	Joint Spacing ft	Standard Width Slabs											Tied PCC Shoulder						Widened Slabs			
		No Base			Aggregate Base E = 30 klb/in <sup>2</sup>			Stabilized Base					Aggregate Base						Aggregate Base E = 30 klb/in <sup>2</sup>			
		k, lbf/in <sup>2</sup> /in			k, lbf/in <sup>2</sup> /in			E = 500 klb/in <sup>2</sup>			E = 1,000 klb/in <sup>2</sup>		Stress LTE = 20% †			Stress LTE = 10% ‡			k, lbf/in <sup>2</sup> /in			
		100	200	400	100	200	400	100	200	400	100	200	400	100	200	400	100	200	400	100	200	400
1.0	12.0	7.50	7.25	6.75	7.50	7.25	6.75	7.50	7.00	6.50	7.25	6.75	6.50	6.75	6.50	6.50	7.00	6.75	6.50	6.50	6.50	6.50
1.0	15.0	7.75	7.50	6.75	7.75	7.50	6.75	7.75	7.25	6.50	7.50	7.25	6.50	6.75	6.50	6.50	7.25	6.75	6.50	6.50	6.50	6.50
1.0	18.0	8.25	7.75	6.75	8.00	7.75	6.75	8.00	7.50	6.50	7.75	7.25	6.50	7.00	6.50	6.50	7.50	7.00	6.50	6.50	6.50	6.50
1.0	20.0	8.25	7.75	6.75	8.25	7.75	6.75	8.25	7.50	6.50	8.00	7.50	6.50	7.00	6.50	6.50	7.75	7.00	6.50	6.50	6.50	6.50
5.0	12.0	8.25	8.00	7.75	8.25	8.00	7.75	8.25	7.75	7.50	8.00	7.75	7.50	7.25	7.00	6.50	7.75	7.50	7.00	6.50	6.50	6.50
5.0	15.0	8.75	8.50	8.25	8.50	8.50	8.25	8.50	8.50	8.00	8.50	8.25	8.00	7.50	7.25	6.50	8.00	8.00	7.50	6.50	6.50	6.50
5.0	18.0	9.00	9.00	8.75	9.00	9.00	8.75	9.00	9.00	8.50	9.00	8.75	8.25	8.00	7.50	6.50	8.50	8.25	7.50	7.00	6.50	6.50
5.0	20.0	9.50	9.50	8.75	9.50	9.50	8.75	9.25	9.25	8.50	9.25	9.00	8.25	8.25	7.75	6.50	8.75	8.50	7.50	7.25	6.50	6.50
10.0	12.0	8.50	8.25	8.25	8.50	8.25	8.25	8.50	8.25	8.00	8.25	8.00	8.00	7.50	7.25	6.75	8.00	7.75	7.50	6.50	6.50	6.50
10.0	15.0	9.00	9.00	9.00	9.00	9.00	8.75	8.75	8.75	8.75	8.75	8.75	8.50	8.00	7.75	7.25	8.50	8.25	8.00	6.75	6.50	6.50
10.0	18.0	9.50	9.75	9.50	9.50	9.75	9.50	9.50	9.50	9.50	9.25	9.50	9.25	8.50	8.25	7.50	9.00	9.00	8.50	7.50	6.50	6.50
10.0	20.0	10.00	10.25	10.00	10.00	10.25	10.00	9.75	10.00	9.75	9.75	10.00	9.50	8.75	8.50	7.50	9.25	9.25	8.50	7.75	7.25	6.50
20.0	12.0	8.75	8.75	8.50	8.75	8.75	8.50	8.75	8.50	8.50	8.50	8.50	8.25	7.75	7.50	7.25	8.25	8.00	8.00	6.75	6.50	6.50
20.0	15.0	9.25	9.25	9.50	9.25	9.25	9.50	9.25	9.25	9.25	9.00	9.00	9.25	8.25	8.25	8.00	8.75	8.75	8.75	7.25	7.00	6.50
20.0	18.0	10.00	10.25	10.50	10.00	10.25	10.50	9.75	10.00	10.25	9.75	10.00	10.25	8.75	8.75	8.25	9.25	9.50	9.50	8.00	7.75	6.50
20.0	20.0	10.50	10.75	11.25	10.50	10.75	11.25	10.25	10.75	11.00	10.25	10.50	11.00	9.25	9.25	8.50	9.75	10.00	10.00	8.50	8.50	6.50
50.0	12.0	9.25	9.00	9.00	9.00	9.00	9.00	9.00	9.00	9.00	9.00	8.75	8.75	8.25	8.00	8.00	8.50	8.50	8.50	7.00	6.75	6.50
50.0	15.0	9.75	9.75	10.25	9.75	9.75	10.25	9.50	9.75	10.00	9.50	9.75	10.00	8.75	8.75	8.75	9.00	9.25	9.50	7.75	7.75	7.50
50.0	18.0	10.50	10.75	11.50	10.50	10.75	11.50	10.25	10.75	11.50	10.25	10.75	11.25	9.25	9.50	9.75	9.75	10.25	10.75	8.50	9.00	10.25
50.0	20.0	11.00	11.50	12.50	11.00	11.50	12.50	11.00	11.50	12.25	10.75	11.50	12.25	9.75	10.25	10.50	10.50	11.00	11.50	9.25	10.25	12.25
100.0	12.0	9.25	9.25	9.50	9.25	9.25	9.50	9.25	9.25	9.25	9.25	9.00	9.25	8.50	8.25	8.25	8.75	8.75	8.75	7.25	7.25	7.00
100.0	15.0	10.00	10.25	10.75	10.00	10.25	10.75	9.75	10.00	10.50	9.75	10.00	10.50	9.00	9.00	9.25	9.50	9.75	10.00	8.00	8.25	8.50
100.0	18.0	10.75	11.25	12.25	10.75	11.25	12.25	10.75	11.25	12.00	10.50	11.25	12.00	9.75	10.25	10.75	10.25	10.75	11.50	9.00	9.75	11.50
100.0	20.0	11.25	12.25	13.25	11.25	12.25	13.25	11.25	12.00	13.00	11.25	12.00	13.00	10.25	11.00	11.75	10.75	11.50	12.50	9.75	11.25	13.25

†Representative of monolithically placed PCC shoulder; ‡Representative of separately placed PCC shoulder

1 in = 25.4 mm  
1 ft = 0.3 m

Table 46. JPCP slab thickness design table for dry-nonfreeze climate (50 percent design reliability).

Traffic million ESAL's	Joint Spacing ft	Standard Width Slabs												Tied PCC Shoulder						Widened Slabs		
		No Base			Aggregate Base E = 30 klb/in <sup>2</sup>			Stabilized Base						Aggregate Base						Aggregate Base E = 30 klb/in <sup>2</sup>		
		k, lbf/in <sup>2</sup> /in			k, lbf/in <sup>2</sup> /in			E = 500 klb/in <sup>2</sup>			E = 1,000 klb/in <sup>2</sup>			Stress LTE = 20% †			Stress LTE = 10% ‡			k, lbf/in <sup>2</sup> /in		
		100	200	400	100	200	400	100	200	400	100	200	400	100	200	400	100	200	400	100	200	400
1.0	12.0	7.75	7.50	7.50	7.75	7.50	7.50	7.75	7.50	7.25	7.50	7.25	7.00	7.00	6.50	6.50	7.25	7.00	6.75	6.50	6.50	6.50
1.0	15.0	8.25	8.25	8.00	8.25	8.25	8.00	8.00	8.00	7.75	8.00	8.00	7.50	7.25	7.00	6.50	7.75	7.50	7.00	6.50	6.50	6.50
1.0	18.0	8.75	8.75	8.50	8.75	8.75	8.50	8.75	8.75	8.00	8.50	8.50	8.00	7.75	7.25	6.50	8.25	8.00	7.25	7.00	6.50	6.50
1.0	20.0	9.25	9.25	8.75	9.25	9.25	8.75	9.00	9.25	8.25	9.00	9.00	8.25	8.00	7.25	6.50	8.50	8.25	7.25	7.50	6.50	6.50
5.0	12.0	8.50	8.50	8.50	8.50	8.50	8.50	8.50	8.25	8.25	8.25	8.25	8.25	7.50	7.50	7.25	8.00	8.00	7.75	6.50	6.50	6.50
5.0	15.0	9.00	9.25	9.50	9.00	9.25	9.50	9.00	9.25	9.50	8.75	9.00	9.25	8.00	8.00	8.00	8.50	8.75	9.00	7.25	7.50	7.50
5.0	18.0	9.75	10.25	10.75	9.75	10.25	10.75	9.75	10.00	10.50	9.50	10.00	10.50	8.75	9.00	9.25	9.25	9.50	9.75	8.25	9.25	10.50
5.0	20.0	10.25	10.75	11.50	10.25	10.75	11.50	10.25	10.75	11.50	10.00	10.75	11.25	9.25	9.50	9.50	9.75	10.25	10.50	9.25	10.25	12.50
10.0	12.0	8.75	8.75	9.00	8.75	8.75	9.00	8.75	8.75	8.75	8.50	8.50	8.75	7.75	7.75	7.75	8.25	8.25	8.25	7.00	6.75	6.75
10.0	15.0	9.50	9.75	10.00	9.50	9.75	10.00	9.25	9.50	10.00	9.25	9.50	10.00	8.50	8.75	9.00	9.00	9.25	9.50	7.75	8.00	9.25
10.0	18.0	10.25	10.75	11.50	10.25	10.75	11.50	10.00	10.75	11.50	10.00	10.50	11.25	9.25	9.75	10.00	9.75	10.00	10.75	9.00	9.75	11.75
10.0	20.0	10.75	11.50	12.50	10.75	11.50	12.50	10.75	11.50	12.50	10.50	11.25	12.25	9.75	10.25	11.00	10.25	11.00	11.75	9.75	11.25	13.50
20.0	12.0	9.00	9.00	9.25	9.00	9.00	9.25	9.00	9.00	9.25	8.75	8.75	9.00	8.00	8.00	8.25	8.50	8.50	8.75	7.25	7.25	7.50
20.0	15.0	9.75	10.00	10.50	9.75	10.00	10.50	9.50	10.00	10.50	9.50	9.75	10.50	8.75	9.00	9.50	9.25	9.50	10.00	8.00	8.75	9.75
20.0	18.0	10.50	11.25	12.25	10.50	11.25	12.25	10.50	11.25	12.25	10.25	11.00	12.00	9.50	10.00	11.00	10.00	10.75	11.50	9.25	10.50	12.50
20.0	20.0	11.25	12.25	13.25	11.25	12.25	13.25	11.25	12.00	13.25	11.00	12.00	13.25	10.25	11.00	12.00	10.75	11.50	12.75	10.00	12.00	14.25
50.0	12.0	9.25	9.50	9.75	9.25	9.50	9.75	9.25	9.25	9.75	9.25	9.25	9.50	8.50	8.50	8.75	8.75	9.00	9.25	7.50	7.75	8.00
50.0	15.0	10.00	10.50	11.25	10.00	10.50	11.25	10.00	10.50	11.25	10.00	10.25	11.00	9.25	9.50	10.25	9.50	10.00	10.75	8.50	9.25	10.50
50.0	18.0	11.00	11.75	13.00	11.00	11.75	13.00	11.00	11.75	13.00	10.75	11.75	13.00	10.00	10.75	12.00	10.50	11.25	12.50	9.75	11.25	13.25
50.0	20.0	11.75	12.75	14.25	11.75	12.75	14.25	11.75	12.75	14.25	11.50	12.75	14.25	10.75	11.75	13.25	11.25	12.25	13.75	10.75	12.75	15.00
100.0	12.0	9.50	9.75	10.00	9.50	9.75	10.00	9.50	9.50	10.00	9.50	9.50	10.00	8.75	8.75	9.25	9.00	9.25	9.50	7.75	8.00	8.75
100.0	15.0	10.25	10.75	11.75	10.25	10.75	11.75	10.25	10.75	11.75	10.25	10.75	11.50	9.50	10.00	10.75	9.75	10.25	11.25	8.75	9.50	11.00
100.0	18.0	11.25	12.25	13.50	11.25	12.25	13.50	11.25	12.25	13.50	11.25	12.25	13.50	10.50	11.25	12.75	10.75	11.75	13.00	10.00	11.75	13.75
100.0	20.0	12.25	13.25	15.00	12.25	13.25	15.00	12.00	13.25	14.75	12.00	13.25	14.75	11.25	12.50	14.00	11.75	12.75	14.50	11.25	13.25	15.00

†Representative of monolithically placed PCC shoulder; ‡Representative of separately placed PCC shoulder

1 in = 25.4 mm  
1 ft = 0.3 m



Table 47. JPCP slab thickness design table for wet-freeze climate (50 percent design reliability).

Traffic million ESAL's	Joint Spacing ft	Standard Width Slabs												Tied PCC Shoulder						Widened Slabs			
		No Base			Aggregate Base E = 30 klb/in <sup>2</sup>			Stabilized Base						Aggregate Base						Aggregate Base E = 30 klb/in <sup>2</sup>			
		k, lbf/in <sup>2</sup> /in			k, lbf/in <sup>2</sup> /in			E = 500 klb/in <sup>2</sup>			E = 1,000 klb/in <sup>2</sup>			Stress LTE = 20% †			Stress LTE = 10% ‡			k, lbf/in <sup>2</sup> /in			
		100	200	400	100	200	400	100	200	400	100	200	400	100	200	400	100	200	400	100	200	400	100
1.0	12.0	7.75	7.50	7.25	7.75	7.50	7.25	7.75	7.50	7.00	7.50	7.25	7.00	7.00	6.50	6.50	7.25	7.00	6.75	6.50	6.50	6.50	
1.0	15.0	8.25	8.00	7.75	8.25	8.00	7.75	8.00	7.75	7.50	8.00	7.75	7.25	7.25	7.00	6.50	7.75	7.50	7.00	6.50	6.50	6.50	
1.0	18.0	8.50	8.50	8.00	8.50	8.50	8.00	8.50	8.25	7.75	8.25	8.25	7.50	7.50	7.25	6.50	8.00	7.75	7.00	7.00	6.50	6.50	
1.0	20.0	8.75	8.75	8.00	8.75	8.75	8.00	8.75	8.50	7.75	8.50	8.25	7.50	7.75	7.25	6.50	8.25	8.00	7.00	7.25	6.50	6.50	
5.0	12.0	8.50	8.25	8.25	8.50	8.25	8.25	8.25	8.25	8.25	8.25	8.00	8.00	7.50	7.25	7.25	8.00	7.75	7.75	6.75	6.50	6.50	
5.0	15.0	9.00	9.00	9.00	9.00	9.00	9.00	8.75	8.75	9.00	8.75	8.75	8.75	8.00	8.00	7.75	8.50	8.50	8.50	7.25	7.25	7.25	
5.0	18.0	9.50	9.75	10.00	9.50	9.75	10.00	9.50	9.75	9.75	9.25	9.50	9.50	8.50	8.50	8.00	9.00	9.00	9.00	8.00	8.25	7.75	
5.0	20.0	10.00	10.25	10.50	10.00	10.25	10.25	9.75	10.25	10.25	9.75	10.00	10.00	8.75	8.75	8.25	9.50	9.50	9.25	8.50	9.00	8.00	
10.0	12.0	8.75	8.50	8.75	8.75	8.50	8.75	8.50	8.50	8.50	8.50	8.25	8.50	7.75	7.75	7.50	8.25	8.00	8.00	6.75	6.75	6.75	
10.0	15.0	9.25	9.25	9.75	9.25	9.25	9.75	9.00	9.25	9.50	9.00	9.25	9.50	8.25	8.25	8.25	8.75	8.75	9.00	7.50	7.75	8.00	
10.0	18.0	10.00	10.25	10.75	10.00	10.25	10.75	9.75	10.25	10.50	9.75	10.00	10.50	9.00	9.00	9.00	9.25	9.75	10.00	8.50	9.00	10.00	
10.0	20.0	10.50	11.00	11.50	10.50	11.00	11.25	10.25	10.75	11.25	10.25	10.75	11.25	9.25	9.50	9.50	9.75	10.25	10.50	9.00	10.00	11.75	
20.0	12.0	9.00	9.00	9.00	9.00	9.00	9.00	8.75	8.75	9.00	8.75	8.75	8.75	8.00	8.00	8.00	8.50	8.50	8.50	7.00	7.25	7.25	
20.0	15.0	9.50	9.75	10.25	9.50	9.75	10.25	9.50	9.75	10.00	9.25	9.50	10.00	8.50	8.75	9.00	9.00	9.25	9.50	7.75	8.25	8.75	
20.0	18.0	10.25	10.75	11.50	10.25	10.75	11.50	10.25	10.75	11.25	10.00	10.50	11.25	9.25	9.75	10.00	9.75	10.25	10.75	8.75	9.75	11.25	
20.0	20.0	10.75	11.50	12.25	10.75	11.50	12.25	10.75	11.50	12.25	10.75	11.25	12.00	9.75	10.25	10.75	10.25	11.00	11.50	9.75	11.00	12.75	
50.0	12.0	9.25	9.25	9.50	9.25	9.25	9.50	9.25	9.25	9.25	9.00	9.00	9.25	8.25	8.25	8.50	8.75	8.75	9.00	7.50	7.50	7.75	
50.0	15.0	10.00	10.25	10.75	10.00	10.25	10.75	9.75	10.25	10.75	9.75	10.00	10.50	9.00	9.25	9.75	9.50	9.75	10.25	8.25	8.75	9.75	
50.0	18.0	10.75	11.25	12.25	10.75	11.25	12.25	10.75	11.25	12.25	10.50	11.25	12.00	9.75	10.25	11.00	10.25	10.75	11.75	9.25	10.50	12.25	
50.0	20.0	11.25	12.25	13.25	11.25	12.25	13.25	11.25	12.00	13.25	11.25	12.00	13.00	10.50	11.25	12.00	10.75	11.75	12.75	10.25	11.75	13.75	
100.0	12.0	9.50	9.50	9.75	9.50	9.50	9.75	9.50	9.50	9.75	9.25	9.25	9.50	8.50	8.50	8.75	9.00	9.00	9.25	7.50	7.75	8.25	
100.0	15.0	10.25	10.50	11.25	10.25	10.50	11.25	10.00	10.50	11.25	10.00	10.50	11.00	9.25	9.50	10.25	9.75	10.00	10.75	8.50	9.00	10.25	
100.0	18.0	11.00	11.75	12.75	11.00	11.75	12.75	11.00	11.75	12.75	11.00	11.75	12.75	10.00	10.75	11.75	10.50	11.25	12.25	9.75	11.00	12.75	
100.0	20.0	11.75	12.75	14.00	11.75	12.75	14.00	11.75	12.50	13.75	11.50	12.50	13.75	10.75	11.75	12.75	11.25	12.25	13.25	10.75	12.25	14.25	

†Representative of monolithically placed PCC shoulder; ‡Representative of separately placed PCC shoulder

1 in = 25.4 mm

1 ft = 0.3 m

Table 48. JPCP slab thickness design table for wet-nonfreeze climate (50 percent design reliability).

Traffic million ESAL's	Joint Spacing ft	Standard Width Slabs											Tied PCC Shoulder						Widened Slabs			
		No Base			Aggregate Base E = 30 klb/in <sup>2</sup>			Stabilized Base					Aggregate Base						Aggregate Base E = 30 klb/in <sup>2</sup>			
		k, lbf/in <sup>2</sup> /in			k, lbf/in <sup>2</sup> /in			E = 500 klb/in <sup>2</sup>			E = 1,000 klb/in <sup>2</sup>		Stress LTE = 20% †			Stress LTE = 10% ‡			k, lbf/in <sup>2</sup> /in			
		100	200	400	100	200	400	100	200	400	100	200	400	100	200	400	100	200	400	100	200	400
1.0	12.0	8.00	8.00	7.75	8.00	8.00	7.75	7.75	7.75	7.75	7.75	7.50	7.25	7.00	6.75	7.50	7.50	7.25	6.50	6.50	6.50	
1.0	15.0	8.50	8.50	8.50	8.50	8.50	8.50	8.25	8.50	8.50	8.25	8.25	8.25	7.50	7.50	7.25	8.00	8.00	8.00	7.00	7.25	7.25
1.0	18.0	9.00	9.25	9.25	9.00	9.25	9.25	9.00	9.00	9.00	8.75	9.00	8.75	8.00	8.00	7.50	8.50	8.75	8.50	7.75	8.00	8.00
1.0	20.0	9.50	9.75	9.50	9.50	9.75	9.50	9.25	9.50	9.25	9.25	9.50	9.25	8.50	8.25	7.50	9.00	9.00	8.50	8.50	9.00	9.00
5.0	12.0	8.50	8.50	8.75	8.50	8.50	8.75	8.50	8.50	8.75	8.50	8.50	8.50	7.75	7.75	7.75	8.25	8.25	8.25	7.00	7.25	7.50
5.0	15.0	9.25	9.50	9.75	9.25	9.50	9.75	9.00	9.50	9.75	9.00	9.25	9.75	8.25	8.50	8.75	8.75	9.00	9.25	7.75	8.25	9.25
5.0	18.0	10.00	10.50	11.00	10.00	10.50	11.00	9.75	10.25	11.00	9.75	10.25	10.75	9.00	9.50	9.75	9.50	10.00	10.25	9.00	9.75	11.00
5.0	20.0	10.50	11.00	11.75	10.50	11.00	11.75	10.50	11.00	11.75	10.25	11.00	11.50	9.50	10.00	10.25	10.00	10.50	11.00	9.75	10.75	12.50
10.0	12.0	8.75	9.00	9.25	8.75	9.00	9.25	8.75	8.75	9.00	8.75	8.75	9.00	8.00	8.00	8.25	8.50	8.50	8.75	7.25	7.50	8.00
10.0	15.0	9.50	9.75	10.25	9.50	9.75	10.25	9.50	9.75	10.25	9.25	9.75	10.25	8.75	9.00	9.50	9.00	9.50	9.75	8.00	8.75	9.75
10.0	18.0	10.25	11.00	11.75	10.25	11.00	11.75	10.25	10.75	11.50	10.25	10.75	11.50	9.50	10.00	10.50	9.75	10.50	11.00	9.25	10.25	11.75
10.0	20.0	11.00	11.75	12.50	11.00	11.75	12.50	10.75	11.50	12.50	10.75	11.50	12.50	10.00	10.75	11.25	10.50	11.25	12.00	10.00	11.50	13.50
20.0	12.0	9.00	9.25	9.50	9.00	9.25	9.50	9.00	9.00	9.50	9.00	9.00	9.25	8.25	8.25	8.50	8.75	8.75	9.00	7.50	7.75	8.25
20.0	15.0	9.75	10.25	10.75	9.75	10.25	10.75	9.75	10.00	10.75	9.75	10.00	10.75	9.00	9.25	10.00	9.25	9.75	10.25	8.50	9.25	10.25
20.0	18.0	10.75	11.25	12.25	10.75	11.25	12.25	10.50	11.25	12.25	10.50	11.25	12.25	9.75	10.50	11.25	10.25	11.00	11.75	9.50	10.75	12.50
20.0	20.0	11.25	12.25	13.25	11.25	12.25	13.25	11.25	12.25	13.25	11.25	12.00	13.25	10.50	11.25	12.25	10.75	11.75	12.75	10.50	12.00	14.00
50.0	12.0	9.50	9.50	10.00	9.50	9.50	10.00	9.25	9.50	9.75	9.25	9.25	9.75	8.50	8.75	9.00	9.00	9.00	9.50	7.75	8.00	8.75
50.0	15.0	10.25	10.75	11.50	10.25	10.75	11.50	10.00	10.50	11.25	10.00	10.50	11.25	9.25	9.75	10.50	9.75	10.25	11.00	8.75	9.50	10.75
50.0	18.0	11.00	12.00	13.00	11.00	12.00	13.00	11.00	11.75	13.00	11.00	11.75	13.00	10.25	11.00	12.00	10.75	11.50	12.50	10.00	11.25	13.25
50.0	20.0	11.75	12.75	14.25	11.75	12.75	14.25	11.75	12.75	14.25	11.75	12.75	14.00	11.00	12.00	13.25	11.25	12.50	13.75	11.00	12.75	14.75
100.0	12.0	9.75	9.75	10.25	9.75	9.75	10.25	9.50	9.75	10.00	9.50	9.75	10.00	8.75	9.00	9.25	9.25	9.25	9.75	8.00	8.25	9.00
100.0	15.0	10.50	11.00	11.75	10.50	11.00	11.75	10.25	11.00	11.75	10.25	10.75	11.75	9.50	10.00	11.00	10.00	10.50	11.25	9.00	9.75	11.25
100.0	18.0	11.50	12.25	13.50	11.50	12.25	13.50	11.25	12.25	13.50	11.25	12.25	13.50	10.50	11.50	12.75	11.00	12.00	13.00	10.25	11.75	13.75
100.0	20.0	12.25	13.25	14.75	12.25	13.25	14.75	12.25	13.25	14.75	12.00	13.25	14.75	11.25	12.50	14.00	11.75	12.75	14.25	11.25	13.25	15.00

†Representative of monolithically placed PCC shoulder; ‡Representative of separately placed PCC shoulder

1 in = 25.4 mm

1 ft = 0.3 m

hold the cracks tightly together, and cracks that were supposed to remain tight have severely deteriorated, resulting in significant reduction in pavement service life.

Over the years, significant progress has been made in steel design procedures for both JRCP and CRCP, providing much more reliable designs. These procedures are discussed in the sections entitled *Reinforcement Design for JRCP* and *Reinforcement Design for CRCP* of this report. Although slab thickness is an important input to the steel design procedures, little work has been done to address thickness design directly for JRCP and CRCP. Most studies on slab thickness design focus on JPCP, and the use of the same thickness as the JPCP thickness remains the only guideline for the thickness design of JRCP and CRCP.

There are two questions that must be addressed in order to optimize slab thickness design of JRCP and CRCP:

- Is the full thickness of JPCP necessary for JRCP and CRCP? The answer depends in part on the amount of reinforcement. The greater the amount of reinforcement, the less the required slab thickness. JRCP and CRCP are designed to accommodate cracking; however, adequate slab thickness must be provided to prevent punchouts and rapid crack deterioration. One study found that the maximum deflection at the cracks and differential deflection across the cracks to be a significant factor affecting the rate of crack deterioration.<sup>(37)</sup> Base type and subgrade stiffness are other important factors influencing the deflection (and subsequent deterioration) of transverse cracks.
- In applying the conventional guidelines, "use the same thickness as JPCP," what is the appropriate joint spacing to use? As discussed in the previous section, joint spacing is one of the more sensitive factors affecting thickness design of JPCP. The required slab thickness is significantly greater for longer slabs.

Further research is needed to develop mechanistic procedures for thickness design of JRCP and CRCP that simultaneously considers thickness and reinforcement requirements. The empirical JRCP crack deterioration model developed under this study includes slab thickness as a parameter, but slab thickness is not a significant factor affecting crack deterioration in this model. For example, the model shows that the amount of deteriorated cracks increases by only 1.5 percent for 3 in (76 mm) reduction in slab thickness (9 in to 6 in [229 mm to 152 mm]). Such a reduction in slab thickness will likely result in uncontrolled cracking or punchouts, and reducing the slab thickness based on this model is therefore inappropriate.

Other prediction models include slab thickness and reinforcement content for JRCP (see references 10 and 11) and for CRCP (see reference 111). Further research is needed to develop a mechanistic model that can address slab shattering or punchout problem as well as crack deterioration.

In the meantime, JPCP thickness design procedures may be used to determine reasonable thickness for JRCP and CRCP, applying the "same thickness as the JPCP" guideline for a joint spacing of approximately 15 ft (4.6 m).

### Concrete Pavement Type Selection Considerations

Throughout the discussion in this chapter, guidelines and design recommendations have been provided on specific elements of JPCP, JRCP, and CRCP designs in order to increase their performance and life. However, no mention has been made regarding the suitability or appropriateness of the different PCC pavement types. Many factors should be considered in the selection of one of these pavement types for a particular roadway, including the following:

- Anticipated traffic levels.
- Initial construction cost or overall life cycle cost.
- Service life.
- Future maintenance and rehabilitation requirements.
- Reliability.
- Subgrade type and condition.
- Agency policies.
- Contractor experience.
- Climatic region.
- Location (urban or rural setting).
- Functional class of roadway (freeway, collector, arterial, local).
- Geometrics.
- Presence of underground utilities.
- Presence of adjacent lanes and curbs.
- Duration of construction and availability of alternate routes.
- Local experience and past performance.

Table 49 has been prepared to summarize relative strengths, weaknesses, and applications of the various PCC pavement types with respect to the above listing. Each pavement type has the potential to provide a long-lasting, smooth-riding roadway, although a particular pavement type may be better suited for certain situations.

JPCP designs are proven, reliable designs that are believed to be applicable in nearly all locations. They are the least complex of the PCC pavement types, and have become by far the most widely used PCC pavement type throughout the world in the last 20 years. Perhaps the most critical design element essential to their success is an effective transverse joint design, consisting of the selection of an effective joint spacing, the provision of adequate load transfer, and provision of a well-designed joint sealant reservoir. However, because of the increased number of joints, this design does have greater joint maintenance requirements. Furthermore, the future rehabilitation of JPCP designs generally calls for careful consideration given to the condition of the transverse joints and their potential impacts on rehabilitation performance.

Table 49. Summary of PCC pavement types.

Pavement Type	Advantages	Disadvantages	Key Design Elements	Applications
JPCP	<ul style="list-style-type: none"> <li>• Reliable design</li> <li>• Can be used in all locations (including intersections)</li> </ul>	<ul style="list-style-type: none"> <li>• Increased joint cost</li> <li>• Increased joint maintenance</li> <li>• Joints may impair future rehabilitation performance</li> </ul>	<ul style="list-style-type: none"> <li>• Effective joint design (joint spacing, load transfer, sealant)</li> </ul>	<ul style="list-style-type: none"> <li>• All locations</li> </ul>
JRCP	<ul style="list-style-type: none"> <li>• Fewer joints</li> <li>• Less concern about random cracking as steel reinforcement is expected to hold cracks together</li> </ul>	<ul style="list-style-type: none"> <li>• Crack deterioration (if inadequate steel)</li> <li>• Joint sealant failures</li> <li>• Joint deterioration</li> <li>• Joints may impair future rehabilitation performance</li> </ul>	<ul style="list-style-type: none"> <li>• Effective joint design (joint spacing, load transfer, sealant)</li> <li>• Effective steel reinforcement design</li> </ul>	<ul style="list-style-type: none"> <li>• Rural and urban freeways and collectors</li> <li>• Not for intersections in urban areas</li> </ul>
CRCP	<ul style="list-style-type: none"> <li>• No joints (except construction joints)</li> <li>• Smooth ride</li> <li>• Low maintenance</li> <li>• Long service life</li> </ul>	<ul style="list-style-type: none"> <li>• High initial cost</li> <li>• Complex to construct</li> <li>• Requires experienced contractor</li> <li>• Rehabilitation (patching) is costly and difficult</li> <li>• Box outs and utility cuts are troublesome</li> </ul>	<ul style="list-style-type: none"> <li>• Effective steel reinforcement design (including splicing)</li> <li>• Strong foundation support</li> <li>• Construction joint design</li> </ul>	<ul style="list-style-type: none"> <li>• High volume urban freeways (but not where utilities are present)</li> <li>• Rural freeways</li> <li>• Not for use in short runs or with complex geometrics</li> </ul>

JRCP designs are an attractive design alternative because they employ fewer transverse joints, which are inherently a weak point in a PCC pavement. However, the performance of JRCP has been hindered by poor joint design (in particular excessive joint spacings that resulted in large joint movements and subsequent joint deterioration) and by inadequate steel reinforcement contents. Nevertheless, with the movement to shorter joint spacings and increased steel reinforcement contents on JRCP, these pavement types can provide excellent performance. They are perhaps most suited to rural and urban freeways and highways, and have had some problems in urban intersections. As with JPCP, future rehabilitation options for JRCP calls for careful consideration given to the condition of the transverse joints and their potential impacts on rehabilitation performance

CRCP designs are high-type, premium pavements suitable for most high-volume freeways. They are an expensive first cost pavement, but should not require substantial maintenance. CRCP are perhaps most applicable in urban areas, where their long life and low maintenance requirements are attractive to highway agencies who want to avoid frequent shut downs or other traffic disruptions. However, they are also suited to rural freeways and Interstates, again where a long-lasting, low-maintenance pavement is desired. Although a few highway agencies have not had good experience with CRCP (most likely because of poor design, construction, and

support conditions), CRCP is widely used by several highway agencies on many high-volume roadways.

Rehabilitation of CRCP can be difficult and costly, particularly if significant full-depth repairs are required. However, full-depth repairs in CRCP generally perform well until a structural improvement is needed; both AC and unbonded PCC overlays have worked well.

In summary, the selection of a particular PCC pavement type must consider all of the previous factors listed while recognizing the different design requirements and performance capabilities of each pavement type. Each construction situation is unique in terms of location and design, and some of the factors listed previously will be of greater importance in some situations than in others. The conduct of a life-cycle cost analysis is one attractive method used by many agencies to aid in the selection of a pavement type, but this should be supplemented with engineering judgment and tempered with local experience to identify the most appropriate pavement type for a given situation.

## Summary

The preceding sections have described recommendations for various aspects of concrete pavement design. As mentioned earlier, it is critical that the entire pavement be designed as a system, and not as a collection of design features and elements derived independently. The relative effects of each individual design feature on the performance of the pavement must be directly considered and evaluated prior to its inclusion.

Several basic design requirements must be met in order for the pavement to perform as intended. These include:

- Provision of adequate subgrade support, through either replacement or stabilization of deficient material.
- Provision of positive drainage to remove excess water from pavement structure.
- Provision of nonerodible or permeable base to minimize pumping and loss of support.
- Provision of a granular subbase beneath a treated base course to control erosion and facilitate drainage.
- Consideration of need for longitudinal edge support:
  - Widened PCC slabs in most rural areas.
  - Tied PCC shoulders in most urban areas (formed monolithically with mainline pavement preferred).
- Provision of a competent joint design:
  - selection of joint spacing for JPCP to minimize slab curling effects.
  - inclusion of dowel bars for pavements designed for 5 million ESAL's or more.

- in suitable locations, selection of long-lasting joint sealant in a properly designed joint reservoir.
- Provision of adequately tied longitudinal joints to prevent horizontal and vertical separation.
- Provision of adequate reinforcement in JRCP (minimum 0.10 percent) and in CRCP (minimum 0.60 percent).
- Provision of adequate PCC strength for load carrying capacity, durability, and wear resistance.
- Provision of adequate slab thickness to carry traffic loading and prevent fatigue cracking.

Recommendations have been developed for each of these key elements, and these are summarized in tables 50, 51, and 52. These tables merely summarize the recommendations described in the chapter; the specific section in the chapter should be consulted for a complete treatment on the topic.

For very heavily-trafficked roadways (design ESAL's greater than 20 million), consideration should be given to adopting several positive design features in order to maximize the performance of the pavement and increase its reliability. For example, European researchers have defined four classes of "modernity elements," factors that are expected to contribute to the overall performance of the pavement.<sup>(79)</sup> The four classes are:

- Nonerosible base course (specifically, lean concrete base).
- Positive pavement drainage.
- Strengthened structure (thickened slab, doweled joints, or continuously reinforced concrete pavement [CRCP]).
- Optimization of the use of materials with respect to loading (widened PCC slabs or trapezoidal cross sections).

One other factor that should perhaps be added to this list is the inclusion of a granular subbase layer (beneath the base course and on top of the subgrade) to help control erosion, facilitate drainage, and to provide additional support and frost protection.

Based on the performance of the European sections (documented in volume IV of this report), pavements with 3 or 4 modernity elements exhibit outstanding performance in the face of very heavy traffic loadings. It is recommended that heavily-trafficked pavements in the U.S. be designed in a similar fashion in order to increase both the reliability of the design and the overall level of performance.

Table 50. Summary of structural design recommendations for medium- and heavy-trafficked roadways.

Design Aspect	Design/Construction/Performance Impacts	Recommended Use	Design Recommendation
Subgrade Preparation	<ul style="list-style-type: none"> <li>Stronger subgrade facilitates construction activities.</li> <li>Stronger support decreases slab stresses.</li> <li>Important to preventing volumetric changes.</li> </ul>	<ul style="list-style-type: none"> <li>Should be considered on every paving project depending on in situ soils.</li> </ul>	<ul style="list-style-type: none"> <li>Minimum CBR of 6 obtained through                             <ul style="list-style-type: none"> <li>Stabilization (using appropriate stabilizing agent)</li> <li>Replacement of existing soil with high quality material.</li> </ul> </li> <li>Increase uniformity by subcutting, remixing, and compacting.</li> <li>Thick granular layer considered in frost areas.</li> </ul>
Drainage	<ul style="list-style-type: none"> <li>Reduced faulting, pumping, and erosion potential by removing excess moisture from pavement structure.</li> </ul>	<ul style="list-style-type: none"> <li>On all projects in which:                             <ul style="list-style-type: none"> <li>need for drainage exists (according to procedure described in text), and.</li> <li>design traffic &gt; 5 million ESALs.</li> </ul> </li> <li>Must be able to offset additional costs with corresponding increase in life.</li> </ul>	<ul style="list-style-type: none"> <li>Permeable base drainage system consisting of:                             <ul style="list-style-type: none"> <li>Permeable base (stabilized or nonstabilized)</li> <li>Separator layer</li> <li>Pipe collector system</li> </ul> </li> <li>Nonerrodible base constructed with permeable base beneath the shoulders and edge drains placed within the shoulder.</li> </ul>
Base Type (and subbase)	<ul style="list-style-type: none"> <li>Stable base facilitates construction and aids in obtaining smooth surface.</li> <li>Stabilized bases reduce load stresses, but also increase curling stresses.</li> <li>Drainage and frost protection provided by base.</li> </ul>	<ul style="list-style-type: none"> <li>Permeable base or LCB for most medium- and high-trafficked roadways.</li> <li>Stabilized bases and aggregate bases for low to medium-trafficked roadways.</li> <li>Granular subbase beneath all base types for medium and high traffic.</li> </ul>	<ul style="list-style-type: none"> <li>Permeable base minimum 4 in thick; stabilized or nonstabilized; designed and constructed in accordance with guidelines.</li> <li>LCB: minimum 4 in thick; minimum 8% cement; perhaps notched and bonded to slab.</li> <li>ATB/CTB: minimum 4 in thick; minimum 6% AC or 8% cement; plant-mixed for high quality.</li> <li>Aggregate: minimum 6 in thick; compacted to 95% density.</li> <li>Granular subbase: minimum 6 in thick.</li> </ul>
Shoulder Type/ Edge Support	<ul style="list-style-type: none"> <li>Widened PCC slabs and tied PCC shoulders reduce critical edge stresses and corner deflections.</li> </ul>	<ul style="list-style-type: none"> <li>Tied PCC shoulders on most high-type roadways, especially in urban areas.</li> <li>Widened lanes on most medium- and high-type roadways.</li> </ul>	<ul style="list-style-type: none"> <li>Tied PCC shoulders:                             <ul style="list-style-type: none"> <li>Tied with minimum No. 5 bar, 30-in long, at 30 in spacings</li> <li>Monolithic paving preferred, with same thickness as mainline.</li> <li>Joints match mainline pavement</li> </ul> </li> <li>Widened PCC slabs:                             <ul style="list-style-type: none"> <li>Maximum 14 ft (4.3 m) total slab width.</li> </ul> </li> </ul>
JRCP Reinforcement	<ul style="list-style-type: none"> <li>Greater amounts of reinforcing steel reduces deteriorated transverse cracks.</li> </ul>	<ul style="list-style-type: none"> <li>On all JRCP projects.</li> </ul>	<ul style="list-style-type: none"> <li>Absolute minimum reinforcement content of 0.10%, with minimum levels of 0.15 to 0.20% recommended in severe climates.</li> </ul>
CRCP Reinforcement	<ul style="list-style-type: none"> <li>Greater amounts of reinforcing steel reduces punchouts and deteriorated transverse cracks.</li> </ul>	<ul style="list-style-type: none"> <li>On all CRCP projects.</li> </ul>	<ul style="list-style-type: none"> <li>Absolute minimum reinforcement content of 0.60%, with minimum levels of 0.65 to 0.70% recommended in severe climates (additional steel increases design reliability more than increases in thickness).</li> </ul>
PCC Strength	<ul style="list-style-type: none"> <li>Greater strength increases fatigue life and increases durability and wear resistance.</li> </ul>		<ul style="list-style-type: none"> <li>Minimum 28-day flexural strength of 650 lbf/in<sup>2</sup>.</li> </ul>
PCC Thickness	<ul style="list-style-type: none"> <li>Greater slab thickness increases fatigue life.</li> </ul>		<ul style="list-style-type: none"> <li>Designed in accordance with approved procedure, but checked with design tables included in chapter.</li> </ul>



Table 51. Summary of transverse joint design recommendations for medium- and heavy-trafficked roadways.

Design Aspect	Design/Construction/Performance Impacts	Recommended Use	Design Recommendation
Sawcut Timing	<ul style="list-style-type: none"> <li>Late transverse joint sawing results in uncontrolled random transverse cracking.</li> </ul>		<ul style="list-style-type: none"> <li>Saw as early as possible without causing significant raveling, generally within 4 to 12 hours.</li> <li>Sawcut timing can be related to concrete compressive strength (see guidelines).</li> </ul>
Sawcut Depth	<ul style="list-style-type: none"> <li>Inadequate sawcut depths of transverse joints result in uncontrolled random transverse cracking.</li> </ul>		<ul style="list-style-type: none"> <li>Minimum sawcut depth of 25 percent of the slab thickness, but this might need to be increased to a depth of 33 percent of the slab thickness for slabs placed on permeable or stabilized bases.</li> </ul>
JPCP Joint Spacing	<ul style="list-style-type: none"> <li>Shorter joint spacings reduce curling stresses and joint movements.</li> <li>Increased maintenance requirements associated with greater number of joints.</li> </ul>		<ul style="list-style-type: none"> <li>Joint spacing a function of slab thickness, climate, traffic, and subgrade support (see guidelines).</li> <li>Generally between 15 and 18 ft, with 20 ft the absolute maximum.</li> </ul>
JRCP Joint Spacing	<ul style="list-style-type: none"> <li>Shorter joint spacings reduce curling stresses and joint movements.</li> </ul>		<ul style="list-style-type: none"> <li>Mixed performance results, but current trends are to shorter spacings (e.g., 30 ft).</li> </ul>
Variable Joint Spacing	<ul style="list-style-type: none"> <li>Reduction in rhythmic response of vehicles due to joint faulting.</li> </ul>	<ul style="list-style-type: none"> <li>Unknown if nonuniform joints are warranted for the wheel bases and suspension systems of today's vehicles.</li> <li>Unknown if nonuniform joints are necessary on doweled pavements.</li> <li>Not recommended for JRCP designs.</li> </ul>	<ul style="list-style-type: none"> <li>If used, shorter joint spacing combinations with smaller deviations between slab sizes (e.g., 12-15-13-14 ft) have performed better.</li> </ul>
Joint Orientation	<ul style="list-style-type: none"> <li>Theoretical reduction in joint stresses and deflections due to axle wheels not crossing joint at the same time.</li> </ul>	<ul style="list-style-type: none"> <li>Recommended for use on nondoweled pavements only.</li> </ul>	<ul style="list-style-type: none"> <li>Maximum skew of 2 ft in 12 ft, with some suggesting no more than 1 ft in 10 ft.</li> </ul>
Joint Load Transfer	<ul style="list-style-type: none"> <li>Reduction in key joint distress (pumping, faulting, loss of support, corner breaks).</li> </ul>	<ul style="list-style-type: none"> <li>Dowel bars recommended on all pavements designed for 5 million or more ESAL applications.</li> </ul>	<ul style="list-style-type: none"> <li>Dowel diameter primarily a function of slab thickness.</li> <li>Minimum diameter of 1.25 in for most medium-trafficked roadways; 1.50 for high-trafficked roadways.</li> <li>Dowel bars 18 in long, epoxy-coated for corrosion protection, and spaced uniformly across the joint at 12-in intervals.</li> </ul>
Joint Sealant/Reservoir Design	<ul style="list-style-type: none"> <li>Prevention of water and incompressibles from infiltrating in joint and pavement structure.</li> </ul>	<ul style="list-style-type: none"> <li>Recommended on most jointed pavements (unless local experience and conditions dictate otherwise).</li> </ul>	<ul style="list-style-type: none"> <li>Joint sealant reservoirs should be designed with consideration given to the type of sealant, the anticipated movements, and the recommended shape factor (see guidelines).</li> <li>Preformed joint sealants provide the best performance of all joint sealants.</li> </ul>

1 in = 25.4 mm; 1 ft = 0.305 m

Table 52. Summary of longitudinal lane-lane contraction joint design recommendations for medium- and heavy-trafficked roadways.

Design Aspect	Design/Construction/Performance Impacts	Recommended Use	Design Recommendation
Forming Method	<ul style="list-style-type: none"> <li>Inadequate longitudinal joint forming leads to development of uncontrolled longitudinal cracking.</li> </ul>		<ul style="list-style-type: none"> <li>Sawcutting of longitudinal joints is more effective for creating the weakened plane than plastic ribbon inserts.</li> </ul>
Sawcut Timing	<ul style="list-style-type: none"> <li>Late longitudinal joint sawing results in uncontrolled random longitudinal cracking.</li> </ul>		<ul style="list-style-type: none"> <li>Saw as early as possible without causing significant raveling, generally within 4 to 12 hours.</li> <li>Sawcut timing can be related to concrete compressive strength (see guidelines).</li> </ul>
Sawcut Depth	<ul style="list-style-type: none"> <li>Inadequate sawcut depths of longitudinal joints result in uncontrolled random longitudinal cracking.</li> </ul>		<ul style="list-style-type: none"> <li>Minimum sawcut depth of 33 percent of the slab thickness.</li> </ul>
Joint Spacing	<ul style="list-style-type: none"> <li>Excessive spacing between longitudinal joints causes uncontrolled random longitudinal cracking.</li> </ul>		<ul style="list-style-type: none"> <li>Minimum 12 ft and maximum 14 ft spacings between longitudinal joints.</li> </ul>
Tie Bars	<ul style="list-style-type: none"> <li>Hold lanes together to prevent separation and excessive vertical movements.</li> </ul>	<ul style="list-style-type: none"> <li>All longitudinal joints (up to a maximum of 3 lanes tied together).</li> </ul>	<ul style="list-style-type: none"> <li>Minimum No. 5 bar placed at 30-in intervals.</li> <li>Larger diameter bars at closer spacings should be considered for areas frequently crossed by trucks (e.g., ramps).</li> <li>Tie bars placed at mid-depth of the slab.</li> </ul>

1 in = 25.4 mm; 1 ft = 0.305 m

## REFERENCES

1. *The Long-Term Pavement Performance Program Guide*, Federal Highway Administration, LTPP Division, Washington, DC, December 1993.
2. Smith, K. D., D. G. Peshkin, M. I. Darter, A. L. Mueller, and S. H. Carpenter, *Performance of Jointed Concrete Pavements, Volume I: Evaluation of Concrete Pavement Performance and Design Features*, FHWA-RD-89-136, Federal Highway Administration, Washington, DC, March 1990.
3. Smith, K. D., A. L. Mueller, M. I. Darter, and D. G. Peshkin, *Performance of Jointed Concrete Pavements, Volume II: Evaluation and Modification of Concrete Pavement Design and Analysis Models*, FHWA-RD-89-137, Federal Highway Administration, Washington, DC, July 1990.
4. Smith, K. D., D. G. Peshkin, M. I. Darter, and A. L. Mueller, *Performance of Jointed Concrete Pavements, Volume III: Summary of Research Findings*, FHWA-RD-89-138, Federal Highway Administration, Washington, DC, November 1990.
5. Smith, K. D., D. G. Peshkin, M. I. Darter, A. L. Mueller, and S. H. Carpenter, *Performance of Jointed Concrete Pavements, Volume IV: Appendix A—Project Summary Reports and Summary Tables*, FHWA-RD-89-139, Federal Highway Administration, Washington, DC, March 1990.
6. Smith, K. D., D. G. Peshkin, M. I. Darter, A. L. Mueller, and S. H. Carpenter, *Performance of Jointed Concrete Pavements, Volume V: Appendix B—Data Collection and Analysis Procedures*, FHWA-RD-89-140, Federal Highway Administration, Washington, DC, March 1990.
7. Mueller, A. L., D. G. Peshkin, K. D. Smith, and M. I. Darter, *Performance of Jointed Concrete Pavements, Volume VI: Appendix C—Synthesis of Concrete Pavement Design Methods and Analysis Models, and Appendix D—Summary of Analysis Data for the Evaluation of Predictive Models*, FHWA-RD-89-141, Federal Highway Administration, Washington, DC, July 1990.
8. *Long-Term Pavement Performance Information Management System—Data User's Guide*, FHWA-RD-93-094, Federal Highway Administration, LTPP Division, Washington, DC, July 1993.
9. Ioannides, A. M., Y. H. Lee, and M. I. Darter, "Control of Faulting Through Jointed Load Transfer Design," *Transportation Research Record* 1286, Transportation Research Board, Washington, DC, 1990.
10. Darter M. I., J. M. Beck, M. B. Snyder, and R. E. Smith, *Portland Cement Concrete Pavement Evaluation System-COPES*, NCHRP Report 277, Transportation Research Board, Washington, DC, 1985.

11. Simpson, A. L., J. B. Rauhut, P. R. Jordahl, E. Owusu-Antwi, M. I. Darter, and R. Ahmad, *Early Analysis of LTPP General Pavement Studies Data, Volume 3: Sensitivity Analyses for Selected Pavement Distresses*, Report SHRP-P-393, Strategic Highway Research Program, Washington, DC, 1994.
12. Wu, C. L., J. W. Mack, P. A. Okamoto, and R. G. Packard, "Prediction of Faulting of Joints in Concrete Pavements," *Proceedings, Fifth International Conference on Concrete Pavement Design and Rehabilitation*, Vol. 2., Purdue University, West Lafayette, Indiana, April 1993.
13. Darter, M.I., and E.J. Barenberg, *Design of Zero-Maintenance Plain Jointed Concrete Pavement, Volume 1—Development of Design Procedures*, FHWA-RD-77-111, Washington, DC, 1977.
14. Heinrichs, K. W., M. J. Liu, M. I. Darter, S.H. Carpenter, and A. M. Ioannides, *Rigid Pavement Analysis and Design*, FHWA-RD-88-068, Federal Highway Administration, Washington, DC, 1989.
15. Friberg, B. F., "Design of Dowels in Transverse Joints of Concrete Pavements", *Transactions, American Society of Civil Engineers*, Vol. 105, 1940.
16. *AASHTO Guide for Design of Pavement Structures*, American Association of Highway and Transportation Officials, Washington, DC, 1986.
17. *S-PLUS for Windows: User's Manual*, Vol.1 and Vol. 2, Statistical Science Inc., Seattle, WA, March 1993.
18. *S-PLUS for Windows: Reference Manual*, Vol.1 and Vol. 2, Statistical Science Inc., Seattle, WA, March 1993.
19. Ray, M. and J. P. Christory, "Combatting Concrete Pavement Slab Pumping: State of the Art and Recommendations," *Proceedings, Fourth International Conference on Concrete Pavement Design and Rehabilitation*, Purdue University, West Lafayette, Indiana, 1989.
20. Ioannides, A. M., M. R. Thompson, and E. J. Barenberg, "Westergaard Solution Reconsidered," *Transportation Research Record 1043*, Transportation Research Board, Washington, DC, 1985.
21. Foxworthy, P.T., *Concepts for the Development of a Nondestructive Testing and Evaluation System for Rigid Airfield Pavements*, Ph.D. Thesis, University of Illinois, 1985.
22. Dempsey, B.J., W.A. Herlache, and A.J. Patel, *The Climatic-Materials-Structural Pavement Analysis Program User's Manual*, FHWA/RD-82/126, Federal Highway Administration, Washington, DC, 1986.

23. Eisenmann, J., and G. Leykauf, "Simplified Calculation Method of Slab Curling Caused by Surface Shrinkage," *Proceedings, 2nd International Workshop on Theoretical Design of Concrete Pavements*, Madrid, Spain, 1990.
24. Eisenmann, J., and G. Leykauf, "Effects of Paving Temperatures on Pavement Performance," *Proceedings, 2nd International Workshop on Theoretical Design of Concrete Pavements*, Madrid, Spain, 1990.
25. Salsilli, R.A., E.J. Barenberg, and M.I. Darter, "Calibrated Mechanistic Design Procedure to Prevent Transverse Cracking of Jointed Plain Concrete Pavements," *Proceedings of the 5<sup>th</sup> International Conference on Concrete Pavement Design and Rehabilitation*, Purdue University, 1993.
26. Westergaard, H. M., "New Formulas for Stresses in Concrete Pavements of Airfields," *Transactions, American Society of Civil Engineers*, Volume 113, 1948.
27. Seiler, W.J., "Expedient Stress Analysis of Jointed Concrete Pavement Loaded by Aircraft with Multiwheel Gear," *Transportation Research Record 1370*, Transportation Research Board, Washington, DC, 1993.
28. Benekohal, R.F., K.T. Hall, and H.W. Miller, "Effects of Lane Widening on Lateral Distribution of Truck Wheels," *Transportation Research Record 1286*, Transportation Research Board, Washington, DC, 1990.
29. Bradbury, R. D., *Reinforced Concrete Pavements*, Wire Reinforcement Institute, 1938.
30. Westergaard, H. M., "Analysis of Stresses in Concrete Pavements Due to Variations of Temperature," *Proceedings, Sixth Annual Meeting*, Highway Research Board, Washington, DC, 1926.
31. Miner, M. A., "Cumulative Damage in Fatigue," *Transactions, ASME*, Volume 67, 1945.
32. Darter, M.I., *A Comparison Between Corps of Engineers and ERES Consultants, Inc. Rigid Pavement Design Procedures*, Technical Report Prepared for the United States Air Force SAC, Urbana, IL, 1988.
33. Treybig, H.J., B.F. McCullough, P. Smith, and H. Von Quintus, *Overlay Design and Reflection Cracking Analysis for Rigid Pavements*, Volume 2, Design Procedures, FHWA-RD-77-67, Federal Highway Administration, Washington, DC, 1977.
34. Darter, M. I., K. T. Hall, and C. M. Kuo, *Support Under Portland Cement Concrete Pavements*, NCHRP Report 372, Transportation Research Board, Washington, DC, 1995.

35. Armaghani, J.M., T.J. Larsen, and L.L. Smith, "Temperature Response of Concrete Pavements," *Transportation Research Record 1121*, Transportation Research Board, Washington, DC, 1987.
36. Snyder, M.B., "Effect of Reinforcement Design and Foundation Stiffness on the Deterioration of Transverse Cracks in Jointed Reinforced Concrete Pavements," *Proceedings, Third International Workshop on the Design and Evaluation of Concrete Roads*, Vienna, Austria, 1994.
37. Bruinsma, J.E., Z.I. Raja, M.B. Snyder, and J.M. Vandenbossche, *Factors Affecting the Deterioration of Transverse Cracks in JRCP*, Final Report, Contract 90-0973, Michigan Department of Transportation, Lansing, MI, 1995.
38. *Subgrade Stability Manual*, Policy Mat-10, Illinois Department of Transportation, Springfield, IL, 1982.
39. *Report on the 1992 U.S. Tour of European Concrete Highways*, Federal Highway Administration, FHWA-SA-93-012, Washington, DC, January 1993.
40. Larson, R. M., S. Vanikar, and S. Forster, *Summary Report—U.S. Tour of European Concrete Highways (U.S. TECH)—Follow-up Tour of Germany and Austria*, Federal Highway Administration, FHWA-SA-93-080, Washington, DC, October 1993.
41. Carpenter, S. H., M. R. Crovetti, K. L. Smith, E. H. Rmeili, and T. P. Wilson, *Soil and Base Stabilization and Associated Drainage Considerations, Volume I: Pavement Design and Construction Considerations*, FHWA-SA-93-004, Federal Highway Administration, Washington, DC, December 1992.
42. *Soil-Cement Laboratory Handbook*, Engineering Bulletin EB052SC, Portland Cement Association, Skokie, IL, 1992.
43. *Soil-Cement Construction Handbook*, Engineering Bulletin EB003SC, Portland Cement Association, Skokie, IL, 1995.
44. *A Basic Asphalt Emulsion Manual*, Manual Series No. 19 (MS-19), The Asphalt Institute, Lexington, KY, 1987.
45. *Lime Stabilization: Reactions, Properties, Design, and Construction*, Transportation Research Board, State of the Art Report 5, Washington, DC, 1987.
46. Barenberg, E. J. and M. R. Thompson, *Lime-FlyAsh-Stabilized Bases and Subbases*, NCHRP Synthesis of Highway Practice No. 37, Transportation Research Board, Washington, DC, 1976.
47. *Guide to Earthwork Construction*, Transportation Research Board, State of the Art Report 8, Washington, DC, 1990.

48. Cole, L.W. and M.J. Hall, Relative Costs of Various Concrete Pavement Features, paper presented at 1997 Annual Meeting of the Trans. Research Board, Wash., D.C.. 1997.
49. Carpenter, S. H., M. I. Darter, B. J. Dempsey, and S. Herrin, *A Pavement Moisture Accelerated Distress (MAD) Identification System*, FHWA/RD-81/079, Federal Highway Administration, Washington, DC, 1981.
50. *AASHTO Guide for Design of Pavement Structures — 1993*, American Association of State Highway and Transportation Officials, Washington, DC, 1993.
51. *Drainable Pavement Systems*, FHWA-SA-92-008, Federal Highway Administration, Washington, DC, 1992.
52. *Highway Design Manual*, Fifth Edition, California Department of Transportation, Sacramento, CA, 1995.
53. Hoffman, G. L., "Importance of Pavement Drainage," *Virginia Pavement Drainage Workshop*, Virginia Department of Transportation, Williamsburgh, VA, 1990.
54. Kazmierowski, T. J., A. Bradbury, and J. Hajek, "Field Evaluation of Various Types of Open-Graded Drainage Layers," *Transportation Research Record 1440*, Transportation Research Board, 1994.
55. *Design Criteria for Portland Cement Concrete Pavements (PCCP)*, Design Information Bulletin Number 80 (draft), California Department of Transportation, Sacramento, CA, November 1995.
56. *WSDOT Pavement Guide*, Volume 1—Pavement Policy, Washington State Department of Transportation, Olympia, WA, February 1995.
57. *Permeable Aggregate Base Drainage Systems*, Design Guidelines, Minnesota Department of Transportation, St. Paul, MN, April 1994.
58. *The New York State Thickness Design Manual for New and Reconstructed Pavements*, Technical Report, New York State Department of Transportation, New York, NY, April 1993.
59. *Policy Statement for Future MHTD Pavement Design*, Missouri Highway and Transportation Department, Jefferson City, MO, January 8, 1993.
60. *AASHTO Design Procedures for New Pavements*, FHWA-HI-94-023, National Highway Institute/Federal Highway Administration, Washington, DC, 1994.
61. Casagrande, A. and W. L. Shannon, "Base Course Drainage for Airport Pavements," *Transactions*, Vol 117, American Society of Civil Engineers, New York, NY, 1952.

62. Cedergren, H. R., *Seepage, Drainage, and Flow Nets*, John Wiley and Sons, New York, NY, 1967.
63. Moulton, L. K., *Highway Subdrainage Design*, FHWA-TS-80-224, Federal Highway Administration, Washington, DC, 1980.
64. Wells, G. K., *Evaluate Stripping of Asphalt Treated Permeable Base*, Minor Research Report 65332-638047-39303, California Department of Transportation, Sacramento, CA, 1993.
65. Crovetti, J. A. and B. J. Dempsey, "Hydraulic Requirements of Permeable Bases," *Transportation Research Record 1425*, Transportation Research Board, Washington, DC, 1993.
66. Wells, G. K., "Improving Pavement Performance," *Virginia Pavement Drainage Workshop*, Virginia Department of Transportation, Williamsburgh, VA, 1990.
67. Koerner, R. M., G. R. Koerner, A. K. Fahim, and R. F. Wilson-Fahmy, *Long-Term Performance of Geosynthetics in Drainage Applications*, NCHRP Report 367, Transportation Research Board, 1994.
68. Allen, D. L. and J. Fleckenstein, "Evaluation and Performance of Geocomposite Edgedrains in Kentucky," *Transportation Research Record 1329*, Transportation Research Board, Washington, DC, 1991.
69. Solberg, C., "Open Graded Bases Under PCC," *Virginia Pavement Drainage Workshop*, Virginia Department of Transportation, Williamsburgh, VA, 1990.
70. Reed, C. M., "Impact of Open-Graded Drainage Layers on the Construction of Concrete Pavements in Illinois," *Transportation Research Record 1478*, Transportation Research Board, Washington, DC, 1995.
71. Steffes, R. F., V. J. Marks, and K. L. Dirks, "Video Evaluation of Highway Drainage Systems," *Transportation Research Record 1329*, Transportation Research Board, Washington, DC, 1991.
72. Ahmed, Z. and T. D. White, "Methodology for Inspection of Collector Systems," *Transportation Research Record 1425*, Transportation Research Board, Washington, DC, 1995.
73. Allen, D., "Kentucky's Experience with Longitudinal Edge Drains," *Virginia Pavement Drainage Workshop*, Virginia Department of Transportation, Williamsburgh, VA, 1990.
74. *1985 Wisconsin Interstate Pavement Rehabilitation Study*, Wisconsin Department of Transportation, Madison, WI, 1985.



75. *Combating Concrete Pavement Slab Pumping by Interface Drainage and Use of Low-Erodability Materials: State of the Art and Recommendations*, Permanent International Association of Road Congresses, Paris, France, 1987.
76. Christory, J., "Assessment of PIARC Recommendation on the Combating of Pumping in Concrete Pavements," *6th International Symposium on Concrete Roads*, Madrid, Spain, 1990.
77. Van Wijk, A. J. and C. W. Lovell, "Prediction of Subbase Erosion Caused by Pavement Pumping," *Transportation Research Record 1099*, Transportation Research Board, Washington, DC, 1986.
78. Hall, M., "Cement-Stabilized Open-Graded Base Strength Testing and Field Performance Versus Cement Content," *Transportation Research Record 1440*, Transportation Research Board, Washington, DC, 1994.
79. Christory, J. P., "COPES System, Europe-USA Cooperation," *Proceedings*, Volume 190.7.B, XIXth World Road Congress, Marrakech, Morocco, September 22-28, 1991.
80. Wells, G. K., *Summary Report to Improve Jointed Plain Concrete Pavement (JPCP) Performance*, Minor Research Report, California Department of Transportation, Sacramento, CA, 1993.
81. Yu, H. T., K. D. Smith, and M. I. Darter, *Field and Analytical Evaluation of the Effects of Tied PCC Shoulder and Widened Slabs on Performance of JPCP*, Final Report, Colorado Department of Transportation, Denver, CO, October 1995.
82. *Materials for Aggregate and Soil-Aggregate Subbase, Base, and Surface Courses*, AASHTO Specification M147-65, American Association of State Highway and Transportation Officials, Washington, DC, 1991.
83. *The AASHO Road Test*, Special Report 61E, Highway Research Board, Washington, DC, 1962.
84. Tayabji, S. D., D. G. Zollinger, G. T. Korovesis, P. J. Stephanos, and J. S. Gagnon, *Performance of CRC Pavements, Volume 1: Annotated Bibliography and Summary of Practice*, FHWA-RD-94-178, Federal Highway Administration, Washington, DC, 1994.
85. Tayabji, S. D., P. J. Stephanos, J. S. Gagnon, and D. G. Zollinger, *Performance of CRC Pavements, Volume 2: Field Investigations of CRC Pavements*, FHWA-RD-94-179, Federal Highway Administration, Washington, DC, 1994.
86. Tayabji, S. D., D. G. Zollinger, J. R. Vederey, and J. S. Gagnon, *Performance of CRC Pavements, Volume 3: Analysis and Evaluation of Field Test Data*, FHWA-RD-94-180, Federal Highway Administration, Washington, DC, 1994.

87. *Concrete Pavement Joints*, Technical Advisory T 5040.30, Federal Highway Administration, Washington, DC, November 30, 1990.
88. Wells, G. K. and W. A. Nokes, *Field Review—PCC Shoulder Performance Near Geyserville*, Minor Research Report 65328-637378-30088, California Department of Transportation, Sacramento, CA, 1990.
89. Vyce, J. M., *A Summary of Experimental Concrete Pavements in New York*, Report FHWA/NY-RR-88/141, New York State Department of Transportation, Albany, NY, 1988.
90. Fuchs, F., and A. Jasienski, *The Design and Maintenance of Contraction Joints: Behaviour of the Namur Test Roads After 10 Years of Traffic*, Proceedings, Sixth International Conference on Concrete Roads, Madrid, Spain, October 1990.
91. Okamoto, P. A., P. J. Nussbaum, K. D. Smith, M. I. Darter, T. P. Wilson, C. L. Wu, and S. D. Tayabji, *Guidelines for Timing Contraction Joint Sawing and Earliest Loading for Concrete Pavements, Volume I—Final Report*, FHWA-RD-91-079, Federal Highway Administration, Washington, DC, October 1991.
92. Okamoto, P. A., P. J. Nussbaum, K. D. Smith, M. I. Darter, T. P. Wilson, C. L. Wu, and S. D. Tayabji, *Guidelines for Timing Contraction Joint Sawing and Earliest Loading for Concrete Pavements, Volume II—Appendix*, FHWA-RD-91-080, Federal Highway Administration, Washington, DC, October 1991.
93. *Benefits of Using Dowel Bars*, Technical Paper 89-03, Federal Highway Administration, Washington, DC, 1989.
94. Wells, G. K. and W. A. Nokes, *Synthesize PCCP Design Parameters Research by Caltrans and Others*, Minor Research Report 65328-637391-31111, California Department of Transportation, Sacramento, CA, 1991.
95. Ayton, G. P., "Concrete Highway Pavements in Australia," *Proceedings*, Fifth International Conference on Concrete Pavement Design and Rehabilitation, Purdue University, West Lafayette, IN, April 20–22, 1993.
96. McGhee, K. H., *Design, Construction, and Maintenance of PCC Pavement Joints*, Synthesis of Highway Practice 211, Transportation Research Board, Washington, DC, 1995.
97. Kelleher, K. and R. M. Larson, "The Design of Plain Doweled Jointed Concrete Pavement," *Proceedings*, Fourth International Conference on Concrete Pavement Design and Rehabilitation, Purdue University, West Lafayette, IN, April 18-20, 1989.

98. Ioannides, A. M. and G. T. Korovesis, "Aggregate Interlock: A Pure-Shear Load Transfer Mechanism," *Transportation Research Record 1286*, Transportation Research Board, Washington, DC, 1990.
99. Snyder, M. B., M. J. Reiter, K. T. Hall, and M. I. Darter, *Rehabilitation of Concrete Pavements, Volume I: Repair Rehabilitation Techniques*, FHWA-RD-88-071, Federal Highway Administration, Washington, DC, 1989.
100. *Guide to Sealing Joints in Concrete Structures*, ACI Committee 504, American Concrete Institute, Detroit, MI, 1990.
101. *Techniques for Pavement Rehabilitation, Participants Manual*, National Highway Institute, Federal Highway Administration, Washington, DC, 1993.
102. Tons, E., *A Theoretical Approach to Design of a Road Joint Seal*, Highway Research Board Bulletin 229, Highway Research Board, Washington, DC, 1959.
103. Smith, K. D., D. G. Peshkin, M. I. Darter, A. L. Mueller, and S. H. Carpenter, *Performance of Jointed Concrete Pavements, Volume I: Evaluation of Concrete Pavement Performance and Design Features*, FHWA-RD-89-136, Federal Highway Administration, Washington, DC, 1990.
104. Darter, M. I., *Initial Evaluation of Michigan JRCR Crack Deterioration*, Technical Report, Michigan Concrete Paving Association, Lansing, MI, February 1989.
105. Kunt, M. M. and B. F. McCullough, *Improved Design and Construction Procedures for Concrete Pavements Based on Mechanistic Modeling Techniques*, Research Report 1169-5F, Texas Department of Transportation, Austin, TX, June 1992.
106. *Jointed Concrete Pavements Reinforced with Welded Wire Fabric*, Wire Reinforcement Institute, Inc., 1975.
107. Iwama, S., *Experimental Studies on the Structural Design of Concrete Pavement*, Technical Report, Public Works Research Institute, Ministry of Construction, Japan, May 1964.
108. Nakamura, T. and T. Iijama, "Evaluation of Performance and Structural Design Methods of Cement Concrete Pavements in Japan," *Proceedings, Session 1, Seventh International Symposium on Concrete Roads*, Vienna, Austria, October 3-5, 1994.
109. Older, C., "Highway Research in Illinois," *Transactions*, Volume 87, paper 1546, American Society of Civil Engineers, 1924.
110. *Mechanistic Pavement Design*, Supplement to Section 7 of the Illinois Department of Transportation Design Manual, Illinois Department of Transportation, Springfield, IL, August 1989.

111. Lee, Y. H. and M. I. Darter, *Development of Pavement Prediction Models*, FHWA-IL-UI-250, Illinois Department Of Transportation, Springfield, IL, July 1994.
112. Won, M., K. Hankins, and B. F. McCullough, *Mechanistic Analysis of CRC Pavements Considering Material Characteristics, Variability, and Fatigue*, Report No. 1169-2, Texas Department of Transportation, Austin, TX, April 1990.
113. LaCoursiere, S. A., M. I. Darter, and S. A. Smiley, *Performance of Continuously Reinforced Concrete Pavement in Illinois*, FHWA-IL-UI-172, Illinois Department of Transportation, Springfield, IL, 1978.
114. Zollinger, D. G. and E. J. Barenberg, *Continuously Reinforced Pavements: Punchouts and Other Distresses and Implications for Design*, FHWA/IL/UI/227, Illinois Department of Transportation, Springfield, IL, 1990.
115. Burke, J. E., and J. S. Dhamrait, "A Twenty-Year Report on the Illinois Continuously Reinforced Pavement," *Highway Research Record No. 239*, Highway Research Board, Washington, DC, 1968.
116. Roman, R. J. and M. I. Darter, *Pavement Distress Study for Interstate Route 77, Fairfield and Chester Counties, South Carolina*, Final Report, South Carolina Department of Highways and Public Transportation, Columbia, SC, 1988.
117. Dhamrait, J. S. and R. K. Taylor, *Behavior of Experimental CRC Pavements in Illinois*, FHWA-IL-PR-82, Illinois Department of Transportation, Springfield, IL, March 1979.
118. *Continuously Reinforced Concrete Pavement*, FHWA Technical Advisory T 5080.14, Federal Highway Administration, Washington, DC, 1990.
119. Betenson, W.B., *The Evolution of Portland Concrete Pavements (PCCP) in Utah*, 7th Annual FHWA Region 8 Concrete Pavement Workshop, Utah Department of Transportation, Salt Lake City, Utah, February 6-8, 1996.
120. Tayabji, S. D., C. G. Ball, and P. A. Okamoto, *Effect of Concrete Shoulders on Concrete Pavement Performance*, FHWA/MN/RD-83/05, Minnesota Department of Transportation, St. Paul, MN, 1983.